

NUREG/CR-2256
EPRI NP-2013
WCAP-9891

PWR FLECHT SEASET

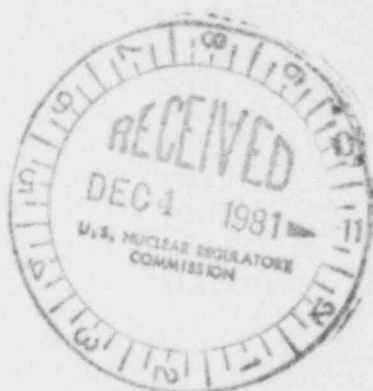
Unblocked Bundle, Forced and Gravity Reflood Task

Data Evaluation and Analysis Report

NRC/EPRI/Westinghouse Report No. 10

Prepared by N. Lee, S. Wong, H. C. Yeh, L. E. Hochreiter

Jointly Sponsored by
USNRC, EPRI, and Westinghouse



8112170476 811130
PDR NUREG
CR-2256 R PDR

NOTICE

This report was prepared as an account of work sponsored by an agency of the United States Government. Neither the United States Government nor any agency thereof, or any of their employees, makes any warranty, expressed or implied, or assumes any legal liability or responsibility for any third party's use, or the results of such use, of any information, apparatus product or process disclosed in this report, or represents that its use by such third party would not infringe privately owned rights.

Available from

GPO Sales Program
Division of Technical Information and Document Control
U. S. Nuclear Regulatory Commission
Washington, D. C. 20555
Printed copy price: \$14.00

and

National Technical Information Service
Springfield, Virginia 22161

FLECHT SEASET Program
NRC/EPRI/Westinghouse Report No. 10
NUREG/CR-2256
EPRI NP-2013
WCAP-9891

PWR FLECHT SEASET
UNBLOCKED BUNDLE, FORCED AND
GRAVITY REFLOOD TASK
DATA EVALUATION AND ANALYSIS REPORT

November 1981

N. Lee
S. Wong
H. C. Yeh
L. E. Hochreiter

prepared for

United States Nuclear Regulatory Commission
Washington, DC 20555

Electric Power Research Institute
3412 Hillview Avenue
Palo Alto, California 94303

and

Westinghouse Electric Corporation
Nuclear Energy Systems
P.O. Box 355
Pittsburgh, Pennsylvania 15230

by

Westinghouse Electric Corporation
under
Contract No. NRC-04-77-127, EPRI Project No. RP959-1

Program Management Group
NRC - L. H. Sullivan
EPRI - K. H. Sun
Westinghouse - H. W. Massie, Jr.

NRC FIN B6204

LEGAL NOTICE

This report was prepared as an account of work sponsored by the U.S. Nuclear Regulatory Commission, the Electric Power Research Institute, Inc., and the Westinghouse Electric Corporation. Neither the United States government nor any agency thereof, nor the Institute or members thereof, nor the Westinghouse Electric Corporation, nor any of their employes, makes any warranty, expressed or implied, or assumes any legal liability or responsibility for any third party's use or the results of such use of any information, apparatus, product, or process disclosed in this report or represents that its use by such third party would not infringe privately owned rights.

ABSTRACT

This analysis of the unblocked bundle task data provides further understanding of reflood heat transfer mechanisms, which can be used for assessing prediction models. A new heat transfer correlation has been developed and shown to predict the FLECHT SEASET data as well as the older FLECHT data. The scaling logic of maintaining the same integrated power per unit flow area has been proved valid, and a method has been developed to calculate steam quality just above the quench front. Improved models for estimating effluence rate and preliminary exploration of the transition zone above the quench front are discussed. Droplet size and velocity data deduced from high-speed movies taken during the tests have led to better understanding of these parameters. A model has been proposed to predict the onset of droplet entrainment, and an analytical expression to predict critical void fraction developed. A network analysis of radiation heat exchange and calculation of convective heat transfer are among efforts expected to give better prediction for heat transfer and wall temperature transients. Recommendations evolving from the data analysis are also included.

ACKNOWLEDGMENTS

The work of the following Westinghouse Nuclear Energy Systems contributors is hereby acknowledged:

PWR PROJECTS L. Chajson

SAFEGUARDS DEVELOPMENT

R. P. Vijuk
A. Tong
E. R. Rosa
M. J. Loftus
C. E. Dodge
K. Beatty
D. H. Dixon
M. A. Emery
D. P. Kitzmiller
D. W. Sklarsky
K. F. McNamee

FACILITIES ENGINEERING

L. R. Katz
B. R. Sinwell
P. M. Brumbaugh
M. M. Valkovic

TEST OPERATIONS

C. E. Fuchs
P. F. Orangis
F. L. Lilly
J. T. Martin
N. Washington
J. Kalo
M. Mulligan
J. Tomasic
J. Letta

The work of the following members of the Program Management Group, their colleagues, and their consultants is hereby acknowledged:

EPRI - K. H. Sun, R. B. Duffey, L. B. Thompson
NRC-NRR - W. Hodges
EG&G - G. Wilson, D. Ogden
NUS Corporation - D. A. Prelewicz

GLOSSARY

This glossary explains definitions, acronyms, and symbols included in the text which follows.

Analysis -- The examination of data to determine, if possible, the basic physical processes that occur and the interrelation of the processes. Where possible, physical processes will be identified from the data and will be related to first principles.

Average fluid conditions -- average thermodynamic properties (for example, enthalpy, quality, temperature, pressure) and average thermal-hydraulic parameters (for example, void fraction, mass flow rate) which are derived from appropriately reduced data for a specified volume or a specified cross-sectional area

Axial peaking factor -- ratio of the peak-to-average power for a given power profile

Blocked -- a situation in which the flow area in the rod bundle or single tube is purposely obstructed at selected locations so as to restrict the flow

Bottom of core recovery (BOCR) -- a condition at the end of the refill period in which the lower plenum is filled with injected ECC water as the water is about to flood the core

Bundle -- a number of heater rods, including spares, which are assembled into a matrix with CRG-type rods, using necessary support hardware to meet the Task Plan design requirements

Carryout -- same as carryover

Carryout rate fraction -- the fraction of the inlet flooding flow rate which flows out the rod bundle exit by upflowing steam

Carryover -- the process in which the liquid is carried in a two-phase mixture out of a control volume, that is, the test bundle

Computational methods -- the procedure of reducing, analyzing, and evaluating data or mathematical expressions, either by hand calculations or by digital computer codes

Computer code -- a set of specific instructions in computer language to perform the desired mathematical operations utilizing appropriate models and correlations

Computer data acquisition system (CDAS) -- the system which controls the test and records data for later reduction and analysis

Computer tape -- magnetic tapes that store FLECHT SEASET data

Core rod geometry (CRG) -- a nominal rod-to-rod pitch of 12.6 mm (0.496 inch) and outside nominal diameter of 9.50 mm (0.374 inch) representative of various nuclear fuel vendors' new fuel assembly geometries (commonly referred to as the 17x17 or 16x16 assemblies)

Correlation -- a set of mathematical expressions, based on physical principles and experimental data but resting primarily on experimental data, which describes the thermal-hydraulic behavior of a system

Cosine axial power profile -- the axial power distribution of the heater rods in the CRG bundle that contains the maximum (peak) linear power at the midplane of the active heated rod length. This axial power profile will be used on all FLECHT SEASET tests as a fixed parameter.

Data -- recorded information, regardless of form or characteristic, of a scientific or technical nature. It may, for example, document research, experimental, developmental, or engineering work, or be usable to define a design or process or to procure, produce, support, maintain, or operate material. The data may be graphic or pictorial delineations in media such as drawings or photographs, text in specifications or related performance or design type documents, or computer printouts. Examples of data include research and engineering data, engineering drawings and associated lists, specifications, standards, process sheets, manuals, technical reports, catalog item identifications and related information, computer programs, computer codes, computer data bases, and computer software documentation. The term data

does not include financial, administrative, cost and pricing, and management information or other information incidental to contract administration.

Data validation -- a procedure used to ensure that the data generated from a test meet the specified test conditions, and that the instrumentation was functioning properly during the test

Design and procurement -- the design of the system, including the specification (consistent with the appropriate Task Plan) of the material, component, and/or system of interest; and the necessary purchasing function to receive the material, component, and/or system on the test site. This does not preclude Contractor from constructing components and systems on the test site to meet requirements of the Task Plan.

ECC -- emergency core cooling

Entrainment -- the process by which liquid, typically in droplet form, is carried in a flowing stream of gas or two-phase mixture

Evaluation -- the process of comparing the data with similar data, other data sets, existing models and correlations, or computer codes to arrive at general trends, consistency, and other qualitative descriptions of the results

Faliback -- the process whereby the liquid in a two-phase mixture flows countercurrent to the gas phase

FLECHT -- Full-Length Emergency Core Heat Transfer test program

FLECHT SEASET -- Full-Length Emergency Core Heat Transfer - Systems Effects and Separate Effects Tests

FLECHT SET -- Full-Length Emergency Core Heat Transfer - Systems Effects Tests

Heat transfer mechanisms -- the process of conduction, convection, radiation, or phase changes (for example, vaporization, condensation, boiling) in a control volume or a system

Hypothetical -- conjectured or supposed. It is understood that this program is concerned with study of physical phenomena associated with reactor accidents that have an extremely low probability and are therefore termed hypothetical.

Loss-of-coolant accident -- a break in the pressure boundary integrity resulting in loss of core cooling water

Model -- a set of mathematical expressions generated from physical laws to represent the thermal-hydraulic behavior of a system. A model rests on physical principles.

PMG -- Program Management Group

Pressurized water reactor (PWR) -- a nuclear reactor type in which the system pressure exceeds saturation pressure, thus preventing gross vapor formation under normal operating conditions

Reduce data -- convert data from the measured signals to engineering units. In some cases the data are manipulated in a simple fashion to calculate quantities such as flows.

Separation -- the process whereby the liquid in a two-phase mixture is separated and detached from the gas phase

Silicon-controlled rectifier (SCR) -- a rectifier control system used to supply dc current to the bundle heater rods

Spacer grids -- the metal matrix assembly (egg crate design) used to support and space the heater rods in a bundle array

Test section -- lower plenum, bundle, and upper plenum

Test site -- the location of the test facilities where tests will be conducted

Transducer -- the devices used in experimental systems that sense the physical quantities, such as temperature, pressure, pressure difference, or power, and transform them into electrical outputs, such as volts

Unblocked -- the situation in which the flow area in the rod bundle or a single tube is not purposely obstructed

TABLE OF CONTENTS

Section	Title	Page
1	INTRODUCTION	1-1
	1-1. Background	1-1
	1-2. Task Objectives	1-3
	1-3. Data Evaluation and Analysis Objectives	1-3
	1-4. Report Organization	1-4
2	TEST DESCRIPTION	2-1
	2-1. Introduction	2-1
	2-2. Test Facility	2-1
	2-3. Heater Rod Bundle	2-2
	2-4. System Design Features	2-6
	2-5. Low Mass Housing	2-6
	2-6. Bundle Differential Pressure Cells	2-7
	2-7. Heater Rod Seals	2-7
	2-8. Steam Probes	2-7
	2-9. Pressure Control	2-9
	2-10. Facility and Bundle Operation	2-9
	2-11. Power Measurement	2-9
	2-12. Coolant Injection System	2-10
	2-13. Test Procedure	2-10
	2-14. Summary of Run Conditions and Test Results	2-12
3	PARAMETRIC EFFECTS	3-1
	3-1. Introduction	3-1
	3-2. Flooding Rate Effect	3-6
	3-3. Pressure Effect	3-7
	3-4. Subcooling Effect	3-14
	3-5. Initial Clad Temperature Effect	3-20

TABLE OF CONTENTS (cont)

Section	Title	Page
	3-6. Rod Peak Power Effect	3-20
	3-7. Variable Flooding Rate Effect	3-27
	3-8. Transient Subcooling Effect	3-27
	3-9. Data Repeatability	3-35
	3-10. Overlap Tests	3-40
 4	BUNDLE FLOW CONDITIONS	 4-1
	4-1. Introduction	4-1
	4-2. Mass and Energy Balance in Bundle	4-1
	4-3. General Mass and Energy Balance	4-2
	4-4. Mass and Energy Balance Above Quench Front	4-3
	4-5. Mass and Energy Balance Below Quench Front	4-6
	4-6. Coupling of Mass and Energy Balance at Quench Front	4-8
	4-7. Axial Dependence of Bundle Mass Flows and Qualities	4-10
 5	EFFLUENCE RATE AND TRANSITION ZONE	 5-1
	5-1. Introduction	5-1
	5-2. Available Models for Mass Effluence Rate	5-1
	5-3. Yeh/Hochreiter Model for Predicting Mass Effluence	5-1
	5-4. New Mass Effluence Rate Model	5-7
	5-5. Implementation of Models in FLEMB	5-13
	5-6. Comparisons With Data	5-14
	5-7. Transition Zone Above Quench Front	5-14

TABLE OF CONTENTS (cont)

Section	Title	Page
6	EVALUATION OF DISPERSED DROPLET FLOW CONDITIONS AND HEAT TRANSFER MECHANISMS DURING REFLOOD	6-1
	6-1. Introduction	6-1
	6-2. Energy Absorption by Droplets Above Quench Front	6-2
	6-3. Flow Regimes Above Quench Front	6-6
	6-4. Basic Relations for Two-Phase Flow Properties in Dispersed Flow Regime	6-8
	6-5. Basic Heat Transfer Components in Dispersed Flow Regime	6-11
	6-6. Analysis of Radiative Heat Exchange in Rod Bundles	6-12
	6-7. FLECHI SEASET Test Runs Analyzed	6-16
	6-8. Calculated Flow Conditions and Basic Heat Transfer Components in Dispersed Flow Regime	6-19
7	MECHANISTIC MODEL FOR DISPERSED FLOW HEAT TRANSFER	7-1
	7-1. General	7-1
	7-2. Model Description	7-1
	7-3. Results and Data Comparisons	7-3
8	HEAT TRANSFER CORRELATION	8-1
	8-1. Introduction	8-1
	8-2. Quench Correlation	8-2
	8-3. Heat Transfer Coefficient Correlation	8-6
9	CONCLUSIONS AND RECOMMENDATIONS	9-1
Appendix A	MASS STORAGE IN BUNDLE	A-1
Appendix B	MASS AND ENERGY BALANCE (FLEMB) RESULTS	B-1

TABLE OF CONTENTS (cont)

Section	Title	Page
Appendix C	INPUT AND OUTPUT SUMMARY OF DATA EVALUATION MODELS	C-1
Appendix D	CALCULATION OF LOCAL QUALITY IN BUNDLE	D-1
Appendix E	ANALYSIS OF FLECHT SEASET DROPLET MOVIE DATA	E-1
Appendix F	CALCULATION OF DROPLET SIZE AND DROP VELOCITY IN DISPERSED FLOW REGIME	F-1
Appendix G	COMPARISON OF HEAT TRANSFER CORRELATION WITH DATA FOR OVERLAP RUNS	G-1
Appendix H	COMPARISON OF HEAT TRANSFER CORRELATION WITH DATA FOR NONOVERLAP RUNS	H-1
Appendix I	HEAT TRANSFER CORRELATION COMPUTER PROGRAM	I-1

LIST OF ILLUSTRATIONS

Figure	Title	Page
2-1	Flow Diagram for Forced Reflood Configuration (FLECHT SEASET Unblocked Bundle)	2-3
2-2	Bundle Cross Section	2-5
2-3	FLECHT SEASET Unblocked Bundle Test Section Housing Differential Pressure Cell Hookup	2-8
3-1	Flooding Rate Effect on Heat Transfer [1.83 m (72 in.) Elevation]	3-8
3-2	Flooding Rate Effect on Temperature	3-8
3-3	Flooding Rate Effect on Carryout Fraction	3-9
3-4	Quench Front Advances at Various Flooding Rates	3-9
3-5	Temperature Rise Comparisons at Various Flooding Rates	3-10
3-6	Quench Time Versus Flooding Rate	3-11
3-7	Temperature Rise Versus Flooding Rate and Rod Peak Power	3-12
3-8	Quench Time Versus Flooding Rate and Rod Peak Power	3-13
3-9	Pressure Effect on Heat Transfer	3-15
3-10	Pressure Effect on Temperature	3-15
3-11	Pressure Effect on Carryout Fraction	3-16
3-12	Pressure Effect on Quench Front Advance	3-16
3-13	Pressure Effect on Temperature Rise and Quench Time	3-17
3-14	Subcooling Effect on Heat Transfer	3-18
3-15	Subcooling Effect on Temperature	3-18
3-16	Subcooling Effect on Carryout Fraction	3-19
3-17	Subcooling Effect on Quench Front Advance	3-19
3-18	Subcooling Effect on Temperature Rise and Quench Time	3-21
3-19	Initial Clad Temperature Effect on Heat Transfer	3-22
3-20	Initial Clad Temperature Effect on Temperature	3-22
3-21	Initial Clad Temperature Effect on Carryout Fraction	3-23
3-22	Initial Clad Temperature Effect on Quench Front Advance	3-23
3-23	Initial Clad Temperature Effect on Temperature Rise and Quench Time	3-24

LIST OF ILLUSTRATIONS (cont)

Figure	Title	Page
3-24	Peak Power Effect on Heat Transfer	3-25
3-25	Peak Power Effect on Temperature	3-25
3-26	Peak Power Effect on Carryout Fraction	3-26
3-27	Peak Power Effect on Quench Front Advance	3-26
3-28	Peak Power Effect on Temperature Rise and Quench Time	3-28
3-29	Initial Flooding Rate Effect on Heat Transfer, Run 32333	3-29
3-30	Initial Flooding Rate Effect on Temperature, Run 32333	3-29
3-31	Initial Flooding Rate Effect on Heat Transfer, Run 32235	3-30
3-32	Initial Flooding Rate Effect on Temperature, Run 32235	3-30
3-33	Initial Flooding Rate Effect on Carryout Fraction, Run 32333	3-31
3-34	Initial Flooding Rate Effect on Carryout Fraction, Run 32235	3-31
3-35	Initial Flooding Rate Effect on Quench Curve, Runs 32333 and 31805	3-32
3-36	Initial Flooding Rate Effect on Quench Curve, Runs 32235 and 34209	3-32
3-37	Initial Flooding Rate Effect on Temperature Rise and Quench Time	3-33
3-38	Low Plenum Temperature Comparison	3-34
3-39	Subcooling Transient Effect on Heat Transfer	3-36
3-40	Subcooling Transient Effect on Temperature	3-36
3-41	Individual Channel Comparisons for Repeat Tests	3-37
3-42	Average Temperature Comparison for Repeat Tests	3-38
3-43	Average Heat Transfer Coefficient Comparison for Repeat Tests	3-38
3-44	Comparison of Quenching Behavior in Repeat Tests	3-39
3-45	Overlap Test Quench Curve Comparison, FLECHT SEASET Run 31263 and Cosine Run 03113	3-43

LIST OF ILLUSTRATIONS (cont)

Figure	Title	Page
3-46	Overlap Test Quench Curve Comparison, FLECHT SEASET Run 30817 and Cosine Run 00904	3-44
3-47	Overlap Test Quench Curve Comparison, FLECHT SEASET Run 30619 and Cosine Run 03709	3-45
3-48	Overlap Test Quench Curve Comparison, FLECHT SEASET Run 31805 and Cosine Run 02414	3-46
3-49	Overlap Test Heat Transfer Coefficient Comparison, FLECHT SEASET Run 31203 and Cosine Run 03113	3-47
3-50	Overlap Test Heat Transfer Coefficient Comparison, FLECHT SEASET Run 30817 and Cosine Run 00904	3-48
3-51	Overlap Test Heat Transfer Coefficient Comparison, FLECHT SEASET Run 30619 and Cosine Run 03709	3-49
3-52	Overlap Test Heat Transfer Coefficient Comparison, FLECHT SEASET Run 31805 and Cosine Run 02414	3-50
4-1	Control Volumes	4-4
4-2	Local Quality at Various Elevations, Run 31504	4-12
4-3	Equilibrium Quality at Various Elevations, Run 31504	4-12
4-4	Vapor Temperature at Various Elevations, Run 31504	4-15
4-5	Local Quality at 1.83 m (72 in.), Run 31504	4-15
4-6	Mass Effluence Rate, Run 31504	4-16
5-1	FLECHT SEASET Froth Level, Collapsed Liquid Level, and Saturation Level Data	5-4
5-2	Comparison of Calculated and Measured Void Fraction, Run 31504 (2 sheets)	5-5
5-3	Comparison of Calculated and Measured Mass Storage Rate, Run 31504	5-8
5-4	Assumptions in Model Development	5-10
5-5	Mass Effluence Fraction Compared With Model Predictions, Run 31504	5-15
5-6	Typical Conditions in Rod Bundle During Reflood	5-16

LIST OF ILLUSTRATIONS (cont)

Figure	Title	Page
5-7	Temperature and Heat Transfer Coefficient Curve, Showing Transition Zone (II)	5-18
5-8	Schematic Construction of Transition Zone Curve	5-19
5-9	Transition Front Curve, Run 31203	5-20
5-10	Transition Front Curve, Run 31302	5-20
5-11	Transition Front Curve, Run 31504	5-2
5-12	Transition Front Curve, Run 31805	5-21
5-13	Transition Front Curve, Run 31922	5-22
5-14	Transition Front Curve, Run 32013	5-22
5-15	Transition Front Curve, Run 31701	5-23
5-16	Transition Front Curve, Run 34006	5-23
5-17	Comparison of Temperature Histories of Rod and Thimble Thermocouples and Steam Probe at 2.03 m (96 in.) Elevation, Run 31504	5-24
6-1	Comparisons of Bundle Heat Release and Heat Absorption by Droplets, Run 31504	6-4
6-2	Comparisons of Bundle Heat Release and Heat Absorption by Droplets, Run 31302	6-5
6-3	Schematic Diagram of Characteristic Vapor Quality and Void Fraction During Reflood	6-7
6-4	Six Radiation Nodes for Calculating Radiation Heat Transfer in FLECHT SEASET 161-Rod Bundle	6-13
6-5	Radiation Network for Calculating Radiation Heat Transfer in FLECHT SEASET 161-Rod Bundle	6-14
6-6	Data-Based Wall Temperature, Steam Temperature, and Steam Quality	6-21
6-7	Calculated Vapor Void Fraction in Dispersed Flow Regime	6-22
6-8	Calculated Vapor Reynolds Number in Dispersed Flow Regime	6-23

LIST OF ILLUSTRATIONS (cont)

Figure	Title	Page
6-9	Calculated Optical Thickness in Dispersed Flow Regime	6-24
6-10	Calculated Drop Sizes in Dispersed Flow Regime	6-25
6-11	Calculated Drop and Vapor Velocities in Dispersed Flow Regime	6-26
6-12	Relative Contribution of Convective Heat Flux During Reflood at 1.83 m (72 in.) and 3.05 m (120 in.) Elevations	6-29
6-13	Calculated Nusselt Number (Based on Heater Rod Total Heat Flux) Versus Vapor Reynolds Number	6-31
6-14	Calculated Nusselt Number (Based on Heater Rod Convective Heat Flux) Versus Vapor Reynolds Number	6-32
6-15	Typical Wall Heat Flux Axial Distribution for a Cosine-Shaped Power Profile Heater Rod During Reflood	6-34
6-16	Calculated Nusselt Number (Based on Heater Rod Convective Heat Flux) Versus Liquid Volume Fraction	6-36
7-1	Predicted Droplet Heat Absorption Rate Between 1.83 and 2.29 m (72 and 90 in.) Elevations	7-4
7-2	Predicted Droplet Heat Absorption Rate Between 2.90 and 3.05 m (114 and 120 in.) Elevations	7-5
7-3	Comparisons of Predicted Steam Quality With Data-Based Steam Quality	7-7
7-4	Comparisons of Predicted Vapor Temperature With Data, 1.83 m (72 in.) Elevation	7-8
7-5	Comparisons of Predicted Vapor Temperature With Data, 3.05 m (120 in.) Elevation	7-9
7-6	Comparisons of Predicted Wall Temperature (Rod 8H) With Data, 1.83 m (72 in.) Elevation	7-10
7-7	Comparisons of Predicted Wall Temperature With Data, 3.05 m (120 in.) Elevation	7-11
8-1	Quench Correlation Versus Data, FLECHT SEASET Run 31203	8-8

LIST OF ILLUSTRATIONS (cont)

Figure	Title	Page
8-2	Quench Correlation Versus Data, FLECHT Cosine Run 03113	8-9
8-3	Quench Correlation Versus Data, FLECHT Skewed Profile Run 11618	8-10
8-4	Present Correlation, WCAP-9183 Correlation, and WCAP-8638 Correlation Versus Data, FLECHT Cosine Run 06638	8-11
8-5	Present Correlation, WCAP-9183 Correlation, and WCAP-8838 Correlation Versus Data, FLECHT Cosine Run 03113	8-12
8-6	Present Correlation, WCAP-9183 Correlation, and WCAP-8838 Correlation Versus Data, FLECHT Cosine Run 02414	8-13
8-7	Adiabatic, Developing, and Quasi-Steady Periods in Heat Transfer Coefficient Correlation	8-15
8-8	Comparison of Time of First Droplet Observation in FLECHT Movies and Time When Heat Transfer Coefficient Starts To Increase	8-17
8-9	Time of First Droplet Observed in FLECHT Movies	8-19
8-10	Comparison of Heat Transfer Coefficient Correlation With Data From FLECHT SEASET Run 31203	8-25
8-11	Comparison of Heat Transfer Coefficient Correlation With Data From Cosine Power Run 03113	8-26
8-12	Comparison of Heat Transfer Coefficient Correlation With Data From Skewed Power Run 11618	8-27
8-13	Comparison of Present Heat Transfer Coefficient Correlation With Previous Correlations, Cosine Power Run 02414	8-29
8-14	Comparison of Present Heat Transfer Coefficient Correlation With Previous Correlations, Cosine Power Run 03113	8-30
8-15	Comparison of Present Heat Transfer Coefficient Correlation With Previous Correlations, Cosine Power Run 06638	8-31

LIST OF ILLUSTRATIONS (cont)

Figure	Title	Page
8-16	Comparison of Predicted and Measured Quench Front Elevations for a Semiscale Test	8-32
8-17	Comparison of Predicted and Measured Clad Surface Temperatures for a Semiscale Test	8-33
8-18	Comparison of Predicted and Measured Heat Transfer Coefficients for a BWR FLECHT Test	8-34

LIST OF TABLES

Table	Title	Page
1-1	Comparison of PWR Vendors' Fuel Rod Geometries (Old and New)	1-2
2-1	FLECHT SEASET Unblocked Bundle Reflood Test Data Summary	2-13
3-1	Summary of Run Numbers and Range of Parameters	3-2
3-2	Subcooling Transient Effect	3-34
3-3	Repeat and Previous Test Data Comparison [1.83 m (72 in.)]	3-41
3-4	Overlap Test Conditions	3-42
4-1	Runs Analyzed by FLEMB	4-11
6-1	Reflood Test Runs With Available Droplet Distribution Data Analyzed by HEAT-II Code	6-17
6-2	Reflood Test Runs With An Input SMD at Transition Front Analyzed by HEAT-II Code	6-18
6-3	Basic Heat Transfer Components in Dispersed Droplet Flow During Reflood	6-27
7-1	Summary of Input and Output Variables for Dispersed Flow Heat Transfer Model	7-2
8-1	Overlap Runs	8-7

SECTION 1 INTRODUCTION

1-1. BACKGROUND

The present nonproprietary data base for reflood heat transfer in a simulated pressurized water reactor (PWR) is limited to heater rod bundles that are typified by the Westinghouse 15x15 design and results from the Full-Length Emergency Core Heat Transfer (FLECHT) tests. These tests utilized rod bundles built to the Westinghouse 15x15 (or 14x14) dimensions which are representative of all the PWR vendors' dimensions (table I-1, old fuel assembly dimensions). PWR reactor and PWR fuel vendors are currently utilizing new fuel assembly dimensions (smaller fuel rod diameter and pitch) in their nuclear power plants, as shown in table I-1; therefore, there is a need for testing smaller fuel assembly dimensions. The tests planned under this task - Unblocked Bundle, Forceo and Gravity Reflood Task - utilized a new core rod geometry (CRG)⁽¹⁾ that is typified by the Westinghouse 17x17 fuel rod design, as presented in table I-1. This CRG is representative of all current vendors' PWR fuel assembly geometries.

Models which predict the dependence of reflood heat transfer and mass carryout rate fractions (CRF) as a function of fuel bundle geometry (particularly rod diameter and pitch) have not been fully established ... either phenomenological or correlational form. Carryout rate fraction models have been developed utilizing an energy balance method by Sun and Duffey⁽²⁾ and similarly by Yeh and Hochreiter.⁽³⁾ However, these models could benefit from experimental verification relative to fuel rod geometries other than the 15x15 type rod geometry.

-
1. The CRG is defined in this program as a nominal rod-to-rod pitch of 12.6 mm (0.496 in.) and outside nominal diameter of 9.5 mm (0.374 in.) representative of various nuclear vendors' new fuel assembly geometries and commonly referred to as the 17x17 or 16x16 assemblies.
 2. Sun, K. H., and Duffey, R. B., "A Generalized Model for Predicting Mass Effluences During Reflooding," Nucl. Tech. 43, 22-27 (1979).
 3. Yeh, H. C., and Hochreiter, L. E., "Mass Effluence During FLECHT Forced Reflood Experiments," Trans. Amer. Nucl. Soc. 24, 301-302 (1976).

TABLE I-1

COMPARISON OF PWR VENDORS' FUEL
ROD GEOMETRIES (OLD AND NEW)

Vendor	Rod Diameter [mm (in.)]	Rod Pitch [mm (in.)]
NEW FUEL ASSEMBLIES (CRG)		
Westinghouse	9.5 (0.374)	12.6 (0.496)
Babcock & Wilcox	9.63 (0.379)	12.8 (0.502)
Combustion Engineering	9.7 (0.382)	12.9 (0.506)
OLD FUEL ASSEMBLIES		
Westinghouse	10.7 (0.422)	14.3 (0.563)
Babcock & Wilcox	10.9 (0.430)	14.4 (0.568)
Combustion Engineering	11.2 (0.440)	14.7 (0.580)

The tests performed in this task are classified as separate effects tests. In this case the bundle is isolated from the system and the thermal-hydraulic conditions are prescribed at the bundle entrance and exit. Within the bundle, the dimensions are full scale, compared to a PWR, with the exception of overall radial dimension. The low mass housing used in these test series was designed to minimize the wall effects such that the rods one row or more away from the housing in the FLECHT bundle are representative of any region in a PWR core. Examination of the housing performance for the skewed axial profile FLECHT tests indicates that it does simulate this radial boundary condition and that only the rods immediately adjacent to the housing are principally affected by the housing presence. To preserve proper thermal scaling of the FLECHT facility with respect to a PWR, the power to flow area ratio is nearly the same as that of a PWR fuel assembly. In this fashion, the steam vapor superheat, entrainment, and fluid flow behavior should be similar to that expected in a PWR for the same boundary conditions.

1-2. TASK OBJECTIVES

The objectives of the unblocked bundle task (with a bundle having a cosine axial profile) are to develop a data base which meets the following objectives:

- To aid in the development or verification of computational methods used by others to predict the reflood thermal-hydraulic behavior of CRG rod arrays
- To establish a baseline for comparison with the flow blockage task (Task 3.2.3⁽¹⁾) data to determine the effect of blockage
- To evaluate the effects of bundle geometry on reflood heat transfer in comparison with previous FLECHT 15x15 unblocked tests
- To provide and evaluate data for single-phase steam cooling heat transfer correlation development

1-3. DATA EVALUATION AND ANALYSIS OBJECTIVES

The objectives followed in evaluating and analyzing the FLECHT-SEASET unblocked bundle task data were as follows:

- To present parametric effects and compare with previous tests
- To apply the data for calculation of bundle average flow properties at several elevations in the bundle and use these properties to help identify heat transfer mechanisms which are important in reflood heat transfer
- To develop more comprehensive models for mass effluent fractions and compare these with the data and with available models
- To develop empirical heat transfer correlations which are applicable to different bundle geometries

1. Conway, C. E., et al., "PWR FLECHT Separate Effects and Systems Effects Test (SEASET) Program Plan," NRC/EPRI/Westinghouse-1, December 1977.

- To develop an improved understanding of the two-phase phenomenon at the quench front

I-4. REPORT ORGANIZATION

Section 2 of this report presents a brief discussion of test hardware and procedure. Sections 3 through 6 present the results of the data evaluation and model developments.

Section 3 presents parametric effects on heat transfer, temperature transients, and bundle mass effluent. The following parameters are included:

- Flooding rate
- Peak power
- Pressure
- Subcooling
- Initial clad temperature
- Initial flooding rate for variable flooding rate tests
- Rod diameter

The data are compared with existing FLECHT data, and data repeatability is examined.

Section 4 presents the results of the calculation of the bundle average mass flow and quality at several elevations within the bundle. Both the actual nonequilibrium and equilibrium qualities are calculated.

Section 5 examines overall aspects of the mass effluence rate, including development of a new model. Mass and energy balance are used in sections 4 and 5. The balances were applied to the region above the quench front in the data analyses of previous FLECHT tests. These were extended to the region below the quench front in the present data analyses.

Section 6 presents detailed analysis of the heat transfer data to assess different heat transfer mechanisms.

Section 7 develops empirical heat transfer correlations which are applicable to various bundle geometries.

It should be mentioned that the posttest examination of this heater bundle revealed rod distortions in the region of the 1.83 m (72 in.) elevation, as indicated in the data report.⁽¹⁾ A statistical analysis has pinpointed the test cycles in which the bundle distortion could be an important factor. The results are shown in appendix F of the data report.

1. Loftus M. J., et al., "PWR FLECHT SEASET Unblocked Bundle, Forced and Gravity Reflood Task Data Report," NRC/EPRI/Westinghouse-7, June 1980.

SECTION 2

TEST DESCRIPTION

2-1. INTRODUCTION

The facility and test information provided in this section is sufficient for a clear understanding of the data evaluation and analyses in subsequent sections. Detailed descriptions of the test facility instrumentation, test procedures, and test matrix are contained in the data report.⁽¹⁾

2-2. TEST FACILITY

The facility used for the FLECHT low flooding rate (LFR) skewed test series⁽²⁾ was modified to conduct the unblocked bundle, forced and gravity reflood tests as shown in figure 2-1.

The facility with modifications consists of:

- A new low mass housing test section and upper and lower plenums
- The 161-rod bundle and related instrumentation

The existing pressurized water supply accumulator and injection line with three rotameters and a turbine meter to measure injection rates from 10 mm/sec (0.4 in./sec) in forced flooding tests to 6.49 kg/sec (14.3 lb/sec) in gravity reflood tests were used. The pressure control system developed in the previous FLECHT tests was also used.

A close-coupled carryover tank connected to the test section upper plenum had a minimum capacity of 65.8 kg (145 lb). A commercially available steam separator with a capacity of 0.315 kg/sec (2500 lb/hr) and a liquid collection tank with a volume of 9.5 kg (21 lb) to collect liquid entrained in the exhaust line was connected to the test section

-
1. Loftus, M. J., et al., "PWR FLECHT SEASET Unblocked Bundle, Forced and Gravity Reflood Task Data Report," NRC/EPRI/Westinghouse-7, June 1980.
 2. Rosal, E. R., et al., "FLECHT Low Flooding Rate Skewed Test Series Data Report," WCAP-9108, May 1977.

upper plenum. The steam separator had a storage capacity of approximately 193 kg (425 lb). The exhaust piping had a system pressure control valve and an orifice plate flowmeter to measure exhaust steam flow rate. A commercially available electric steam boiler with a capacity of 0.016 kg/sec (125 lb/hr) was used to establish initial loop pressure and temperature.

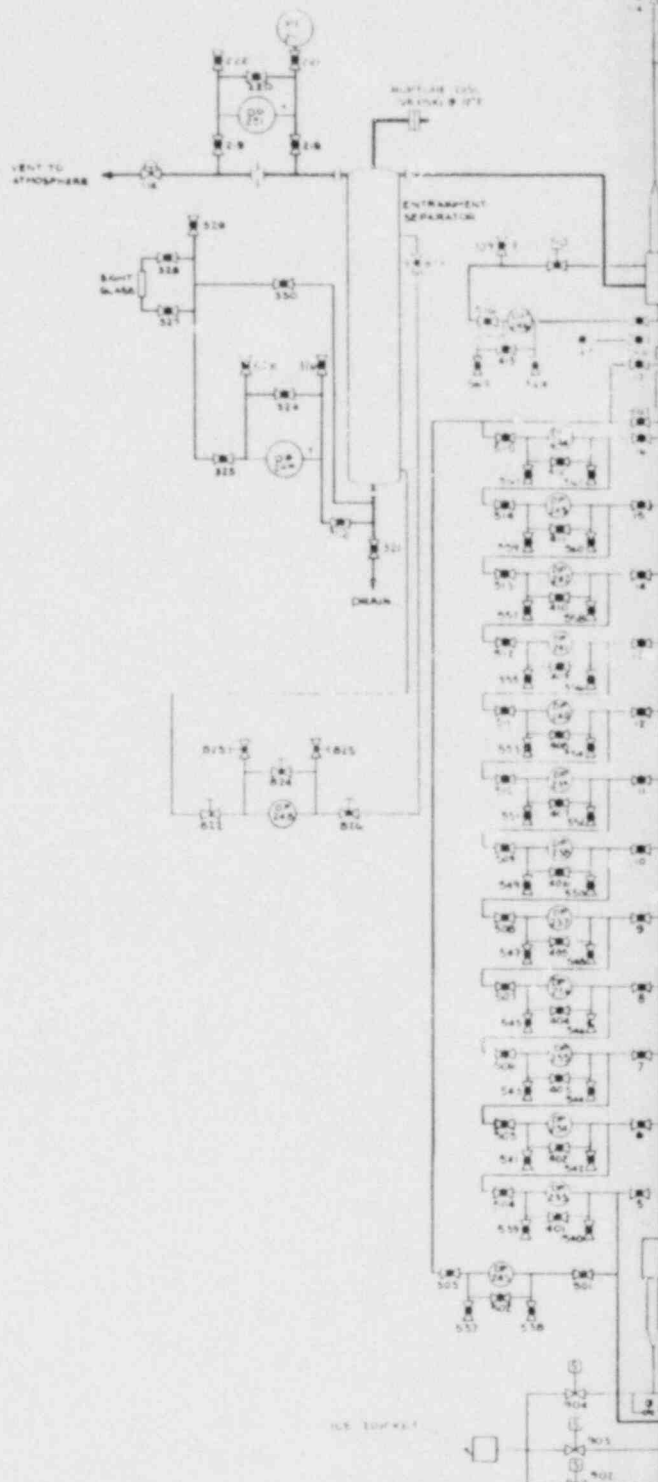
During operation, coolant flow from the 1.51 m^3 (400 gal) capacity water supply accumulator entered the test section housing through a flow redistribution skirt in the lower plenum to assure proper flow distribution. The flow was regulated manually through a series of hand valves or automatically through a hydraulic control valve or series of solenoid valves.

Test section pressure was initially established by the electric steam boiler, which is connected to the upper plenum of the test section. During the experimental run, the boiler was valved out of the system and the pressure was maintained by a pneumatically operated control valve located in the exhaust line.

Liquid effluent leaving the test section was separated in the upper plenum and collected in the close-coupled carryover tank. A baffle assembly in the upper plenum was used to improve liquid carryout separation and minimize liquid entrainment into the exhaust vapor. An entrainment separator located in the exhaust line was used to separate any remaining entrained liquid carryout from the vapor. Dry steam flow leaving the separator was measured at an orifice section before exhausting to atmosphere. To help ensure single-phase flow measurement, the piping upstream of the orifice section was heated to a temperature well above the saturation temperature.

2-3. HEATER ROD BUNDLE

A cross section of the test bundle is shown in figure 2-2 in the original configuration. The bundle comprised 161 heater rods (93 noninstrumented and 68 instrumented), 4 thimbles instrumented with wall thermocouples, 12 steam probes, 8 solid triangular fillers, and 8 grids. The triangular fillers were welded to the grids to maintain the proper grid location. The fillers also reduced the amount of excess flow area from 9.3 to 4.7 percent.



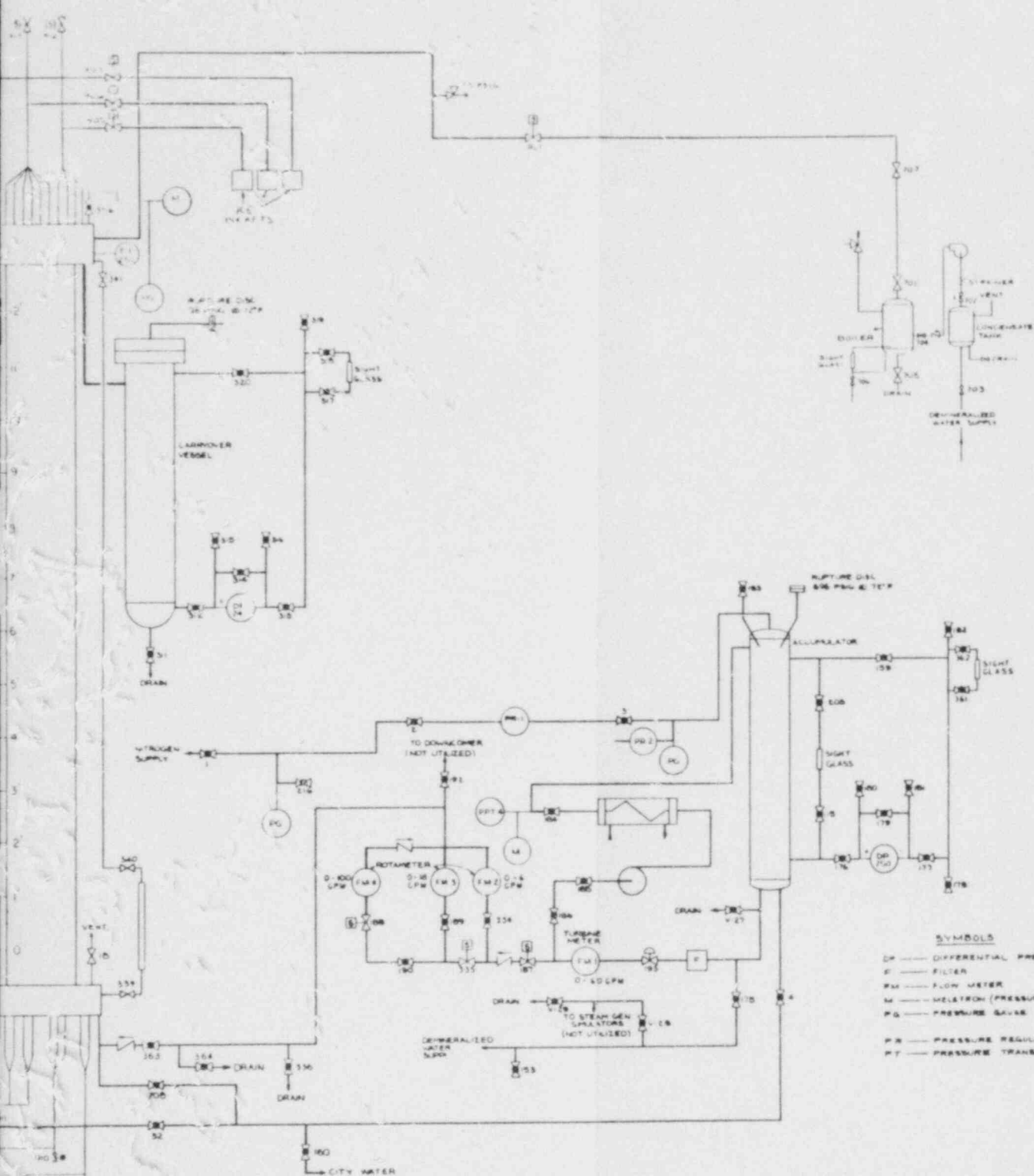
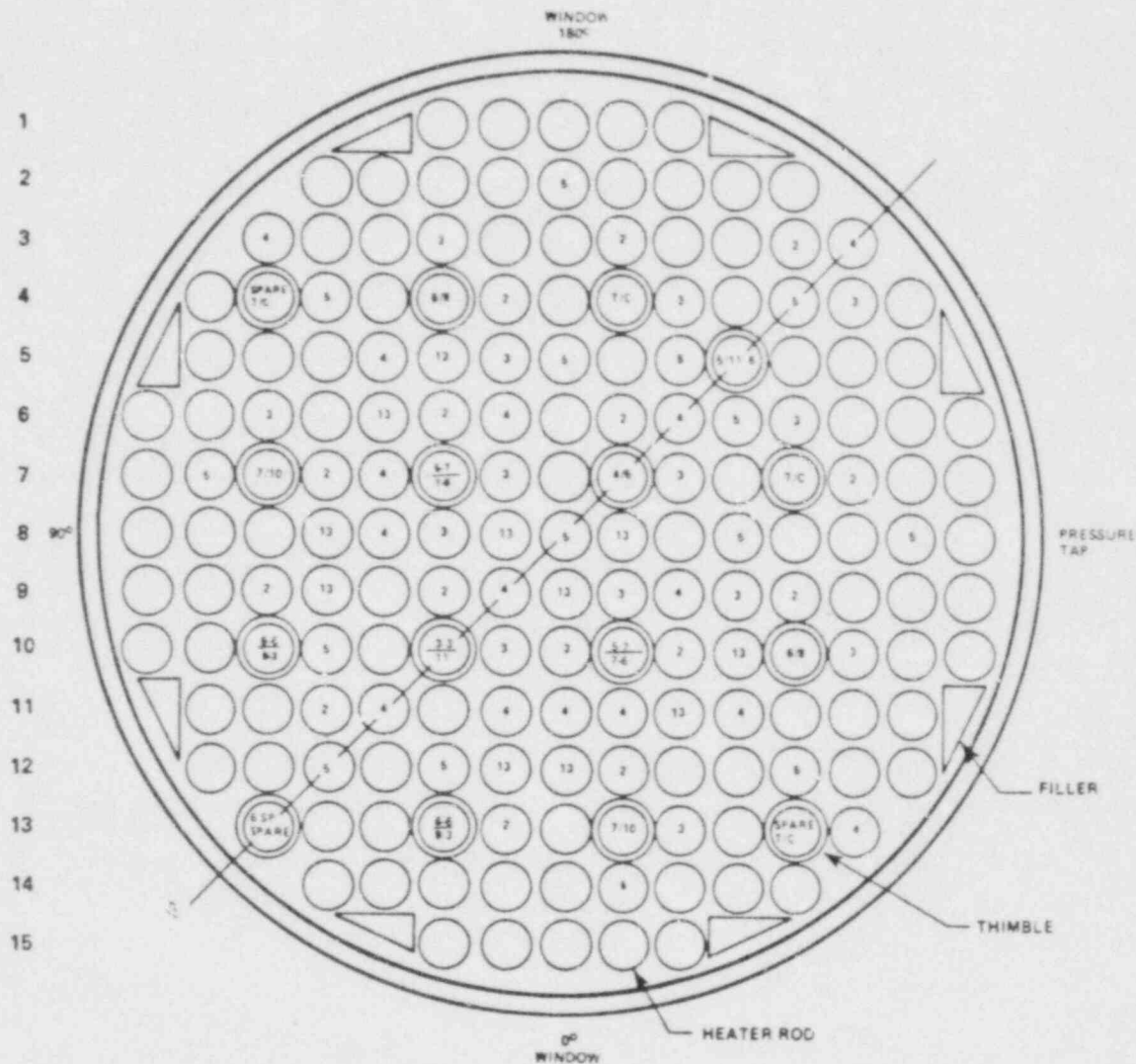


Figure 2-1. Flow Diagram for Forced Reflood Configuration (FLECHT SEASET Unblocked Bundle)

A B C D E F G H I J K L M N O



BUNDLE STATISTICS

HOUSING INSIDE DIAMETER	194.0 mm (7.625 in.)
HOUSING WALL THICKNESS	5.08 mm (0.200 in.)
ROD DIAMETER	9.50 mm (0.374 in.)
THIMBLE DIAMETER	12.0 mm (0.474 in.)
ROD PITCH	12.6 mm (0.496 in.)
CROSS-SECTIONAL FLOW AREA	15571 mm ² (24 136 in. ²)
FILLER DIMENSIONS	18.8 x 8.43 mm (0.741 x 0.332 in.)
161 HEATER RODS	— —
16 THIMBLES	— —
8 FILLERS	— —

Figure 2-2. Bundle Cross Section

2-4. SYSTEM DESIGN FEATURES

The following paragraphs describe the major design features utilized for the FLECHT SEASET unblocked bundle test series.

2-5. Low Mass Housing

A low mass housing design was utilized in the previous FLECHT LFR Skewed Test series to minimize the housing effects. The behavior of the skewed test low mass housing was studied by performing two tests with the same initial conditions except for the housing wall initial temperature.⁽¹⁾ The effect of the housing temperature on rod surface temperature and the corresponding heat transfer coefficient was found to be negligible. In addition, the housing temperature did not affect the quench front along the bundle. It was concluded that performing reflood tests with an unheated low mass housing is acceptable, since a cold housing does not significantly affect the reflood heat transfer and hydraulic behavior of the rod bundle.

A low mass housing design was utilized again for the unblocked bundle test series. The present design is a low mass cylindrical housing with a 19.37 cm (7.625 in.) ID by 0.478 cm (0.188 in.) wall. The wall thickness, the minimum thickness allowed by the ASME Code, was chosen so that the housing would absorb and hence release the minimum amount of heat to the rod bundle.

The inside diameter of the housing was made as close to the diameter of the rod bundle as possible to minimize excess flow area. The excess flow area was further minimized by the solid fillers mentioned in paragraph 2-3. The housing was constructed of 304 stainless steel rated for 0.52 MPa (60 psig) at 816°C (1500°F). The design allowed for 1000 pressure and temperature cycles. The housing was provided with end flanges to mate with the upper and lower plenums used in the previous test series. Two commercial quartz sight glasses were located 180 degrees apart at the 0.91, 1.83, and 2.74 m (36, 72, and 108 in.) elevations for viewing and photographic study. The sight glass configuration allowed back lighting in addition to front lighting for the purpose of photographic studies. The sight glasses had clamp-on heaters to raise the quartz

I. Rosal, E. R., et al., "FLECHT Low Flooding Rate Skewed Test Series Data Report," WCAP-9108, May 1977.

temperature at the initiation of reflood to approximately 260°C (500°F). This eliminated the formation of a liquid film on the quartz during a run.

2-6. Bundle Differential Pressure Cells

The test section differential pressure cells provided data used in determining mass balance and bundle void fraction. Low range [$\pm 0.0069 \text{ MPa} (\pm 1 \text{ psid})$] pressure transducers were used to improve the accuracy of the data. The cells were located every 0.30 m (12 in.) along the test section, arranged as shown in figure 2-3. The differential pressure cell manifold was carefully bled to eliminate any trapped air and thus improve the repeatability of the readings.

2-7. Heater Rod Seals

The bundle heater rods passed through polyurethane O-ring seals in the upper and lower seal plates. This design was improved by sealing each rod individually with an O-ring sleeve. The O-rings were inserted into the sleeve. In the previous FLECHT tests, the O-ring was located in a groove in the seal plate. The new design allowed for the removal and replacement of individual O-rings, which was not possible in previous designs. This feature permitted the replacement of heater rods in the bundle without a total bundle disassembly.

2-8. Steam Probes

Steam probes were located in the bundle and in the test section outlet pipe. The bundle steam probes, which were located in the thimble tubes, were redesigned from the previous FLECHT test series. The probe was designed to separate moisture from the high-temperature steam, and to aspirate the steam across the thermocouple and into an ice bucket. Because of the larger number of probes, the probes were controlled to limit the amount of steam aspirated from the test section. This was accomplished by manifolding the aspiration lines for common elevations of steam probes together and closing the lines when the particular elevation had quenched. The mass flow through the probes represented about 0.7 to 5 percent of the injected mass; the average was 1.42 percent. A steam probe was installed in the elbow of the test section outlet pipe, to measure the temperature of the steam leaving the test section. This probe was designed to measure steam temperature in the same manner as the bundle probes.

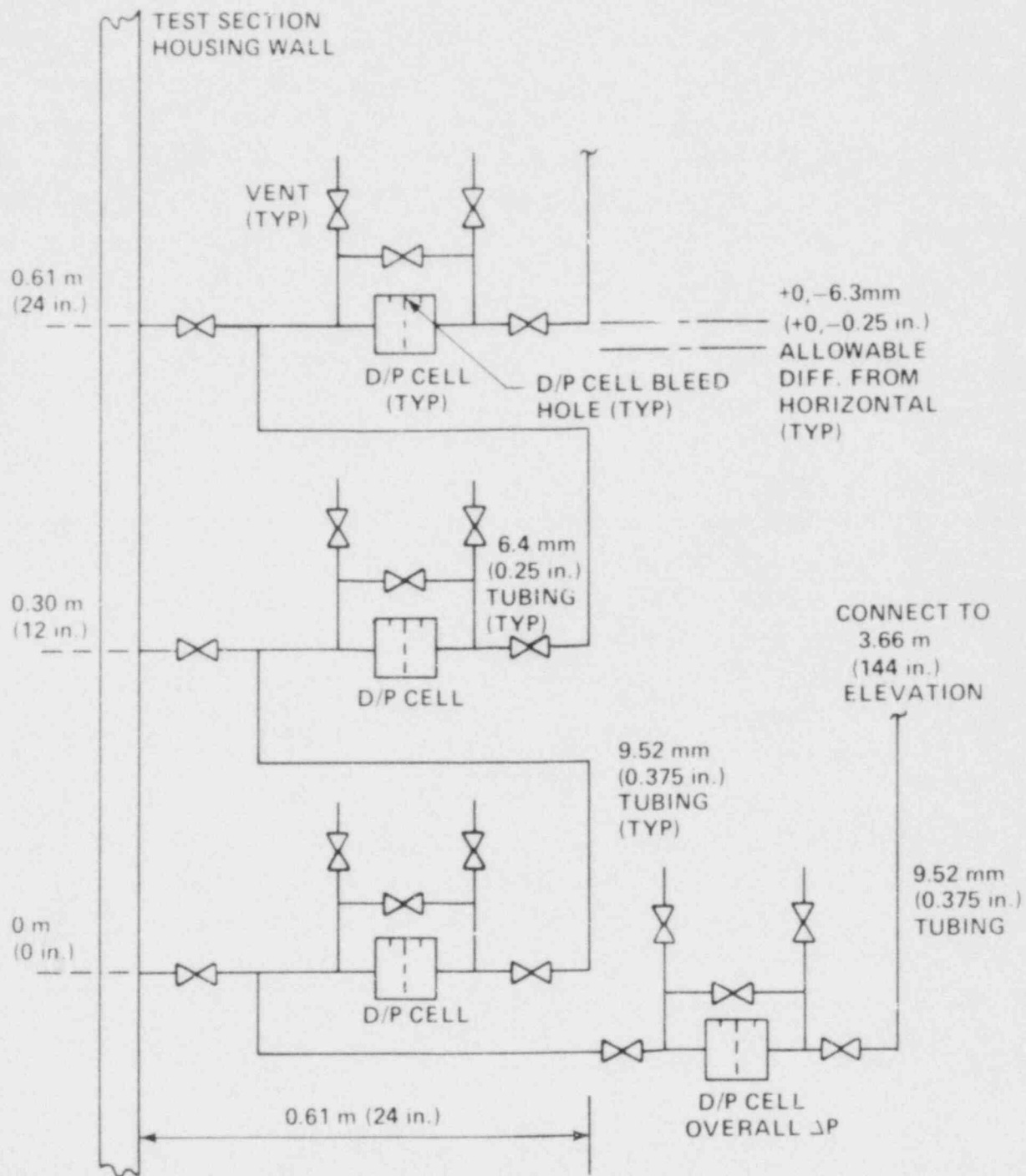


Figure 2-3. FLECHT SEASET Unblocked Bundle Test Section Housing Differential Pressure Cell Hookup

2-9. Pressure Control

Maintaining a constant upper plenum pressure had been a difficult problem in previous FLECHT test programs. In an effort to reduce the pressure oscillations, several modifications were made to the facility for the FLECHT Skewed Test series. The first modification was to increase the volume of the steam separator to help reduce the magnitude of the oscillations. The second modification was to replace the existing air-operated globe exhaust control valve with an air-operated V-ball control valve. The V-ball valve had a larger flow loss coefficient (254 maximum) and a more linear operating characteristic. These same modifications were used to help minimize the pressure oscillations in the unblocked bundle tests.

2-10. Facility and Bundle Operation

The test facility was designed for automatic operation whenever critical functions required a high degree of sophistication, safety, or repeatability. The Computer Data Acquisition System (CDAS) was the heart of the operation; it monitored, protected, and controlled the facility operation as well as collected data. Both contact and analog outputs were used to control pressure, power, and flow during the test. The CDAS software monitored critical safety parameters during the test and used corresponding outputs to run the test. These outputs included the safety interlock for proper operation of the bundle power control system.

2-11. Power Measurement

The technique of bundle power measurement was improved for the FLECHT low flooding rate skewed test series, and the improved technique was utilized again for the present unblocked bundle test series. The bundle power measurement systems were improved by the addition of a secondary independent power measurement system and the adoption of a system calibration. A secondary power-measuring system consisting of wide band Hall-effect watt transducers and stepdown current and potential transformers was installed in each power zone as a check on the primary. With the two data channels measuring the same parameter, any change in one system was detected by the other.

2-12. Coolant Injection System

The facility configuration provided for both forced and gravity reflood injection. The injection system consisted of a hydraulic valve for programmed flow and a turbine meter in series with three rotameters. The flow out of the rotameters went either to the lower plenum of the test section for forced reflood or to the bottom elbow of the downcomer for gravity reflood. Solenoid valves were used to initiate flood and channel the flow through the desired rotameter. A bidirectional turbo-probe in the downcomer crossover pipe measured the flow between the downcomer and the test section in gravity reflood tests.

In the forced flooding configuration, the flooding rate into the test section lower plenum was measured directly by a turbine meter with a range of 3.78×10^{-5} to $3.78 \times 10^{-3} \text{ m}^3/\text{sec}$ (0.6 to 60 gal/min) or by one of three rotameters with ranges of 0 to 3.78×10^{-4} , 0 to 1.14×10^{-3} , and 0 to $6.31 \times 10^{-3} \text{ m}^3/\text{sec}$ (0 to 6, 0 to 18, and 0 to 100 gal/min). The desired flow through each rotameter was preset using the hand throttling valves located upstream of the rotameters.

In the gravity reflood configuration, the injection flow rate into the bottom elbow of the downcomer was measured by the 0 to $9.46 \times 10^{-3} \text{ m}^3/\text{sec}$ (0 to 150 gal/min) turbine meter, with the rotameters providing the backup measurement.

2-13. TEST PROCEDURE

The following is a general procedure used to establish initial test conditions and perform a typical FLECHT SEASET unblocked bundle reflood test.

The accumulator is filled with water and heated to the desired coolant temperature of 53°C (127°F) nominal.

The boiler is turned on and brought up to nominal gage pressure of 0.42 MPa (75 psig).

The carryover vessel, entrainment separator, separator drain tank, test section upper plenum, and test section outlet piping (located before the entrainment separator) are

heated while empty to slightly above the saturation temperature corresponding to the test run pressure. The exhaust line between the separator and exhaust orifice is heated to 260°C (500°F) nominal and the test section lower plenum is heated to the temperature of the coolant temperature in the accumulator. The above component heating is accomplished by using clamp-on strip heaters.

The test section, carryover vessel, and exhaust line components are pressurized to the desired system pressure of 0.14 MPa to 0.41 MPa (20 to 60 psia) by valving the boiler into the system and setting the exhaust line air-operated control valve to the desired pressure.

The coolant in the accumulator is pressurized to 2.76 MPa (400 psia). Water is then injected into the test section lower plenum until it reaches the beginning of the heated length of the bundle heater rods. Coolant is circulated and drained to assure that the water in the lower plenum and injection line are at the specified temperature prior to the run.

Power is then applied to the test bundle and the rods are allowed to heat up. When the temperature in any two designated bundle thermocouples reaches the preset value of 260°C to 871°C (500° to 1600°F), the computer automatically initiates flood and controls power decay. Solenoid valves in conjunction with a hydraulic control valve control coolant injection into the test section. The exhaust control valve regulates the system pressure at the preset value by releasing steam to the atmosphere.

After all the designated heater rods have quenched, as indicated by the rod thermocouples, power to the heater rods is terminated, coolant injection is terminated, the entire system is depressurized by opening a control valve, and the CDAS is deactivated. Water stored in all components is drained and weighed.

During the test series, the facility was modified to perform gravity reflood tests. The same procedure was used to perform the gravity, reflood tests with the following exception: After flood was initiated, the flooding rate was adjusted if necessary to assure that the level in the downcomer did not go past the 4.88 m (192 in.) elevation.

After runs 30123 through 30817 had been conducted, a modification was made to the above test procedure. This modification consisted of power pulsing the bundle to approximately 260°C (500°F) prior to applying full power and subsequently venting the bundle steam probe lines before achieving the designated flood temperature. This procedure was followed to dry out the bundle thimbles and steam probes, in order to achieve faster response and higher reliability of the steam probes.

2-14. SUMMARY OF RUN CONDITIONS AND TEST RESULTS

Data from 63 reflood and steam cooling tests performed during the FLECHT SEASET unblocked bundle test program met the specified test conditions. The initial run conditions and summary results are listed in table 2-1. The summary results for the reflood tests include the following information:

- Location of the hottest temperature recorded during the test, which is characterized by the radial location of the rod in the bundle and the thermocouple nominal elevation with respect to the bottom of the heated length
- Initial and maximum temperature of the hot rod
- Turnaround time, which is the time after the start of flooding at which the hot rod maximum temperature was recorded
- Hottest rod quench time, which is the time after the start of flooding at which the temperature of the hottest rod started to drop very rapidly
- Bundle quench time, which is the time after the start of flooding at which all thermocouples in the bundle had quenched. On the average, the thermocouples located at the 3.35 m (132 in.) elevation quenched last.

TABLE
FLECHT SEASET UNBLOCKED BUND

Test No.	Run No.	Actual Test Conditions					
		Upper Plenum Pressure [MPa (psia)]	Rod Initial T _{clad} at 1.83m (72 in.) [°C(°F)]	Rod Peak Power [kw/m (kw/ft)]	Flooding Rate [mm/sec (in./sec)]	Coolant Temperature [°C(°F)]	Radial Power Distribution
CONSTANT FLOODING RATE							
1	31701	0.28 (40)	872 (1601)	2.3 (0.70)	155 (6.1)	53 (127)	Uniform
2	31302	0.28 (40)	869 (1597)	2.3 (0.69)	76.5 (3.01)	52 (126)	Uniform
3	31203	0.28 (40)	872 (1601)	2.3 (0.70)	38.4 (1.51)	52 (126)	Uniform
	33903	0.28 (40)	881 (1619)	2.3 (0.70)	40.1 (1.58)	52 (125)	Uniform
	34103	0.28 (40)	885 (1626)	2.4 (0.74)	38.1 (1.50)	51 (123)	Uniform
4	31504	0.28 (40)	863 (1585)	2.3 (0.70)	24 (0.97)	51 (123)	Uniform
	35304(a)	0.28 (40)	915 (1679)	2.4 (0.74)	25.9 (1.02)	51 (124)	Uniform
5	31805	0.28 (40)	871 (1600)	2.3 (0.70)	21 (0.81)	51 (124)	Uniform
6	34006	0.27 (39)	882 (1620)	1.3 (0.40)	15 (0.59)	51 (124)	Uniform
7	34907(a,b)	0.28 (40)	897 (1648)	1.4 (0.42)	11 (0.45) 76 (3.0)	51 (123)	Uniform
	35807(a)	0.28 (40)	886 (1628)	0.89(0.27)	10 (0.41)	50 (121)	Uniform
PRESSURE AT CONSTANT FLOODING RATE							
8	31108	0.13 (19)	871 (1600)	2.3 (0.70)	79.0 (3.11)	33 (91)	Uniform
9	34209	0.14 (20)	889 (1636)	2.4 (0.72)	27.2 (1.07)	32 (90)	Uniform

- a. Significant rod bundle distortion occurred between 1.52 and 2.27 m (60 and 90 in.)
- b. Scrammed at 279 seconds because of high rod temperature

LE REFLOOD TEST DATA SUMMARY

Results							
Hottest Rod T/C and Elevation [m(in.)]	Initial Temperature [$^{\circ}\text{C}({}^{\circ}\text{F})$]	Maximum Temperature [$^{\circ}\text{C}({}^{\circ}\text{F})$]	Temperature Rise [$^{\circ}\text{C}({}^{\circ}\text{F})$]	Turn-around Time (sec)	Quench Time (sec)	Bundle Quench Time (sec)	Disconnected Rod Location
9I-1.78(70)	893 (1640)	923 (1694)	30 (54)	5	55	114	4G, 5G
8E-1.70(67)	889 (1631)	932 (1710)	43 (79)	8	124	262	4G, 5G, 6J, 11G
9L-1.93(76) 7K-1.98(78)	870 (1597) 868 (1594)	1037 (1898) 1048 (1919)	167 (301) 180 (325)	63 68	246 220	435 335	4G, 5G 4G, 5G, 11I, 11J, 11K, 12IJK, 13JK
7K-1.98(78)	872 (1601)	1089 (1992)	217 (391)	71	241	381	4G, 5G, 11IJK, 12IJK, 13JK
8K-1.98(78)	820 (1507)	1150 (2101)	330 (593)	130	325	594	4G, 5G
9F-1.93(76)	797 (1467)	1230 (2246)	433 (779)	125	249	499	4G, 5G, 11IJK, 12IJK, 13JK,
11K-1.98(78)	851 (1563)	1232 (2250)	381 (687)	134	419	691	4G, 5G
7K-1.98(78)	864 (1587)	1163 (2126)	299 (539)	175	327	566	4G, 5G, 11IJK, 12IJK, 13JK
9F-1.98(78)	836 (1538)	1230 (2246)	394 (708)	203	326	385	4G, 5G, 11IJK, 12IJK, 13JK
9F-1.88(74)	849 (1560)	1182 (2160)	333 (600)	217	368	734	4G, 5G, 11IJK, 12IJK, 13JK
9I-1.78(70)	884 (1624)	938 (1720)	54 (96)	10	156	364	4G, 5G
7K-1.98(78)	854 (1570)	1161 (2121)	307 (551)	127	427	701	4G, 5G, 11IJK, 12IJK, 13JK

TABLE 2
FLECHT SEASET UNBLOCKED

Test No.	Run No.	As-Run Test Conditions					
		Upper Plenum Pressure [MPa (psia)]	Rod Initial T _{clad} at 1.83m (72 in.) [°C(°F)]	Rod Peak Power [kw/m (kw/ft)]	Flooding Rate [mm/sec (in./sec)]	Coolant Temperature [°C(°F)]	Radial Power Distribution
10	34610	0.14 (20)	892 (1637)	1.4 (0.42)	21 (0.82)	32 (90)	Uniform
11	34711(a)	0.13 (19)	888 (1630)	1.4 (0.42)	17 (0.67)	33 (91)	Uniform
12	35212(a,c) 35912(a)	0.14 (20)	879 (1613)	1.4 (0.42)	11 (0.43) 178 sec 79 (3.1) 11 (0.42)	32 (89)	Uniform
13	32013	0.41 (60)	887 (1629)	2.3 (0.70)	26.4 (1.04)	66 (150)	Uniform
SUBCOOLING							
14	32114	0.28 (40)	893 (1639)	2.3 (0.70)	25→31 (1.0→1.22)	125 (257)	Uniform
	35114	0.28 (40)	892 (1638)	2.4 (0.74)	25 (0.98)	123 (253)	Uniform
15	31615 34815(a)	0.14 (20) 0.14 (20)	876 (1609) 895 (1643)	2.3 (0.70) 2.4 (0.74)	0 (0) 25 (0.98)	94 (221)	Uniform Uniform
16	34316	0.28 (40)	889 (1631)	2.4 (0.74)	25 (0.97)	51→119 (124→246)	Uniform
INITIAL CLAD TEMPERATURE							
17	30817	0.27 (39)	531 (987)	2.3 (0.70)	38.6 (1.52)	53 (128)	Uniform
18	30518	0.28 (40)	256 (494)	2.3 (0.70)	38.9 (1.53)	52 (126)	Uniform
19	30619	0.134 (19.5)	256 (494)	2.3 (0.70)	38.9 (1.53)	36 (96)	Uniform

c. Scrammed at 178 seconds because of high rod temperature

-1 (cont)

BUNDLE REFLOOD TEST DATA SUMMARY

Results							
Hottest Rod T/C and Elevation [m(in.)]	Initial Temperature [$^{\circ}\text{C}$ ($^{\circ}\text{F}$)]	Maximum Temperature [$^{\circ}\text{C}$ ($^{\circ}\text{F}$)]	Temperature Rise [$^{\circ}\text{C}$ ($^{\circ}\text{F}$)]	Turn-around Time (sec)	Quench Time (sec)	Bundle Quench Time (sec)	Disconnected Rod Location
6D-1.88 (74)	845 (1554)	1052 (1926)	207 (372)	137	310	507	4G, 5G, 11IJK, 12IJK, 13JK
9E-1.93 (76)	855 (1571)	1119 (2045)	264 (474)	135	361	600	4G, 5G, 11IJK, 12IJK, 13JK
9E-1.83 (72)	830 (1526)	1231 (2247)	401 (721)	173	236	294	4G, 5G, 11IJK, 12IJK, 13JK
9G-2.29 (90)	802 (1476)	1128 (2062)	326 (586)	289	558	789	4G, 5G, 11IJK, 12IJK, 13JK
6L-1.93 (76)	846 (1555)	1171 (2139)	325 (584)	115	269	461	4G, 5G
6L-1.88 (74)	840 (1544)	1189 (2172)	349 (628)	114	405	633	4G, 5G
9D-1.83 (72)	886 (1628)	1192 (2178)	306 (550)	123	394	651	4G, 5G, 11IJK, 12IJK, 13JK
11H-1.70 (67)	881 (1617)	1220 (2228)	339 (611)	57	-	-	4G, 5G
7J-1.83 (72)	870 (1597)	1178 (2152)	308 (555)	132	562	919	4G, 5G, 11IJK, 12IJK, 13JK
6D-1.88 (74)	849 (1560)	1207 (2206)	358 (646)	107	349	592	4G, 5G, 11IJK, 12IJK, 13JK
10J-1.98 (78)	519 (965)	832 (1530)	313 (565)	84	219	395	4G, 5G
8H-1.98 (78)	246 (475)	653 (1208)	407 (732)	96	187	344	4G, 5G
2H-1.98 (78)	243 (469)	727 (1340)	484 (871)	142	292	572	4G, 5G

TABLE
FLECHT SEASET UNBLOCK

Test No.	Run No.	As-Run Test Conditions					
		Upper Plenum Pressure [MPa (psia)]	Rod Initial T _{clad} at 1.83m (72 in.) [°C(°F)]	Rod Peak Power [kw/m (kw/ft)]	Flooding Rate [mm/sec (in./sec)]	Coolant Temperature [°C(°F)]	Radial Power Distribution
20	34420	0.27 (39)	1119 (2045)	2.4 (0.74)	38.9 (1.53)	51 (124)	Uniform
ROD PEAK POWER							
21	30921(d) 31021	0.27 (39) 0.28 (40)	879 (1614) 880 (1615)	1.3 (0.40) 1.3 (0.40)	38.9 (1.53) 38.6 (1.52)	52 (126) 52 (126)	Uniform Uniform
22	31922	0.14 (20)	883 (1621)	1.3 (0.40)	27.2 (1.07)	35 (95)	Uniform
23	30223 30323	0.27 (39) 0.27 (39)	258 (497) 259 (499)	1.3 (0.40) 1.3 (0.40)	37.8 (1.49) 38.6 (1.52)	54 (129) 52 (126)	Uniform Uniform
24	34524	0.28 (40)	878 (1612)	3.0 (1.0)	39.9 (1.57)	52 (125)	Uniform
RADIAL POWER DISTRIBUTION							
25	Not run						
26	35426(a) 36026(a)	0.28 (40) 0.28 (40)	886 (1627) 900 (1651)	2.54 (0.773) 2.42 (0.737) 2.08 (0.633) 2.42 (0.737) 2.31 (0.703) 2.19 (0.667)	25.7 (1.01) 25 (1.0)	52 (126) 51 (124)	FLECHT FLECHT
27	Not run						
28	Not run						
REPEAT TESTS							
29	35304						

d. Scrammed because of high-temperature thermocouple failure at 125 seconds

E 2-1 (cont)

ED BUNDLE REFLOOD TEST DATA SUMMARY

Results							
Hottest Rod T/C and Elevation [m(in.)]	Initial Temperature [$^{\circ}\text{C}({}^{\circ}\text{F})$]	Maximum Temperature [$^{\circ}\text{C}({}^{\circ}\text{F})$]	Temperature Rise [$^{\circ}\text{C}({}^{\circ}\text{F})$]	Turn-around Time (sec)	Quench Time (sec)	Bundle Quench Time (sec)	Disconnected Rod Location
7J-1.83 (72)	1102 (2016)	1207 (2205)	105 (189)	34	222	376	4G, 5G, 11IJK, 12IJK, 13JK
9I-1.78 (70)	887 (1629)	949 (1740)	62 (111)	17	152	158	4G, 5G
9H-1.78 (70)	891 (1635)	941 (1726)	50 (91)	14	158	271	4G, 5G
6F-1.83 (72)	883 (1621)	975 (1787)	92 (166)	70	229	435	4G, 5G
6F-1.93 (76)	261 (501)	455 (852)	194 (351)	44	113	181	None
6F-1.98 (78)	256 (494)	459 (859)	203 (365)	57	115	171	None
7J-1.83 (72)	873 (1604)	1204 (2199)	331 (595)	89	266	520	4G, 5G, 11IJK, 12IJK, 13JK
9F-1.93 (76)	814 (1497)	1229 (2243)	415 (746)	113	240	485	4G, 5G, 11IJK, 12IJK, 13JK
11F-1.88 (74)	862 (1583)	1174 (2145)	312 (562)	113	286	475	4G, 5G, 11IJK, 12IJK, 13JK

FLECHT SEASET UNBLOCK

Test No.	Run No.	As-Run Test Conditions					
		Upper Plenum Pressure [MPa (psia)]	Rod Initial T _{clad} at 1.83m (72 in.) [°C(°F)]	Rod Peak Power [kw/m (kw/ft)]	Flooding Rate [mm/sec (in./sec)]	Coolant Temperature [°C(°F)]	Radial Power Distribut
30	Not run						
VARIABLE FLOODING RATE							
31	Not run						
32	Not run						
33	32333	0.28 (40)	889 (1631)	2.3 (0.70)	162 (6.36) 5 sec 21 (0.82) onward	52 (125)	Uniform
34	Not run						
35	32235	0.14 (20)	888 (1630)	2.3 (0.70)	166 (6.53) 5 sec 25 (0.98) 200 sec 16 (0.62) onward Injection Rate kg/sec (lbm/sec)	31 (88)	Uniform
GRAVITY REFLOOD							
36	33436	0.27 (39)	878 (1611)	2.3 (0.70)	5.80 (12.8) 15 sec 0.785 (1.73) onward	52 (125)	Uniform
37	Not run						
38	33338	0.28 (40)	871 (1600)(e) 591 (1096)(f)	2.3 (0.70)(e) 1.3 (0.40)(f)	5.9 (13) 15 sec 0.807 (1.78) onward	52 (125)	Hot/ cold channels

e. Hot channel

f. Cold channel

LE 2-1 (cont)

REF BUNDLE REFLOOD TEST DATA SUMMARY

Results							
Hottest Rod T/C and Elevation [m(in.)]	Initial Temperature [$^{\circ}$ C ($^{\circ}$ F)]	Maximum Temperature [$^{\circ}$ C ($^{\circ}$ F)]	Temperature Rise [$^{\circ}$ C ($^{\circ}$ F)]	Turn-around Time (sec)	Quench Time (sec)	Bundle Quench Time (sec)	Disconnected Rod Location
6L-1.93 (76)	843 (1550)	1148 (2099)	305 (549)	131	337	639	4G, 5G
6K-1.98 (78)	823 (1514)	1146 (2096)	323 (582)	142	546	964	4G, 5G
10H-1.78 (70)	891 (1636)	910 (1670)	19 (34)	4	121	174	4G, 5G
10H-1.78 (70)	906 (1664)	925 (1697)	19 (33)	6	76	181	4G, 5G

TAB
FLECHT SEASET UNBLOC

Test No.	Run No.	As-Run Test Conditions					
		Upper Plenum Pressure [MPa (psia)]	Rod Initial T _{clad} at 1.83m (72 in.) [°C(°F)]	Rod Peak Power [kw/m (kw/ft)]	Injection Rate [kg/sec (lbm/sec)]	Coolant Temperature [°C(°F)]	Radial Power Distribu
39	Not run						
HOT AND COLD CHANNELS							
40	Not run						
41	Not run						
42	Not run						
43	Not run						
AXIAL TEMPERATURE DISTRIBUTION							
44	33544	0.27 (39)	196 (385)(g) (0 to 3) 874 (1605)	2.3 (0.69)	5.85 (12.9) 15 sec 0.780 (1.72) onward	52 (125)	Uniform
	33644	0.27 (39)	182 (359)(g) (0 to 3) 877 (1610)	2.3 (0.70)	5.81 (12.8) 15 sec 0.789 (1.76) onward	52 (125)	Uniform
STEAM COOLING							
45	32652 through 33056						
46	36160 through 37170						
OVERLAP COSINE TESTS							
47	Not run						
48	Not run						

g. Axial temperature distribution - simulated gravity reflood

TABLE 2-1 (cont)

REFLOODED BUNDLE REFLOOD TEST DATA SUMMARY

	Results							
Location	Hottest Rod T/C and Elevation [m(in.)]	Initial Temperature [$^{\circ}$ C($^{\circ}$ F)]	Maximum Temperature [$^{\circ}$ C($^{\circ}$ F)]	Temperature Rise [$^{\circ}$ C($^{\circ}$ F)]	Turn-around Time (sec)	Quench Time (sec)	Bundle Quench Time (sec)	Disconnected Rod Location
	11K-1.93 (76)	877 (1610)	908 (1668)	31 (58)	8	121	213	4G, 5G
	7D-1.93 (76)	884 (1623)	930 (1705)	46 (82)	9	104	250	4G, 5G

TABL
FLECHT SEASET UNBLOCKE

Test No.	Run No.	As-Run Test Conditions					
		Upper Plenum Pressure [MPa (psia)]	Rod Initial T _{clad} at 1.83m (72 in.) [°C(°F)]	Rod Peak Power [kw/m (kw/ft)]	Flooding Rate [mm/sec (in./sec)]	Coolant Temperature [°C(°F)]	Radial Power Distribution
COMPARISON WITH WESTINGHOUSE PROPRIETARY REFLOOD DATA							
49	33749 33849(h)	0.27 (39) 0.28 (40)	745 (1374) 745 (1374)	1.9 (0.57) 1.9 (0.57)	26.9 (1.06) 25.9 (1.02)	61 (142) 58 (138)	Uniform Uniform
50	35050(a)	0.14 (20)	758 (1397)	1.6 (0.48)	25.9 (1.02)	43 (109)	Uniform
POWER DECAY							
51	Not run						

h. Rod 12J failed during test.

E 2-1 (cont)

ED BUNDLE REFLOOD TEST DATA SUMMARY

	Results							
on	Hottest Rod T/C and Elevation [m(in.)]	Initial Temperature [$^{\circ}\text{C} (^{\circ}\text{F})$]	Maximum Temperature [$^{\circ}\text{C} (^{\circ}\text{F})$]	Temperature Rise [$^{\circ}\text{C} (^{\circ}\text{F})$]	Turn-around Time (sec)	Quench Time (sec)	Bundle Quench Time (sec)	Disconnected Rod Location
	11K-1.88 (74) 8K-1.98 (78)	730 (1346) 705 (1302)	1017 (1861) 1025 (1878)	287 (515) 320 (576)	103 105	250 254	430 437	4G, 5G 4G, 5G
	9D-1.83 (72)	758 (1397)	958 (1758)	200 (361)	98	243	433	4G, 5G, 11JK, 12JK, 13JK

SECTION 3

PARAMETRIC EFFECTS

3-1. INTRODUCTION

This section is a qualitative presentation of the effects of the principal test parameters. Overlap tests have been used to determine bundle geometry effects. No attempt has been made to analyze the causes of the observed trends. A detailed quantitative analysis of heat transfer mechanisms and their effects is treated in section 4.

Trends in temperature rise and quench time are also compared with previous results. Comparison of skewed and cosine power shapes for the same test conditions indicate that the skewed profile is less severe than the cosine; that is, for the same test conditions, including peak power, the skewed profile usually resulted in lower temperature rises than either the 17x17 or 15x15 cosine power shape.

Parametric effects examined are flooding rate, pressure, subcooling, initial cladding temperature, peak power, and initial flooding rate for variable flooding rate tests. Table 3-1 presents the range of parameters and relevant runs used for each comparison. The effect of each parameter on heat transfer, temperature transients, and mass effluent fractions are presented. Temperature rise and quench time trends are then compared with previous FLECHT results. For these latter comparisons, the test conditions are usually not the same. However, the main purpose of these comparisons is to examine the trends with each parameter, rather than the absolute values of temperature rise or quench time. In particular, the quench times plotted for the skewed tests are 3.04 m (120 in.) values; for cosine (FLECHT final, low flooding cosine and SEASET), the 1.83 m (72 in.) values are plotted. This typically results in much longer quench times for the skewed tests.

Time-integrated values of mass effluent fractions are presented as a function of time rather than the instantaneous values. Fluctuations in the instantaneous values during a

TABLE 3-1

SUMMARY OF RUN NUMBERS AND RANGE OF PARAMETERS

Parameter	Run	Pressure [MPa (psi)]	Rod Initial Temperature [°C (°F)]	Rod Peak Power [kw/m (kw/ft)]	Flooding Rate [mm/sec (in./sec)]	Subcooling [°C (°F)]
Flooding rate	31504	0.28 (40)	863 (1585)	2.3 (0.7)	24.6 (0.97)	80 (144)
	31805	0.28 (40)	871 (1600)	2.3 (0.7)	20.6 (0.81)	79 (143)
	31203	0.28 (40)	872 (1601)	2.3 (0.7)	38.4 (1.51)	78 (141)
	31302	0.28 (40)	869 (1597)	2.3 (0.7)	76.5 (3.01)	78 (141)
	31701	0.28 (40)	872 (1601)	2.3 (0.7)	154 (6.1)	78 (140)
	34006	0.27 (39)	882 (1620)	1.3 (0.4)	15.0 (0.59)	79 (142)
	31021	0.28 (40)	879 (1615)	1.3 (0.4)	38.6 (1.52)	78 (141)
Pressure	31504	0.28 (40)	863 (1585)	2.3 (0.7)	24.6 (0.97)	80 (144)
	34209	0.14 (20)	891 (1636)	2.3 (0.7)	27.2 (1.07)	98 (177)
	31013	0.14 (20)	887 (1629)	2.3 (0.7)	26.4 (1.04)	65 (117)
	31302	0.28 (40)	869 (1597)	2.3 (0.7)	76.5 (3.01)	78 (141)
Initial clad temperature	31108	0.13 (19)	871 (1600)	2.3 (0.7)	79.0 (3.11)	98 (176)
	31203	0.28 (40)	872 (1601)	2.3 (0.7)	38.4 (1.51)	78 (141)
	30817	0.27 (39)	531 (987)	2.3 (0.7)	38.6 (1.52)	77 (139)
	30518	0.28 (40)	257 (494)	2.3 (0.7)	38.6 (1.52)	78 (141)

TABLE 3-1 (cont)

SUMMARY OF RUN NUMBERS AND RANGE OF PARAMETERS

Parameter	Run	Pressure [MPa (psi)]	Rod Initial Temperature [°C (°F)]	Rod Peak Power [kw/m (kw/ft)]	Flooding Rate [mm/sec (in./sec)]	Subcooling [°C (°F)]
Subcooling	31504	0.28 (40)	863 (1585)	2.3 (0.7)	24.6 (0.97)	80 (144)
	35114	0.28 (40)	892 (1638)	2.4 (0.74)	24.9 (0.98)	8 (14)
Peak power	34209	0.14 (20)	891 (1636)	2.4 (0.72)	27.2 (1.07)	98 (177)
	31922	0.14 (20)	883 (1621)	1.3 (0.4)	27.2 (1.07)	96 (172)
	31203	0.28 (40)	872 (1601)	2.3 (0.7)	38.4 (1.51)	78 (141)
	31021	0.28 (40)	879 (1615)	1.3 (0.4)	38.6 (1.52)	78 (141)
	34524	0.28 (40)	878 (1612)	3.3 (1.0)	39.9 (1.57)	79 (142)
Initial flooding rate (variable flooding rate runs)	31805	0.28 (40)	871 (1600)	2.3 (0.7)	20.6 (0.81)	79 (143)
	32333	0.28 (40)	888 (1631)	2.3 (0.7)	162 (6.36) 5 sec 21 (0.82) onward	79 (142)

TABLE 3-1 (cont)

SUMMARY OF RUN NUMBERS AND RANGE OF PARAMETERS

Parameter	Run	Pressure [MPa (psi)]	Rod Initial Temperature $^{\circ}\text{C}$ ($^{\circ}\text{F}$)	Rod Peak Power [kw/m (kw/ft)]	Flooding Rate [mm/sec (in./sec)]	Subcooling $^{\circ}\text{C}$ ($^{\circ}\text{F}$)
	34259	0.14 (20)	891 (1636)	2.4 (0.72)	2.72 (1.07)	98 (177)
	32235	0.14 (20)	888 (1630)	2.3 (0.7)	166 (6.53) 5 sec 25 (0.98) 200 sec 16 (0.62) on 3rd	99 (179)
Transient subcooling	31504	0.28 (40)	863 (1585)	2.3 (0.7)	24.6 (0.97)	80 (144)
	34316	0.28 (40)	888 (1631)	2.4 (0.74)	24.6 (0.97)	79 → 11.7 (143 → 21)
	35114	0.28 (40)	892 (1638)	2.4 (0.74)	24.9 (0.98)	8 (14)

TABLE 3-1 (cont)

SUMMARY OF RUN NUMBERS AND RANGE OF PARAMETERS

Parameter	Run	Pressure [MPa (psi)]	Rod Initial Temperature [°C (°F)]	Rod Peak Power [kw/m (kw/ft)]	Flooding Rate [mm/sec (in./sec)]	Subcooling [°C (°F)]
Repeat	31203	0.28 (40)	872 (1601)	2.3 (0.7)	38.4 (1.51)	78 (141)
	34103	0.28 (40)	886 (1626)	2.4 (0.74)	38.1 (1.50)	80 (144)

run tend to obscure the small run-to-run differences in mass effluent fraction. On the figures, r_{out} versus time is plotted. The parameter r_{out} is defined as follows:

$$r_{out}(t) = \frac{M_{in}(t) - M_{st}(t)}{M_{in}(t)} \quad (3-1)$$

where

$M_{in}(t)$ = total mass injected up to time t

$M_{st}(t)$ = total mass stored in the bundle up to time t

It will be noted that some of the r_{out} curves tend to show large values early in time. On physical grounds, r_{out} must be zero at time zero, since mass must enter the bundle some finite time before it leaves the bundle. The large values of r_{out} in the first 10 to 20 seconds of the runs are artifacts of the uncertainty in the mass balance measurements and the definition of r_{out} which, by equation (3-1), becomes indefinite at time zero. The mass effluent fraction curves presented in the following discussions have been modified to use extrapolations at the early time period.

The heat transfer and temperature transients in the following discussions represent typical results measured by rod thermocouples at least two rows from the bundle housing and failed rods.

3-2. FLOODING RATE EFFECT

An abundant amount of data is available on the effect of flooding rate with a cosine power shape.⁽¹⁾ In WCAP-8838, it was shown that temperature rise and quench time trends were consistent among all the cosine data. WCAP-9183⁽²⁾ indicates that the skewed power shaped test also showed the same trends.

-
1. Lilly, G. P., et al., "PWR FLECHT Cosine Low Flooding Rate Test Series Evaluation Report," WCAP-8838, March 1977.
 2. Lilly, G. P., et al., "PWR FLECHT Skewed Profile Low Flooding Rate Test Series Evaluation Report," WCAP-9183, November 1977.

Figure 3-1 and 3-2 present the variation of heat transfer coefficient and peak temperatures at the 183 m (72 in.) elevation versus time for the runs in which only flooding rate was varied. The figures show the expected orderly increase in heat transfer at all times as flooding rate increased. Temperatures show more rapid turnaround and increasingly lower peak temperatures as the flooding rate was increased.

Figure 3-3 presents the variation of time-integrated mass effluent fraction versus time. The higher the flooding rate, the more rapidly the mass effluent fraction approaches its asymptotic value. This is expected, simply because of the accelerated pace of events in higher flooding rate runs. The same trend was observed in the previous tests. Of course, the principal effect of increasing flooding rate is to proportionately increase the mass flow above the quench front.

Figure 3-4 shows the quench front progress. As expected, the higher the flooding rate, the faster the quench front moves up.

Figures 3-5 and 3-6 reproduce data from the skewed profile tests, with the addition of new FLECHT SEASET results. Figure 3-5, for temperature rise, shows that the unblocked FLECHT SEASET data exhibit the same trend as the previous data of increasing temperature rise with decreasing flooding rate. This trend is expected. Figure 3-6 shows the quench time versus flooding rate. The trends of quench time with flooding rate observed in the previous FLECHT tests could be observed in the present data.

The temperature rise and quench time data of FLECHT SEASET [1.83 m (72 in.) elevation] are replotted in figures 3-7 and 3-8 against the ratio of flooding rate and peak power. The results of a comparable run of the previous cosine power shape test are also shown in the figures. The results are fairly well aligned.

3-3. PRESSURE EFFECT

Pressure and subcooling were two parameters which showed opposite trends with respect to temperature rise for the skewed profile and the two cosine power shape tests. Trends of quench time were the same for all parameters for both power shapes.

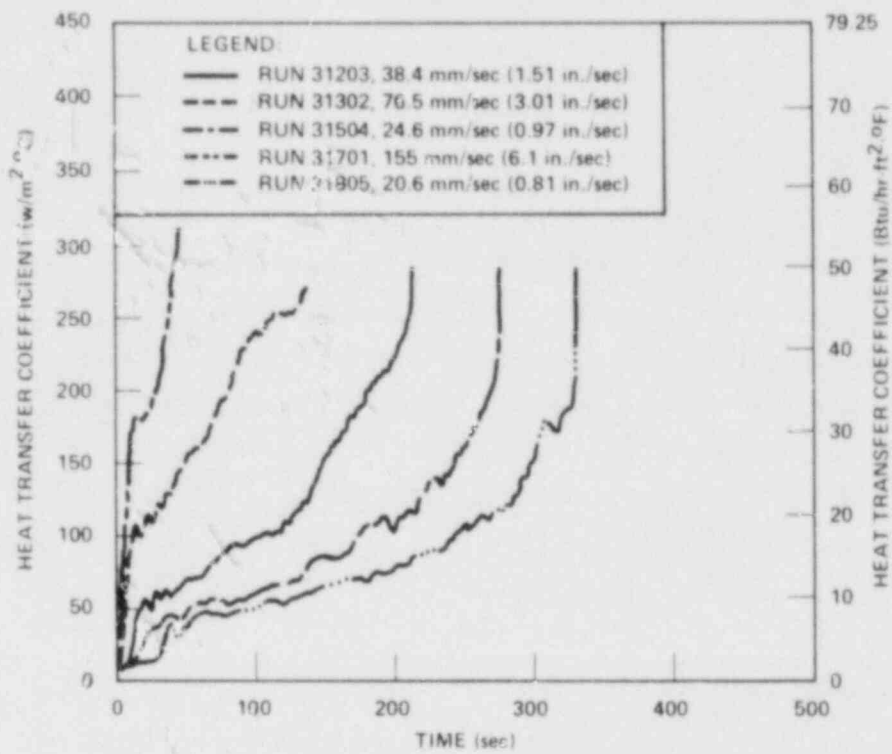


Figure 3-1. Flooding Rate Effect on Heat Transfer
[1.83 m (72 in.) Elevation]

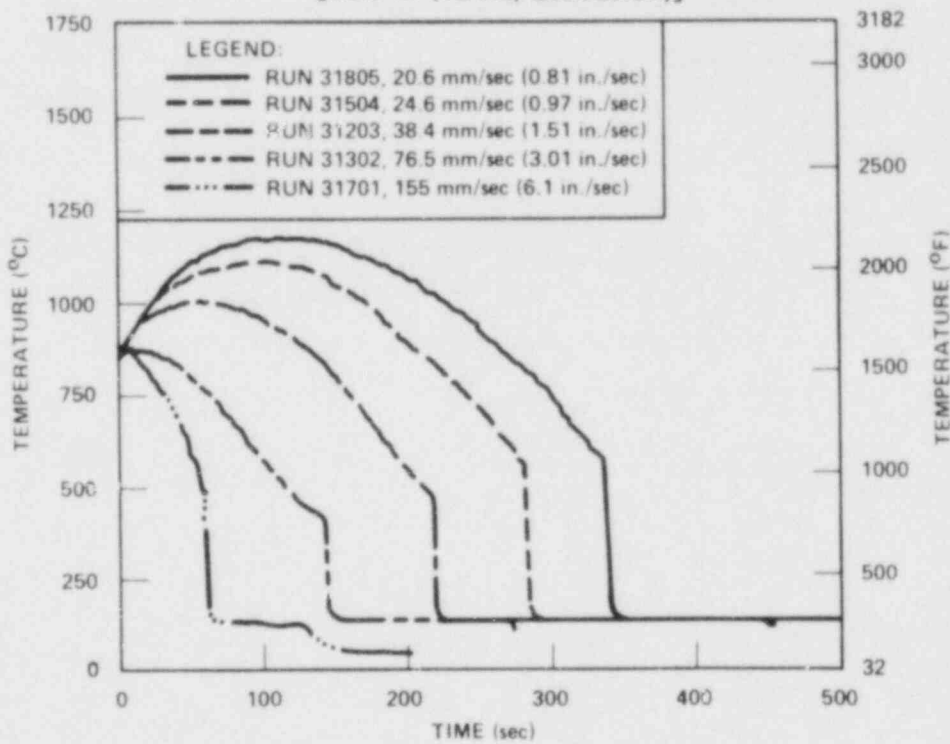


Figure 3-2. Flooding Rate Effect on Temperature

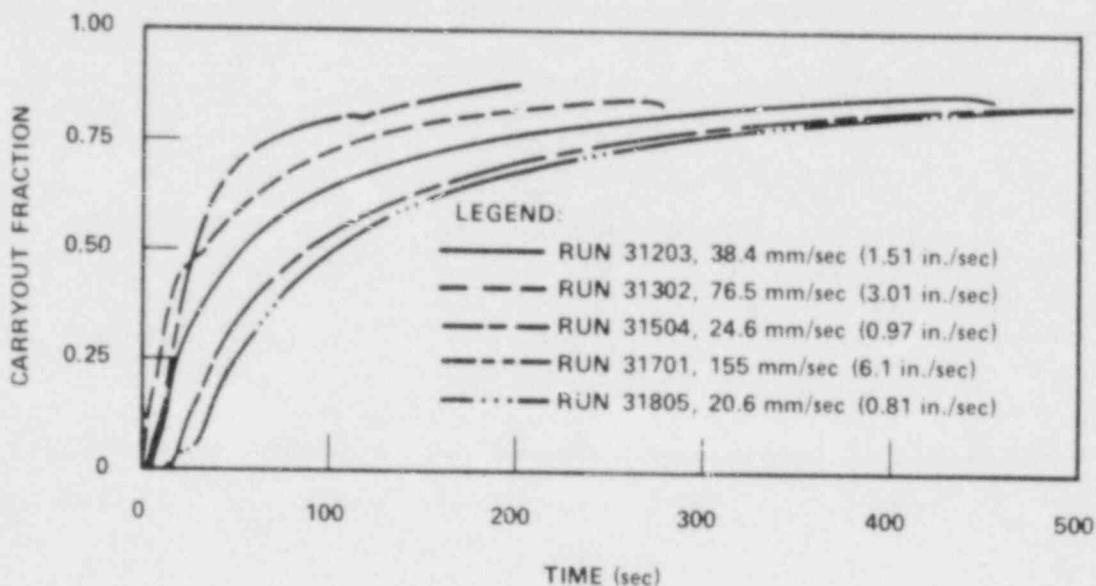


Figure 3-3. Flooding Rate Effect on Carryout Fraction

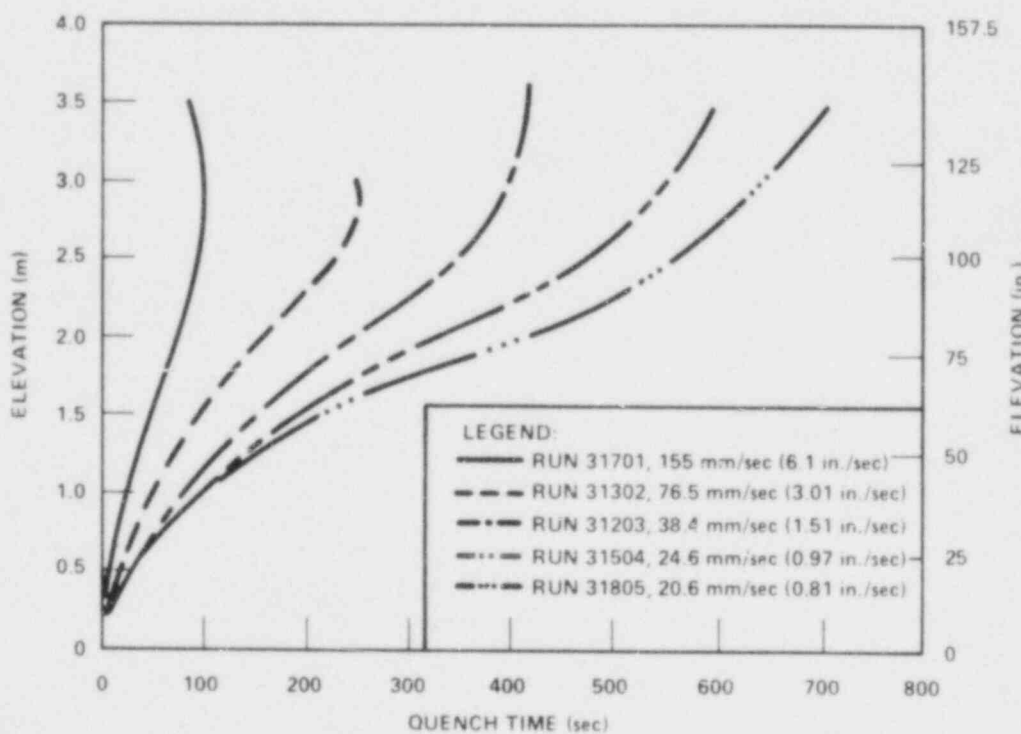
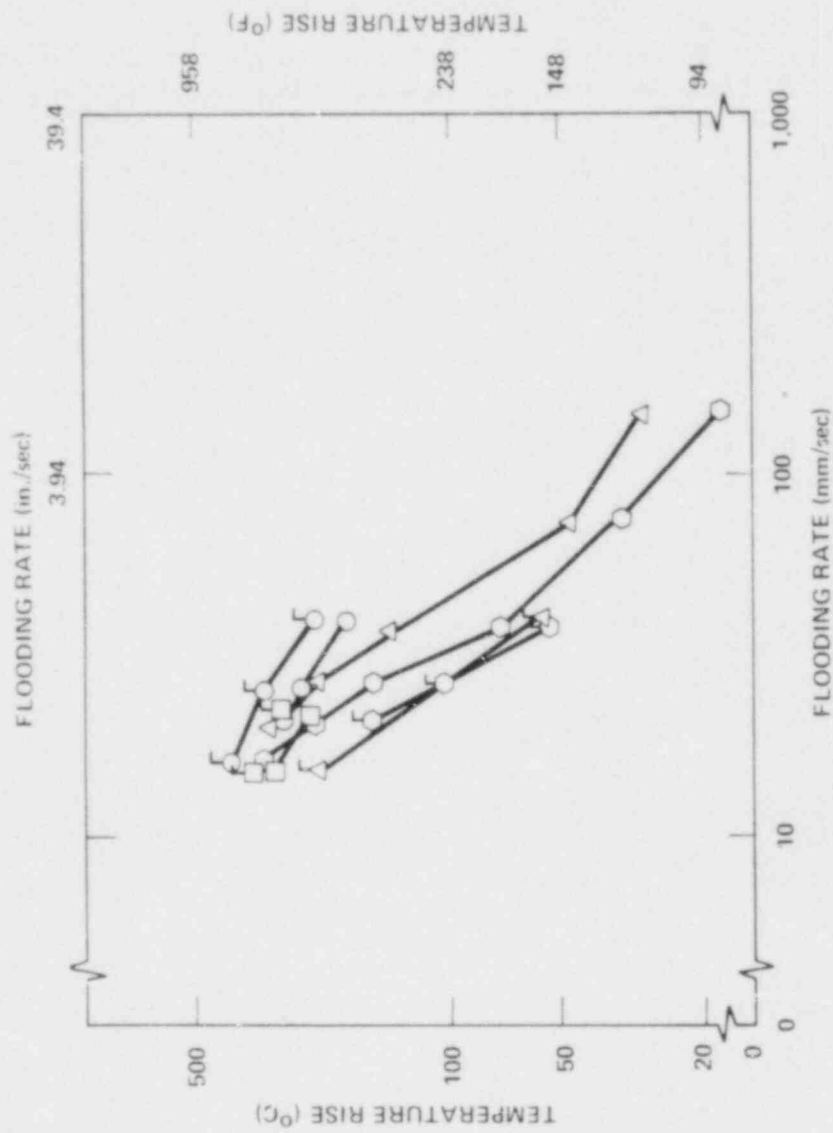


Figure 3-4. Quench Front Advances at Various Flooding Rates



SYMBOL	TEST	PRESSURE [MPa (psia)]	POWER [kw/m (kW/ft)]	SUBCOOLING [°C (°F)]	INITIAL TEMPERATURE [°C (°F)]	ELEVATION [m (ft)]
Δ	FLECHT SEASET	0.28 (40)	1.3 (0.40)	78 (140)	882 (1620)	1.83 (72)
△	FLECHT SEASET	0.28 (40)	2.3 (0.70)	69 (125)	871 (1600)	1.83 (72)
○	SKewed	0.28 (40)	2.3 (0.70)	78 (140)	871 (1600)	3.05 (120)
○	COSINE	0.28 (40)	3.1 (0.95)	22 (40)	871 (1600)	1.83 (72)
○	COSINE	0.28 (40)	3.1 (0.95)	22 (40)	871 (1600)	1.98 (78)
○	COSINE	0.28 (40)	2.4 (0.73)	78 (140)	871 (1600)	1.83 (72)
□	COSINE	0.28 (40)	2.5 (0.75)	78 (140)	871 (1600)	1.98 (78)
□	SKewed	0.14 (20)	2.3 (0.70)	50 (90)	871 (1600)	3.05 (120)

Figure 3-5. Temperature Rise Comparisons at Various Flooding Rates

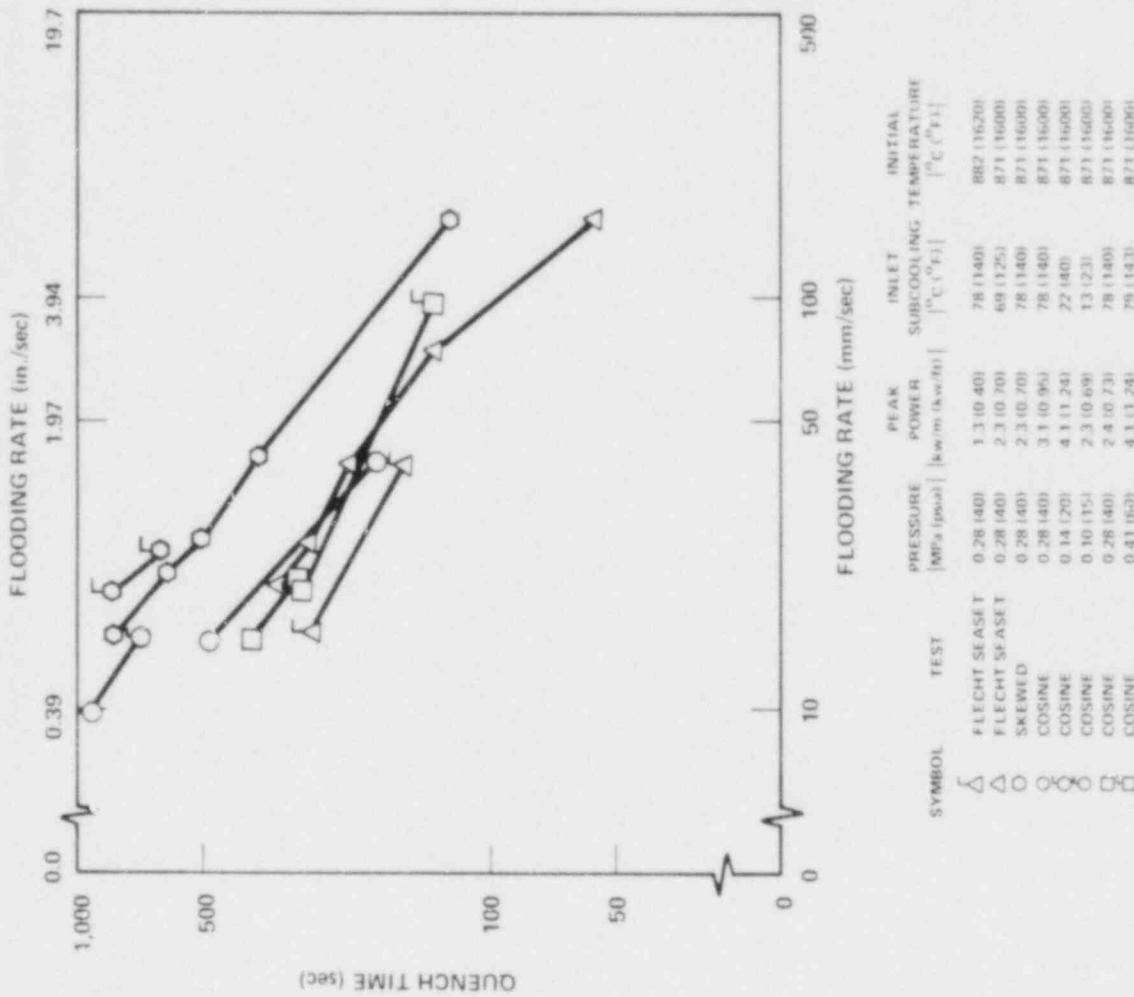


Figure 3-6. Quench Time Versus Flooding Rate

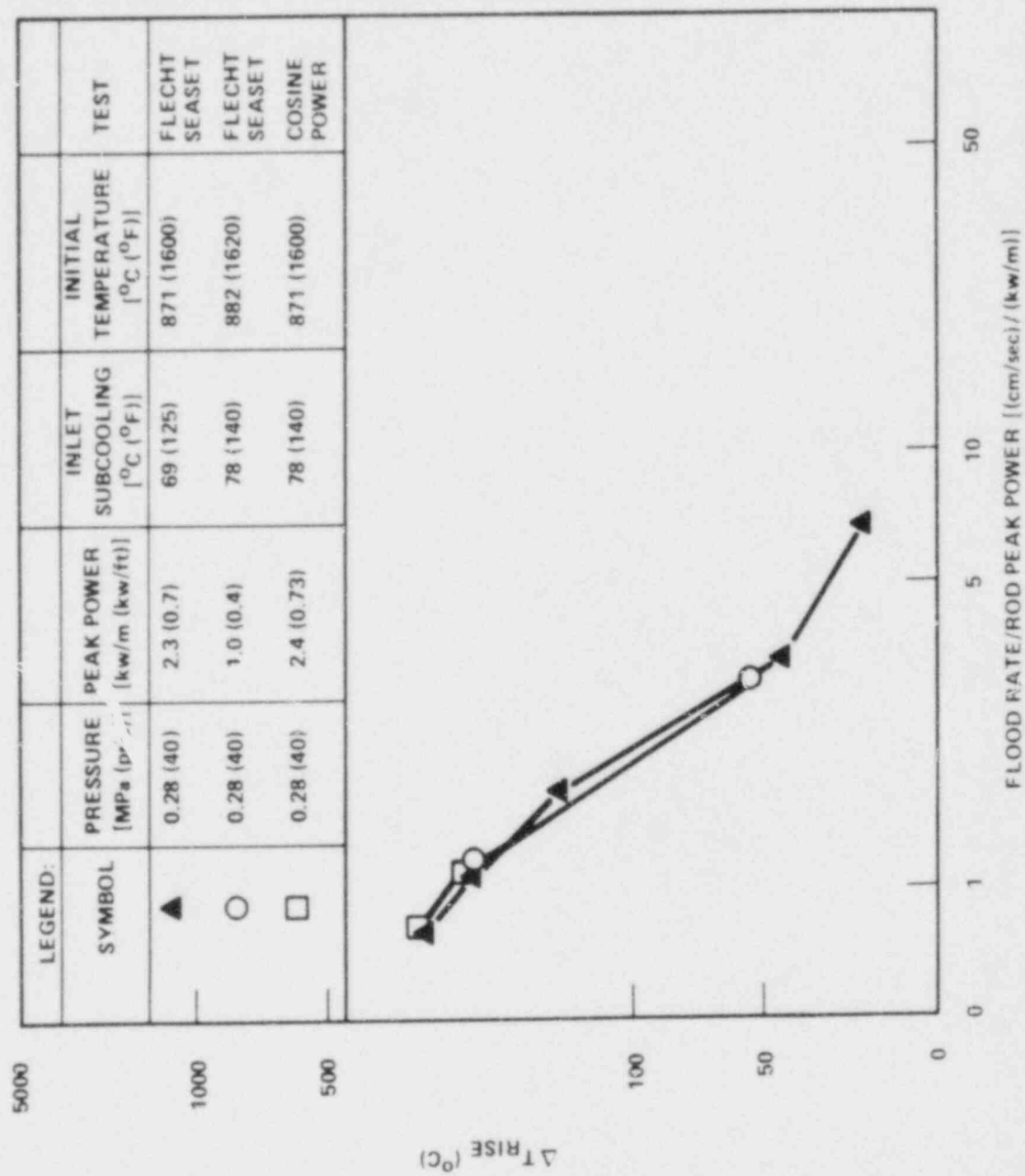


Figure 3-7. Temperature Rise Versus Flooding Rate and Rod Peak Power

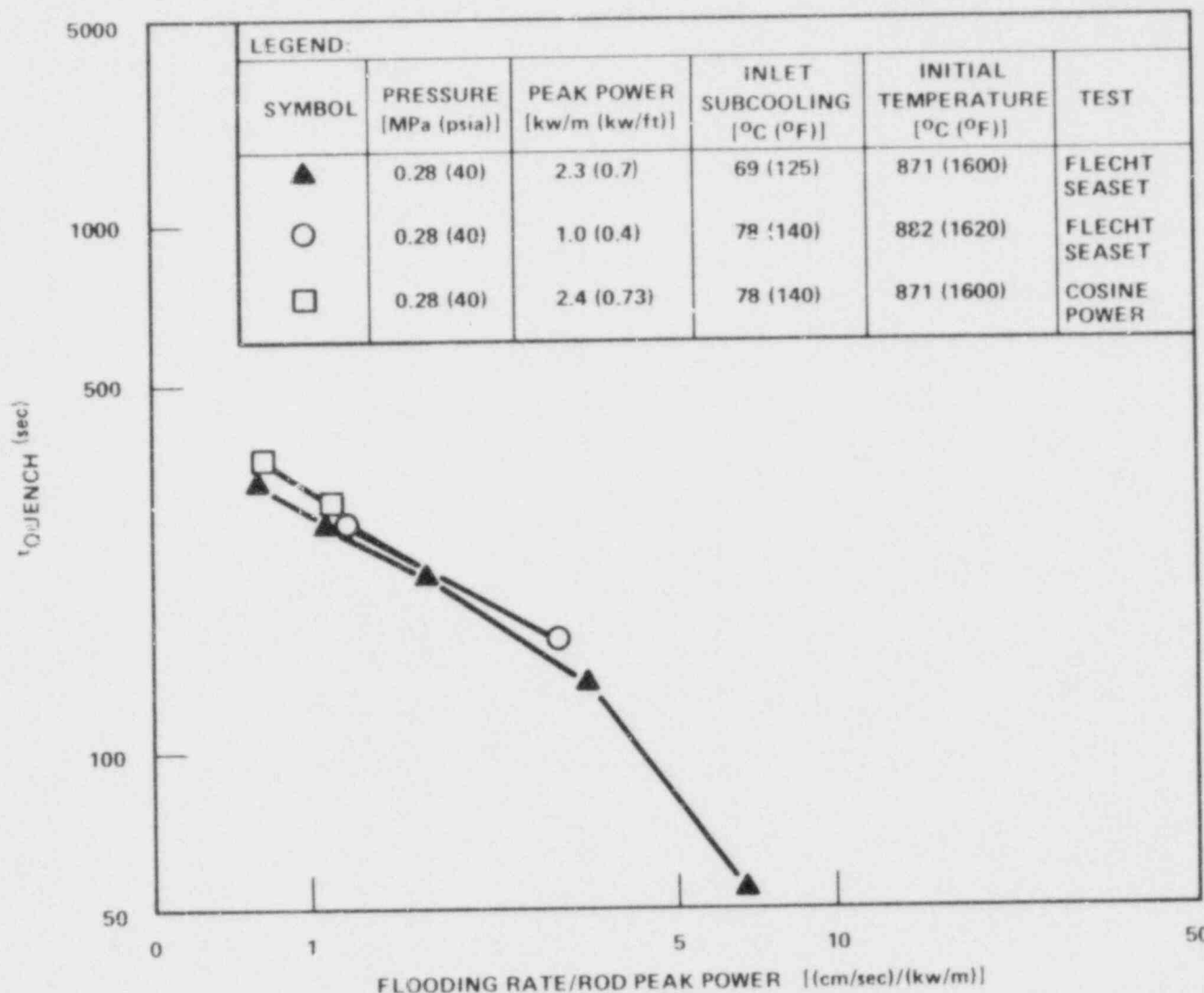


Figure 3-8. t_{Quench} Vs. Flood Rate/Rod Peak Power

Figure 3-8. Quench Time Versus Flooding Rate and Rod Peak Power

Figures 3-9 and 3-10 present the heat transfer coefficient and temperature transients for the sequence of FLECHT SEASET tests at 25.4 mm/sec (1 in./sec).

Figure 3-11 displays the effect of pressure on integrated mass effluent fraction. The low-pressure tests show a higher carryout fraction early in time. This same effect was observed for the previous FLECHT tests. This trend could be expected, since lower pressure will lead to higher void formation for the same steam generation. This phenomenon will tend to reduce storage below the quench front. Figure 3-12 presents the effect of pressure on quench front progression.

Figure 3-13 plots temperature rise and quench time versus pressure for both FLECHT and FLECHT SEASET tests at the 1.83 m (72 in.) elevation for FLECHT SEASET and FLECHT cosine tests, and at 3.05 m (120 in.) for FLECHT skewed power tests. The FLECHT SEASET data indicate that the temperature rise is a weak function of pressure. The trend of the quench time is consistent with the previous FLECHT data. However, it must be noted that the temperature rise seems to increase with pressure for the skewed tests and decrease with pressure for the cosine tests. This difference is believed to be due to the earlier entrainment and higher steam flow which occurred in the skewed tests as a result of the large amount of stored and generated energy in the first 0.6 m (24 in.) of the bundle.

3-4. SUBCOOLING EFFECT

Run 35114 was used to study subcooling effect, even though the bundle may have been deformed. This run also experienced pressure oscillation, which influences the void fraction distribution as a function of time in the bundle.

Figures 3-14 and 3-15 show higher heat transfer and more rapid turnaround for the higher value of subcooling.

The integrated carryout fraction increased markedly with decreased subcooling, as shown in figure 3-16. This phenomenon, which was also observed for the previous cosine and skewed tests, is expected since the lower subcooling results in more vapor generation for the same heat input. Figure 3-17 shows the effect of subcooling on the quench front progression.

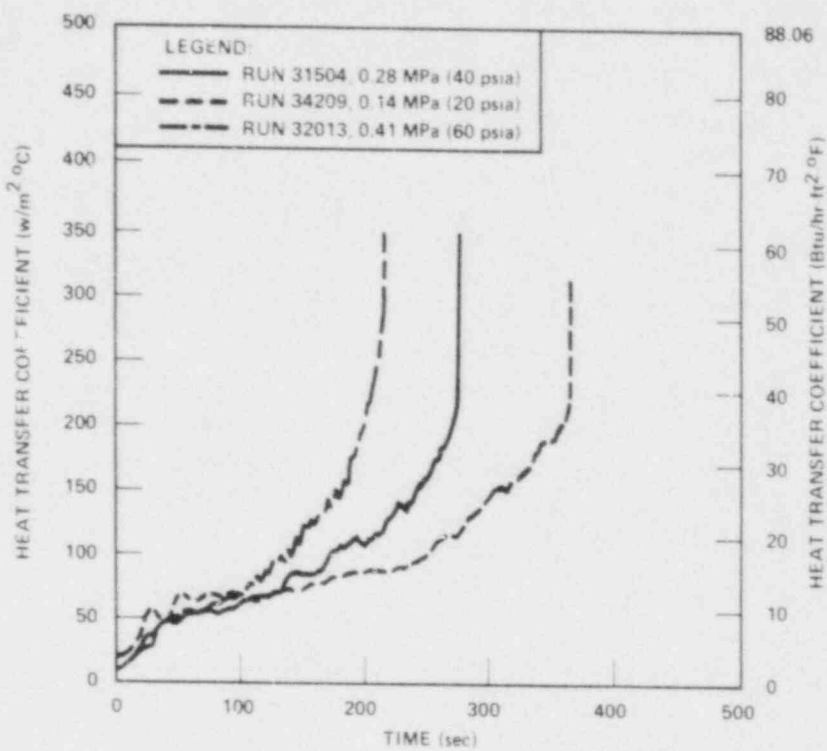


Figure 3-9. Pressure Effect on Heat Transfer

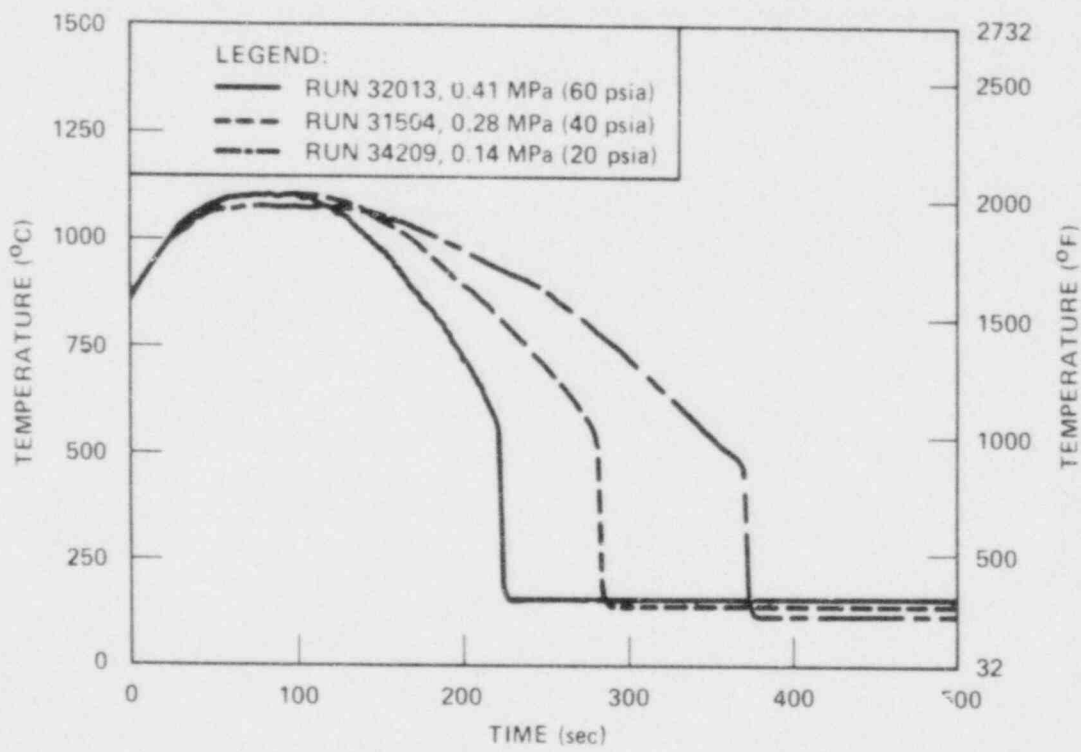


Figure 3-10. Pressure Effect on Temperature

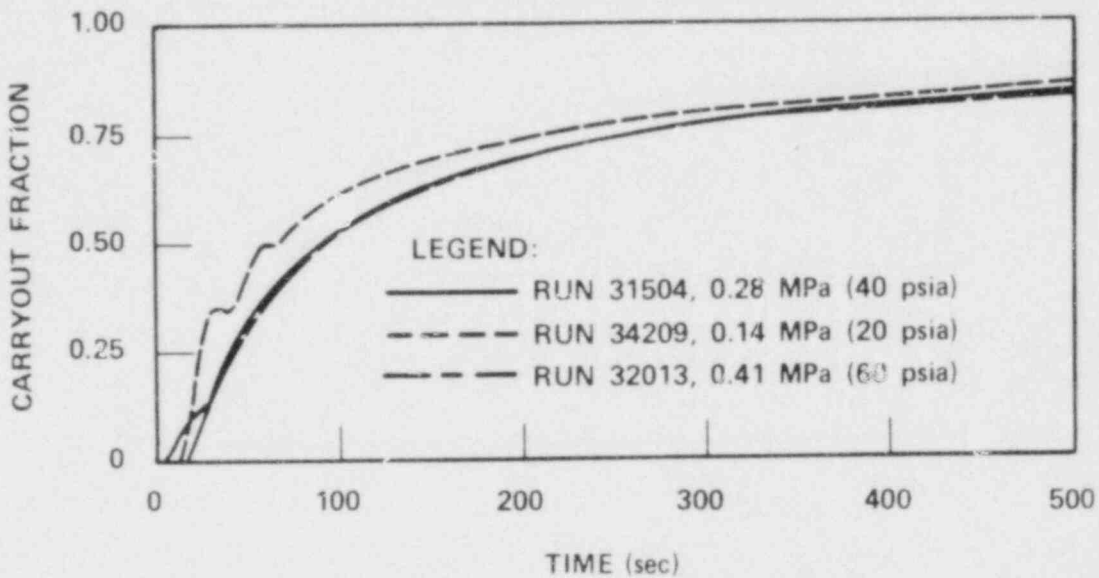


Figure 3-11. Pressure Effect on Carryout Fraction

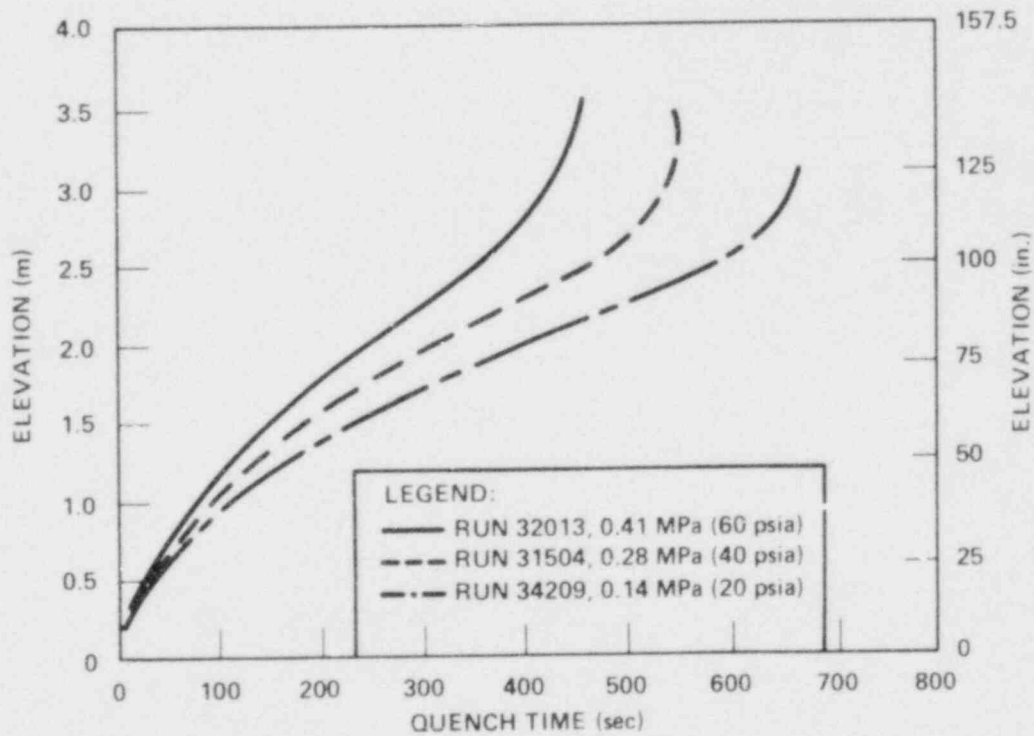


Figure 3-12. Pressure Effect on Quench Front Advance

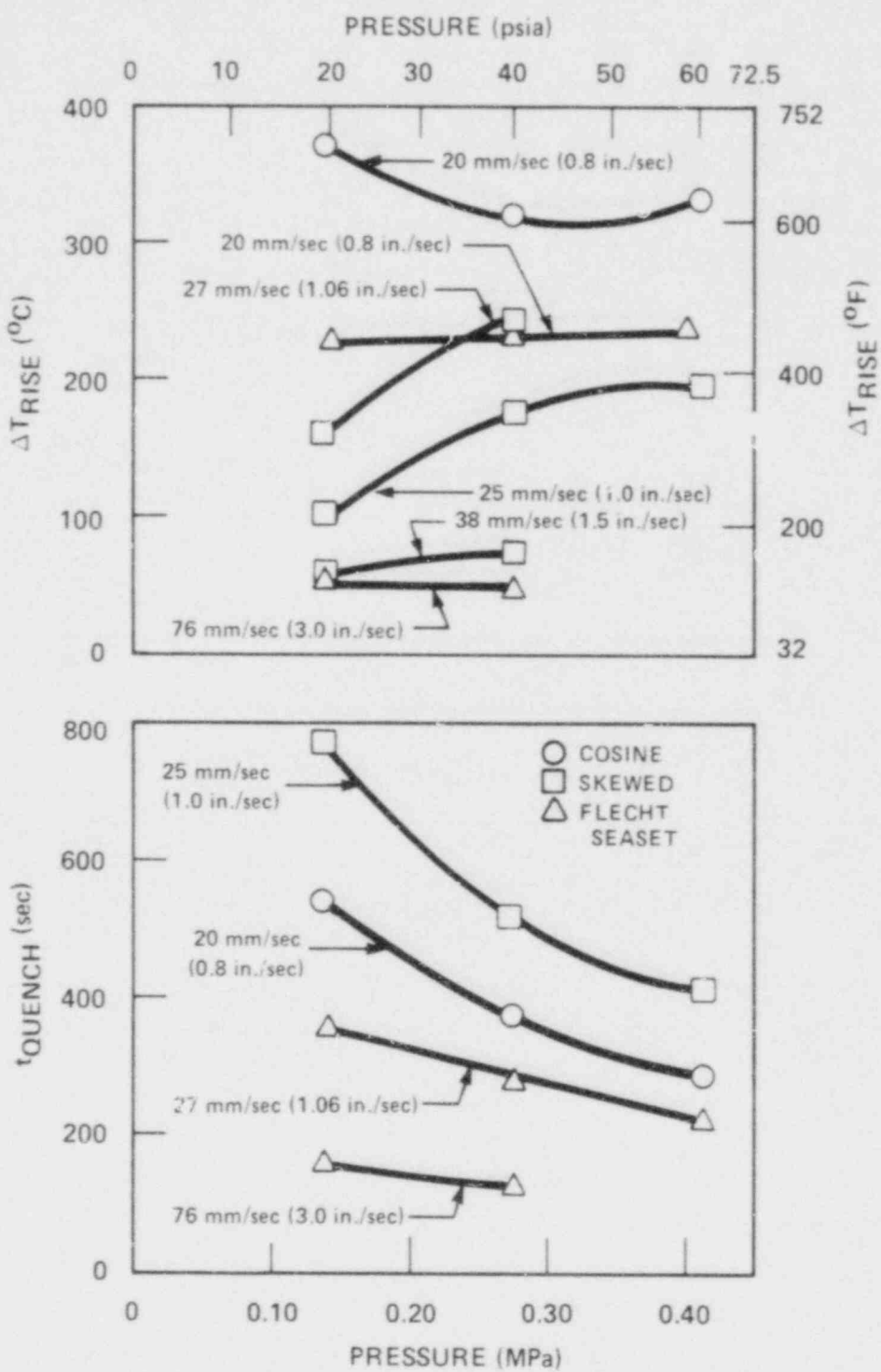


Figure 3-13. Pressure Effect on Temperature Rise and Quench Time

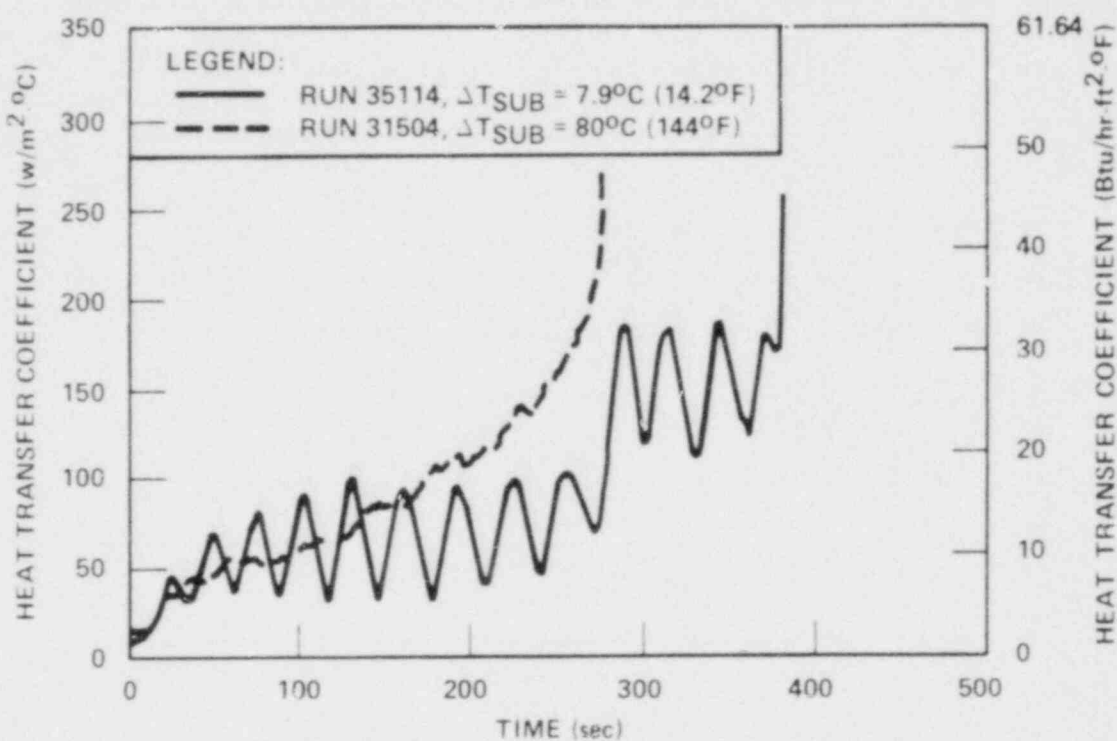


Figure 3-14. Subcooling Effect on Heat Transfer

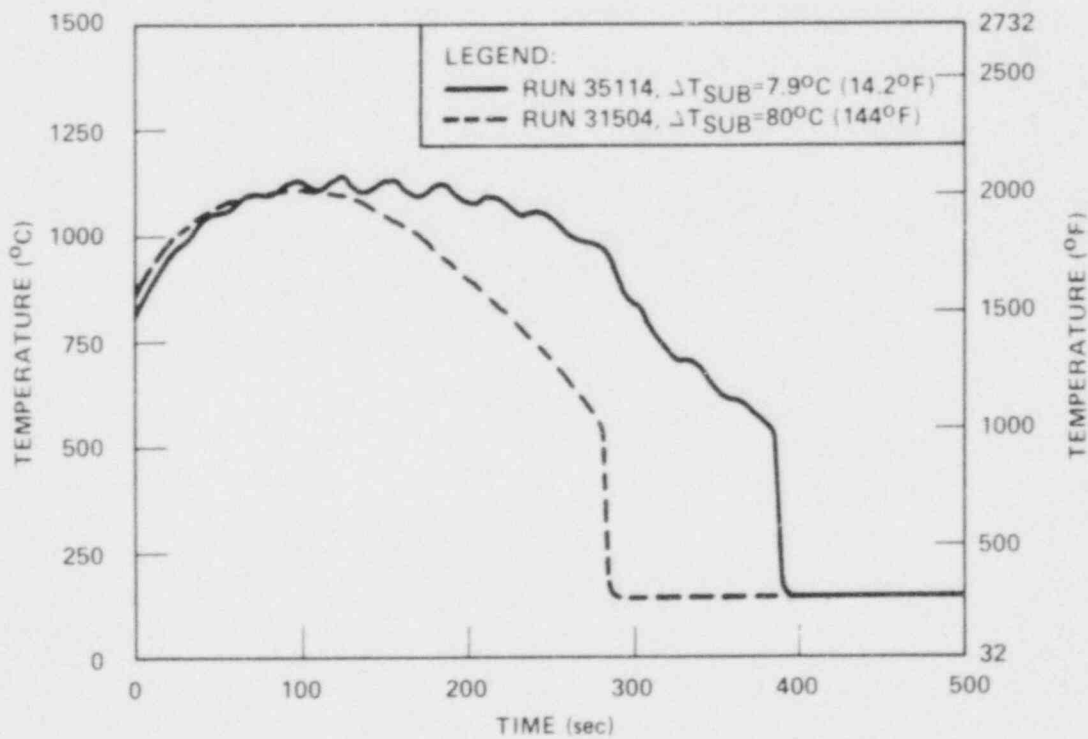


Figure 3-15. Subcooling Effect on Temperature

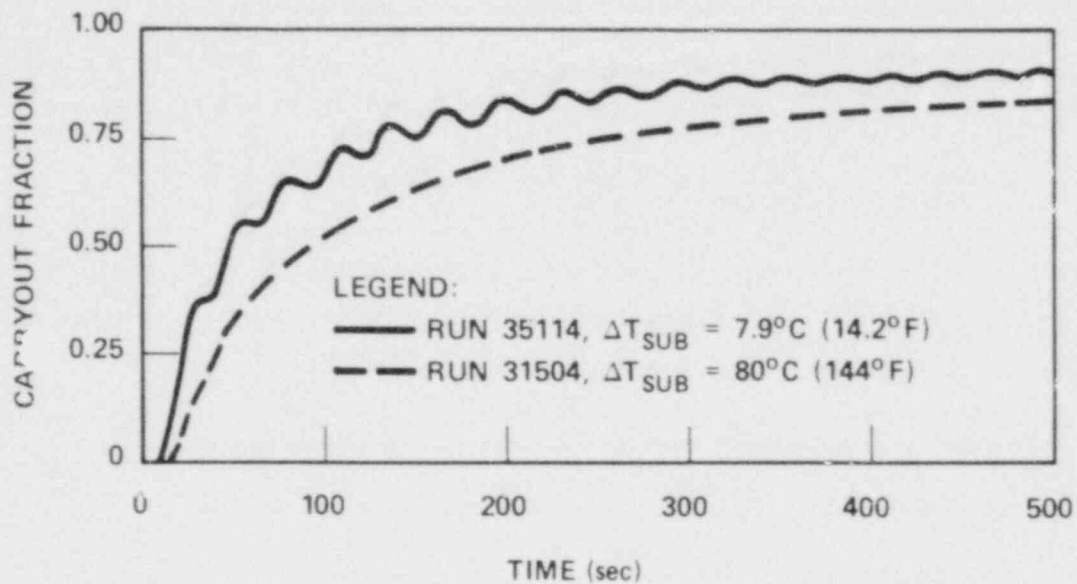


Figure 3-16. Subcooling Effect on Carryout Fraction

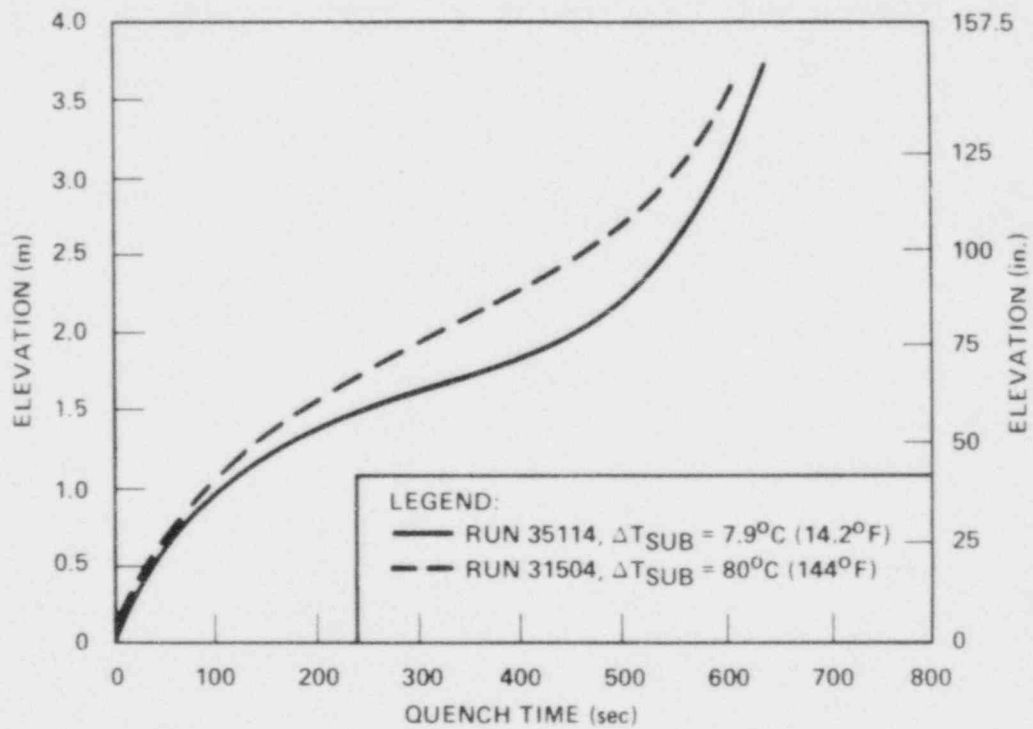


Figure 3-17. Subcooling Effect on Quench Front Advance

The effect of subcooling on temperature rise for the present test is very weak, as shown in figure 3-18, which plots FLECHT SEASET and cosine test data from 1.83 m (72 in.) and skew test data from 3.05 m (120 in.). The same effect was observed in the previous cosine tests. It is noted that the skewed tests showed a stronger effect of subcooling, and the trend was opposite. This could be due to the higher energy input in the skewed tests as explained above.

3-5. INITIAL CLAD TEMPERATURE EFFECT

Heat transfer coefficients and wall temperatures are compared in figures 3-19 and 3-20 to show the effect of initial clad temperature. Figure 3-21 shows the mass effluence comparison. The delay in carryout for the lower clad temperatures is to be expected, because less vapor formation and liquid entrainment are occurring at the lower temperatures. Therefore, the solid water level (or the saturation line) will penetrate farther into the bundle for lower initial clad temperature early in time. Figure 3-22 compares quench front progress in the various tests.

Initial clad temperature effects [figure 3-23, 1.83 m (72 in.) for FLECHT SEASET and cosine, 3.05 m (120 in.) for skew] for the present tests parallel closely the trends observed in the previous cosine and skew tests. These effects are, basically, higher temperature rises and shorter quench times as the initial cladding temperature decreases.

3-6. ROD PEAK POWER EFFECT

Predictably, for the FLECHT SEASET tests, the higher power runs show higher heat transfer before turnaround (figure 3-24). The power effect still dominates, however, leading to higher peak temperatures and longer quench time for higher power (figure 3-25). The same trends have been observed in the previous cosine and skewed power profile tests.

The mass effluent fractions (figure 3-26) increase with power. The lower powers lead to lower void formation below the quench front and hence more storage below the quench front and also faster quench velocity. Figure 3-27 shows quench front behaviors.

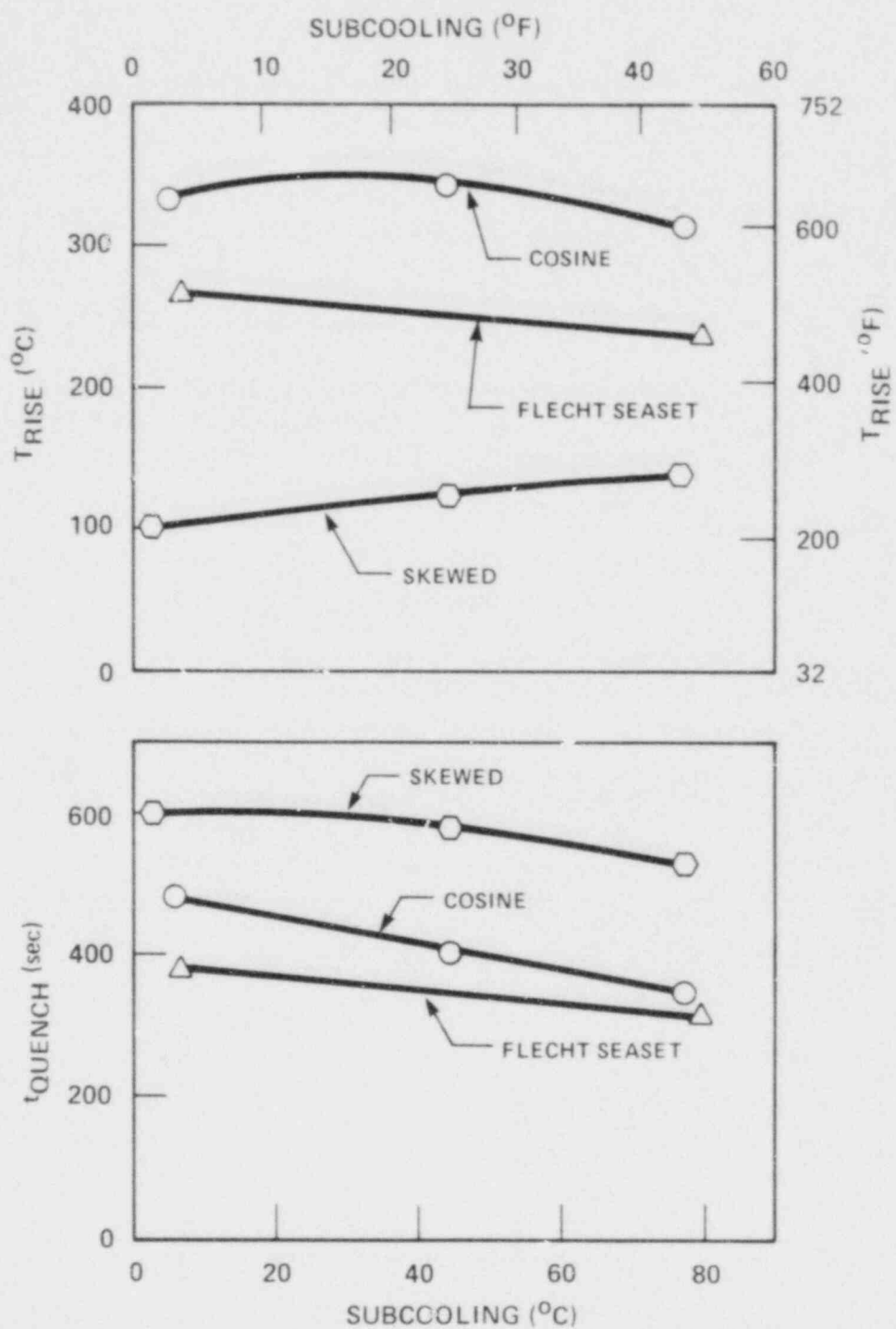


Figure 3-18. Subcooling Effect on Temperature Rise and Quench Time

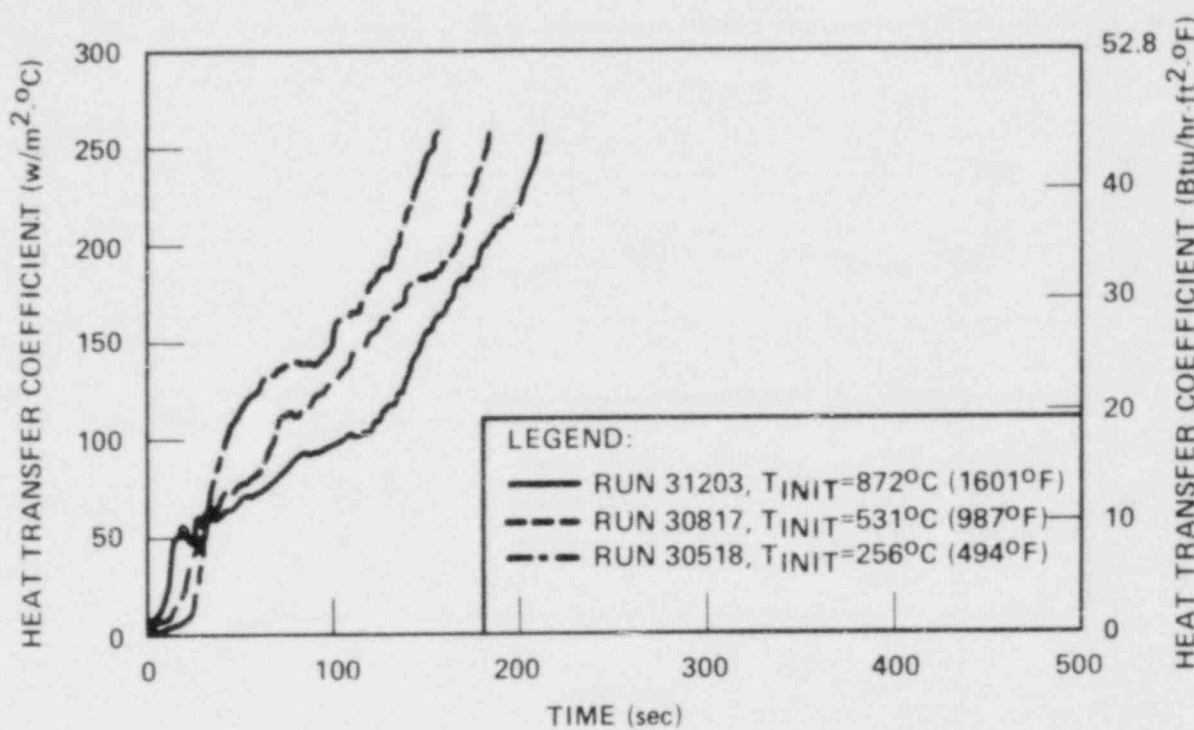


Figure 3-19. Initial Clad Temperature Effect on Heat Transfer

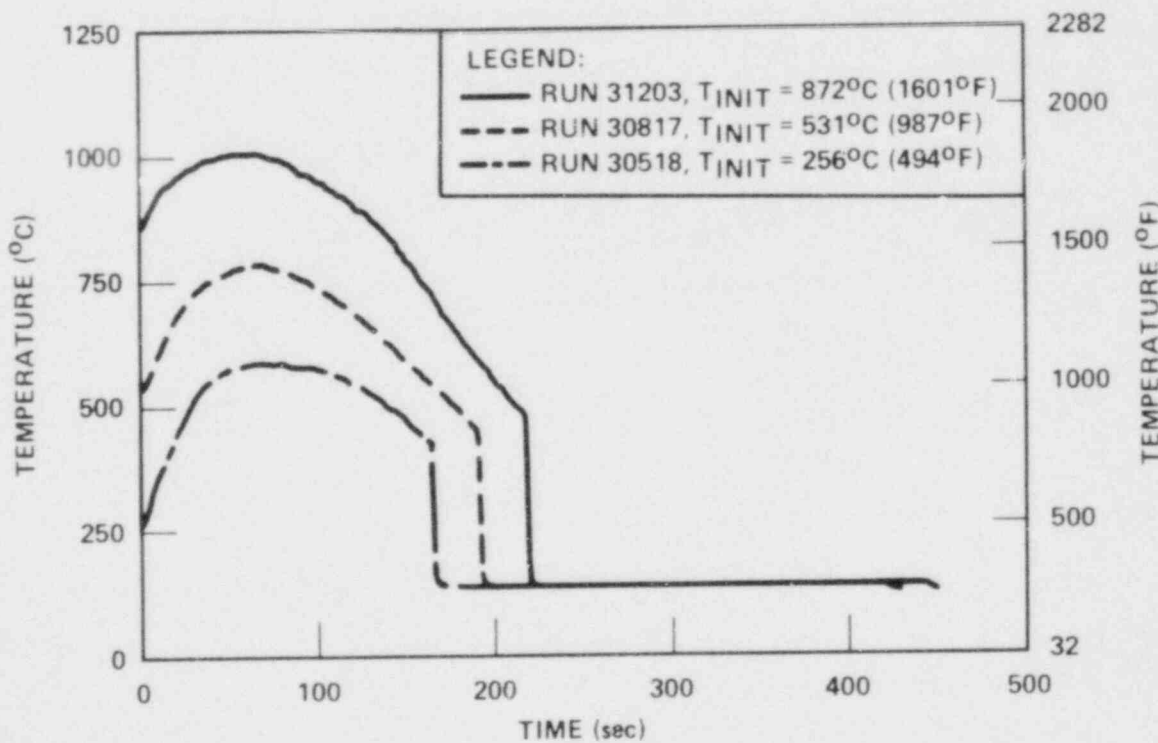


Figure 3-20. Initial Clad Temperature Effect on Temperature

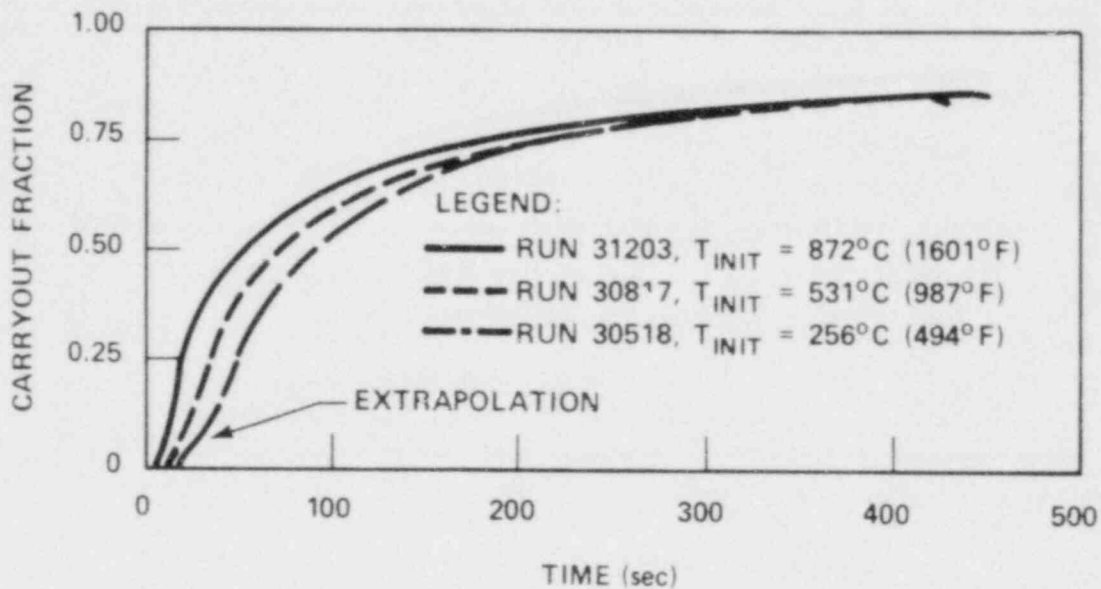


Figure 3-21. Initial Clad Temperature Effect on Carryout Fraction

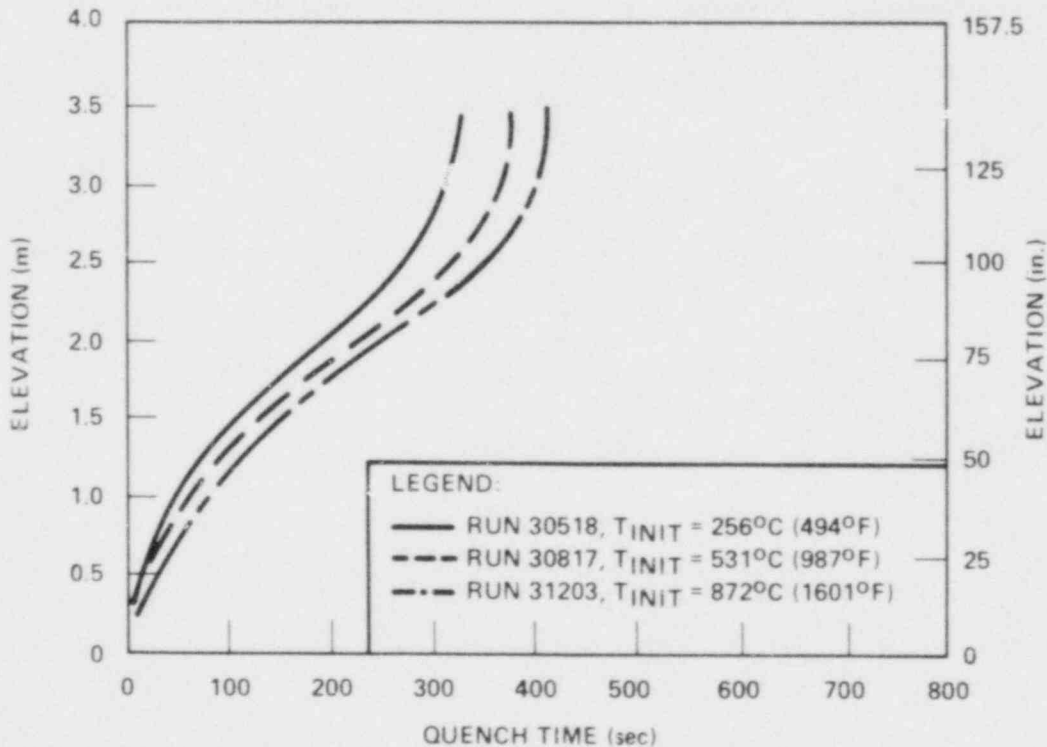


Figure 3-22. Initial Clad Temperature Effect on Quench Front Advance

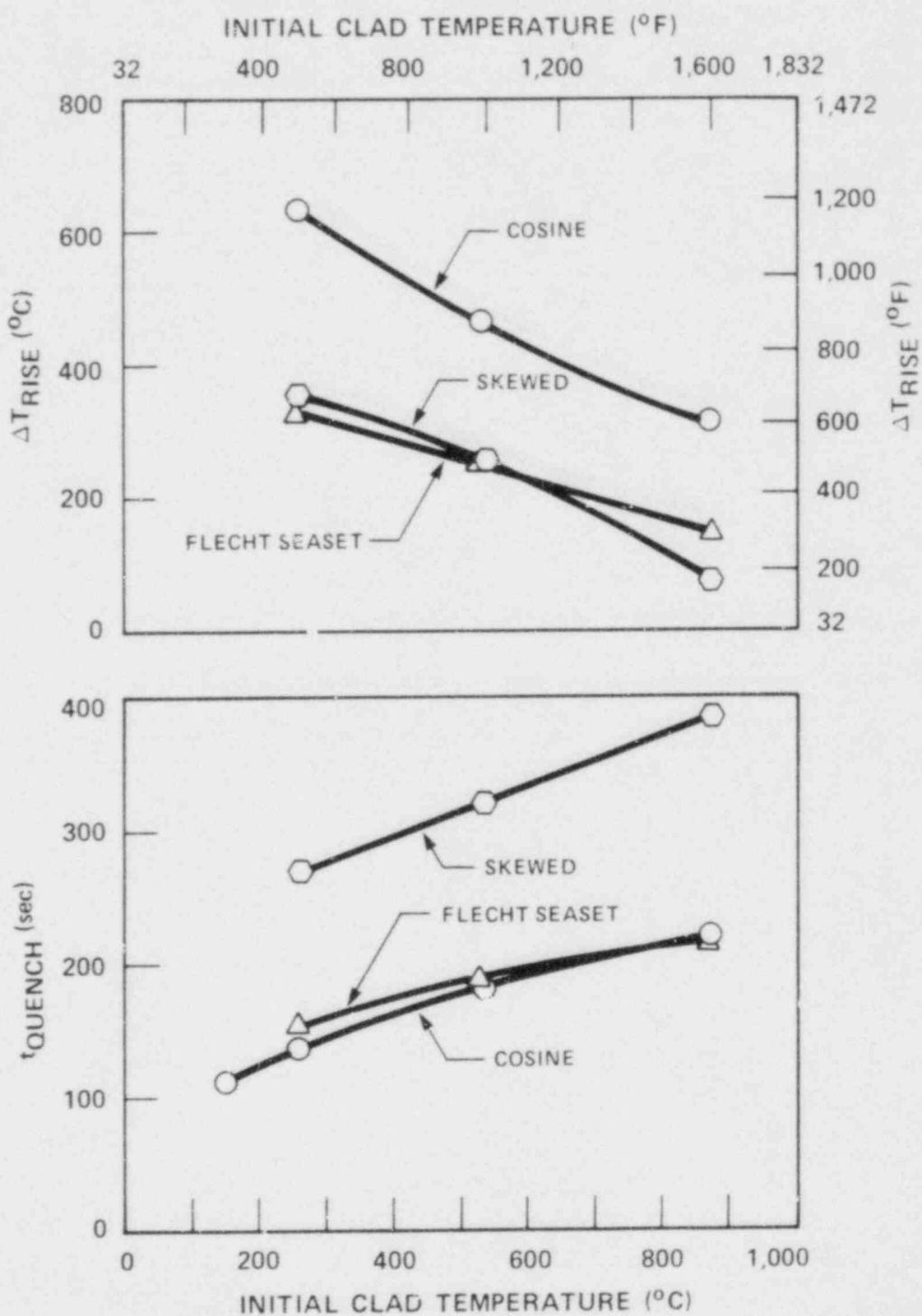


Figure 3-23. Initial Clad Temperature Effect on Temperature Rise and Quench Time

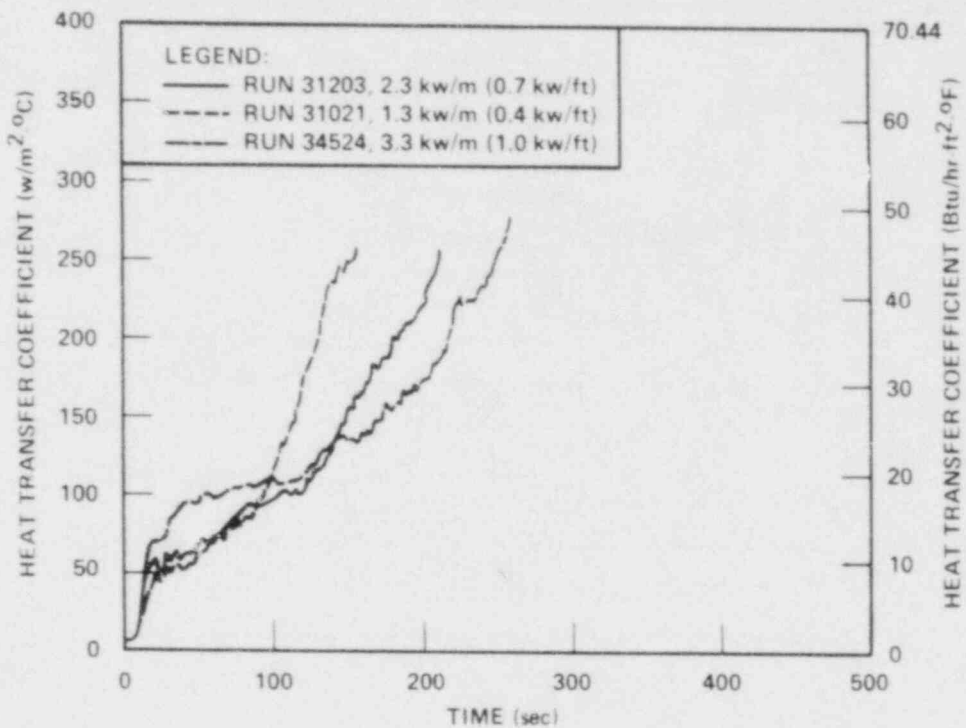


Figure 3-24. Peak Power Effect on Heat Transfer

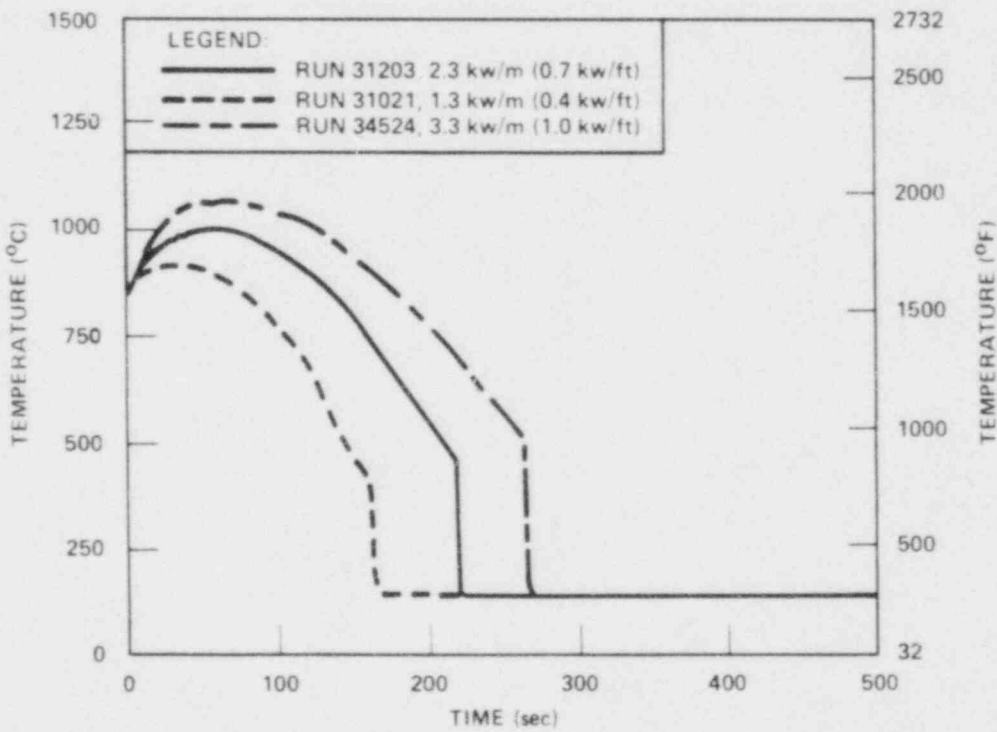


Figure 3-25. Peak Power Effect on Temperature

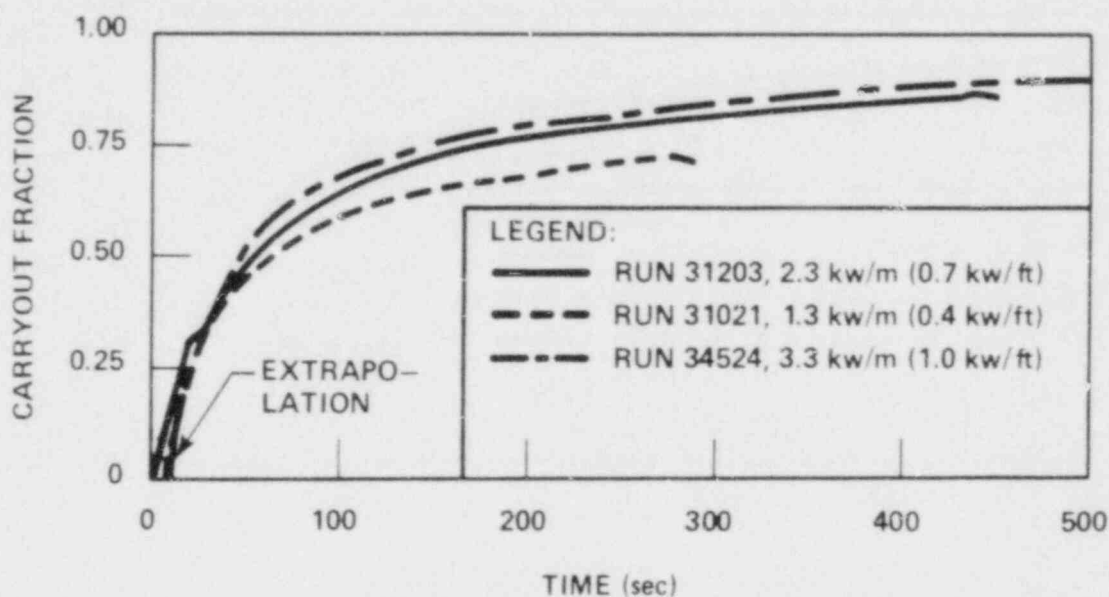


Figure 3-26. Peak Power Effect on Carryout Fraction

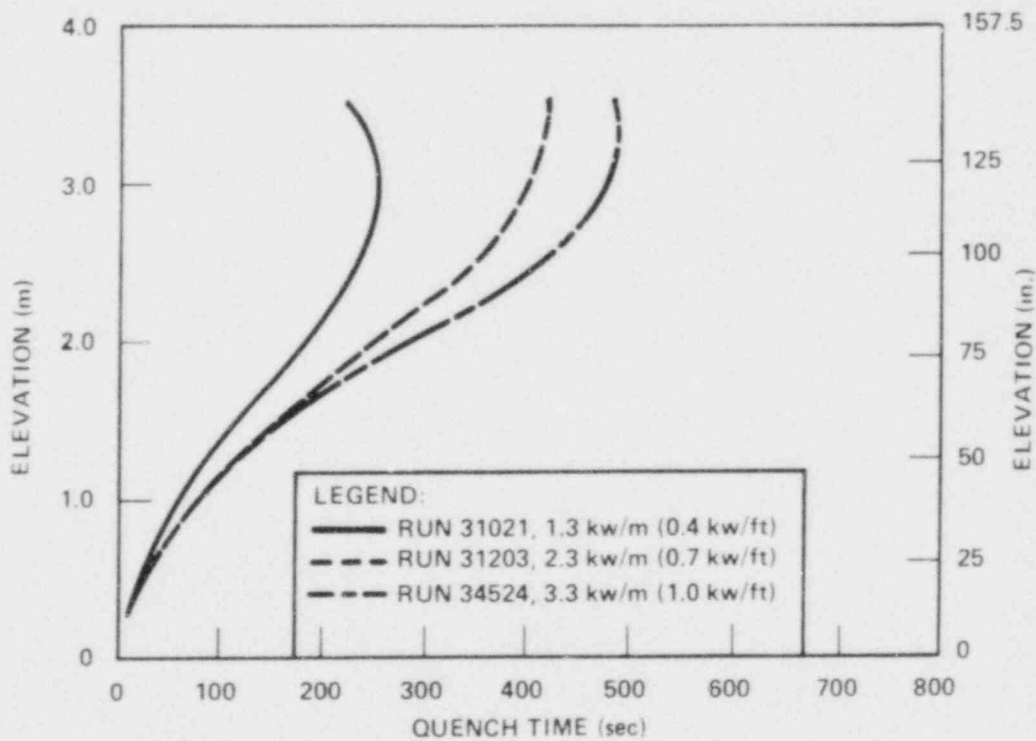


Figure 3-27. Peak Power Effect on Quench Front Advance

Decreasing peak power decreases both temperature rise and quench time. This is shown in figure 3-28 at the 1.83 m (72 in.) elevation for FLECHT SEASET and cosine tests and at the 3.05 m (120 in.) elevation for the skew tests.

3-7. VARIABLE FLOODING RATE EFFECT

The variable flooding rate tests examined the effect of an initial period of high flooding rate on an otherwise constant low flooding rate run. One run (32333), at 0.28 MPa (40 psia), was initiated with a high flooding rate [162 mm/sec (6.36 in./sec)] for 5 seconds, followed by a step down to 21 mm/sec (0.82 in./sec) for the remainder of the run. The run at 0.14 MPa (20 psia) (32235) was initiated with 166 mm/sec (6.53 in./sec) flooding rate for 5 seconds, followed by a step down to 25 mm/sec (0.98 in./sec). This lower flow rate continued for 200 seconds and then the rate was stepped down again to 16 mm/sec (0.62 in./sec) for the remainder of the run.

Heat transfer coefficients and temperature transients for the present tests are presented in figures 3-29 through 3-32. Figures 3-33 and 3-34 show the integrated mass effluent fraction for the tests. The fact that a high proportion of the water injected in the initial period is carried out of the bundle is responsible for the improved heat transfer. Figures 3-35 and 3-36 compare quench front progressions.

The variable flooding rate tests indicate that temperature rise and quench times decrease as increasing amounts of water are injected in the initial period. This is displayed in figure 3-37 at the 1.83 m (72 in.) elevation for FLECHT SEASET and cosine tests and at the 3.05 m elevation for the skewed tests. Where the amount of water in the initial period was directly proportional to the initial flooding rate. The decrease of temperature rise and quench time were observed in the previous skewed and cosine tests.

3-8. TRANSIENT SUBCOOLING EFFECT

During run 34316, the subcooling was changed from 79°C to 12°C (143°F to 21°F). This run was compared with the fixed subcooling tests (runs 31504 and 35114) to see the transient effect. Figure 3-38 compares the low plenum fluid temperatures to show the fluid temperature changes. Temperature rises and quench times of the runs at

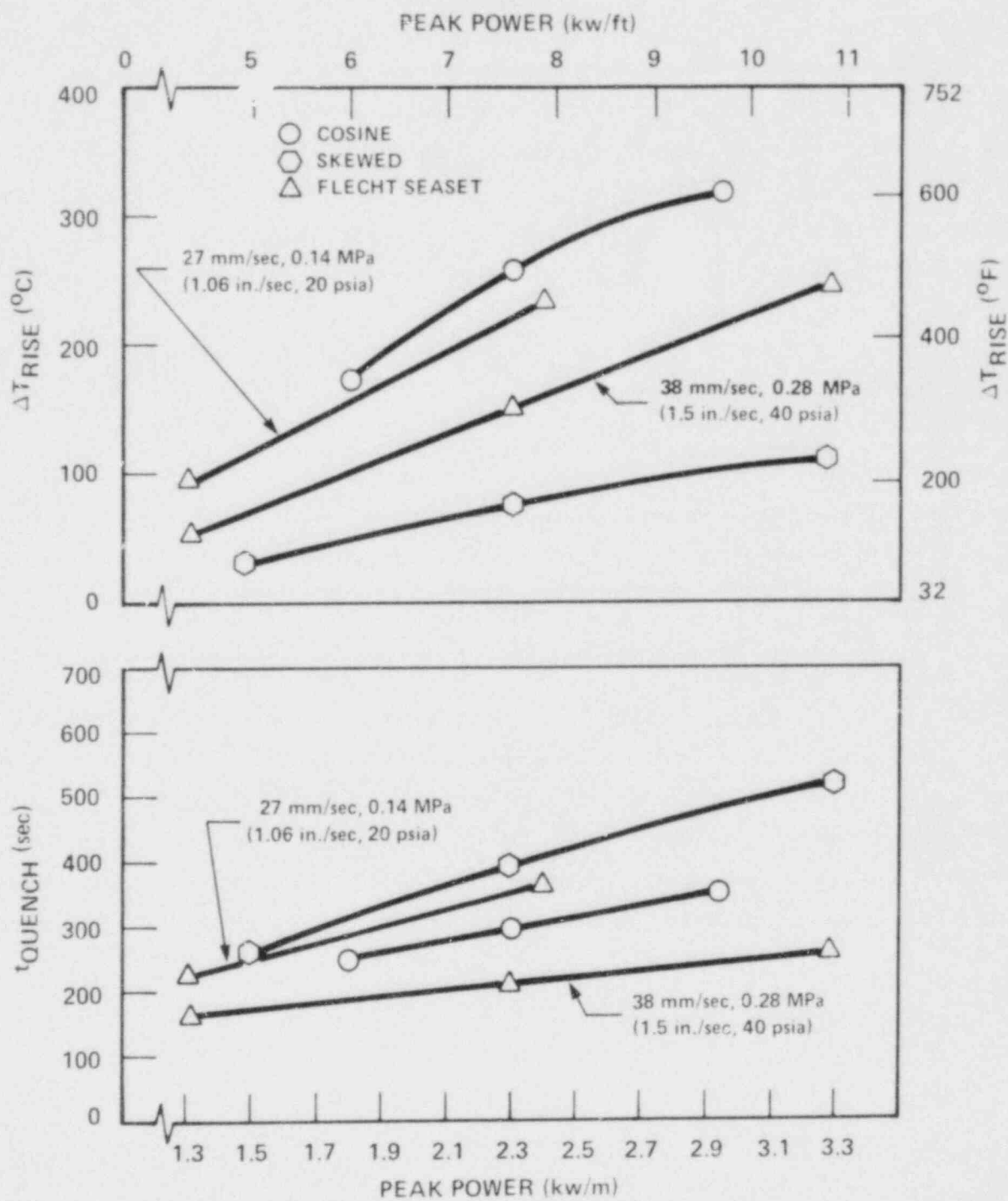


Figure 3-28. Peak Power Effect on Temperature Rise and Quench Time

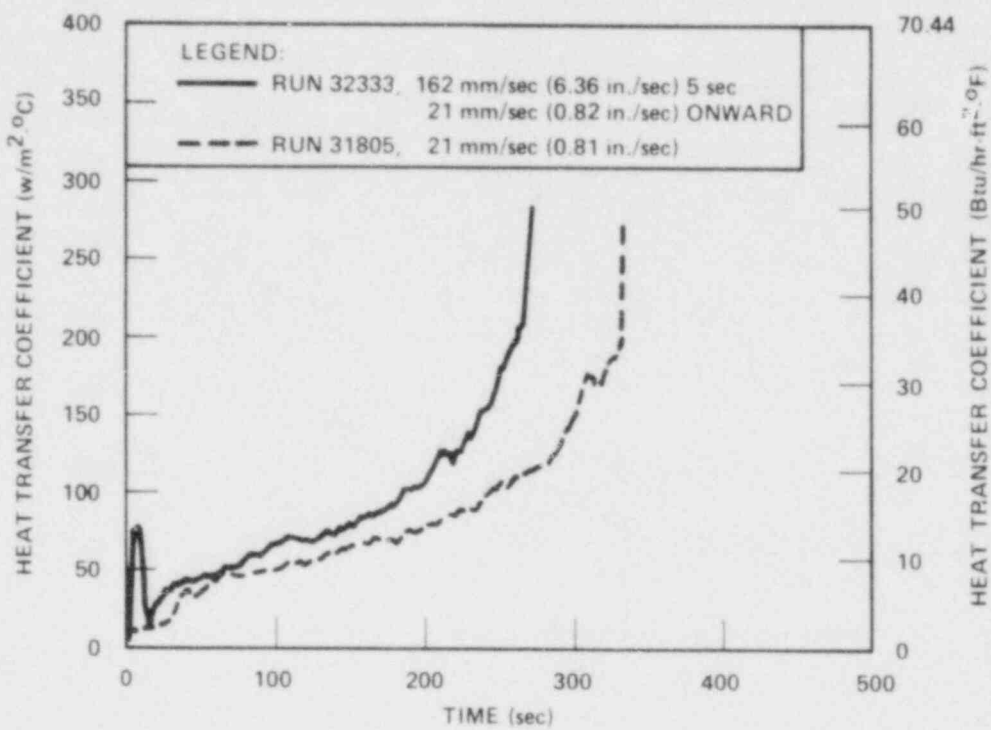


Figure 3-29. Initial Flooding Rate Effect on Heat Transfer Run 32333

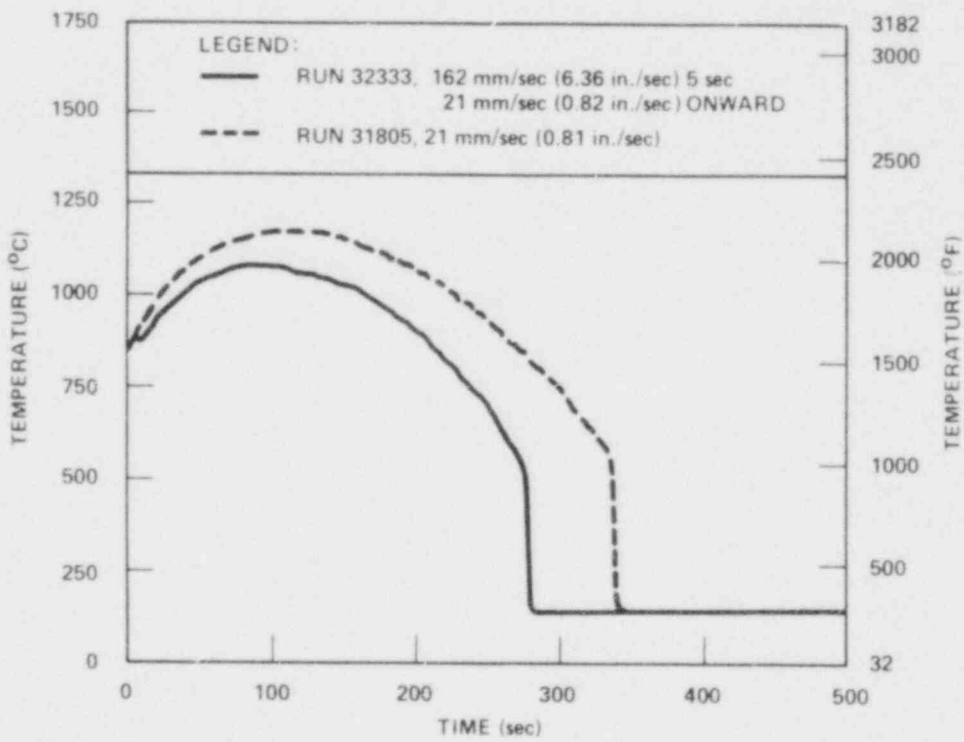


Figure 3-30. Initial Flooding Rate Effect on Temperature, Run 32333

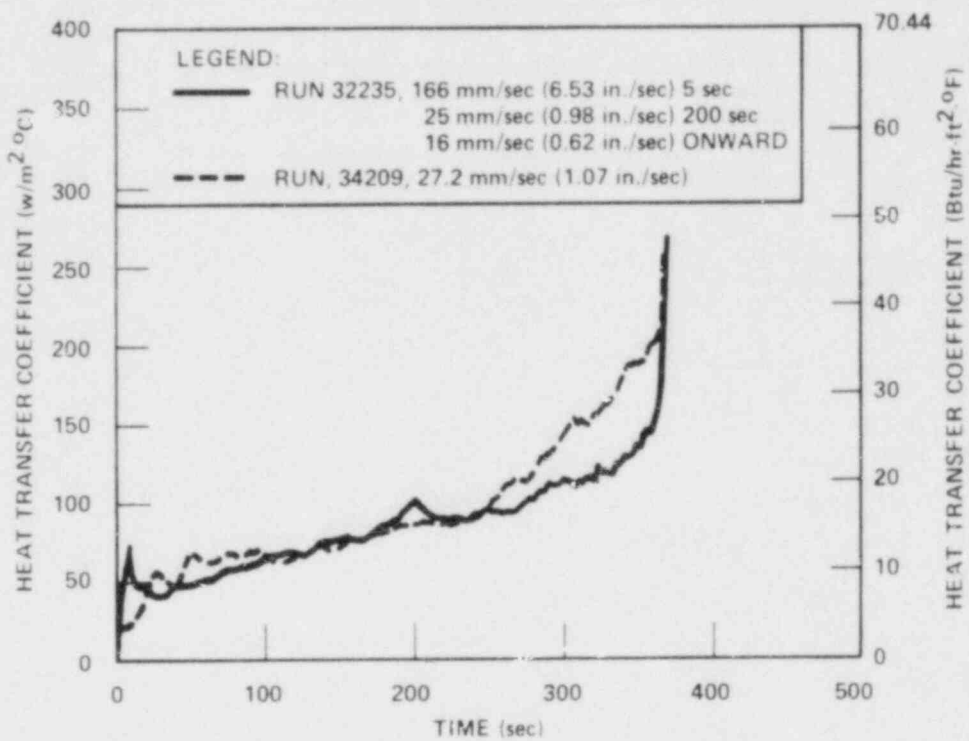


Figure 3-31. Initial Flooding Rate Effect on Heat Transfer Run 32235

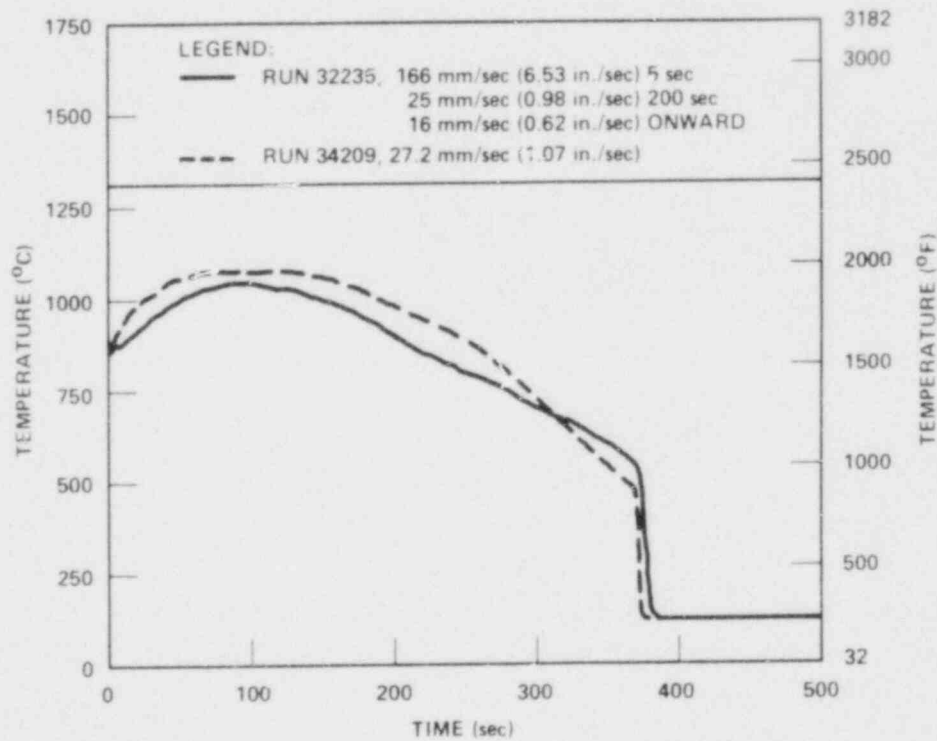


Figure 3-32. Initial Flooding Rate Effect on Temperature, Run 32235

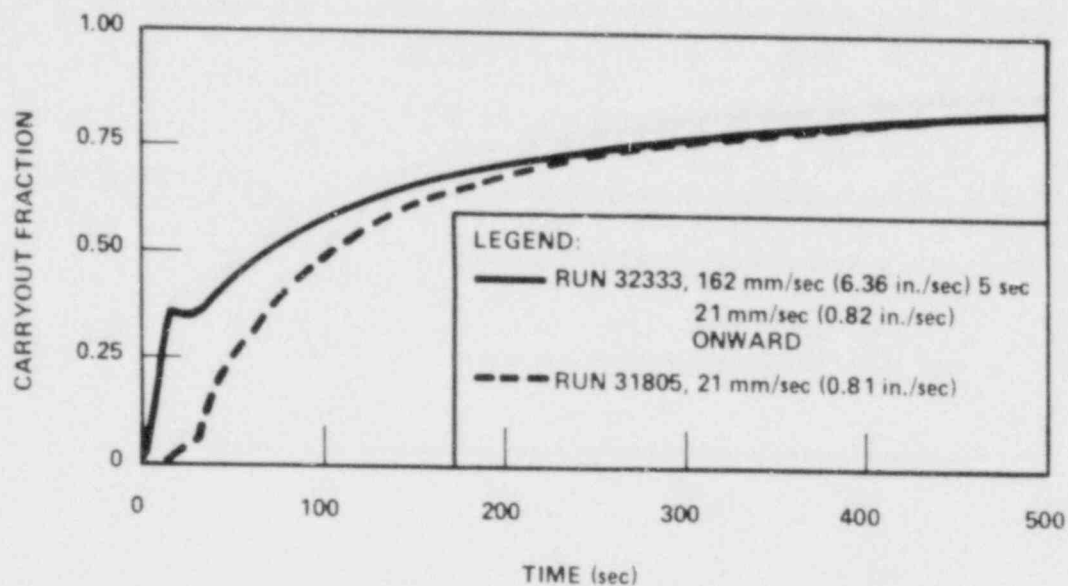


Figure 3-33. Initial Flooding Rate Effect on Carryout Fraction, Run 32333

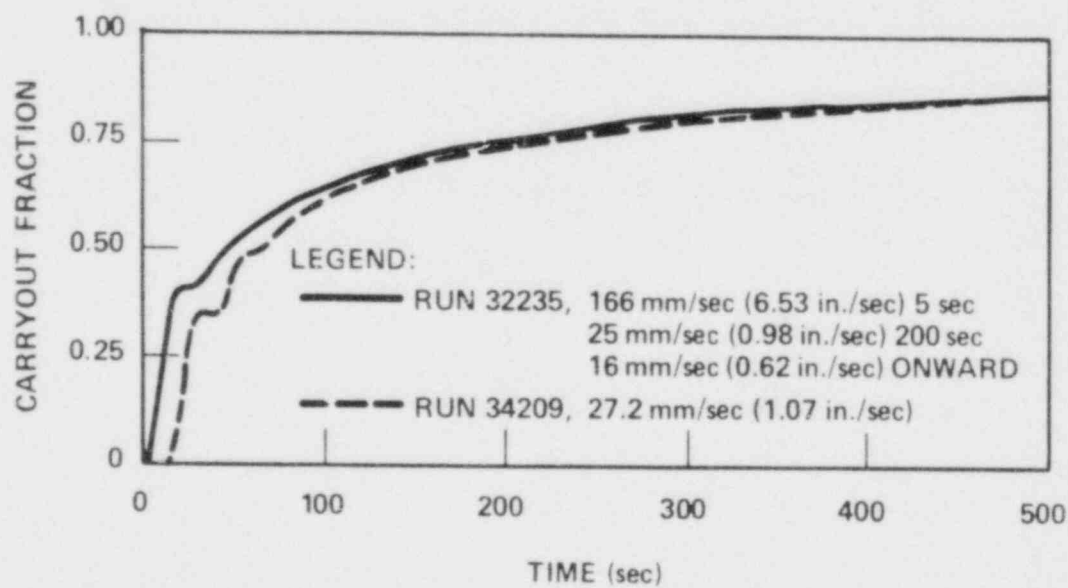


Figure 3-34. Initial Flooding Rate Effect on Carryout Fraction, Run 32235

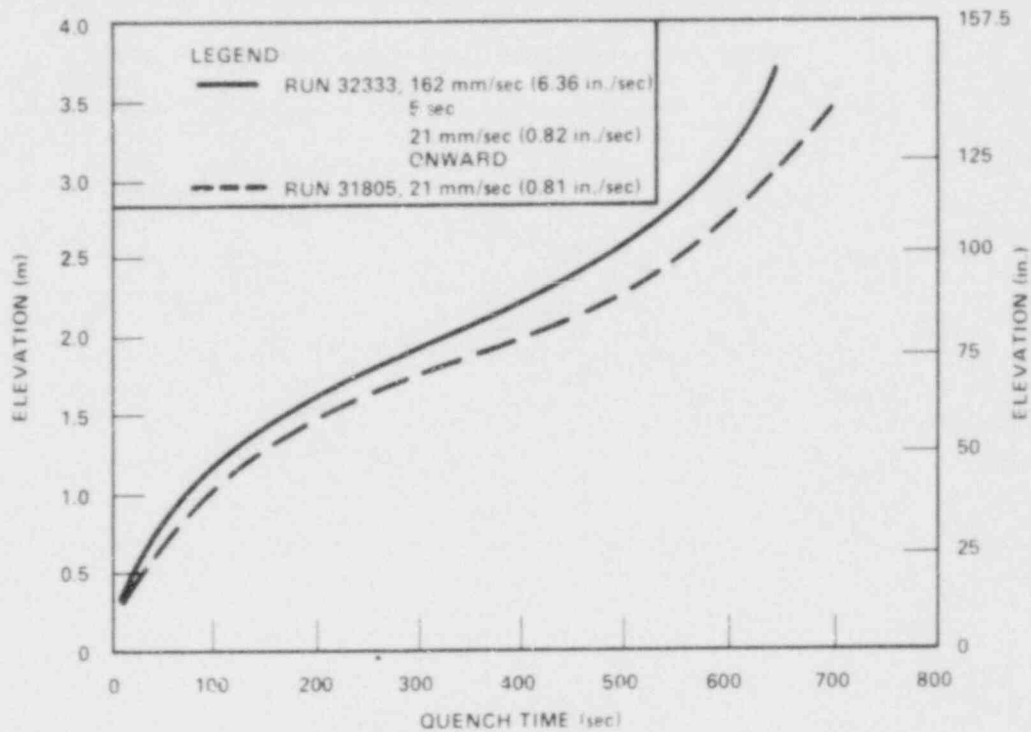


Figure 3-35. Initial Flooding Rate Effect on Quench Curve, Runs 32333 and 31805

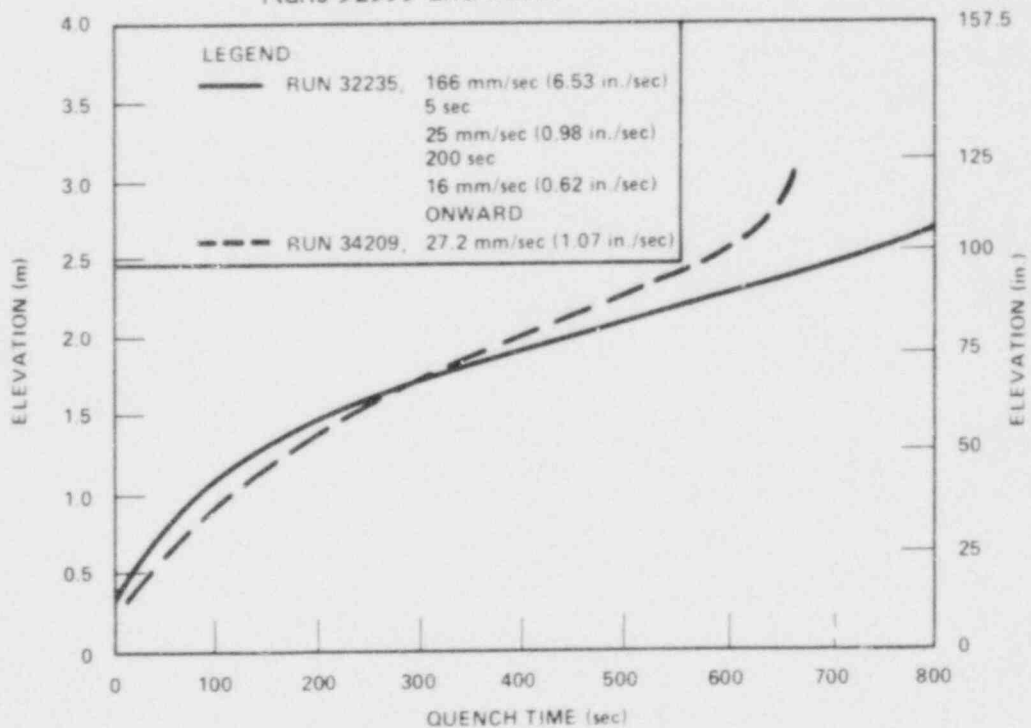


Figure 3-36. Initial Flooding Rate Effect on Quench Curve, Runs 32235 and 34209

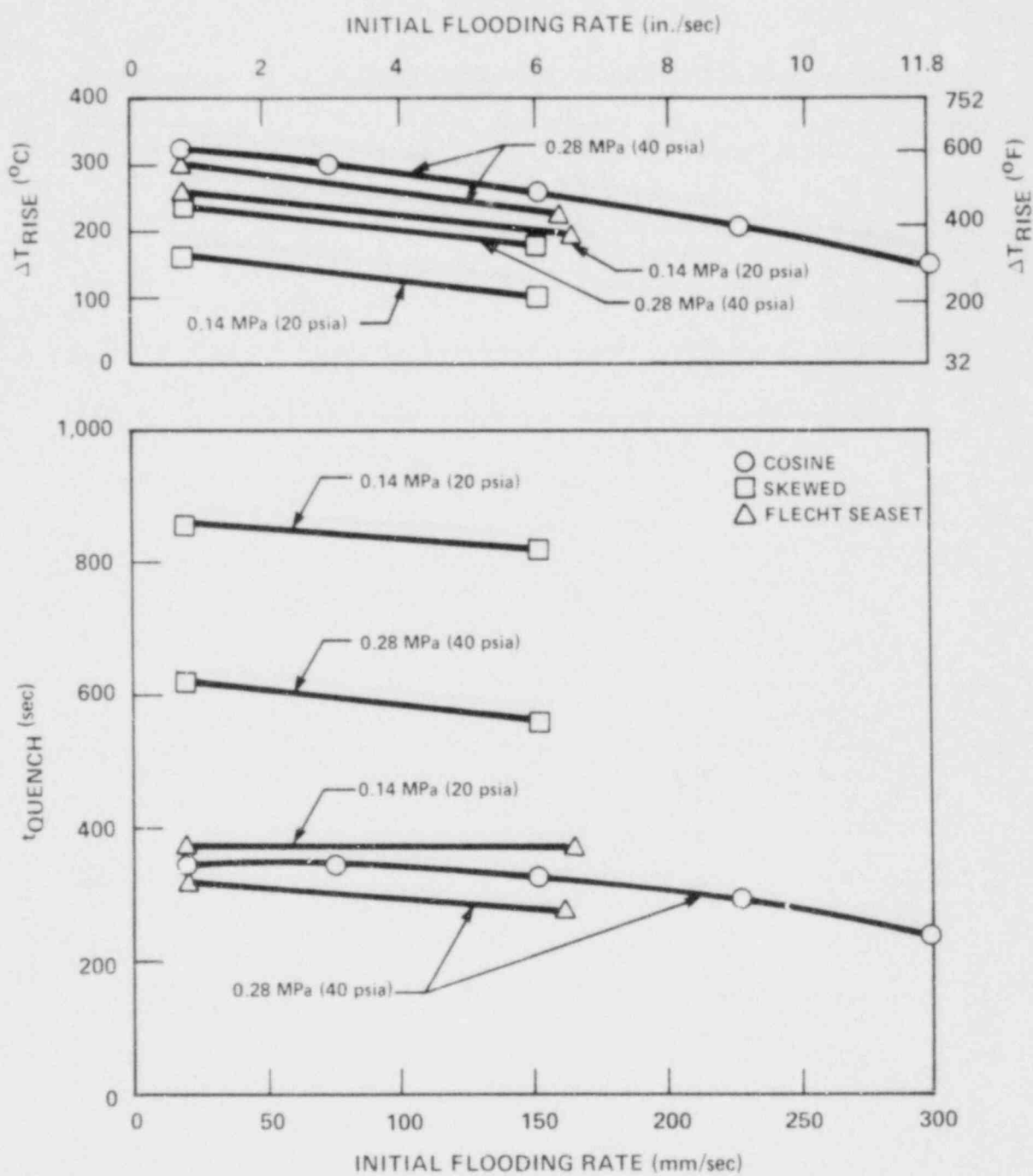


Figure 3-37. Initial Flooding Rate Effect on Temperature Rise and Quench Time

TABLE 3-2
SUBCOOLING TRANSIENT EFFECT

Run	Subcooling [°C (°F)]	Temperature Rise [°C (°F)]	Quench Time (sec)
34316	79 → 11.7 (143 → 21)	278 (500)	311
31504	80 (144)	233 (419)	272
35114	8 (14)	267 (481)	380

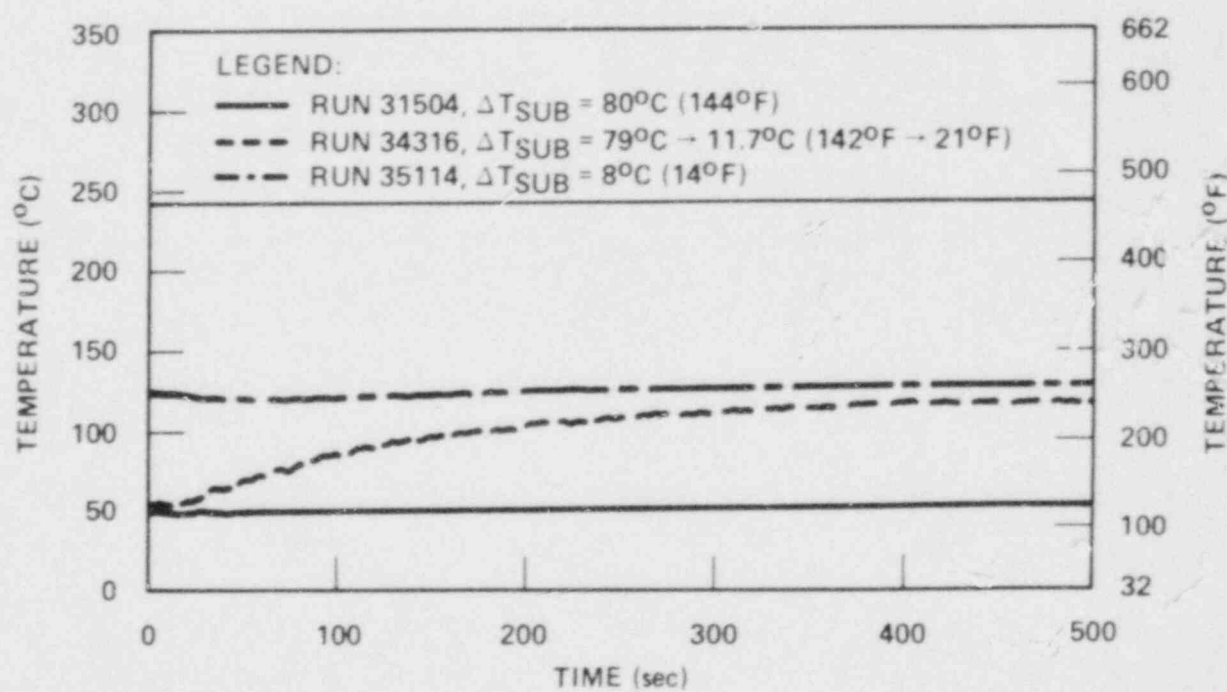


Figure 3-38. Low Plenum Temperature Comparison

the 1.83 m (72 in.) elevation are compared in table 3-2. Although the trend of quench time is as expected, the temperature rise trend is not easy to understand. It is believed that run 35114 had a higher temperature rise than run 34316, contrary to the data. These unexpected results could be due to the pressure oscillation observed during run 35114. Figures 3-39 and 3-40 compare the heat transfer coefficients and temperature histories, respectively. As indicated in the discussion of subcooling effect, run 35114 experienced a flow oscillation. Therefore, for convenience of comparison, a dotted line is also shown in figure 3-39 to indicate the change of the averaged values of the heat transfer coefficient of run 35114. The trends are as expected.

3-9. DATA REPEATABILITY

The data repeatability of this test series has been examined in the data report. A few additional discussions are presented here, using runs 31203 and 34103. The test conditions of these runs are summarized in table 3-1. The data repeatability analysis could be done in two ways: individual channel base and overall behavior.

Individual channel comparisons are one-to-one comparisons among corresponding thermocouple measurements when the corresponding thermocouples are located at the same position for the compared runs. A comparison at the 1.83 m (72 in.) elevation is shown in figure 3-41. It appears that, based on the individual channels, the repeatability is good except for the quench time data. Considering the slight differences in the operating conditions in the repeat tests, the repeatability is better than the figures show.

Overall tests of data repeatability could be approached in several ways: comparisons of characteristic temperatures and heat transfer coefficient transients, or comparisons of quench curves and overall quench characteristics like temperature rise, turnaround time, quench time, and maximum temperature.

Figures 3-42 and 3-43 present comparisons of the average temperature and heat transfer coefficient transients of the repeat tests. Factoring in the differences of operational conditions, it is considered that the repeatability is acceptable. Figure 3-44 compares average quench curves of the repeat tests.

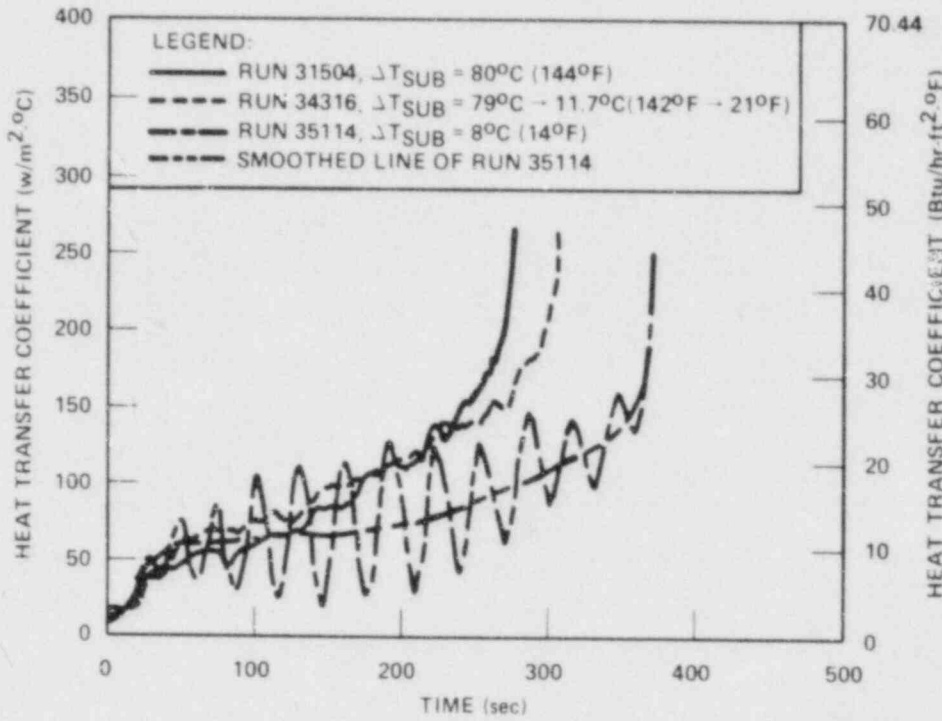


Figure 3-39. Subcooling Transient Effect on Heat Transfer

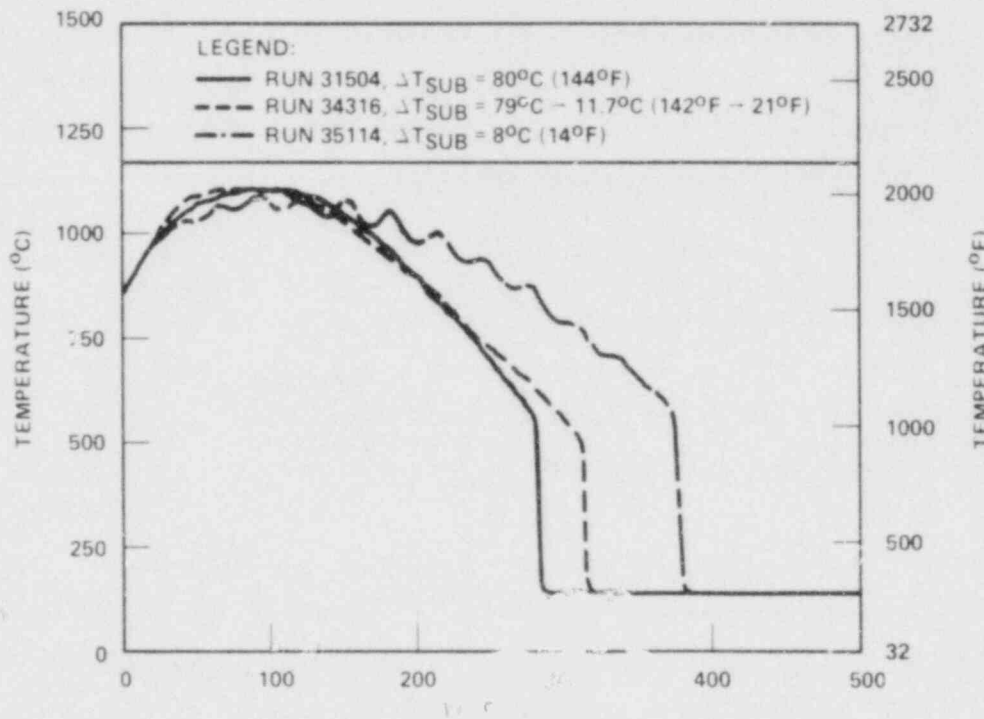


Figure 3-40. Subcooling Transient Effect on Temperature

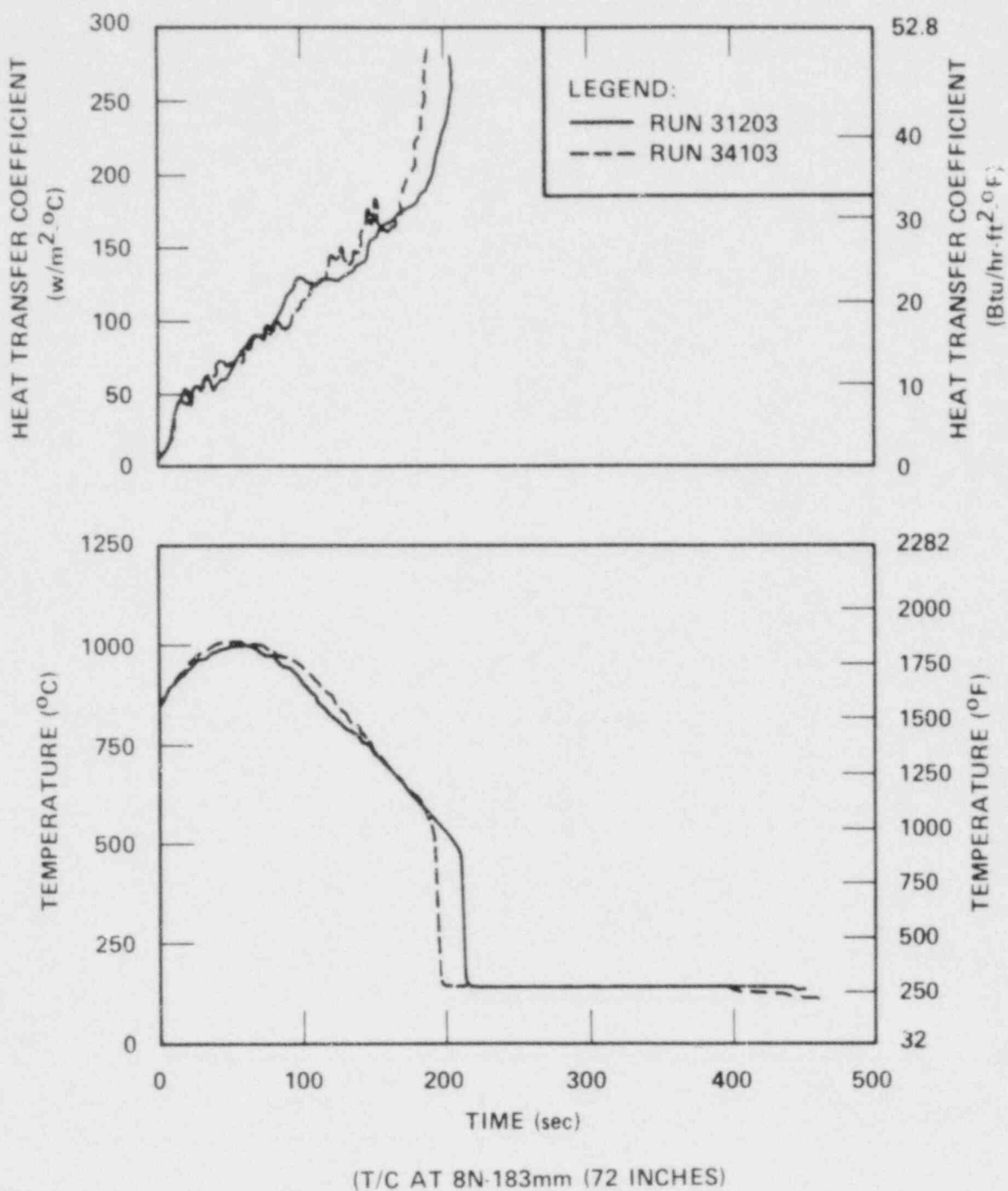


Figure 3-41. Individual Channel Comparisons for Repeat Tests

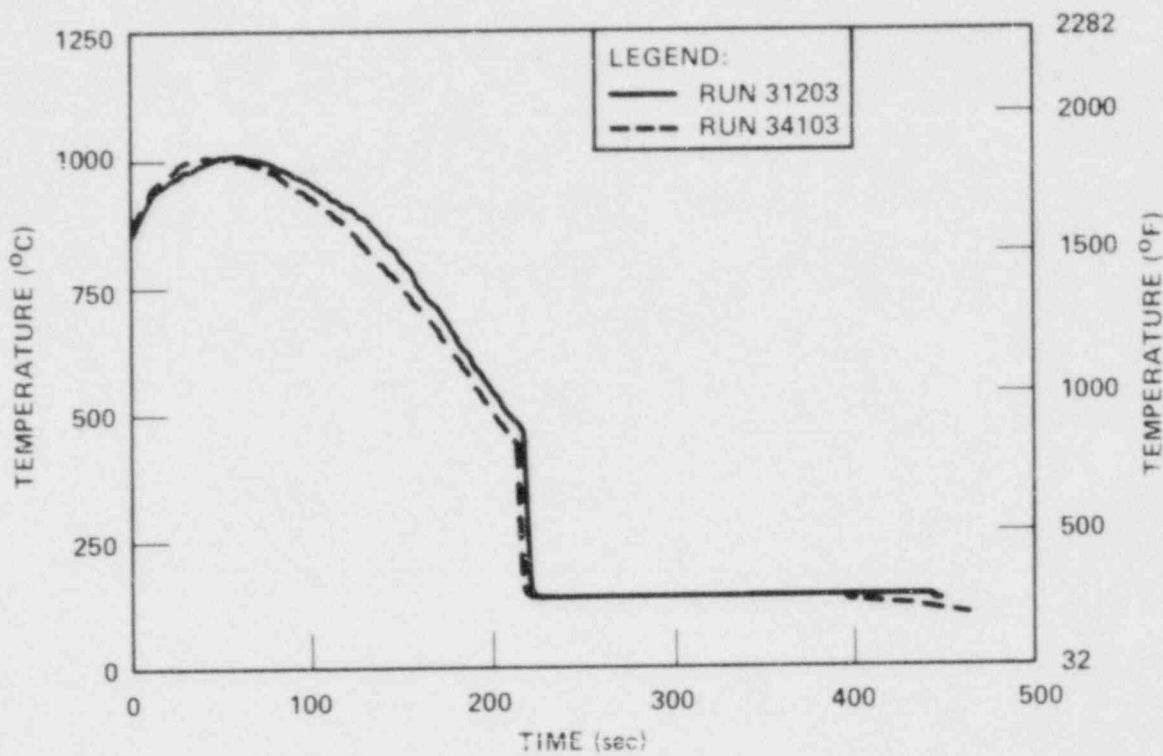


Figure 3-42. Average Temperature Comparison for Repeat Tests

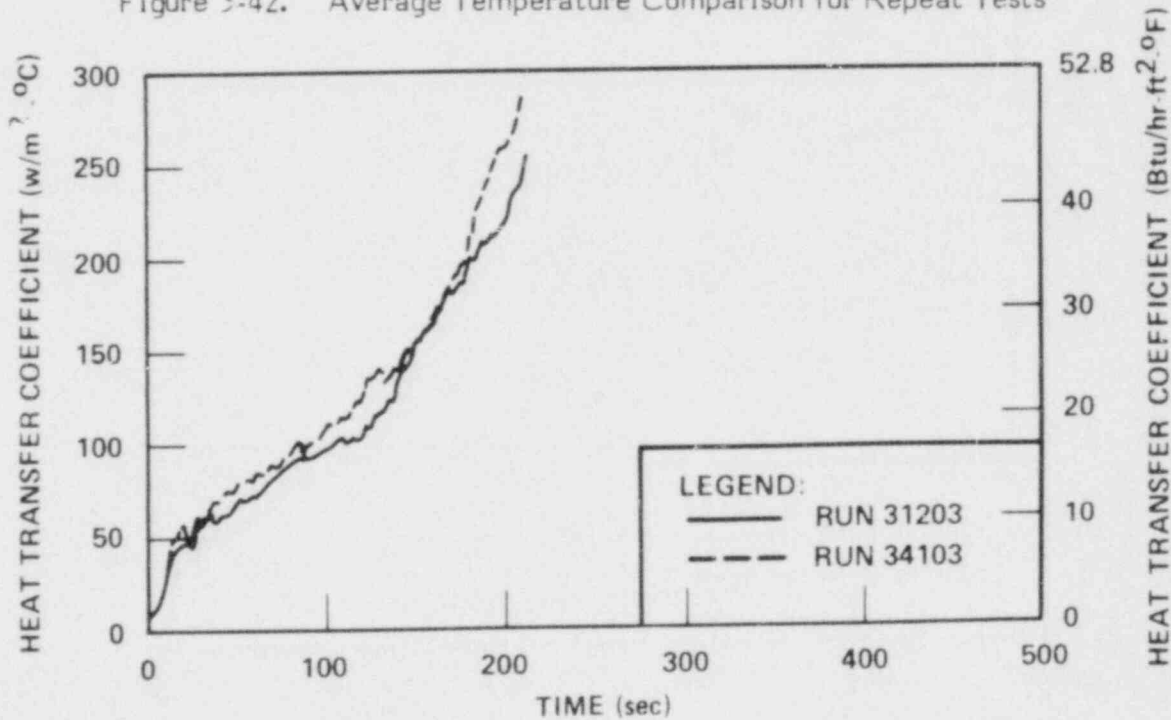


Figure 3-43. Average Heat Transfer Coefficient Comparison for Repeat Tests

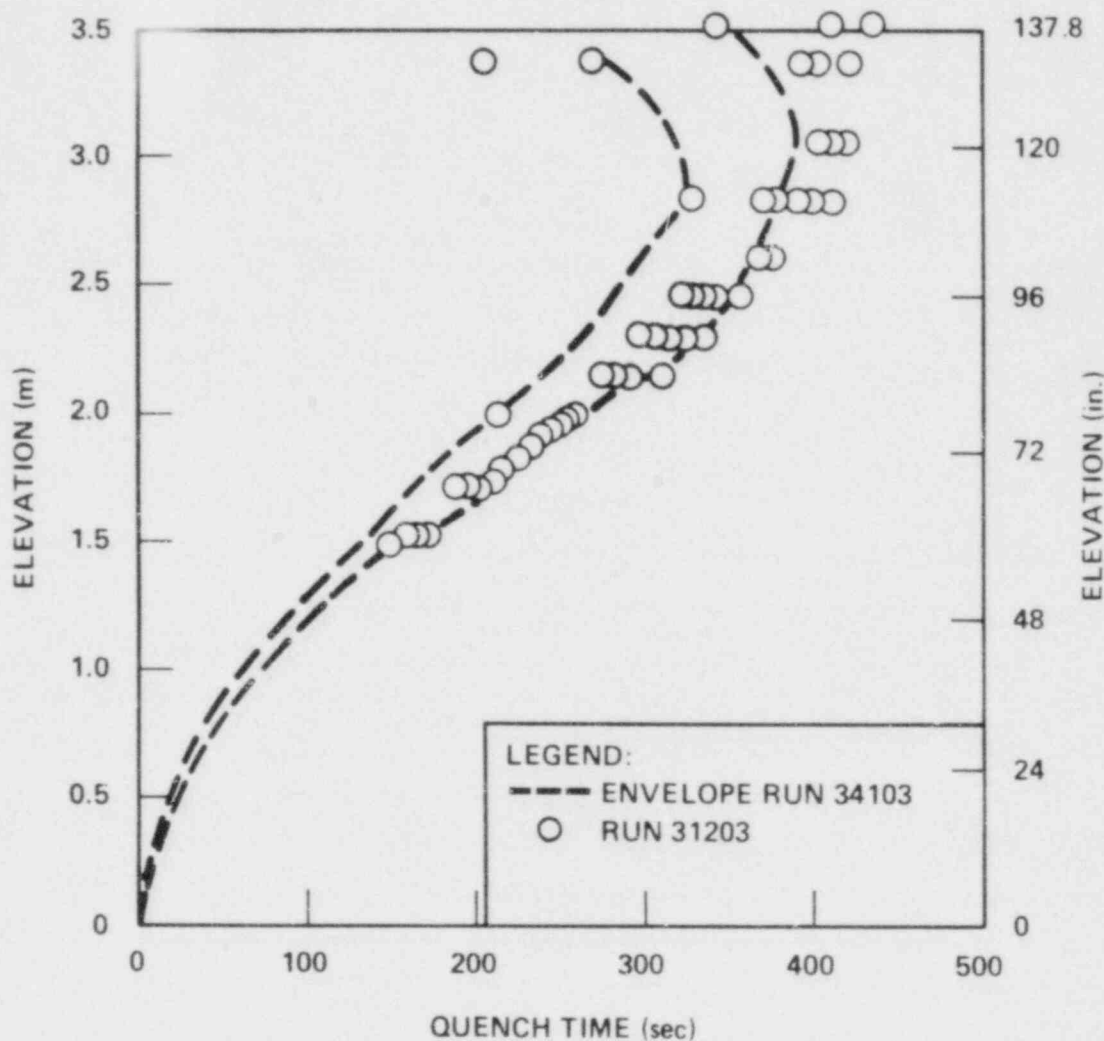


Figure 3-44. Comparison of Quenching Behavior in Repeat Tests

A few quench characteristics at the 1.83 m (72 in.) elevation are compared in table 3-3. For reference purposes, the same information is available for the similar runs of the previous cosine and skewed power profile tests. The variations of the FLECHT SEASET variables are larger than those of the cosine test but comparable to those of the skewed test.

3-10. OVERLAP TESTS

Some overlap tests linking the previous 15x15 FLECHT low flooding rate cosine tests with the current 17x17 array tests have been performed. Table 3-4 lists the overlap tests with their operational conditions.

The method used to rescale the 15x15 tests conditions preserves both generated power and stored energy per unit flow area. The detailed equational forms of the scaling methods are presented in the FLECHT SEASET unblocked bundle task plan.⁽¹⁾ Based on the philosophy behind choosing test conditions in this way, the following two hypotheses could be proposed:

- Quench times at given elevations for both the tests are the same if the integrated power per unit flow area up to the elevations is the same.
- Heat transfer coefficients are the same if the integrated power per unit flow area up to the elevations is the same.

The first hypothesis can be checked out by comparing quench curves, because the two bundles have same integrated power per unit flow area up to the same elevations. The results are shown in figures 3-45 through 3-48. It can be observed from the figures that the quench curves do not show any significant effect of the bundle geometry difference up to the time when the secondary quench fronts from the top are significant.

The second hypothesis can be tested by using heat transfer coefficients of the two test series at the same elevations. The heat transfer coefficients at the 1.83 m (72 in.) elevation are compared in figures 3-49 through 3-52.

I. Hochreiter, L. E., et al., "PWR FLECHT SEASET Unblocked Bundle Forced and Gravity Reflood Task: Task Plan Report," NRC/EPRI/Westinghouse-3, March 1978.

TABLE 3-3

REPEAT AND PREVIOUS TEST DATA COMPARISON [1.83 m (72 in.)]

Run	Test Series	Quench Time (sec)	Turnaround Time (sec)	Temperature Rise [$^{\circ}\text{C}$ ($^{\circ}\text{F}$)]	Maximum Temperature [$^{\circ}\text{C}$ ($^{\circ}\text{F}$)]
31203	FLECHT	217.7	55.6	148.8 (267.9)	993.7 (1820.6)
34103	SEASET	203.8	52.8	155.1 (279.1)	1011 (1851.8)
04748	Cosine	207.4	66.7	188.3 (338.9)	1036.9 (1893.4)
04831		210.3	69.5	194.7 (350.5)	1043.8 (1910.8)
13303	Skewed	384	35.8	73.7 (132.6)	913 (1676)
11003		337.4	23	54.5 (98.1)	893 (1640)
17136	Skewed	453	143	157.9 (284.3)	1008 (1847)
13404		518.4	7.2	175.2 (315.3)	1015 (1859)

TABLE 3-4

OVERLAP TEST CONDITIONS

Run	Test Series	Rod Peak Power [kw/m (kw/ft)]	Flooding Rate [mm/sec (in./sec)]	Rod Initial Temperature [°C (°F)]	Subcooling [°C (°F)]	Pressure [MPa (psi)]
03113	Cosine	2.7 (0.81)	38.1 (1.5)	87 (1600)	76 (136)	0.26 (38)
31203	FLECHT SEASET	2.3 (0.7)	38.1 (1.5)	87 (1600)	78 (140)	0.28 (40)
00904	Cosine	2.8 (0.85)	38.1 (1.5)	537 (998)	78 (140)	0.28 (41)
30817	FLECHT SEASET	2.3 (0.7)	38.1 (1.5)	538 (1000)	78 (140)	0.28 (40)
03709	Cosine	2.7 (0.81)	38.1 (1.5)	317 (603)	78 (141)	0.14 (20)
30619	FLECHT SEASET	2.3 (0.7)	38.1 (1.5)	260 (500)	78 (140)	0.14 (20)
02414	Cosine	2.8 (0.84)	20.6 (0.81)	871 (1600)	77 (138)	0.28 (40)
31805	FLECHT SEASET	2.3 (0.7)	20.3 (0.8)	871 (1600)	78 (140)	0.28 (40)

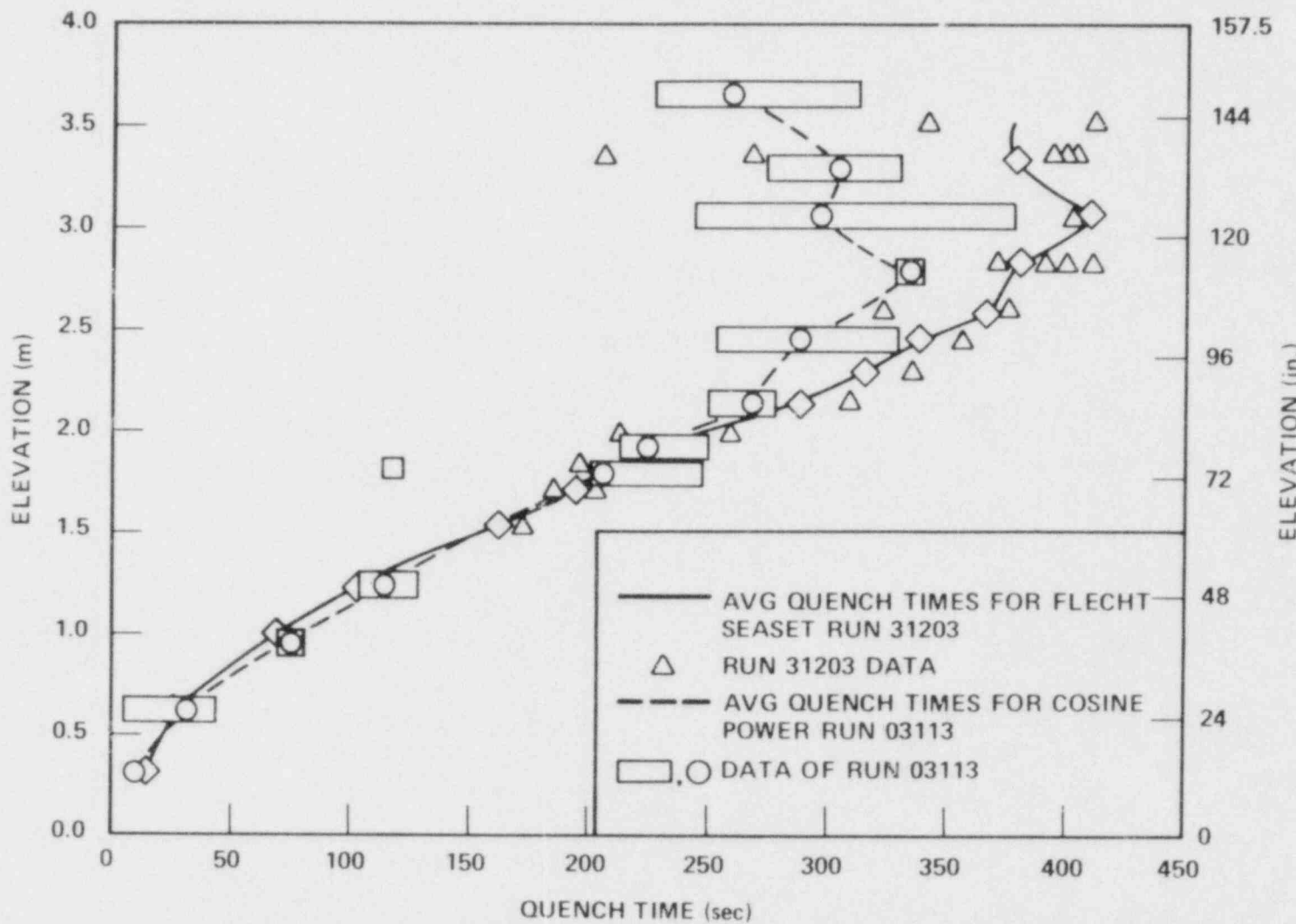


Figure 3-45. Overlap Test Quench Curve Comparison, FLECHT SEASET Run 31203 and Cosine Run 03113

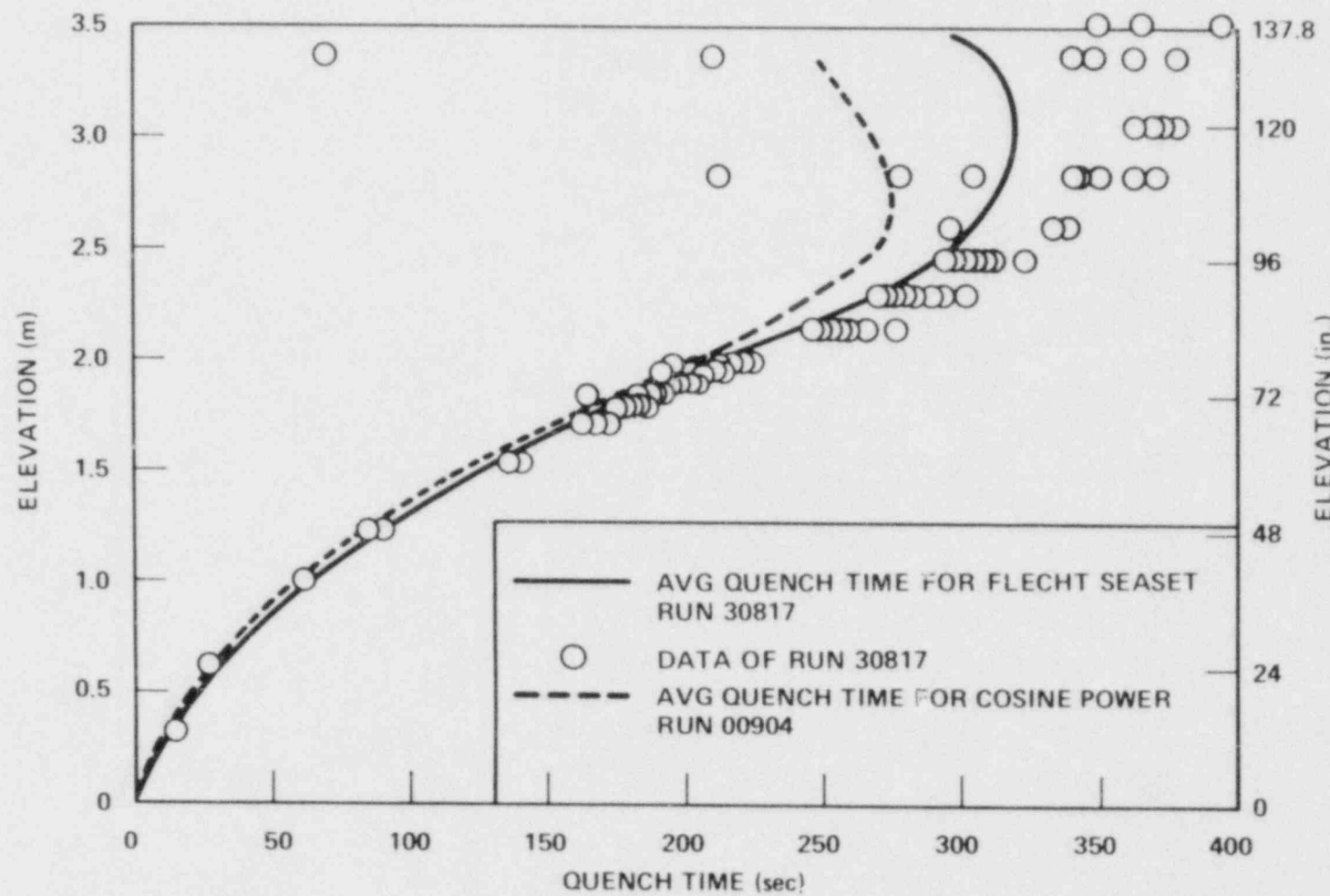


Figure 3-46. Overlap Test Quench Curve Comparison, FLECHT SEASET Run 30817 and Cosine Run 00904

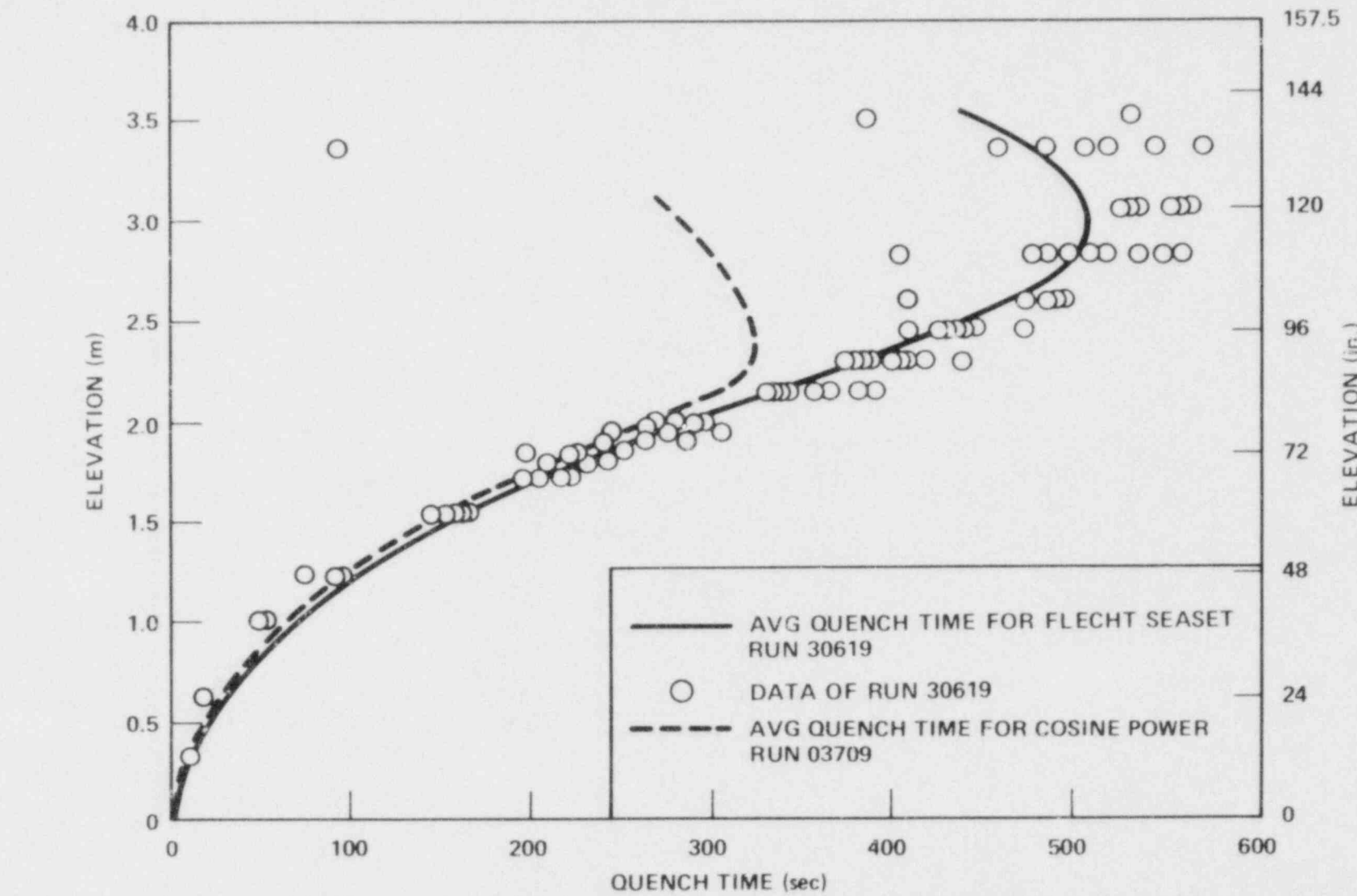


Figure 3-47. Overlap Test Quench Curve Comparison, FLECHT SEASET Run 30619 and Cosine Run 03709

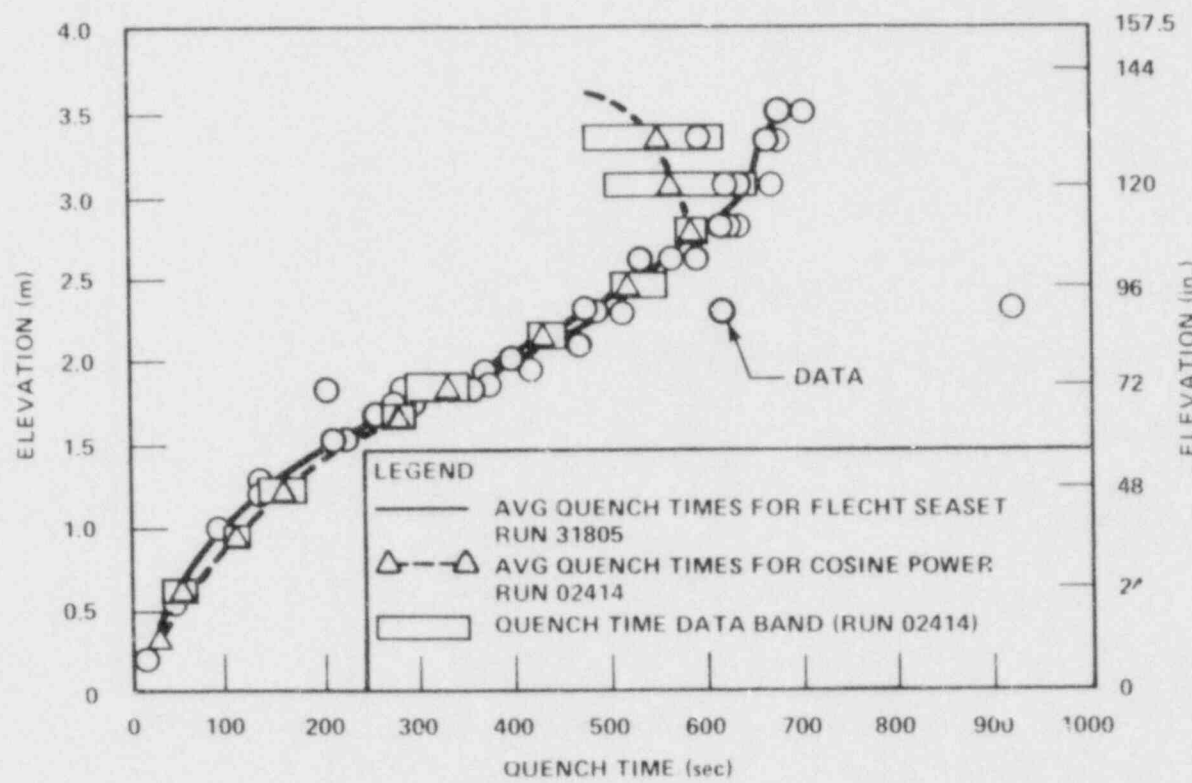


Figure 3-48. Overlap Test Quench Curve Comparison, FLECHT SEASET Run 31805 and Cosine Run 02414

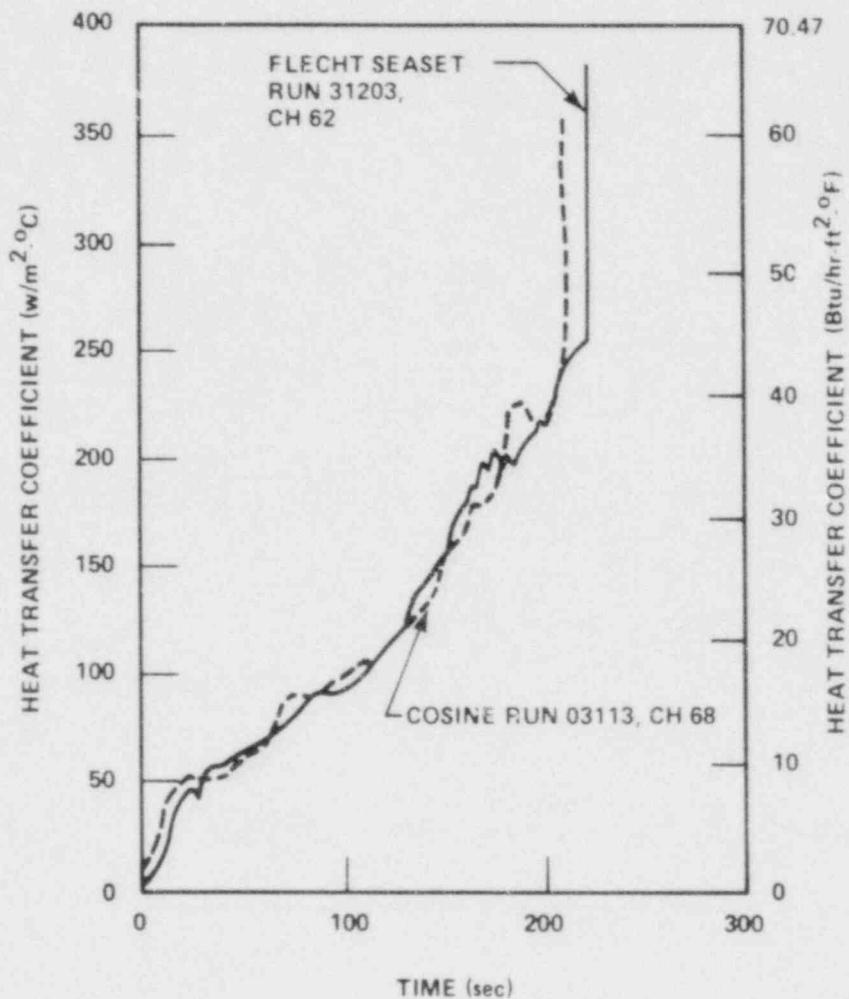


Figure 3-49. Overlap Test Heat Transfer Coefficient Comparison,
FLECHT SEASET Run 31203 and Cosine Run 03113

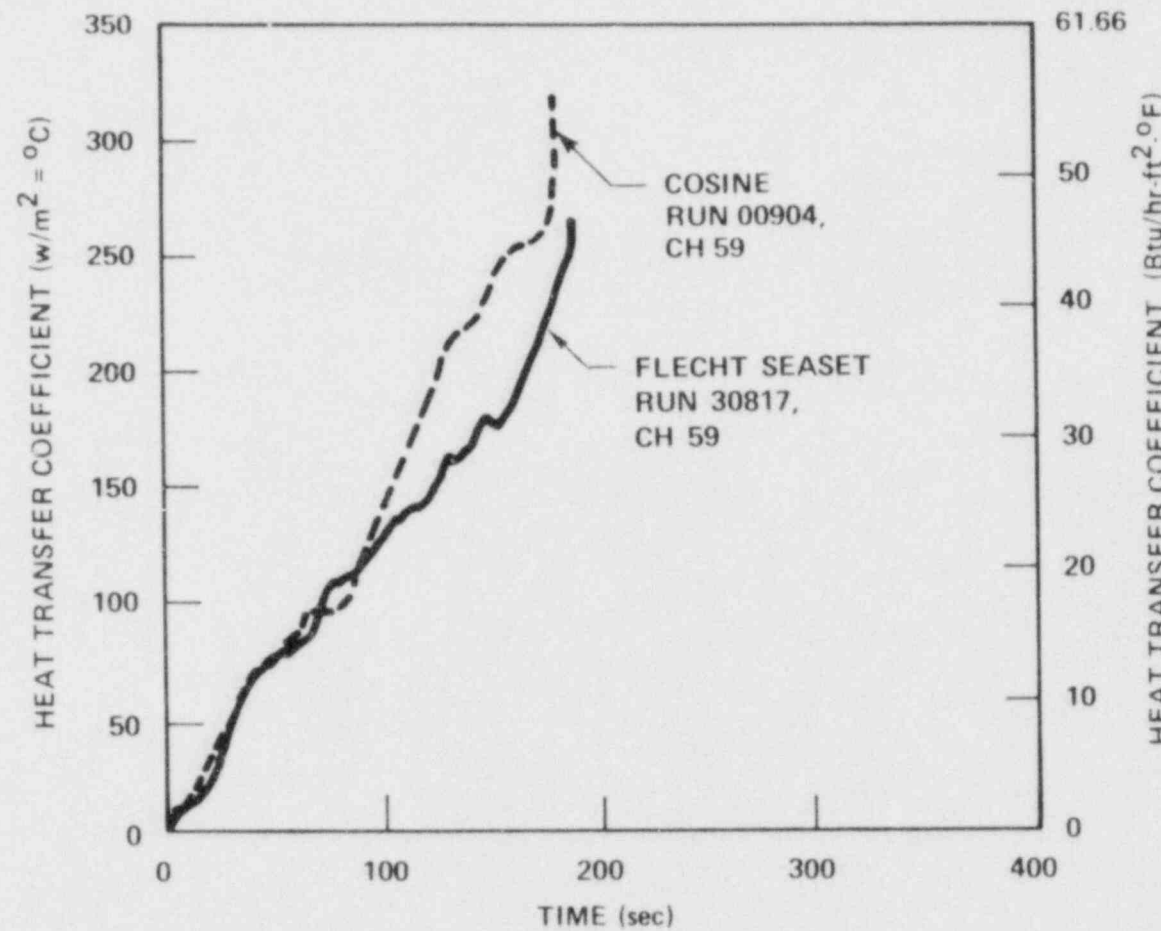


Figure 3-50. Overlap Test Heat Transfer Coefficient Comparison,
FLECHT SEASET Run 30817 and Cosine Run 00904

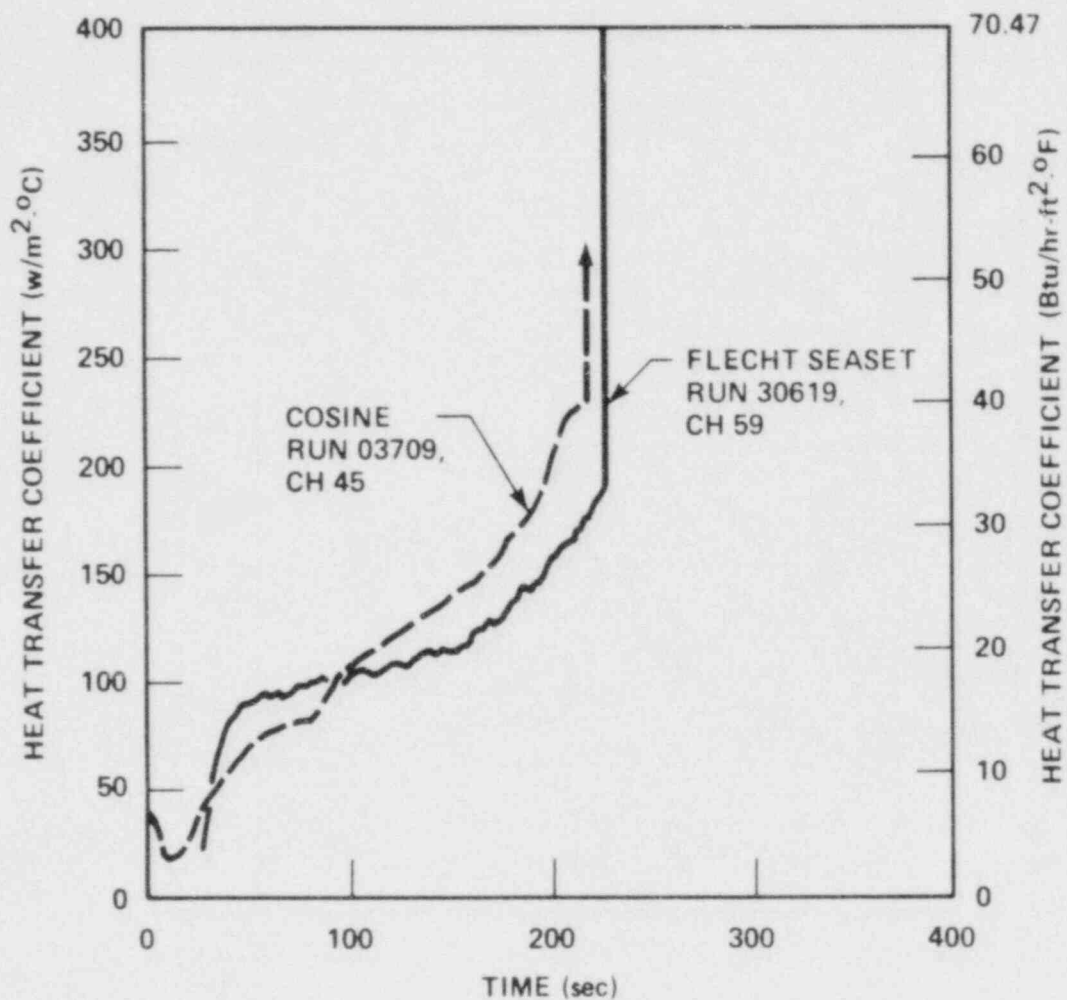


Figure 3-51. Overlap Test Heat Transfer Coefficient Comparison,
FLECHT SEASET Run 30619 and Cosine Run 03709

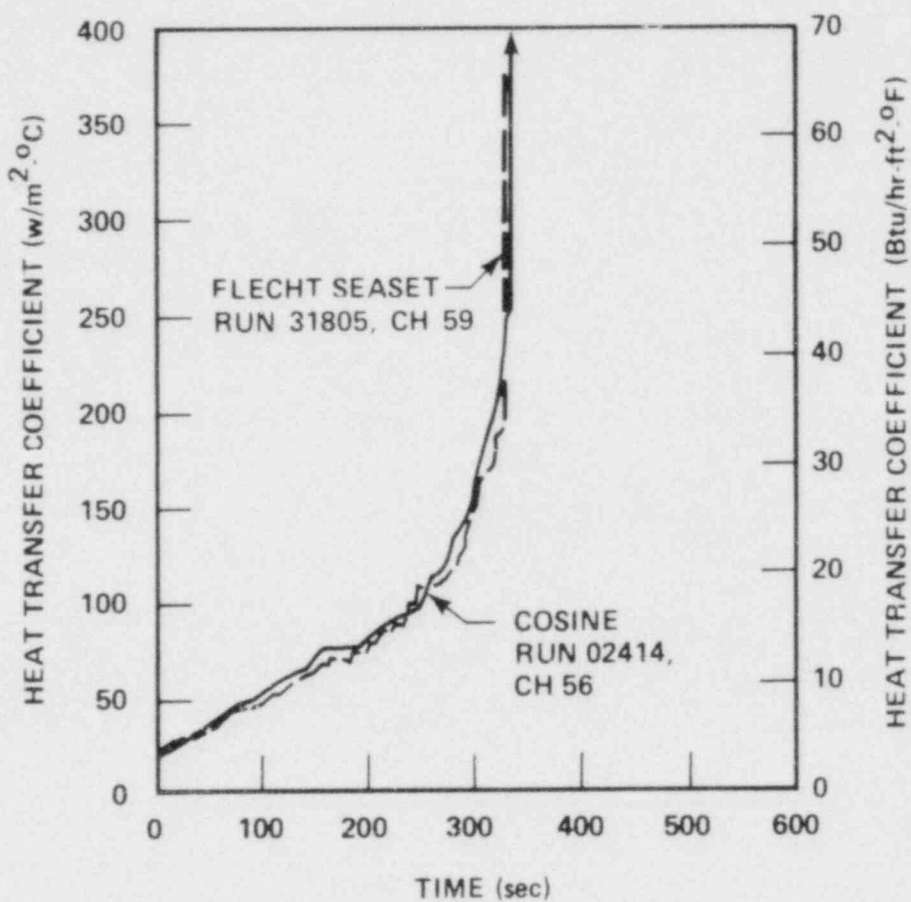


Figure 3-52. Overlap Test Heat Transfer Coefficient Comparison,
FLECHT SEASET Run 31085 and Cosine Run 02414

The heat transfer coefficient curves compare reasonably well for runs 31203 and 03113. This is also true for runs 31805 and 02414. Runs 30817 and 00904 show good agreement up to about 100 seconds and then start to deviate. A possible reason for the deviation at the later period could be the fall-back effect. Runs 30619 and 03709 show poor agreement, but the general trends of the heat transfer coefficient curves are the same.

It is concluded from the above observations that the effect of the bundle geometry difference on heat transfer characteristics during a reflooding period is minimal.

SECTION 4

BUNDLE FLOW CONDITIONS

4-1. INTRODUCTION

Methods were developed to calculate mass and energy balance above the quench front for the previous FLECHT tests. The procedure discussed in WCAP-8838 and WCAP-9183 allows calculation of the mass velocity and nonequilibrium quality at several bundle elevations where steam temperatures are available. Equilibrium quality is also calculated for reference conditions, assuming saturated vapor temperature at the elevations. These calculations, along with a radiation heat transfer model, allow the separation of the total heat flux into its basic components: radiation to surface, radiation to vapor, radiation to drops entrained in the flow, and forced convection of vapor. Examination of the wall heat flux split for different test conditions, times, and elevations makes it possible to investigate various heat transfer models or correlations in relation to the physical picture calculated from the data. These heat transfer mechanisms are discussed in section 6.

An effort has been made in the present analyses to extend and improve the mass and energy balance methods applied to the region above the quench front in the previous FLECHT tests.

The method of analysis has some limitations which should be recognized. Completely one-dimensional flow was assumed and all quantities calculated represent bundle averages. Many calculated values rest rather heavily on the steam probe measurements; one or two measurements at each elevation are assumed to give the average vapor temperature for the whole cross section. This assumption is fairly valid, since the steam temperature measurements do not show much scatter.

4-2. MASS AND ENERGY BALANCE IN BUNDLE

A procedure using a mass and energy balance above the quench front to calculate bundle mass flows and qualities was detailed in section 4 and appendix A of

WCAP-8838. This procedure had been programmed into the computer code FLEMB, and this code was used for data analyses of several key skewed and cosine runs.

This code has been updated and improved in many areas for the analysis of the unblocked bundle test data, as discussed in the following paragraphs. Also, the analysis has been extended to the region below the quench front.

4-3. General Mass and Energy Balance

General mass and energy balance equations are developed herein to provide a uniform approach in the calculations for both below and above the quench front. The one-dimensional continuity equation of fluid in the test section can be written as

$$\frac{\partial \rho}{\partial t} + \frac{\partial(\rho u)}{\partial z} = 0 \quad (4-1)$$

where

ρ = fluid density

u = fluid velocity

t = time

z = coordinate of axial direction

Equation (4-1) can be integrated between two axial levels to get a mass balance equation for the control volume bounded by the two levels, as follows:

$$(\rho u)_{Z_2} - (\rho u)_{Z_1} = - \int_{Z_1}^{Z_2} \frac{\partial(\rho)}{\partial t} dz \quad (4-2)$$

In the same way, the energy equation can be written as

$$\frac{\partial(\rho h)}{\partial t} + \frac{\partial}{\partial Z} (\rho hu) = Q''' \quad (4-3)$$

where

h = fluid enthalpy

Q''' = energy addition rate per unit fluid volume

For a control volume bounded by two axial levels in the test bundle, equation (4-3) can be integrated to give

$$(\rho hu)_{Z_2} - (\rho hu)_{Z_1} = \int_{Z_1}^{Z_2} Q''' dZ - \int_{Z_1}^{Z_2} \frac{\partial(\rho h)}{\partial t} dZ \quad (4-4)$$

The general balance equations, equations (4-2) and (4-4), can be applied to the region of interest in the bundle, as shown in the following paragraphs.

4-4. Mass and Energy Balance Above Quench Front

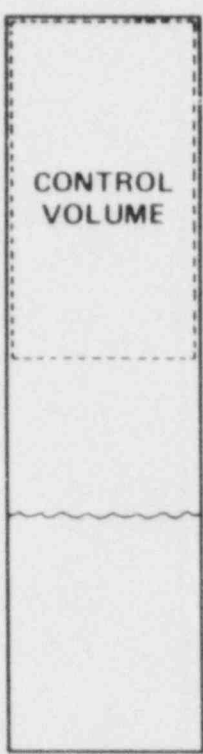
A control volume in the zone above a quench front can be taken as the volume between the bundle exit and the axial elevation where a quality is to be determined (figure 4-1a). Since Z_1 and Z_2 are fixed for this case, equations (4-2) and (4-4) can be rewritten as

$$(\rho u)_{Z_2} - (\rho u)_{Z_1} = - \frac{d}{dt} \int_{Z_1}^{Z_2} \rho dZ \quad (4-5)$$

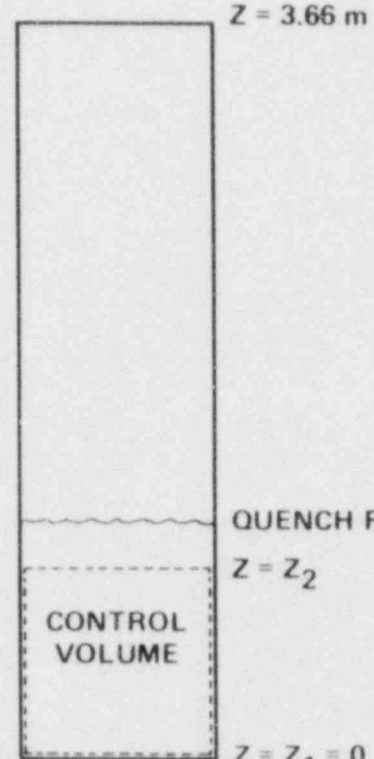
and

$$(\rho hu)_{Z_2} - (\rho hu)_{Z_1} - \int_{Z_1}^{Z_2} Q''' dZ = - \frac{d}{dt} \int_{Z_1}^{Z_2} (\rho h) dZ \quad (4-6)$$

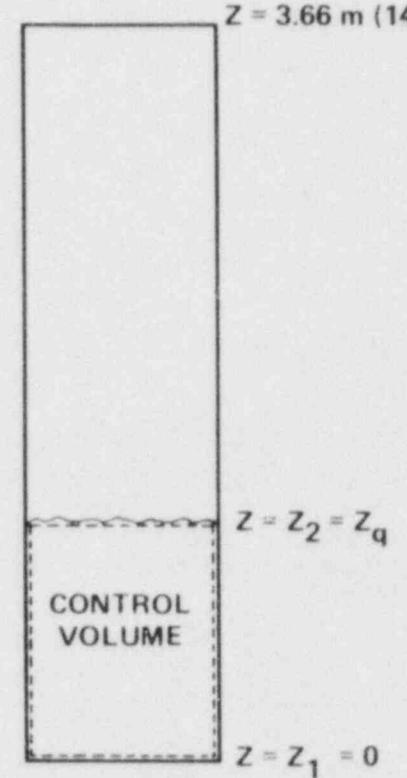
4



(A) ABOVE
QUENCH FRONT



(B) BELOW
QUENCH FRONT



(C) COUPLING OF ABOVE
AND BELOW QUENCH FRONTS

Figure 4-1. Control Volumes

The Leibnitz formula has been utilized in the derivation of the above equations. Further, the terms on the right-hand side of equations (4-5) and (4-6) can be shown to be negligible, as described in appendix A.

Therefore, equations (4-5) and (4-6) become, when $Z_2 = 3.66$ m,

$$(\rho u)_o - (\rho u)_{Z_1} = 0 \quad (4-7)$$

$$(\rho hu)_{Z_2} - (\rho hu)_{Z_1} = \int_{Z_1}^{3.66} Q''' dZ \quad (4-8)$$

The subscript o denotes the bundle exit [$Z = 3.66$ m (144 in.)]. Dividing each term in equation (4-8) by the total mass flow rate, utilizing $AQ''' = Q'$ and equation (4-7) gives

$$h_o - (h)_{Z_1} = \frac{1}{\dot{m}_t} \int_{Z_1}^{3.66} Q' dZ \quad (4-9)$$

where \dot{m}_t is total mass flow rate and Q' is total heat release rate per foot. This equation can be further modified using the relation of $h = X h_v + (1-X) h_l$ and the fact that $h_{l_o} = (h_l)_{Z_1}$ as follows:

$$(X)_{Z=Z_1} = \frac{1}{(h_v - h_{l_o})_{Z_1}} \left[X_o (h_{v_o} - h_{l_o}) - \frac{1}{\dot{m}_t} \int_{Z_1}^{3.66} Q' dZ \right] \quad (4-10)$$

where

h_{l_o} = saturation liquid enthalpy

h_v = vapor enthalpy

X_o = outlet quality

Equation (4-10) allows the calculation of local quality (X) when the data of m_t , Q' , X_o , h_{v_o} , and h_v are available.

4-5. Mass and Energy Balance Below Quench Front

A control volume in the zone below a quench front can be taken as the volume between the bundle bottom and the axial elevation where a quality is to be determined, as indicated in figure 4-1b. The same conservation equations, equations (4-5) and (4-6), can be applied for this case also. As discussed in appendix A, the right-hand-side terms of equations (4-5) and (4-6) are negligible even below a quench front. Therefore, the equations can be simplified as follows:

$$(\rho u)_{Z_2} - (\rho u)_{Z_1} = 0 \quad (4-11)$$

$$(\rho hu)_{Z_2} - (\rho hu)_{Z_1} = \int_{Z_1}^{Z_2} Q''' dz \quad (4-12)$$

Since the total mass flow rate in the bundle can be expressed as

$$\dot{m}_t = \rho u A$$

where A is the total flow area, equations (4-11) and (4-12) can be rewritten as

$$\dot{m}_{in} = (\dot{m}_t)_{Z=0} = (\dot{m}_t)_{Z_2} \quad (4-13)$$

$$\dot{m}_t \left[(h)_{Z_2} - (h)_{Z=0} \right] = \int_0^{Z_2} Q' dz \quad (4-14)$$

By definition, the enthalpies in equation (4-14) are related as

$$(h)_{Z_2} = (x h_v + (1-x) h_{f_0})_{Z_2} \quad (4-15)$$

$$(h)_{Z=0} = (h)_{f_0} = h_{f_0} - C_p \Delta T_{SUB} \quad (4-16)$$

where X is a local quality and ΔT_{SUB} and C_p are the degree of subcooling of inlet water and water heat capacity, respectively.

Equations (4-13), (4-15), and (4-16) can be used to rearrange equation (4-14) as follows:

$$(X)_{Z_2} = \frac{\int_0^{Z_2} Q' dz - \dot{m}_{in} C_p \Delta T_{SUB}}{\dot{m}_{in} h_{fg}} \quad (4-17)$$

where h_{fg} is heat of evaporation.

Further, it is known that the heat release rate (Q') below the quench front is due to the generated power only and is

$$Q'(t,z) = Q'_{max} P_{dec}(t) F_{ax}(z) \quad (4-18)$$

where

Q'_{max} = peak power at time $t=0$

$P_{dec}(t)$ = power decay factor

$F_{ax}(z)$ = axial power distribution factor defined as $Q'(t,Z)/Q'(t,1.83\text{ m})$

Therefore, equations (4-17) and (4-18) make it possible to calculate local qualities below the quench front.

4-6. Coupling of Mass and Energy Balance at Quench Front

Mass and energy balances in the regions below and above a quench front have been developed in the previous two sections. The relationships can be coupled to each other by considering mass and energy balance in a control volume bounded by the bottom of the bundle and the quench front, as indicated in figure 4-1c. An overall mass balance over the control volume is written as

$$\dot{m}_e = \dot{m}_{in} - A \frac{d}{dt} \int_0^{Z_q} \rho dz \quad (4-19)$$

where

\dot{m}_e = mass flow rate just above quench front

Z_q = quench front

It should be noted that the general mass balance equation [equation (4-2)] is not used here because this equation does not give the mass flow rate above the quench front because of the moving upper boundary.

Since the upper boundary of the present control volume is a function of time and the lower level is fixed at $Z=0$, equation (4-19) can be reformulated, with the help of the Leibnitz formula, into

$$\dot{m}_e = \dot{m}_{in} - A \rho_q \frac{dZ_q}{dt} - A \int_0^{Z_q} \frac{\partial \rho}{\partial t} dz \quad (4-20)$$

where ρ_q indicates the two-phase density just below the quench front. Further, it is assumed that the rate of density change in the bundle is small except around the quench front (appendix A). Then, since $\frac{dZ_q}{dt}$ is a quench velocity (V_q), equation (4-20) is reduced to

$$\dot{m}_e = \dot{m}_{in} - A \rho_q (A_q V_q) \quad (4-21)$$

As indicated in paragraph 4-4, the mass accumulation above the quench front is negligible. Therefore, equation (4-21) provides a method for estimating a mass effluence from the bundle. A detailed discussion of mass effluence is presented in section 5.

Further, the quality just above the quench front can be estimated by considering the mass flow rate above the quench front (\dot{m}_e) and the heat release at the quench front. The steam generated below a quench front is calculated from equation (4-17) as follows:

$$(\dot{m}_v)_{Z=0 \sim Z_q} = \frac{\int_0^{Z_q} Q' dz - \dot{m}_{in} C_p \Delta T_{SUB}}{h_{fg}} \quad (4-22)$$

Additional energy is released at the quench front because of the release of rod latent heat. This can be estimated as

$$\dot{Q}_q = (\rho C_p A)_{rod} (T_q - T_{sat}) V_q \quad (4-23)$$

where

T_q = wall temperature at quench time

T_{sat} = saturation temperature

Housing heat release is neglected, because of the low mass housing design, and heat loss through the housing is also neglected.

Then the total steam flow rate at the quench front is

$$(\dot{m}_v)_{Z_q} = \frac{\int_0^{Z_q} Q' dz - \dot{m}_{in} C_p \Delta T_{SUB} + \dot{Q}_q}{h_{fg}} \quad (4-24)$$

Thus the quality just above the quench front is

$$x_q = \frac{(\dot{m}_v)_{Z_q}}{\dot{m}_e} \quad (4-25)$$

The quality calculated by equation (4-25) can be compared with the quality calculated by the method used in WCAP-9183, where the vapor temperature at the quench front was assumed to be the average of the wall temperature and saturation temperature.

It must be noted that the quality just below the quench front is

$$x_{Z=Z_q} = \frac{(\dot{m}_v)_{Z=0-Z_q}}{\dot{m}_{in}} \quad (4-26)$$

4-7. AXIAL DEPENDENCE OF BUNDLE MASS FLOWS AND QUALITIES

The new developments discussed above have been incorporated into the existing mass and energy balance (FLEMB) code. The resultant FLEMB code has been used to analyze data from selected runs of the FLECHT SEASET unblocked bundle tests, as listed in table 4-1.

The results of the quality and mass flow calculation for run 31504 are presented and discussed for illustration. The results of other runs are summarized in appendix B.

Figures 4-2 and 4-3 present the calculated axial dependence of local and equilibrium quality for run 31504. The quench times at 1.83 m (72 in.) and 2.29 m (90 in.) are also indicated in figure 4-2. The local quality is calculated based on the vapor temperature at the location, and the equilibrium quality is based on the saturation vapor temperature. Therefore, the difference between the local and equilibrium quality is a measure of the steam superheating.

TABLE 4-1

RUNS ANALYZED BY FLEMB

Run	Pressure [MPa (psi)]	Rod Initial Clad Temperature [°C (°F)]	Rod Peak Power [kw/m (kw/ft)]	Flooding Rate [mm/sec (in./sec)]	Subcooling [°C (°F)]
31203	0.28 (40)	872 (1601)	2.3 (0.7)	38.4 (1.51)	78 (141)
31302	0.28 (40)	869 (1597)	2.3 (0.7)	76.5 (3.01)	78 (141)
31504	0.28 (40)	863 (1585)	2.3 (0.7)	24.6 (0.97)	80 (144)
31701	0.28 (40)	872 (1601)	2.3 (0.7)	155 (6.1)	78 (140)
31805	0.28 (40)	871 (1600)	2.3 (0.7)	20.6 (0.81)	79 (143)
31922	0.14 (20)	883 (1621)	1.3 (0.4)	27.2 (1.07)	96 (172)
32013	0.41 (60)	887 (1629)	2.3 (0.7)	26.4 (1.04)	62 (117)
34006	0.27 (39)	882 (1620)	1.3 (0.4)	15.0 (0.59)	79 (142)

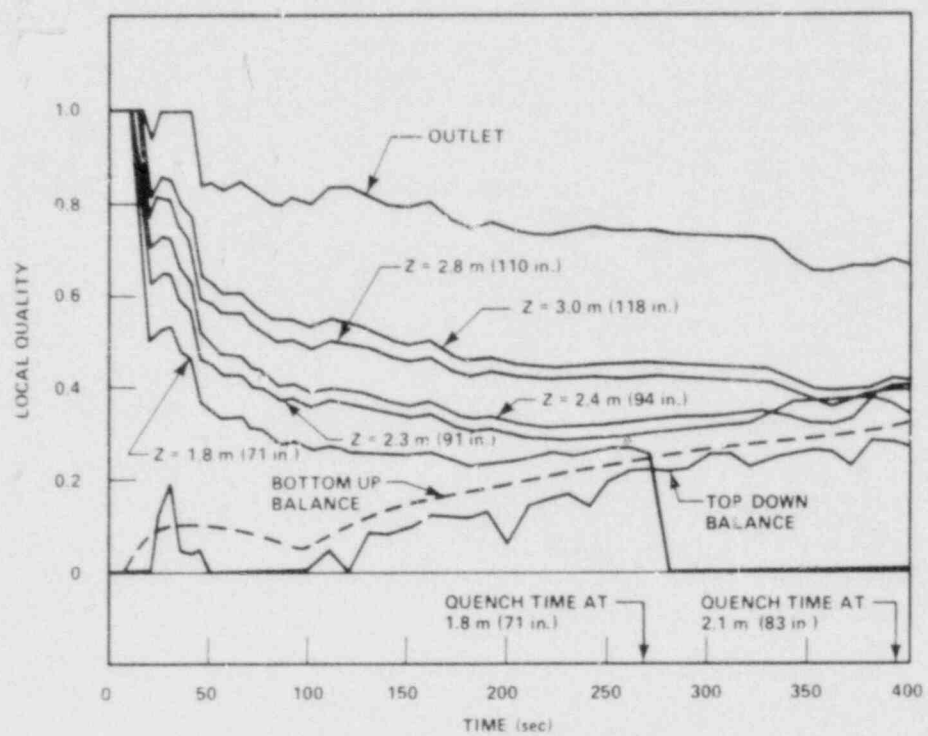


Figure 4-2. Local Quality at Various Elevations, Run 31504

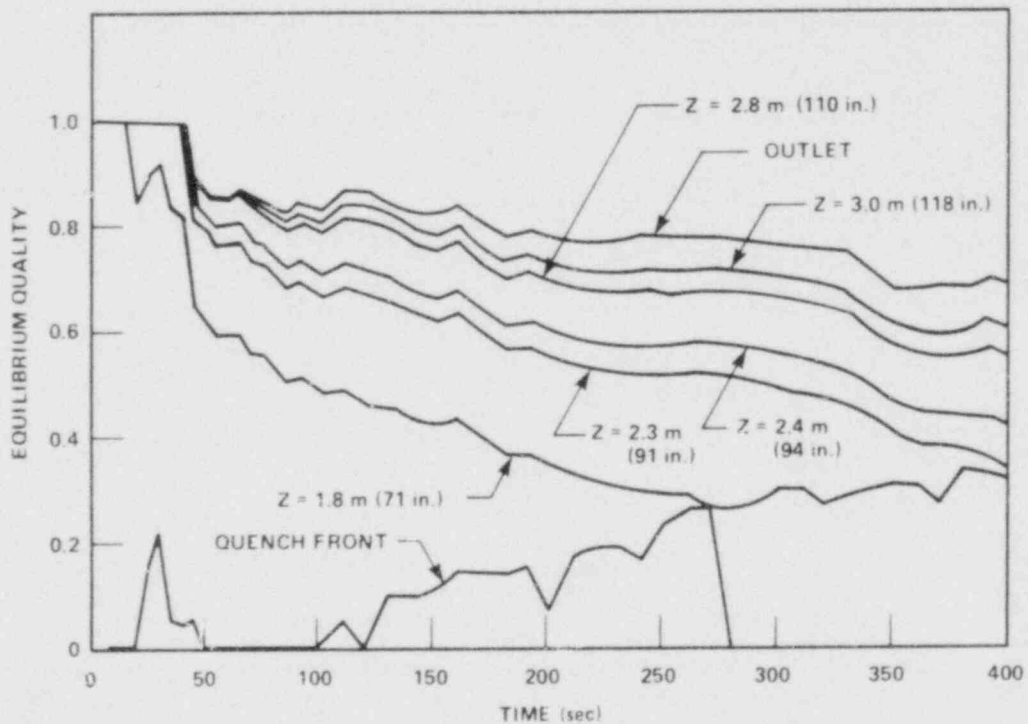


Figure 4-3. Equilibrium Quality at Various Elevations, Run 31504

As described in appendix C, the steam probe measurements at five elevations, 1.83, 2.29, 2.44, 2.82, and 3.05 m (72, 90, 96, 111, and 120 in.), in the bundle were used for all cases except run 34006. This run was executed at a low power and low flooding rate, so that steam probe measurements up to 3.51 m (138 in.) were available.

The quality and vapor temperature at the housing exit were measured in the tests. These data can be utilized to calculate the local qualities in the bundle using equation (4-10), as described in appendix D. It must be noted that the outlet qualities provided here are not the local qualities at the bundle exit, but those at the housing exit. The steam probe measurements at the housing exit indicate that most steam desuperheating occurred in the upper plenum region. The quality at the bundle exit could not be estimated because of the lack of vapor temperature information there.

The qualities at the quench fronts were calculated by two methods: equation (4-25) and assumed vapor temperatures at the quench fronts. The second method assumes the vapor temperature at a quench front as the average of the saturation and wall temperature. This method was used in the data analyses for the skewed power profile FLECHT tests. The solid line for the quench front quality in figure 4-2 is based on the assumed vapor temperature. The dotted line in the figure is based on the method using equation (4-25), in which the vapor temperature is assumed to be at the saturation temperature.

Figure 4-2 shows that the quench front qualities predicted by equation (4-25) are in good agreement with the qualities based on the steam temperatures at 1.83 and 2.29 m (72 and 90 in.) when the quench front is at these elevations, that is, assuming that the vapor is at the saturation temperature (equilibrium). This fact is also observed in other runs under various test conditions, as shown in appendix B. Therefore it is believed that the quench front quality can be predicted by equation (4-25) with confidence. Thus, it is recommended that thermodynamic equilibrium be assumed when estimating quench front qualities.

As shown in figure 4-2, the quality starts at a low value at the quench front and progressively increases with increasing elevation; this is physically reasonable. The quality at upper elevations decreases slowly with time. Equilibrium qualities are higher than the local qualities early in time, reflecting the highly superheated vapor in the

bundle. Figure 4-4 shows the vapor temperatures measured at the various elevations. Superheats up to 816°C (1500°F) could be observed at the midsection of the bundle. Figure 4-5 presents the quality history at the 1.83 m (72 in.) elevation. The method developed in paragraph 4-5 was used to estimate the quality when the quench front was located above 1.83 m (72 in.).

Figure 4-6 presents the mass flow fraction above the quench front in the bundle for run 31504. Because of the low storage rate above the quench front in the bundle, the mass flow rates at the steam probe elevations are the same when they are above the quench front.

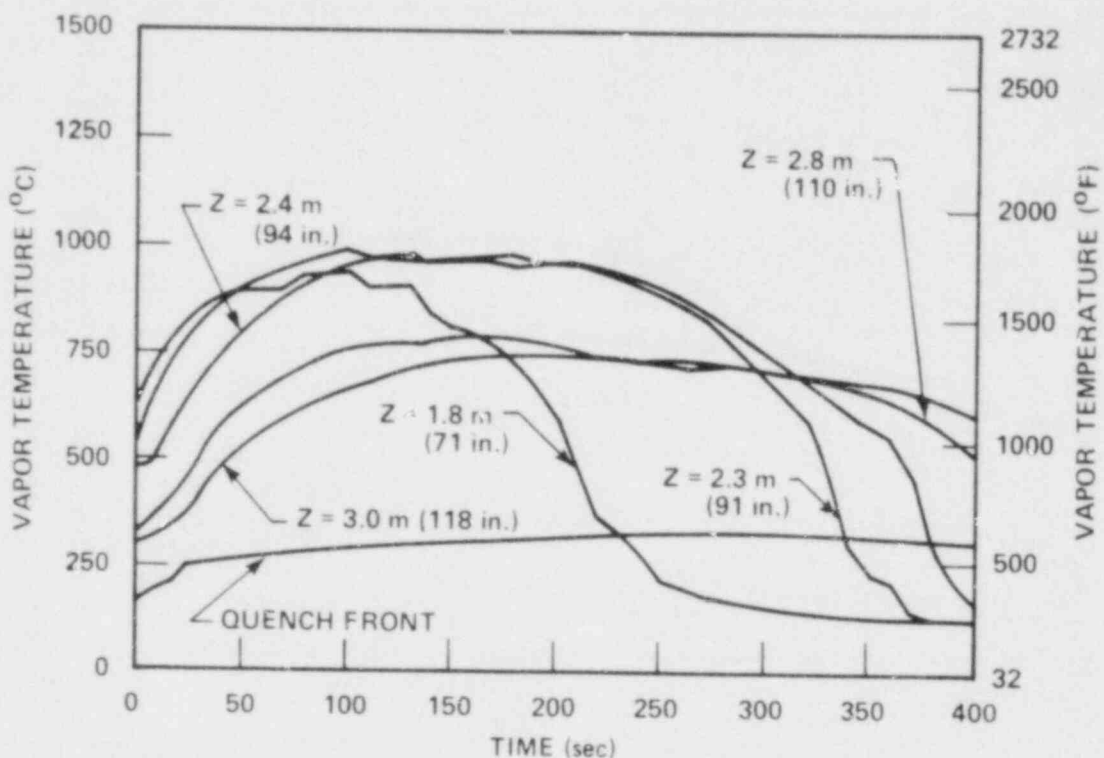


Figure 4-4. Vapor Temperature at Various Elevations, Run 31504

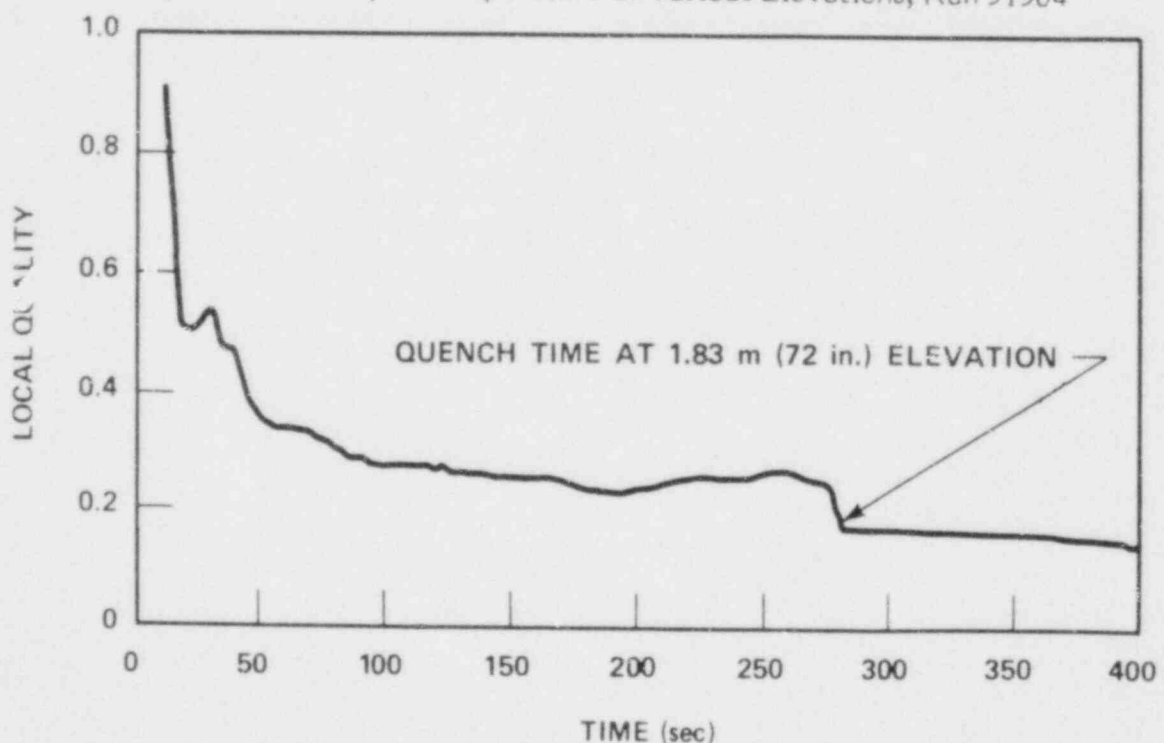


Figure 4-5. Local Quality at 1.83 m (72 in.), Run 31504

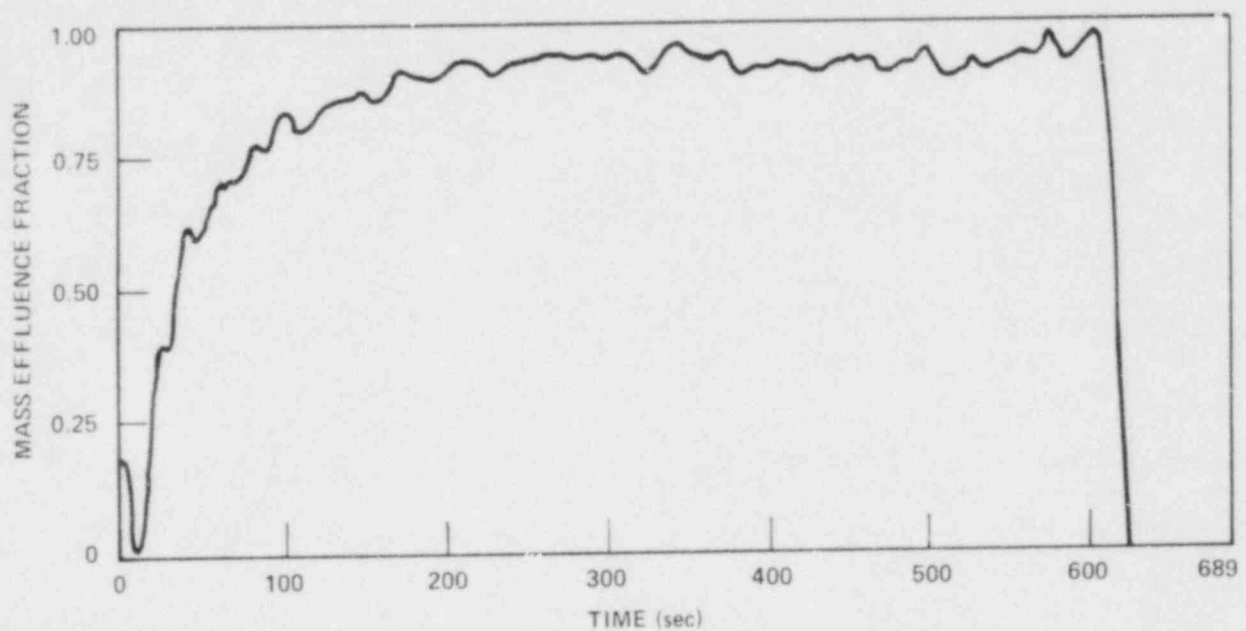


Figure 4-6. Mass Effluence Rate, Run 31504

SECTION 5

EFFLUENCE RATE AND TRANSITION ZONE

5-1. INTRODUCTION

Equation (4-21) was derived to calculate the mass flow rate above a quench front. It has also been shown that the mass accumulation rate above a quench front is so low that the mass flow rate obtained by the equation can be considered as a mass effluence rate. A discussion of the methods of calculating mass effluence rate is provided in this section.

Also provided here are some preliminary discussions on the transition zone just above a quench front, where the flow regime is not yet a dispersed flow.

5-2. AVAILABLE MODELS FOR MASS EFFLUENCE RATE

Yeh and Hochreiter developed a model for mass effluence during a reflooding process.^(1,2) Their approach was based on an empirical void fraction correlation derived from the data of the low flooding rate tests. This model is applicable to the low flooding rate tests only. Sun and Duffey⁽³⁾ tried to remove the shortcomings of the Yeh and Hochreiter model and found the importance of quench velocity in predicting effluence rate. A new model to extend their approach is provided here.

5-3. YEH/HOCHREITER MODEL FOR PREDICTING BUNDLE MASS EFFLUENCE

The model for calculating the mass flow above the froth level (or simply mass effluence) and void fraction below the froth level has been formulated. This model has been

-
1. Yeh, H. C., and Hochreiter, L. E., "Mass Effluence During FLECHT Forced Reflood Experiments," Trans. Am. Nucl. Soc. 24, 301-302 (1976).
 2. Yeh, H. C., and Hochreiter, L. E., "Mass Effluence During FLECHT Forced Reflood Experiments," Nucl. Eng. Des. 60, 413 (1980).
 3. Sun, K. H., and Duffey, R. B., "A Generalized Model for Predicting Mass Effluences During Reflooding," Nucl. Tech. 43, 22-27 (1979).

compared with the 15x15 FLECHT cosine and skewed power data,⁽¹⁾ with good agreement. Here this model is compared with the FLECHT SEASET unblocked test data to justify the applicability of the model to the 17x17 rod array.

The model utilizes the Lagrangian method of describing fluid motion to compute the fluid velocity and steam generation, and uses the Yeh void fraction correlation to compute the void fraction below the quench front. The rate of mass effluence, m_f , is then computed by

$$\dot{m}_f = \dot{m}_{in} \left[1 - \left(\frac{1}{V_{in}} \right) \left(\frac{dZ_{Lf}(t)}{dt} \right) \right] = \dot{m}_{in} r_f$$

where \dot{m}_{in} and V_{in} are the inlet mass flow rate and velocity, respectively, and $Z_{Lf}(t)$ is the collapsed liquid height (net liquid height if all bubbles were collapsed) below the froth level. The froth level is defined as the interface between the region of continuous vapor phase (dispersed flow) and the region of continuous liquid phase (flow boiling), and $r_f = m_f/m_{in}$ is the mass effluent ratio.

In FLECHT cosine power low flooding rate tests, the froth level detected from the pressure drop data was found to be in the scattering band of the quench front data. Therefore, the froth level and quench front elevation are assumed to be the same for the low flooding rate test data. The collapsed liquid level $Z_{Lf}(t)$ is obtained by computing the void fraction and integrating the liquid up to the froth level. The void fraction is obtained by computing superficial steam velocity (steam volumetric flux) and using Yeh's void fraction correlation. The superficial steam velocity is obtained by computing heat release from the heater rods. The calculated mass effluent ratio, r_f , and the void fraction for the FLECHT cosine power and skewed power low flooding rate tests are in good agreement with the test data.

The model can also be applied to the recent FLECHT SEASET tests. As in the previous FLECHT tests, the froth level was found to be in the scattering band of the quench front data for the low flooding rate. Therefore, the froth level is assumed to be the same as the quench front elevation for a low flooding rate. Figure 5-1 plots the froth

I. Lilly, G. P., et al., "PWR FLECHT Cosine Low Flooding Rate Test Series Evaluation Report," WCAP-8838, March 1977.

level (or the quench front elevation) and the saturation line. Also plotted in figure 5-1 are the collapsed liquid level, $Z_{Lf}(t)$, from this model and that measured from the pressure drop data. The calculated $Z_{Lf}(t)$ is in excellent agreement with data. Figure 5-2 shows that the comparison of the calculated average void fraction over 0.30 m (12 in.) intervals and that reduced from pressure drop data is not as good as the comparison of the collapsed liquid level $Z_{Lf}(t)$ (figure 5-1). At this point it should be noted that the collapsed liquid level data are more accurate than the average void fraction data for the following reasons.

One reason is that the average void fraction data were reduced from the pressure drop measured only over 0.30 m (12 in.) intervals, which can be small in the high void fraction region. Therefore, experimental uncertainty will be larger at the higher void fraction. On the other hand, the collapsed liquid level is reduced from the pressure drop measured over the distance between the bottom of the bundle and the froth front. Furthermore, it always contains the high-density region at the lower part of the bundle. Therefore, the pressure drop is large and experimental error is expected to be small.

Another reason is that the pressure taps of the 0.30 m (12 in.) interval differential pressure cells can be in the bubbly flow region; the pressure measurement may be disturbed by the bubbles. The pressure between the bottom of the bundle and the froth level was measured with one of the pressure taps at the bottom of the bundle, in which the fluid is a single-phase liquid, and another pressure tap at the elevation just above the froth level, in which the fluid is mostly steam with some droplets. Therefore, the pressure measurement could not be disturbed by the bubbles. Thus, the collapsed liquid level data are more accurate than the average void fraction data. Since the calculated collapsed liquid level is in excellent agreement with the 17x17 FLECHT data, it is concluded that the model and void fraction correlation are applicable to the 17x17 rod array.

To compare the calculated r_f , it should be noted that, since the void fraction is large above the froth level and the mass storage (and hence the rate of mass storage) is small above the froth level, the mass flow ratio, r_f , above the froth level should be about the same as the ratio of mass flow out of the bundle, r_o . This is confirmed for the 15x15 cosine power bundle and skewed power bundle by comparing the calculated

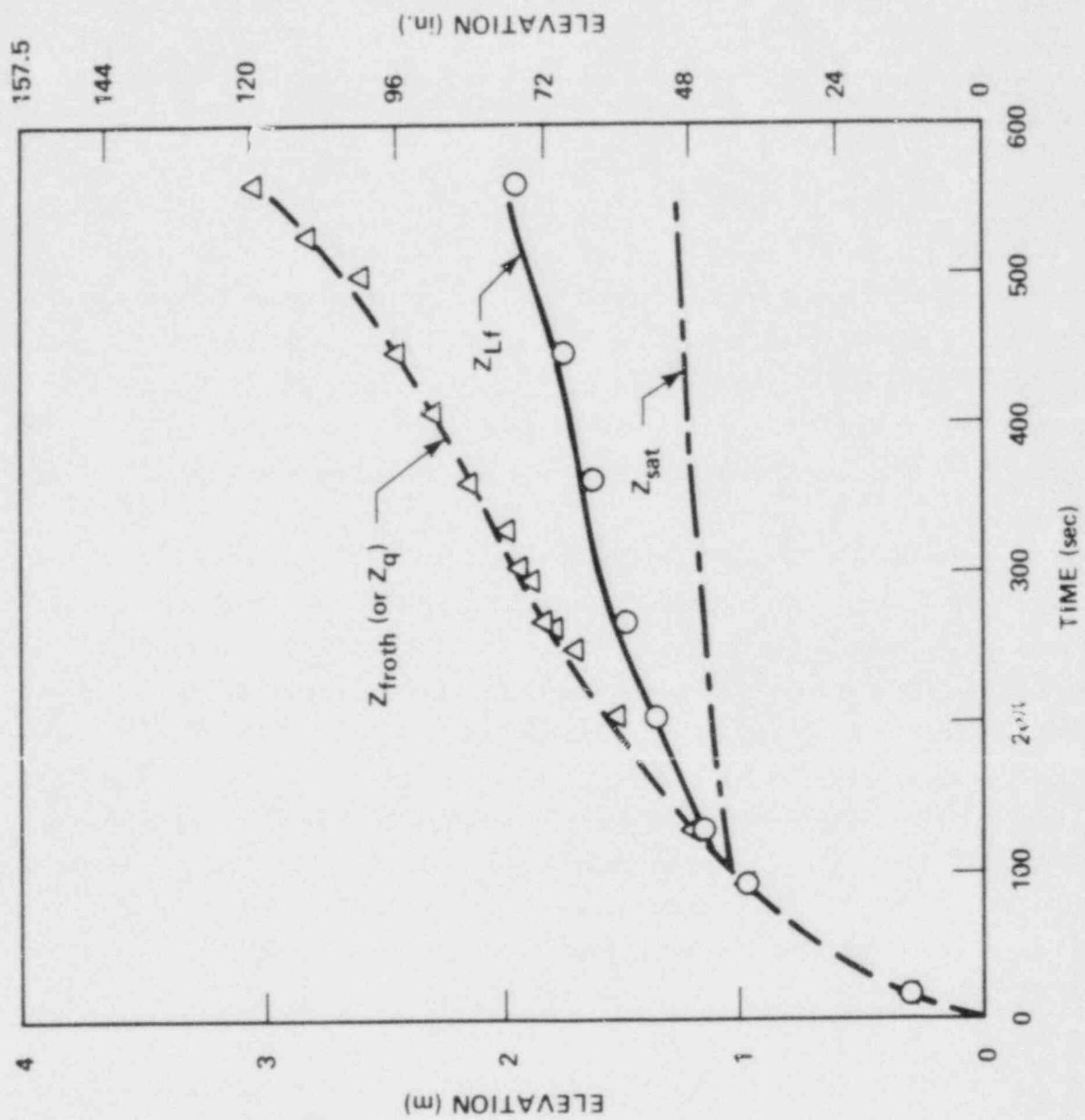


Figure 5-1. FLECHT SEASET Froth Level, Collapsed Liquid Level, and Saturation Level Data

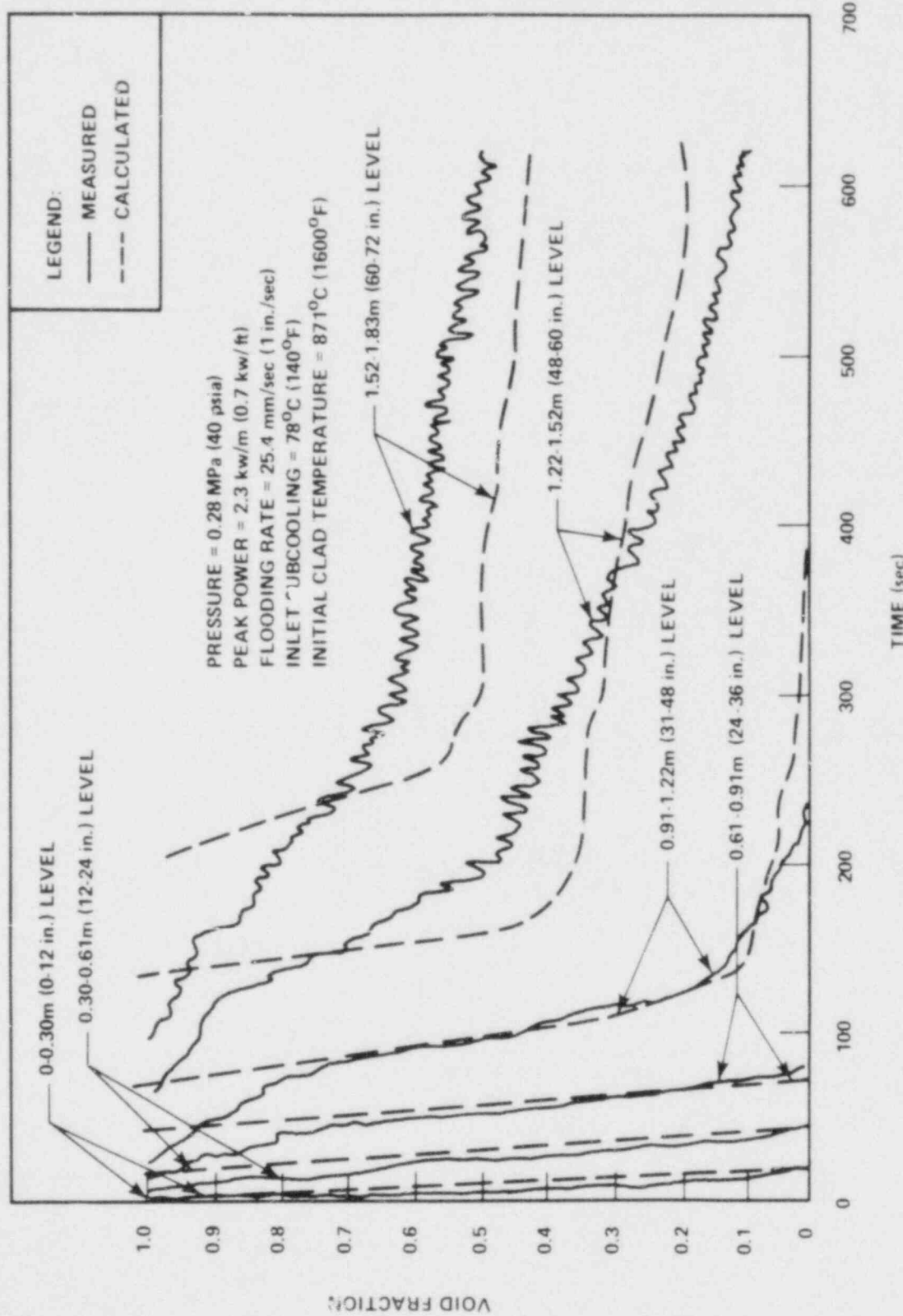


Figure 5-2.
 Comparison of Calculated and Measured Void Fraction, Run 31504
 (sheet 1 of 2)

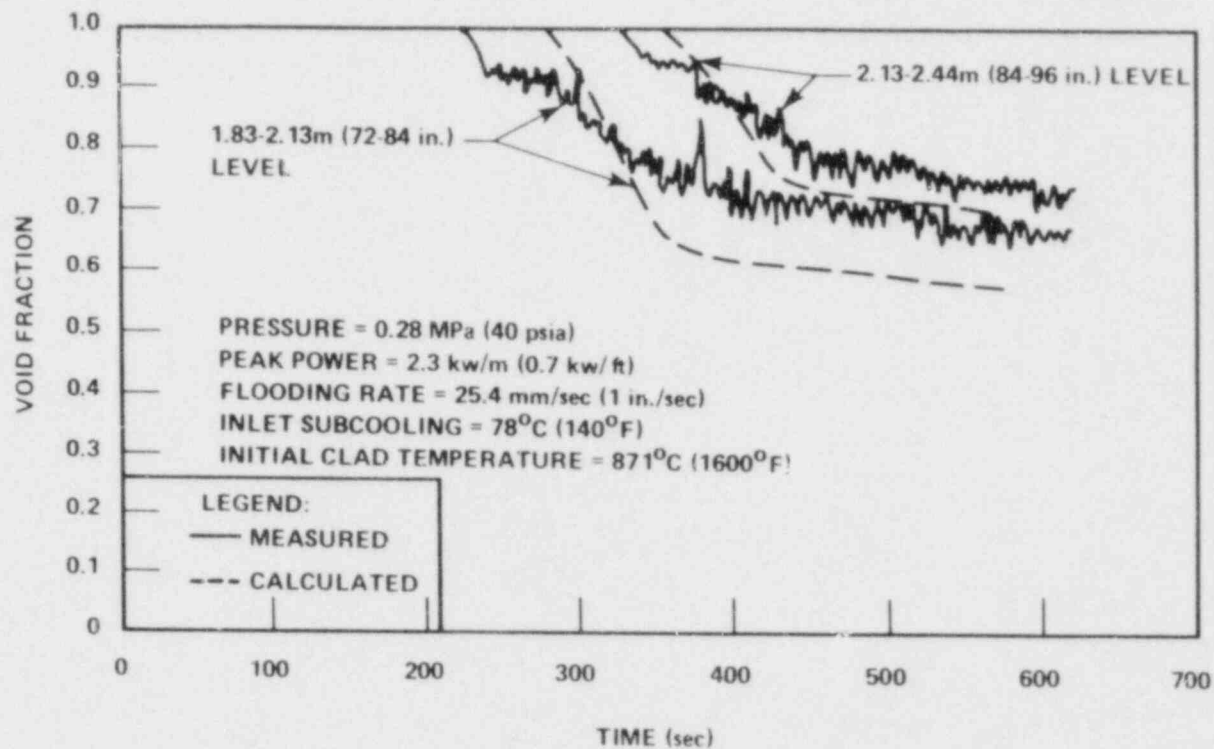


Figure 5-2. Comparison of Calculated and Measured Void Fraction, Run 31504
(sheet 2 of 2)

r_f with the measured r_o . Figure 5-3 shows that the calculated r_f and measured r_o for a FLECHT SEASET test are also in excellent agreement.

The pressure drop data indicate that in runs in which the flooding rate is equal to or greater than 76 mm/sec (3 in./sec), the froth level is higher than the quench front elevation, which means that there is film boiling above the quench front for these runs. Since an appropriate method for computing the void fraction is not available at present, the calculation for these runs was not made.

Appendix C contains additional comparisons of the collapsed liquid level, the void fraction, and the mass flow ratio, r_f , above the froth level for the low flooding rate.

From the agreement of the above comparisons and the comparisons of WCAP-8838 and WCAP-9108 for the cosine and the skewed power shapes, it can be inferred that the model is applicable to any power shape, and to both 15x15 and 17x17 assemblies.

5-4. NEW MASS EFFLUENCE RATE MODEL

As pointed out in the introduction, equation (4-21) can be used to calculate effluence rate. In addition to this, a new simple model has been developed.

A mass balance over a bundle is written as

$$\dot{m}_{in} - \dot{m}_{out} = A \frac{d}{dt} \int_0^L [\alpha \rho_v + (1-\alpha) \rho_l] dz \quad (5-1)$$

where

\dot{m}_{in} = mass flow rate at bottom of bundle

\dot{m}_{out} = mass flow rate at top of bundle

A = total bundle flow area

L = axial length of bundle

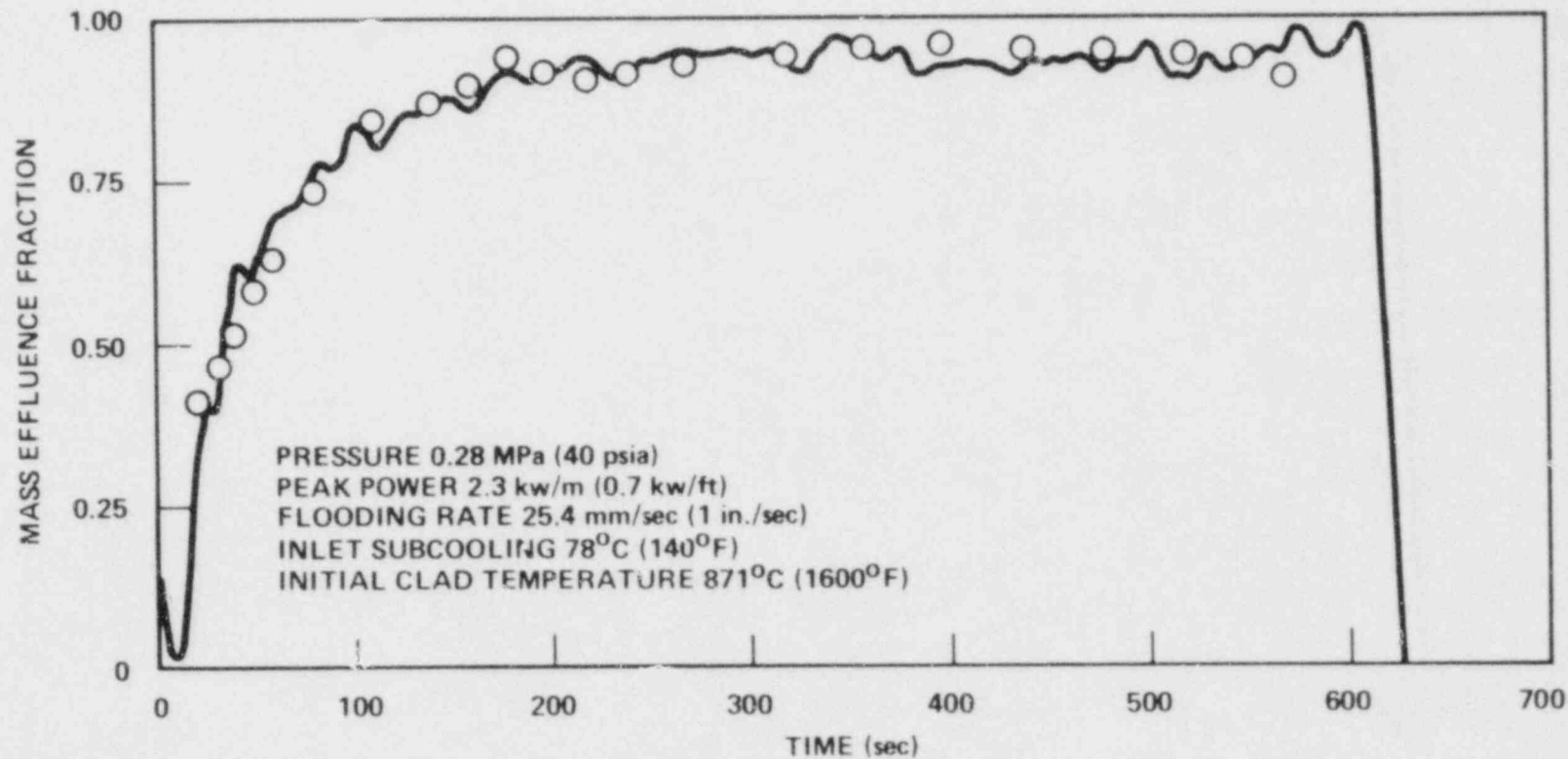


Figure 5-3. Comparison of Calculated and Measured Mass Storage Rate, Run 31504

α = void fraction

ρ = density

v = subscript for vapor

l = subscript for liquid water

It is clear that effluence rate (\dot{m}_{out}) can be calculated from equation (5-1) if the void fraction distribution in the bundle is provided as a function of elevation and time. But the void fraction information, $\alpha(z,t)$, is not usually available. However, it is still possible to develop a relation to calculate the effluence rate approximately, using physically reasonable assumptions.

One possible approach is to assume that the void fraction distribution in the bundle, $\alpha(z,t)$, can be expressed as a function of $(z - V_q t)$ for any short time period when V_q is a quench front velocity. This assumption means that the profile of the axial void distribution at $t = t_i + \Delta t$ is the same as that at $t = t_i$ and simply shifted by $(V_q \Delta t)$, as shown in figure 5-4 when Δt is small. It is further assumed that

$$\alpha(L,t + \Delta t) = \alpha(L,t) \quad (5-2)$$

That is, there is an interval ($L_1 \sim L$) where the void fraction does not change for a small Δt at the top of the bundle, and

$$\alpha(L_1,t) = \alpha(L,t) \quad (5-3)$$

It must be noted that dL_1/dt is the same as the quench velocity, according to the first assumption. These assumptions are not true when Δt is large. But for small values of Δt , they are reasonably applicable in view of the relatively slow progress of the quench front. These assumptions are useful because equation (5-1) does not have any term involving an integration over time.

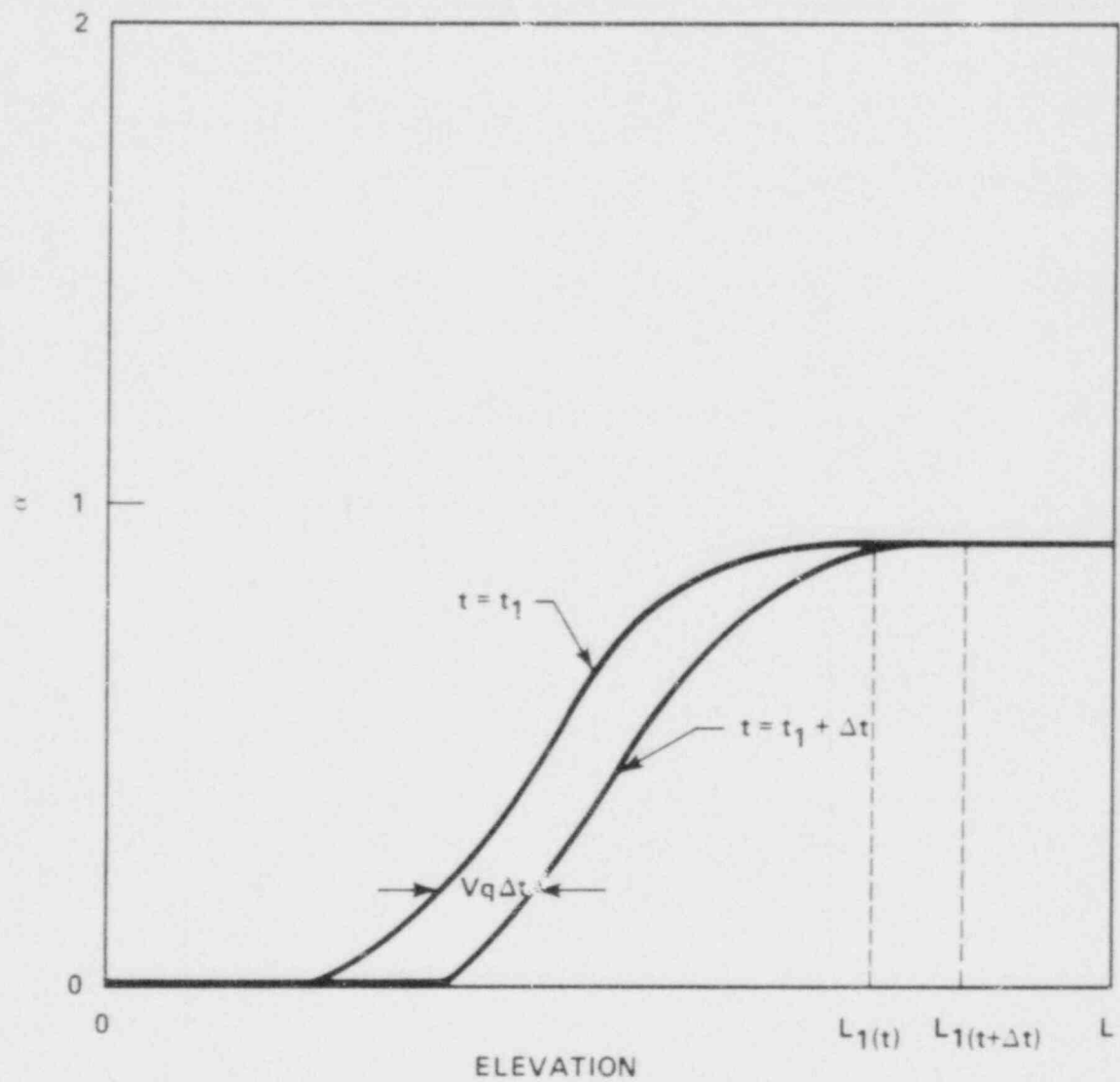


Figure 5-4. Assumptions in Model Development

Using the above assumptions, equation (5-1) can be modified as shown below. When the liquid density is assumed to be constant, the integration term in equation (5-1) can be simplified as

$$\frac{d}{dt} \int_0^L [\alpha \rho_v + (1 - \alpha) \rho_l] dz = (\rho_v - \rho_l) \frac{d}{dt} \int_0^L \alpha dz \quad (5-4)$$

The integration of the right-hand side of equation (5-4) can be modified as follows, using the above assumptions:

$$\frac{d}{dt} \int_0^L \alpha dz = \frac{d}{dt} \left(\int_{L_1}^L \alpha dz + \int_{L_1}^L \alpha dz \right) \quad (5-5)$$

where L_1 is the axial elevation where a constant void fraction near the top of a bundle starts. The first assumption provides that the first integration term on the right-hand side of equation (5-5) is constant. Also, utilizing Leibnitz' rule, it can be shown that equation (5-5) can be simplified as

$$\frac{d}{dt} \int_0^L \alpha dz = \int_{L_1}^L \frac{d\alpha}{dt} dz - \frac{dL_1}{dt} \alpha(L_1, t) \quad (5-6)$$

Since the void fraction at the top of the bundle is a weak function of time, the first term on the right-hand side of equation (5-6) becomes negligible. Further, the term dL_1/dt is V_q and $\alpha(L_1, t) = \alpha(L, t)$. Therefore, equation (5-6) can be simplified as

$$\frac{d}{dt} \int_0^L \alpha dz = - V_q \alpha(L, t) \quad (5-7)$$

Using equations (5-4) and (5-7), equation (5-1) can be modified as

$$\dot{m}_{in} - \dot{m}_{out} = A(\rho_l - \rho_v)V_q \alpha(L, t) \quad (5-8)$$

Since $\dot{m}_{in} = A \rho_{in} V_{in}$, equation (5-8) can be rewritten as

$$\frac{\dot{m}_{\text{out}}}{\dot{m}_{\text{in}}} = 1 - \frac{1}{V_{\text{in}} \rho_{\text{in}}} \left[(\rho_{\text{L}})_{\text{sat}} - \rho_{\text{v}} \right] \alpha(L,t) V_q \quad (5-9)$$

where V_{in} and ρ_{in} are reflooding velocity and the water density at the bottom of the bundle, respectively. For practical purposes, the liquid density is much larger than the vapor density. Therefore equation (5-9) becomes

$$\frac{\dot{m}_{\text{out}}}{\dot{m}_{\text{in}}} = 1 - \frac{(\rho_{\text{L}})_{\text{sat}} \alpha(L,t)}{V_{\text{in}} \rho_{\text{in}}} V_q \quad (5-10)$$

This is a general relation to calculate mass flow rate at the top of the bundle; it shows that the effluence rate is controlled not only by the quench front velocity as found by Sun and Duffey, but also by the void fraction at the top of the bundle.

As a special case, when the exit quality is unity (which is approximately true for the case with a very low flooding rate), equation (5-10) is reduced to

$$\frac{\dot{m}_{\text{out}}}{\dot{m}_{\text{in}}} = 1 - \frac{(\rho_{\text{L}})_{\text{sat}}}{V_{\text{in}} \rho_{\text{in}}} V_q \quad (5-11)$$

This is the same as the equation developed by Duffey and Porthouse⁽¹⁾ for an ideal case in which the void fraction distribution is a step function where the void fractions below and above the quench front are zero and one, respectively.

A general relation for estimating the mass effluence rate during a reflooding process has been developed. It was found that the effluence rate is governed by the quench velocity, as claimed by Sun and Duffey. But the rate is also controlled by the exit void fraction or the density at the top of the quench front.

I. Duffey, R. B., and Porthouse, D. T. C., "The Physics of Rewetting in Water Reactor Emergency Core Cooling," Nucl. Eng. Des. 25, No. 3, 379-394 (1973).

In summary, three relations for effluence rate have been provided:

-- General case I

$$\frac{\dot{m}_{out}}{\dot{m}_{in}} = 1 - \frac{(\rho_q)_{sat} \alpha(L,t)}{\rho_{in} V_{in}} V_q \quad (5-12)$$

-- Special case of general case I, when $\alpha(L,t) = 1$

$$\frac{\dot{m}_{out}}{\dot{m}_{in}} = 1 - \frac{(\rho_q)_{sat}}{\rho_{in} V_{in}} V_q \quad (5-13)$$

-- General case II

$$\frac{\dot{m}_{out}}{\dot{m}_{in}} = 1 - \frac{\rho(z_q)}{\rho_{in} V_{in}} V_q \quad (5-14)$$

5-5. IMPLEMENTATION OF MODELS IN FLEMB

The implementation of the three models in FLEMB requires knowledge of the quench front velocity, the density just below the quench front, and the void fraction at the top of the bundle. Since these variables were measured or calculated for these tests, it is possible to check out the models, using the data. For more general application of the models, the quench velocity can be reasonably predicted using an empirical or theoretical correlation. The determinations of the void fraction and density can also be done using an empirical relation like the Yeh void fraction correlation.⁽¹⁾

The density just below the quench front and the void fraction at the top of the bundle are readily available from the results of FFLOW, which is explained in the FLECHT SEASET unblocked bundle data report.⁽²⁾ The quench front velocity can be calculated

1. Cunningham, J. P., and Yeh, H. C., "Experiments and Void Correlation for PWR Small-Break LOCA Conditions," Trans. Am. Nucl. Soc. 17, 369-370 (1973).
2. Loftus, M. J., et al., "PWR FLECHT SEASET Unblocked Bundle, Forced and Gravity Reflood Task Data Report," NRC/EPRI/Westinghouse-7, June 1980.

from the quench curve. A quench curve generally rises rapidly at the start of a reflooding and the slope reduces to a more or less constant level for some time after the initial period. Therefore, a quench curve could be divided into two parts: an early period and a later period. The sections of these two periods were separately curve-fit by polynomials.

5-6. COMPARISONS WITH DATA

Figure 5-5 compares the predictions of the models with the experimental data for run 31504. The data were calculated using the rate of mass stored in the bundle. The figure contains four different predictions: those of equations (5-12), (5-13), (5-14), and the Yeh and Hochreiter model. Generally they predict the effluence rate fairly well. The predictions made by equations (5-12) and (5-13) are very close to each other, to be expected because this run is a low flooding rate test. In run 31701, where the flooding rate was 152 mm/sec (6 in./sec), the difference between the two predictions is about 7 percent. (See figure B-11.) Therefore, for practical purposes equation (5-13) is a fairly good tool for predicting the effluence rate when the flooding rate is low. More data comparisons of all methods are provided in appendix B.

5-7. TRANSITION ZONE ABOVE QUENCH FRONT

It has been known that there is a transition zone above a quench front where the flow regime is not quite a dispersed flow (figure 5-6). Therefore, the heat transfer mechanism in the zone should be different from those in a dispersed flow and below the quench front. There have been efforts to delineate heat transfer mechanisms in a dispersed flow above the quench front and to predict heat transfer above the quench front. But the length of the transition zone should be known to apply the theories of dispersed flow heat transfer to a proper region.

Murao⁽¹⁾ observed that in-bundle temperature history curves during reflood show sudden slope increases and stay at the constant levels for some time before quench.

I. Murao, Y., et al., "Experimental and Analytical Modeling of the Reflood Phase During PWR LOCA," paper presented at the 19th National Heat Transfer Conference, Orlando, FL (ASME), July 27-30, 1980.

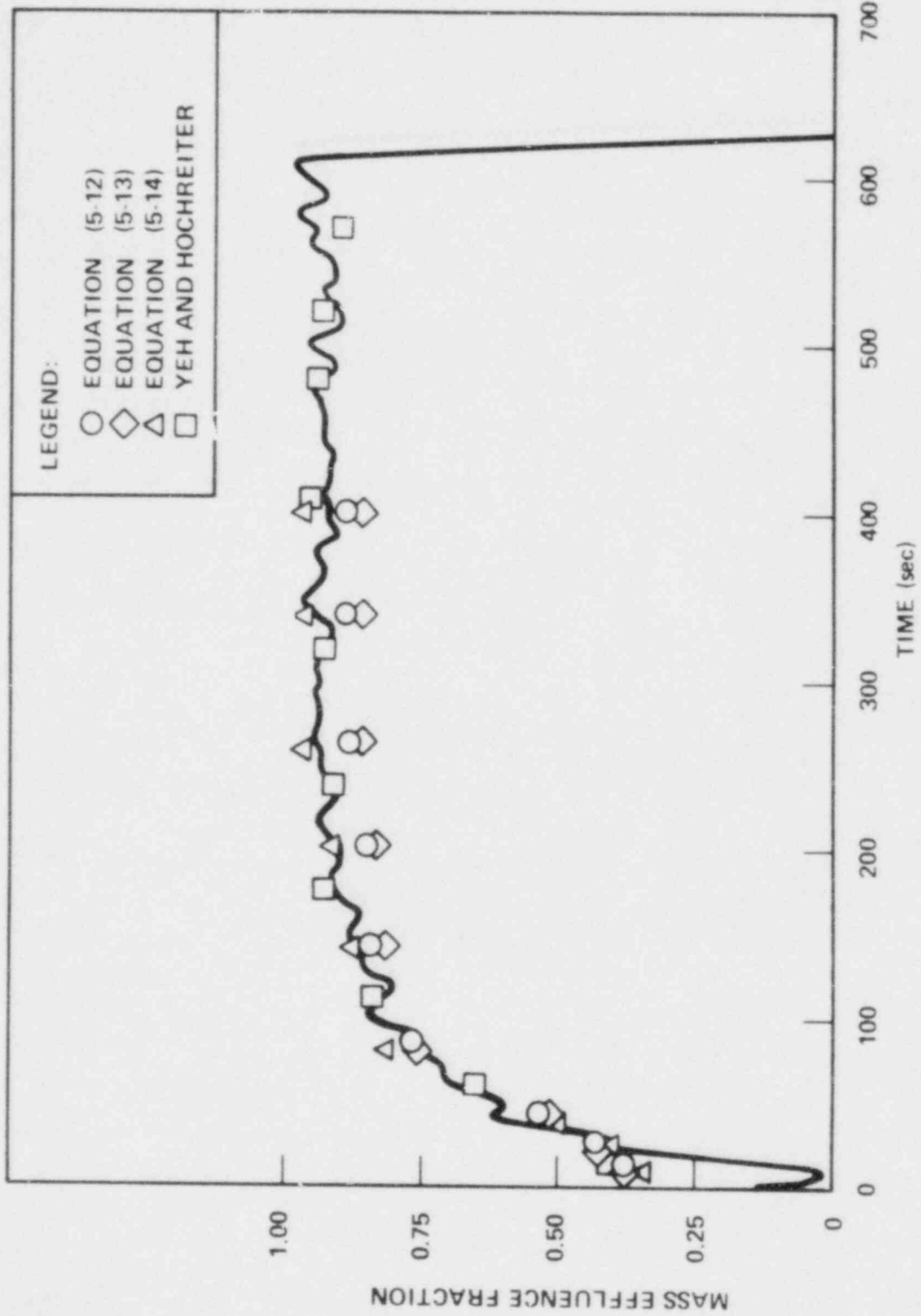


Figure 5-5. Mass Effluence Fraction Compared With Model Predictions, Run 31504

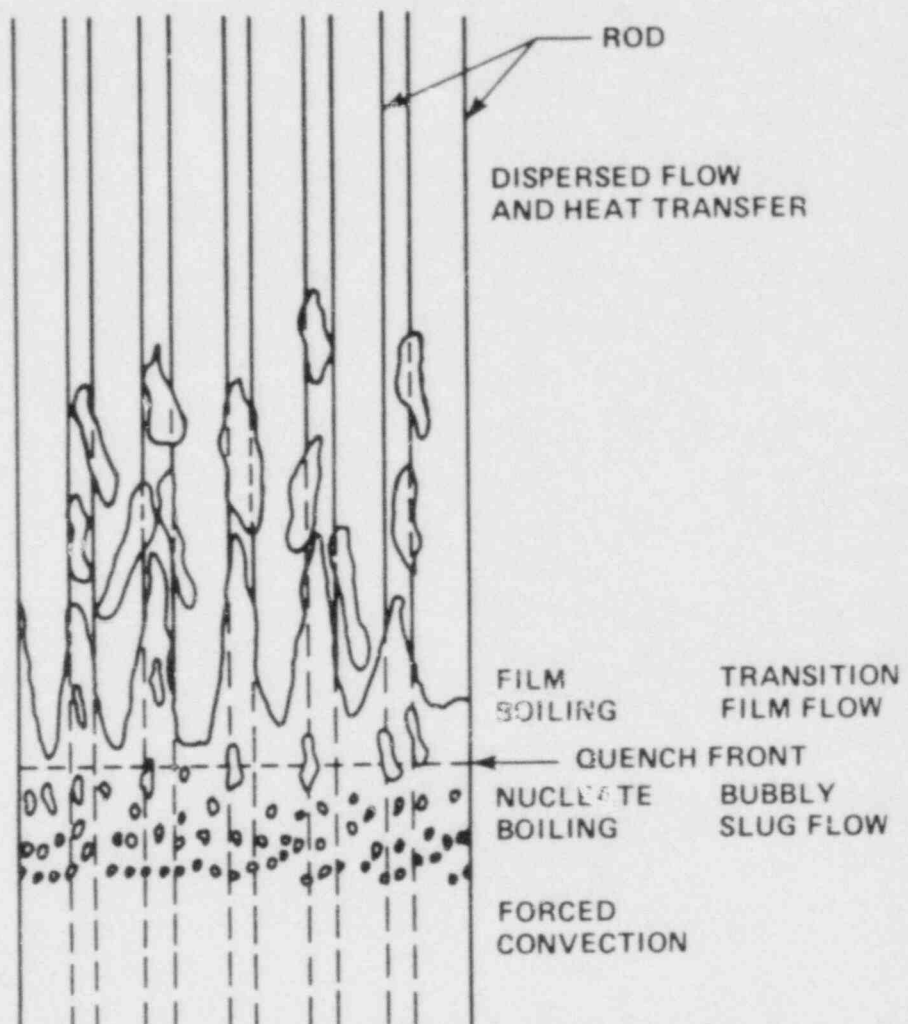


Figure 5-6. Typical Conditions in Rod Bundle During Reflood

He related the slope change to the flow regime change above the quench front. Most of the rod temperature measurements of the FLECHT SEASET unblocked bundle tests also indicated such behavior, as shown in figure 5-7 and section 3.

If it is postulated that the slope change is due to the advance of the transition zone above the quench front, it is possible to distinguish three different flow conditions at each bundle elevation, as indicated in figure 5-7. The first period (I) is when the elevation sees a dispersed droplet flow around it after a short period of single-phase steam flow. The second (II) is when the transition zone right above the quench front surrounds the elevation, and the third period (III) is when it is below the quench front. These different flow regimes are distinguished in heat transfer coefficient curves, as shown in figure 5-7. The relatively moderate increase in heat transfer during the first period is followed by a rather sharp increase during the second period and then quench produces a sudden increase. This trend is consistent with the heat transfer characteristics of the relevant flow regimes.

Based on the above discussions, the advances of the transition zone fronts during the unblocked bundle tests have been measured. A schematic way to construct the transition front curve is shown in figure 5-8. The resulting curves for eight runs are presented in figures 5-9 through 5-16. Corresponding quench data are shown to indicate the length of the transition zones. It is observed that the transition zone could be about 0.30 m (12 in.) at a 25.4 mm/sec (1 in./sec) reflooding rate, and it could be 0.91 m (36 in.) at a 76.2 mm/sec (3 in./sec) reflooding rate.

It is of interest to compare heater rod temperatures to steam probe measurements and thimble temperatures at the same elevation, as shown in figure 5-17. It is observed that the steam and thimble temperatures drop down to the saturation temperature when the second period is reached at a particular elevation.

From these observations, it is concluded that there is a transition zone of finite length above a quench front. Further, the vapor in the zone is under a saturated condition. It has been observed that the transition zone length is a strong function of flooding rate.

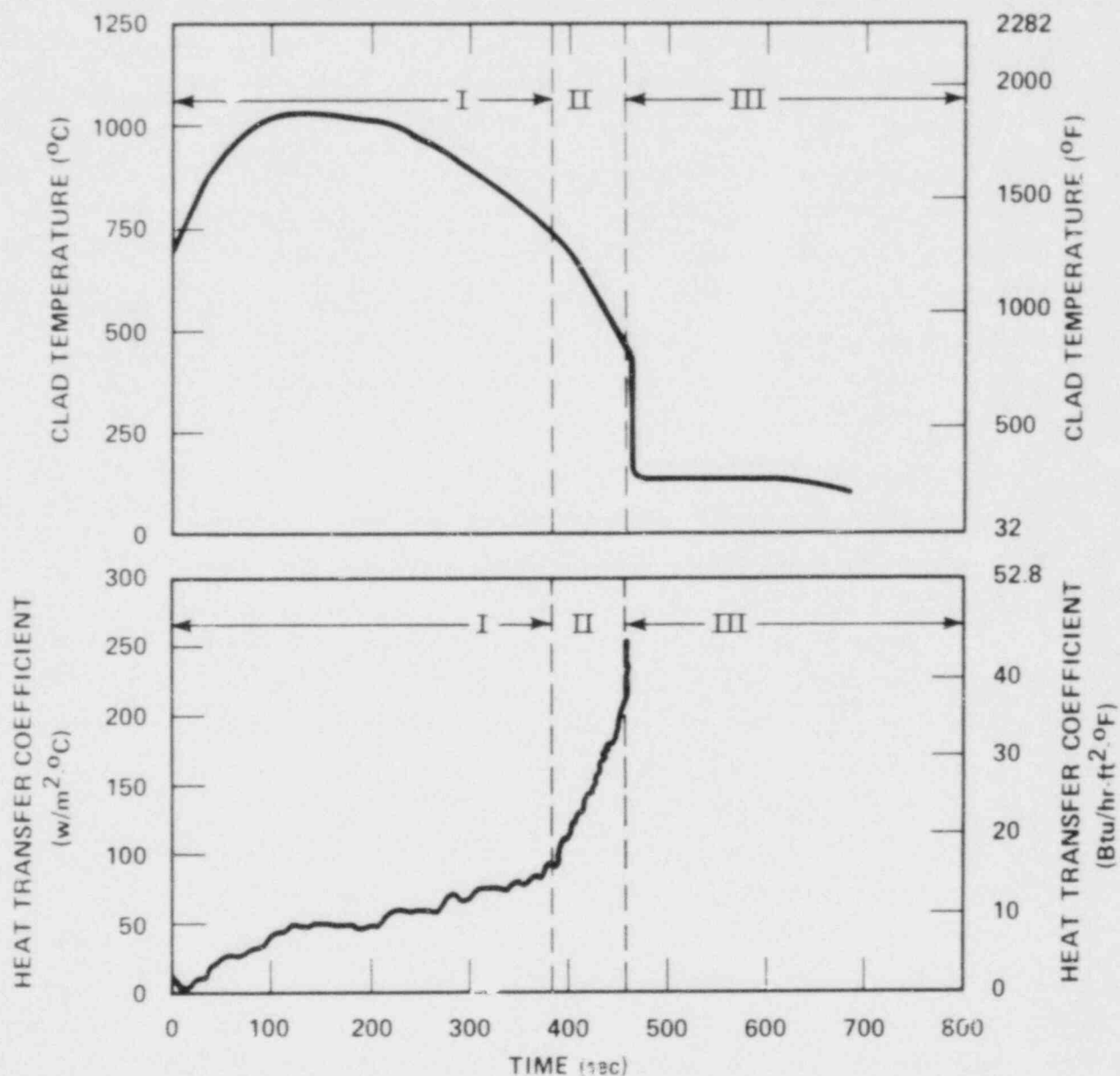


Figure 5-7. Temperature and Heat Transfer Coefficient Curve, Showing Transition Zone (II)

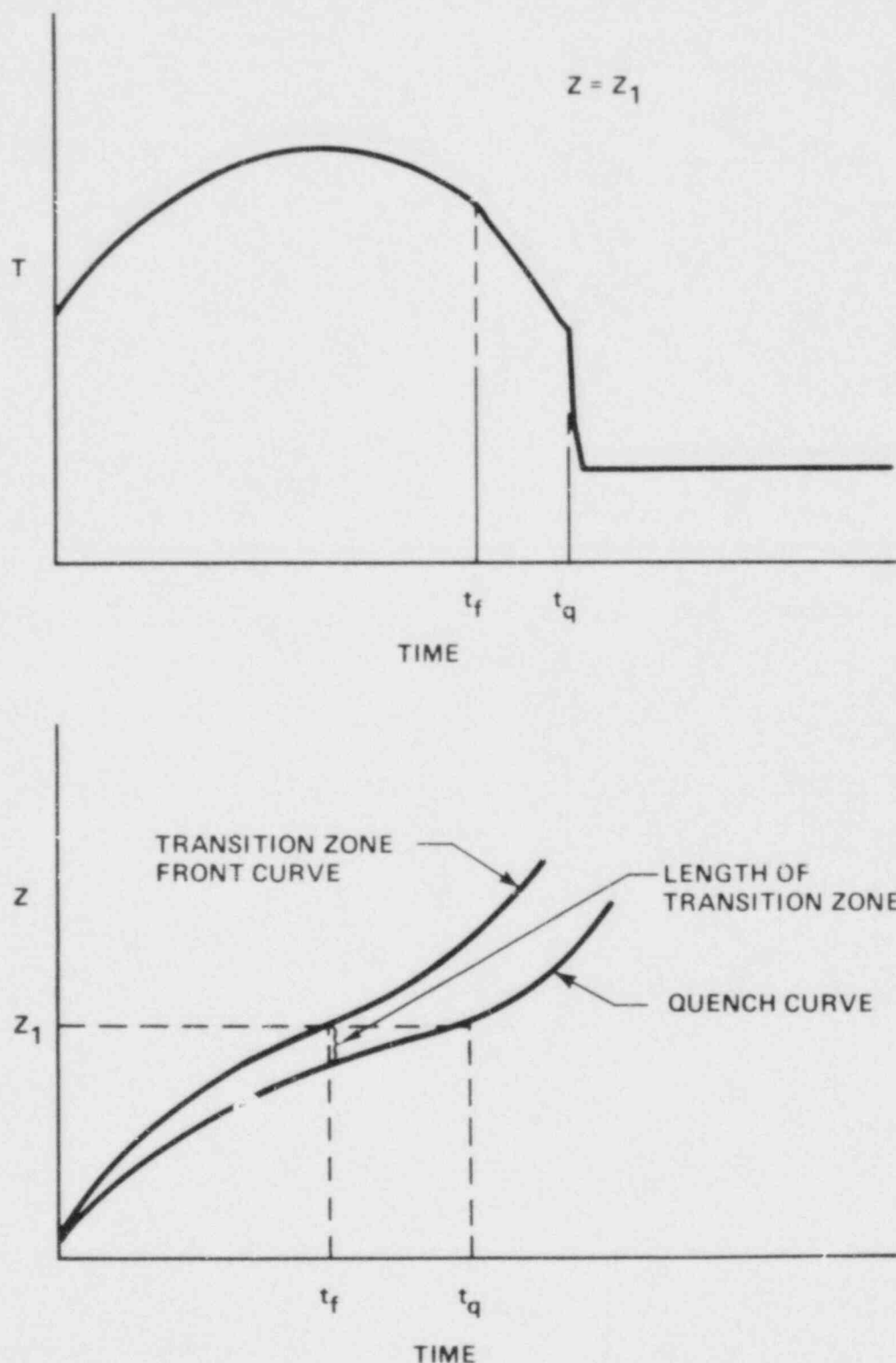


Figure 5-8. Schematic Construction of Transition Zone Curve

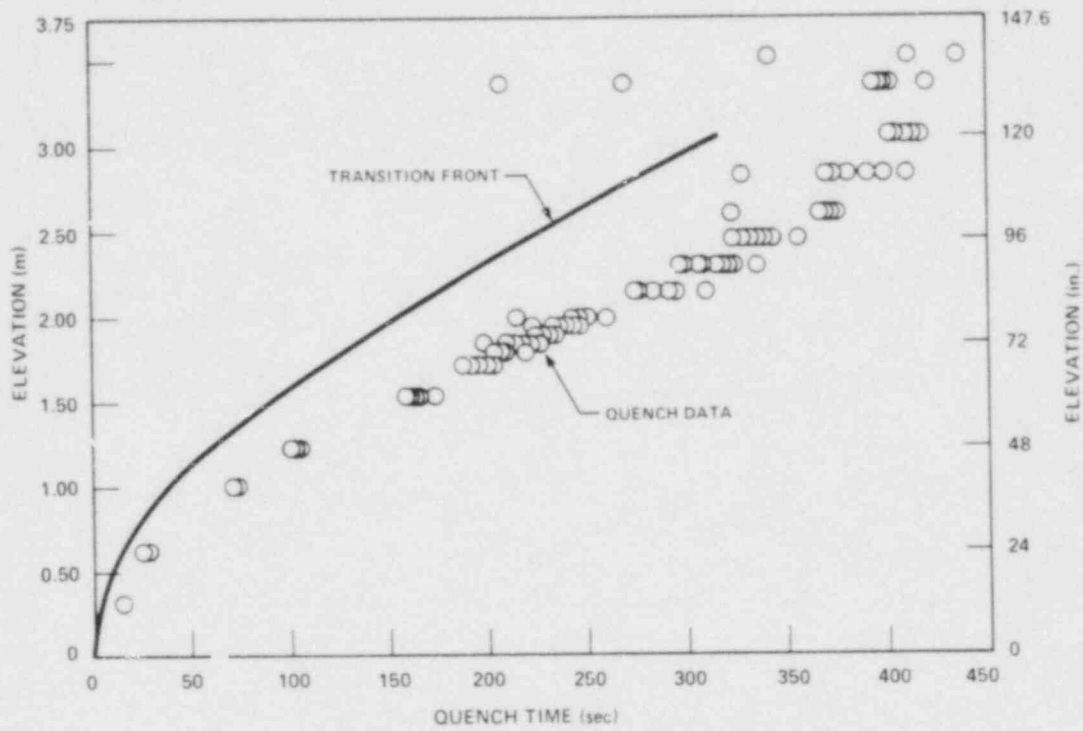


Figure 5-9. Transition Front Curve, Run 31203

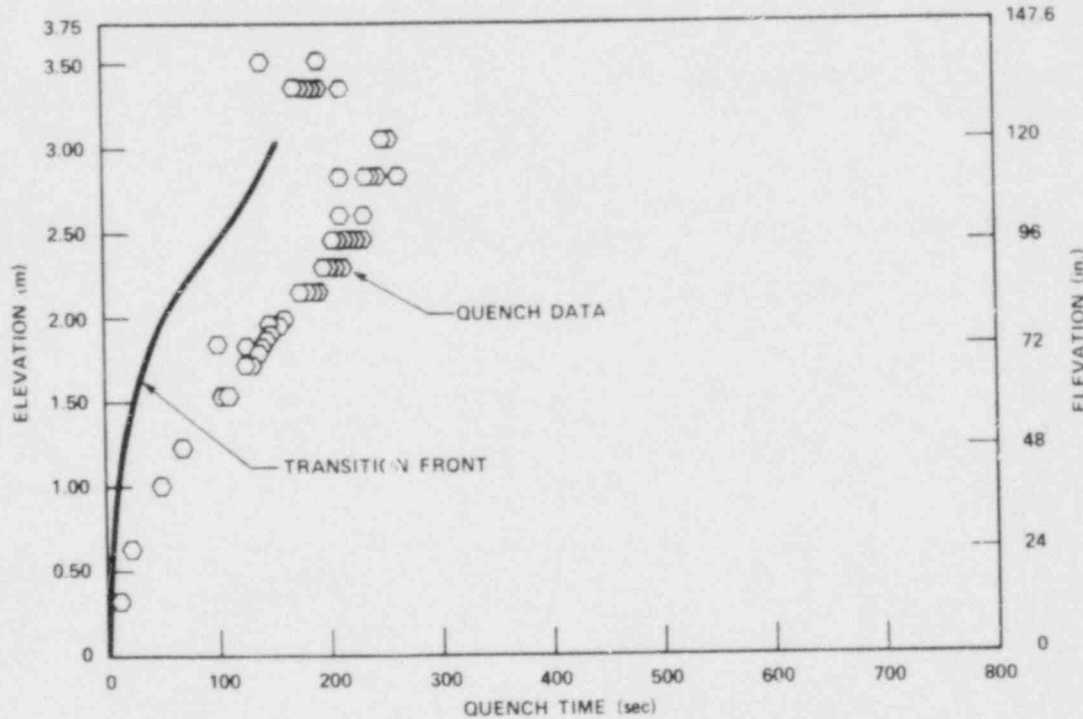


Figure 5-10. Transition Front Curve, Run 31302

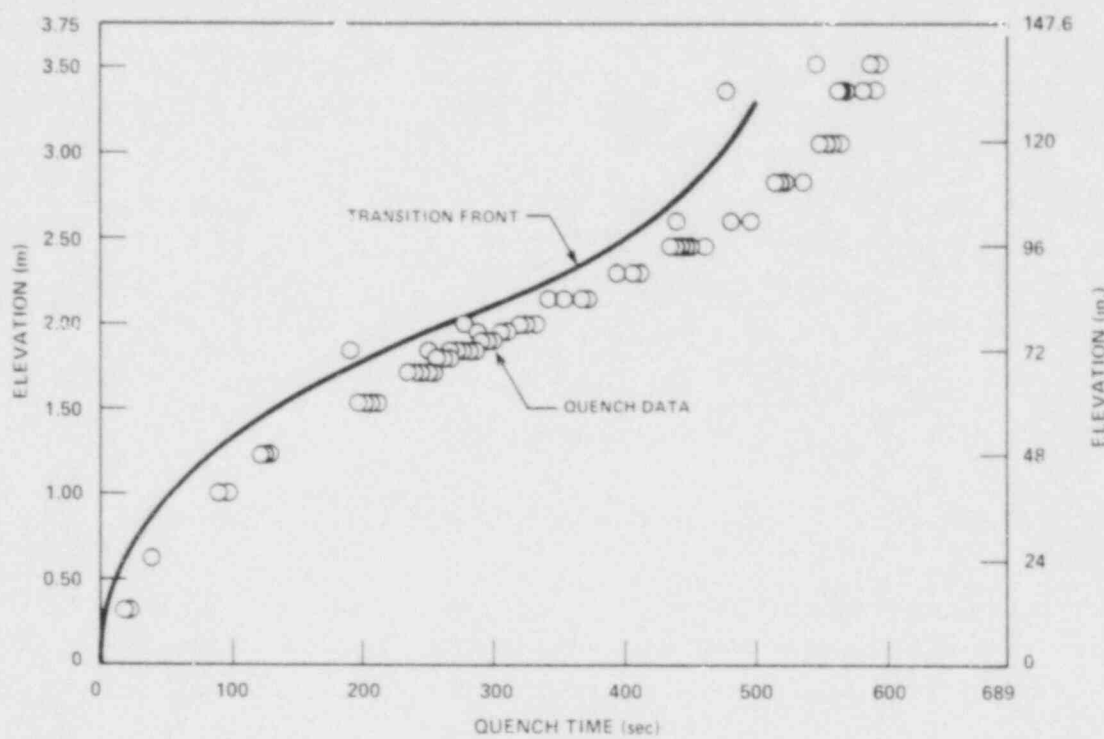


Figure 5-11. Transition Front Curve, Run 31504

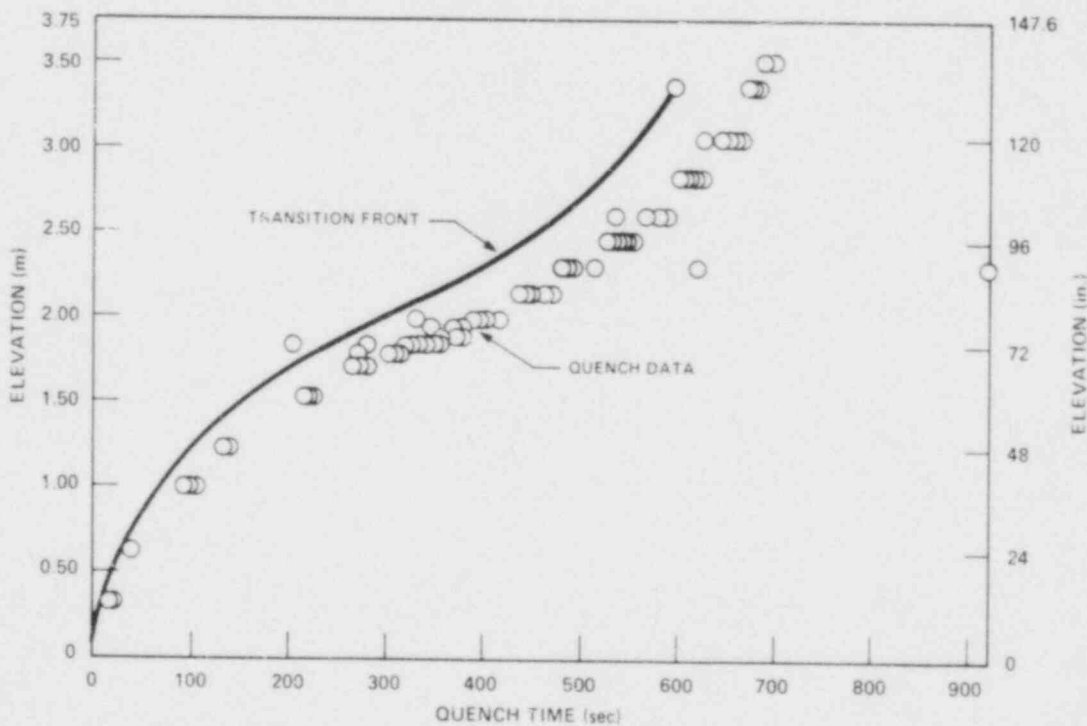


Figure 5-12. Transition Front Curve, Run 31805

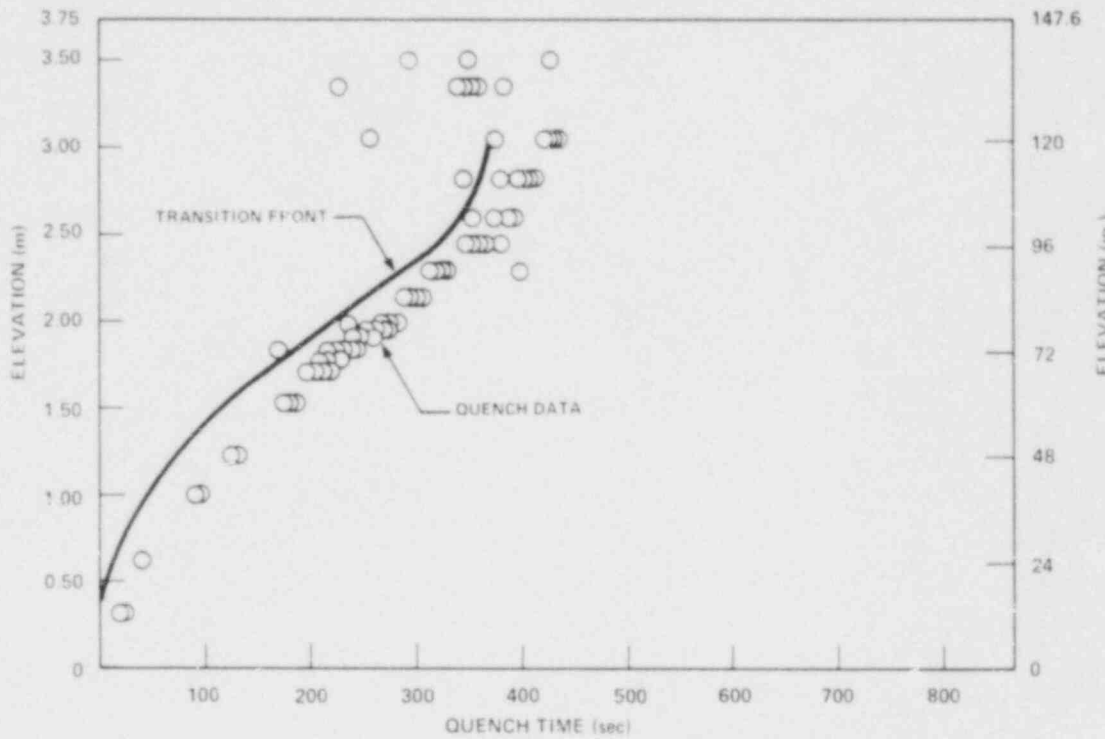


Figure 5-13. Transition Front Curve, Run 31922

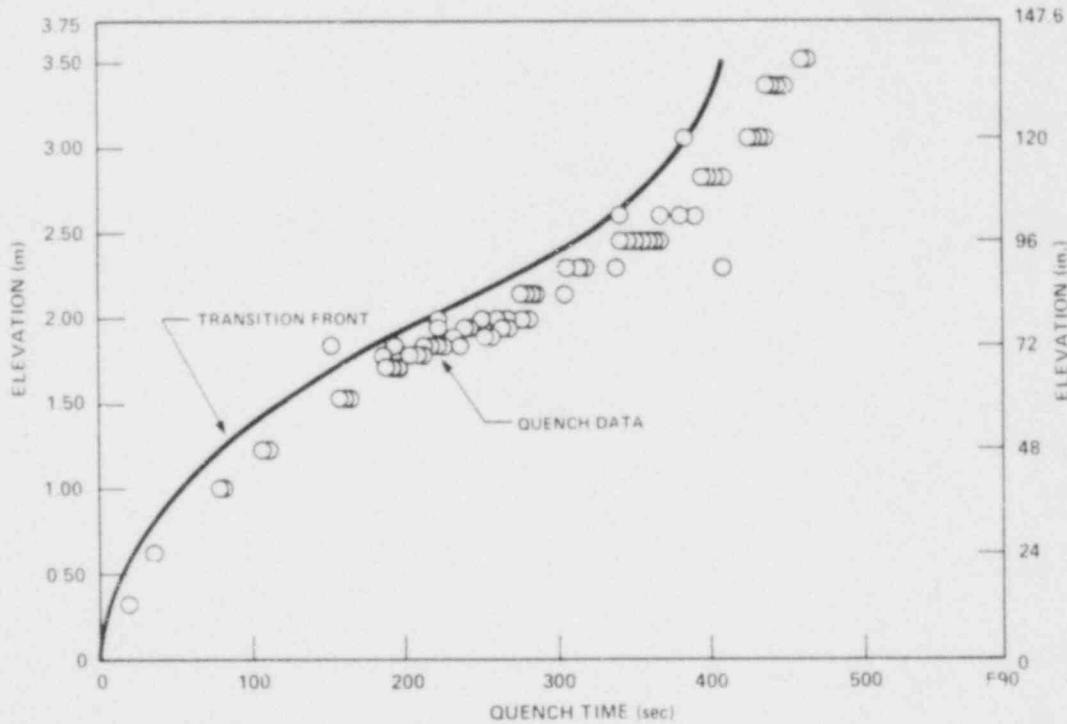


Figure 5-14. Transition Front Curve, Run 32013

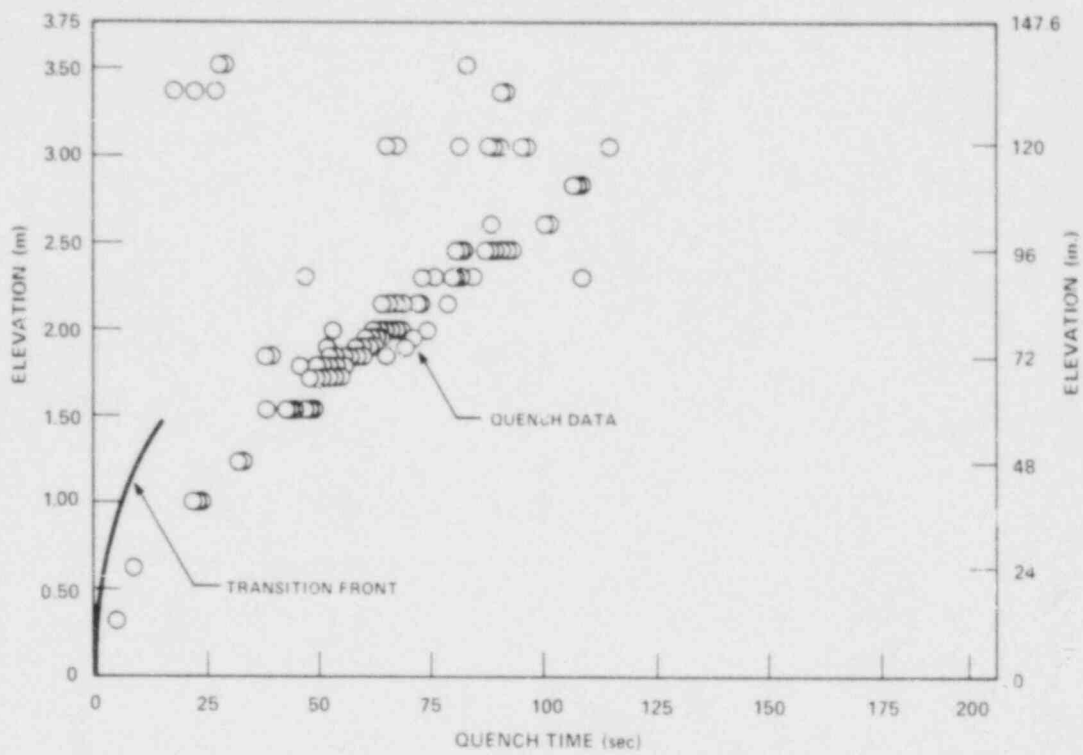


Figure 5-15. Transition Front Curve, Run 31701

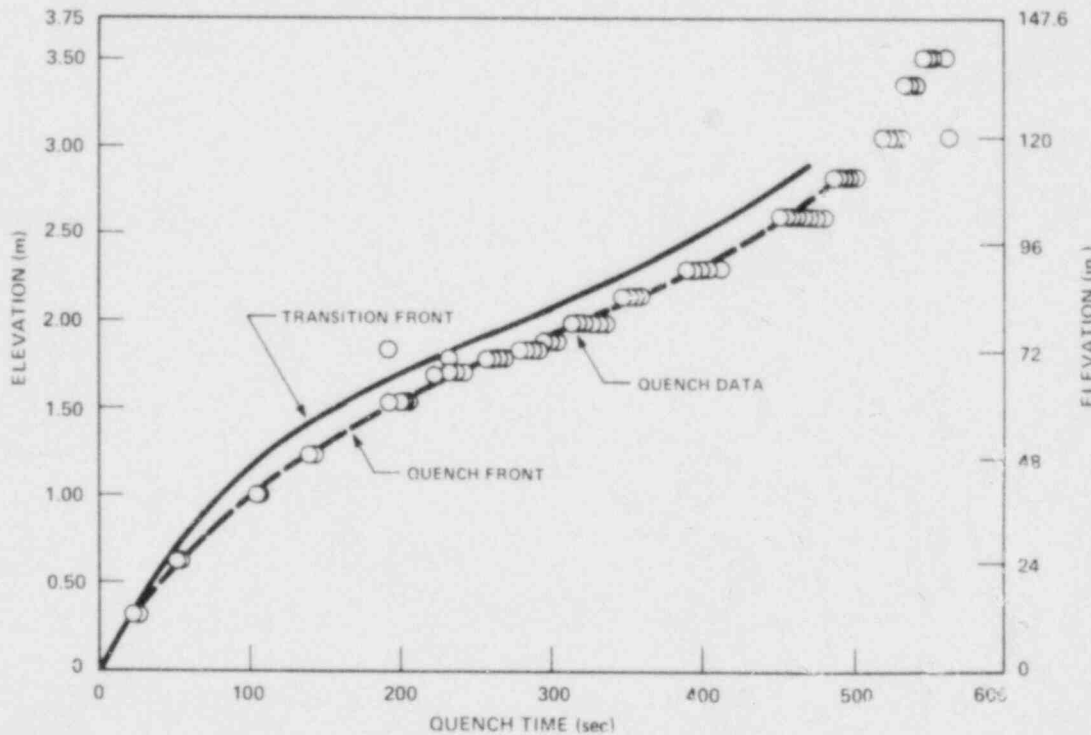


Figure 5-16. Transition Front Curve, Run 34006

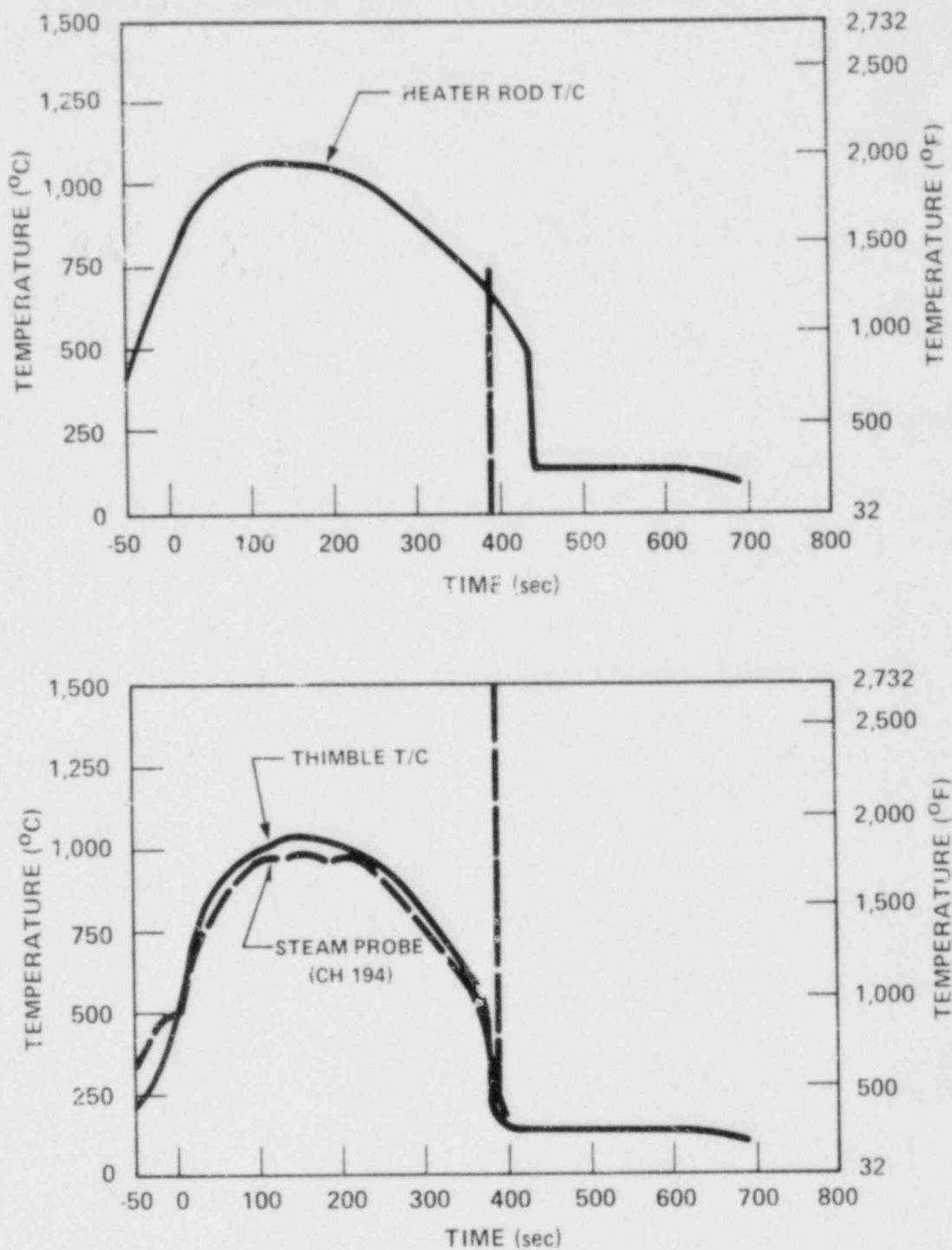


Figure 5-17. Comparison of Temperature Histories of Rod and Thimble Thermocouples and Steam Probe at 2.03 m (96 in.) Elevation, Run 31504

SECTION 6

EVALUATION OF DISPERSED DROPLET FLOW CONDITIONS AND HEAT TRANSFER MECHANISMS DURING REFLOOD

6-1. INTRODUCTION

Previous sections and the FLECHT SEASET 161-rod unblocked bundle task plan and data report describe how FLECHT SEASET reflood data were recorded and then reduced by various computer codes to obtain useful reflood flow conditions and heat transfer information. To summarize, raw data (system pressure, steam temperatures, thimble wall and heater rod inner clad surface temperatures, heater rod power, bundle inlet and outlet fluid temperatures, bundle and water collection tank pressure drops, and flowmeter readings) were recorded by the CATALOG code; heater rod quench time, turnaround time, quench temperature, and turnaround temperature were calculated by the QUENCH code; mass flow above the quench front was calculated by the FFLOW code; bundle mass and energy balance and actual nonequilibrium steam quality were calculated by the FLEMB code.

Fluid states and heat transfer above the quench front during reflood have been investigated extensively by previous authors.⁽¹⁾ However, most earlier works have been limited to tube experiments, or there were insufficient data to determine the local fluid conditions (for example, droplet size distribution was not measured). The FLECHT SEASET reflood experiments were performed in a full-length 161-rod bundle, adequately instrumented such that local fluid conditions (for instance, nonequilibrium steam quality) could be determined. Also, droplet size distributions and velocities were measured (see appendixes E and F) at several locations in the bundle. In this section, local flow conditions in the dispersed flow regime are calculated. In the dispersed flow regime, quasi-steady-state one-dimensional axial flow is assumed, and all flow quantities referred to in this section are bundle cross-sectional averaged values. The important axial variation of flow conditions is evaluated in this section. The calculated

I. For instance, Seban, R.A., et al., "Predictions of Drop Models for the Dispersed Flow Downstream of the Quench Front in Tube Reflood Experiments," ASME paper 80-WA/HT-47.

flow conditions are then used to evaluate the basic heat transfer components, forced convection and thermal radiation, in the dispersed flow regime.

In analysis of the data, maximum use is made of the available data and data-based heat transfer quantities; assumptions and physical models are introduced only when absolutely necessary to calculate dispersed flow conditions and the basic heat transfer components. A mechanistic heat transfer model is developed in section 7, using boundary condition information provided in this section to predict local flow conditions and heat transfer in the dispersed flow regime.

6-2. ENERGY ABSORPTION BY DROPLETS ABOVE QUENCH FRONT

The FLECHT cosine and skewed power profile reflood experiments^(1,2) and the present FLECHT SEASET reflood experiments show that two-phase dispersed droplet flow exists above the quench front even for low flooding rates [less than 25.4 mm/sec (1 in./sec)]. The water droplets above the quench front serve as very effective heat sinks, and the resulting heat transfer between the heated walls and the two-phase flow is much higher than that which could be predicted by conventional single-phase heat transfer correlations (for example, the Dittus-Boelter correlation), in which no droplet evaporation is assumed.⁽²⁾

Peak clad temperature during reflood is determined by the heat transfer between the heated wall and the dispersed droplet flow. Hence it is most important to understand the basic heat transfer mechanisms above the quench front and the role of the water droplets in these mechanisms.

Because of the high wall temperatures above the quench front, direct wall and droplet contact is not anticipated. The droplets absorb heat by convection and thermal radiation from surrounding superheated steam, and by thermal radiation from the hot walls. Neglecting heat release and absorption by the housing solid fillers, and thimble guide tubes, an energy balance in the bundle gives the following relationship:

-
1. Lilly, G.P., et al., "PWR FLECHT Cosine Low Flooding Rate Test Series Evaluation Report," WCAP-8838, March 1977.
 2. Lilly, G.P., et al., "PWR FLECHT Skewed Profile Low Flooding Rate Test Series Evaluation Report," WCAP-9183, November 1977.

$$Q_{\text{rod}}(z_1, z_2) = Q_{\text{vapor}}(z_1, z_2) + Q_{\text{droplet}}(z_1, z_2) \quad (6-1)$$

where

$$Q_{\text{rod}}(z_1, z_2) = \text{total heat release by heater rods between elevations } z_1 \text{ and } z_2 [\text{kw (Btu/sec)}]$$

$$Q_{\text{vapor}}(z_1, z_2) = \text{total heat absorption by vapor between elevations } z_1 \text{ and } z_2 [\text{kw (Btu/sec)}]$$

$$Q_{\text{droplet}}(z_1, z_2) = \text{total heat absorption by droplets between elevations } z_1 \text{ and } z_2 [\text{kw (Btu/sec)}]$$

Heat exchange in the axial direction is also neglected in equation (6-1). Assuming quasi-steady-state and the droplets at saturation condition, $Q_{\text{droplet}}(z_1, z_2)$ can be calculated if the actual steam quality is known:

$$Q_{\text{droplet}}(z_1, z_2) = h_{fg} m_T [x(z_2) - x(z_1)] \quad (6-2)$$

where

$$x(z) = \text{actual steam quality at elevation } z$$

$$h_{fg} = \text{latent heat of vaporization [kw-sec/kg (Btu/lbm)]}$$

$$m_T = \text{total mass flow in the bundle [kg/sec (lbf/sec)]}$$

Using the steam quality calculated by the FLEMB code, Q_{droplet} was calculated and compared with Q_{rod} . Typical results are shown in figures 6-1 and 6-2. It may be noted that even for a low flooding rate case [run 31504, 24.6 mm/sec (0.97 in./sec)], energy absorption by droplets was significant and could not be neglected compared to the total heat release by the heater rods. As flooding rate increased, Q_{droplet} became more important and represented an even larger fraction of Q_{rod} . When Q_{droplet} was greater than Q_{rod} , as shown in the figures, Q_{vapor} in equation (6-1) was negative or the vapor desuperheated (returned to equilibrium). Vapor desuperheating usually occurred at higher elevations of the bundle.

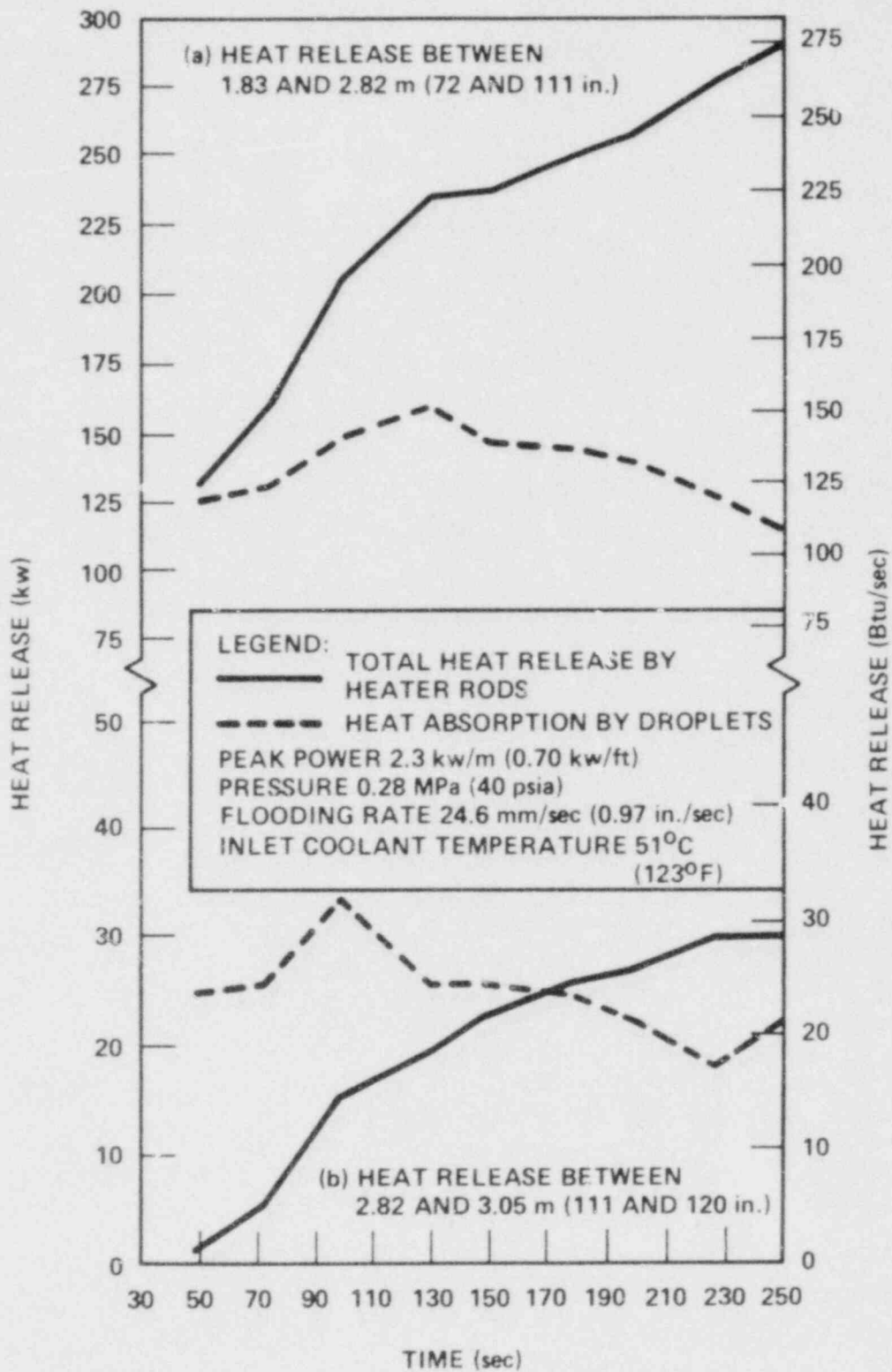


Figure 6-1. Comparisons of Bundle Heat Release and Heat Absorption by Droplets, Run 31504

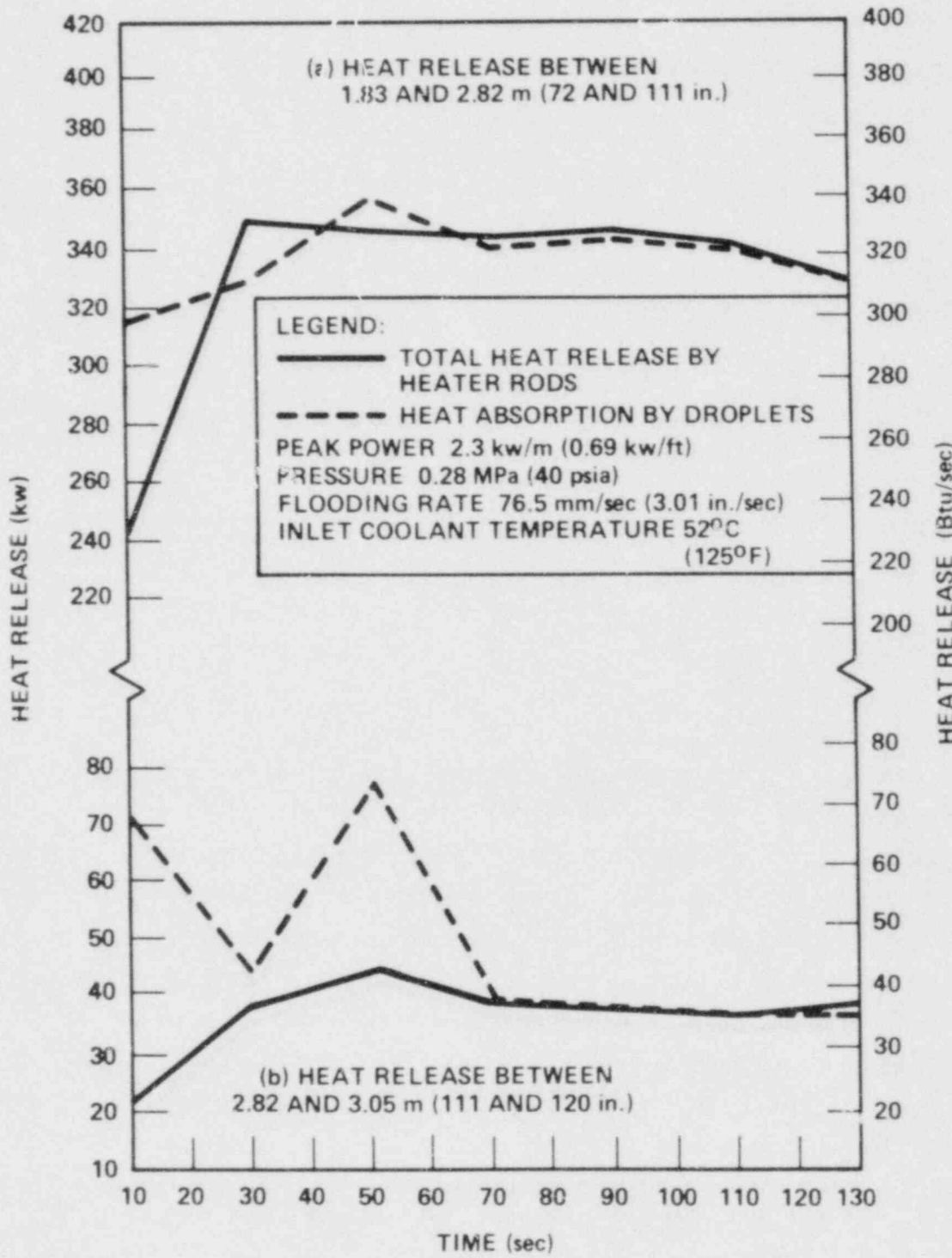


Figure 6-2. Comparisons of Bundle Heat Release and Heat Absorption by Droplets, Run 31302

From the results presented above, it is apparent that the droplets play an important role in the heat transfer processes above the quench front during reflood. Adequate modeling of the heat transfer processes that take place above the quench front requires a better knowledge of the droplet size, the droplet velocity, and the droplet-vapor interactions. In the following paragraphs, local dispersed flow conditions and basic heat transfer components above the quench front are evaluated.

6-3. FLOW REGIMES ABOVE QUENCH FRONT

As discussed in section 5, a transition flow regime exists right above the quench front. In the transition regime, the flow is nonsteady, large chunks of liquid may exist, droplets may collide and interact with one another, vapor superheat is low, and steam quality and void fraction increase rapidly. Above the top of the transition flow regime (or transition front), a dispersed droplet flow regime exists. In the dispersed flow regime, the flow is quasi-steady, vapor superheat is high, the void fraction is high enough that droplets do not interact with one another, and drops are entrained upward and do not make direct contact with the hot walls. Figure 6-3 illustrates the characteristic vapor quality and void fraction in these two flow regimes above the quench front. The discontinuities at the quench front are due to the rapid release of stored heat from the hot rods.

The distinction between the transition and dispersed flow regimes is important, particularly when calculating heat transfer from the hot walls to the two-phase flow. Researchers generally distinguish between these two regimes by assuming that dispersed flow exists when the vapor void fraction exceeds a certain preassigned value, but offer no data nor convincing theories to support the values they choose. In section 5, a method is proposed to distinguish between the transition and dispersed flow regimes by observing the time-slope of the heater rod temperature data. In the following paragraphs, no attempt is made to calculate flow conditions in the transition flow regime. Local flow conditions and basic heat transfer components in the dispersed flow regime are evaluated; that is, all calculations presented in this section began at the transition front and ended at the bundle exit. The transition front elevations were input from curves such as those shown in figures 5-9 through 5-14. Steam quality at the transition front was obtained by extrapolating available steam probe data above the transition front. Other input quantities are presented in appendix C.

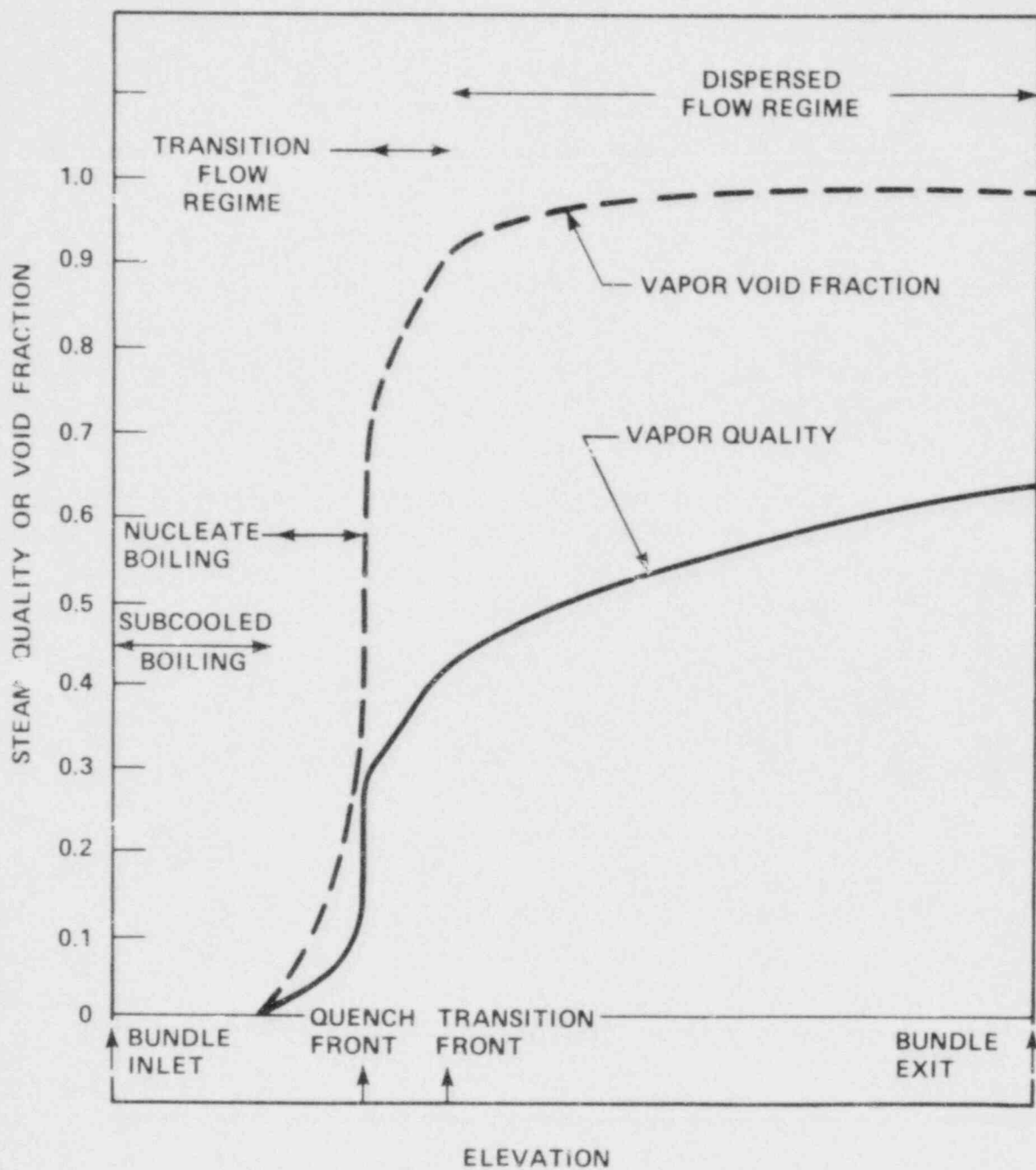


Figure 6-3. Schematic Diagram of Characteristic Vapor Quality and Void Fraction During Reflood

6-4. BASIC RELATIONS FOR TWO-PHASE FLOW PROPERTIES IN DISPERSED FLOW REGIME

In this section, one-dimensional quasi-steady flow is assumed above the transition front during reflood. Two-phase flow properties are calculated as a function of axial positions; they are bundle-averaged values. The required input quantities are summarized in appendix C. To avoid lengthy and tedious equations, the axial dependence is omitted from the symbols.

Methods to calculate drop size, droplet velocity, droplet mass flux, droplet number flux, droplet number density, droplet Reynolds number, liquid volume fraction, vapor void fraction, and vapor Reynolds numbers are described in detail in appendix F. Relations of other dispersed flow properties are summarized below.

The slip ratio, S_i , and the Weber number, We_i , for the i -th drop size group are defined as

$$S_i = \frac{u_v}{u_{di}} \quad (6-3)$$

$$We_i = \frac{\rho_v (u_v - u_{di})^2 d_i}{\sigma_l} \quad (6-4)$$

where

u_v = vapor velocity [m/sec (ft/sec)]

u_{di} = droplet velocity of i -th drop size group [m/sec (ft/sec)]

ρ_v = vapor mass density [kg/m^3 (lbm/ft^3)]

d_i = drop diameter of the i -th drop size group [m (ft)]

σ_l = surface tension for water-vapor interface [kg/sec^2 (lbm/sec^2)]

Under typical reflood conditions, the droplets are in the geometric scattering regime, and the liquid absorption coefficient, a_l , can be computed by⁽¹⁾

$$a_l = \sum_{i=1}^{N_d} 0.185 \pi d_i^2 n_{di} \quad (6-5)$$

where

a_l = liquid absorption coefficient [m^{-1} (ft^{-1})]

N_d = total number of drop size groups

n_{di} = droplet number density of i-th drop size group [drops/ m^3 (drops/ ft^3)]

The vapor absorption coefficient, a_v , is calculated by⁽²⁾

$$a_v = P \left[5.6 \left(\frac{1000}{T_v} \right)^2 - 0.3 \left(\frac{1000}{T_v} \right)^4 \right] \quad (6-6)$$

where

a_v = vapor absorption coefficient (ft^{-1})

P = pressure (atmosphere)

T_v = vapor temperature ($^{\circ}$ Rankine)

-
1. Sun, K.H., et al., "Calculations of Combined Radiation and Convection Heat Transfer in Rod Bundles Under Emergency Cooling Conditions," J. Heat Transfer 98, ASME, 414-420 (1976).
 2. Abu-Romia, M.M., and Tien, C.K., "Appropriate Mean Absorption Coefficients for Infrared Radiation of Gases," J. Heat Transfer 89, ASME, 321-327 (1967).

Equation (6-6) is a curve-fit of the water vapor data presented by Abu-Romia and Tien.⁽¹⁾

The optical thickness of the droplet and vapor media is computed by⁽¹⁾

$$\tau = (a_v + 2.7 a_l) D_h \quad (6-7)$$

where

τ = optical thickness (dimensionless)

D_h = hydraulic diameter based on rod-centered subchannel [m (ft)]

Assuming that the droplet and vapor media are optically thin (that is, the optical thickness is smaller than unity), the drop and vapor emissivities, ϵ_l and ϵ_v , are computed by⁽¹⁾

$$\epsilon_l = 1 - e^{-a_l L_m} \quad (6-8)$$

$$\epsilon_v = 1 - e^{-a_v L_m} \quad (6-9)$$

and the mean beam length, L_m , is defined as

$$L_m = 0.85 D_h \quad (6-10)$$

for a rod bundle geometry.⁽²⁾

-
1. Abu-Romia, M. M., and Tien, C. K., "Appropriate Mean Absorption Coefficients for Infrared Radiation of Gases," J. Heat Transfer 89, ASME, 321-327 (1967).
 2. Hottel, H.C., and Sarofim, A.F., Radiative Transfer, McGraw-Hill, New York, 1967.

6-5. BASIC HEAT TRANSFER COMPONENTS IN DISPERSED FLOW REGIME

The heater rod heat flux in the dispersed flow regime is assumed to be made up of a convective component and a radiation component:

$$\dot{q}_T'' = \dot{q}_{cv}'' + \dot{q}_r'' \quad (6-11)$$

where

$$\dot{q}_T'' = \text{total heat flux } [\text{w/m}^2 (\text{Btu/sec-ft}^2)]$$

$$\dot{q}_{cv}'' = \text{convective heat flux } [\text{w/m}^2 (\text{Btu/sec-ft}^2)]$$

$$\dot{q}_r'' = \text{radiation heat flux } [\text{w/m}^2 (\text{Btu/sec-ft}^2)]$$

The total heat flux, \dot{q}_T'' , is calculated from wall temperature measurements by an inverse conduction code. The radiation component is calculated by a radiation network analysis described in paragraph 6-6. The convective heat flux can then be calculated from equation (6-11) by

$$\dot{q}_{cv}'' = \dot{q}_T'' - \dot{q}_r'' \quad (6-12)$$

It is shown later that the convective heat flux calculated by equation (6-12) is generally much higher than that which would be predicted by conventional single-phase heat transfer correlations (for example, the Dittus-Boelter correlation). Based on information developed in this section, a dispersed flow heat transfer predictive model is proposed. Heat transfer enhancement due to the presence of the droplets is considered and a higher convective heat flux component is calculated. Details of the predictive model are described in section 7.

6-6. ANALYSIS OF RADIATIVE HEAT EXCHANGE IN ROD BUNDLES

The radiative heat exchange between the droplet phase, the vapor phase, and the wall surfaces in a rod bundle system can be calculated by a radiation network. (1,2) To account for the radiative heat exchange between various wall surfaces, the FLECHT SEASET 161-rod bundle system is divided into four radiating nodes, as depicted in figure 6-4: the heater rods in the central bundle (hot rods), the heater rods near the housing (cold rods), the thimble guide tubes, and the housing wall and solid fillers. Together with the droplet and vapor phases, a radiation network with six radiating nodes is solved, as illustrated in figure 6-5.

The radiation resistances are calculated by

$$\frac{1}{R_{ii}} = \frac{\epsilon_w}{1 - \epsilon_w} A_i \quad \left. \begin{array}{l} \\ \\ \end{array} \right\} \quad (6-13)$$

$$\frac{1}{R_{ij}} = (1 - \epsilon_i)(1 - \epsilon_v) A_i F_{ij} \quad \left. \begin{array}{l} \\ \\ \end{array} \right\} \quad i, j = 1, 2, 3, 4 \quad (6-14)$$

$$\frac{1}{R_{ii}} = \epsilon_i(1 - \epsilon_v) A_i \quad \left. \begin{array}{l} \\ \\ \end{array} \right\} \quad (6-15)$$

$$\frac{1}{R_{iv}} = \epsilon_v(1 - \epsilon_i) A_i \quad \left. \begin{array}{l} \\ \\ \end{array} \right\} \quad (6-16)$$

$$\frac{1}{R_{lv}} = \epsilon_i \epsilon_v \sum_{i=1}^4 A_i \quad (6-17)$$

-
1. Sun, K.H., et al., "Calculations of Combined Radiation and Convection Heat Transfer in Rod Bundles Under Emergency Cooling Conditions," J. Heat Transfer 98, ASME, 414-420 (1976).
 2. Yao, S.C., et al., "A Simple Method for Calculating Radiative Heat Transfer in Rod Bundles With Droplets and Vapors as Absorbing Media" (Technical Note), J. Heat Transfer 101, ASME, 736 (1979).

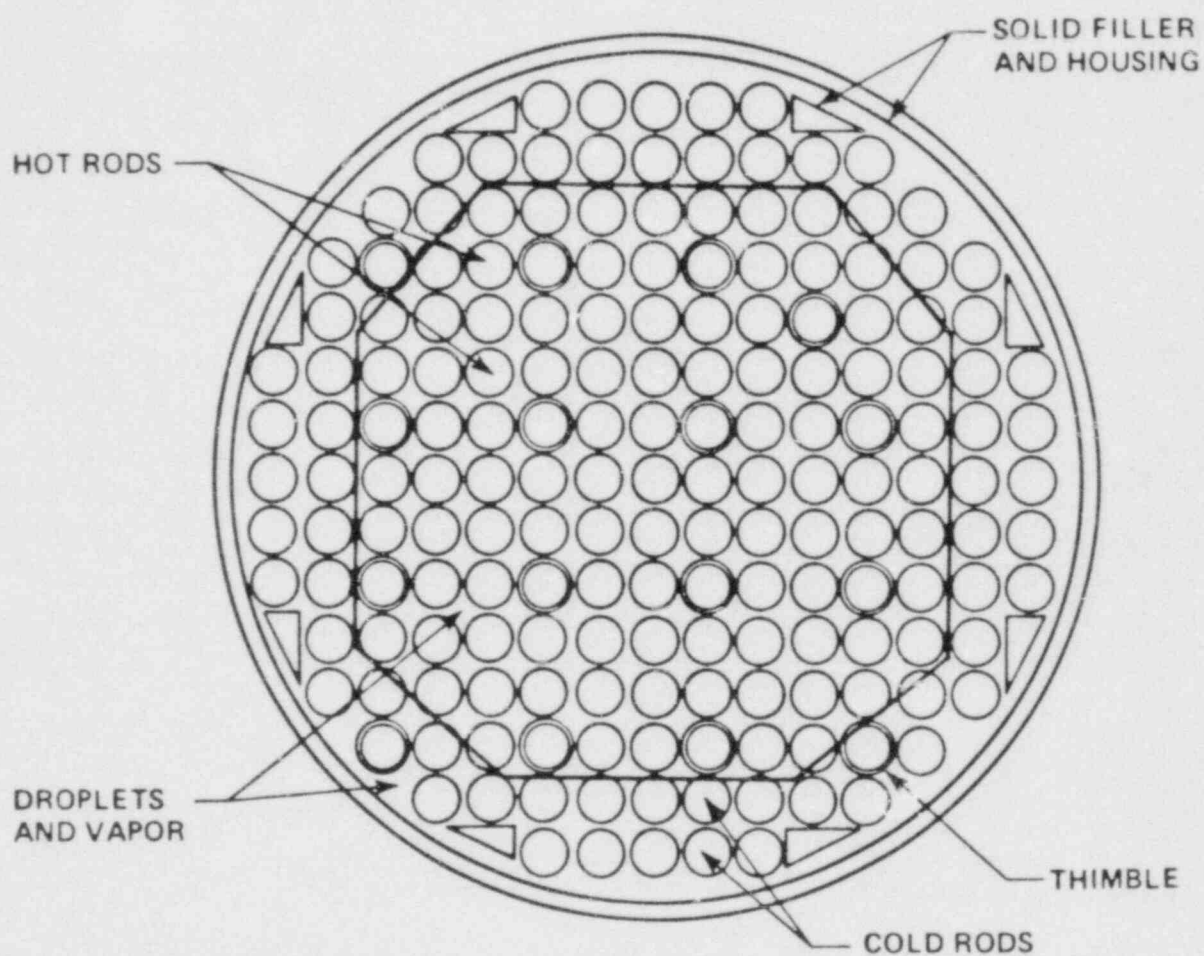


Figure 6-4. Six Radiation Nodes for Calculating Radiation Heat Transfer in FLECHT SEJET 161-Rod Bundle

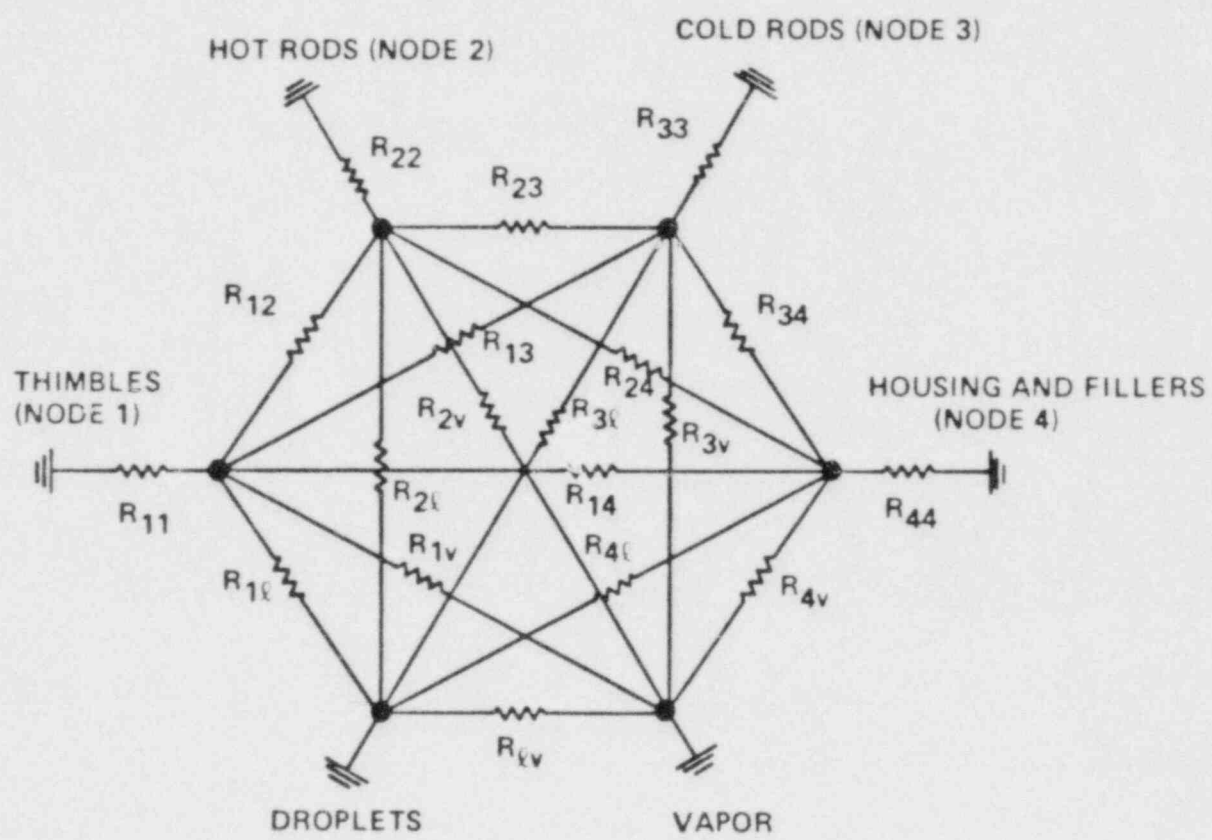


Figure 6-5. Radiation Network for Calculating Radiation Heat Transfer in FLECHT SEASET 161-Rod Bundle

where

A_i = radiating area per unit length for the i -th radiating wall surface group [m (ft)]

ϵ_w = wall emissivity

F_{ij} = view factor from i -th to j -th radiating wall surface group

The view factors between the radiating wall surface groups are calculated by

$$A_i F_{ij} = \sum_{k=1}^{N_i} A_{k\text{-th rod in group } i} \sum_{l=1}^{N_j} F_{k\text{-th rod in group } i \rightarrow l\text{-th rod in group } j} \quad (6-18)$$

where

N_i, N_j = number of rods in i -th and j -th radiating wall surface group, respectively

$A_{k\text{-th rod in group } i}$ = radiating area per unit length of k -th rod in i -th radiating surface group [m (ft)]

$F_{k\text{-th rod in group } i \rightarrow l\text{-th rod in group } j}$ = view factor from k -th rod in i -th radiating surface group to l -th rod in j -th radiating surface group

The view factors between individual rods can be computed from the known geometric configuration (for instance, by the cross string method described by Hottel and Sarofim). In the present work, the view factors between individual rods were calculated by the MOXY computer code as described by Evans.⁽¹⁾

I. Evans, D.R., The MOXY Core Heat Transfer Code: Model Description and User's Guide, Idaho National Engineering Laboratory, PG-R-76-003, December 1976.

Once the radiation resistances have been calculated, the solution of the radiation network is straightforward, and is similar to the solution of an electrical network. Detailed solution are omitted here; sample calculations have been presented by Yao et al.⁽¹⁾

6-7. FLECHT SEASET TEST RUNS ANALYZED

The analysis described in paragraphs 6-4 through 6-6 is programmed in a computer code called HEAT-II. FLECHT SEASET reflood test runs analyzed by HEAT-II are divided into two categories:

- Reflood test runs with available droplet distribution data

Four reflood tests were analyzed by the HEAT-II code using available droplet distribution data at time periods during which droplet movies were taken. These four reflood test runs are summarized in table 6-1 for reference.

- Reflood test runs analyzed by an input Sauter Mean Diameter (SMD) at the transition front

Seven reflood test runs, summarized in table 6-2, were analyzed by the HEAT-II code using an input SMD. The seven reflood tests (excluding run 34006) cover a reasonable range of test parameters and are the same tests chosen for the FLEMB analyzed (see table 4-1). Run 34006 was not analyzed by HEAT-II because the interpolation schemes on FLEMB data, described in appendix C, give negative vapor temperatures near the bundle exit. The input SMD for runs 31504 and 31701 were taken from the time-averaged values in tables F-2 and F-3, respectively. Data-based SMDs for the other five tests in table 6-2 are not available. Because of insufficient data, no attempt has been made to correlate the measured drop size with reflood test parameters. However, it is reasonable to assume that the drop size depends on the flooding rate and increases as the flooding rate increases. For runs 32013, 31922, 31805, and 31203, it was assumed that the SMD is the same as

1. Yao, S.C., et al., "A Simple Model for Calculating Radiative Heat Transfer in Rod Bundles with Droplets and Vapor as Absorbing Media" (Technical Note), J. Heat Transfer 101, ASME, 736 (1979).

TABLE 6-1
 REFLOOD TEST RUNS WITH AVAILABLE DROPLET DISTRIBUTION DATA
 ANALYZED BY HEAT-II CODE^(a)

Run	Time of Movie ^(b) (sec)	Movie Camera Elevation [m (in.)]	Times of Analysis (sec)
30921	20-26	1.83 (72)	20, 23, 26
31504	200-206	1.83 (72)	200, 210
31701	2-9	0.91 (36)	5, 10
31701	1-8	2.74 (108)	5, 10
32114	18-24	0.91 (36)	18, 21, 24
32114	20-30	2.74 (108)	20, 26, 30

a. For test conditions, see table E-4, appendix E.

b. Time zero corresponds to beginning of flooding.

TABLE 6-2
REFLOOD TEST RUNS WITH AN INPUT SMD AT TRANSITION
FRONT ANALYZED BY HF A1-II CODE^(a)

Run	Time of Analysis ^(b) (sec)	SMD ^(c) at Transition Front [mm (in.)]	Runs From Which SMD Was Taken
31203	30, 50, 70, 80, 90, 100, 110, 120	1.18 (0.0463)	31504
31302	10, 20, 30, 40	1.31 (0.0517)	Average of 31504 and 31701
31504	80, 100, 120, 140, 160, 180, 200, 210	1.18 (0.0463)	31504
31701	5, 10, 15, 20	1.45 (0.0570)	31701
31805	80, 100, 130, 160, 200, 230, 260, 280	1.18 (0.0463)	31504
31922	50, 70, 90, 110, 130, 150, 170, 190	1.18 (0.0463)	31504
32013	50, 70, 90, 110, 130, 150, 170, 190	1.18 (0.0463)	31504

- a. For test conditions, see table 4-1.
- b. Time zero corresponds to beginning of flooding.
- c. Sauter Mean Diameter, assumed independent of time

that of run 31504; for run 313L2, the SMD was taken to be the average of those of runs 31504 and 31701. The time period which the analysis covered included a reasonable period of flooding time before or shortly after the 1.83 m (72 in.) elevation was quenched.

It should be noted that run 31504 appears in both tables 6-1 and 6-2. The results from this reflood test are used to establish the validity of characterizing a drop size distribution by the SMD in the present heat transfer analysis.

6-8. CALCULATED FLOW CONDITIONS AND BASIC HEAT TRANSFER COMPONENTS IN DISPERSED FLOW REGIME

A unique feature of the present analysis is the extensive use of the droplet data obtained from the FLECHT SEASET high-speed movies. The movies were analyzed in detail by using a movie projector which had the capability to project and stop the movies frame by frame; droplet size and velocities were then measured by tracing the drops through successive frames. Details of the droplet movie analysis can be found in appendix E.

The droplet information was used to calculate bundle average flow conditions and basic heat transfer components as functions of axial position in the dispersed flow regime (above the transition front) by methods described in appendix F and paragraphs 6-4 through 6-6. A computer code, HEAT-II, was developed to perform the analysis.

Measured drop size distribution is shown in appendix E. Comparisons between measured and calculated drop velocities are shown in figures F-2 through F-7. Calculated drop size distribution and Sauter Mean Diameter (SMD) at the transition front are shown in tables F-1 through F-6. The following paragraphs illustrate typical axial variation of vapor void fraction, vapor Reynolds number, optical thickness of the two-phase media, drop size distribution, and vapor and droplet velocities, using the results of run 31504. Relative contributions of thermal radiation and convection at different elevations during reflood are also illustrated by run 31504. The validity of using the SMD to characterize a drop size distribution is also demonstrated. Finally, the calculated heat flux of all reflood test runs in table 6-2 is correlated with the vapor Reynolds number and droplet volume fraction in order to illustrate the significance of the convective heat transfer enhancement due to the presence of the water droplets.

Typical data-based wall temperature, steam temperature, and quality (see appendix C) are shown in figure 6-6 for reference. The calculated vapor void fraction and vapor Reynolds number are shown in figures 6-7 and 6-8. Note that results for the droplet spectrum and the SMD are practically identical after a short distance above the transition front. The vapor void fraction increases rapidly above the transition front to nearly 1 (>0.99). The vapor Reynolds number is directly proportional to the vapor velocity and inversely proportional to the vapor specific volume or absolute vapor temperature. The effect of vapor temperature dominates and the vapor Reynolds number varies inversely with the vapor temperature (compare figure 6-8 with figure 6-6). The calculated optical thickness for the vapor and droplet media is shown in figure 6-9. Since the optical thickness is generally less than 1, the assumption of an optically thin dispersed medium is valid and the radiation network model described in paragraph 6-6 is applicable.

As shown in figure 6-10, the drop sizes decrease monotonically because of the continuous evaporation in the superheated steam. The increase in evaporation rate, as indicated by the change in slope at the 2.44 m (96 in.) elevation corresponds to the increase in the slope of the input steam quality (figure 6-6). Also, it is to be noted that the smallest drop size group evaporates rapidly and the drop diameter approaches zero near the bundle exit [3.66 m (144 in.) elevation]. Because of the very small drop diameter, drops belonging to this drop size group accelerate very rapidly and approach the vapor velocity (that is, the slip ratio for these drops approaches one) as shown in figure 6-11. In reality, these small drops will be completely evaporated before they reach the bundle exit. As explained at the end of paragraph F-1, these drops were kept in the numerical calculations for the sole purpose of efficient programming. Finally, note again the close agreement of the vapor velocities calculated by using the drop size spectrum and the SMD.

Basic heat transfer components, convection and radiation, were calculated by the method described in paragraphs 6-5 and 6-6; the results are shown in table 6-3 and figure 6-12. It is apparent from table 6-3 that one can obtain satisfactory heat transfer results by replacing the drop spectrum method with the SMD method. Figure 6-12 shows the relative contribution of convective heat flux during reflood, calculated by using an input SMD at the transition front (see table 6-2). At higher

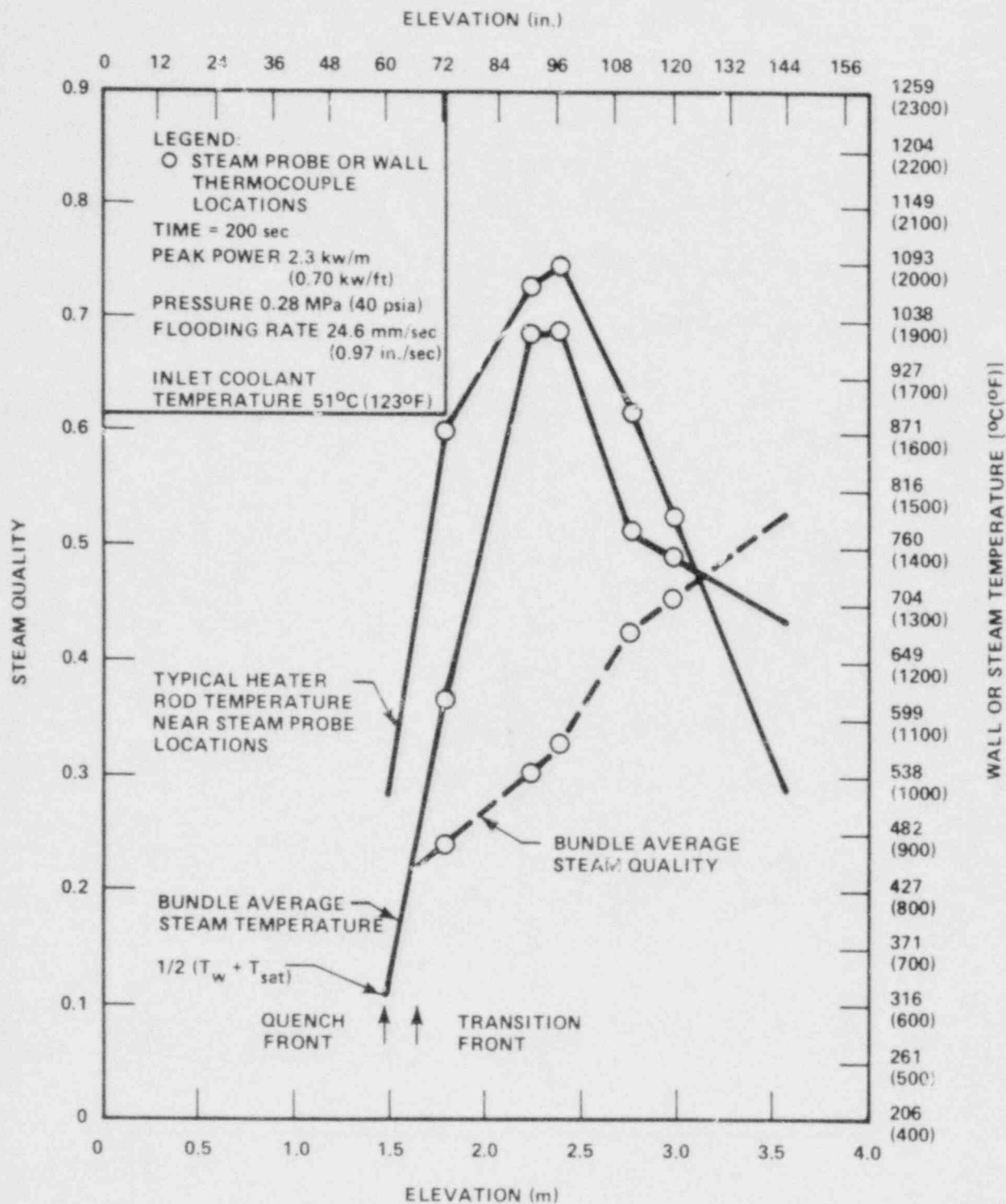


Figure 6-6. Data-Based Wall Temperature, Steam Temperature, and Steam Quality

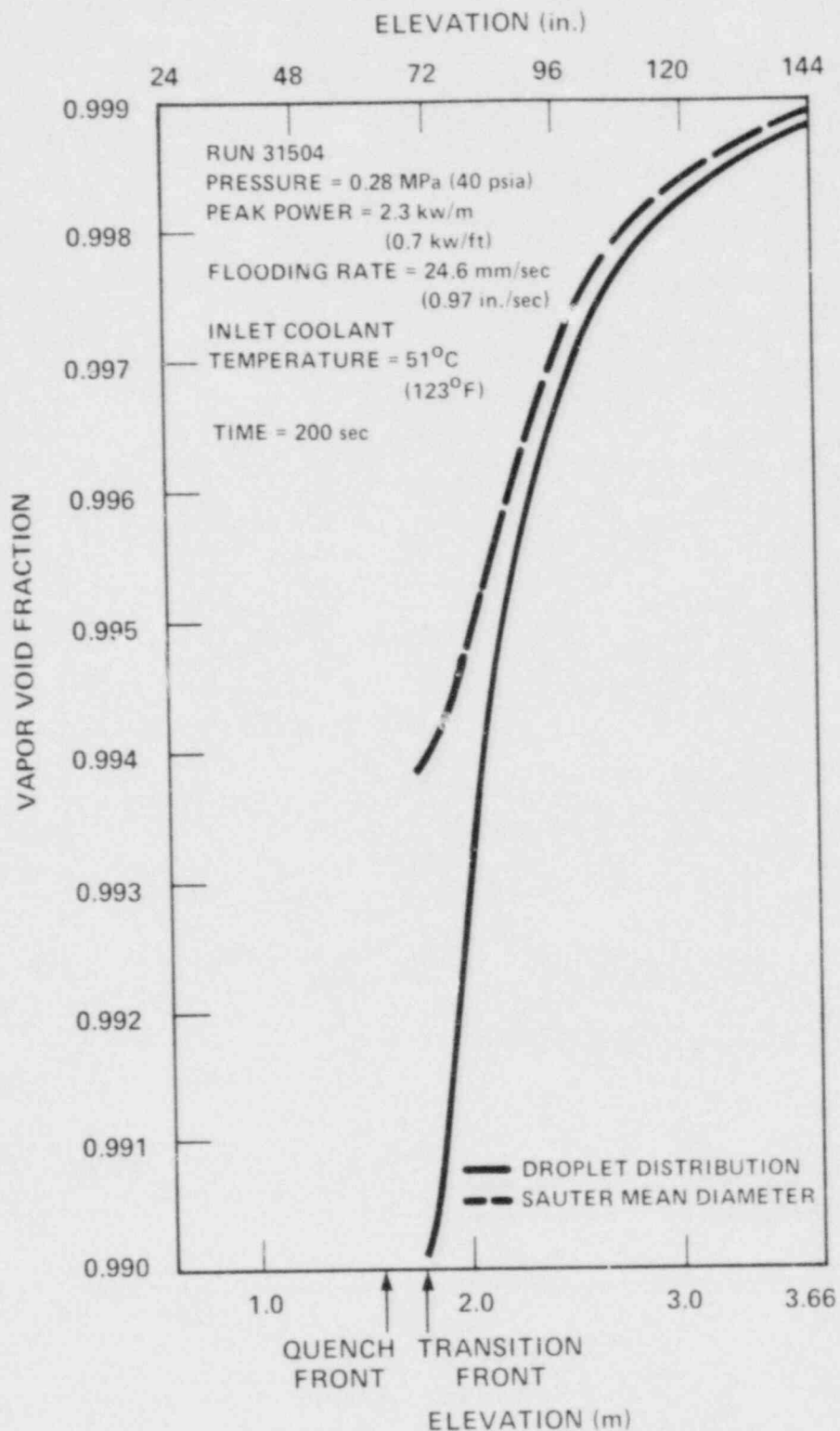


Figure 6-7. Calculated Vapor Void Fraction in Dispersed Flow Regime

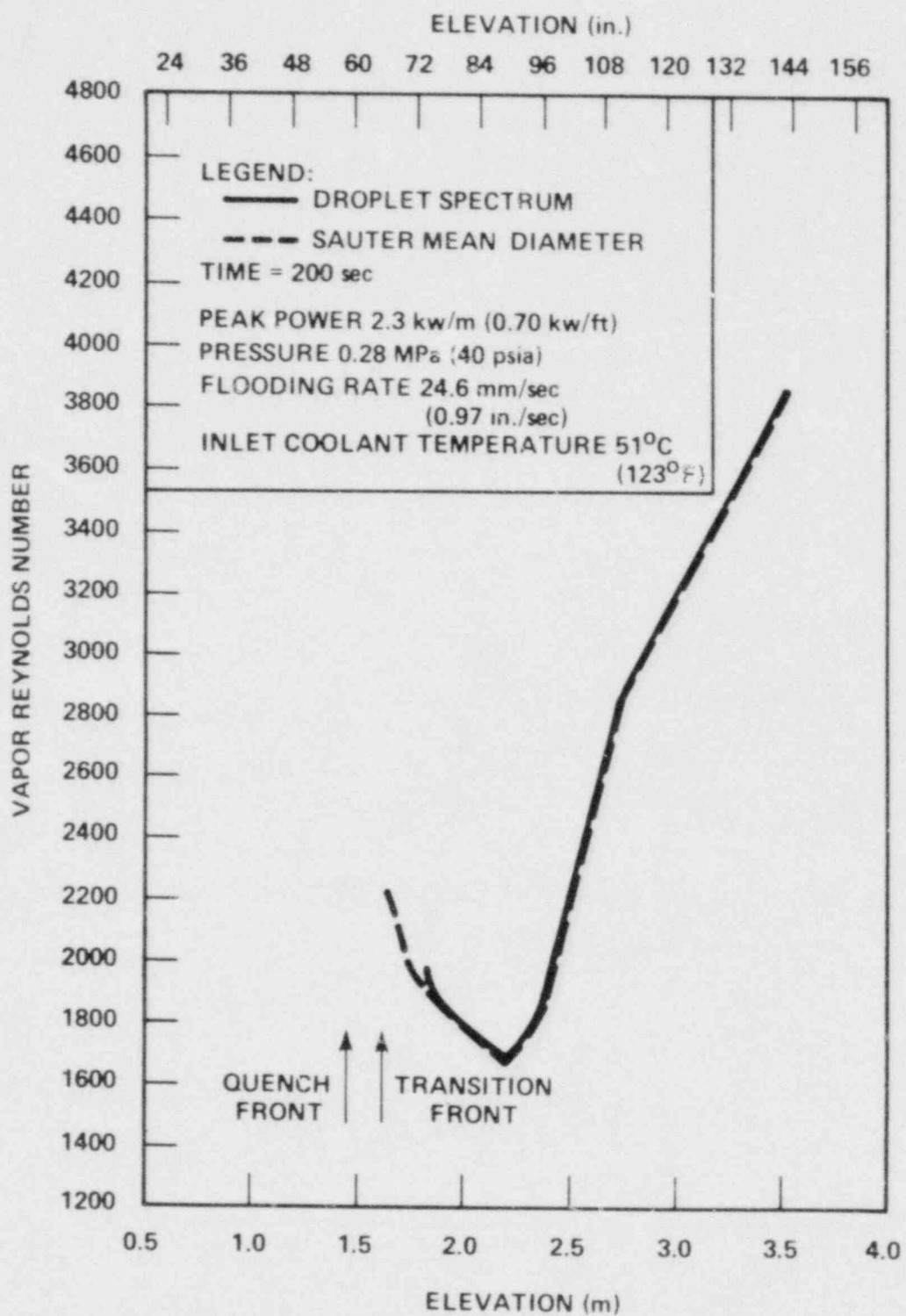


Figure 6-8. Calculated Vapor Reynolds Number in Dispersed Flow Regime

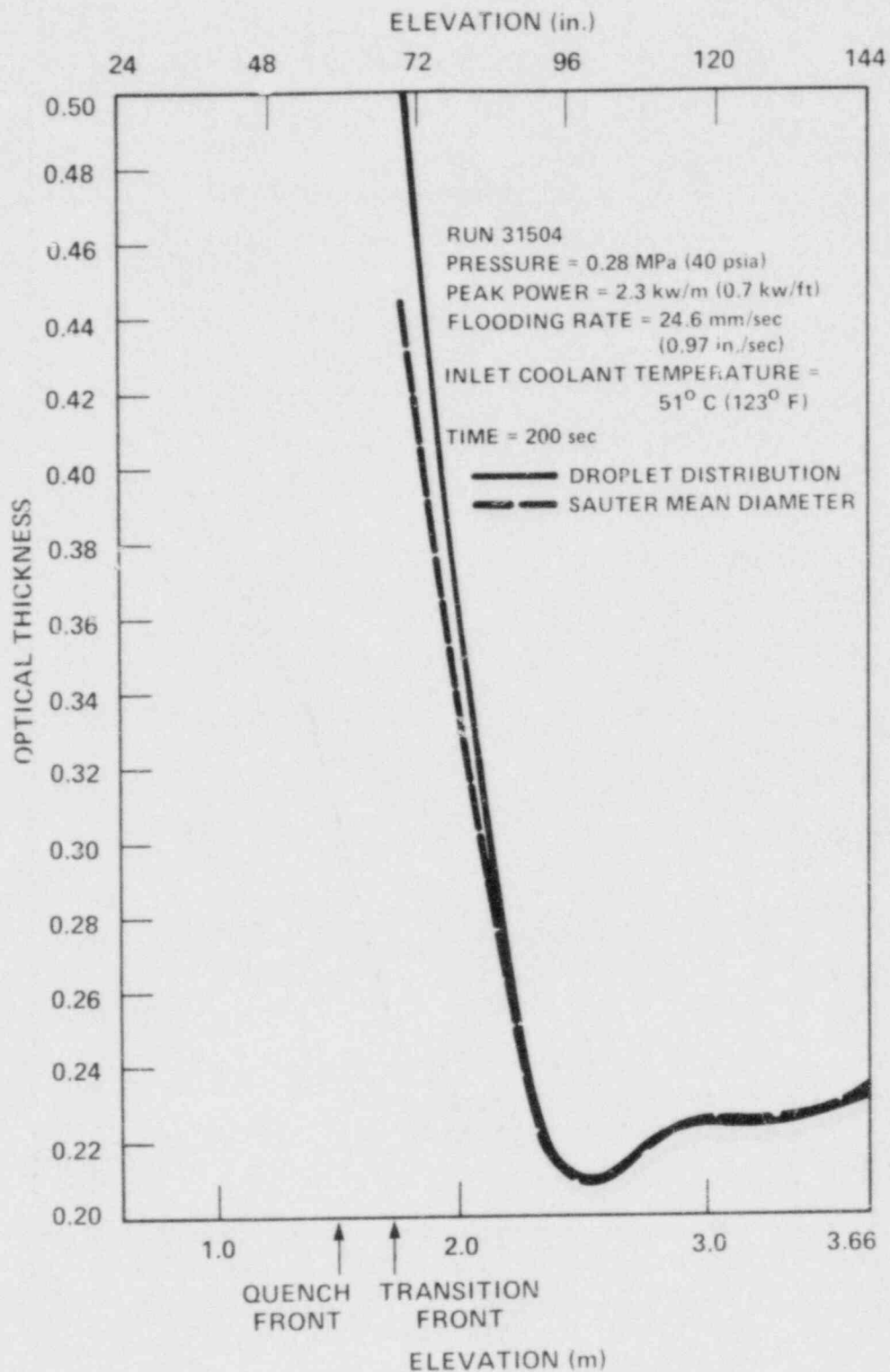


Figure 6-9. Calculated Optical Thickness in Dispersed Flow Regime

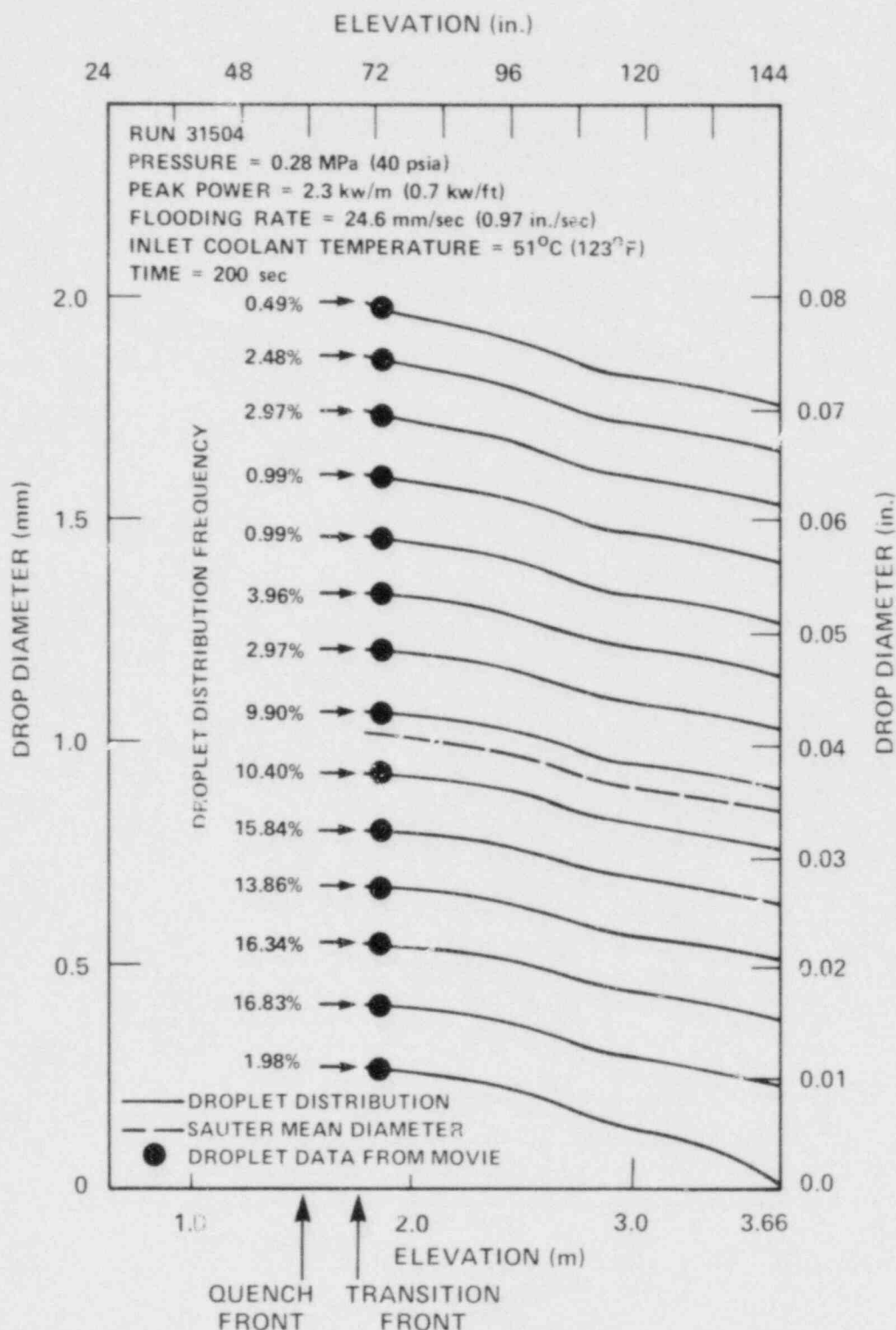


Figure 6-10. Calculated Drop Sizes in Dispersed Flow Regime

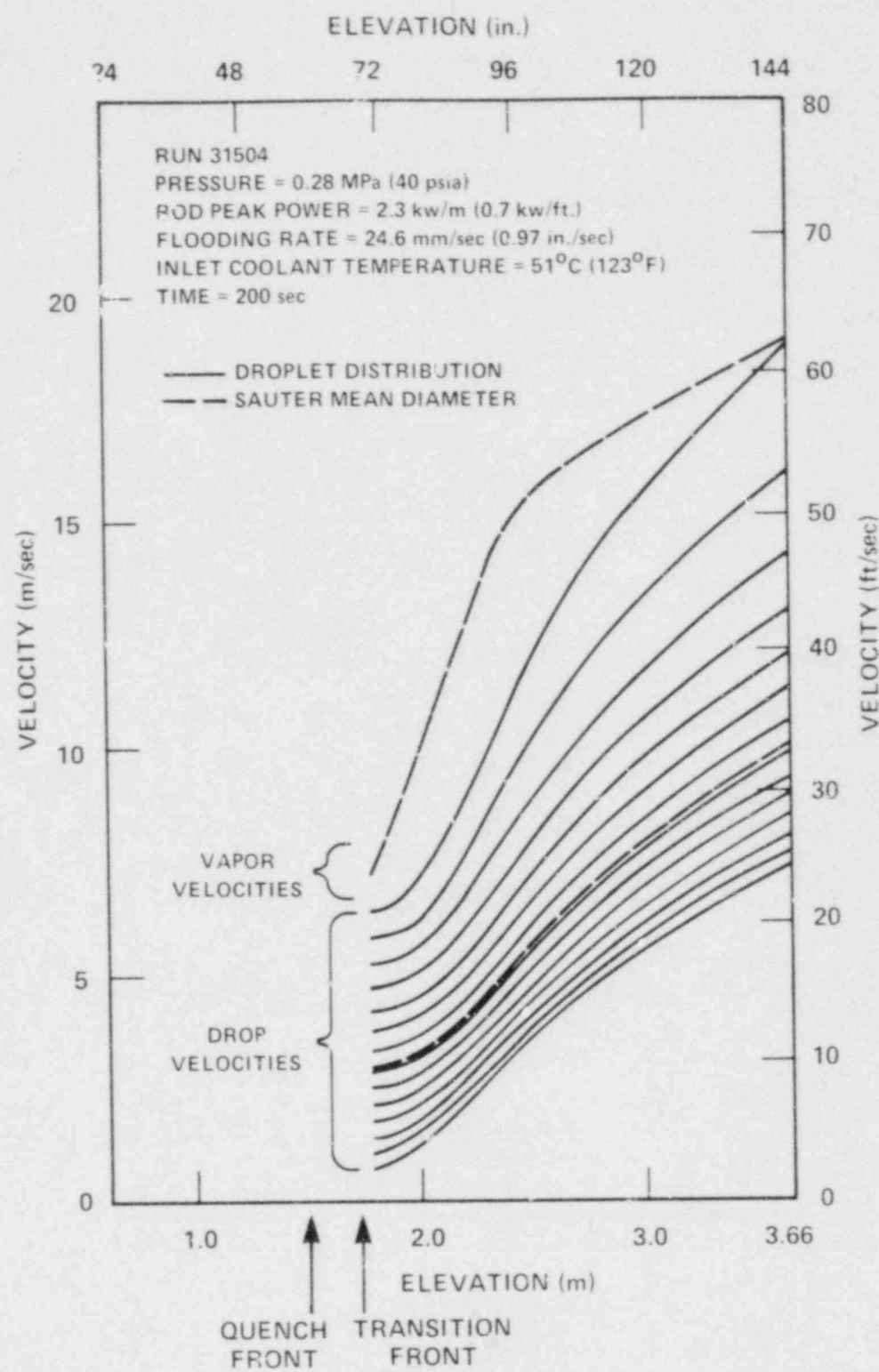


Figure 6-11. Calculated Drop and Vapor Velocities in Dispersed Flow Regime

TABLE 6-3
BASIC HEAT TRANSFER COMPONENTS IN DISPERSED
DROPLET FLOW DURING REFLOOD

Run 31504		Time = 200 sec		
Rod peak power = 2.3 kw/m (0.7 kw/ft)		Quench front = 1.51 m (59.6 in.)		
Flooding rate = 24.6 mm/sec (0.97 in./sec)		Transition front = 1.68 m (66 in.)		
Inlet coolant temp. = 51° C (123° F)		SMD (Sauter Mean Diameter) at transition		
Pressure = 0.28 MPa (40 psia)		front = 1.18 mm (0.0463 in.)		
Parameter ^(a)	Value at Indicated Elevation			
	Near Transition Front [1.83 m (72 in.) Elevation]		Away From Transition Front [3.05 m (120 in.) Elevation]	
	Drop Spectrum Method	SMD Method	Drop Spectrum Method	SMD Method
Q_T (hot) [kw/m (kw/ft)]	242.75 (73.899)	242.45 (73.899)	51.77 (15.78)	51.77 (15.78)
Q_{cv} (hot)/ Q_T (hot)	0.8340	0.8414	0.5304	0.5297
Q_R (hot)/ Q_T (hot)	0.1660	0.1586	0.4696	0.4703
Q_T (cold) [kw/m (kw/ft)]	161.33 (49.173)	161.33 (49.173)	42.12 (12.84)	42.12 (12.84)
Q_{cv} (cold)/ Q_T (cold)	0.7378	0.7441	0.3200	0.3195

a. Q_T = total heat release

Q_{cv} = convective heat release

Q_R = radiative heat release

$\Sigma Q_R = Q_R$ (hot) + Q_R (cold)

hot = hot rods (see figure 6-4)

cold = cold rods (see figure 6-4)

thim = thimbles (see figure 6-4)

hous = housing (see figure 6-4)

TABLE 6-3 (cont)
BASIC HEAT TRANSFER COMPONENTS IN DISPERSED
DROPLET FLOW DURING REFLOOD

Parameter ^(a)	Value at Indicated Elevation			
	Near Transition Front [1.83 m (72 in.) Elevation]		Away From Transition Front [3.05 m (120 in.) Elevation]	
	Drop Spectrum Method	SMD Method	Drop Spectrum Method	SMD Method
Q_R (cold)/ Q_T (cold)	0.2622	0.2559	0.6800	0.6805
ΣQ_R [kw/m (kw/ft)]	82.55 (25.16)	79.74 (24.30)	52.95 (16.14)	53.61 (16.16)
Q_R (hot)/ ΣQ_R	0.4875	0.4823	0.4591	0.4593
Q_R (cold)/ ΣQ_R	0.5125	0.5177	0.5409	0.5407
Q_R (thim)/ ΣQ_R	-0.1189	-0.1284	-0.0509	-0.0506
Q_R (hous)/ ΣQ_R	-0.3224	-0.3397	-0.7020	-0.7011
Q_R (drop)/ ΣQ_R	-0.2867	-0.2349	-0.1347	-0.1363
Q_R (vapor)/ ΣQ_R	-0.2720	-0.2970	-0.1124	-0.1120

a. Q_T = total heat release

Q_{cv} = convective heat release

Q_R = radiative heat release

ΣQ_R = Q_R (hot) + Q_R (cold)

hot = hot rods (see figure 6-4)

cold = cold rods (see figure 6-4)

thim = thimbles (see figure 6-4)

hous = housing (see figure 6-4)

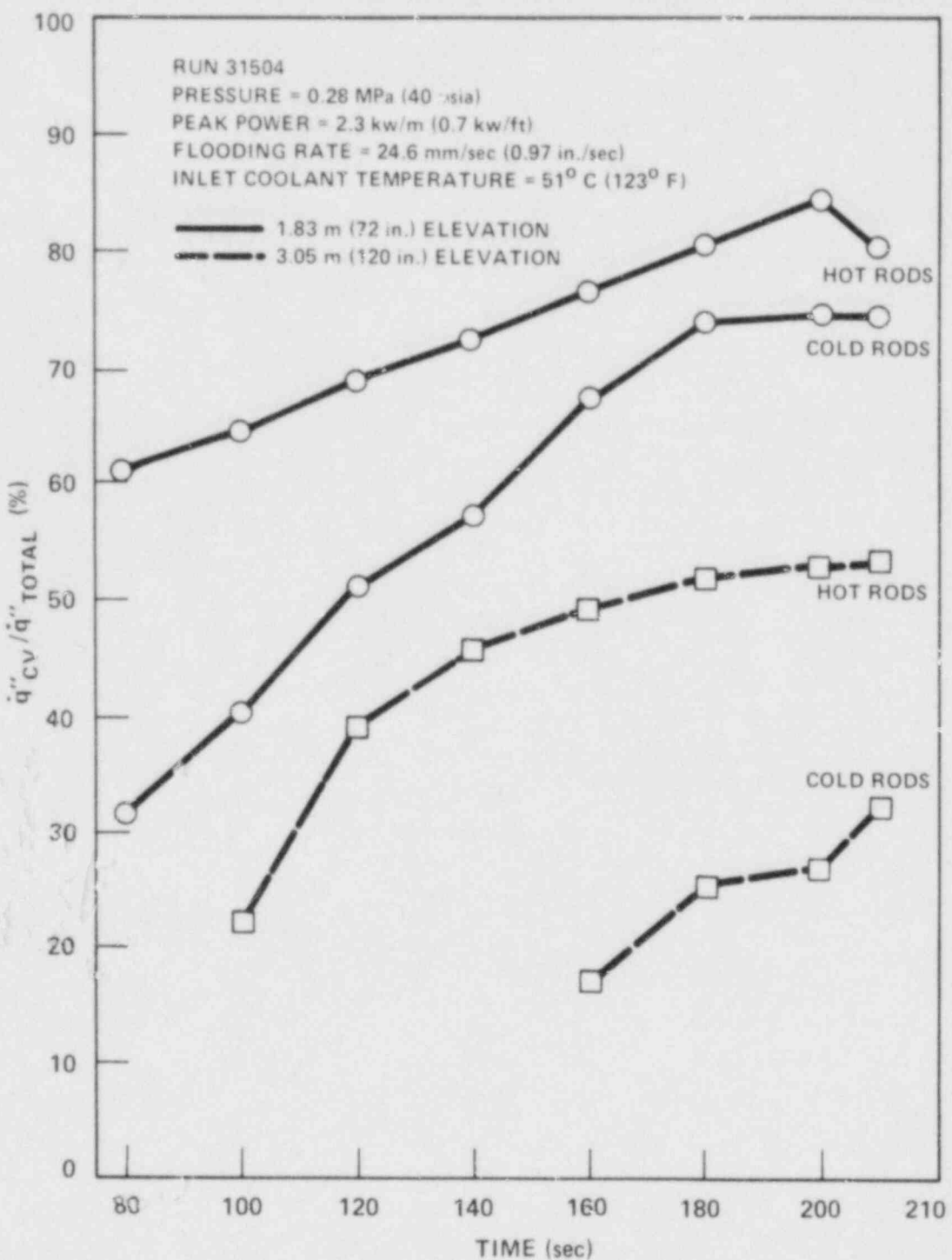


Figure 6-12. Relative Contribution of Convective Heat Flux During Reflood at 1.83 m (72 in.) and 3.05 m (120 in.) Elevations

elevations, because of the lower power, total heat release from the rods is small, and radiation accounts for a large fraction of the total heat release. However, the absolute magnitude of the radiation heat release is smaller at higher elevations than at lower elevations. As the magnitude of the convective heat transfer and radiation to drops decreases at higher elevations, surface-to-surface radiation becomes important.

From the above considerations, it is clear that radiative heat exchange among the vapor and droplet media and the rod bundle system is important during reflood, and cannot be neglected in best-estimate dispersed flow models.

From the calculated total and convective heat flux (paragraph 6-5), the following Nusselt numbers can be defined:

$$Nu_T = \frac{\dot{q}_T''}{T_w - T_v} \frac{D_h}{k} \quad (6-20)$$

$$Nu_{cv} = \frac{\dot{q}_{cv}''}{T_w - T_v} \frac{D_h}{k} \quad (6-21)$$

where

- Nu_T = Nusselt number based on total wall heat flux
- Nu_{cv} = Nusselt number based on convective wall heat flux
- T_w = wall surface temperature [$^{\circ}\text{C}$ ($^{\circ}\text{F}$)]
- T_v = vapor temperature [$^{\circ}\text{C}$ ($^{\circ}\text{F}$)]
- k = vapor conductivity [$\text{w/m-}^{\circ}\text{C}$ ($\text{Btu/ft-sec-}^{\circ}\text{F}$)]

Figures 6-13 and 6-14 show the Nusselt number, based on total and convective wall heat flux, respectively, versus the vapor Reynolds number. It should be noted that all the 1.83 m (72 in.) results in figure 6-13 are well above the Dittus-Boelter correlation. In figure 6-14, only a few points from the 1.83 m (72 in.) elevation are slightly below the Dittus-Boelter correlation. The convective heat flux, however, is based on a radiation model [see equation (6-12)]; the slight discrepancy between the few data

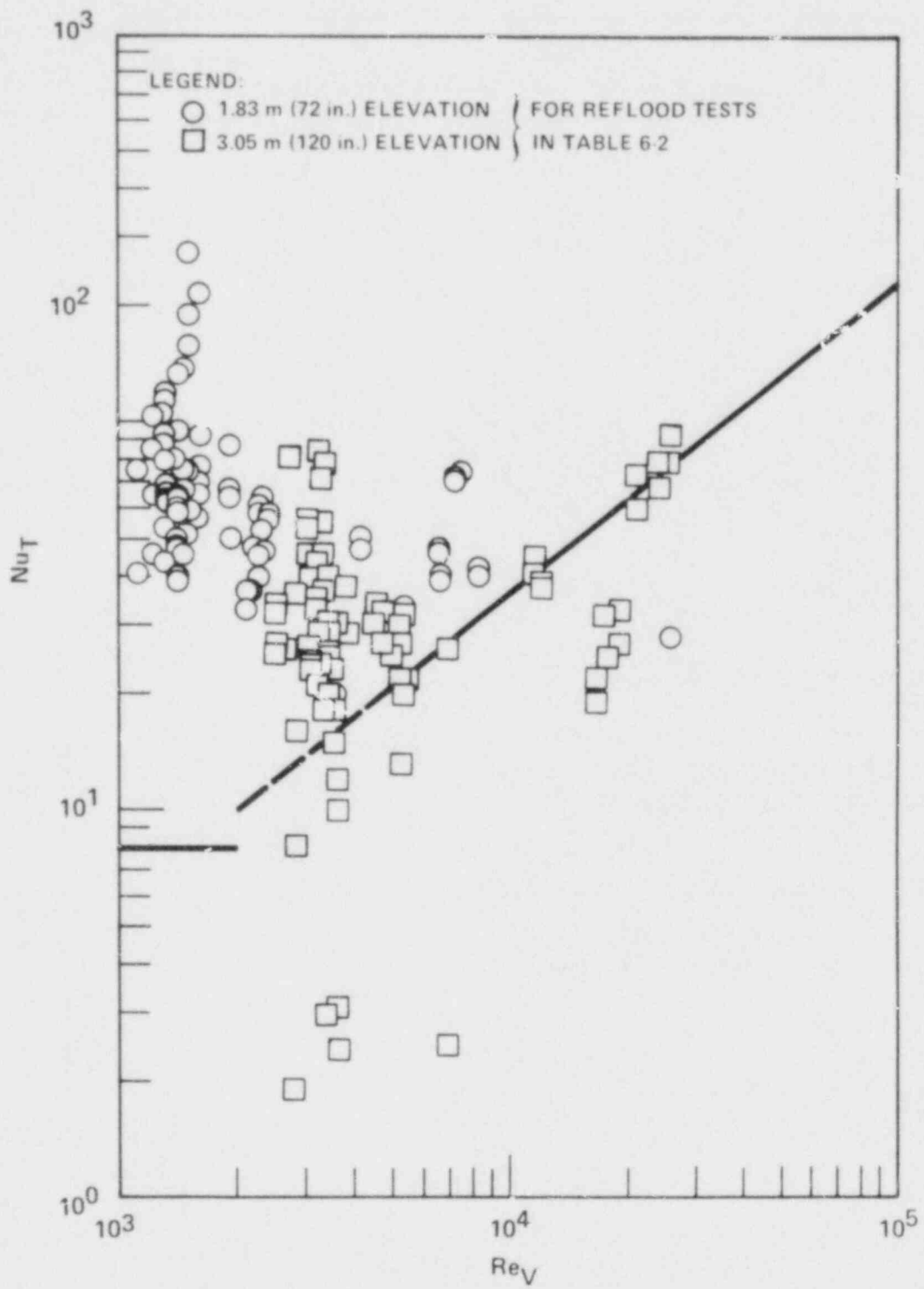


Figure 6-13. Calculated Nusselt Number (Based on Heater Rod Total Heat Flux) Versus Vapor Reynolds Number

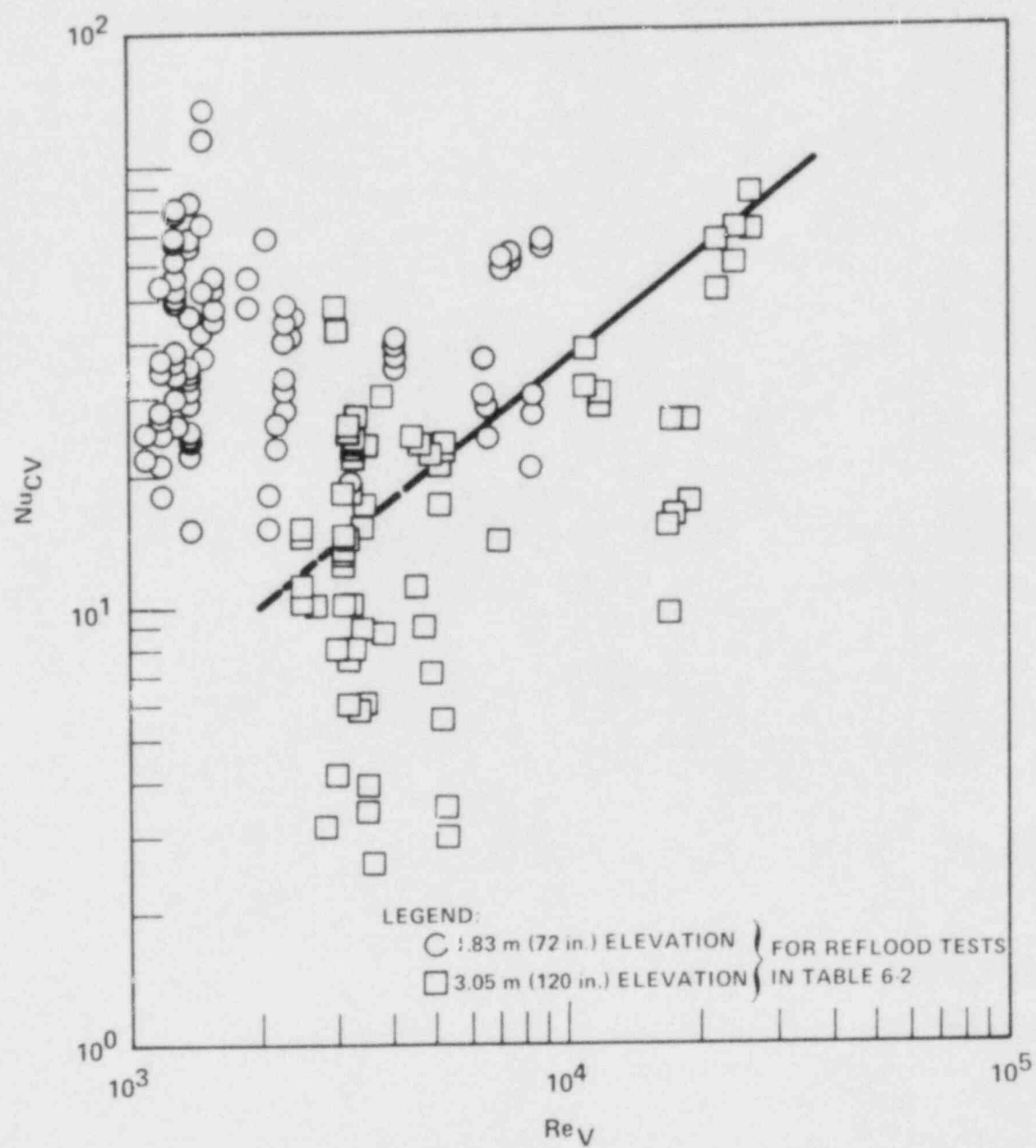


Figure 6-14. Calculated Nusselt Number (Based on Heater Rod Convective Heat Flux) Versus Vapor Reynolds Number

points and the Dittus-Boelter correlation is well within the uncertainties of the radiation model. A typical axial wall heat flux (total) distribution for a cosine-shaped power distribution above the quench front is shown in figure 6-15. The heat flux becomes negative at higher elevations [generally at 3.05 m (120 in.) or above]. The small Nusselt numbers (points well below the Dittus-Boelter correlation) shown in figures 6-13 and 6-14 are from results at the 3.05 m (120 in.) elevation and at times when the heat flux approached zero. (Results for negative heat flux are not plotted in figures 6-13 and 6-14.) Also, for low Reynolds numbers (below 10,000), figures 6-13 and 6-14 show that the Nusselt number tends to decrease as the vapor Reynolds number increases, in contrast to conventional single-phase heat transfer correlations which predict higher Nusselt numbers for higher Reynolds numbers. For higher Reynolds numbers (above 20,000), the results tend to converge to the Dittus-Boelter correlation.

These observations clearly indicate the significance of the role of the droplets in enhancing the heat transfer between the heated wall and the dispersed flow during reflood, especially at low Reynolds numbers. At low Reynolds numbers (in the laminar or laminar-turbulent transition regime) and without the presence of droplets, molecular conduction would be the only means of removing heat from the hot wall surfaces. The presence of evaporating drops may enhance the heat transfer by lowering the bulk vapor temperature and flattening the vapor temperature profile,⁽¹⁾ or by increasing the turbulence level because of the slip between the droplets and vapor phase, which would also increase the effective conductivity of the vapor phase. At high Reynolds numbers (in the fully-developed turbulent regime), the turbulence intensity in the flow is so high that the effects of the modified temperature profile and the additional turbulence generated in the flow become insignificant, so that conventional single-phase correlations generally predict the heat transfer data well. It is reasonable to assume that, at low Reynolds numbers, the heat transfer enhancement is proportional to the droplet number density or liquid volume fraction (or one minus the vapor void fraction).

I. Analytical investigation of the vapor temperature profile in the presence of evaporating droplets was first performed by K.H. Sun, et al., "Calculations of Combined Radiation and Convection Heat Transfer in Rod Bundles Under Emergency Cooling Conditions," J. Heat Transfer 98, 414-426 (1976).

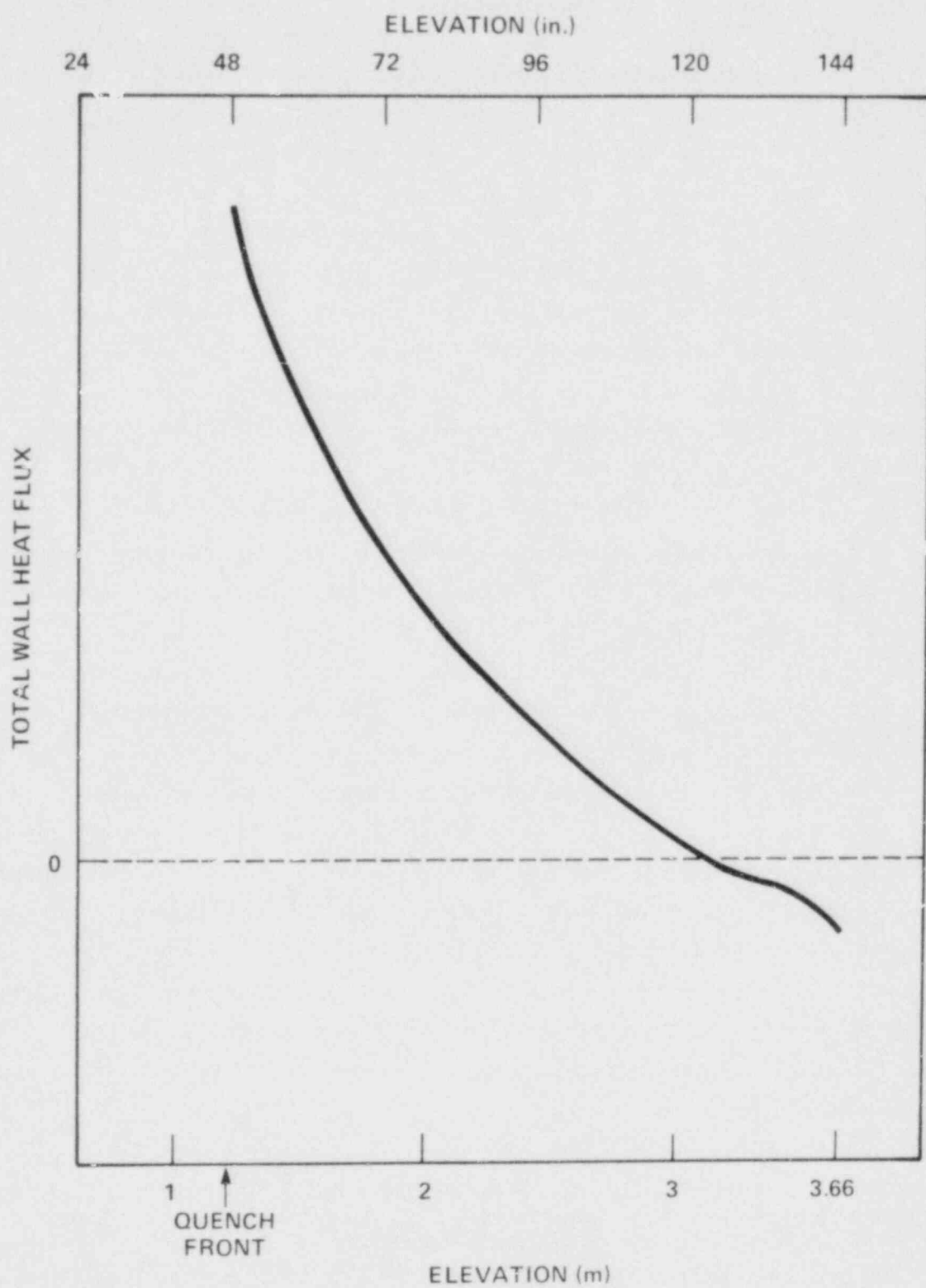


Figure 6-15. Typical Wall Heat Flux Axial Distribution for a Cosine-Shaped Power Profile Heater Rod During Reflood

Figure 6-16 illustrates the relationship between the Nusselt number and liquid volume fraction at low to moderate Reynolds numbers. Figure 6-16 shows a definite increase in heat transfer as the liquid volume fraction increases. The scattering of data in the figure is due to the dependence of heat transfer on other reflood test parameters. Correlation of the heat transfer with the test parameters is given in section 8.

From the above considerations, it is clear that adequate reflood heat transfer modeling must include the effects of the droplets and various radiation components. Using information derived in this section and appendix F as boundary conditions, a predictive dispersed flow heat transfer model is proposed in section 7 which takes into account the enhancement of the convective wall heat flux due to the evaporating drops and the radiation exchange within the rod bundle system.

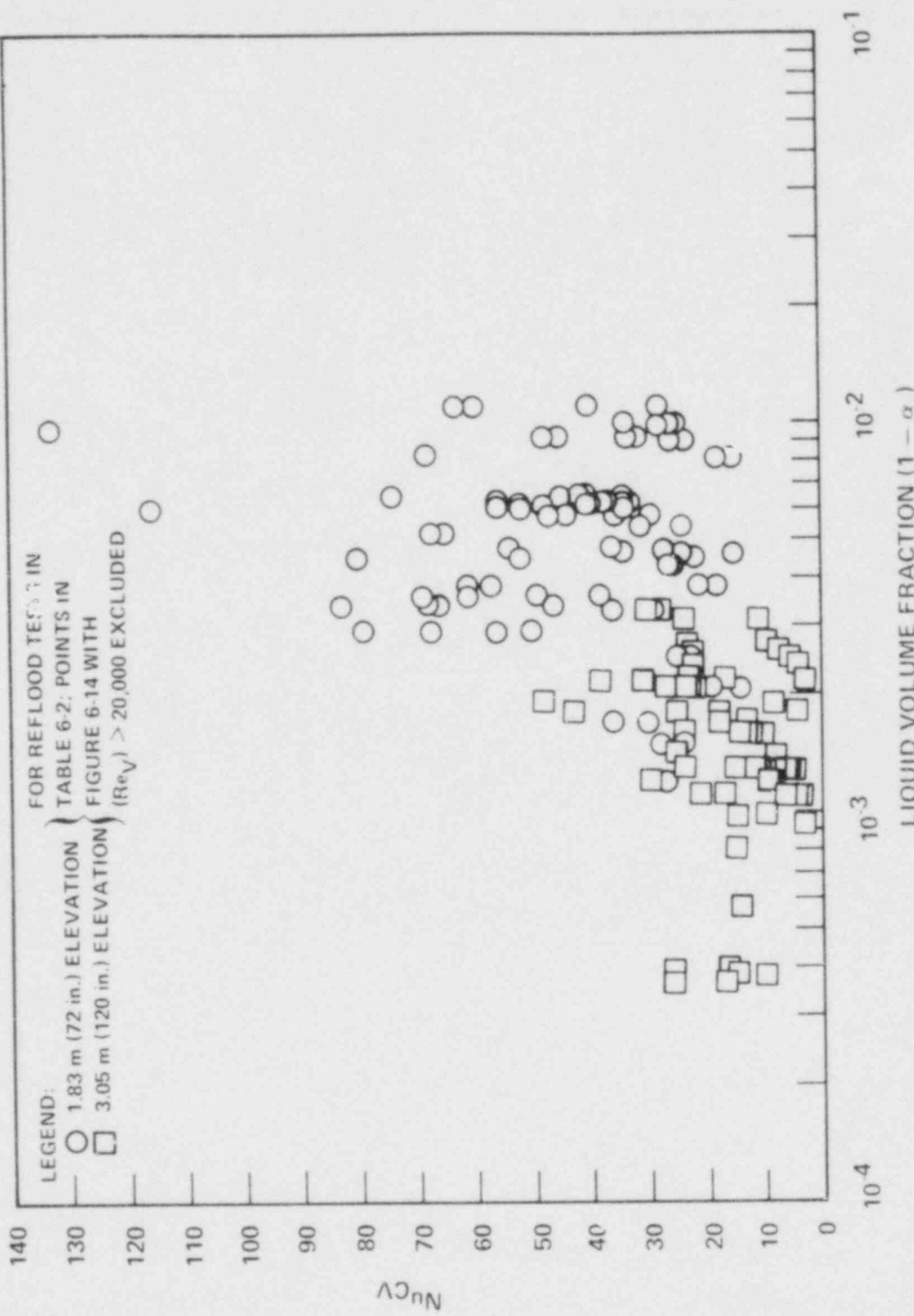


Figure 6-16. Calculated Nusselt Number (Based on Heater Rod Convective Heat Flux) Versus Liquid Volume Fraction

SECTION 7

MECHANISTIC MODEL FOR DISPERSED FLOW HEAT TRANSFER

7-1. GENERAL

In section 6, dispersed flow conditions and heat transfer were evaluated using FLECHT SEASET reflood data. This section presents a mechanistic model to predict the heat transfer and flow properties. Because the model is strictly applicable in the dispersed flow regime, input boundary conditions are required at the transition front. The required input boundary conditions are obtained from information derived from section 6 and appendix F. The model was originally developed for predictions from the FLECHT low flooding rate series cosine and skewed power profile reflood data. With minor modifications, it was also used for the present FLECHT SEASET 161-rod bundle reflood experiments. The model is outlined briefly in the following paragraphs, the input and output variables are summarized, and the calculated results are compared with data.

7-2. MODEL DESCRIPTION

Details of the model have been published;^(1,2) only an outline of the key features is given here. The model is composed of two parts: a quasi-steady-state dispersed flow model and a transient heater rod (or fuel rod) conduction model. The quasi-steady-state dispersed flow model uses input flow conditions at the onset of dispersed flow and rod surface temperature calculated by the transient heater rod model as boundary conditions, and calculates dispersed flow properties and heater rod surface heat flux. The transient heater rod model uses input rod temperature data at the first time step as initial conditions, and then uses the rod surface heat flux calculated by the dispersed flow model as a boundary condition to calculate the rod temperature transient at subsequent time steps. Table 7-1 summarizes the input and output variables of the model.

-
1. Wong, S., "A Model for Dispersed Flow Heat Transfer During Reflood," Ph.D. Thesis, Carnegie-Mellon University, Department of Nuclear Science and Engineering, 1980.
 2. Wong, S., and Hochreiter, L. E., "A Model for Dispersed Flow Heat Transfer During Reflood," paper presented at the 19th National Heat Transfer Conference, Orlando, Florida, July 27-30, 1980.

TABLE 7-1
SUMMARY OF INPUT AND OUTPUT VARIABLES FOR
DISPERSED FLOW HEAT TRANSFER MODEL

Model	Input	Output
Transient rod conduction model	<ul style="list-style-type: none"> o Input from data: Rod temperatures at the initial time step as initial conditions o Input from dispersed flow model at every time step: Calculated wall heat flux as boundary conditions 	Rod temperature transient
Quasi-steady-state dispersed flow model	<ul style="list-style-type: none"> At every time step, input as boundary condition: o Input from data: Transition front elevation, and the following quantities at the transition front: drop size, total mass flux, and steam quality o Input from transient rod model: Calculated rod surface temperature as boundary conditions for vapor temperature field 	Rod surface heat flux and the following flow properties in the dispersed flow regime: drop size, drop velocity, steam velocity, steam quality, steam temperature distributions (three-dimensional), and steam void fraction

The key feature of the model is the calculation of the convective heat flux from the rod surface to the dispersed flow. Conventionally, an empirical correlation is used to calculate this component; in the present model, a mechanistic approach is employed. A three-dimensional energy balance equation is developed for the vapor temperature field in dispersed flow; effects of droplet evaporation, mixing of the newly formed vapor, and effects of radiation heat transfer are accounted for in the energy equation. The vapor temperature distribution is then solved, and the convective heat flux is computed by the normal gradient of the vapor temperature field at the rod surface.

In the published version of the model, the calculations start at quench front. In the present work, however, the calculations start at the transition front. Also, in the previous version, it was determined by fitting the calculated steam quality with data that the best overall predictions of the skewed and cosine low flooding rate heat transfer data could be obtained by assuming the droplet velocity to be equal to the terminal velocity and by using an input drop size of 0.76 mm (0.03 in.). In the present work, an alternative approach is taken. Instead of fitting calculated steam quality with data, the droplet size at the transition front is taken to be the calculated Sauter Mean Diameter, as described in appendix F (tables F-1 through F-6), and the droplet velocity is calculated by the method described in paragraph F-1 (that is, the drop is being accelerated by the drag, gravitational, and buoyancy forces). With these modifications, predictive calculations for flow properties and heater rod temperature transitions were performed as in the previous version, and results are presented in the following paragraphs.

7-3. RESULTS AND DATA COMPARISONS

Typical results of the predictive model are illustrated using run 31504. As mentioned above, the previously published version of the model used an input drop size of 0.76 mm (0.03 in.) and assumed the drop to be at terminal velocity. In the present work, drop size at the transition front is taken to be the calculated Sauter Mean Diameter given in table F-2, and the drops are accelerated according to equation (F-12).

Figures 7-1 and 7-2 show the calculated heat absorption rate by the droplets. It is seen that the present model generally calculates a higher droplet absorption rate than the previous model. Consequently, the steam quality calculated using the present model is

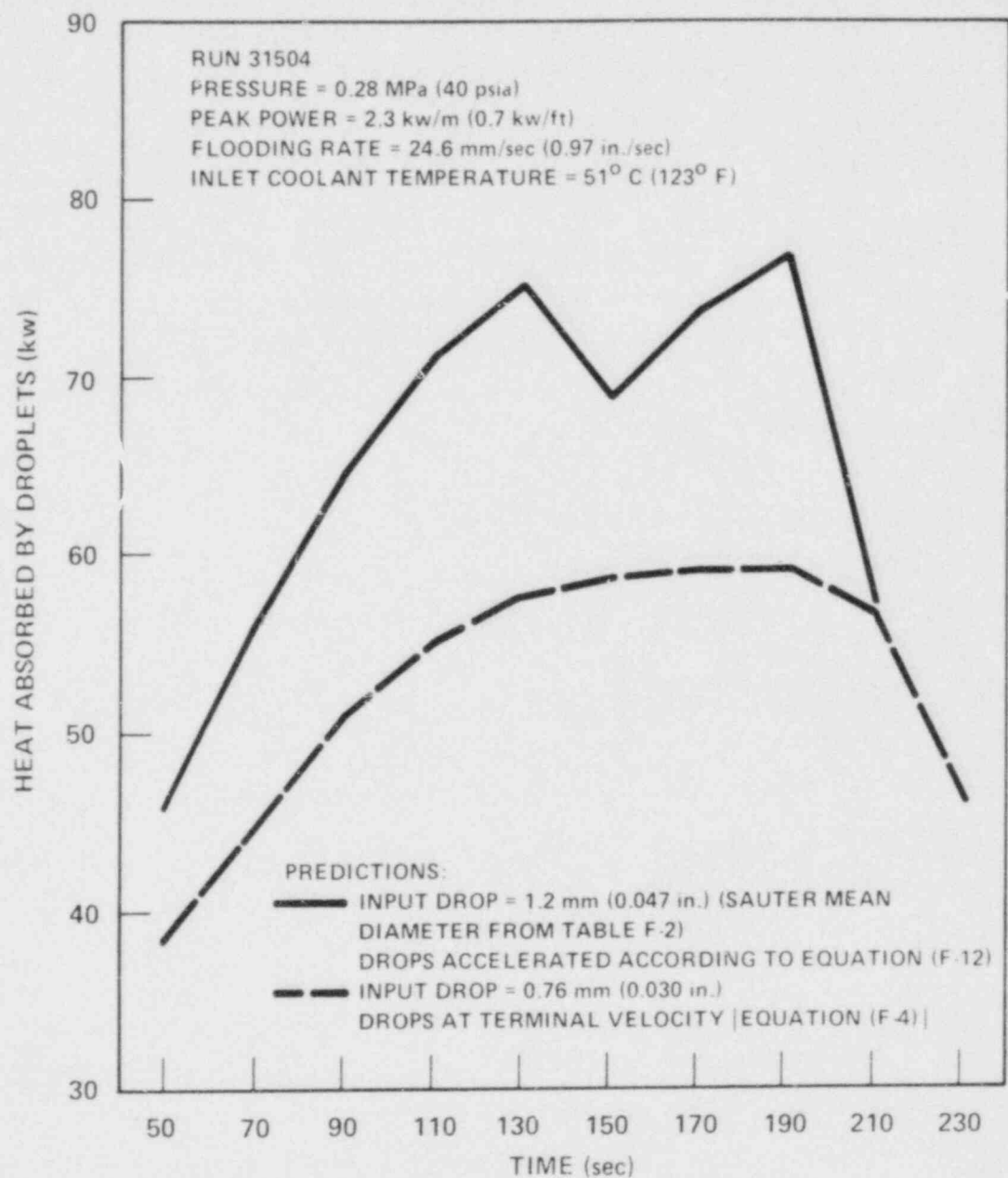


Figure 7-1. Predicted Droplet Heat Absorption Rate Between 1.83 and 2.29 m (72 and 90 in.) Elevations

$\leq L$

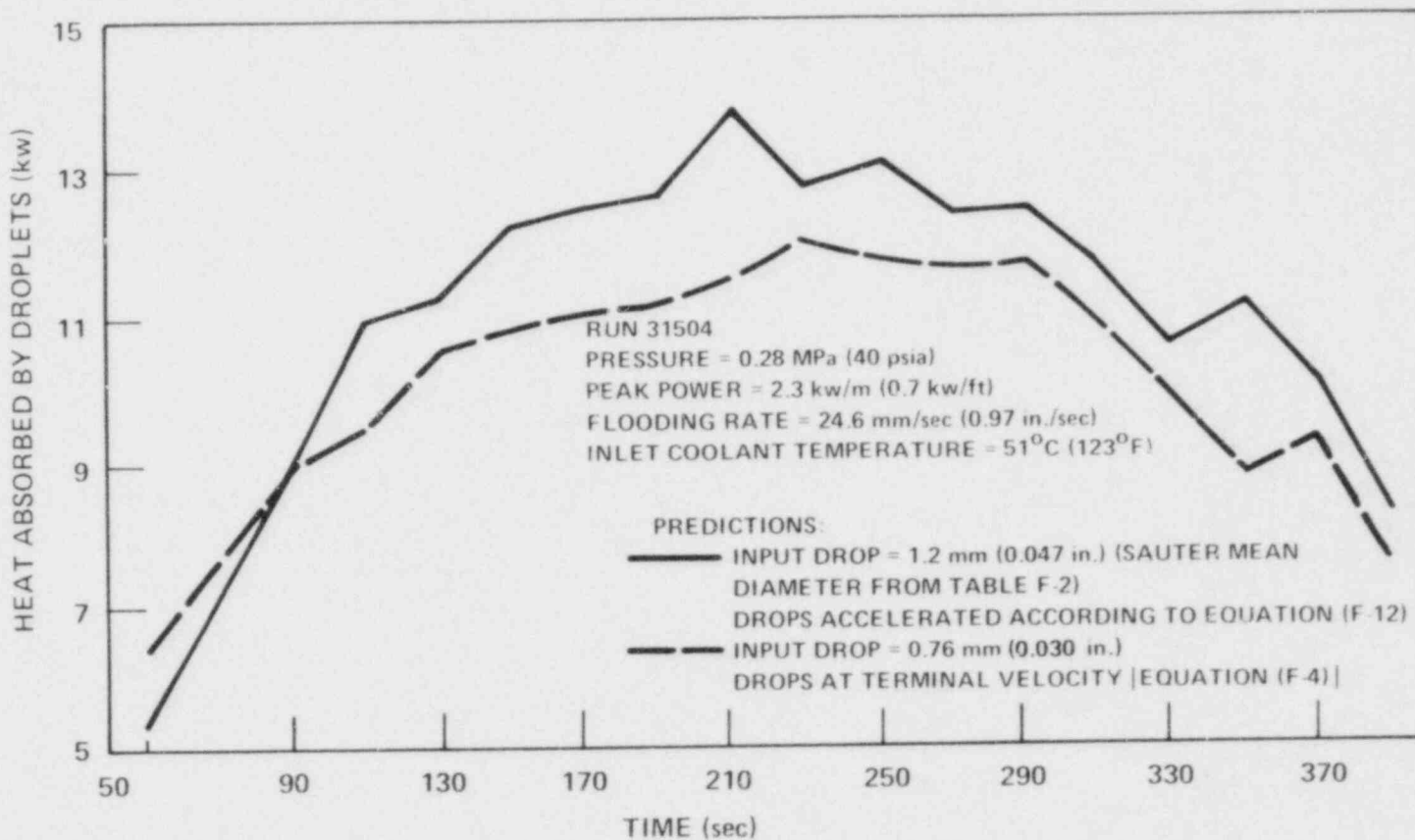


Figure 7-2. Predicted Droplet Heat Absorption Rate Between 2.90 and 3.05 m (114 and 120 in.) Elevations

higher and the calculated vapor temperature is lower, as shown in figures 7-3 through 7-5. Also, because of the higher heat transfer to the droplets, the wall temperature calculated with the present model is lower, as shown in figures 7-6 and 7-7. The wall temperature data are also shown in figures 7-3 through 7-7, for comparison.

Two major uncertainties are thought to contribute to the discrepancies between predictions and data. First, the droplet-vapor heat transfer and the droplet-vapor relative velocity are not precisely known. The present work uses a larger drop size and calculates a smaller relative velocity than the previous version. It is not apparent from the data comparisons in figures 7-3 through 7-7 which model is superior. Hence, more work is required, at a more detailed and fundamental level, on the vapor-droplet hydrodynamic and heat transfer interactions. Second, radiation exchange between different rod and housing surfaces was not accurately calculated in either of the two models. It is shown in section 6 that surface-to-surface radiation could be significant, particularly at higher elevations.

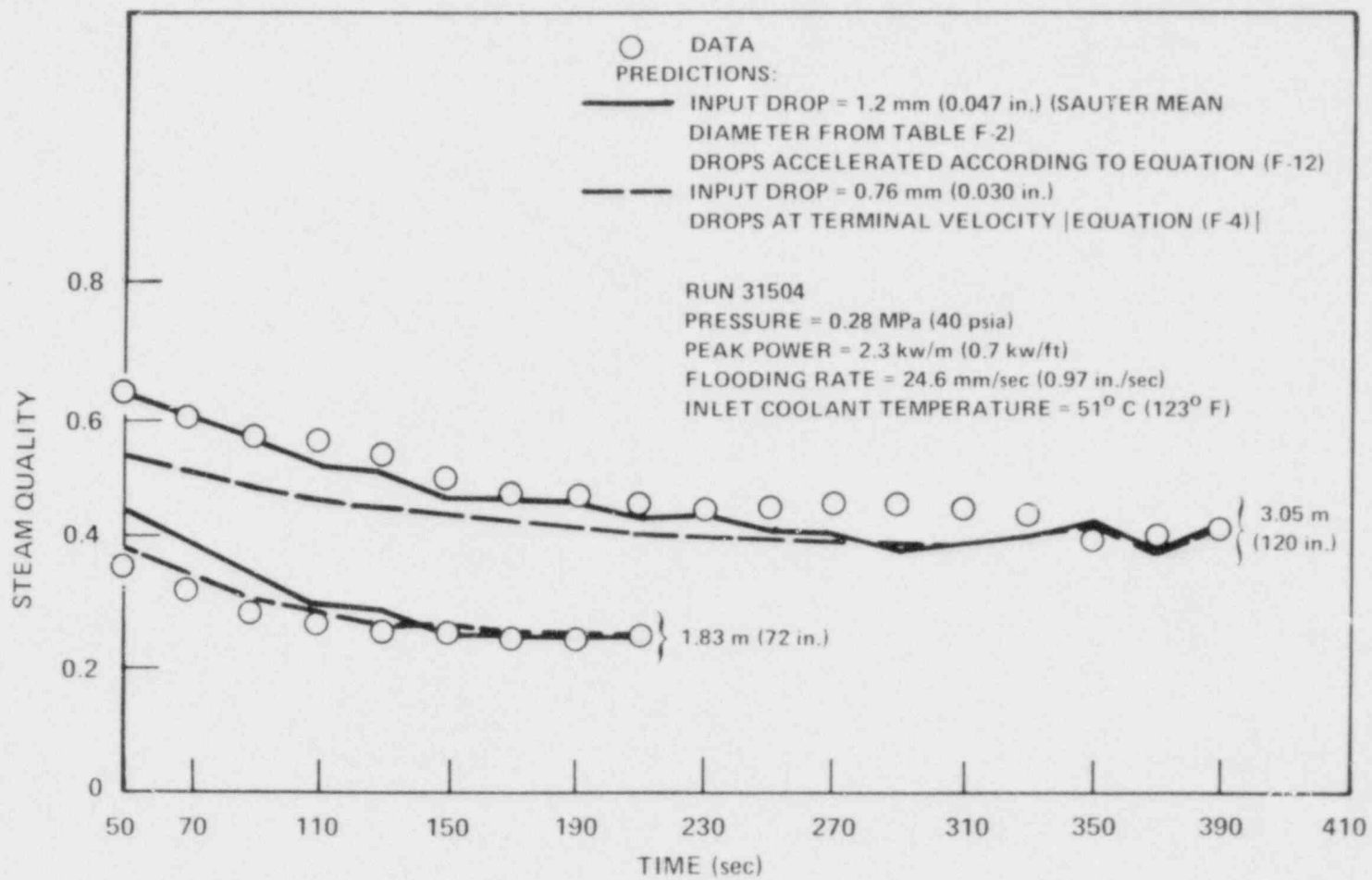


Figure 7-3. Comparisons of Predicted Steam Quality With Data-Based Steam Quality

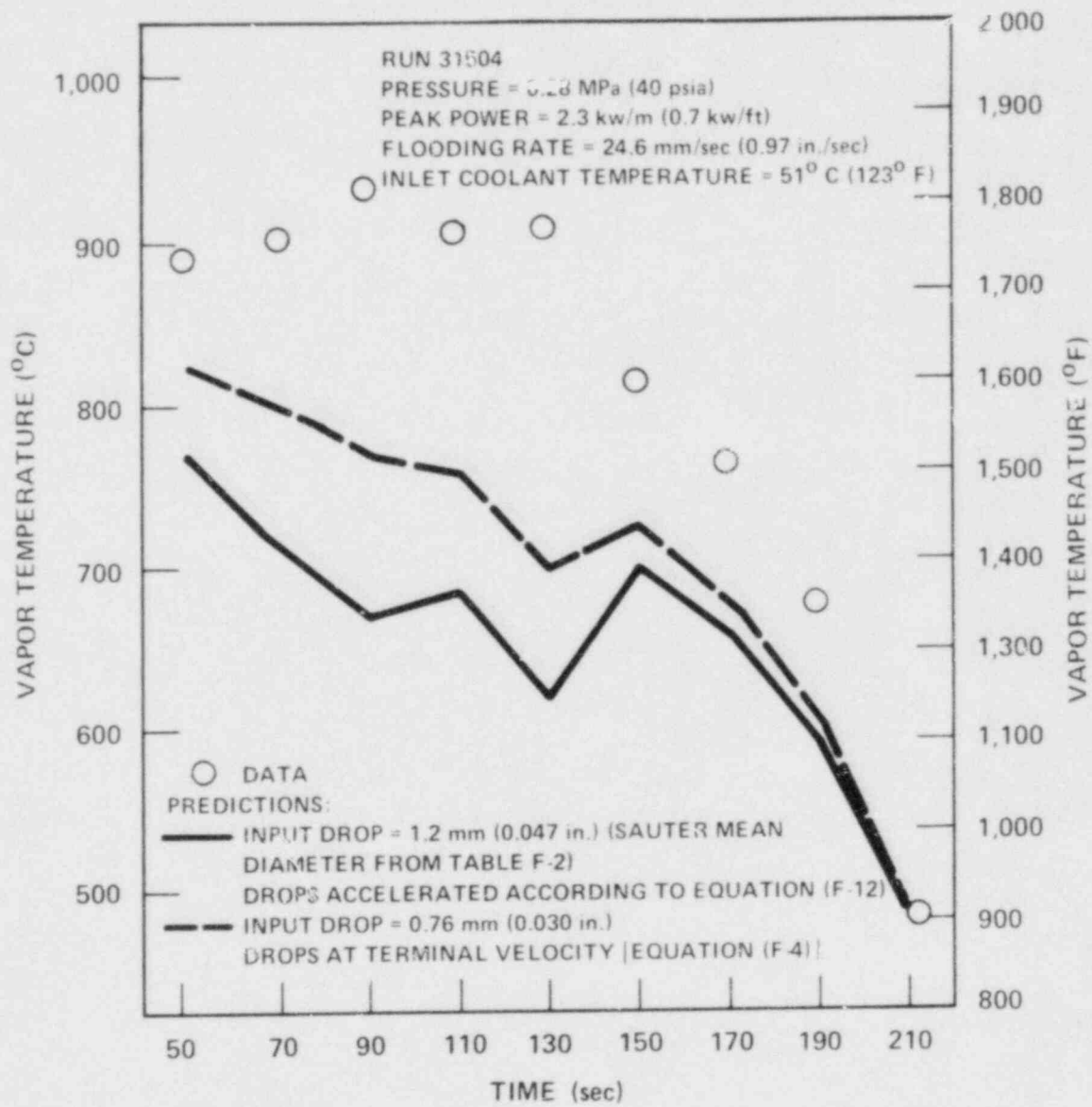


Figure 7-4. Comparisons of Predicted Vapor Temperature With Data, 1.83 m (72 in.) Elevation

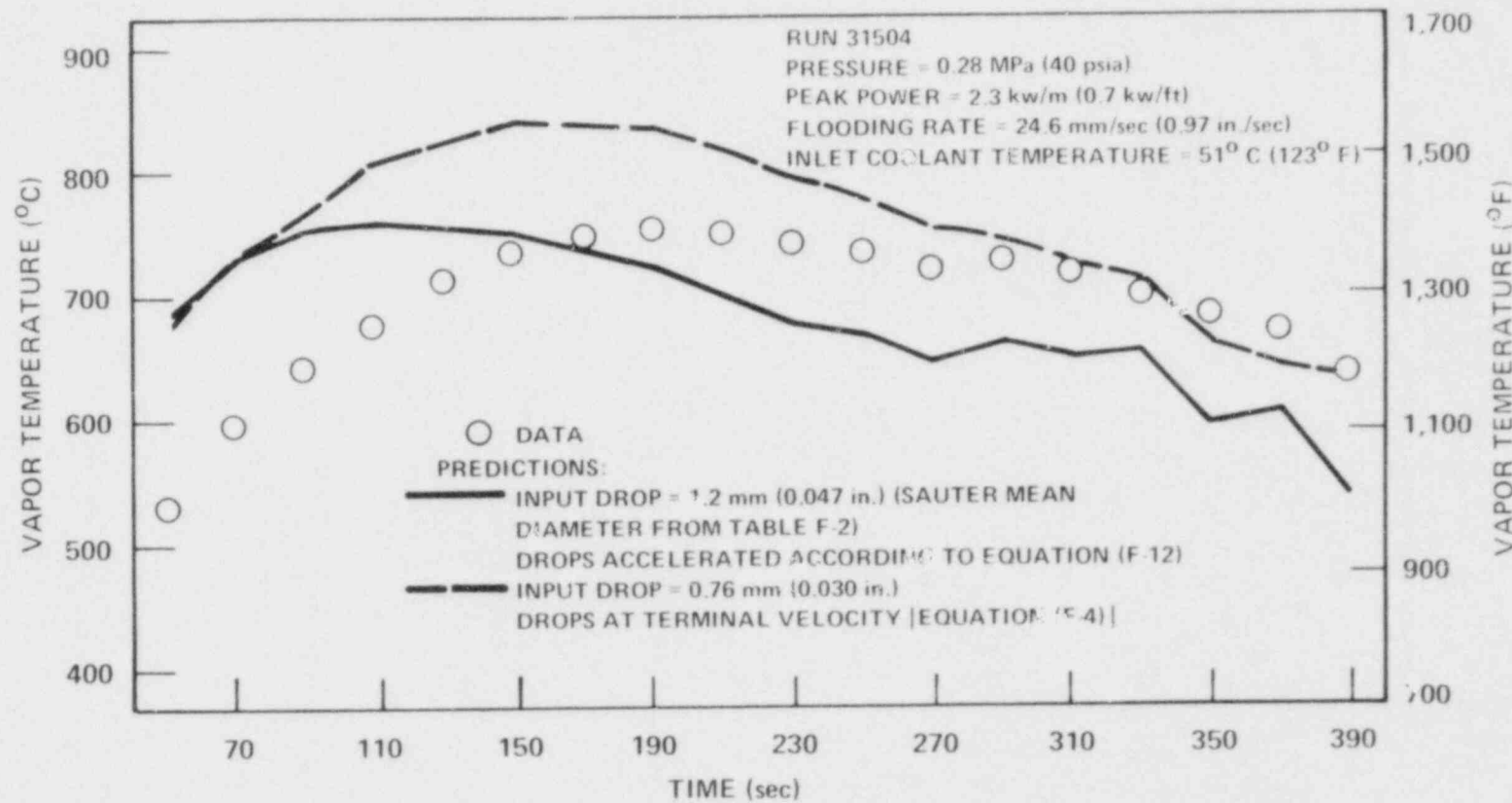


Figure 7-5. Comparisons of Predicted Vapor Temperature With Data, 3.05 m (120 in.) Elevation

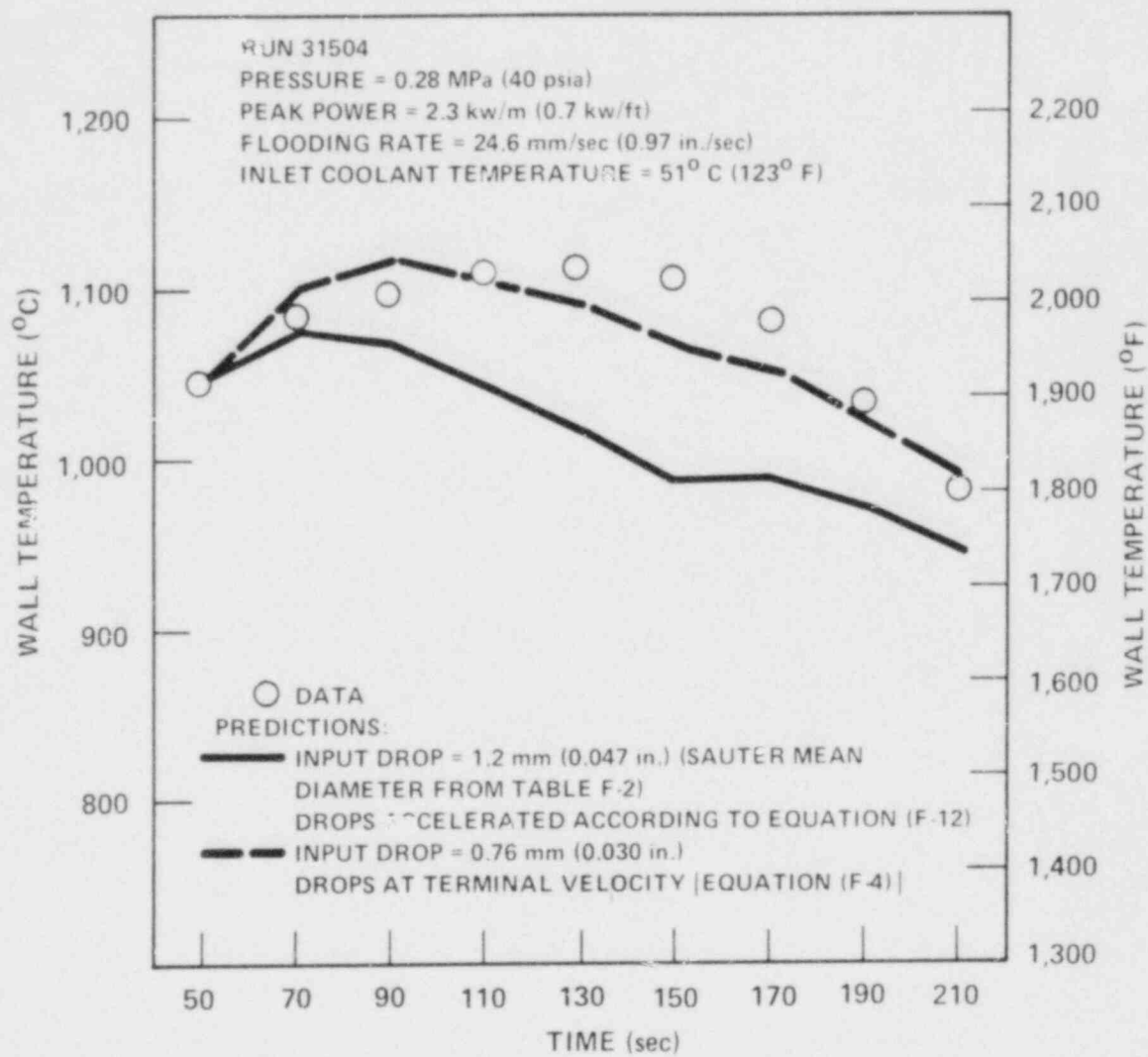


Figure 7-6. Comparisons of Predicted Wall Temperature (Rod 8H) With Data,
 1.83 m (72 in.) Elevation

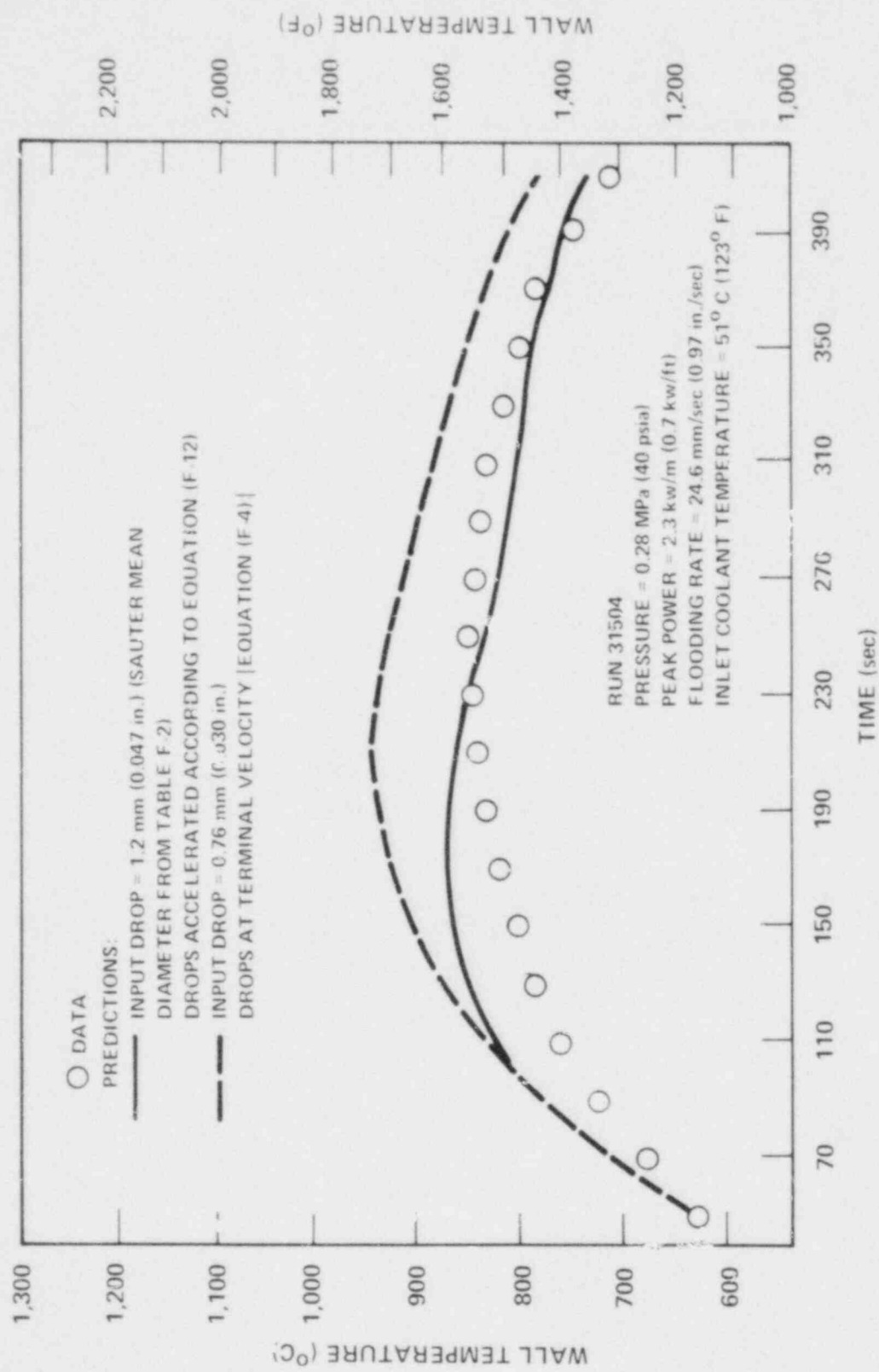


Figure 7-7. Comparisons of Predicted Wall Temperature (Rod 8H) With Data, 3.05 m (120 in.) Elevation

SECTION 8

HEAT TRANSFER CORRELATION

8-1. INTRODUCTION

A heat transfer correlation has been derived based on the concept that the heat transfer coefficient is primarily a function of the distance from the quench front,^(1,2) and the basis of this concept has been explained in detail. The correlation predicts the quench time and the heat transfer coefficient quite well for the FLECHT cosine power tests and the skewed power tests with the 15x15 assembly rod bundle. However, the correlation is not in dimensionless form; therefore, it is not general enough to be applicable to other rod bundle geometries such as the 17x17 assembly rod bundle of the FLECHT SEASET tests.

In this report, the correlation of Yeh and Lilly^(1,2) is reformulated in dimensionless form and modified to provide better agreement with the data of the 15x15 FLECHT cosine power tests and skewed power tests as well as with the data of the 17x17 FLECHT SEASET tests.

The present correlation, like its predecessor, consists of two subcorrelations:

- Quench correlation, which predicts the quench front elevation as a function of time
- Heat transfer coefficient correlation, which predicts the heat transfer coefficient as a function of the distance from the quench front, $Z - Z_q$

The heat transfer coefficient can be computed as a function of time by using the quench correlation, which bridges the space variable Z_q and the time variable t .

-
1. Yeh, H. C., et al., "Reflood Heat Transfer Correlation," Nucl. Tech. 46, 473 (1979).
 2. Lilly, G. P., et al., "PWR FLECHT Skewed Profile Low Flooding Rate Test Series Evaluation Report," WCAP-9183, November 1977.

8-2. QUENCH CORRELATION

The original quench correlation has been modified and reformulated in dimensionless form as follows:⁽¹⁾

$$\frac{t_q V_{in}}{Z_q} = 1 + \frac{\frac{t_q, \text{ peak } V_{in}}{Z_q} \left(Q_r + 0.5 Q_r e^{-9} Q_r^2 \right) - 1}{1 + 50 * \left(\frac{T_{sat} - T_o}{T_o - T_{sat}} \right)} \quad (8-1)$$

where

$$Q_r = \int_0^{Z_q} Q'(Z) dZ / \int_0^{Z_{\text{peak}}} Q'(Z) dZ \quad (8-2)$$

$Q'(Z)$ = linear power at elevation Z of one rod [j/sec-m (Btu/sec-ft)]

Z_q = quench elevation [m (ft)]

Z_{peak} = peak power elevation [m (ft)]

t_q = quench time at elevation Z_q (sec)

V_{in} = flooding rate [m/sec (ft/sec)]

T_o = 204°C (400°F)

T_{sat} = saturation temperature [°C (°F)]

I. Whenever confusion is likely to occur, exponentiation is indicated by**.

$$T_{init, q} = (T_{init} - T_{sat}) \frac{Q'(Z_q)}{Q'(Z_{peak})} + T_{sat}, [^{\circ}\text{C} (^{\circ}\text{F})]$$

T_{init} = cladding temperature at peak power elevation at beginning of flood [$^{\circ}\text{C}$ ($^{\circ}\text{F}$)]

and $t_{q, peak}$ is the quench time at the peak power elevation which is given by

$$\frac{t_{q, peak}}{Z_{q, peak}} = 0.0028 \text{ Re} \left(\frac{\rho_g}{\rho_f} \right)^{-0.262} [F_{t1} (F_{t2} + F_{t3} + F_{t4}) + F_{t5}] \\ \cdot (F_{t6} - F_{t7}) F_{t8} \quad (8-3)$$

where

$$F_{t1} = \exp [-10.09 (C_{pf} \Delta T_{sub} / h_{fg})] 6.458(10^{-5}) \\ \text{Re}^{1.938} / (\rho_g / \rho_f)^{0.5078} (C_Q D_{rod} / Z_{peak})^{1.5} \\ -0.7 \{1 - \exp [-0.00000801 \text{Re} / (\rho_g / \rho_f)^{0.262}] \}$$

$$F_{t2} = 1 + 0.5 \exp [-5.6251 (10^8) (\rho_g / \rho_f)^3]$$

$$F_{t3} = 1.3 \exp [-1.652 (10^{-9}) \text{Re}^2 / (\rho_g / \rho_f)^{0.524}]$$

$$F_{t4} = 17.3 \exp [-5.6251 (10^8) (\rho_g / \rho_f)^3]$$

$$\exp [-7.293 (10^{-9}) \text{Re}^2 / (\rho_g / \rho_f)^{0.524}]$$

$$F_{t5} = 66203 (\rho_g / \rho_f)^{0.2882} / \text{Re}^{1.1}$$

$$-2.8 \exp [-0.000122 \text{Re} / (\rho_g / \rho_f)^{0.262}] F_{t2}$$

$$F_{t6} = 1.01552 + 0.01388 C_T$$

$$F_{t7} = 1.05 \exp (-0.66 + 0.59 C_T) \{ 1 + 0.5/[1 + 50^{**} \\ (2.8137 \times 10^{-5}) Re / (\rho_g / \rho_f)^{0.262}] \}$$

$$F_{t8} = F_{t81} F_{t82}$$

$$F_{t81} = 0.3 + 0.7 \{ 1 - \exp [-10.31(10^{-8}) Re^2 / (\rho_g / \rho_f)^{0.524}] \\ - 2.9 (10^{-11}) Re^3 (\rho_g / \rho_f)^{-0.786} \\ \exp [-9.3 (10^{-8}) Re^2 / (\rho_g / \rho_f)^{0.524}] \\ / \{ 1 + 50^{**} [- 15.75 (C_{pf} \Delta T_{sub} / h_{fg}) + 1.333] \}$$

$$F_{t82} = 1 - 0.16/[1 + 70^{**} 1250 (D_{rod} / Z_{peak}) \\ - 5.45] / [1 + 80^{**} (7.14 C_Q - 4.93)]$$

$$C_Q = \int_0^{Z_{peak}} Q(Z) dZ / (\rho_f / A_f V_{in} h_{fg})$$

$$C_T = (T_{init} - T_{sat}) / (T_{Lei} - T_{sat})$$

$$\rho_f = \text{water density [kg/m}^3 \text{ (lbm/ft}^3\text{)]}$$

$$D_{rod} = \text{rod diameters [m (ft)]}$$

$$A_f = \text{flow area formed by four adjacent rods [m}^2 \text{ (ft}^2\text{)]}$$

$$h_{fg} = \text{latent heat of evaporation [kcal/kg (Btu/lbm)]}$$

$$T_{Lei} = \text{Leider frost temperature} = 260^\circ\text{C (500°F)}$$

$$\Delta T_{sub} = \text{inlet subcooling [}^\circ\text{C (}^\circ\text{F)]}$$

The rationale and the method of deriving equations (8-1) and (8-3) are as follows. In the early FLECHT correlation,⁽¹⁾ the quench time was predicted only for the peak power elevation, which is 1.83 m (72 in.) for the cosine power shape. In the later version^(2,3) and the present version of the FLECHT correlation, since the concept of the heat transfer coefficient h being a function of the distance from the quench front $Z - Z_q$ was used, it is necessary to have a correlation which is able to predict the quench time for all elevations. Since the early FLECHT correlation predicts the quench time at the peak power elevation quite well, it is used as a base correlation in the later and the present versions [equation (8-3)], which is denoted by $t_{q, \text{peak}}$; the quench time of the other elevations is predicted by adjusting $t_{q, \text{peak}}$ with the integral of power Q_r as expressed in equation (8-1).

In the above correlation, the quench time, t_q , is given as a function of the quench elevation, Z_q . In practice, it is necessary to compute the quench elevation as a function of time. This can be accomplished by first computing the quench front velocity, V_q , for a given time t by

$$V_q = \frac{(Z_q + \Delta Z_q) - Z_q}{t_q(Z_q + \Delta Z_q) - t_q(Z_q)} \quad (8-4)$$

where $t_q(Z_q + \Delta Z_q)$ and $t_q(Z_q)$ are the quench times computed from equation (8-1). The quench front elevation at the time $t + \Delta t$ is then computed by

$$Z_q(t + \Delta t) = Z_q(t) + V_q \Delta t \quad (8-5)$$

This method of computing the quench elevation as function of time is also valid for variable flooding rates. Note that, for the variable flooding rate case, the actual time t is different from t_q .^(2,3)

-
1. Lilly, G.P., et al., "PWR FLECHT Cosine Low Flooding Rate Test Series Evaluation Report," WCAP-8838, March 1977.
 2. Yeh, H. C., et al., "Reflood Heat Transfer Correlation," Nucl. Tech. 46, 473 (1979).
 3. Lilly, G. P., et al., "PWR FLECHT Skewed Profile Low Flooding Rate Test Series Evaluation Report," WCAP-9183, November 1977.

It is noted that the power per flow area is preserved in the above correlation through the parameter C_Q . It is also noted that through the use of the dimensionless quench time, $t_q V_{in}/Z_q$, the length effect (originally f-factor^(1,2)) has been taken care of automatically.

The above quench correlation has been compared with the data of the FLECHT SEASET unblocked test series as well as with the data of the 15x15 FLECHT cosine power test series and skewed power test series. In particular, the overlap runs of these three test series have been compared. The overlap tests are the runs which have the same test conditions and the same total energy (the integral of power plus the stored energy) below the peak power elevations, so that the quench time at the peak power elevation is about the same. Table 8-1 lists the overlap or essentially overlapping runs of the three test series. Figures 8-1 through 8-3 compare the above quench correlation with the data of the first set of overlap runs in Table 8-1.

The comparisons of the other sets of the overlap runs can be found in appendix G. All these comparisons show that the quench time at the peak power elevation is about the same in each set of the overlap runs, and that the predicted quench times are in good agreement with the data. The comparisons of nonoverlap runs are given in appendix H.

Figures 8-4 through 8-6 compare the present correlation with previous correlations^(1,2) and with the data. Note that the correlation of WCAP-8838 predicts only the quench time at the peak power elevation. These comparisons indicate that the present correlation is in better agreement with data than the previous correlations.

8-3. HEAT TRANSFER COEFFICIENT CORRELATION

As in all previous FLECHT reports, the heat transfer coefficient h is defined as

$$h = q_{total} / (T_{rod} - T_{sat})$$

-
1. Yeh, H. C., et al., "Reflood Heat Transfer Correlation," Nucl. Tech. 46, 473 (1979).
 2. Lilly, G. P., et al., "PWR FLECHT Skewed Profile Low Flooding Rate Test Series Evaluation Report," WCAP-9183, November 1977.

TABLE 8-1
OVERLAP RUNS

Run	Peak Power [kw/m (kw/ft)]	Flooding Rate [mm/sec (in./sec)]	Initial Clad Temperature [°C (°F)]	Inlet Subcooling [°C (°F)]	Pressure [MPa (psia)]	Bundle Geometry(a)
31203	2.3 (0.7)	38.1 (1.5)	871 (1600)	77 (140)	0.28 (40)	A
03113	2.7 (0.81)	38.1 (1.5)	871 (1600)	76 (136)	0.26 (38)	B
11618	1.5 (0.45)	38.1 (1.5)	881 (1618)	79 (142)	0.28 (41)	C
30817	2.3 (0.7)	38.1 (1.5)	538 (1000)	77 (140)	0.28 (40)	A
00904	2.8 (0.85)	37.6 (1.48)	538 (998)	77 (140)	0.28 (41)	B
11719	1.5 (0.45)	38.1 (1.5)	538 (1001)	79 (142)	0.28 (41)	C
30518	2.3 (0.7)	38.1 (1.5)	260 (500)	77 (140)	0.28 (40)	A
02005	2.8 (0.84)	38.4 (1.51)	274 (525)	78 (141)	0.28 (40)	B
12720	1.5 (0.45)	38.1 (1.5)	262 (508)	78 (141)	0.28 (40)	C
30619	2.3 (0.7)	38.1 (1.5)	260 (500)	77 (140)	0.14 (20)	A
03709	2.7 (0.81)	38.1 (1.5)	317 (603)	78 (141)	0.14 (20)	B
11821	1.5 (0.45)	41.7 (1.64)	263 (506)	79 (143)	0.14 (20)	C
31805	2.3 (0.7)	20.3 (0.8)	871 (1600)	77 (140)	0.14 (40)	A
02414	2.8 (0.84)	20.6 (0.81)	871 (1600)	77 (138)	0.14 (40)	B
34006	1.3 (0.4)	15.2 (0.6)	871 (1600)	77 (140)	0.14 (40)	A
07836	2.4 (0.76)	15.7 (0.62)	871 (1600)	78 (141)	0.14 (40)	B
36026	2.3 (0.7)	25.4 (1)	871 (1600)	77 (140)	0.14 (40)	A
05132	3.1 (0.95)	25.1 (0.99)	871 (1600)	77 (140)	0.14 (40)	B
32333	2.3 (0.7)	152.4 (6) 5 sec 20.3 (0.8) onward	871 (1600)	77 (140)	0.14 (40)	A
04516	3.1 (0.95)	152.4 (6) 5 sec 20.3 (0.8) onward	871 (1600)	77 (140)	0.14 (40)	B

a. A - 17 x 17 cosine power
 B - 15 x 15 cosine power
 C - 15 x 15 skewed power

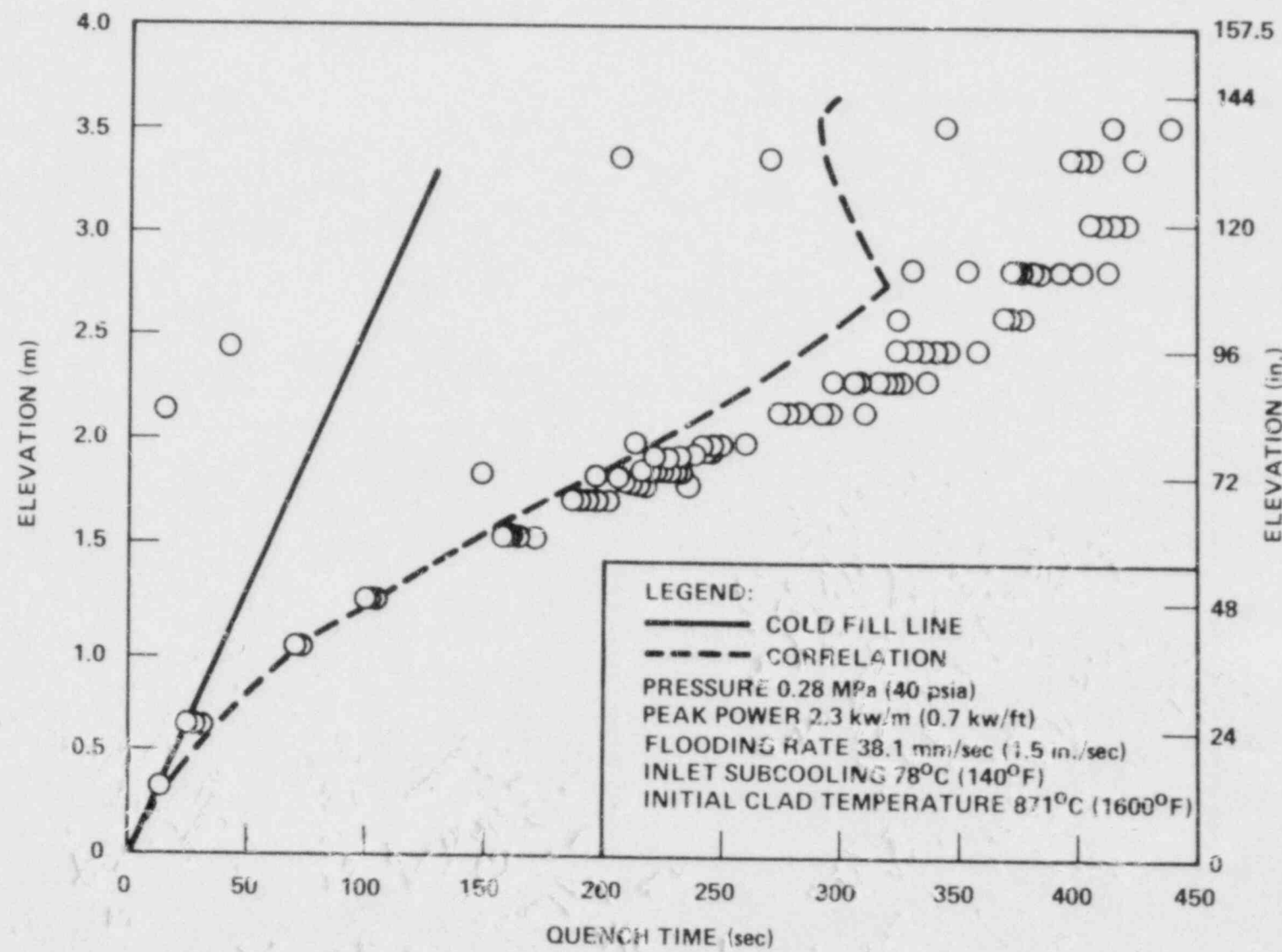


Figure 8-1. Quench Correlation Versus Data, FLECHT SEASET Run 31203

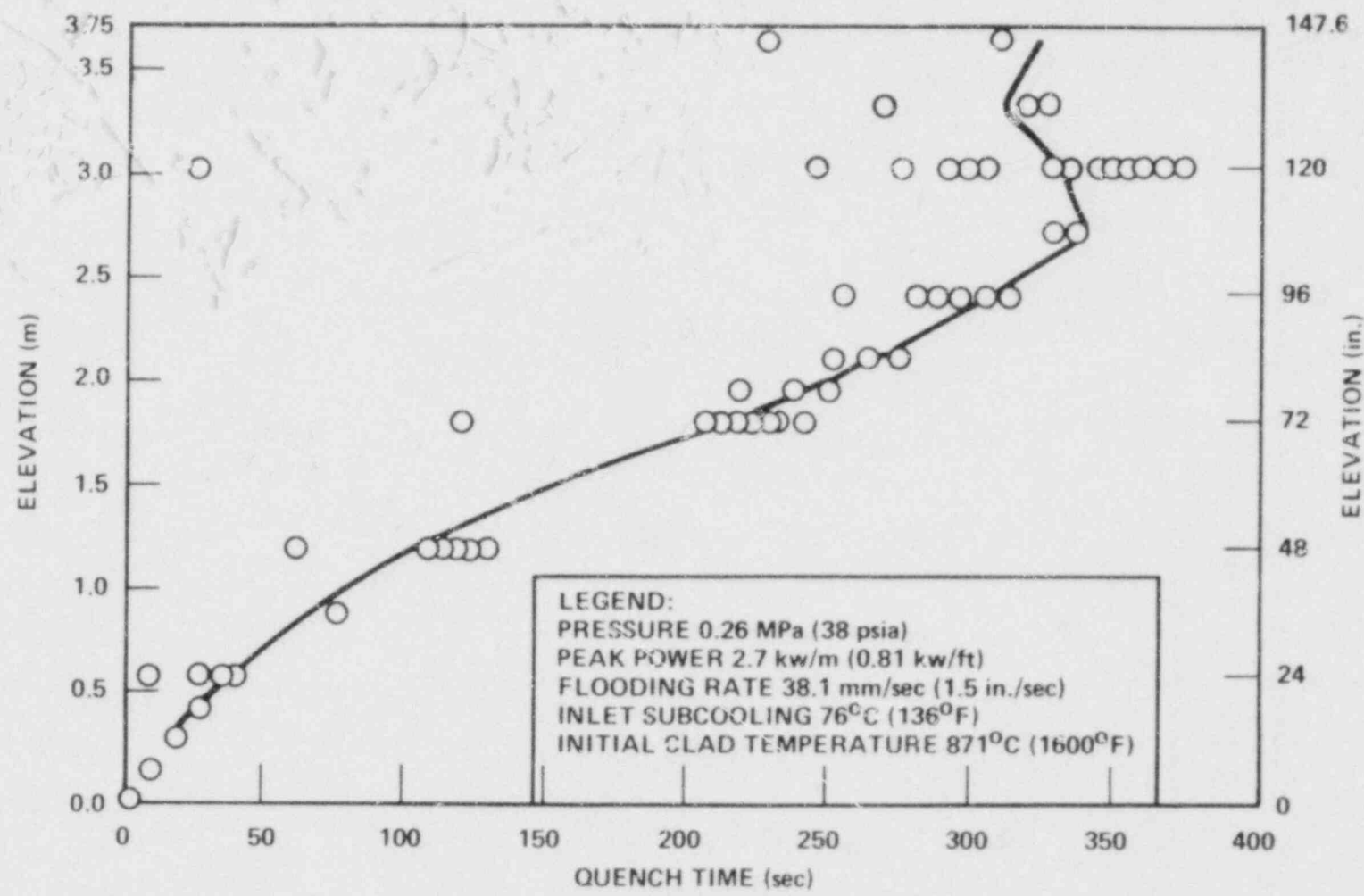


Figure 8-2. Quench Correlation Versus Data, FLECHT Cosine Run 03113

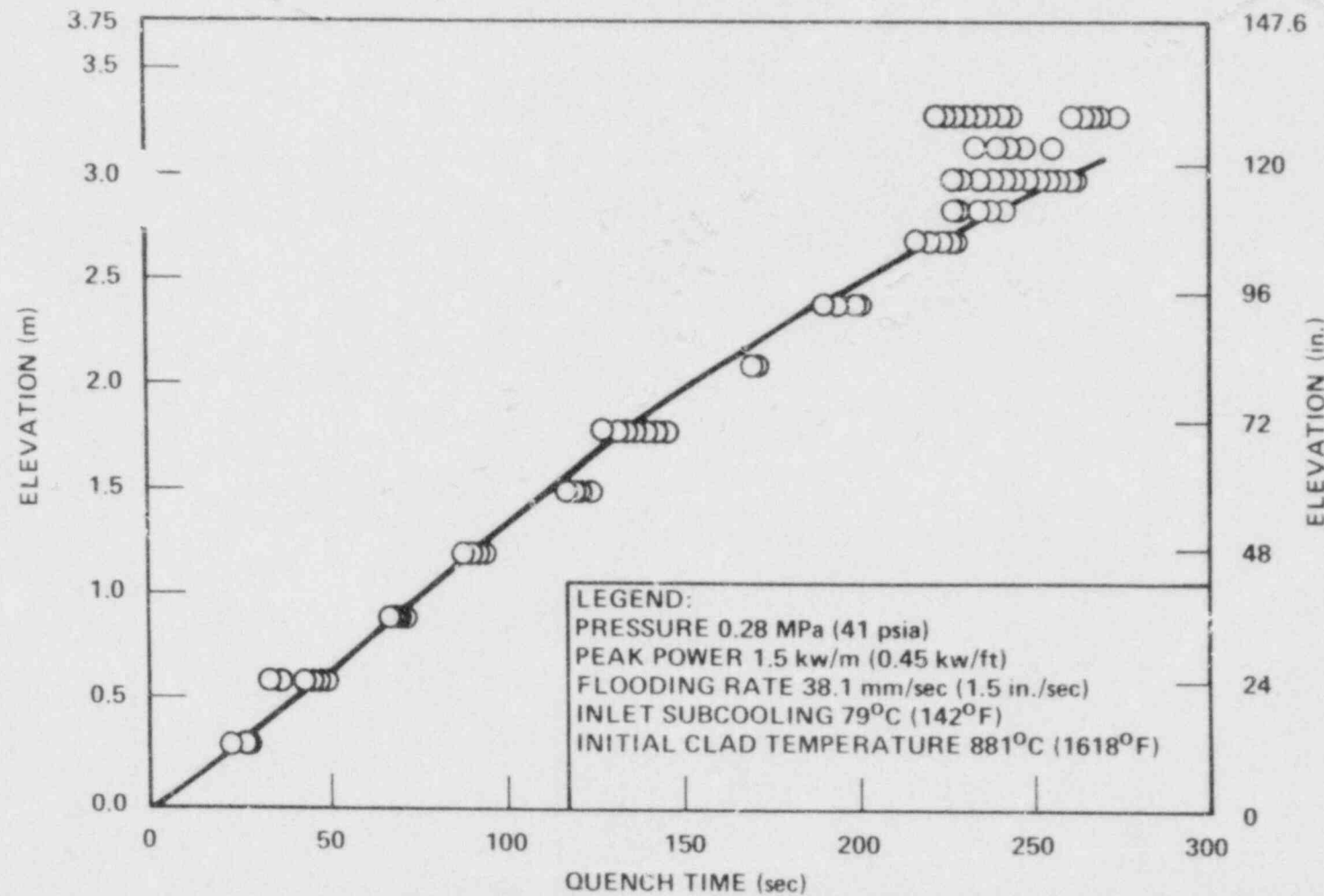


Figure 8-3. Quench Correlation Versus Data, FLECHT Skewed Profile Run 11618

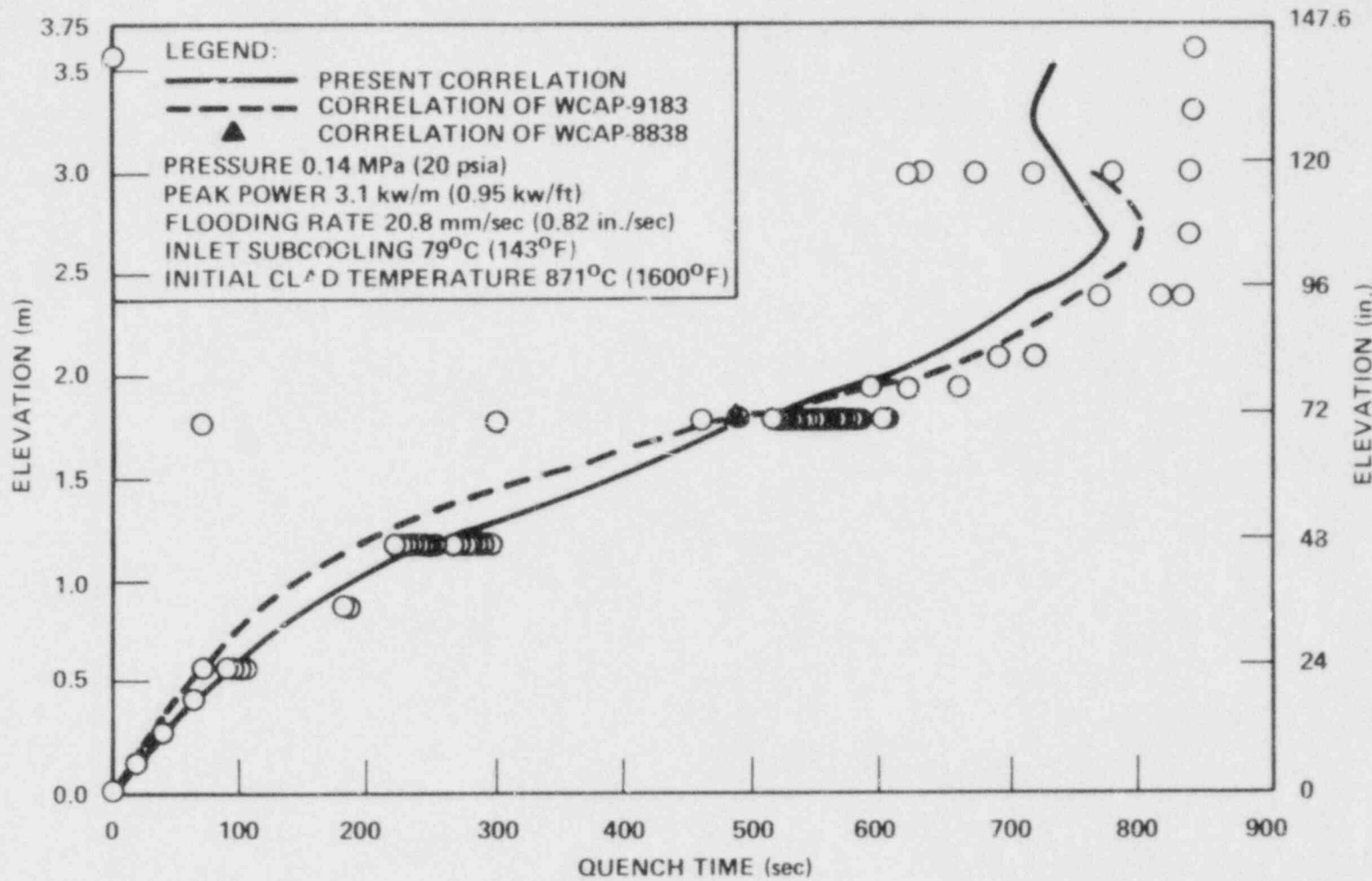


Figure 8-4. Present Correlation, WCAP-9183 Correlation, and WCAP-8838 Correlation Versus Data, FLECHT Cosine Run 06638

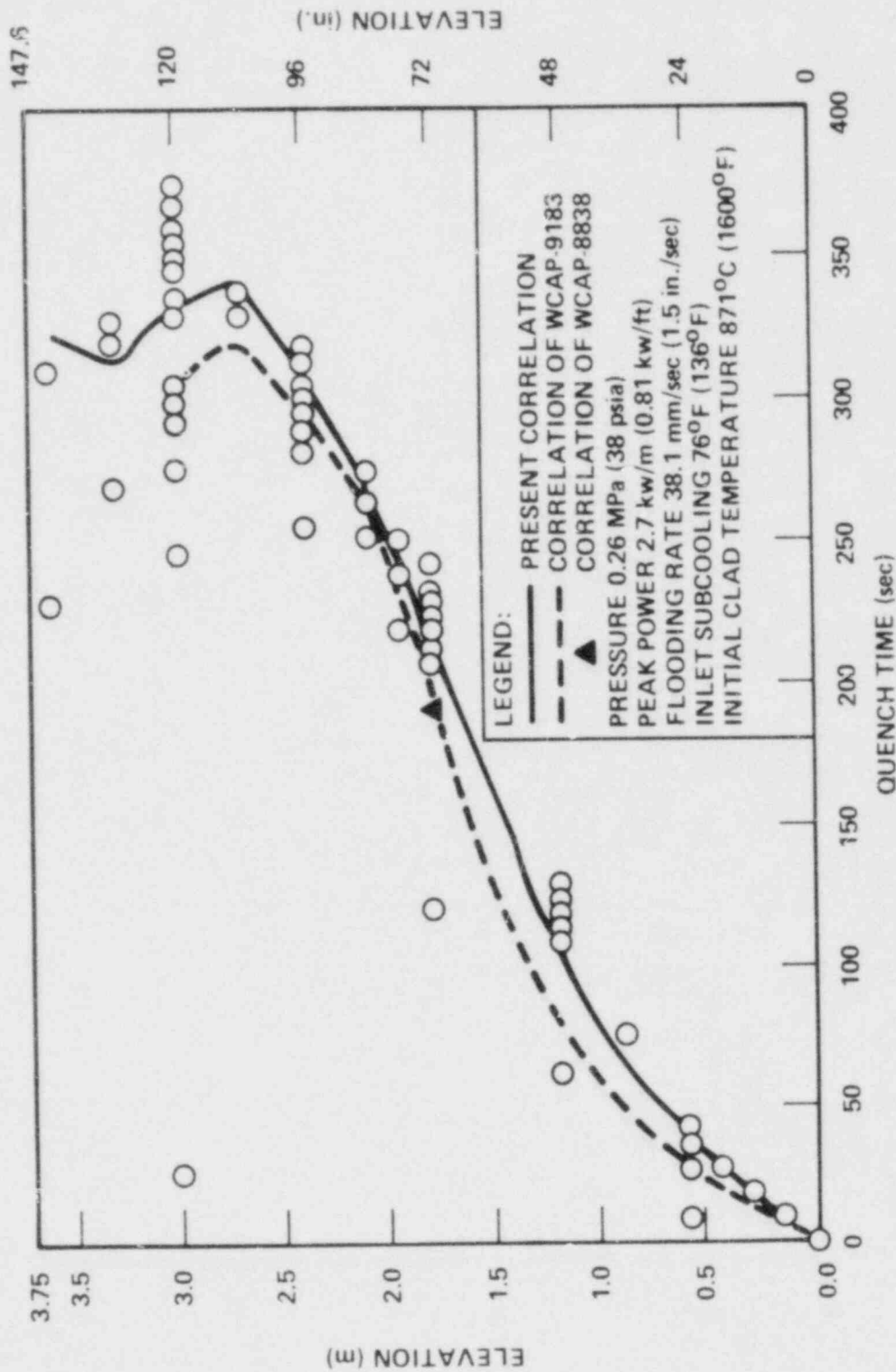


Figure 8-5.
Present Correlation, WCAP-9183 Correlation, and WCAP-8838 Correlation Versus Data,
FLECHT Cosine Run 03113

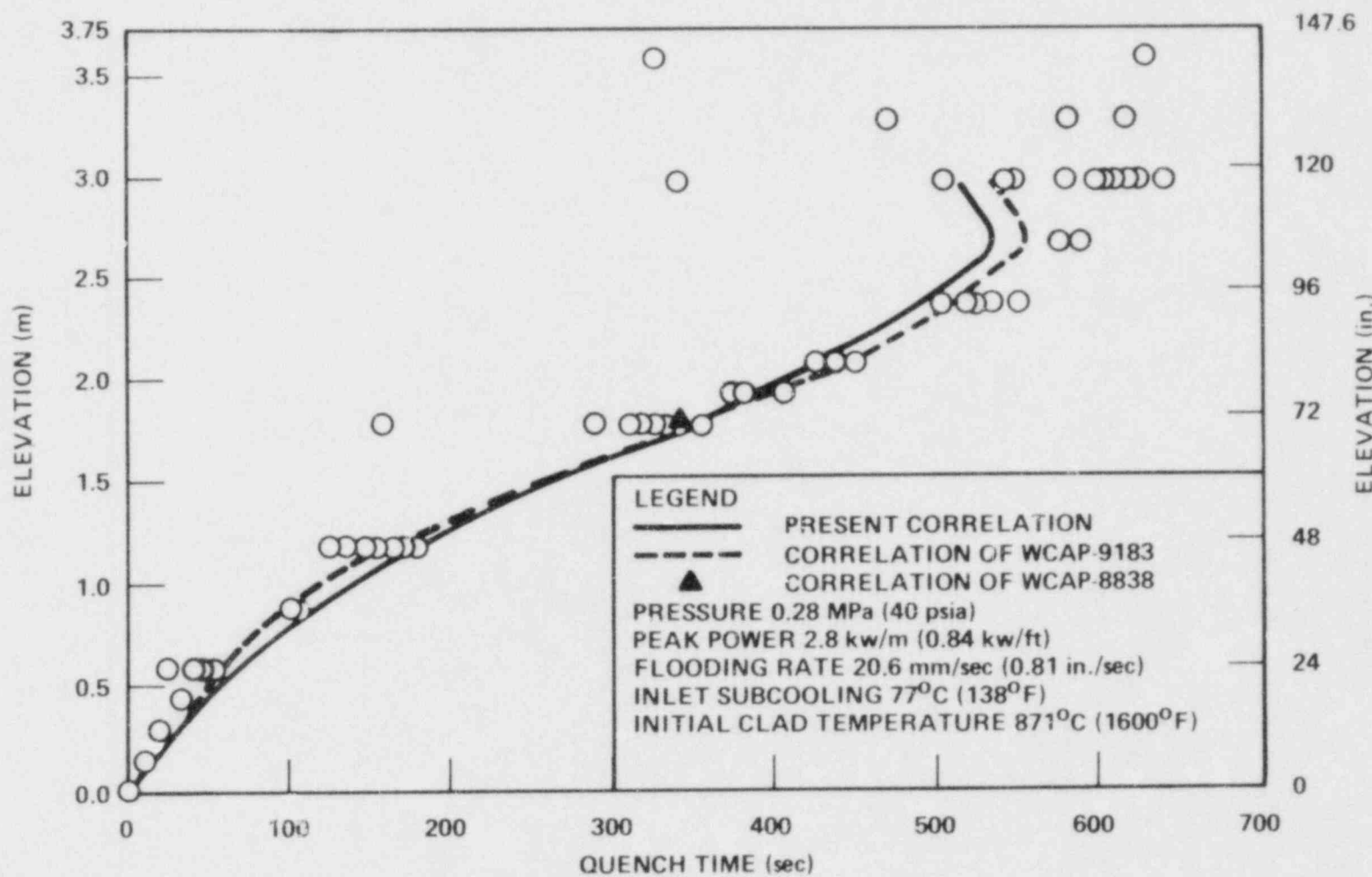


Figure 8-6. Present Correlation, WCAP-9183 Correlation, and WCAP-8838 Correlation Versus Data, FLECHT Cosine Run 02414

where

q_{total} = rod total surface heat flux, which includes radiation and convection

T_{rod} = rod surface (cladding) temperature

T_{sat} = saturation temperature

The present heat transfer coefficient correlation is divided into four parts instead of three parts:⁽¹⁾

-- Radiative Heat Transfer period

The radiative heat transfer period exists only for the case of low initial cladding temperature. For low initial cladding temperature, there is practically no vapor generation at the beginning of flood because the rods are cold at the lower elevation. Therefore the heat transfer during this period is essentially radiative heat transfer.

-- Early developing period

This period extends from the end of the radiative heat transfer period to the time when the heat transfer reaches a quasi-steady state (figure 8-7). During this developing period, the heat transfer mechanism changes from the radiation-dominated prereflood condition to single-phase steam flow. The mechanism then changes to dispersed flow when the steam velocity becomes great enough to carry droplets up the bundle.

These changes were indicated in the movies taken during the FLECHT cosine test by the appearance of the first droplet. Figure 8-8 shows that the heat transfer coefficient started to increase at the time the first droplets were observed.

-
1. Yeh, H. C., et al., "Reflood Heat Transfer Correlation," Nucl. Tech. 46, 473 (1979).
 2. Lilly, G. P., et al., "PWR FLECHT Cosine Low Flooding Rate Test Series Evaluation Report," WCAP-8838, March 1977.

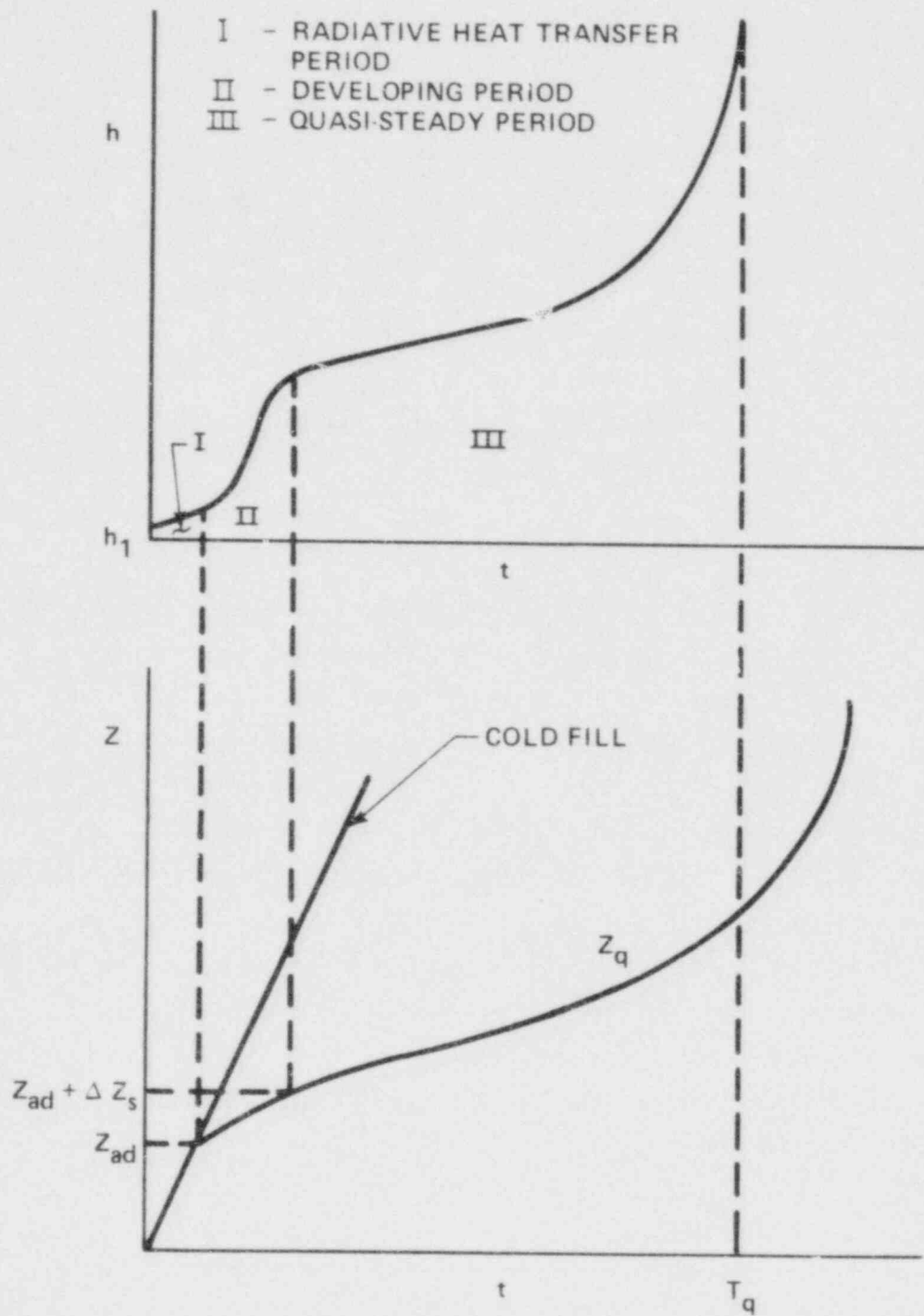


Figure 8-7. Adiabatic, Developing, and Quasi-Steady Periods in Heat Transfer Coefficient Correlation

Figure 8-9 shows that the time of first droplets is primarily a function of flooding rate. For low flooding rate, the dispersed flow eventually becomes quasi-steady-state. For high flooding rate, the heat transfer mechanism further develops into the unstable film boiling which becomes a quasi-steady state.

-- Quasi-steady period

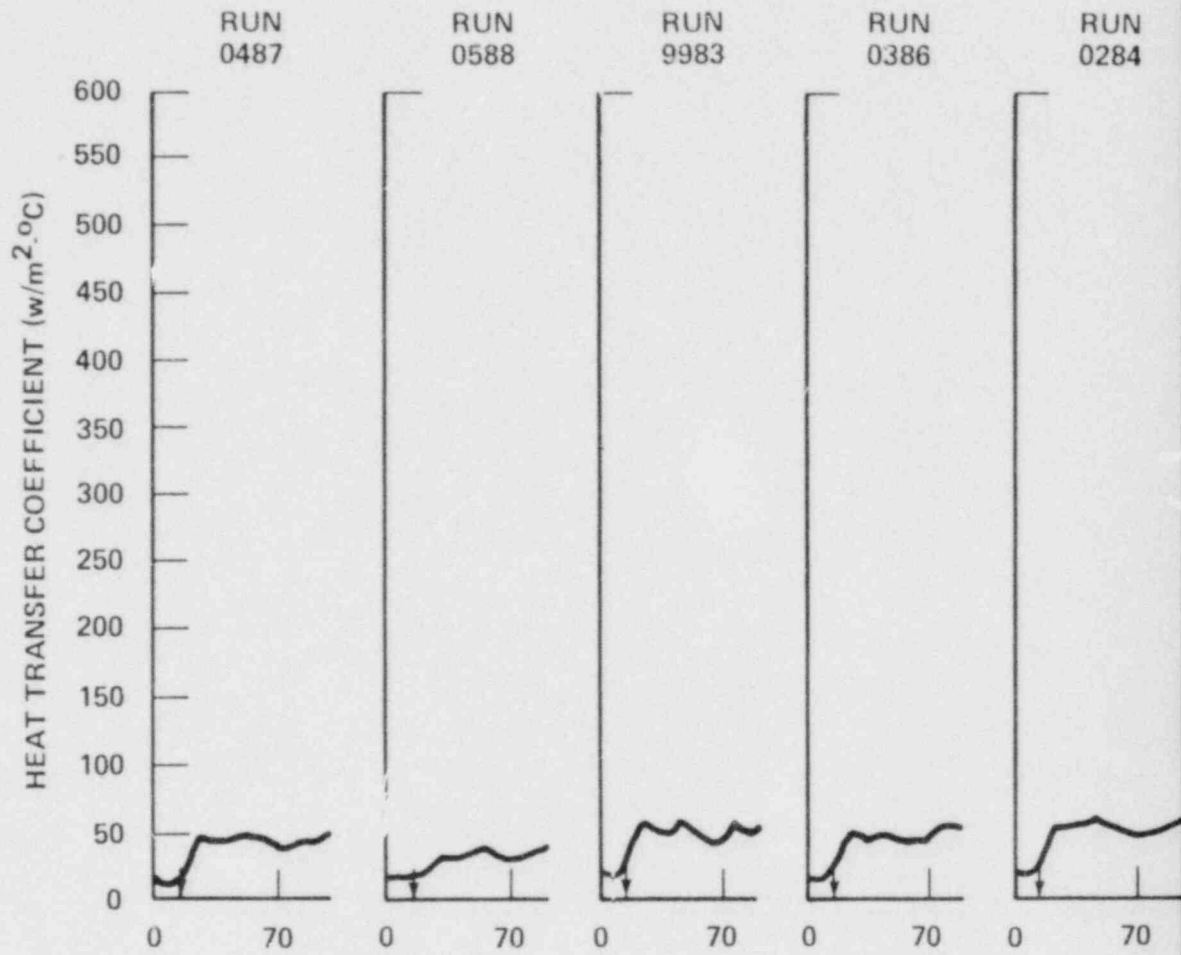
During this period the heat transfer is essentially in a quasi-steady state. This means that the heat transfer pattern moves with the quench front; that is, the heat transfer coefficient versus the distance from the quench front is essentially unchanged with time.

-- Heat transfer coefficient above peak cladding temperature elevation

Because the situation above the peak cladding temperature elevation is different from that below the peak cladding temperature elevation, it must be treated separately. Above the peak cladding temperature elevation, the steam temperature may be greater than the cladding surface temperature, and the heat may be transferred from the steam to heater rods. The FLECHT definition of heat transfer coefficient, saturation temperature equal to sink temperature, implies that the heat transfer coefficient is negative. Below the peak cladding temperature elevation, the steam temperature never becomes greater than the cladding surface temperature. Therefore the heat transfer coefficient never becomes negative.

The transition between the radiative heat transfer period and the developing period occurs when Z_q is equal to Z_{ad} , and the transition between the developing period and the quasi-steady period occurs when Z_q is equal to $Z_{ad} + \Delta Z_s$, where Z_{ad} and ΔZ_s are computed from the following formulas.

The expression of the four-part heat transfer coefficient is as follows:



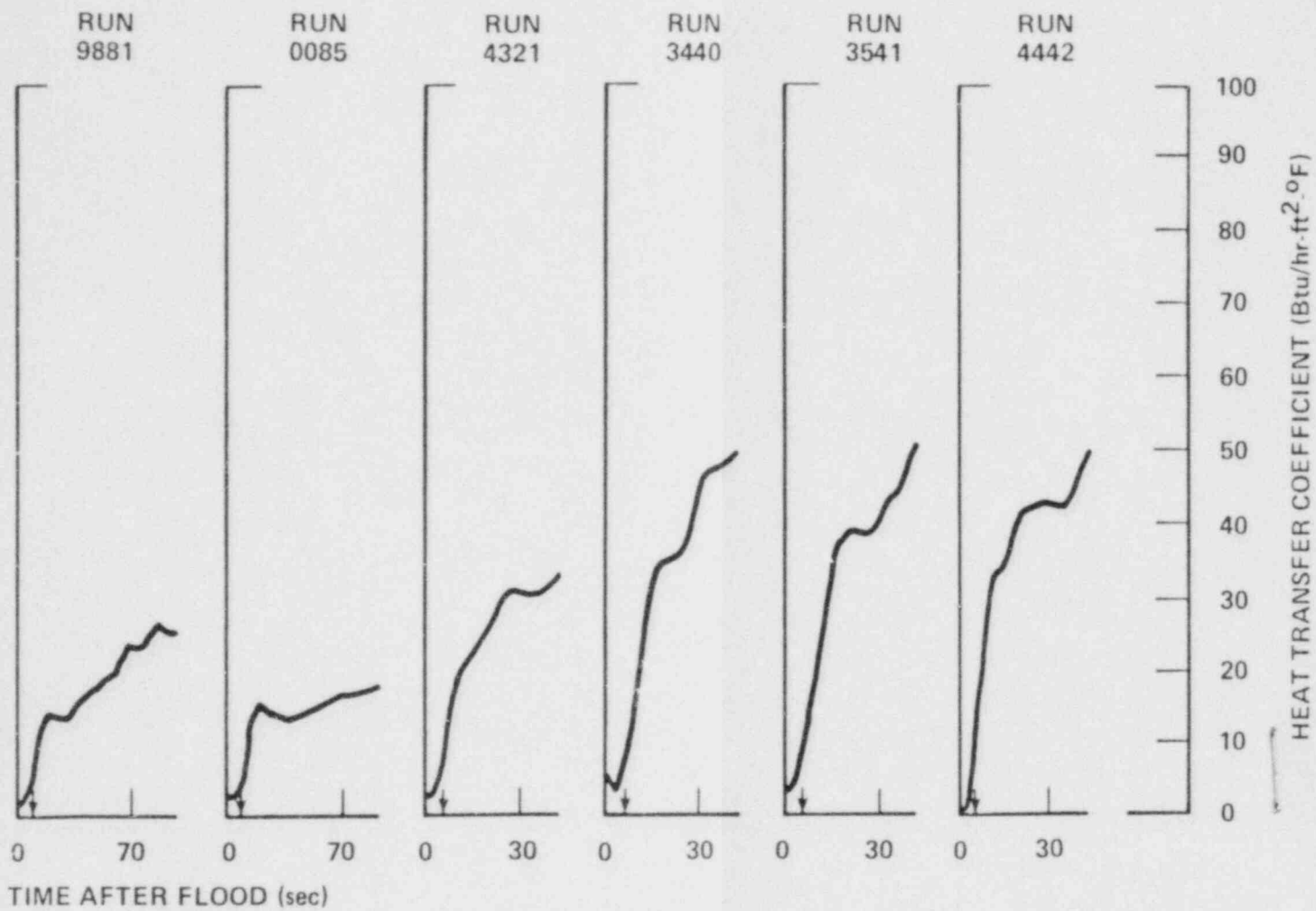


Figure 8-8. Comparison of Time of First
Droplet Observation in FLECHT
Movies and Time When Heat
Transfer Coefficient Starts To
Increase

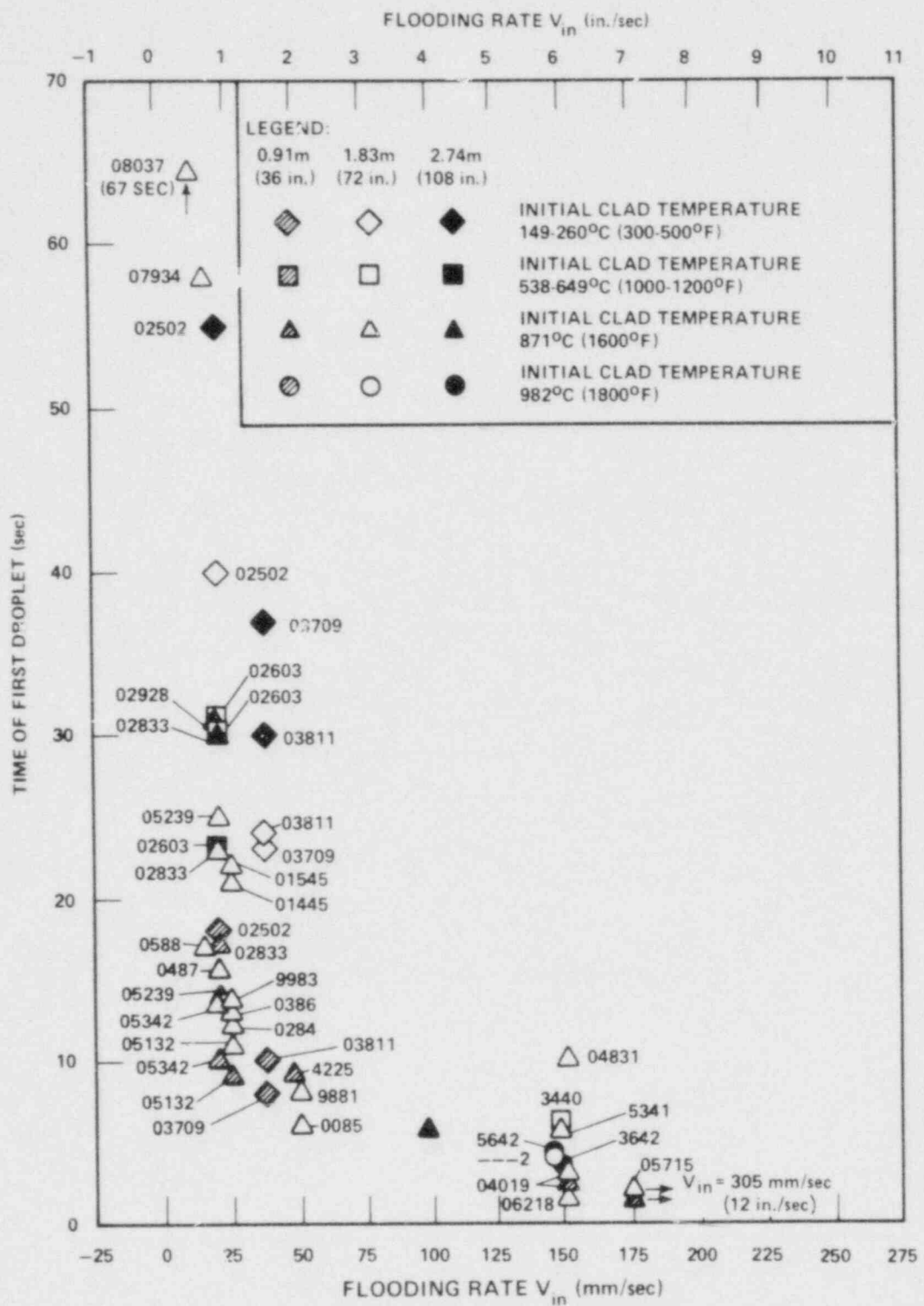


Figure 8-9. Time of First Droplet Observation in FLECHT Movies

-- Radiative heat transfer period ($Z_q < Z_{ad}$)

$$h = h_1 = C \frac{Q'(Z)}{(\rho C_p A)_{rod}} \left[1 - \exp \left(- \frac{T_{initz} - T_{ro}}{\Delta T_r} \right) \right] \quad (8-6)$$

where Z_{ad} is computed from the following dimensionless expression:

$$1 = 51 \frac{(\rho C_p A)_f \Delta T_{sub} V_{in}}{Q'_{max} Z_{ad}} - 0.234 \frac{(\rho C_p A)_{rod} (T_{init} - T_{sat}) V_{in}}{Q'_{max} Z_{ad}} + \frac{Z_o}{Z_{ad}} F_h \quad (8-7)$$

and

$$C = 36745 \text{ J/m}^2 \text{ (0.215 Btu/}^\circ\text{F}^2/\text{ft}^2\text{)}$$

$(\rho C_p A)_{rod}$ = heat capacity of a rod [j/m- $^\circ\text{C}$ (Btu/ft- $^\circ\text{F}$)]

$$T_{initz} = (T_{init} - T_{sat}) \frac{Q'(Z)}{Q'(Z_{peak})} + T_{sat} \quad [^\circ\text{C (}^\circ\text{F)}]$$

$$T_{ro} = 371 \text{ }^\circ\text{C (}700\text{ }^\circ\text{F)}$$

$$\Delta T_r = 224 \text{ }^\circ\text{C (}435\text{ }^\circ\text{F)}$$

$(\rho C_p A)_f$ = heat capacity of water in a channel formed by four adjacent rods
[j/m- $^\circ\text{C}$ (Btu/ft- $^\circ\text{F}$)]

$$Z_o = 0.3496 \text{ m (1.147 ft)}$$

$$h = \text{heat transfer coefficient [j/sec-}^\circ\text{C-m}^2 \text{ (Btu/sec-}^\circ\text{F-ft}^2\text{)}}$$

$$F_h = 1 / \left\{ 1 + 70^{**} [1 - 0.0133 (Z_{peak}/D_{rod})] \right\}$$

It is noted that the radiative heat transfer coefficient h_1 given by equation (8-6) is mainly due to the radiative heat exchange between the rod of interest and its neighboring thimble and rods. Therefore, h_1 depends on the temperature difference between the

rods and the neighboring thimbles. The temperature difference depends on the pre-reflood heatup rate. For example, if the pre-reflood heatup rate is very slow, then the radial temperature will be essentially uniform and the temperature difference practically zero, so that h_1 is also zero. The faster the heatup rate, the larger the temperature difference and hence the larger the h_1 . This mechanism has been discussed in great length in WCAP-7931.⁽¹⁾ The heatup rate is proportional to the local power $Q'(Z)$ and is inversely proportional to the heat capacity $(\rho C_p A)_{\text{rod}}$ of the rod. This leads to the expression of equation (8-6).

-- Developing period ($Z_{\text{ad}} < Z_q < Z_{\text{ad}} + \Delta Z_s$)

$$\text{Nu} = \text{Nu}_1 [1 - \exp(2.5x - 10)] + \{\text{Nu}_2 - \text{Nu}_1 [1 - \exp(2.5x - 10)]\}$$

$$(1 - e^{-x} - 0.9 \times e^{-x^2}) \quad (8-8)$$

where $\text{Nu} = h D_{\text{rod}} / k_g$. When $Z_q = Z_{\text{ad}} + \Delta Z_s$, the heat transfer changes from the developing period to the quasi-steady period, where ΔZ_s is computed from

$$\frac{\Delta Z_s}{V_{\text{in}} \rho_f C_p f D_e^2 / k_f} = 6329 (Re + 4000)^{-1.468} F_h \quad (8-9)$$

Other parameters are computed as follows:

$$\begin{aligned} \text{Nu}_2 = \text{Nu}_3 + 108 \exp[-1.83(10^{-5}) Re / (\rho_g / \rho_f)^{0.262}] \\ \exp[-0.0534 (Z - Z_q) / D_e] \end{aligned} \quad (8-10)$$

Nu_1 and Nu_3 are computed by first calculating h_1 and h_3 , respectively, then using the definition of the Nusselt number as follows:

$$h_1 = \text{from equation (8-6)}$$

$$\text{Nu}_1 = h_1 D_e / k_g$$

I. Cadek, F. F., et al., "PWR FLECHT Final Report Supplement," WCAP-7931
October 1972.

$$\frac{h_3(T_{eff,Z} - T_{sat}) D_{rod}}{Q'_{eff,Z}} = 1.21 \left\{ 1 - \exp \left[-3.05(10^{-5}) Re(\rho_g/\rho_f)^{-0.262} \right] \right\} \\ \left\{ 0.714 + 0.286 \left[1 - \exp (-3.05(10^{-4}) (\rho_g/\rho_f)^{1.524} Re^{-2}) \right] \right\} \quad (8-11)$$

$$Nu_3 = h_3 D_e / k_g$$

The other parameters in the above correlation are

$$\Delta T_{eff} = \Delta T_c \left\{ 1 + 60^{**} \left[1.08 \left(\frac{T_{init} - T_{sat}}{\Delta T_c} \right) - 1.26 \right] \right\}$$

$$\Delta T_c = 427^0C (800^0F)$$

$$T_{eff} = T_{init} + \Delta T_{eff}$$

$$T_{eff,Z} = T_{sat} + (T_{eff} - T_{sat}) \frac{Q'(Z_q)}{Q'(Z_{peak})}$$

$$x = 4(Z_q - Z_{ad})/\Delta Z_s$$

D_e = hydraulic diameter of channel formed by four adjacent rods [m (ft)]

ρ_f = density of water at saturation temperature [kg/m^3 (lbm/ft^3)]

ρ_g = density of steam at saturation temperature [kg/m^3 (lbm/ft^3)]

C_{pf} = specific heat of water at saturation temperature [$\text{j/kg-}^0\text{C}$ ($\text{Btu/lbm-}^0\text{F}$)]

k_f = conductivity of water at saturation temperature [$\text{j/sec-}^0\text{C-m}$ ($\text{Btu/sec-}^0\text{F-ft}$)]

Q'_{eff} = $2297 \text{ w/m} = 2297 \text{ j/sec-m}$ (0.7 kw/ft)

$Q'_{eff,Z}$ = $Q'_{eff} Q'(Z_q)/Q'(Z_{peak})$

k_g = conductivity of steam at saturation temperature
[j/sec- $^{\circ}$ C-m (Btu/sec- $^{\circ}$ F-ft)]

D_{rod} = rod diameter [m (ft)]

$$Re = \rho_f V_{in} D_e / \mu_f$$

-- Quasi-steady period ($Z_q > Z_{ad} + \Delta Z_s$)

$$Nu = Nu_2$$

-- Above peak elevation ($Z > Z_{peak}$)

$$Nu = Nu_4 - 44.2 \left[1 - \frac{Q'(Z)}{Q'(Z_{peak})} \right] \exp \left[-0.00304 (Z - Z_{peak})/D_e \right]$$

where $Nu_4 = Nu_1$ for radiative heat transfer period, Nu_4 = equation (8-8) for developing period, and $Nu_4 = Nu_2$ for quasi-steady period.

It should be noted that, in the above correlation, all expressions are in dimensionless forms except equation (8-6), which is primarily due to the radiation. Therefore consistent units must be used.

The above correlations are valid over the following range of parameters:

Pressure (P)	103 - 414 kPa (15 - 60 psia)
Inlet subcooling (ΔT_{sub})	9 $^{\circ}$ C - 78 $^{\circ}$ C (16 $^{\circ}$ F - 140 $^{\circ}$ F)
Initial temperature (T_{init})	149 $^{\circ}$ C - 1204 $^{\circ}$ C (300 $^{\circ}$ F - 2200 $^{\circ}$ F)
Flooding rate (V_{in})	1.02 - 25.4 cm/sec (0.4 - 10 in./sec)
Equivalent peak power ($Q'_{max, eq}$)	0.984 - 6.56 kw/m (0.3 - 2 kw/ft)

where the equivalent peak power is the power equivalent to the peak power of the FLECHT cosine power shape when the integrated power is preserved. That is,

$$Q'_{\max, \text{eq}} = \int_0^{Z_{\text{peak}}} Q'(Z) dZ \left/ \left(\int_0^{Z_{\text{peak}}} \frac{Q'(Z)}{\overline{Q'(Z)_{\text{peak}}}} dZ \right) \right. \text{FLECHT cosine}$$

$$= Q'_{\max} \int_0^{Z_{\text{peak}}} \frac{Q'(Z)}{\overline{Q'(Z)_{\text{peak}}}} dZ \left/ \left(\int_0^{Z_{\text{peak}}} \frac{Q'(Z)}{\overline{Q'(Z)_{\text{peak}}}} dZ \right) \right. \text{FLECHT cosine}$$

In terms of dimensionless parameters, the above range of parameters can be written as

$C_Q \left[= \int_0^{Z_{\text{peak}}} Q'(Z) dZ / (\rho_f A_f V_{in} h_{fg}) \right]$	0.204 - 1.14
$C_T \left[= (T_{init} - T_{sat}) / (T_{Lei} - T_{sat}) \right]$	0.146 - 6.9
ρ_g / ρ_f	0.000636 - 0.0036
$(C_{\rho_f} \Delta T_{SUB} / h_{fg})$	0.0165 - 0.158
$Re \left[= \rho_f V_{in} D_e / \mu_f \right]$	470 - 8620
$Z_{\text{peak}} / D_{\text{rod}}$	61 - 284

It is also noted that the dominating term in equation (8-3) of the quench correlation is the first term in the expression for F_{t5} . The next dominating term is the brace containing parameter C_Q in the expression for F_{t1} . The third dominating term is the brace containing ΔT_{SUB} in the expression for F_{t1} . As for the heat transfer coefficient correlation, since the expressions are quite simple, nothing can be said about dominating terms.

Figures 8-10 through 8-12 compare the present heat transfer correlation with the data of the first set of overlap runs (table 8-1). The comparisons of the other sets of overlap runs can be found in appendix G. The comparisons of nonoverlap runs are in appendix H. These comparisons are in good agreement except for a few runs in which the quench time prediction is slightly off.

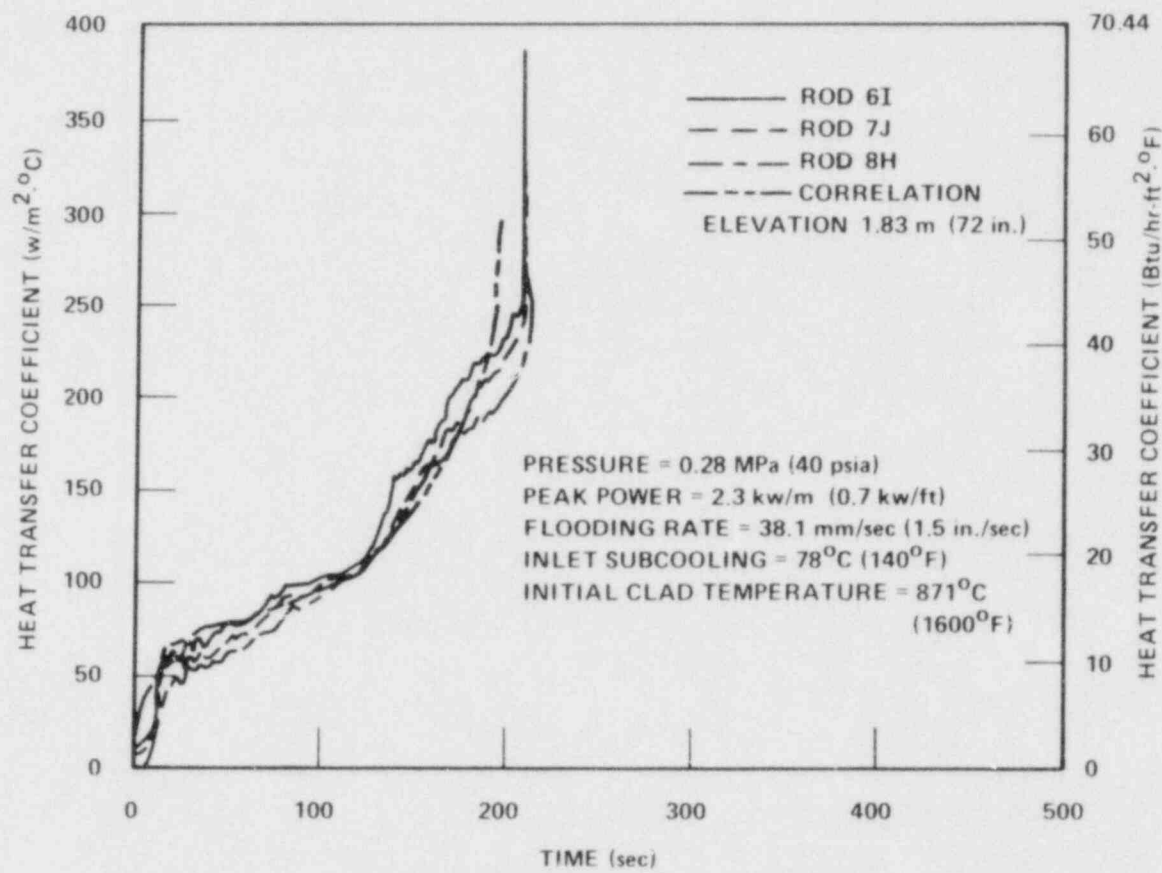


Figure 8-10. Comparison of Heat Transfer Coefficient Correlation With Data From FLECHT SEASET Run 31203

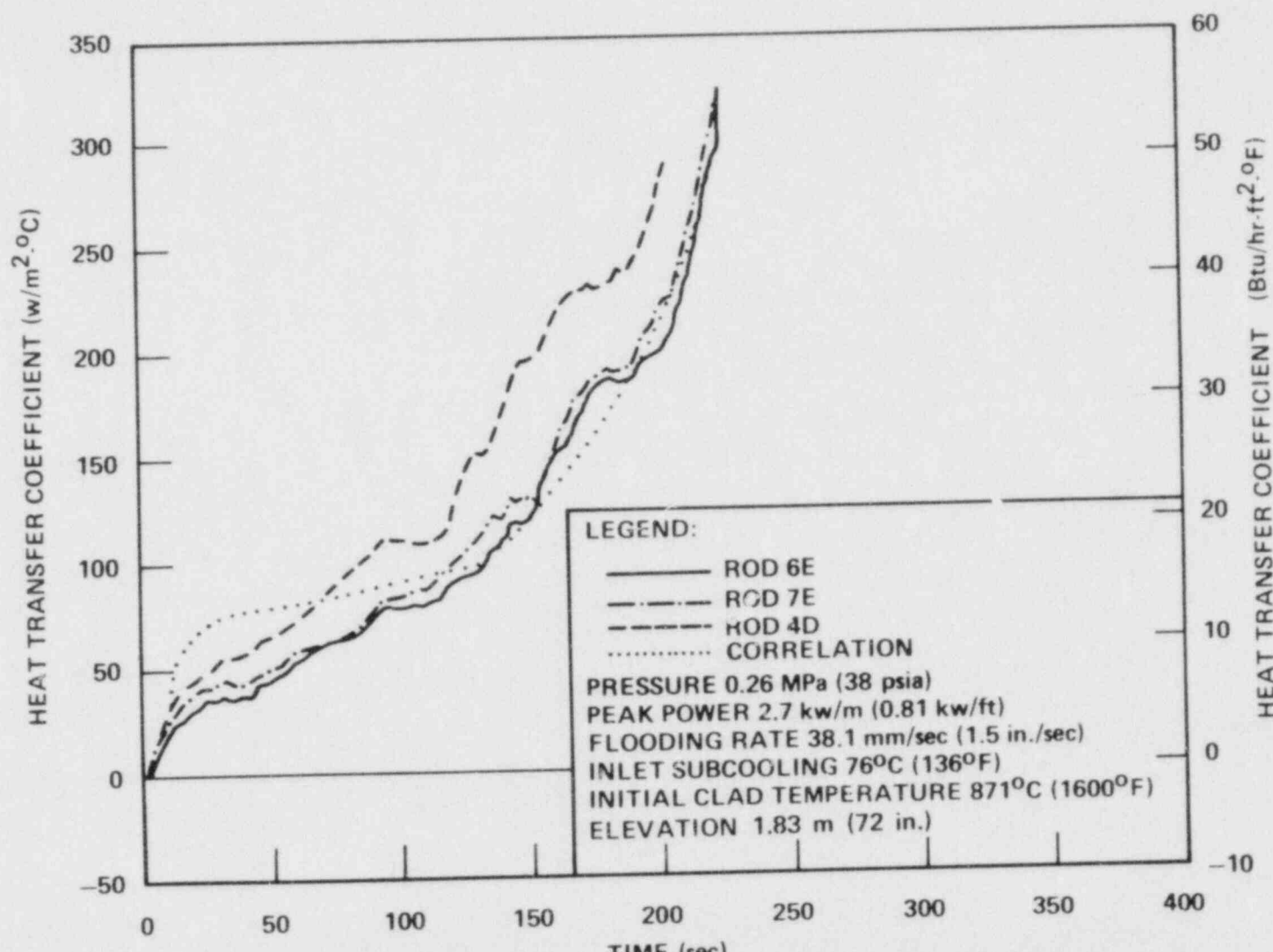


Figure 8-11. Comparison of Heat Transfer Coefficient Correlation With Data From Cosine Power Run 03113

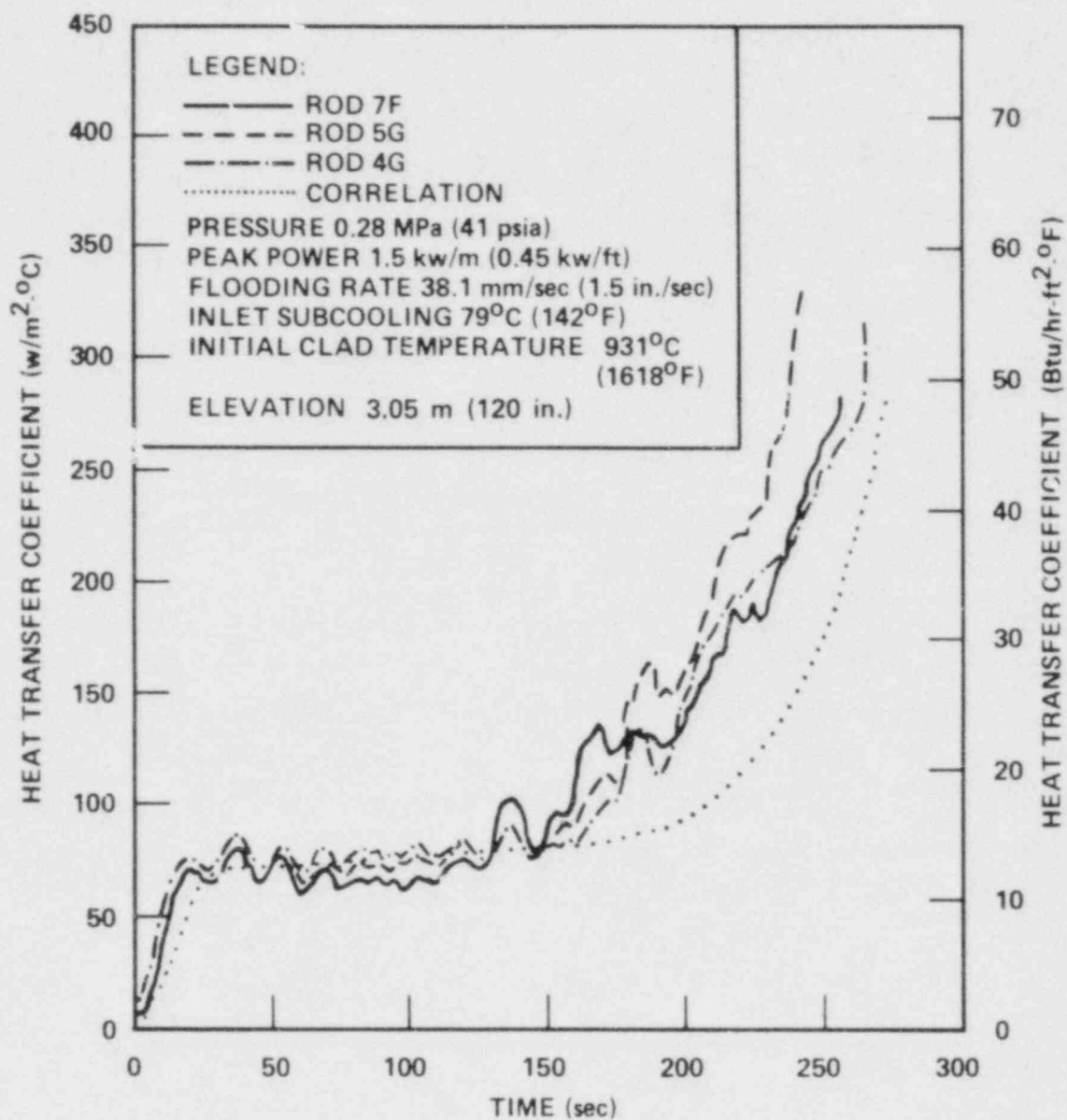


Figure 8-12. Comparison of Heat Transfer Coefficient Correlation With Data From Skewed Power Run 11618

Figures 8-13 through 8-15 compare the present heat transfer correlation with the previous correlations of WCAP-9183 and WCAP-8838 and the data. Again, in general the present correlation is in better agreement with data than the previous correlations.

Comparisons of the present correlation with some of the boiling water reactor (BWR) FLECHT data⁽¹⁾ and Semiscale test data⁽²⁾ were also made, with reasonably good agreement.

Figures 8-16 and 8-17 are typical comparisons of the Semiscale test data. In figure 8-17, the heater rod clad surface temperature rather than the heat transfer coefficient has been compared, since the heat transfer coefficient of the Semiscale tests is not available. The predicted temperature in figure 8-17 was computed by using the heat transfer coefficient predicted from the present correlation. In Semiscale tests, the heated length of the rod bundle is only 1.68 m (66 in.), with the peak power elevation at 0.66 m (26 in.). That is, the power shape is slightly skewed to the bottom. The diameter and filler material of the heater rod of Semiscale tests are the same as those of the FLECHT tests.

Figure 8-18 shows the comparison of the heat transfer correlation with a BWR FLECHT test that had bottom flooding only. The figure shows reasonable agreement between the data and correlation. The test conditions are given in the figure. The BWR FLECHT tests had a flatter cosine power shape (1.47 peak power to average) compared with the PWR FLECHT tests. The rod diameter for the BWR FLECHT tests was also larger [11.45 mm (0.451 in.) versus 10.75 mm (0.423 in.) for the PWR FLECHT rod]. The BWR heater rod was MgO filled instead of BN filled.

The listing of the computer program for the above correlation is reproduced in appendix I. It is recommended that the program listing be used for any calculations using this correlation.

-
1. McConnell, J. W., "Effect of Geometry and Other Parameters on Bottom Flooding Heat Transfer Associated With Nuclear Fuel Bundle Simulators," ANCR-1049, Aerojet Nuclear Company, 1972.
 2. Crapo, H. S., et al., "Experimental Data Report for Semiscale Mod-I Tests S-03-A, S-03-B, S-03-C, and S-03-D (Reflood Heat Transfer Tests)," ANCR-NUREG-1307, Aerojet Nuclear Company, 1976.

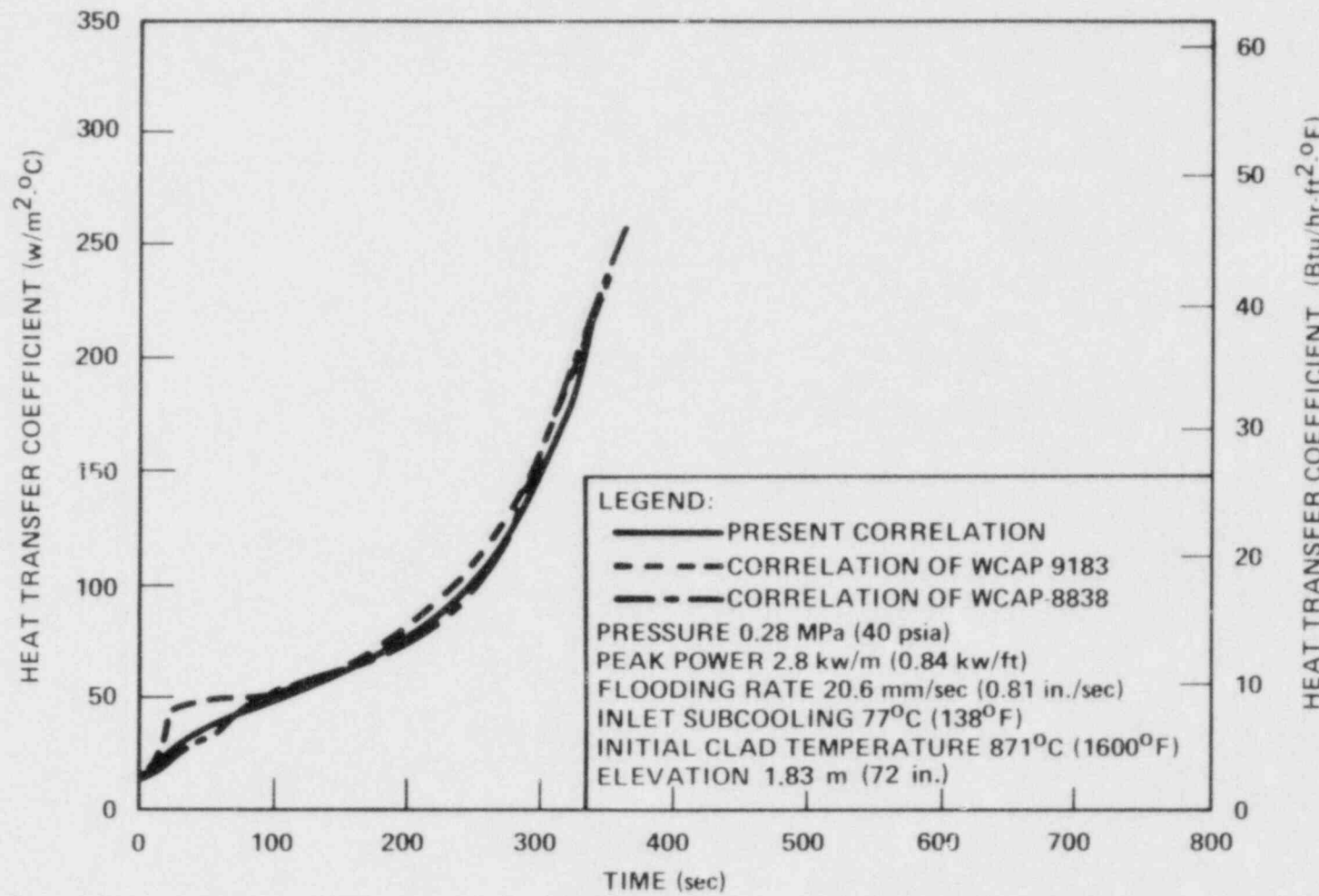


Figure 8-13. Comparison of Present Heat Transfer Coefficient Correlation With Previous Correlations, Cosine Power Run 02414

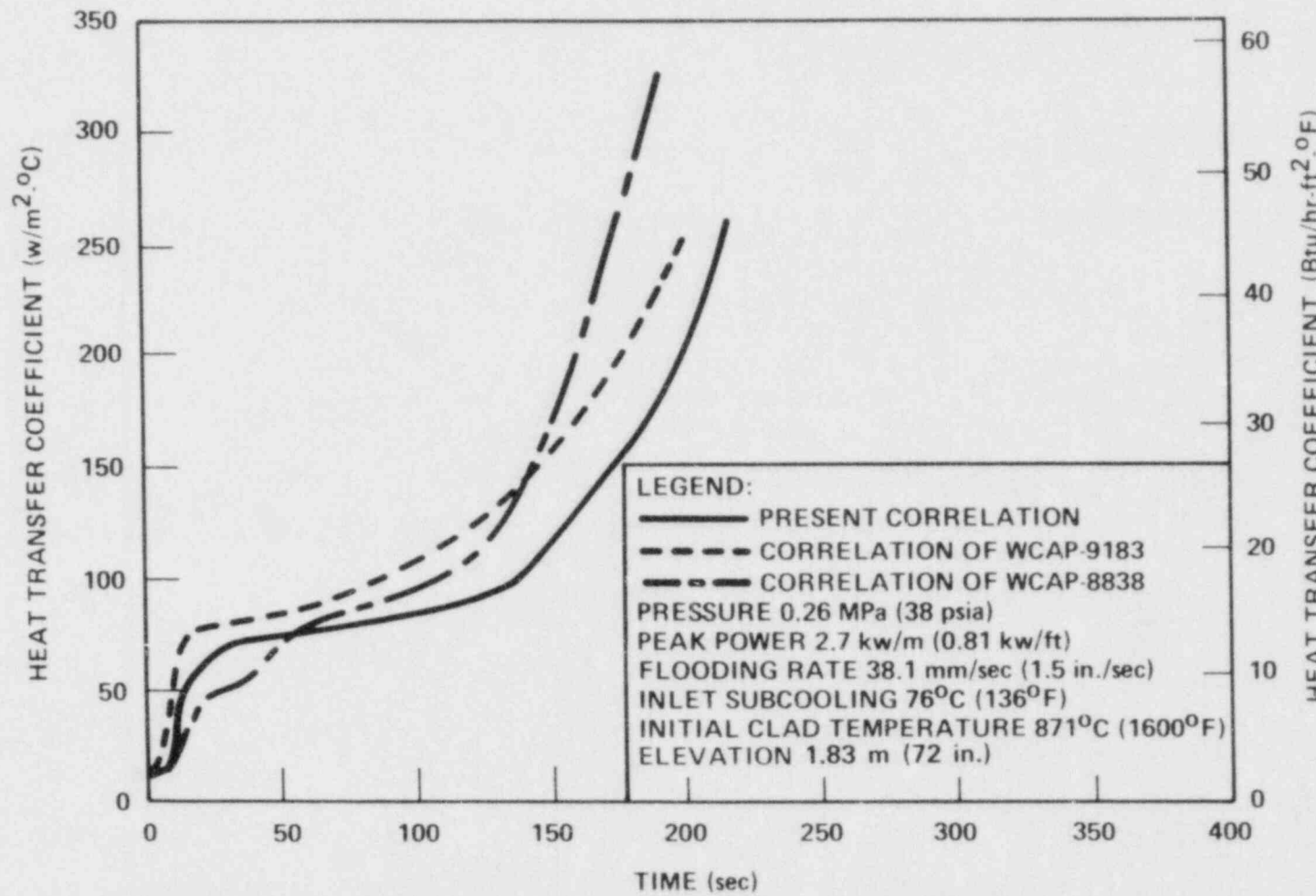


Figure 8-14. Comparison of Present Heat Transfer Coefficient Correlation With Previous Correlations, Cosine Power Run 03113

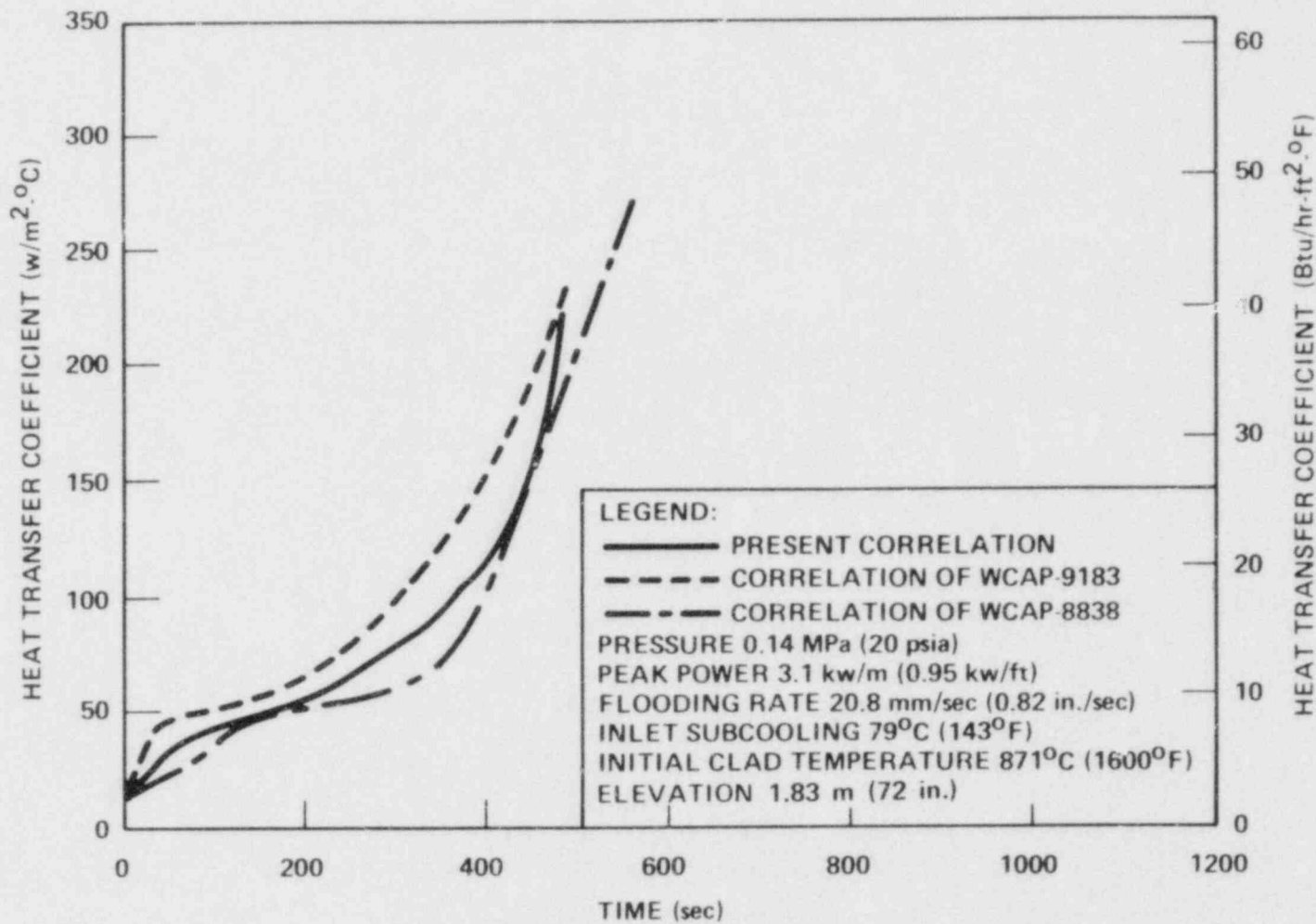


Figure 8-15. Comparison of Present Heat Transfer Coefficient Correlation With Previous Correlations, Cosine Power Run 06638

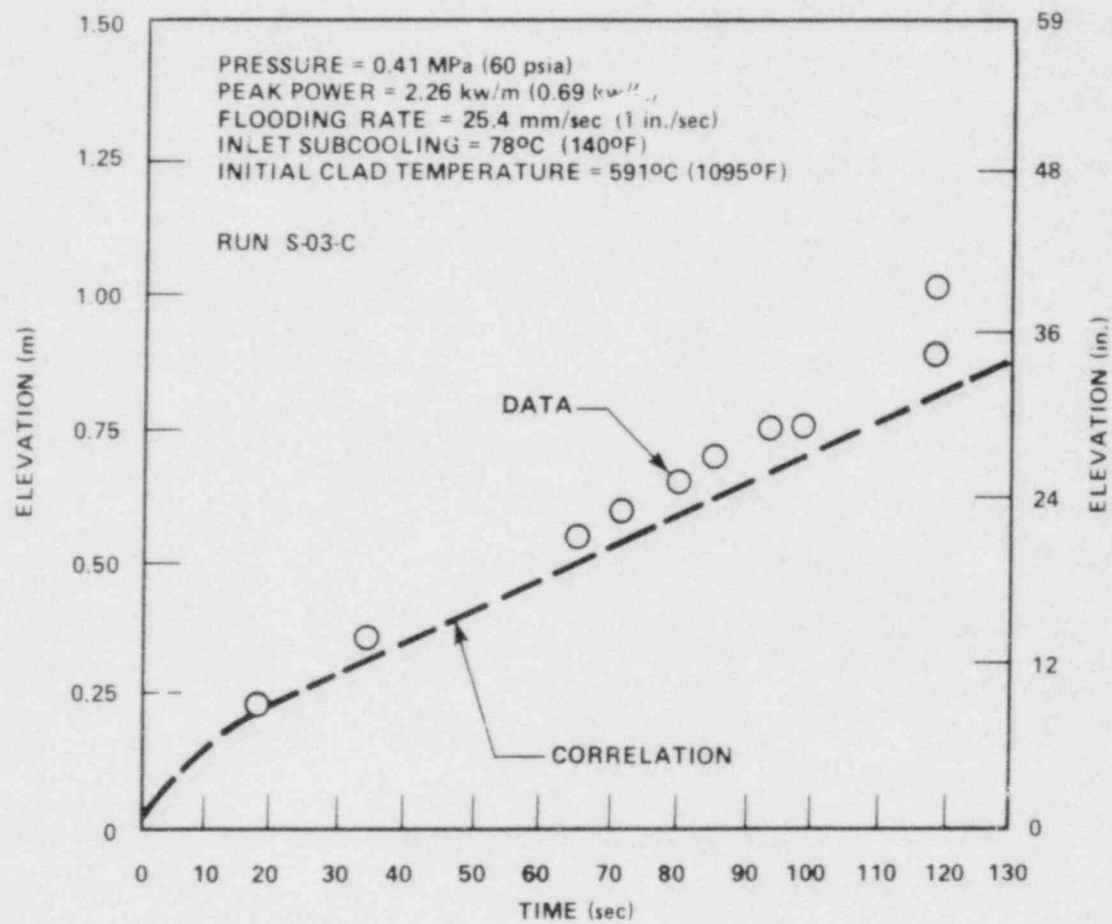


Figure 8-16. Comparison of Predicted and Measured Quench Front Elevations for a Semiscale Test

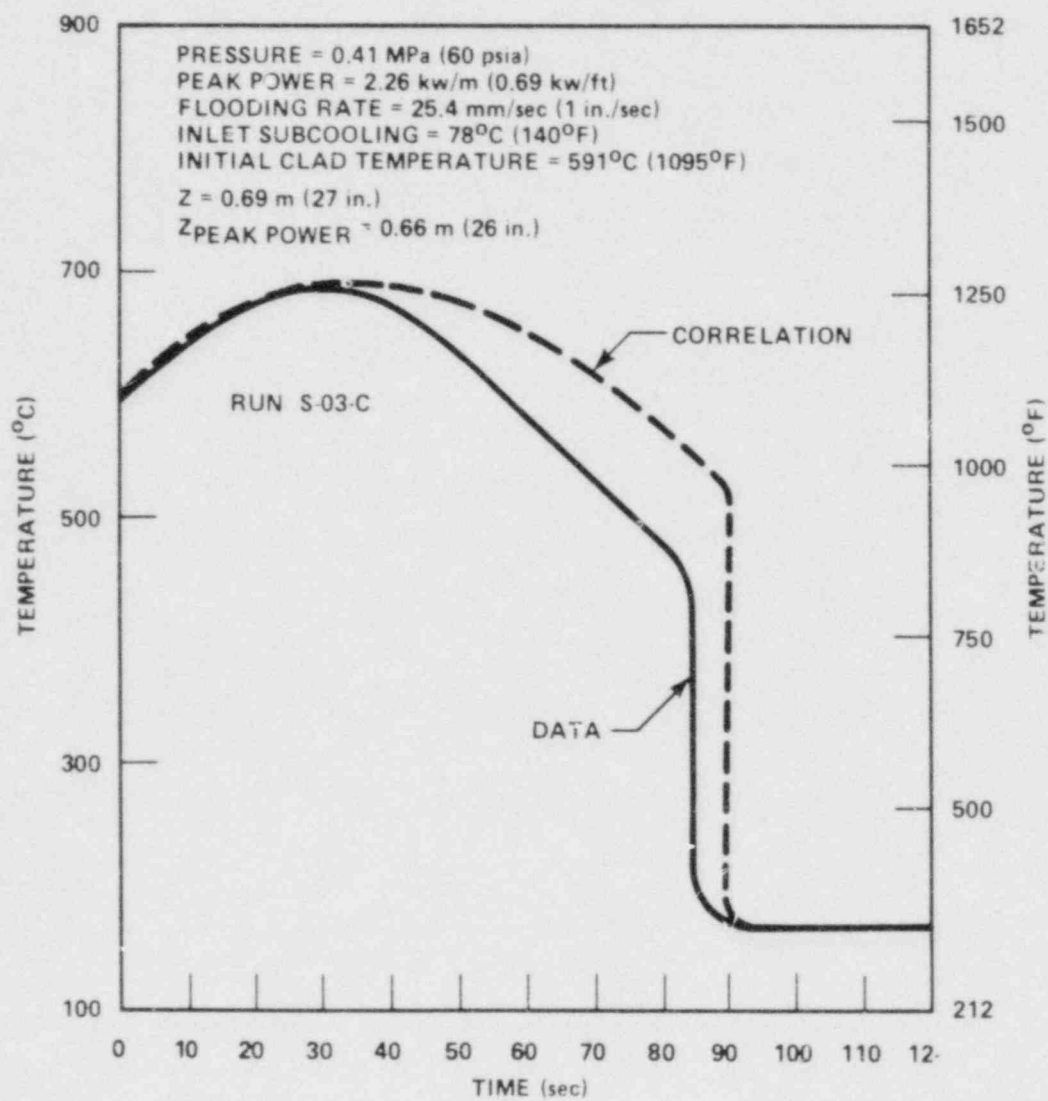


Figure 8-17. Comparison of Predicted and Measured Clad Surface Temperatures for a Semiscale Test

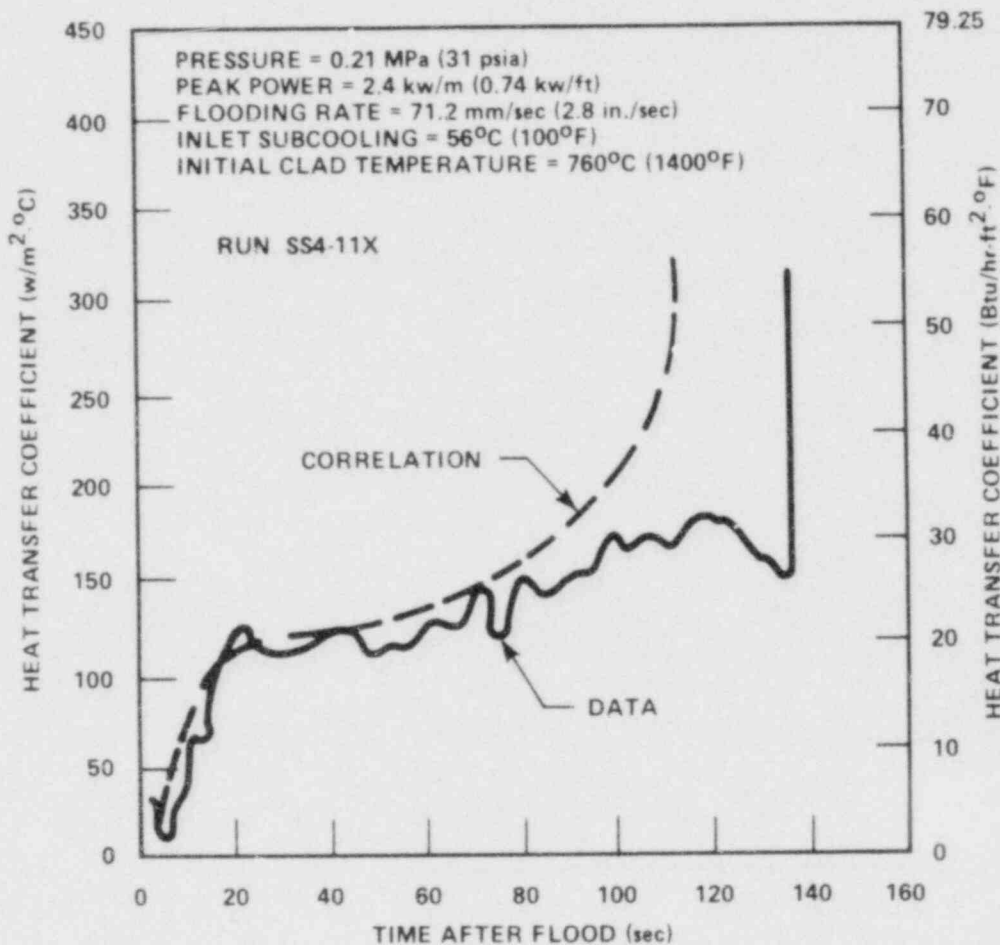


Figure 8-18. Comparison of Predicted and Measured Heat Transfer Coefficients for a BWR FLECHT Test

SECTION 9

CONCLUSIONS AND RECOMMENDATIONS

The objectives of the unblocked bundle task have been achieved. Further understanding of the reflood heat transfer mechanisms is documented in this report and can be used for assessing state-of-the-art prediction models. A new FLECHT-type heat transfer correlation has been provided which can predict the FLECHT SEASET 17x17 data as well as the older FLECHT data. Detailed conclusions and recommendations are given below.

Qualitative trends of the FLECHT SEASET unblocked bundle tests are consistent with the previous findings in the low flooding rate cosine and skewed test series. The effect of bundle geometry (rod diameter and pitch) difference was found to be minimal if the scaling scheme of maintaining the same integrated power per unit flow area is met.

Increased sophistication of test hardware and instrumentation have made possible a significantly better understanding of the reflood heat transfer process. In particular, steam temperatures measured at several elevations in the bundle made it possible to calculate more accurate local quality and to obtain the trend of quality changes in the bundle.

The following items represent the significant results and accomplishments of the present analysis of the unblocked bundle task of FLECHT SEASET:

- The scaling logic of maintaining the same integrated power per unit flow area is valid.
- Local qualities at several elevations in the bundle were estimated to show high nonequilibrium between steam and water above the quench front.
- A method has been developed to calculate the quality just above the quench front using mass and energy balances below the quench front.

- Models for estimating effluence rate have been reviewed and a better understanding has been provided. The new models can be used to estimate the mass effluence rate of high flooding rate tests.
- Preliminary work has been done to aid in understanding of the transition zone above the quench front.

A unique feature of the data evaluation effort was the extensive use of the droplet size and velocity data deduced from the high-speed movies. Making use of the drop size data obtained at movie camera locations, local two-phase flow conditions (such as drop size and velocity, slip ratio, and void fraction) were calculated as a function of axial positions from the transition front (onset of dispersed flow regime) to the bundle exit.

Radiation heat exchange in the rod bundle system was calculated by a network analysis. It was found that radiation to droplets is important near the transition front, and surface-to-surface radiation is important at higher elevations.

By subtracting the radiation component from the total heater rod heat flux (calculated from the measured heater rod temperatures by an inverse conduction technique), the convective heat transfer component was deduced. It was found that the convective heat transfer during reflood was generally higher than that which could be predicted by conventional single-phase heat transfer correlations (when no droplet evaporation was assumed). Also, the droplet was found to play an important role in the transfer enhancement in dispersed flow and the heat transfer enhancement are proportional to the droplet density or droplet volume fraction (1 minus vapor void fraction).

Making use of the information obtained from the data evaluation as boundary conditions, a mechanistic model was proposed to predict the two-phase flow properties and wall temperature transients in the dispersed flow regime. The droplet evaporation rate or heat transfer was overpredicted near the transition front and was underpredicted at higher elevations. As a result, the wall temperature was underpredicted at lower elevations and was overpredicted at higher elevations. Continuing work to improve the droplet model is expected to give better predictions for the heat transfer and wall temperature transients.

A heat transfer correlation in dimensionless form is presented in this report. The correlation is basically developed from the correlation of WCAP-9183, which is based on the theory that the heat transfer coefficient is primarily a function of distance from the quench front. The present correlation is more general, since it is in dimensionless form and preserves power per flow area. Comparison of the correlation with the FLECHT 15x15 cosine power and skewed power data, the FLECHT SEASET 17x17 data, the BWR FLECHT data, and the Semiscale test data shows generally good agreement.

As a result of the data analysis and evaluation effort, areas which may require in-depth technical examination are identified. These areas are as follows:

- Development of instruments to measure steam temperatures in relatively low quality environments. This will allow the calculation of flow quality at the bundle exit which will result in more accurate bundle quality data.
- Continual development for a dispersed flow model with added attention given to the upper elevations
- Development of a mechanistic model for the transition region over a large range of conditions
- Development of state-of-the-art photographic techniques to obtain the details of the transition zone

Using the results of the analysis of the 17x17 FLECHT-SEASET data and the development of dispersed flow models, heat transfer enhancement models, and analysis of the droplet data, it is hoped that state-of-the-art model and code developers can improve and assess their models.

APPENDIX A

MASS STORAGE IN BUNDLE

The change of mass storage in a bundle is due to two phenomena: the advance of the quench front and the density change both below and above the quench front. The concern here is the magnitude of mass storage change due to the second phenomenon.

The mass balance between two fixed elevations either below or above a quench front in a bundle can be written as

$$\dot{M}_{in} - \dot{M}_{out} = A \frac{d}{dt} \int_{Z_1}^{Z_2} \rho dZ \quad (A-1)$$

where

\dot{M}_{in} = mass flow rate at Z_1

\dot{M}_{out} = mass flow rate at Z_2

A = bundle flow area

The right-hand side of equation (A-1) is the change of mass storage in the control volume. Therefore it is necessary to determine the relative magnitudes of the three terms in equation (A-1), to determine the importance of the storage change term.

The storage term in equation (A-1) can be rewritten for the FLECHT SEASET unblocked bundle as

$$\dot{M}_{st} = \frac{d}{dt} \int_{Z_1}^{Z_2} A \rho dZ$$

$$\begin{aligned}
 &= \frac{d}{dt} (A \bar{\rho} \Delta Z) \\
 &= 24 \frac{d(\Delta p^l)}{dt}
 \end{aligned} \tag{A-2}$$

where

$\bar{\rho}$ = average density in the axial interval of $\Delta Z = (Z_2 - Z_1)$

Δp^l = hydrostatic pressure difference along the axial interval of ΔZ

The last relation of equation (A-2) is valid when M_{st} and Δp are expressed in lb/sec and psi, respectively.

The available differential pressure data include the effect of mass storage, acceleration, and friction. But if it is assumed that the components due to acceleration and friction are not a strong function of time,⁽¹⁾ equation (A-2) can be modified as

$$\dot{M}_{st} = 24 \frac{d(\Delta p)}{dt} \tag{A-3}$$

where Δp is a pressure drop measured by differential pressure cells. This relation can be utilized in the comparison of the magnitudes of the terms in equation (A-1) as shown in the following paragraphs.

Figure A-1 shows the differential pressure measurement at the interval of $Z = 0.91$ to 1.22 m (36 to 48 in.) as a function of time for run 31504. The curve can be divided into three periods as indicated in the figure. As discussed in section 5, period I is the period when the transition zone front is below $Z = 0.91$ m (36 in.), period II is the period when the quench front is between 0.91 m (36 in.) and 1.22 m (48 in.), and period III is the

I. Lottus, M. J., et al., "PWR FLECHT SEASET Unblocked Bundle, Forced and Gravity Reflood Task Data Report," NRC/EPRI/Westinghouse-7, June 1980.

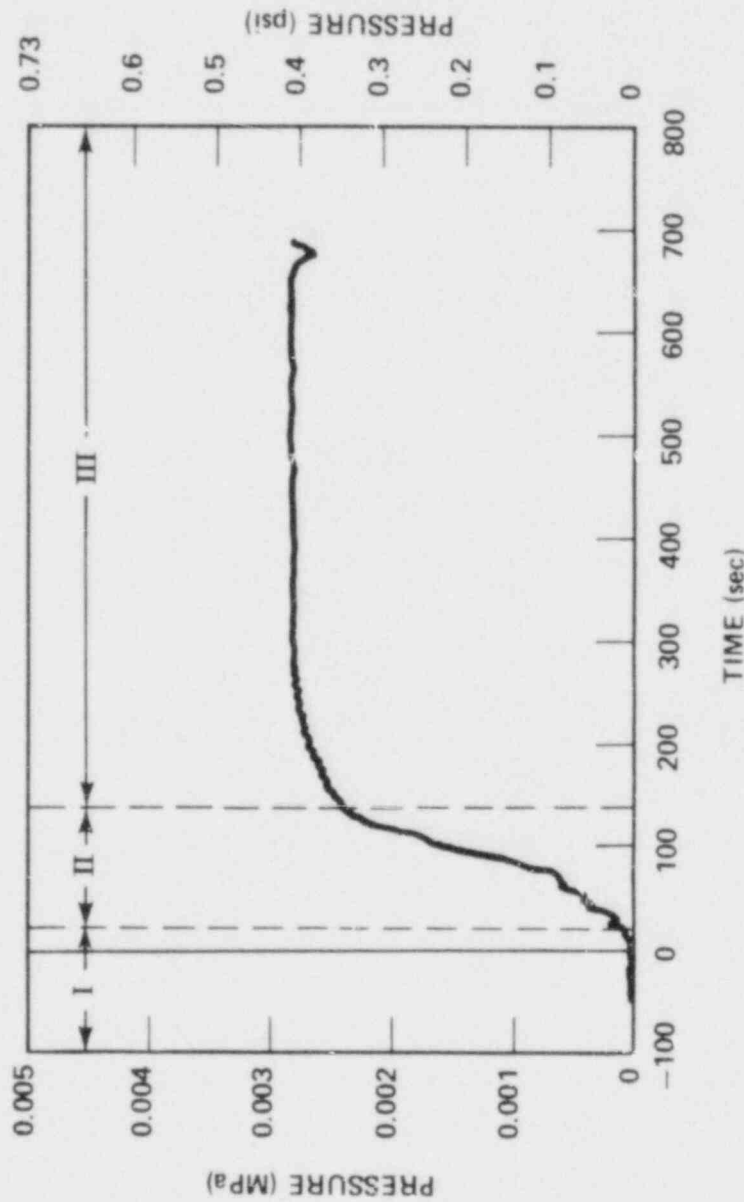


Figure A-1. Differential Pressure Curve at the Int. rvl of 0.91 to 1.22 m
(36 to 48 in.), Run 31504

period when the quench front is above 1.22 m (48 in.). Therefore the mass storage change term of concern for these purposes should be considered during periods I or III. The change in period II is predominantly affected by the advance of the quench front.

When the 0.91 to 1.22 m (36 to 48 in.) interval is located above the quench front, it can be deduced from the figure that

$$\left[\frac{d(\Delta p)}{dt} \right]_{\max} \approx 0$$

Therefore, from equation (A-3), the storage term change is zero. Thus the storage change term in this interval is negligible. The same argument also applies to other intervals, because the same trend was observed for the intervals.

When the interval is immersed in water,

$$\left[\frac{d(\Delta p)}{dt} \right]_{\max} \approx \frac{1}{1800}$$

Therefore, from equation (A-3),

$$\dot{M}_{st} = 5.9 \text{ g/sec (0.013 lb/sec)}$$

The mass flow rate below the quench front is 367 g/sec (0.81 lb/sec) for this case. The flow rate above the quench front at the time when the maximum change is observed is about 336 g/sec (0.74 lb/sec).

Therefore the storage rate is only 1.6 percent of total mass flow rate below the quench front. Since the value taken is the maximum value observed and the rates are lower in other intervals, the accumulation rate is also negligible below the quench front.

A few more runs have been examined, as summarized in table A-1. These runs represent a wide range of flooding rate and power. The results show that the storage change term is relatively insignificant. Further, it must be noted that the estimation uncertainty of the change term is very high because of the differentiation process. Therefore, the inclusion of the storage change term does not guarantee improvement of the analysis.

TABLE A-I
STORAGE RATE CHANGE

Run	Pressure [MPa(psi)]	Peak Power [kw/m (kw/ft)]	Flooding Rate [mm/sec (in./sec)]	Flooding Mass Flow [g/sec (lb/sec)]	$(M_{st})_{max}$ Below Quench Front [g/sec (lb/sec)]	$(M_{st})_{max}$ Above Quench Front [g/sec (lb/sec)]
31504	0.28 (40)	2.3 (0.7)	24.6 (0.97)	367 (0.81)	4.5 (0.01)	0 (0)
34209	0.14 (20)	2.3 (0.7)	27.2 (1.07)	376 (0.83)	4.5 (0.01)	0 (0)
31701	0.28 (40)	2.3 (0.7)	155 (6.1)	2270 (5.0)	0 (0)	0 (0)
34006	0.27 (39)	1.3 (0.4)	15.0 (0.59)	227 (0.5)	9.1 (0.02)	0 (0)

APPENDIX B

MASS AND ENERGY BALANCE (FLEMB) RESULTS

The FLEMB results from run 31504 have been discussed in sections 4 and 5. The results of the additional runs included in table 4-1 are provided in figures B-1 through B-28. The local and equilibrium quality, mass effluence, and the quality transient at the 1.83 m (72 in.) elevation of each run are presented. It must be noted that two quench front qualities are provided.

The trends observed in run 31504 were generally true for the other runs, which were conducted under various other conditions. For all cases, the estimations of the quench front quality are fairly good. Mass effluence estimations are in good agreement with the data, except for the early time period (6 to 20 sec) of a high flooding rate test [152 mm/sec (6 in./sec)]. However, the predictions are in good agreement with the data after 20 seconds even at this high flooding rate.

The discrepancy during the early period for the high flooding rate test can be traced to several possible reasons:

- Inadequate quench velocity data
- Time required to stabilize the test at the start
- Instrumentation response time delay or test time delay

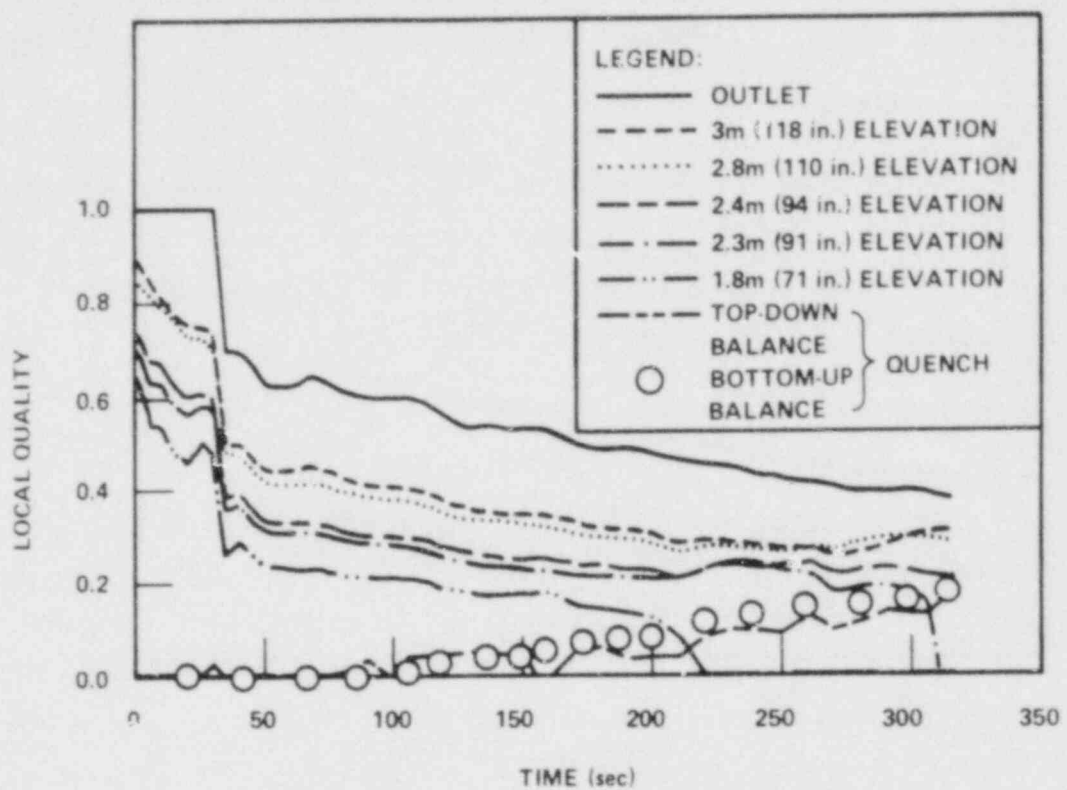


Figure B-1. Local Quality, Run 31203

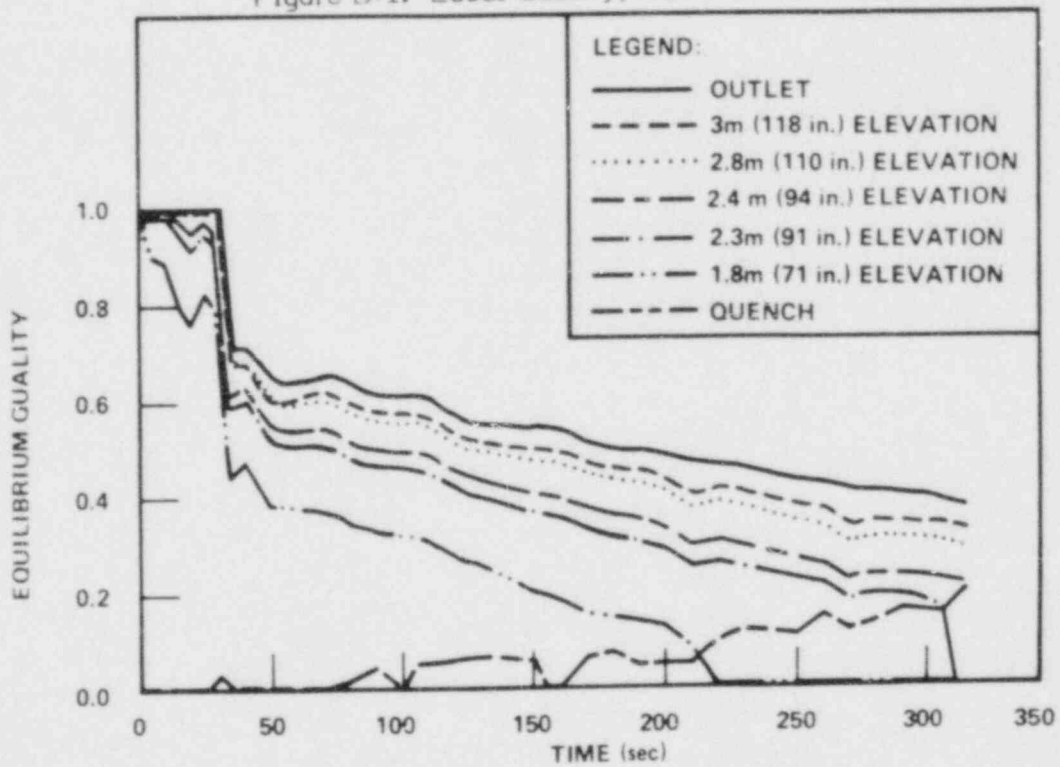


Figure B-2. Equilibrium Quality, Run 31203

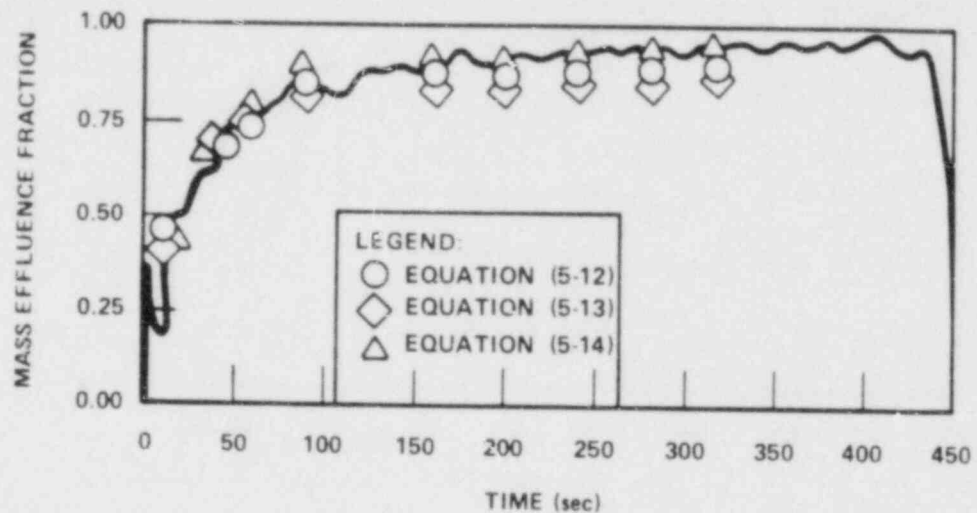


Figure B-3. Mass Effluence, Run 31203

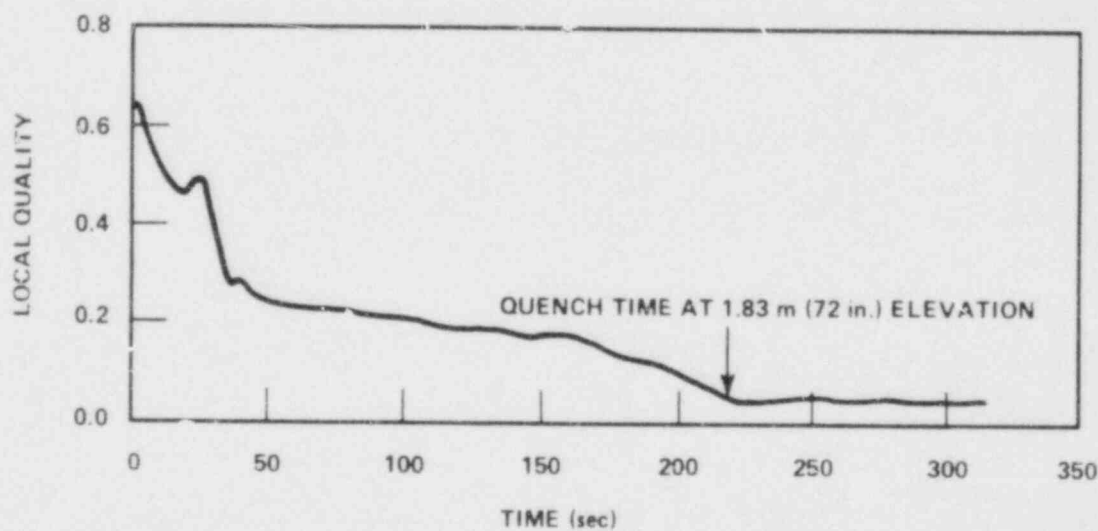


Figure B-4. Quality Transient, 1.83 m (72 in.) Elevation, Run 31203

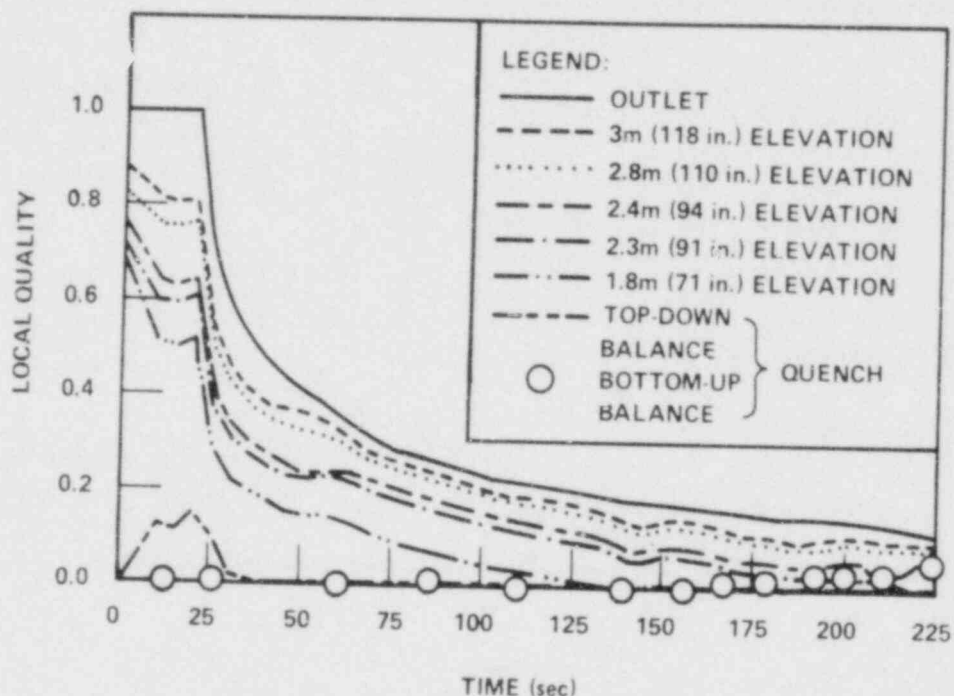


Figure B-5. Local Quality, Run 31302

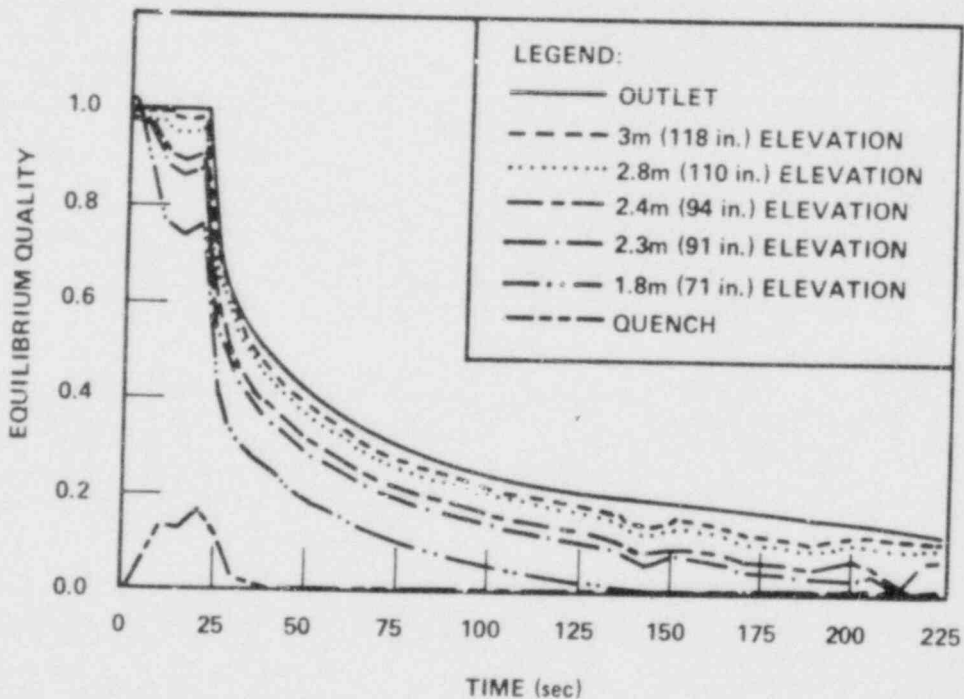


Figure B-6. Equilibrium Quality, Run 31302

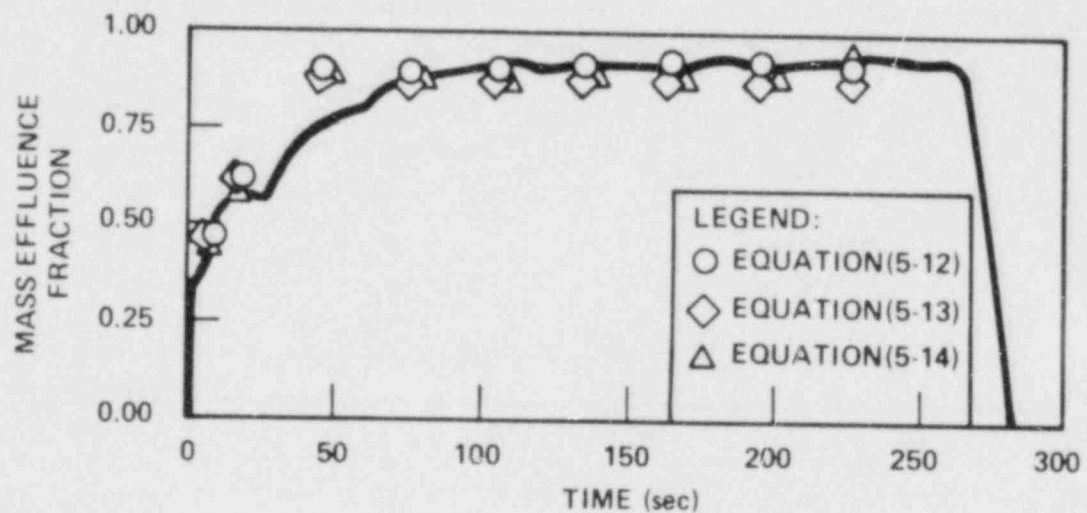


Figure B-7. Mass Effluence, Run 31302

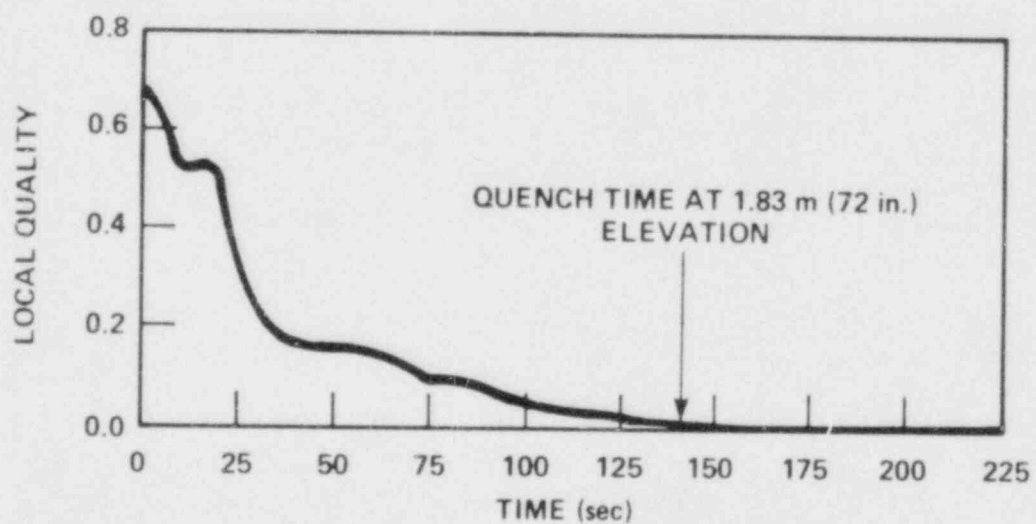


Figure B-8. Quality Transient, 1.83 m (72 in.) Elevation, Run 31302

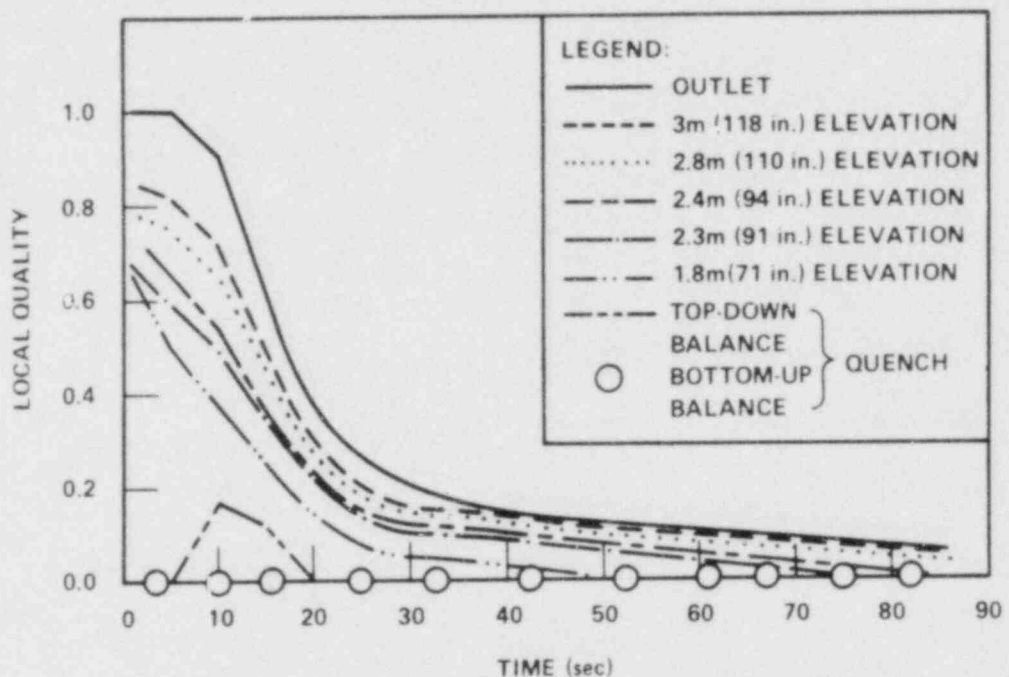


Figure B-9. Local Quality, Run 31701

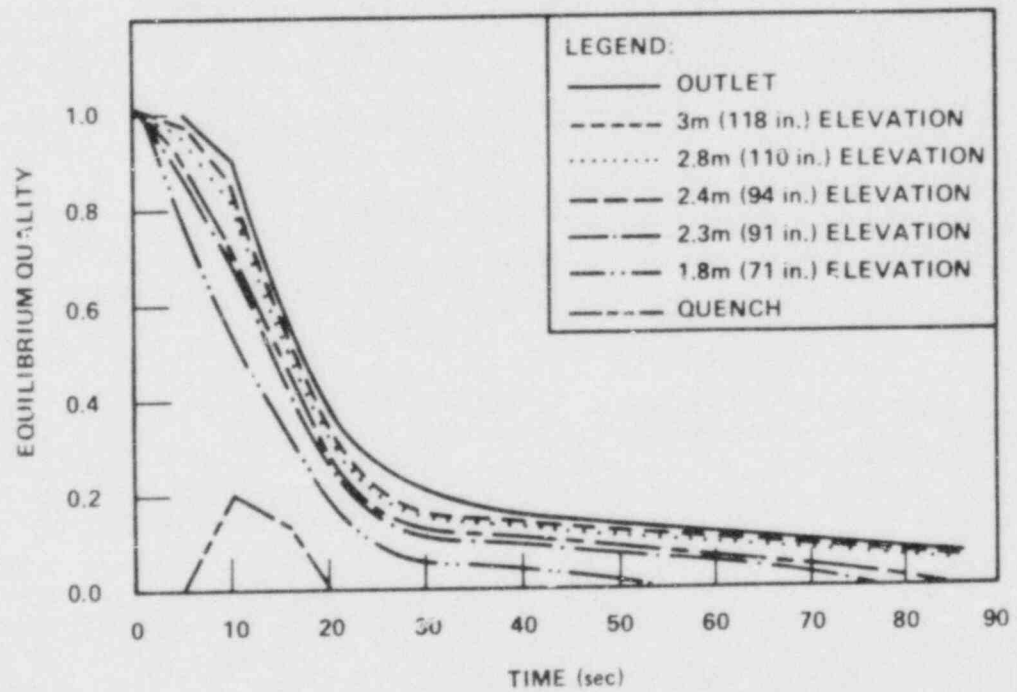


Figure B-10. Equilibrium Quality, Run 31701

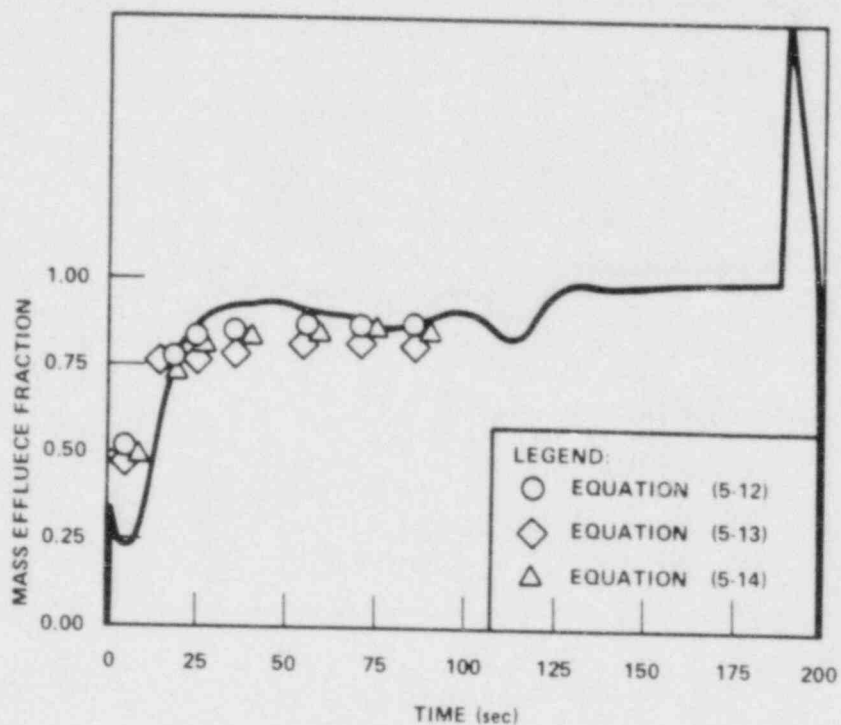


Figure B-11. Mass Effluence, Run 31701

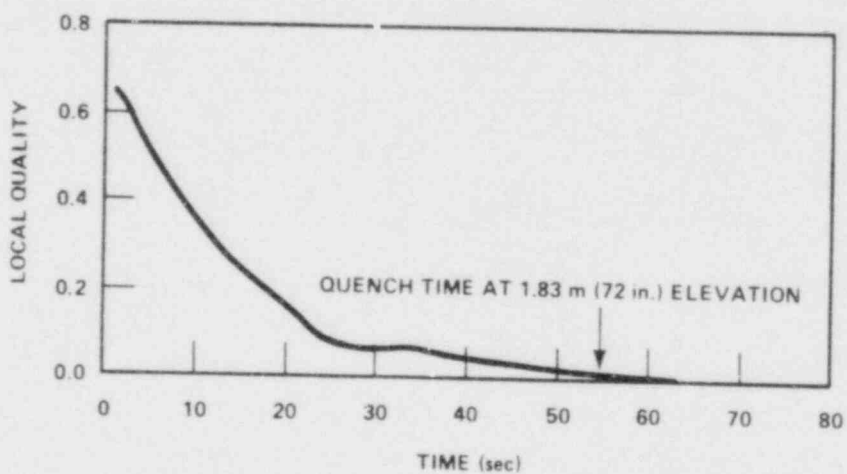


Figure B-12. Quality Transient, 1.83 m (72 in.) Elevation, Run 31701

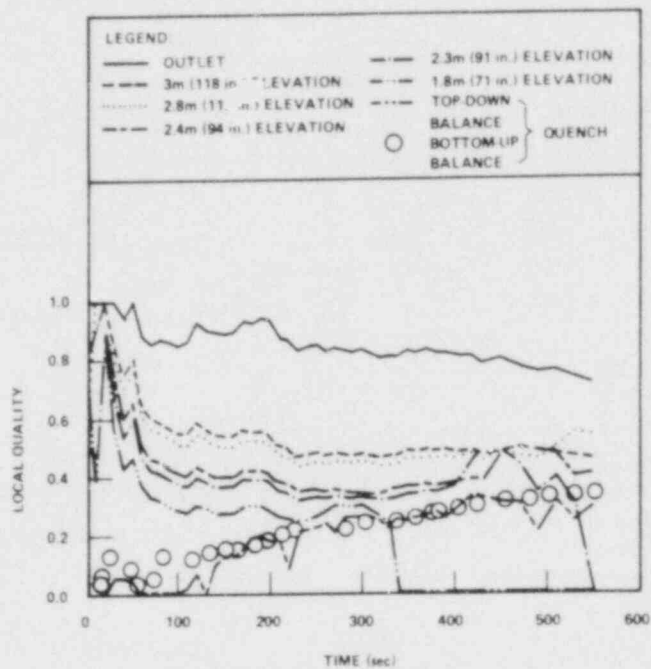


Figure B-13. Local Quality, Run 31805

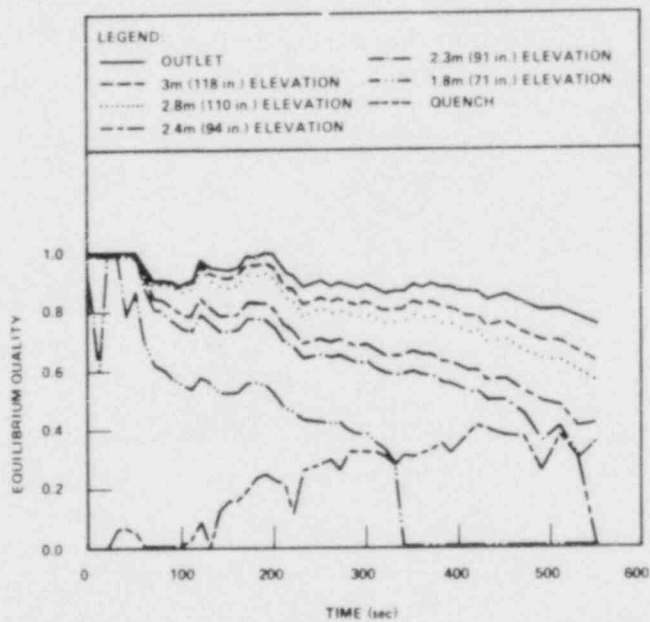


Figure B-14. Equilibrium Quality, Run 31805

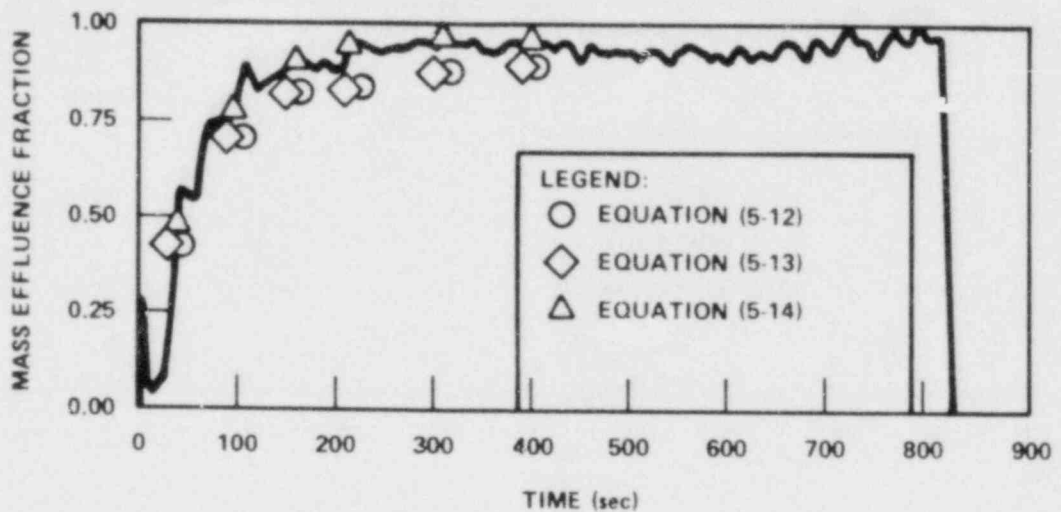


Figure B-15. Mass Effluence, Run 31805

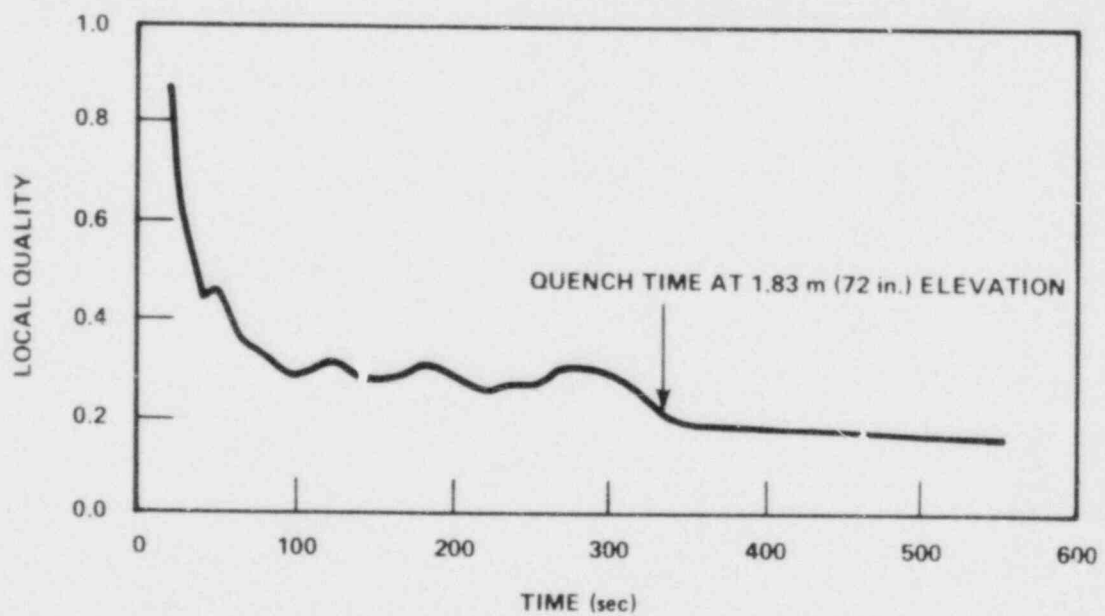


Figure B-16. Quality Transient, 1.83 m (72 in.) Elevation, Run 31805

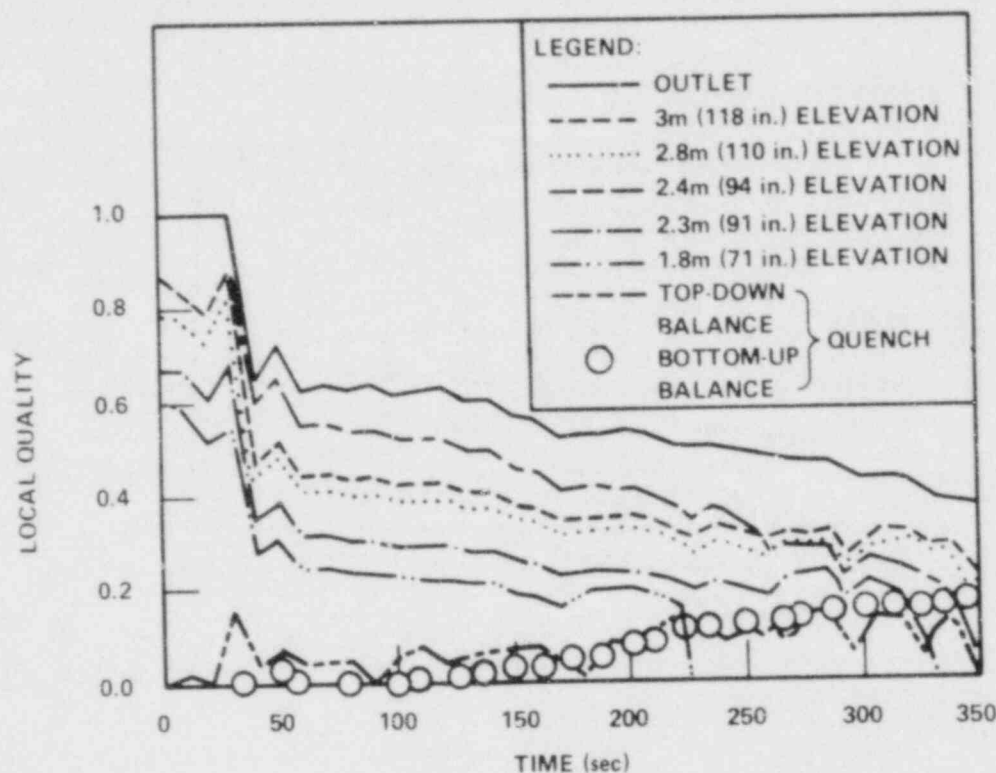


Figure B-17. Local Quality, Run 31922

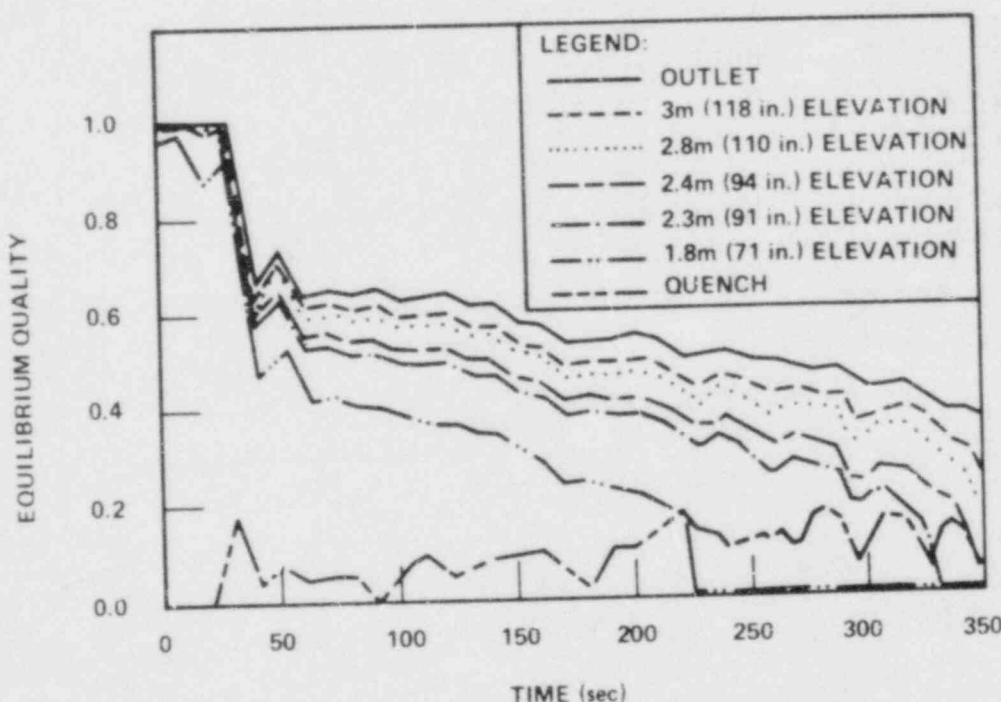


Figure B-18. Equilibrium Quality, Run 31922

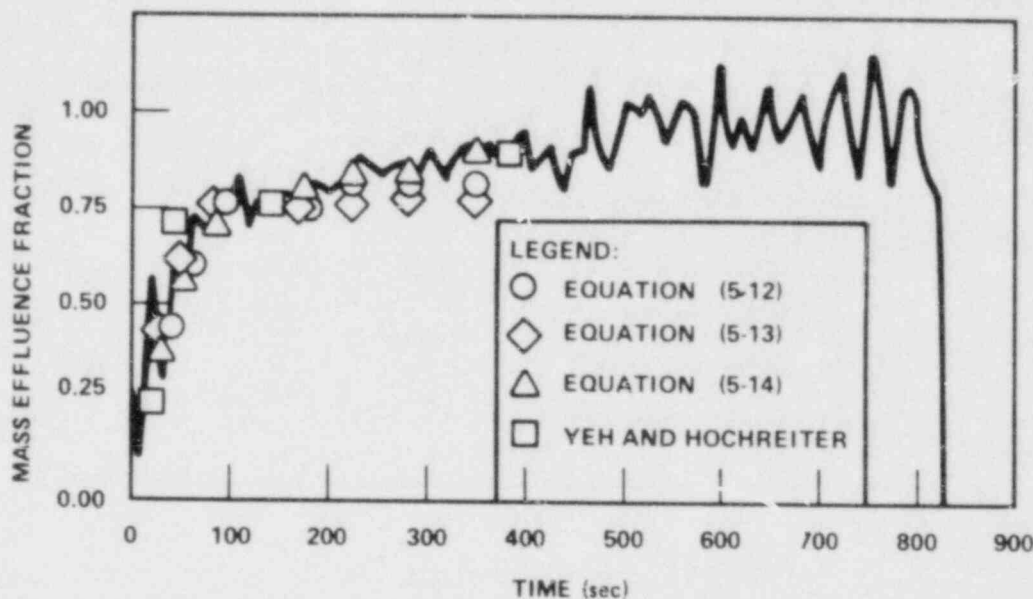


Figure B-19. Mass Effluence, Run 31922

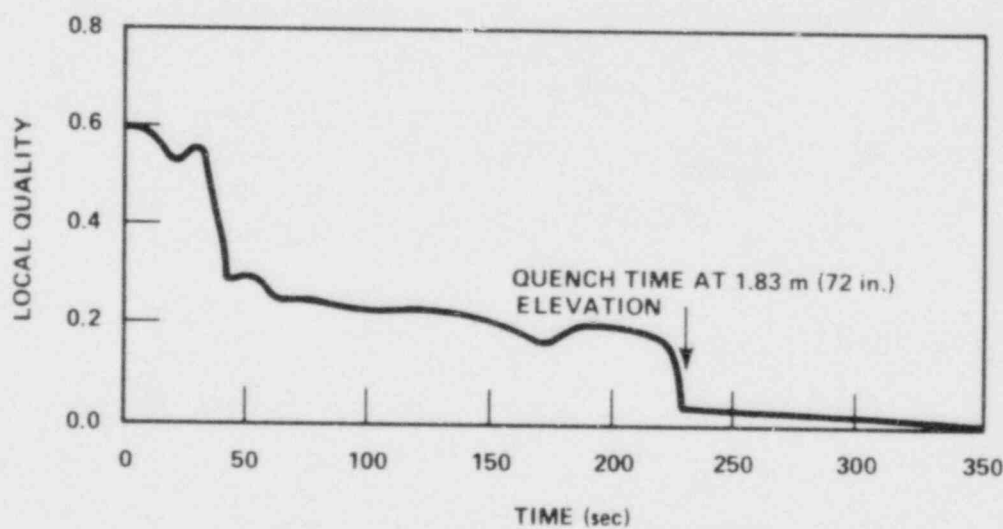


Figure B-20. Quality Transient, 1.83 m (72 in.) Elevation, Run 31922

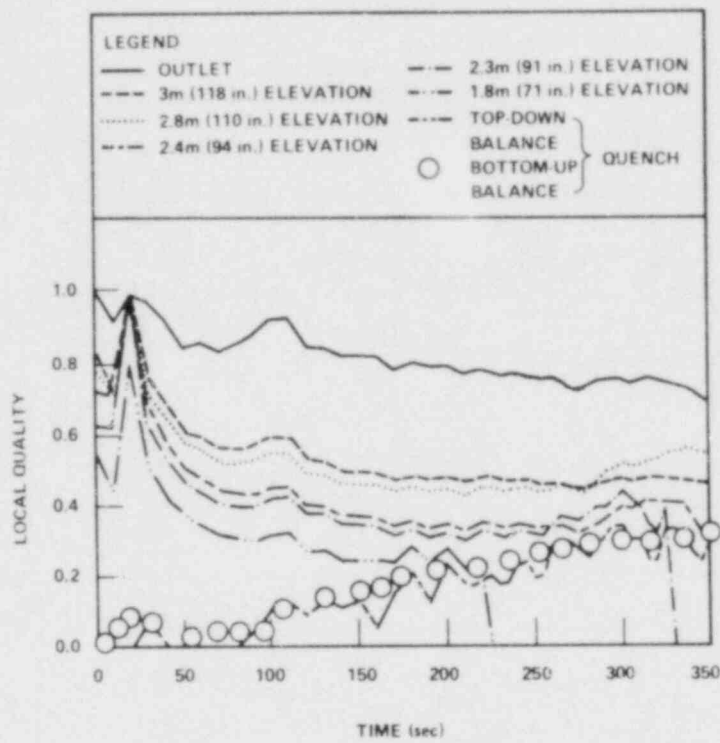


Figure B-21. Local Quality, Run 32013

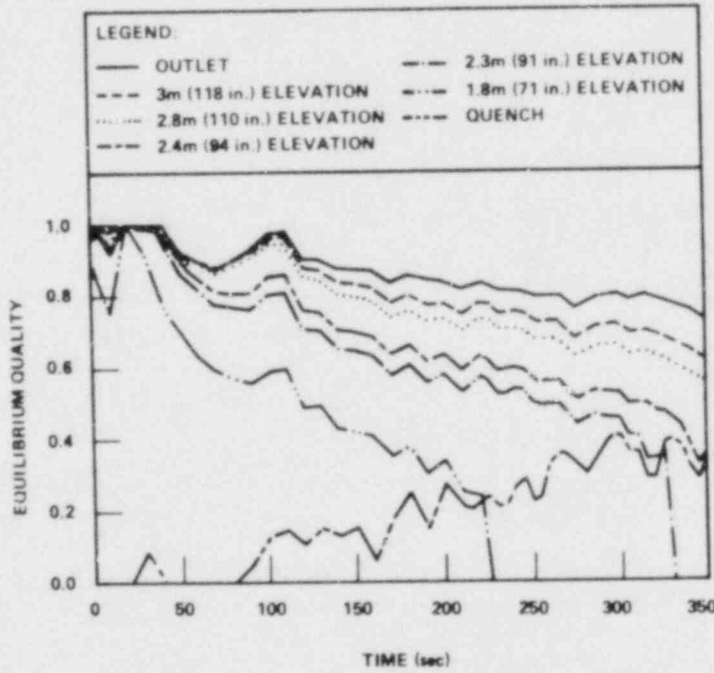


Figure B-22. Equilibrium Quality, Run 32013

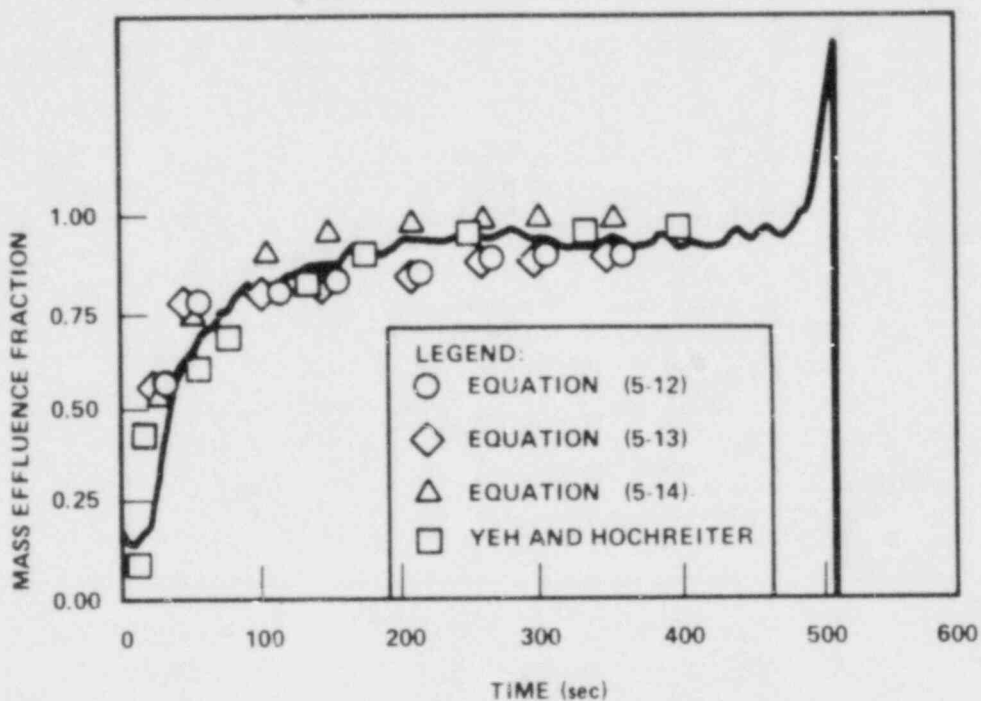


Figure B-23. Mass Effluence, Run 32013

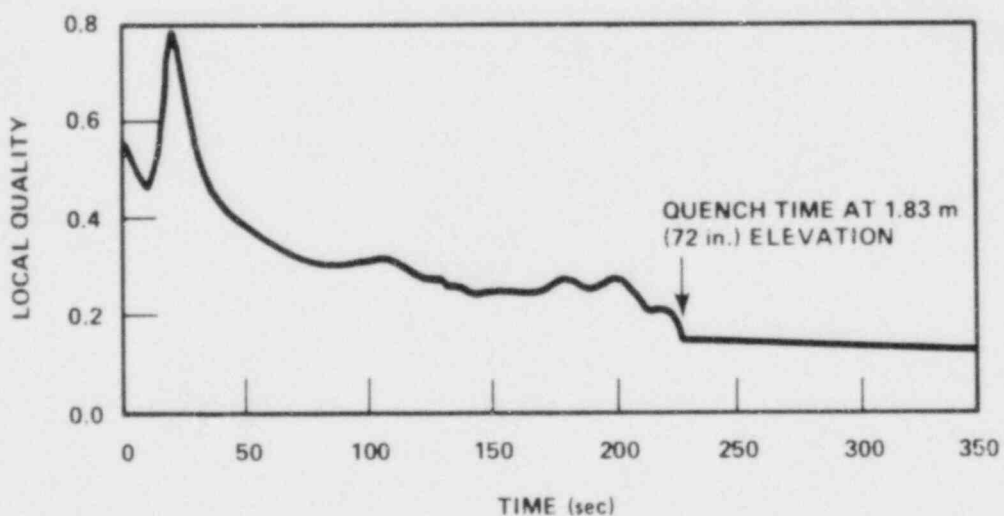


Figure B-24. Quality Transient, 1.83 m (72 in.) Elevation, Run 32013

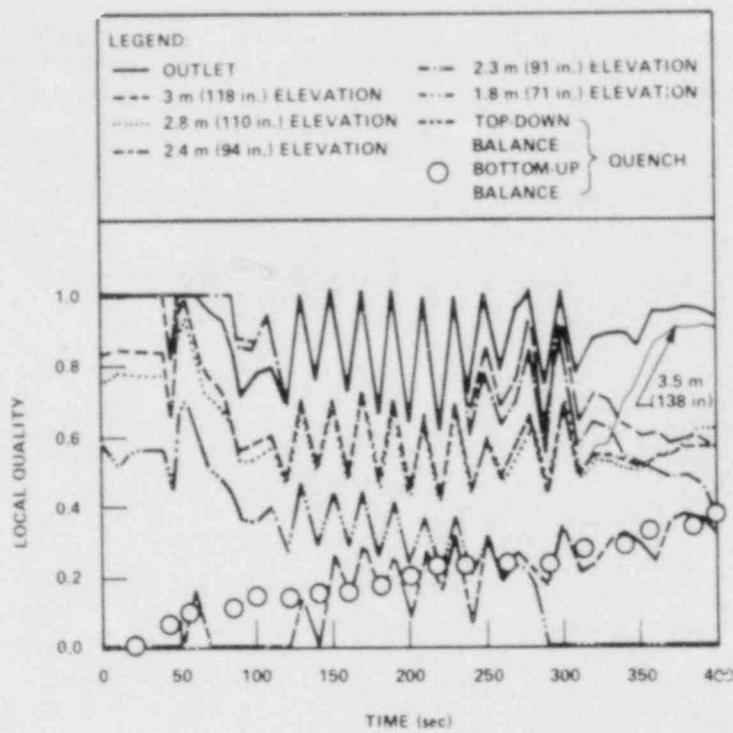


Figure B-25. Local Quality, Run 34006

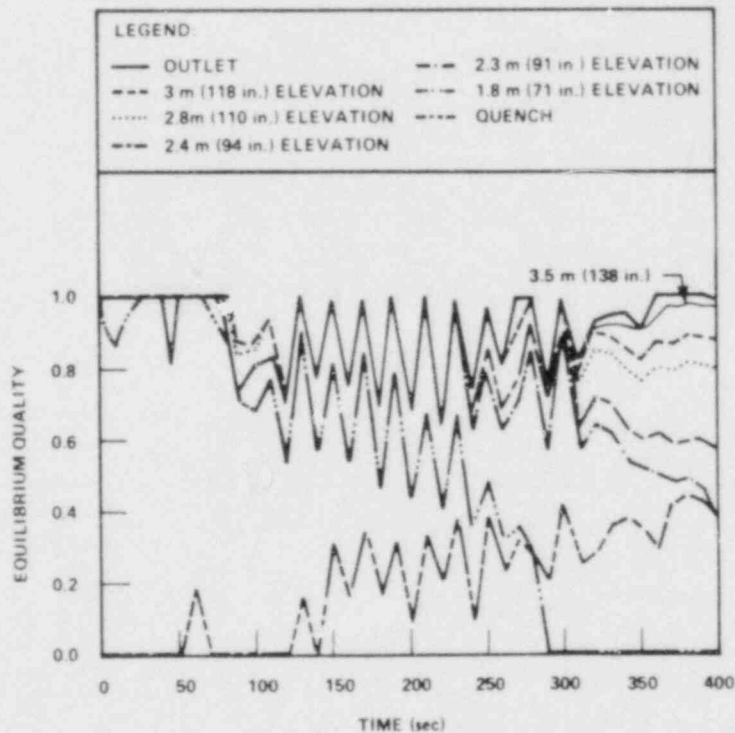


Figure B-26. Equilibrium Quality, Run 34006

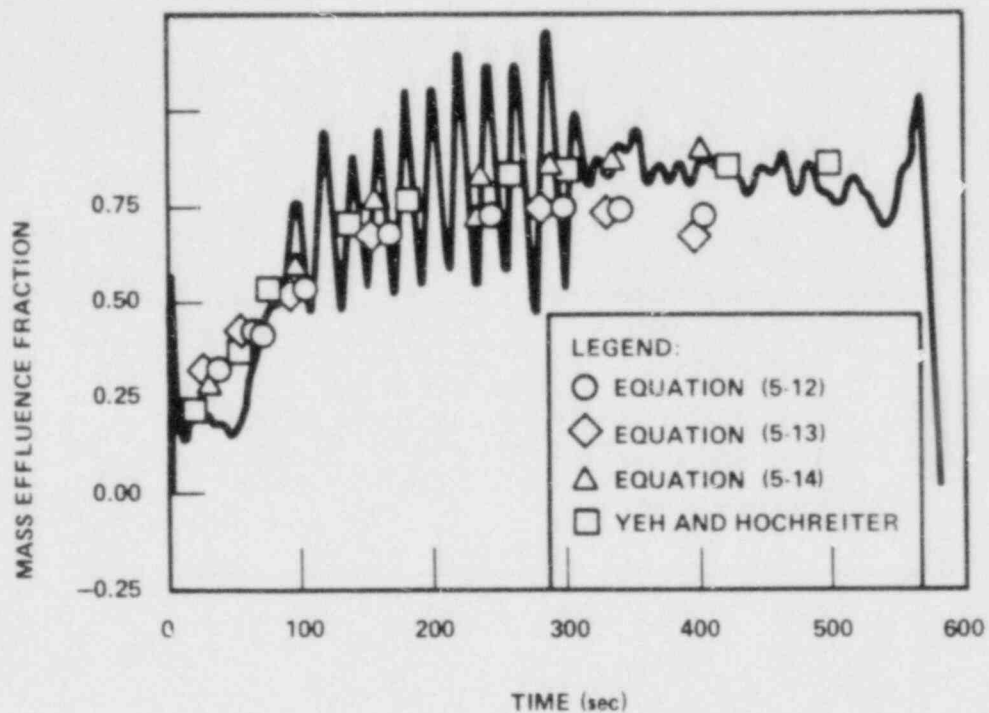


Figure E-27. Mass Effluence, Run 34006

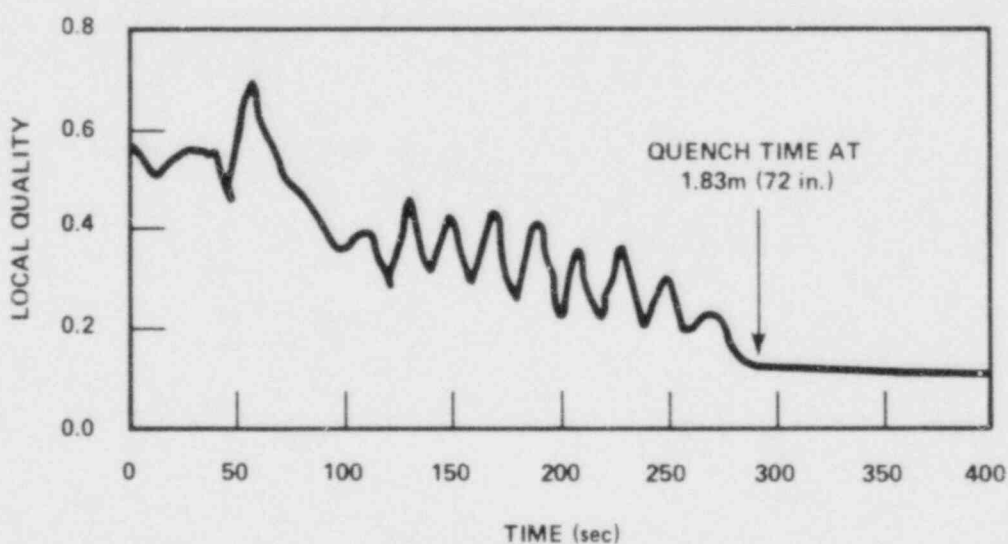


Figure B-28. Quality Transient, 1.83 m (72 in.) Elevation, Run 34006

APPENDIX C

INPUT AND OUTPUT SUMMARY OF DATA EVALUATION MODELS

C-1. INPUT SUMMARY

Table C-1 summarizes the input data used in the evaluation of bundle flow conditions and basic heat transfer components above the transition front by methods described in section 6 and appendix F. Unless otherwise stated, the following schemes were also used:

- The housing temperature was defined to be the average of all available thermocouple measurements at a given elevation; housing temperatures at various times or elevations not directly recorded were obtained by linear interpolation of the two closest available data points.
- Vapor temperatures at the 1.83, 2.29, 2.44, 2.82, and 3.05 m (72, 90, 96, 111, and 120 in.) elevations were taken from steam probe measurements; vapor temperature at the quench front was taken to be equal to the mean of the vapor saturation and the average heater rod wall temperature; vapor temperature above the 3.05 m (120 in.) elevation was obtained by linear extrapolation of the 2.44 and 2.82 m (96 and 111 in.) steam probe data; and vapor temperature at all other locations was obtained by linear interpolation of the two closest steam probe measurements.
- All local vapor physical properties were evaluated at the vapor temperatures specified above, and liquid properties were assumed to be at saturation conditions.
- Except at the transition front, steam quality was evaluated by the same method as vapor temperature; steam quality below the lowest available steam probe measurement to the transition front was obtained by linearly extrapolating data from the next two available steam probe locations.

TABLE C-1

SUMMARY OF INPUT DATA FOR EVALUATION MODELS

Input Data	Source
Drop size distribution and velocity at housing window locations	FLECHT SEASET droplet motion movies
System pressure and thimble guide tube temperature	CATALOG code
Quench front elevation, total mass flow above quench front, vapor temperature, and quality at steam probe locations	FLEMB code
Heater rod surface temperature and heat flux	DATARH code
Housing temperature	FLUKE tape
Top of transition regime (transition front)	Determined from heater rod temperature data (see section 5, figures 5-9 through 5-16)

C-2. OUTPUT SUMMARY

The input data described in the previous paragraph were used in the data evaluation models to calculate the following important information on dispersed flow properties:

- Droplet size distribution and droplet velocity from the transition front to the bundle exit (see appendix F).
- Dispersed flow properties above the transition front such as vapor void fraction, slip ratio, droplet number density, droplet Weber number and Nusselt number, and vapor Reynolds number (see appendix F and paragraph 6-4).
- Basic heat transfer components above the transition front, which include convective heat transfer from heater rod surface to vapor and radiative heat exchange between heater rods, thimble guide tubes, housing wall, vapor, and dispersed droplets (see paragraphs 6-5 and 6-6).

APPENDIX D

CALCULATION OF LOCAL QUALITY IN BUNDLE

D-1. DERIVATION OF EQUATION

Equation (4-10) was developed in section 4 to calculate local quality in a bundle using bundle exit quality and steam temperatures:

$$(x)_{Z=Z_1} = -\frac{1}{(h_v - h_l)} Z_1 \left[x_0 (h_{v_0} - h_{l_0}) - \frac{1}{m_t} \int_{Z_1}^{3.66 \text{ m}} Q' dz \right]$$

where

m_t = total mass flow rate

h_l, h_v = liquid and vapor enthalpy

Q' = total of bundle and housing heat release rate
per foot of elevation

x = quality

o = subscript for bundle exit

Z_1 = elevation in bundle

This equation cannot be applied directly in the present problem because of the lack of bundle exit quality or exit vapor temperature. A method has developed to circumvent this difficulty; it is detailed in the following paragraphs.

Figure D-1 shows instrumentation on the bundle, upper plenum, and a pipe from the upper plenum to the orifice meter. These components can be schematically arranged (figure D-2) to show interrelations among the components. In the flow

diagram, the known (measured) variables are \dot{m}_{v_2} , T_{v_2} , T_{v_1} , \dot{m}'_{l_1} , \dot{m}_{l_2} , and T_o (saturation temperature).

Mass and energy balances over the first block in figure D-2 give equation (4-10). Equations (4-5) and (4-6) can be utilized to set up mass and energy balance over the second block. Since no mass accumulation in the upper plenum occurred in the test, and heat release to the upper plenum wall from the fluid was negligible, the balance equations give

$$\dot{m}_t = \dot{m}'_{l_1} + \dot{m}_{l_1} + \dot{m}_{v_1} \quad (D-1)$$

and

$$X_o h_{v_o} + (1-X_o) h_{l_o} = X_1 h_{v_1} + (1-X_1) h_{l_1} \quad (D-2)$$

Equation (D-2) is modified using the fact that $X_1 = \dot{m}_{v_1} / \dot{m}_t$ as follows:

$$X_o (h_{v_o} - h_{l_o}) = \frac{\dot{m}_{v_1}}{\dot{m}_t} (h_{v_1} - h_{l_1}) \quad (D-3)$$

A similar relation can be derived over the third block by noting that

$$X_2 = \frac{\dot{m}_{v_2}}{\dot{m}_{l_2} + \dot{m}_{v_2}} \quad \text{and} \quad X'_1 = \frac{\dot{m}_{v_1}}{\dot{m}_{l_1} + \dot{m}_{v_1}}$$

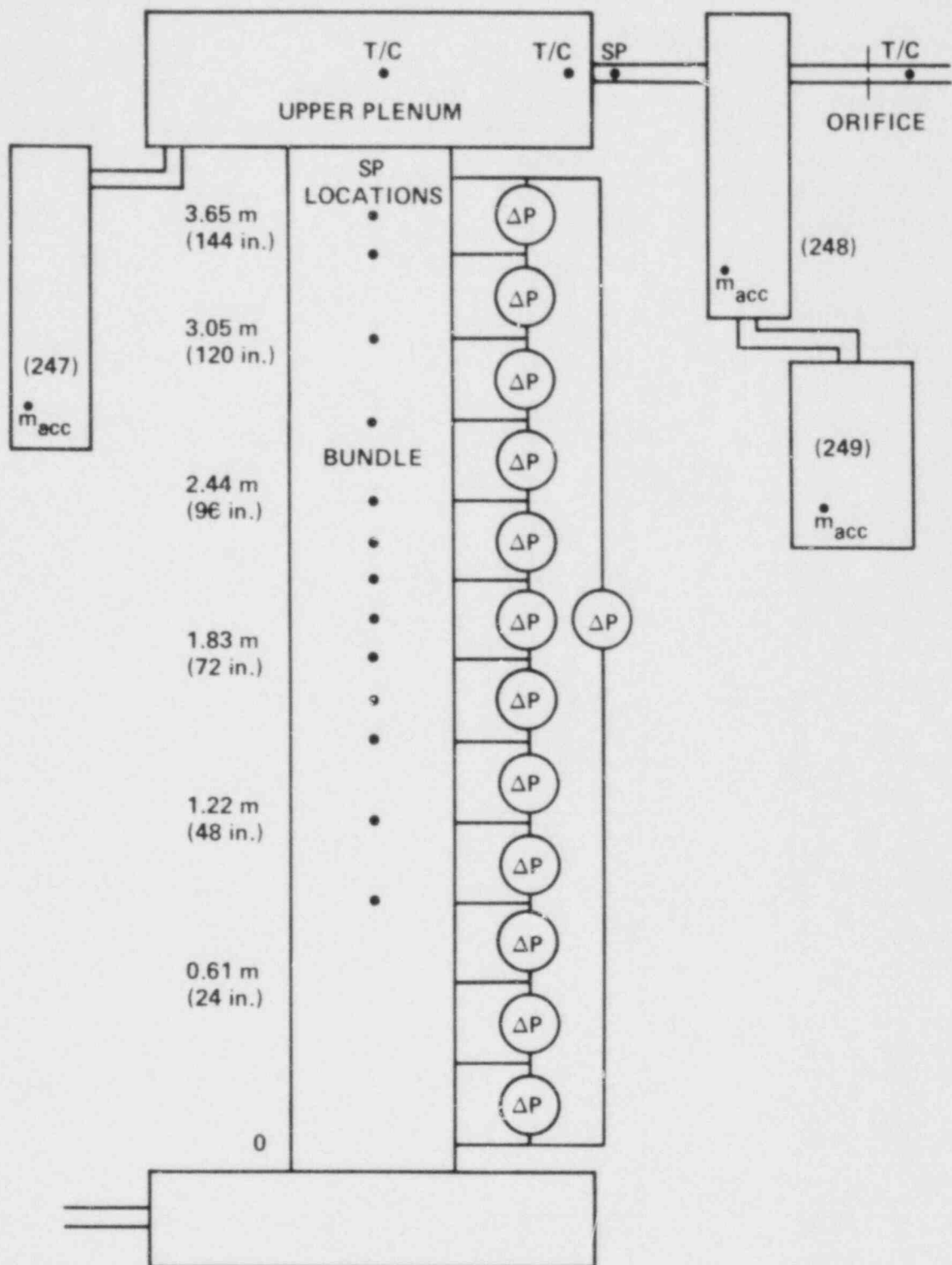
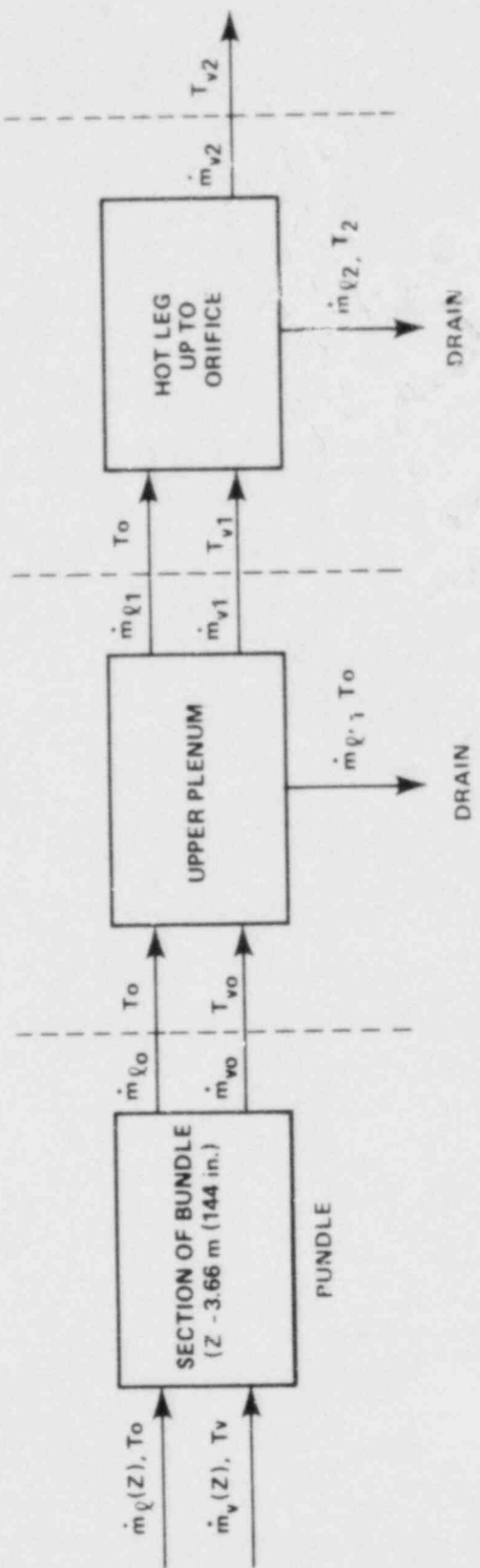


Figure D-1. Schematic Diagram of Test Instrumentation



D-4

Figure D-2. Schematic Diagram of Relations Between Components

The result for the third block is

$$\frac{\dot{m}_{v_2}}{\dot{m}_{t_2} + \dot{m}_{v_2}} (h_{v_2} - h_{t_2}) = \frac{\dot{m}_{v_1}}{\dot{m}_{t_1} + \dot{m}_{v_1}} (h_{v_1} - h_{t_1}) \quad (D-4)$$

$$\dot{m}_{t_1} + \dot{m}_{v_1} = \dot{m}_{t_2} + \dot{m}_{v_2} \quad (D-5)$$

From equations (D-4) and (D-5),

$$\dot{m}_{v_2} (h_{v_2} - h_{t_2}) = \dot{m}_{v_1} (h_{v_1} - h_{t_1}) \quad (D-6)$$

Manipulating equations (D-1), (D-2), and (D-6) gives

$$x_0 (h_{v_0} - h_{t_0}) = \frac{\dot{m}_t (h_{v_2} - h_{t_2})}{\dot{m}_t} \quad (D-7)$$

Equation (D-7) can be substituted into equation (4-10) to give

$$x(z) = \frac{i}{(h_v - h_z)} \left(\frac{\dot{m}_v (h_{v_2} - h_{t_2})}{\dot{m}_t} - \frac{1}{\dot{m}_t} \int_z^{3.66 \text{ m}} Q' dz \right) \quad (D-8)$$

This equation makes it possible to calculate local qualities in the bundle where steam temperatures are known from the information on two-phase flow at the housing exit.

D-2. STEAM PROBE LOCATIONS USED FOR ANALYSES

Steam probes were installed in the bundle as indicated in figure D-1. It was found that the steam probes which were aspirated through the bottom of the bundle were not providing valid steam temperatures. Therefore, these probe measurements were not considered in the present analyses. Some of the steam probes aspirated through the top of the bundle also showed early quenching. The data from the probes which quenched were not used either. From the consideration of data validity, five steam probe locations were selected where reasonable steam temperatures were measured. The locations and number of steam probes used in the present analyses are shown in table D-1.

TABLE D-1
STEAM PROBES USED IN PRESENT ANALYSES

Channel	Elevation [m (in.)]	Radial Location
185	1.83 (72)	7I
192	2.29 (90)	10I
194	2.44 (96)	10L
195	2.82 (111)	10C
196	2.82 (111)	13F
197	3.05 (120)	7C
198	3.05 (120)	13I

D-3. MODIFICATION OF STEAM PROBE MEASUREMENTS

Several steam probe measurements showed quenching pulses [figure D-3(a)]. Apparently the downward pulses did not represent real steam temperatures. Therefore, the measurements were modified to remove such pulses. A typical result of such a modification is shown in figure D-3(b).

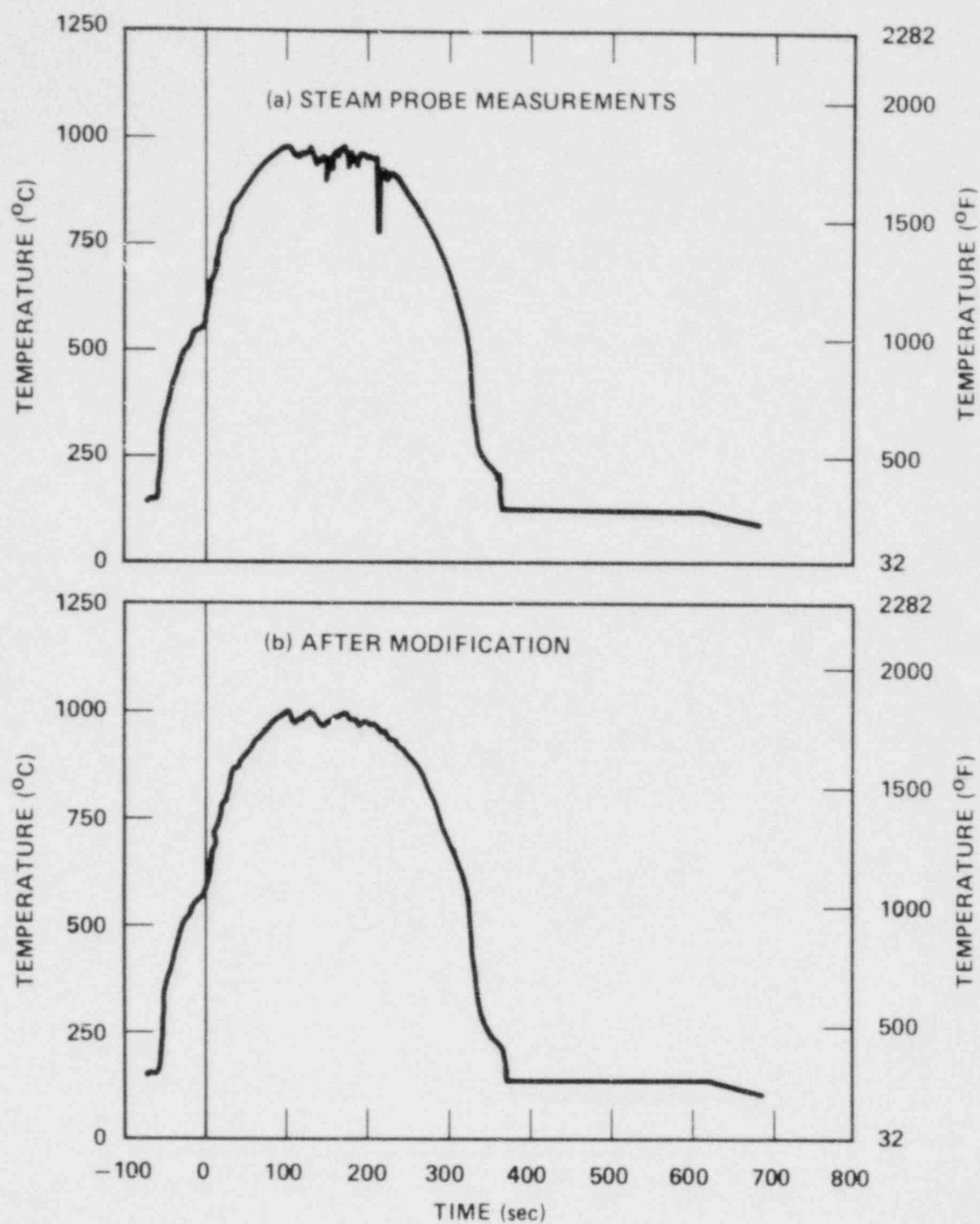


Figure D-3. Modification of Steam Probe Measurements

APPENDIX E

ANALYSIS OF FLECHT SEASET DROPLET MOVIE DATA.

E-1. INTRODUCTION

Information is needed on the density and size distribution of droplets entrained in the flow to provide a calculation of heat transfer in the region of dispersed flow ahead of the quench front during reflood conditions. In addition, information on the droplet velocity is also of considerable importance in modeling the dispersed flow heat transfer. At present, systematic measurements of drop size and velocity distribution under reflood conditions in rod bundles are almost nonexistent.

In the 161-rod unblocked bundle task, high-speed black-and-white motion pictures were taken through the housing windows for some test runs. The results have been reported in the data report. Further analysis of the drop size spectra and the velocity distribution is provided in this appendix, and the results obtained are summarized.⁽¹⁾

E-2. METHOD OF MEASUREMENT

Movie film was projected onto a fine-scale graph paper attached to the wall. A Lafayette Analyst Model D projector, which has frame-by-frame stop control and other features, was used. The window and rods were traced on the graph paper. Measurements of the rod and window diameters were taken and recorded on the graph paper. They were used to calculate the scale factor between the real dimension and the measured dimension. Any clear, distinct droplets observed were traced on the graph paper directly. Among these traced droplets, those which could be seen to travel a considerable distance within the gap were considered for droplet velocity calculation. They were identified with numbers and their initial and final positions were traced. The number of frames between the initial and final positions was also

1. Thanks are due to Y. Y. Hsu of NRC-RSR, and R. Simeneau and E. Walker of NASA Lewis Research Center for providing their expertise in analysis of the high-speed rod bundle movie.

recorded. This was facilitated by the frame-by-frame stop control of the projector, without which the droplet velocity calculation would have been difficult. The small-scale graph paper used (readable to ± 0.5 mm) enabled direct measurement of drop size and distance travelled.

Prints from the movie films were made and are shown in figures E-1 and E-2.

E-3. DATA REDUCTION

The drop diameter and distance travelled were measured directly from the graph paper and recorded in tabular form. To obtain the real drop diameter as well as distance travelled, a scale factor was needed.

Since the real dimensions of the window and the rod diameter were known, either the ratio of the measured window diameter to the real window diameter or that of the measured rod diameter to the real rod diameter could be used as the scale factor.

Because the window diameter was larger than the rod diameter and the window had less susceptibility to optical illusion, the window diameter ratio was preferred. It was found later that the window diameter ratios (defined as measured diameter divided by actual diameter) were always less than the rod diameter ratios. The difference was about 17 percent for the 0.91 m (36 in.) elevation movies and between 30 and 50 percent for the 2.74 m (108 in.) elevation movies. No comparison could be made for the 1.83 m (72 in.) elevation movies because the window perimeter was not visible in those movies. It was suspected that the 17-percent difference in the ratios for the 0.91 m (36 in.) elevation movies was caused by the slight rod misalignment or by optical illusion, which resulted in the larger rod diameter seen in the movies. Most of the 2.74 m (108 in.) elevation movies did not show a completely clear window, and the window diameter had to be estimated roughly. It was suspected that the window diameter was underestimated and the result was a larger difference between the two ratios. It was then decided that the window diameter ratio would be used for 0.91 m (36 in.) elevation movies and the rod diameter ratio with a 17-percent reduction would be used for both the 1.83 m (72 in.) and the 2.74 m (108 in.) elevation movies.

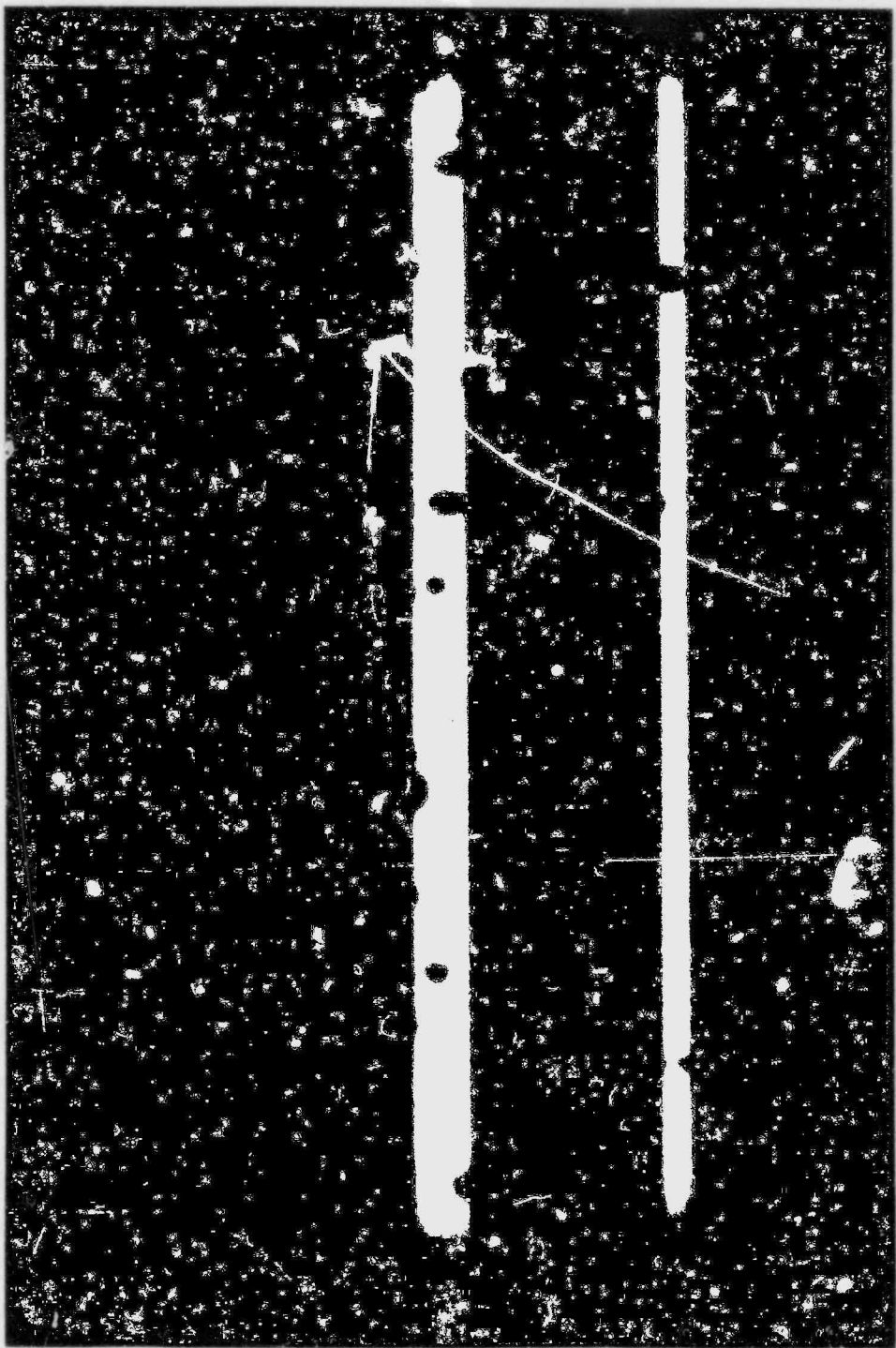


Figure E-1. Droplets From Run 32114, 2.74 m (108 in.) Elevation, ~ 25 Seconds After Flood (sheet 1 of 4)

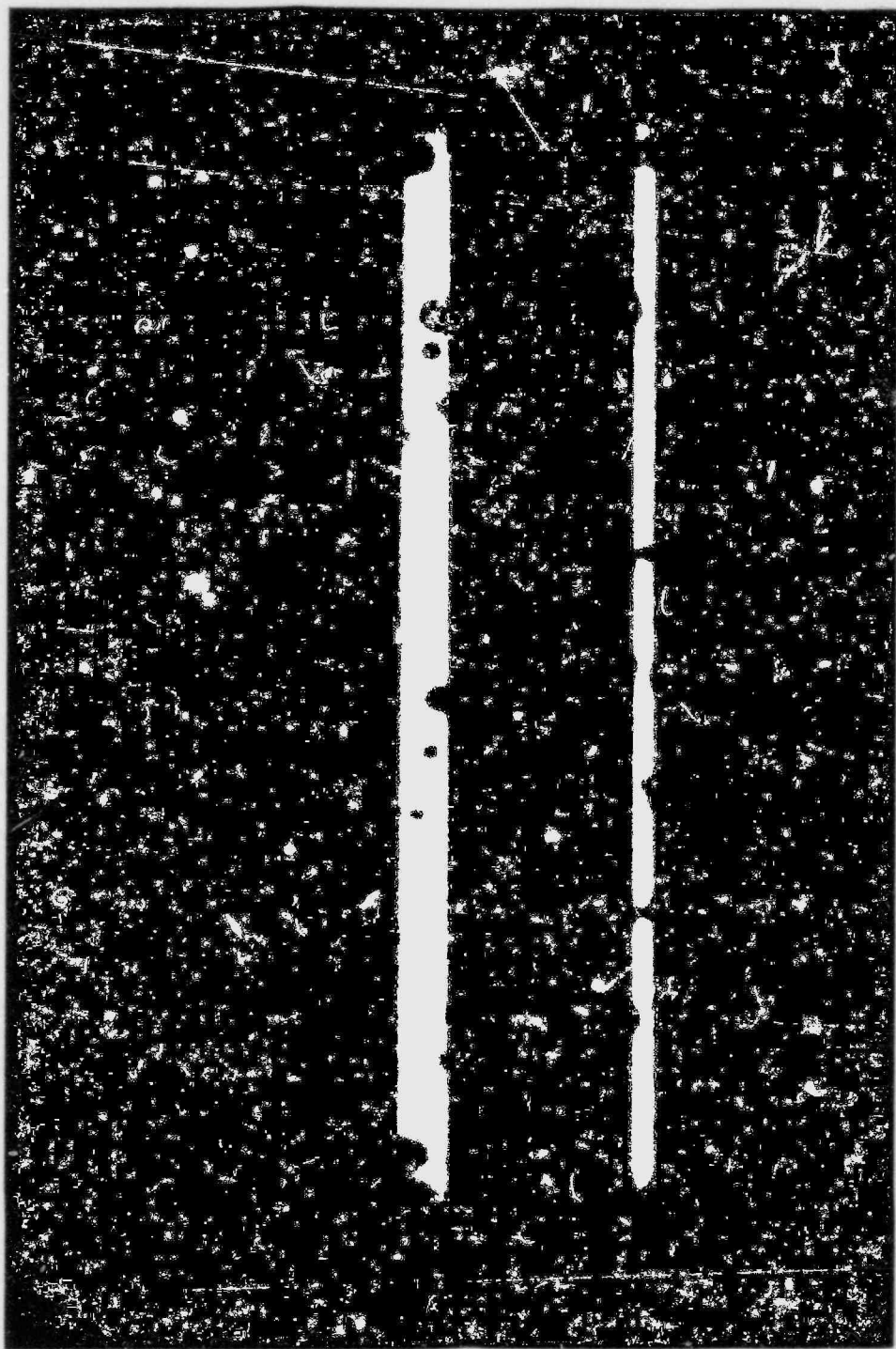


Figure E-1. Droplets From Run 32114, 2.74 m (108 in.) Elevation, ~ 25 Seconds After Flood (sheet 2 of 4)

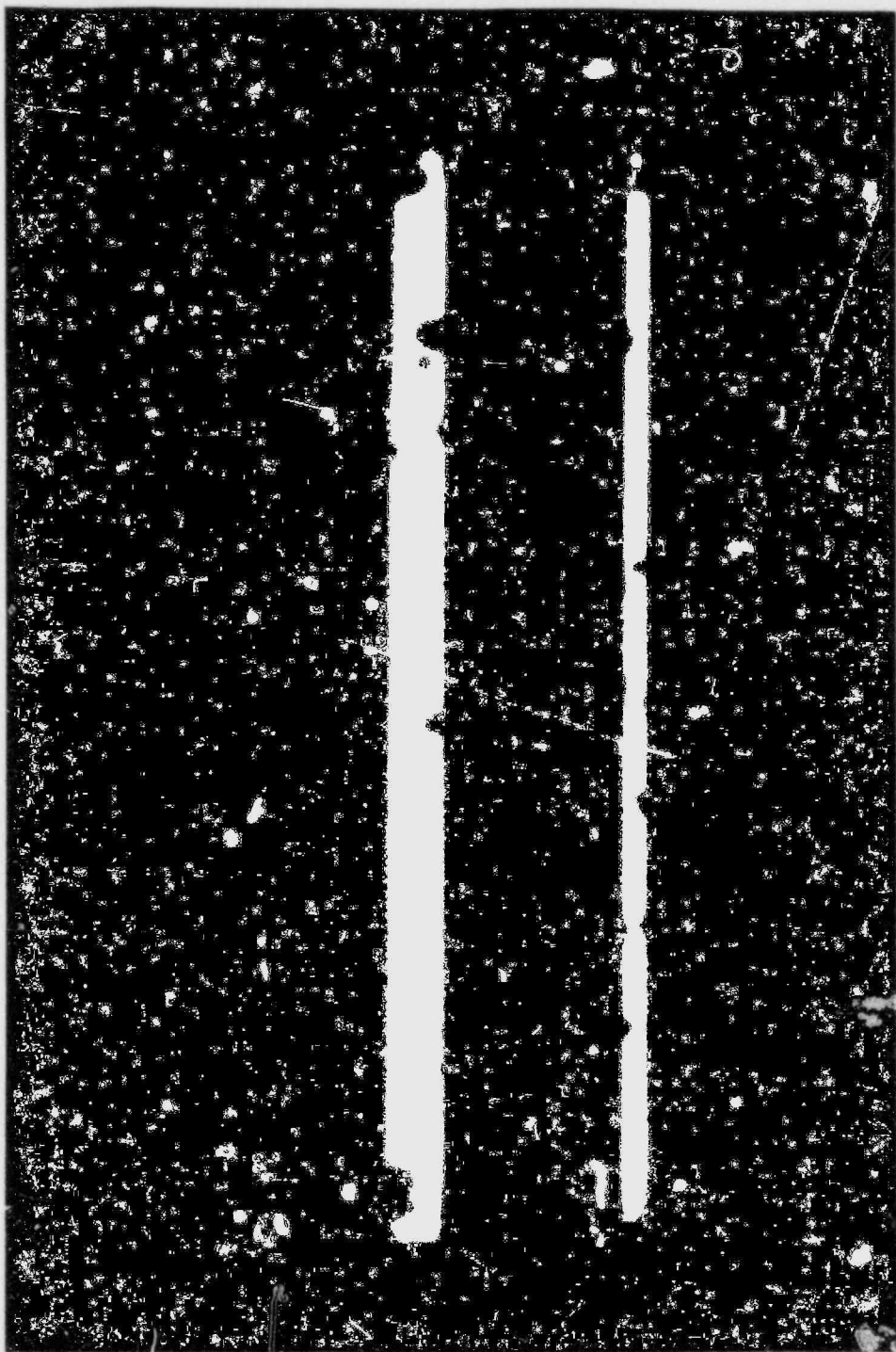


Figure E-1. Droplets From Run 32114, 2.74 m (108 in.) Elevation, ~ 25 Seconds After Flood (sheet 3 of 4)

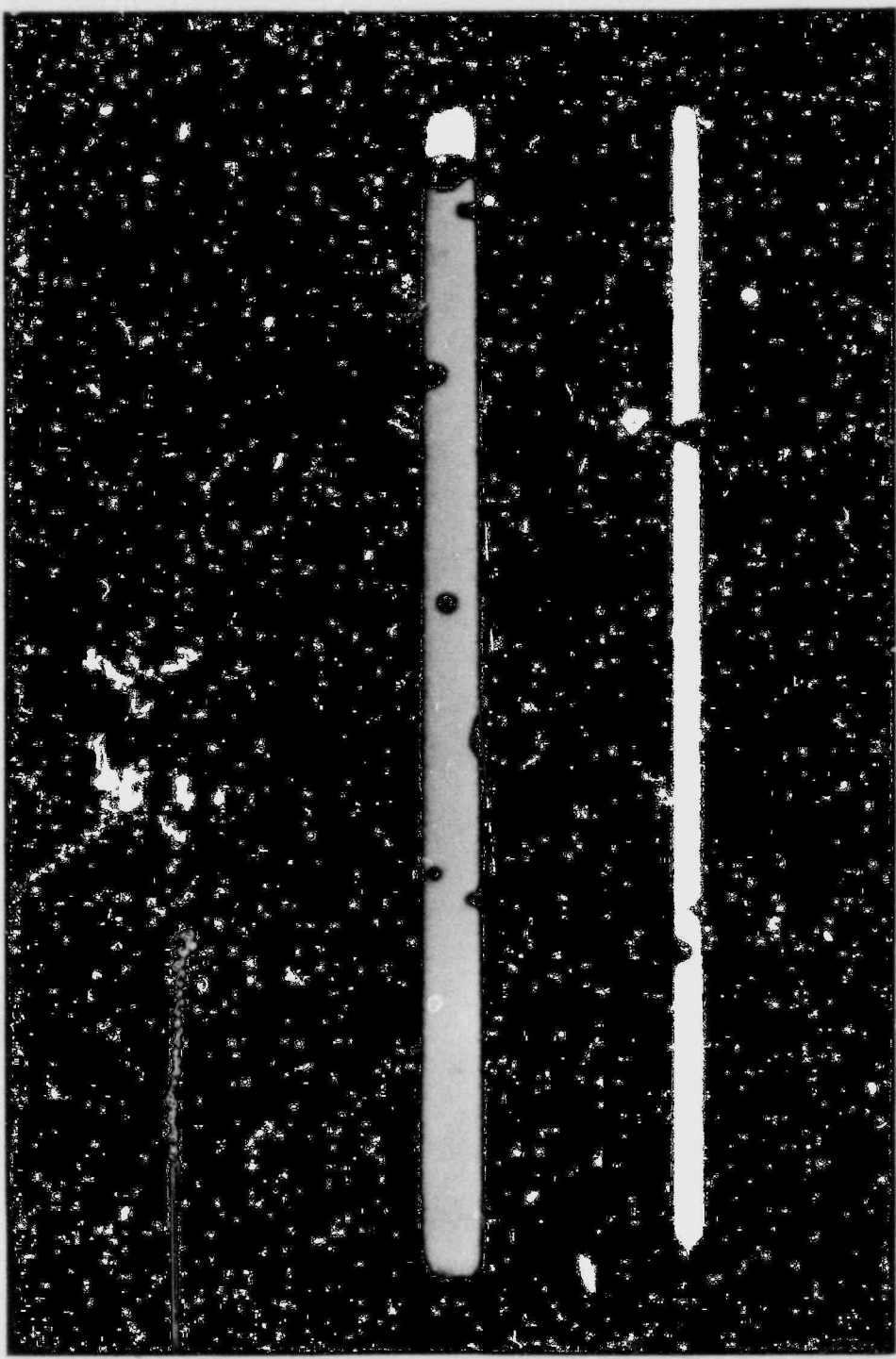


Figure E-1. Droplets From Run 32114, 2.74 m (108 in.) Elevation, ~ 25 Seconds After Flood (sheet 4 of 4)

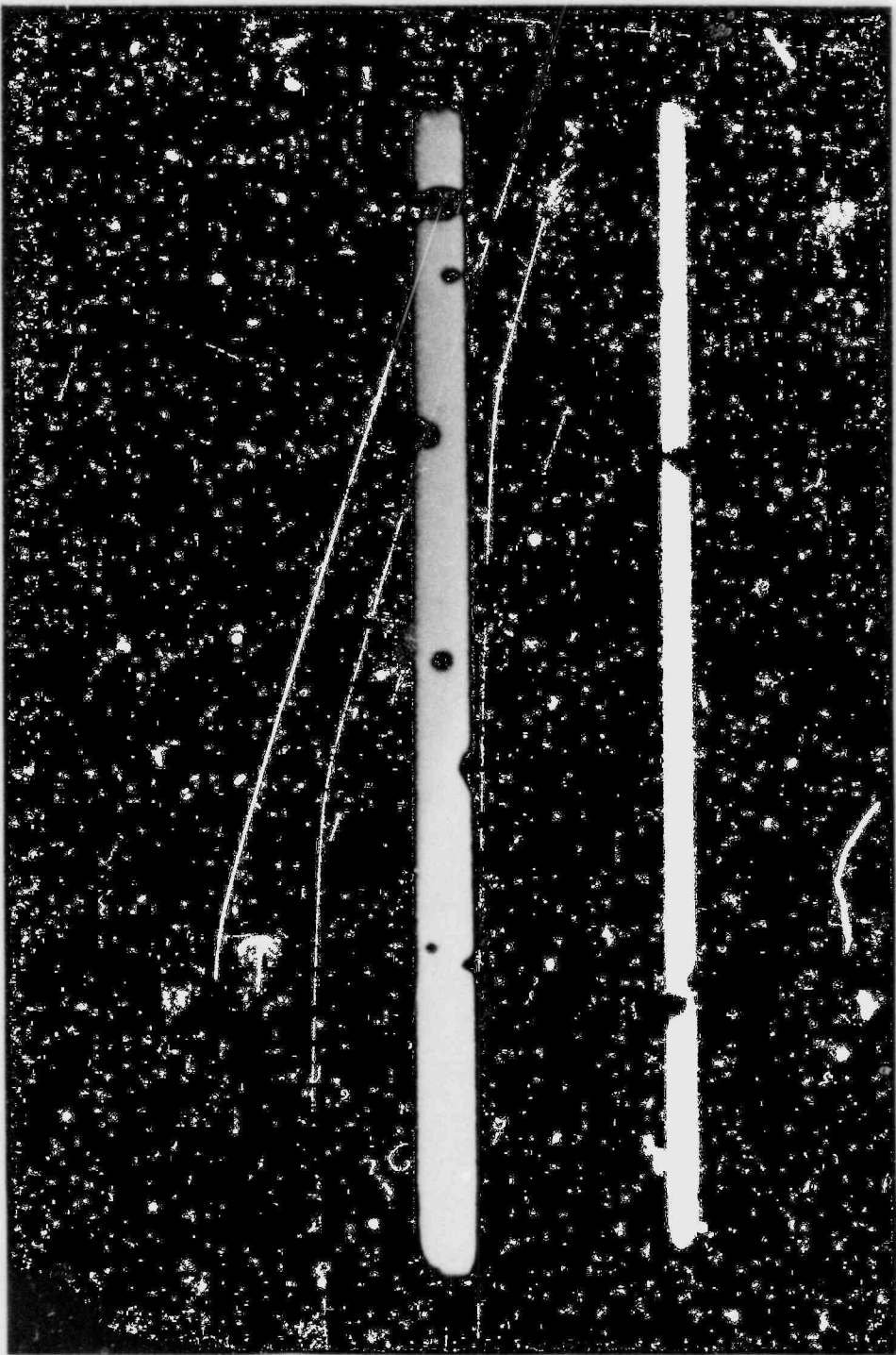


Figure E-2. Droplets From Run 32114, 0.91 m (36 in.) Elevation, ~ 20 Seconds After Flood (sheet 1 of 4)

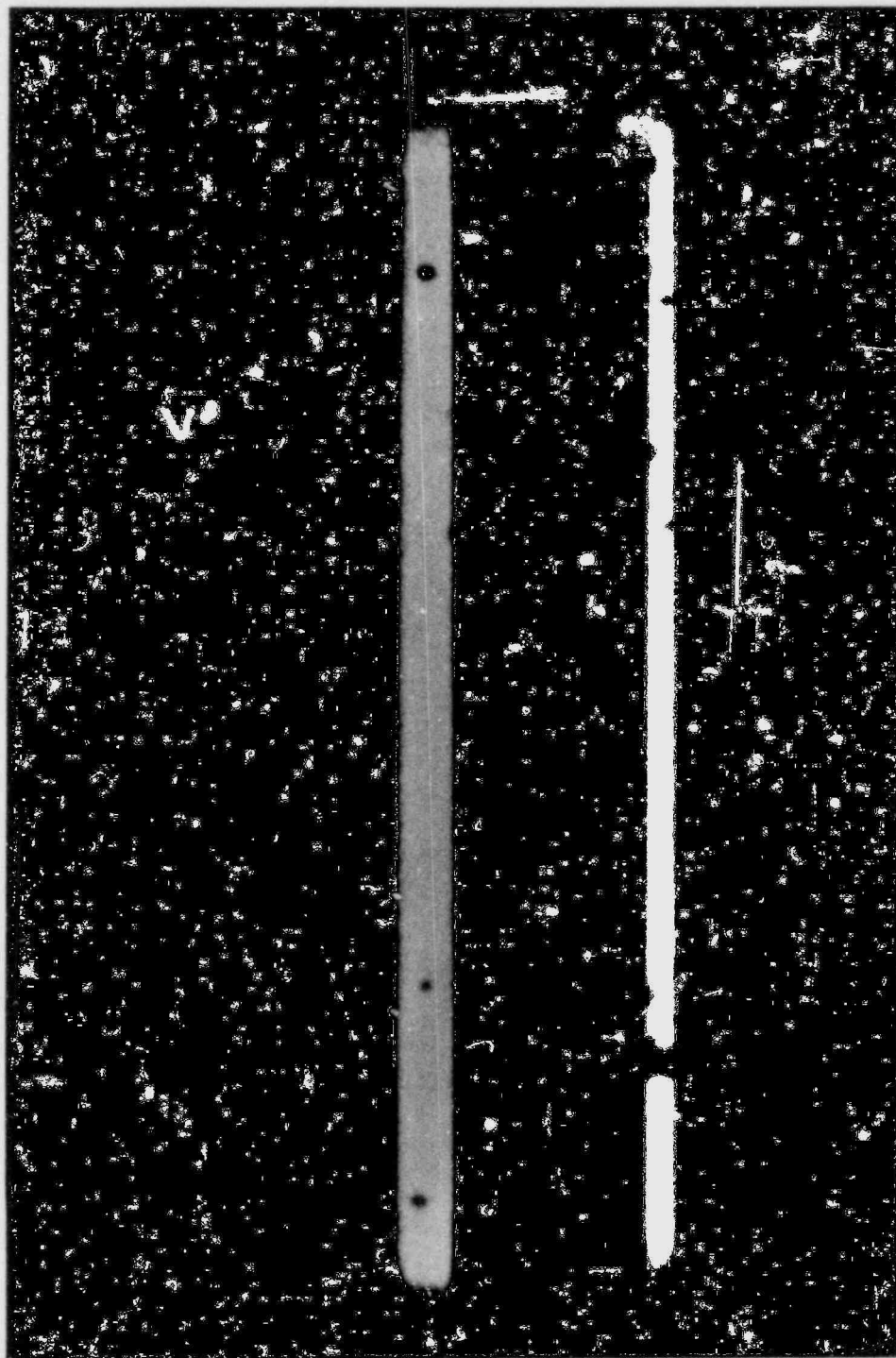


Figure E-2. Droplets From Run 32114, 0.91 m (36 in.) Elevation, ~ 20 Seconds After Flood (sheet 2 of 4)

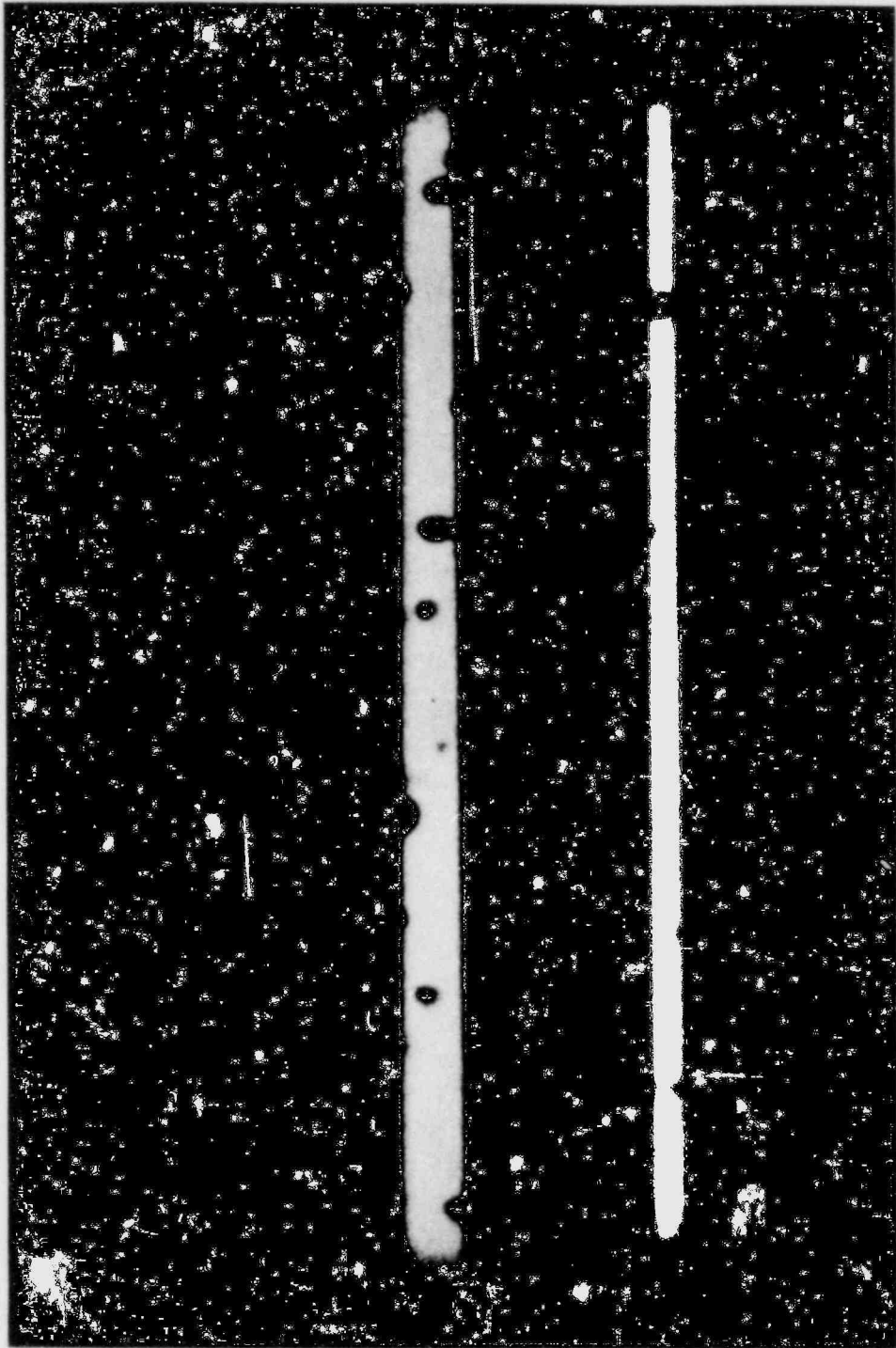


Figure E-2. Droplets From Run 32114, 0.91 m (36 in.) Elevation, ~20 Seconds After Flood (sheet 3 of 4)

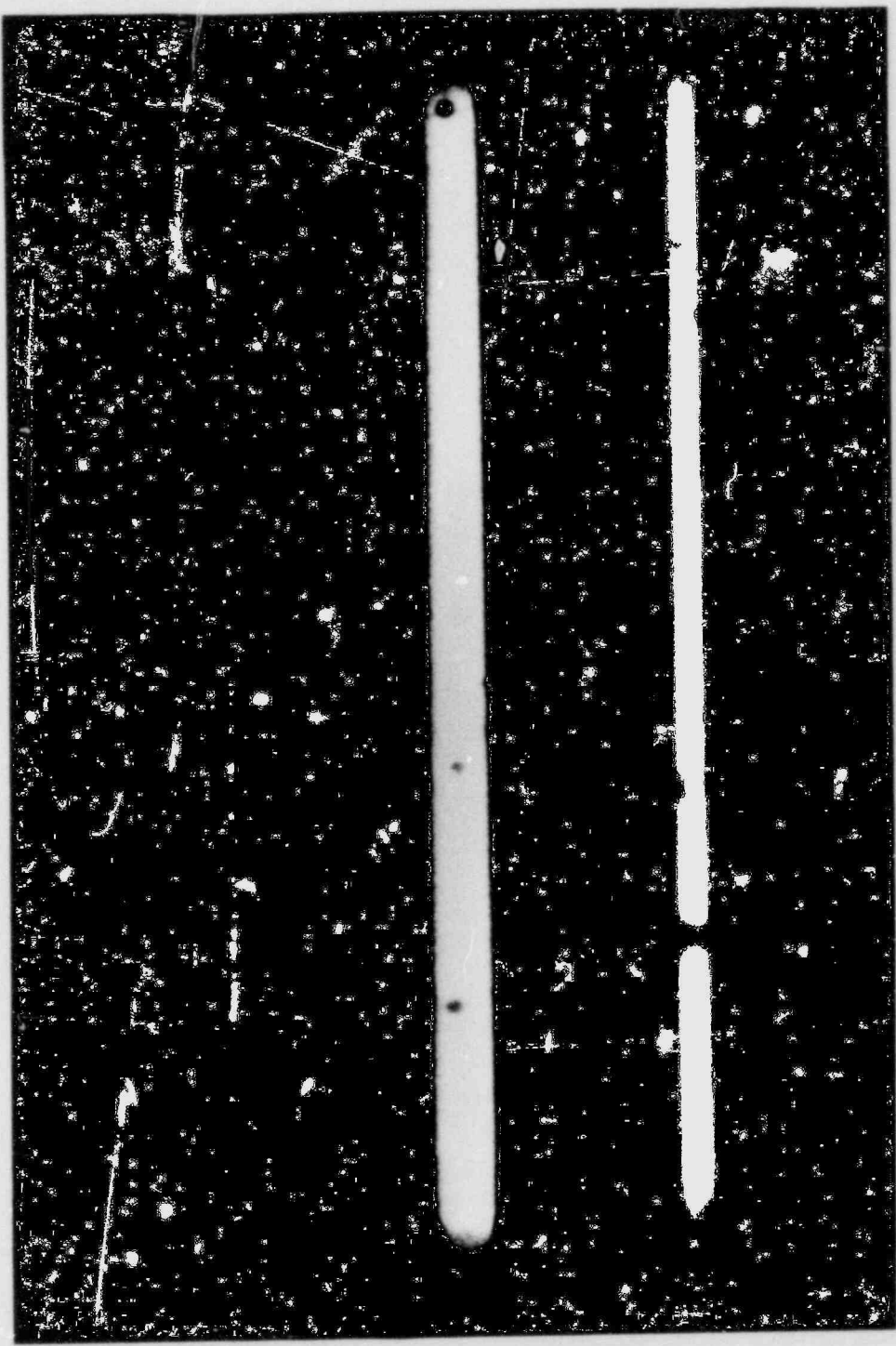


Figure E-2. Droplets From Run 32114, 0.91 m (36 in.) Elevation, ~ 20 Seconds After Flood (sheet 4 of 4)

The real drop diameter and drop velocity were calculated accordingly, using the following simple relationships:

$$D_r = \frac{D_m}{S_f} \quad (E-1)$$

$$WX_r = \frac{WX_m}{S_F} \quad (E-2)$$

$$Wt = \frac{N}{F} \quad (E-3)$$

$$V = \frac{WX_r}{Wt} \times 10^{-3} \quad (E-4)$$

where

- D_r = real drop diameter (mm)
 D_m = measured drop diameter (mm)
 WX_r = real distance traveled (mm)
 WX_m = measured distance traveled (mm)
 S_f = scale factor (measured diameter divided by actual dimension)
 Δt = time interval for the drop to travel the distance WX_r (sec)
 N = number of movie frames taken during the interval Wt
 F = film speed (frames/sec)
 V = drop velocity (m/sec)

E-4. RESULTS AND ANALYSIS

Drop diameter frequency distributions, in the form of histograms, were obtained. They are tabulated in table E-1 and sketched in figures E-3 through E-20. From the summary of continuous distributions in Hahn and Shapiro,⁽¹⁾ the log-normal distribution seemed to be the best choice to represent the drop diameter distribution. To test the appropriateness of the log-normal distribution for representing the drop diameter data,

I. Hahn, G. J., and Shapiro, S. S., Statistical Models in Engineering, John Wiley and Sons, Inc., New York, 1967.

a series of probability plottings were made. These plots are shown in figures E-21 through E-36. In these figures, the common logarithm of measured drop diameter instead of the natural logarithm of real drop diameter was used. Although some data reduction work was saved, the linearity of the curves was still preserved. This probability plotting technique was found to be very simple and convenient to use. If the assumed distribution model is correct, the plotted points will tend to fall in a straight line. If the model is inadequate, the plot will not be linear and the extent and type of departure can be observed. The underlying principle is described in Hahn and Shapiro.

It should be mentioned that many droplets were seen in the 1.83 m (72 in.) elevation movies of runs 30921 and 32333. These movies were divided into several segments, and drop diameter distributions were obtained for each individual segment as well as for the whole film. They are shown in table E-1 and figures E-4 through E-7 and E-17 through E-19 where A, B, and C after the run number refer to the different individual film segments and "total" refers to the whole movie. The plots show that the drop diameter distributions of the different film segments of the same movie agree quite well with one another.

With few exceptions, most of the probability plottings appear to be quite linear. This suggests that the log-normal distribution may be an appropriate representation for the drop size distribution. As a result, the log-normal distribution was used.

The following paragraphs describe briefly the log-normal distribution and explain how the parameters of the distribution were estimated from the drop diameter data.

The probability density function, $f(x)$, for log-normal distribution is given by

$$f(x) = \frac{\eta}{(x-\epsilon)\sqrt{2\pi}} \exp \left\{ -\frac{1}{2} \left[\frac{\gamma^2}{\eta^2} + \ln(x-\epsilon) \right]^2 \right\} \quad (E-5)$$

for $x \geq \epsilon$; $\eta > 0$; $-\infty < \gamma < +\infty$

where ϵ , γ , and η are the parameters characterizing the distribution, with ϵ the lower bound on the random variable x and

DROPLET DIAMETER

Run 30518 Quench front - information not available Total drops - 334

Elevation - 1.83 m (72 in.) Time - information not available

Diameter Range [mm (in.)]	Number of Drops	Percentage of Total
0.11-0.32 (0.004-0.013)	0.5	0.15
0.32-0.52 (0.013-0.020)	31.5	9.43
0.52-0.73 (0.020-0.029)	95.5	28.59
0.73-0.94 (0.029-0.037)	88.5	26.50
0.94-1.15 (0.037-0.045)	62.5	18.71
1.15-1.36 (0.045-0.054)	28.5	8.53
1.36-1.57 (0.054-0.062)	14.0	4.19
1.57-1.78 (0.062-0.070)	8.5	2.54
1.78-1.99 (0.070-0.078)	3.0	0.90
1.99-2.20 (0.078-0.087)	1.5	0.45

Run 30921A Quench front - 0.38 m (14.9 in.)

Total drops - 562

Elevation - 1.83 m (72 in.) Time - 20-26 sec

Diameter Range [mm (in.)]	Number of Drops	Percentage of Total
0.29-0.49 (0.011-0.019)	11	1.96
0.49-0.68 (0.019-0.027)	146.5	26.07
0.68-0.88 (0.027-0.035)	193.5	34.43
0.88-1.07 (0.035-0.042)	102.5	18.24
1.07-1.27 (0.042-0.050)	51.5	9.16
1.27-1.46 (0.050-0.057)	29	5.16
1.46-1.66 (0.057-0.065)	15	2.67
1.66-1.85 (0.065-0.073)	8	1.42
1.85-2.05 (0.073-0.081)	4	0.71
2.05-2.24 (0.081-0.088)	0.5	0.09
2.24-2.44 (0.088-0.096)	0.5	0.09

REQUENCY DISTRIBUTION

Run 30921B	Quench front - 0.38 m (14.9 in.)	Total drops - 641
Elevation - 1.83 m (72 in.)	Time - 20-26 sec	
<hr/>		
Diameter [mm (in.)]	Number of Drops	Percentage of Total
0.27-0.44 (0.011-0.017)	1.5	0.23
0.44-0.62 (0.017-0.024)	93.5	14.59
0.62-0.79 (0.024-0.031)	237	36.97
0.79-0.97 (0.031-0.038)	177	27.61
0.97-1.15 (0.038-0.045)	79.5	12.40
1.15-1.32 (0.045-0.052)	31	4.84
1.32-1.50 (0.052-0.059)	11	1.72
1.50-1.68 (0.059-0.066)	6	0.94
1.68-1.85 (0.066-0.073)	3.5	0.55
1.85-2.03 (0.073-0.080)	1	0.16
<hr/>		
Run 30921C	Quench front - 0.38 m (14.9 in.)	Total drops - 836
Elevation - 1.8 m (72 in.)	Time - 20-26 sec	
<hr/>		
Diameter [mm (in.)]	Number of Drops	Percentage of Total
0.25-0.42 (0.0098-0.017)	7.5	0.90
0.42-0.59 (0.017-0.023)	89.5	10.71
0.59-0.76 (0.023-0.030)	260	31.10
0.76-0.93 (0.030-0.037)	223	26.67
0.93-1.10 (0.037-0.043)	132	15.79
1.10-1.26 (0.043-0.050)	77	9.21
1.26-1.43 (0.050-0.056)	30	3.59
1.43-1.60 (0.056-0.063)	10	1.20
1.60-1.77 (0.063-0.070)	2.5	0.30
1.77-1.94 (0.070-0.076)	3.5	0.42
1.94-2.11 (0.076-0.083)	1	0.12

TABLE

DROPLET DIAMETER F

Run 30921 (Total)	Quench front - information not available	Total drops - 2039
Elevation - 1.83 m (72 in.)	Time - 20-26 sec	
<hr/>		
Diameter Range [mm (in.)]	Number of Drops	Percentage of Total
0.27-0.45 (0.011-0.018)	20	0.98
0.45-0.63 (0.018-0.025)	329.5	16.16
0.63-0.81 (0.025-0.032)	690.5	33.86
0.81-0.99 (0.032-0.039)	502.5	24.64
0.99-0.17 (0.039-0.046)	263	12.90
1.17-1.35 (0.046-0.053)	137	6.72
1.35-1.52 (0.053-0.060)	56	2.75
1.52-1.70 (0.060-0.067)	24	1.18
1.70-1.88 (0.067-0.074)	10	0.49
1.88-2.06 (0.074-0.081)	5	0.25
2.06-2.24 (0.081-0.088)	1.5	0.07
<hr/>		
Run 31504	Quench front - 1.53 m (60.1 in.)	Total drops - 101
Elevation - 1.83 m (72 in.)	Time - 200-206 sec	
Diameter Range [mm (in.)]	Number of Drops	Percentage of Total
0.20-0.33 (0.079-0.013)	2	1.98
0.33-0.47 (0.013-0.019)	17	16.83
0.47-0.60 (0.019-0.024)	16.5	16.34
0.60-0.73 (0.024-0.029)	14	13.86
0.73-0.87 (0.029-0.034)	16	15.84
0.87-0.99 (0.034-0.039)	10.5	10.40
0.99-0.13 (0.039-0.044)	10	9.90
1.13-1.27 (0.044-0.050)	3	2.97
1.27-1.40 (0.050-0.055)	4	3.96
1.40-1.53 (0.055-0.060)	1	0.99
1.53-1.66 (0.060-0.065)	1	0.99
1.66-1.80 (0.065-0.071)	3	2.97
1.80-1.93 (0.071-0.076)	2.5	2.48
1.93-2.06 (0.076-0.081)	0.5	0.50

EQUENCY DISTRIBUTION

Run 31701	Quench front - 0.75 m (29.4 in.)	Total drops - 153
-----------	----------------------------------	-------------------

Elevation - 0.91 m (36 in.)	Time - 2-9 sec
-----------------------------	----------------

Diameter [mm (in.)]	Number of Drops	Percentage of Total
0.41-0.68 (0.016-0.027)	6	3.92
0.68-0.95 (0.027-0.037)	43.5	28.43
0.95-1.23 (0.037-0.048)	44	28.76
1.23-1.50 (0.048-0.059)	32	20.92
1.50-1.77 (0.059-0.070)	12	7.84
1.77-2.04 (0.070-0.080)	8	5.23
2.04-2.32 (0.080-0.091)	4	2.61
2.32-2.59 (0.091-0.102)	3	1.96
2.59-2.86 (0.102-0.113)	0.5	0.33

Run 31701	Quench front - 0.40 m (15.6 in.)	Total drops - 108
-----------	----------------------------------	-------------------

Elevation - 2.74 m (108 in.)	Time - 1-8 sec
------------------------------	----------------

Diameter [mm (in.)]	Number of Drops	Percentage of Total
0.31-0.51 (0.012-0.020)	5	4.63
0.51-0.72 (0.020-0.028)	25	23.15
0.72-0.92 (0.028-0.036)	31.5	29.17
0.92-1.13 (0.036-0.044)	28.5	26.39
1.13-1.33 (0.044-0.052)	9.5	8.80
1.33-1.54 (0.052-0.061)	3	2.78
1.54-1.74 (0.061-0.069)	2.5	2.31
1.74-1.95 (0.069-0.077)	3	2.78

TABLE E-

DROPLET DIAMETER FREQUENCY

Run 31805	Quench front - 0.42 m (15.6 in.)	Total drops - 32
Elevation - 0.91 m (36 in.)	Time - 10-16 sec	
Diameter Range [mm (in.)]	Number of Drops	Percentage of Total
0.46-0.76 (0.018-0.030)	8.5	26.56
0.76-1.07 (0.030-0.042)	21.5	67.19
1.07-1.37 (0.042-0.054)	2	6.25
Run 31805	Quench front - 0.42 m (15.6 in.)	Total drops - 12
Elevation - 1.83 m (72 in.)	Time - 10-16 sec	
Diameter Range [mm (in.)]	Number of Drops	Percentage of Total
0.34-0.57 (0.013-0.022)	1	8.33
0.57-0.80 (0.022-0.031)	2.5	20.83
0.80-1.03 (0.031-0.041)	6	50.00
1.03-1.26 (0.041-0.050)	2.5	20.83

(Cont)

FREQUENCY DISTRIBUTION

Run 32114	Quench front - 0.21 m (8.2 in.)	Total drops - 346
Elevation - 2.74 m (108 in.)	Time - 20-30 sec	
<hr/>		
Diameter [mm (in.)]	Number of Drops	Percentage of Total
0.43-0.60 (0.017-0.024)	23.5	6.79
0.60-0.77 (0.024-0.030)	71	20.52
0.77-0.95 (0.030-0.037)	117.5	33.96
0.95-1.12 (0.037-0.044)	76.5	22.11
1.12-1.29 (0.044-0.051)	31	8.96
1.29-1.46 (0.051-0.057)	15	4.34
1.46-1.63 (0.057-0.064)	4.5	1.30
1.63-1.80 (0.064-0.071)	4.0	1.16
1.80-1.98 (0.071-0.078)	1	0.29
1.98-2.15 (0.078-0.085)	2	0.58
<hr/>		
Run 32114	Quench front - 0.18 m (7.2 in.)	Total drops - 316
Elevation - 0.91 m (36 in.)	Time - 18-24 sec	
<hr/>		
Diameter [mm (in.)]	Number of Drops	Percentage of Total
0.41-0.69 (0.016-0.027)	55.5	17.56
0.69-0.96 (0.027-0.038)	107.5	34.02
0.96-1.24 (0.038-0.049)	53.5	16.93
1.24-1.51 (0.049-0.059)	35	11.08
1.51-1.79 (0.059-0.070)	29	9.18
1.79-2.06 (0.070-0.081)	11.5	3.16
2.06-2.34 (0.081-0.092)	10	3.20
2.34-2.61 (0.092-0.103)	8	2.53
2.61-2.89 (0.103-0.114)	1	0.32
2.89-3.16 (0.114-0.124)	1	0.32
3.16-3.44 (0.124-0.135)	1	0.32
3.44-3.71 (0.135-0.146)	2	0.63
3.71-3.99 (0.146-0.157)	1	0.32

TABLE

DROPLET DIAMETER F

Run 32235	Quench front - 0.20 m (8.0 in.)	Total drops - 53
Elevation - 0.91 m (36 in.)	Time - 0-6 sec	
<hr/>		
Diameter Range [mm (in.)]	Number of Drops	Percentage
0.46-0.77 (0.018-0.030)	13	24.5
0.77-1.07 (0.030-0.042)	15	28.3
1.07-1.38 (0.042-0.054)	11	20.7
1.38-1.69 (0.054-0.067)	3	5.6
1.69-1.99 (0.067-0.078)	5	9.4
1.99-2.30 (0.078-0.091)	3	5.6
2.30-2.61 (0.091-0.103)	3	5.6
<hr/>		
Run 32235	Quench front - 0.16 m (6.2 in.)	Total drops - 79
Elevation - 0.91 m (36 in.)	Time - 0-6 sec	
Diameter Range [mm (in.)]	Number of Drops	Percentage
0.47-0.79 (0.019-0.031)	6.5	8.2
0.79-1.11 (0.031-0.044)	31.5	39.8
1.11-1.42 (0.044-0.056)	20	25.3
1.42-1.74 (0.056-0.069)	12	15.1
1.74-2.05 (0.069-0.081)	4.5	5.7
2.05-2.37 (0.081-0.093)	3	3.8
2.37-3.00 (0.093-0.118)	1.5	1.9

FREQUENCY DISTRIBUTION

Run 32333A Quench front - 0.92 m (36.2 in.)		Total drops - 706	
Elevation - 2.74 m (108 in.)		Time - 50-61 sec	
f Total	Diameter [mm (in.)]	Number of Drops	Percentage of Total
	0.32-0.53 (0.013-0.021)	1.5	0.21
	0.53-0.74 (0.021-0.029)	36.5	5.17
	0.74-0.96 (0.029-0.038)	220.5	31.23
	0.96-1.17 (0.038-0.046)	265	37.54
	1.17-1.38 (0.046-0.054)	132.5	18.77
	1.38-1.59 (0.054-0.063)	38.5	5.45
	1.59-1.81 (0.063-0.071)	9.5	1.35
	1.81-2.02 (0.071-0.080)	1	0.14
	2.02-2.23 (0.080-0.088)	1	0.14
Run 32333B Quench front - 0.92 m (36.2 in.)		Total drops - 768	
Elevation - 2.74 m (108 in.)		Time - 50-61 sec	
f Total	Diameter [mm (in.)]	Number of Drops	Percentage of Total
	0.28-0.46 (0.011-0.018)	0.5	0.07
	0.46-0.65 (0.018-0.026)	80	10.42
	0.65-0.83 (0.026-0.033)	239	31.12
	0.83-1.02 (0.033-0.040)	220.5	28.71
	1.02-1.20 (0.040-0.047)	142	18.49
	1.20-1.39 (0.047-0.055)	54.5	7.10
	1.39-1.58 (0.055-0.062)	20.5	2.67
	1.58-1.76 (0.062-0.069)	8.5	1.11
	1.76-1.95 (0.069-0.077)	2.5	0.33

TABLE

DROPLET DIAMETER F

Run 32333 (Total) Quench front - 0.92 m (36.2 in.)		Total drops - 1474
Elevation - 2.74 m (108 in.)		
Diameter Range [mm (in.)]	Number of Drops	Percentage of Total
0.30-0.49 (0.012-0.019)	2	0.14
0.49-0.69 (0.019-0.027)	116.5	7.90
0.69-0.89 (0.027-0.035)	459.5	31.17
0.89-1.09 (0.035-0.043)	485.5	32.94
1.09-1.29 (0.043-0.051)	274.5	18.62
1.29-1.48 (0.051-0.058)	93	6.31
1.48-1.68 (0.058-0.066)	30	2.04
1.68-1.88 (0.066-0.074)	9.5	0.64
1.88-2.08 (0.074-0.082)	3.5	0.33

-1 (Cont)

FREQUENCY DISTRIBUTION

Run 34524 Quench front - 0.26 m (10.2 in.)		Total drops - 330	
	Elevation - 2.74 m (108 in.)	Time - 0.24 sec	
Total	Diameter [mm (in.)]	Number of Drops	Percentage of Total
	0.29-0.48 (0.011-0.019)	3	0.91
	0.48-0.67 (0.019-0.026)	12	3.64
	0.67-0.86 (0.026-0.034)	46	13.94
	0.86-1.05 (0.034-0.041)	62	18.79
	1.05-1.25 (0.041-0.049)	72	21.82
	1.25-1.44 (0.049-0.057)	58.5	17.73
	1.44-1.63 (0.057-0.064)	37	11.21
	1.63-1.82 (0.064-0.072)	18.5	5.61
	1.82-2.01 (0.072-0.079)	12.5	3.79
	2.01-2.20 (0.079-0.087)	4.5	1.36
	2.20-2.39 (0.087-0.094)	2	0.61
	2.78-2.97 (0.109-0.117)	2	0.61

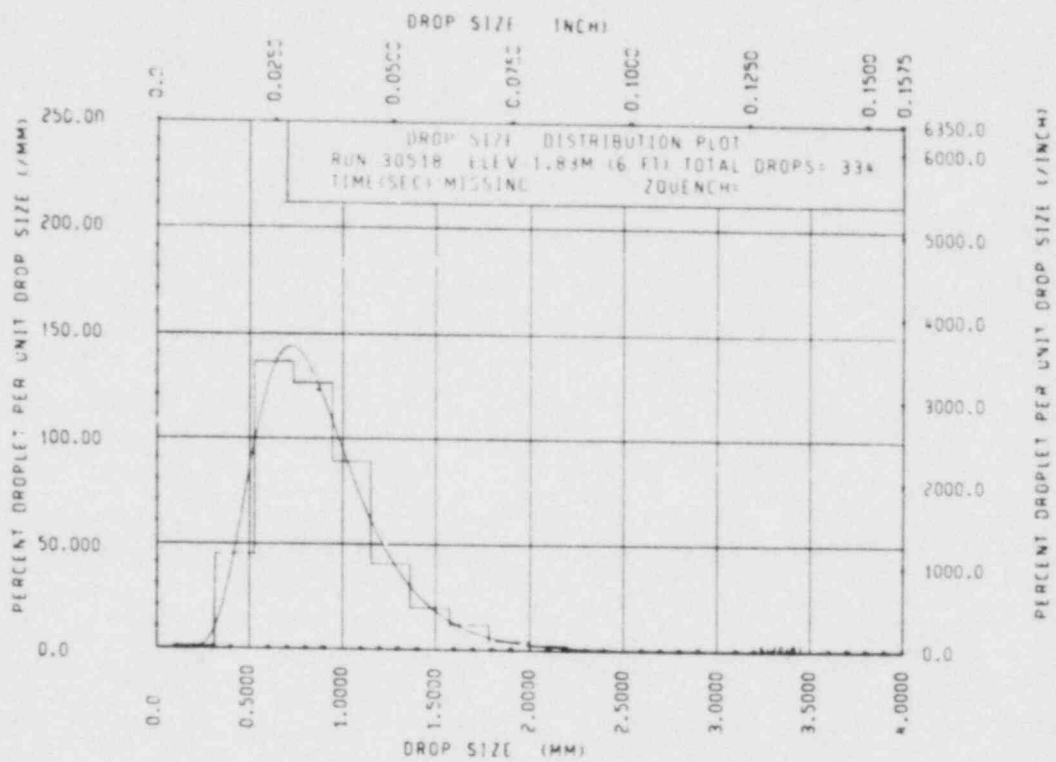


Figure E-3. Drop Size Distribution Plot, Run 30518

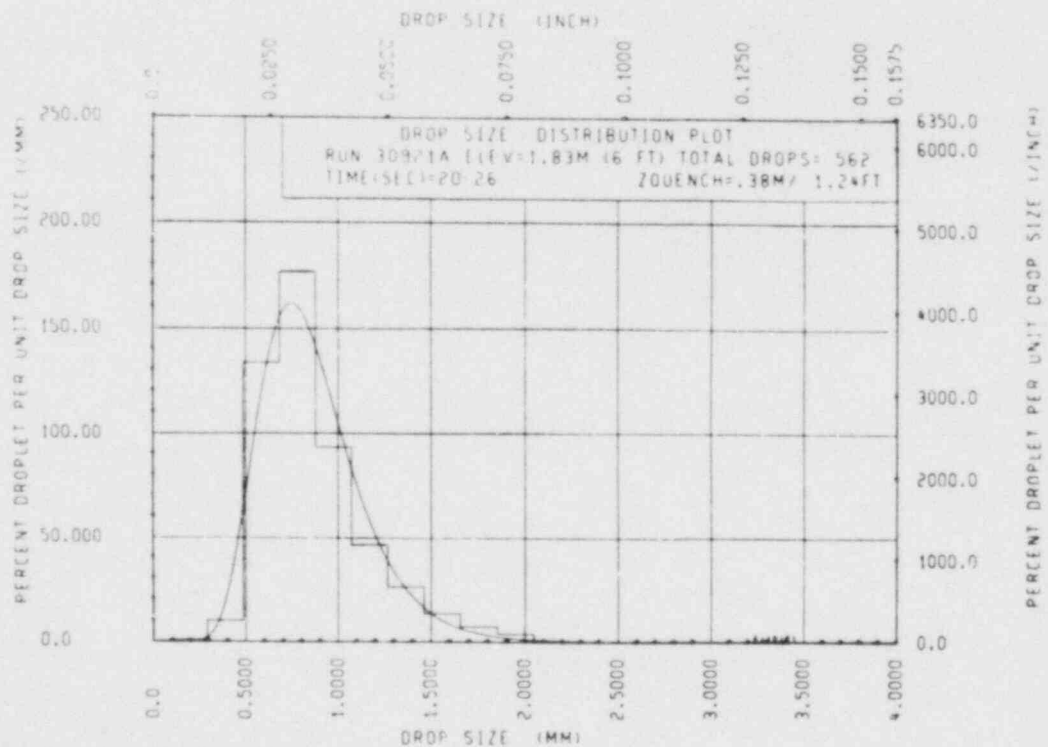


Figure E-4. Drop Size Distribution Plot, Run 30921A

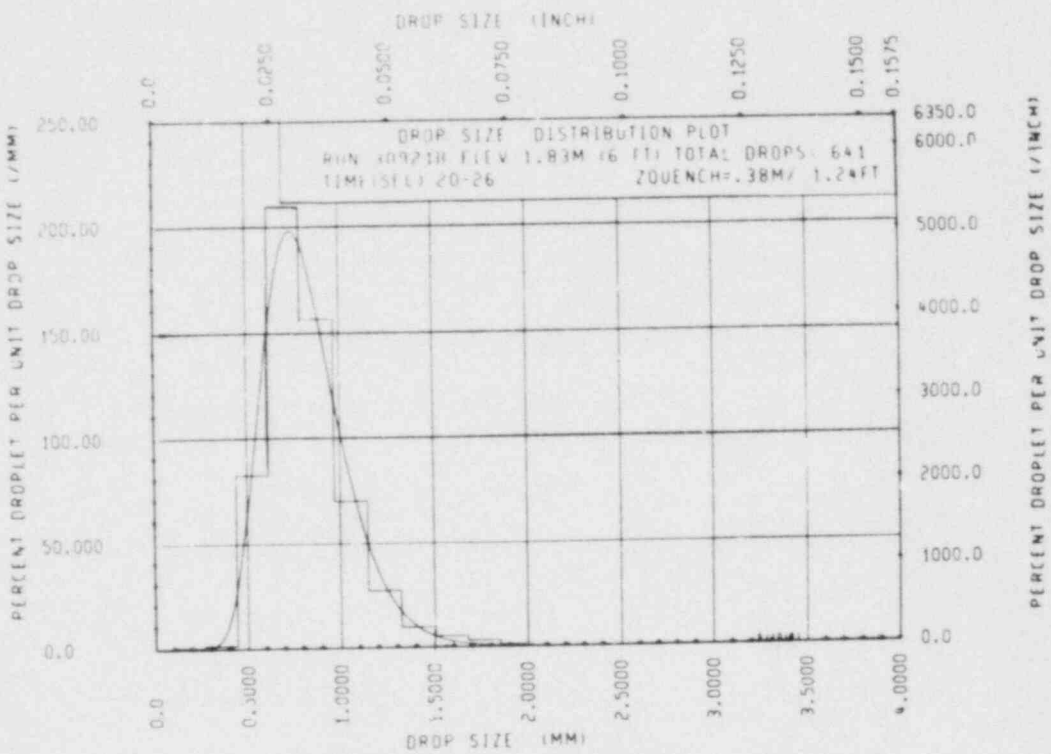


Figure E-5. Drop Size Distribution Plot, Run 30921B

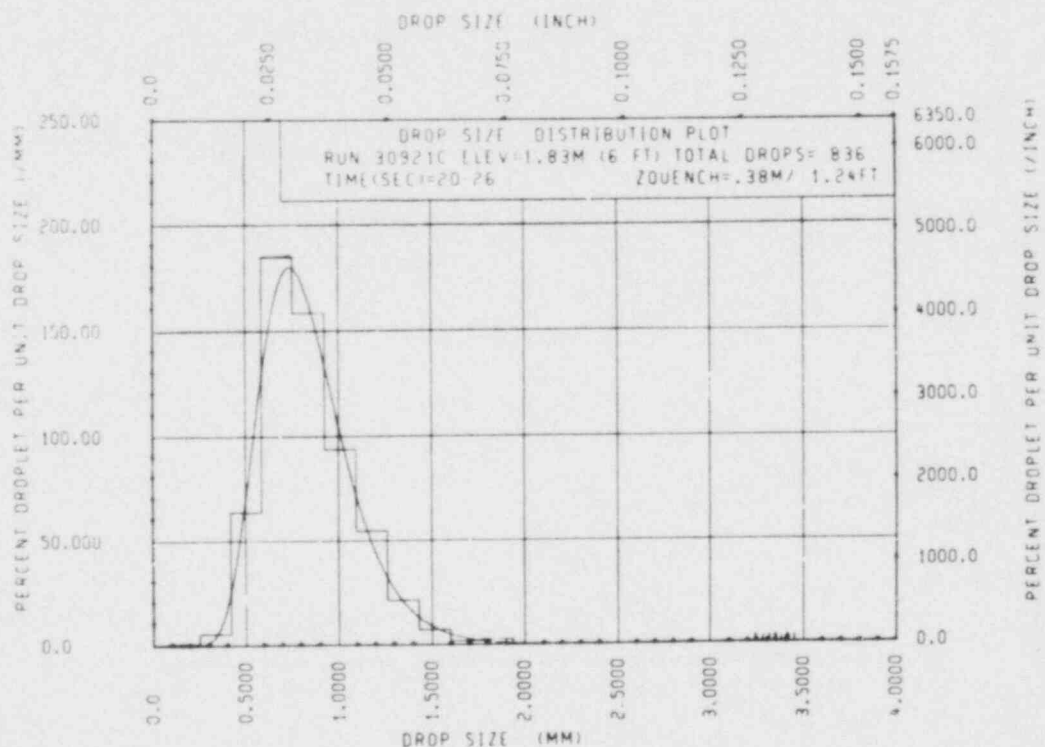


Figure E-6. Drop Size Distribution Plot, Run 30921C

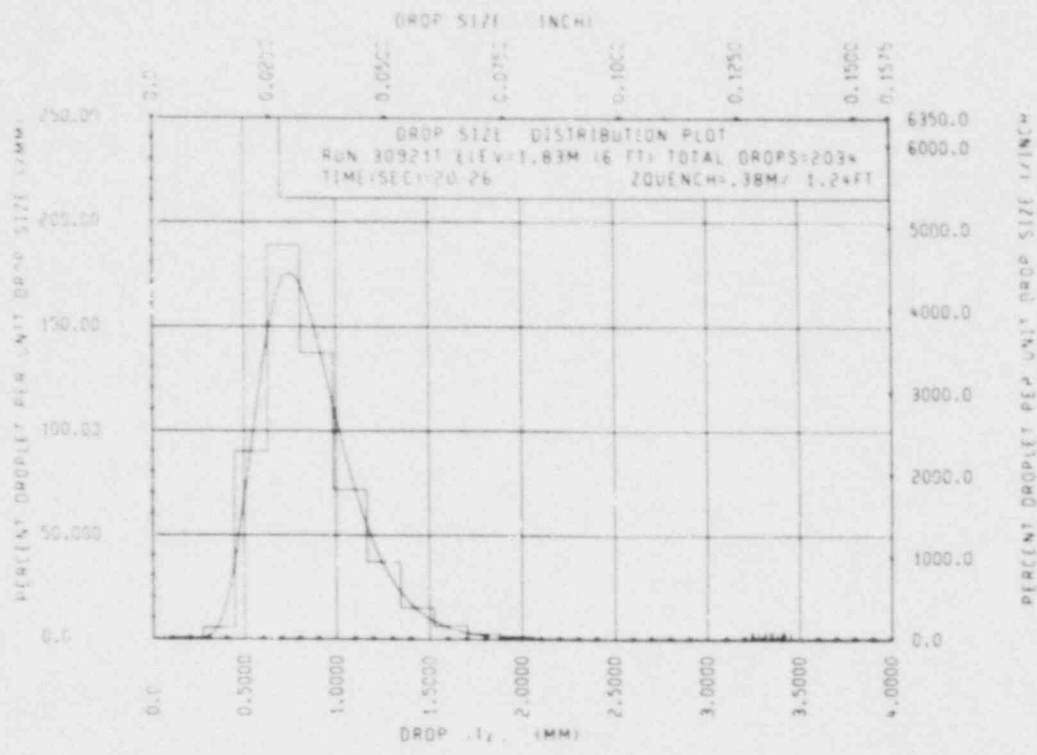


Figure E-7. Drop Size Distribution Plot, Run 30921 (Total)

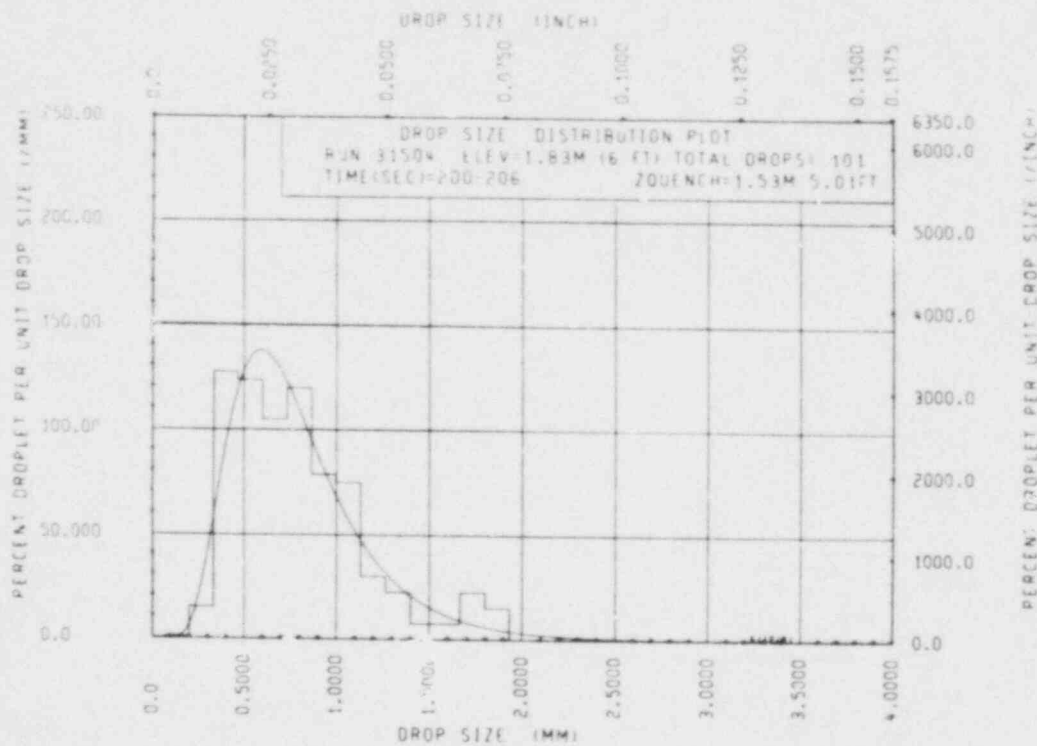


Figure E-8. Drop Size Distribution Plot, Run 31504

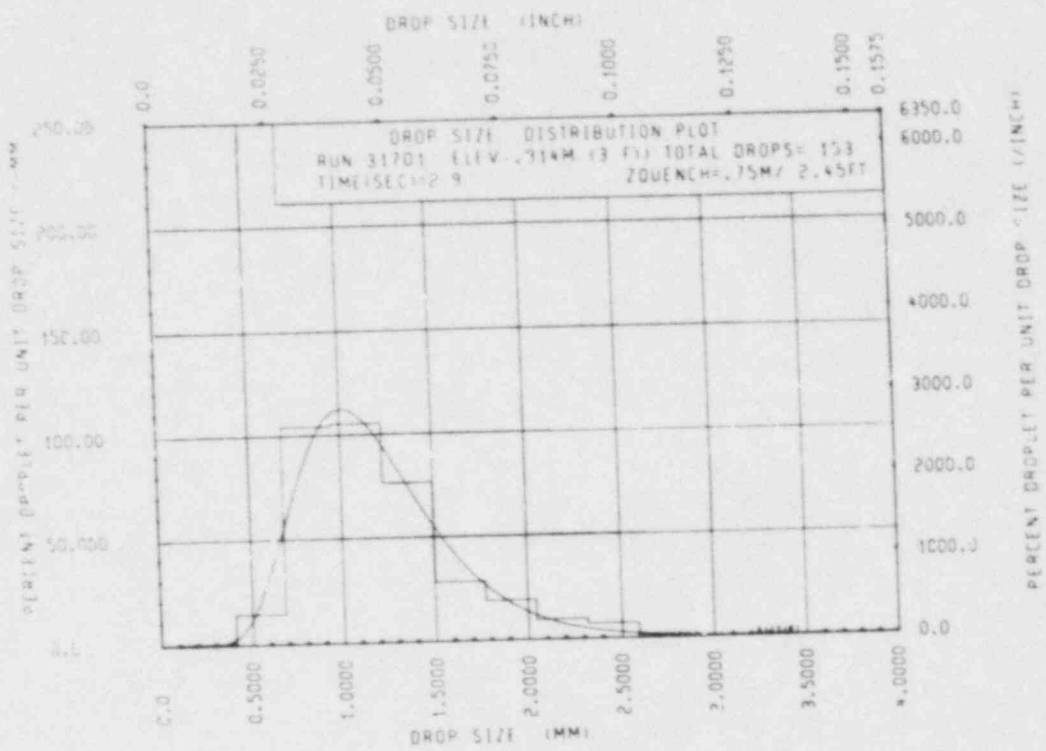


Figure E-9. Drop Size Distribution Plot, Run 31701, 0.91 m (36 in.) Elevation

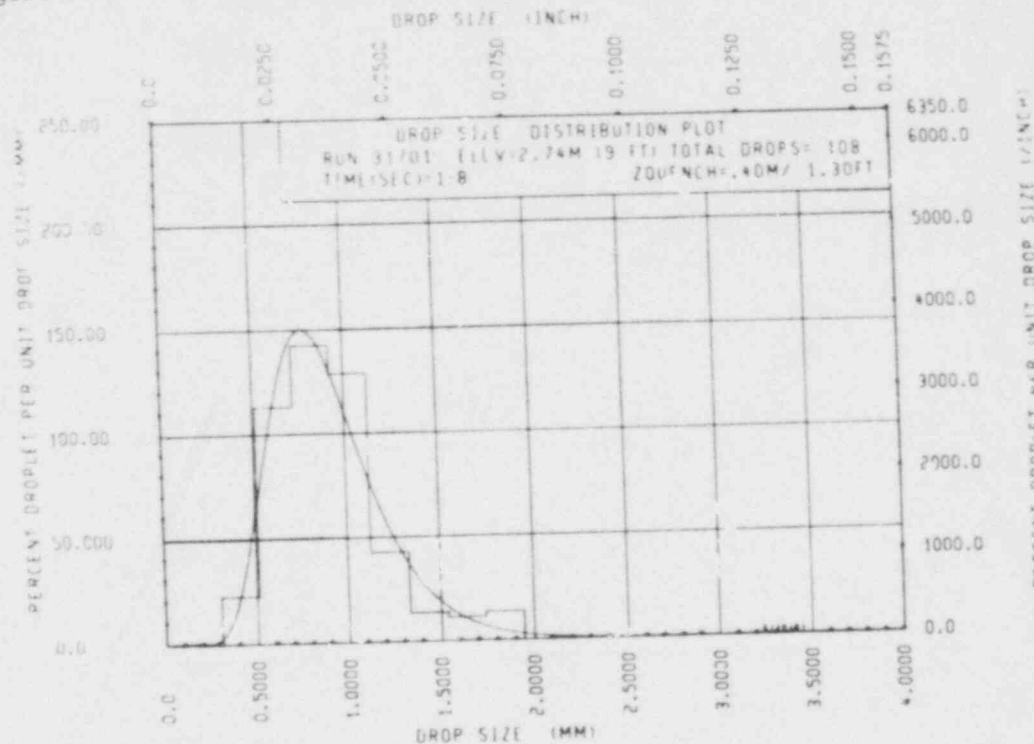


Figure E-10. Drop Size Distribution Plot, Run 31701, 2.74 m (108 in.) Elevation

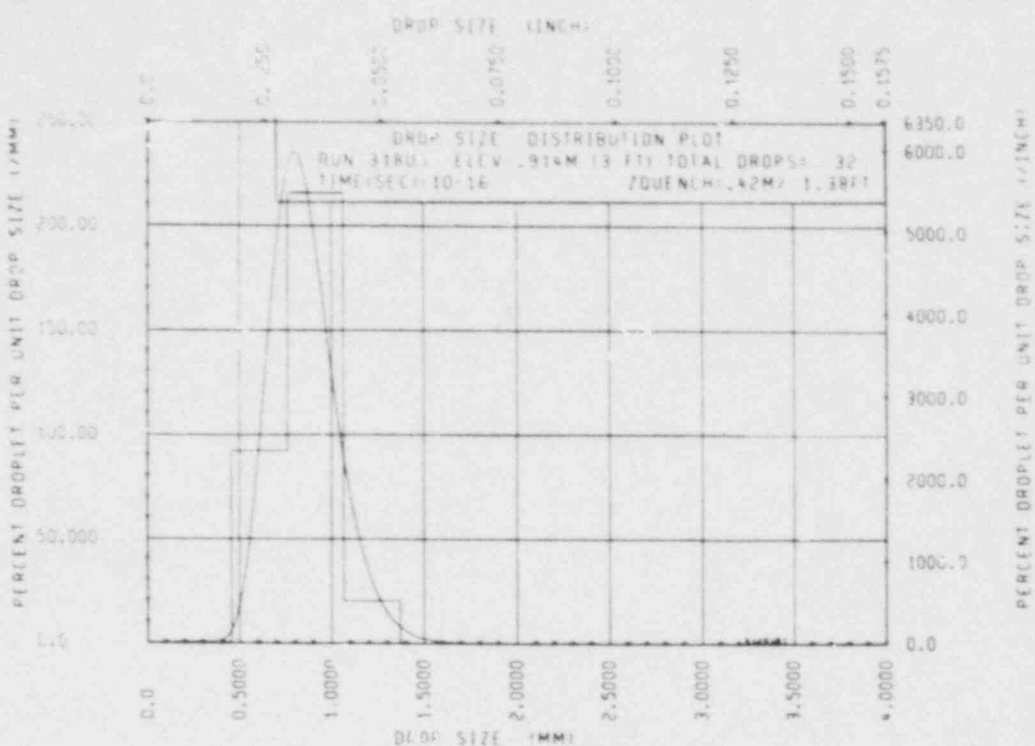


Figure E-11. Drop Size Distribution Plot, Run 31805, 0.91 m (36 in.) Elevation

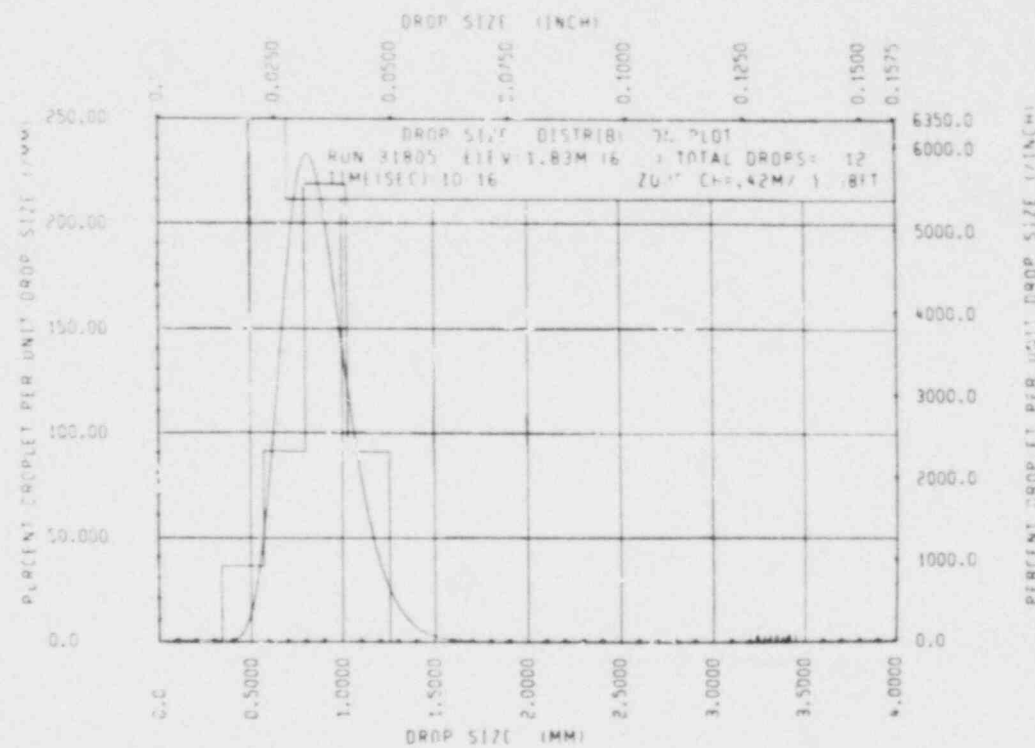


Figure E-12. Drop Size Distribution Plot, Run 31805, 1.83 m (72 in.) Elevation

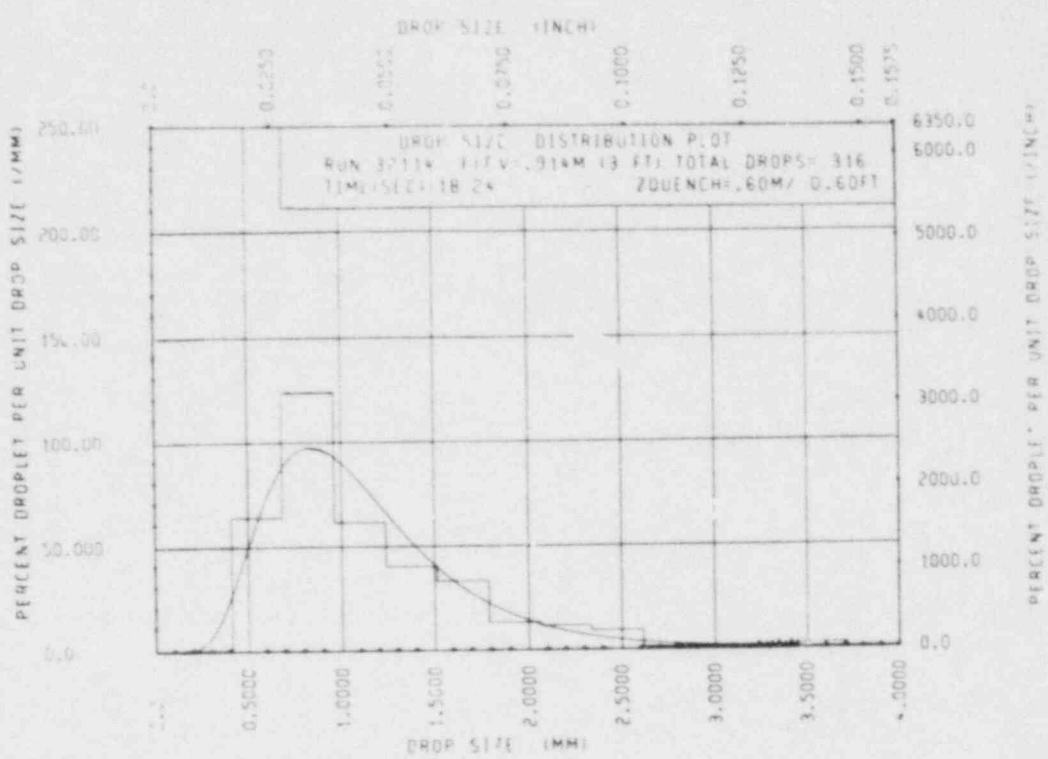


Figure E-13. Drop Size Distribution Plot, Run 32114, 0.91 m (36 in.) Elevation

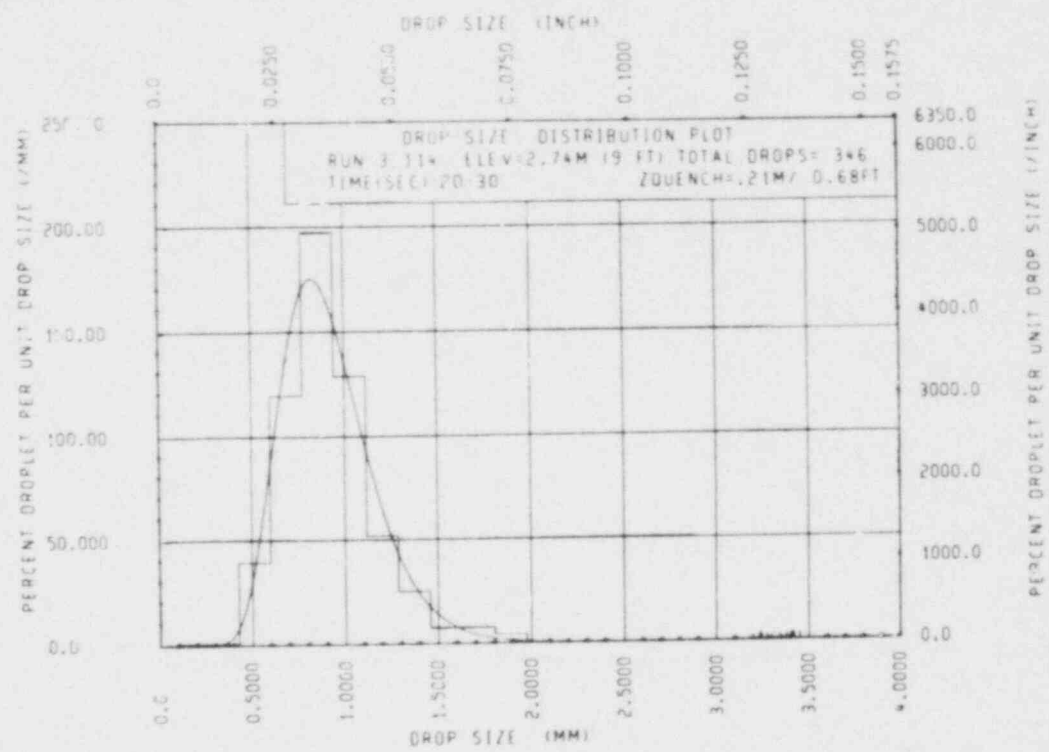


Figure E-14. Drop Size Distribution Plot, Run 32114, 2.74 m (108 in.) Elevation

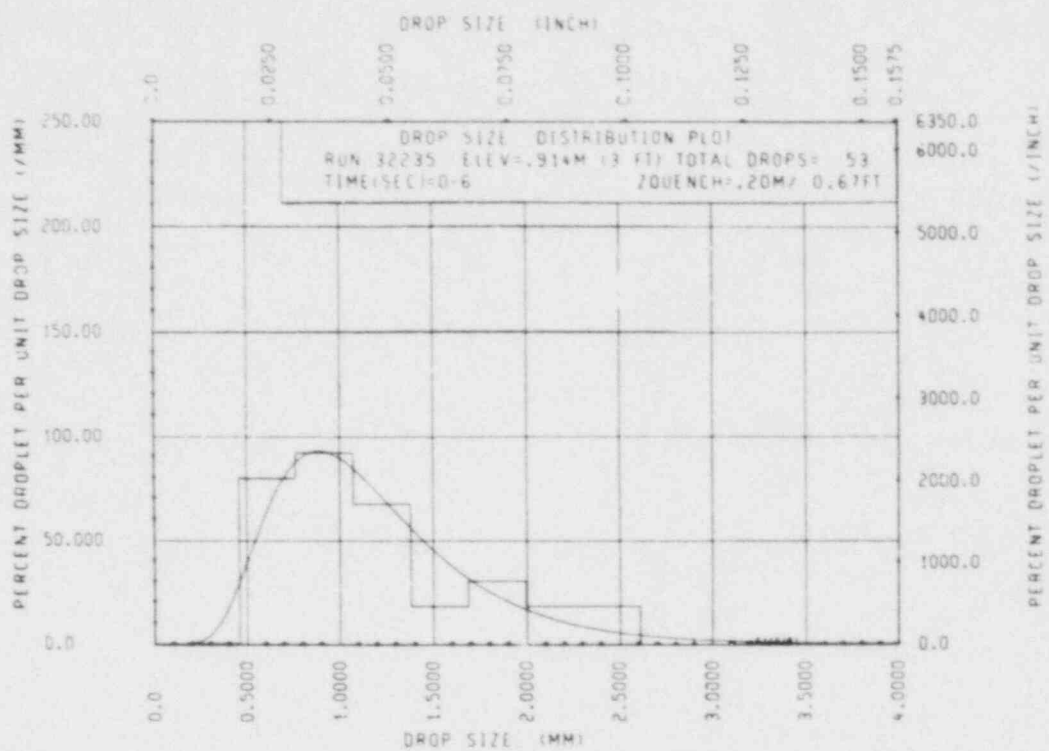


Figure E-15. Drop Size Distribution Plot, Run 32235

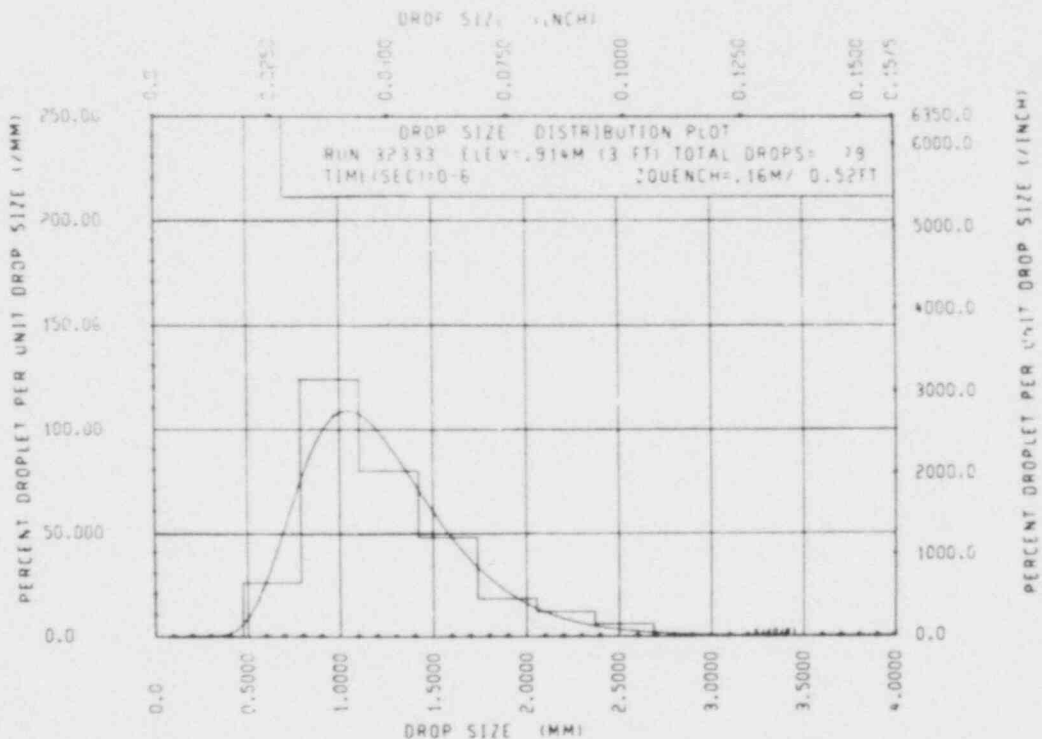


Figure E-16. Drop Size Distribution Plot, Run 32333, 0.91 m (36 in.) Elevation

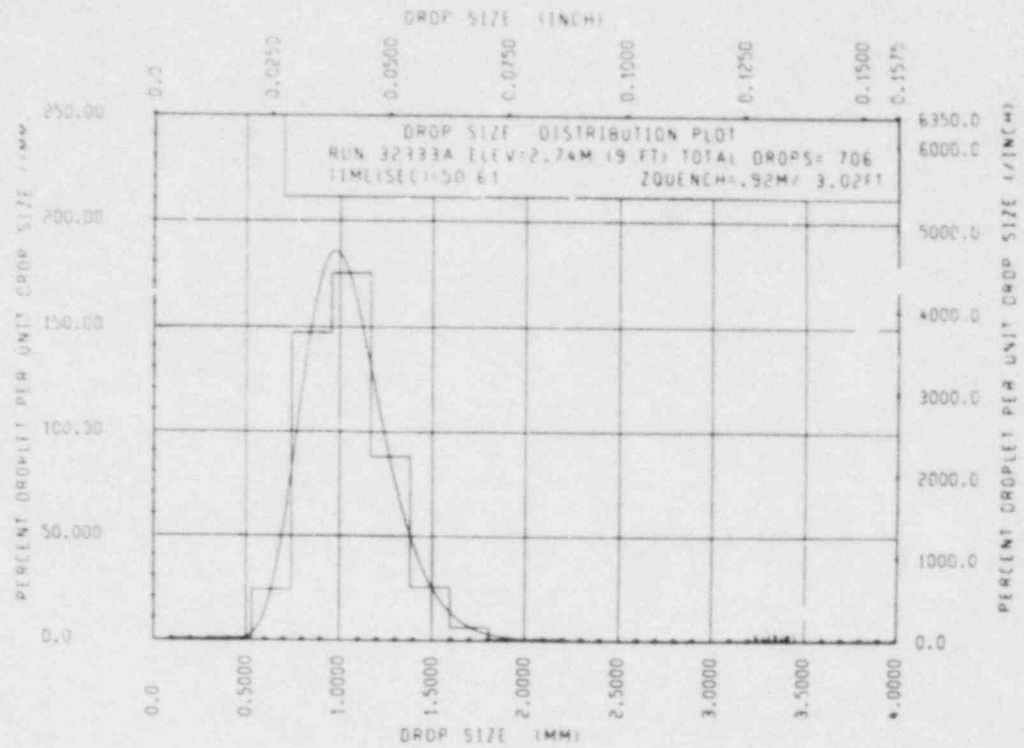


Figure E-17. Drop Size Distribution Plot, Run 32333A, 2.74 m (108 in.) Elevation

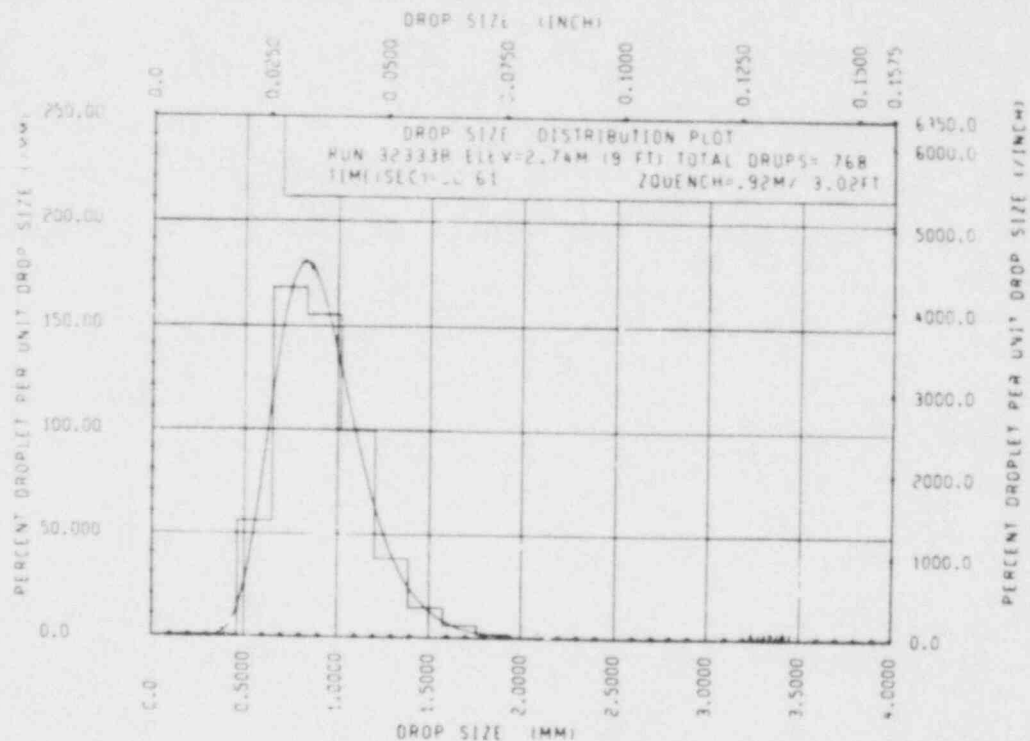


Figure E-18. Drop Size Distribution Plot, Run 32333B, 2.74 m (108 in.) Elevation

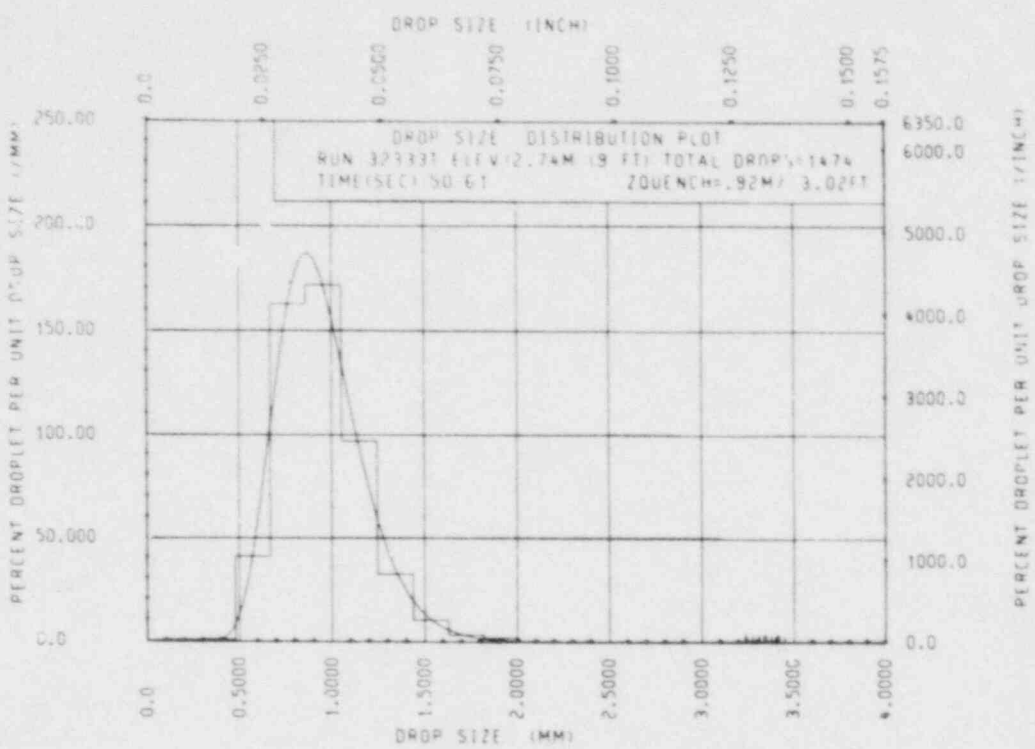


Figure E-19. Drop Size Distribution Plot, Run 323333 (Total), 2.74 m (108 in.) Elevation

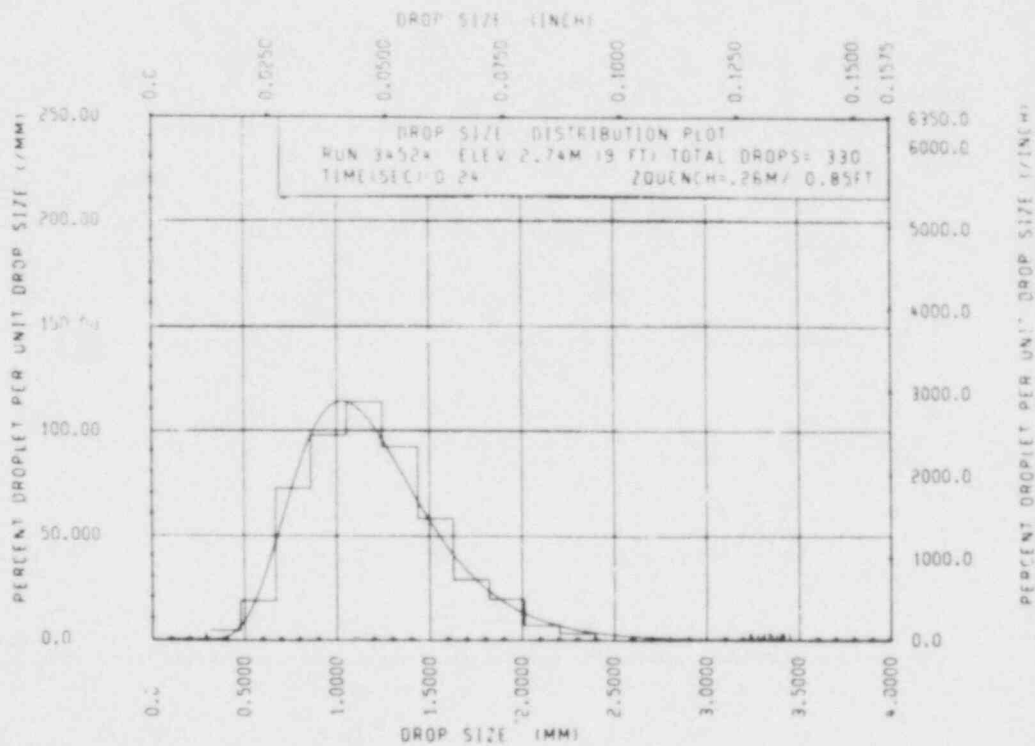


Figure E-20. Drop Size Distribution Plot, Run 34524

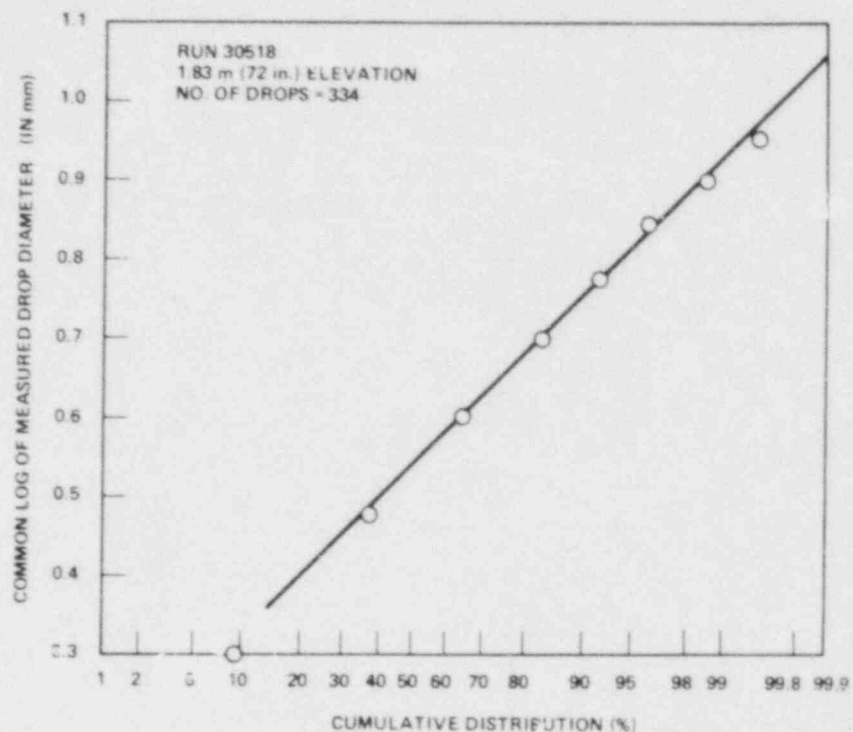


Figure E-21. Log-Normal Distribution Probability Plot, Run 30518

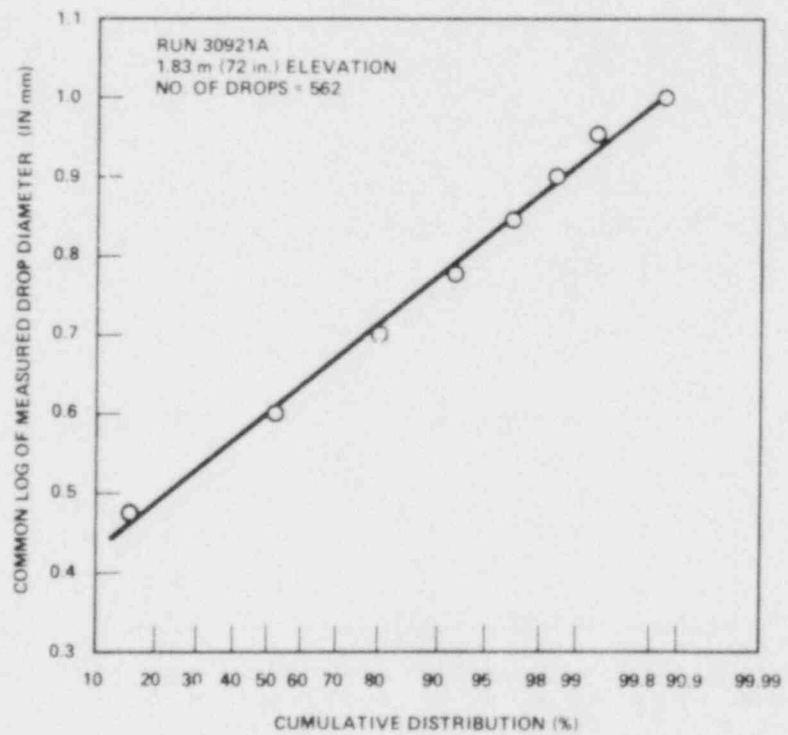


Figure E-22. Log-Normal Distribution Probability Plot, Run 30921A

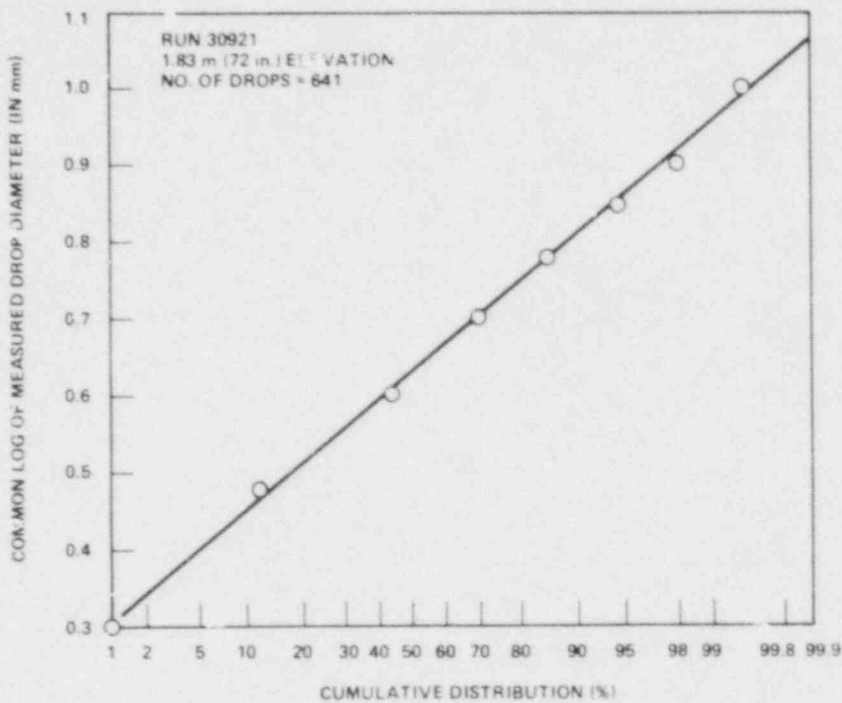


Figure E-23. Log-Normal Distribution Probability Plot, Run 30921B

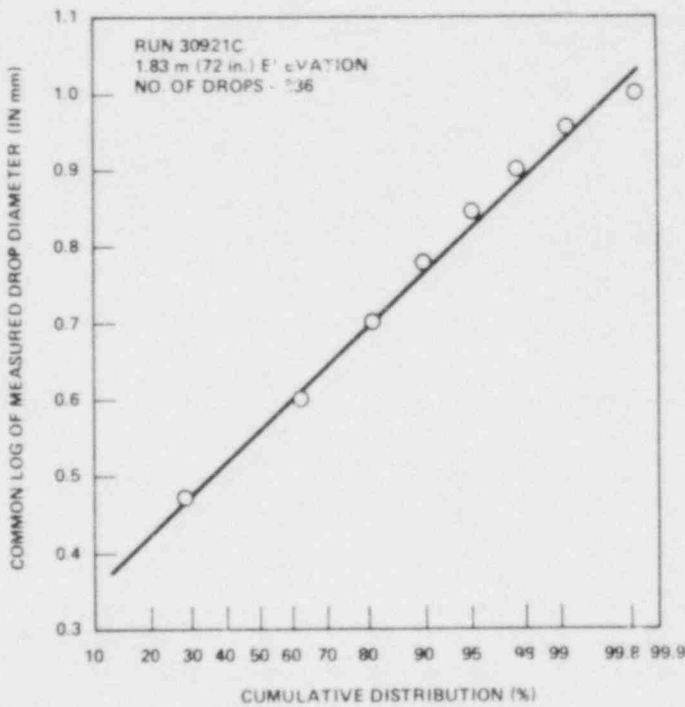


Figure E-24. Log-Normal Distribution Probability Plot, Run 30921C

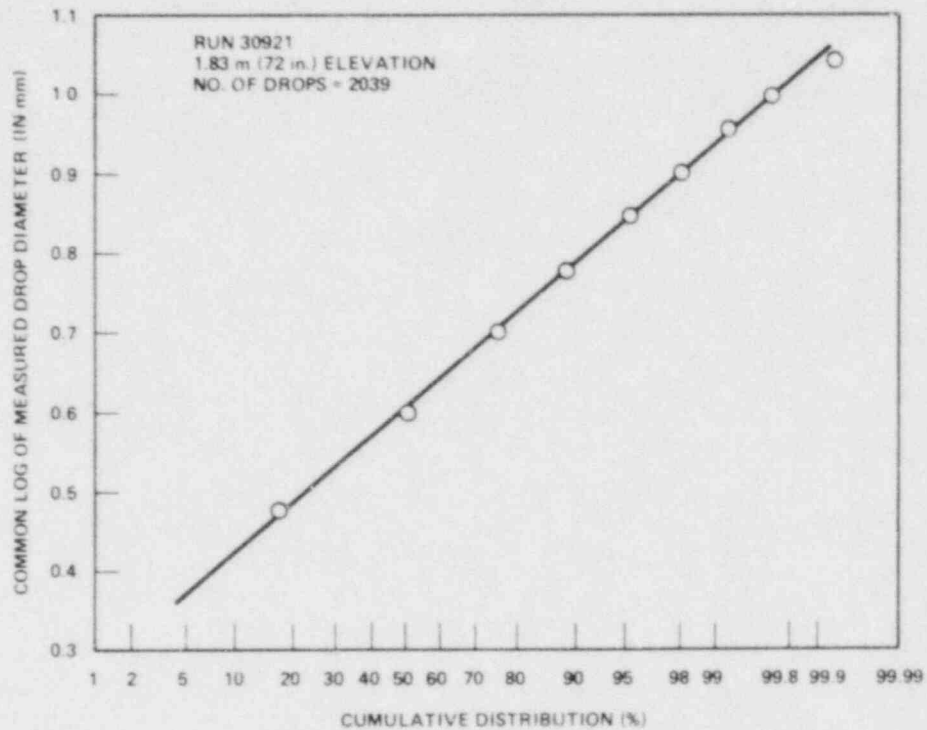


Figure E-25. Log-Normal Distribution Probability Plot, Run 30921 (Total)

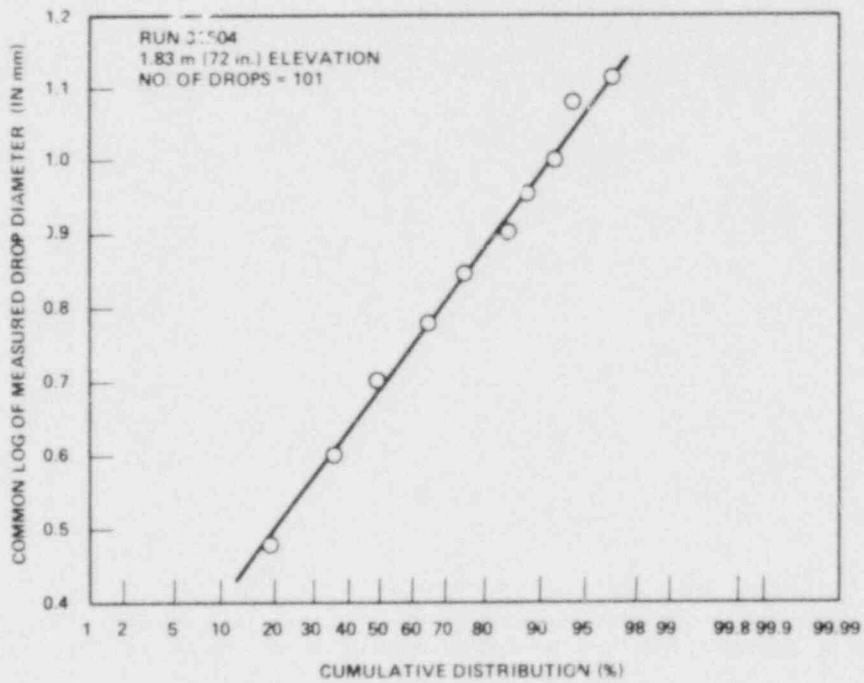


Figure E-26. Log-Normal Distribution Probability Plot, Run 31504

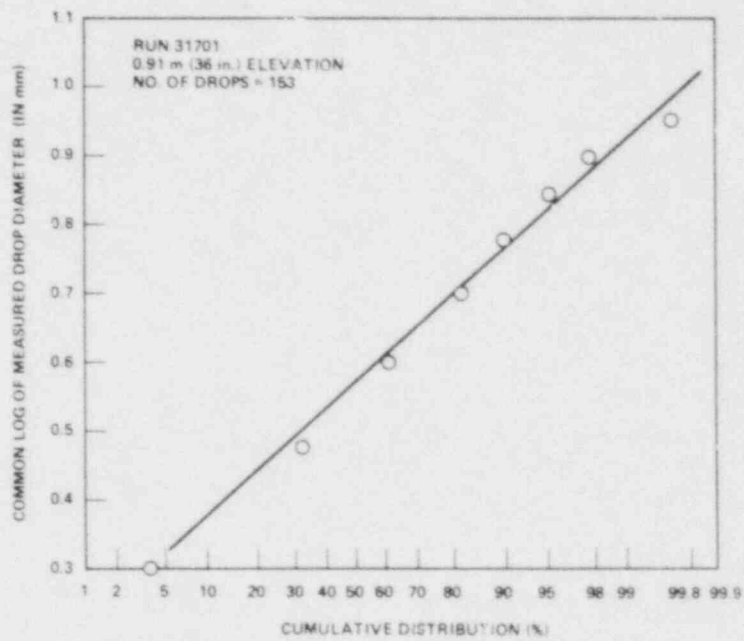


Figure E-27. Log-Normal Distribution Probability Plot, Run 31701, 0.91 m (36 in.) Elevation

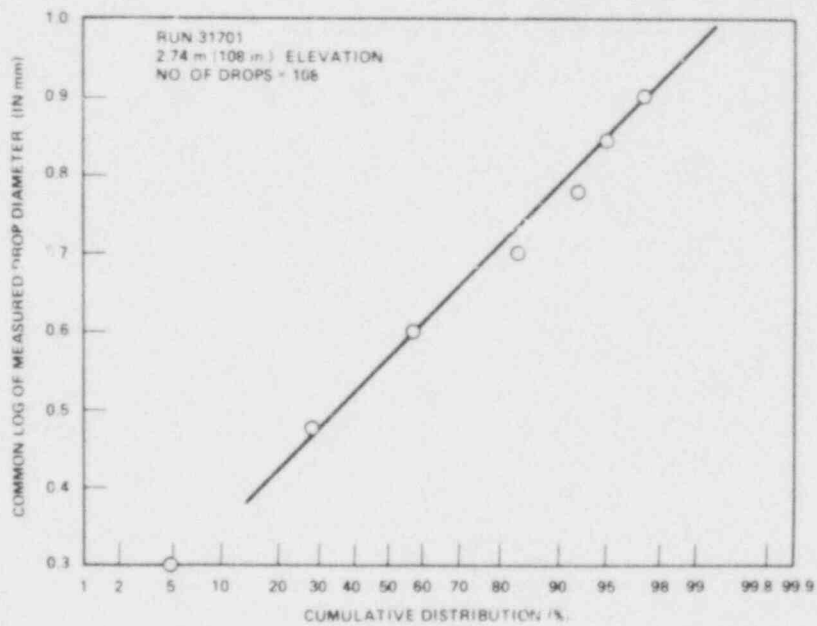


Figure E-28. Log-Normal Distribution Probability Plot, Run 31701, 2.74 m (108 in.) Elevation

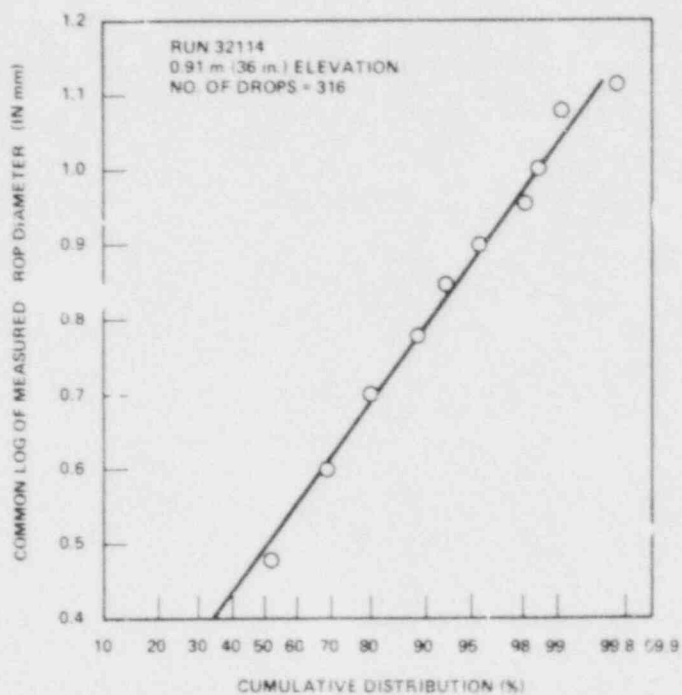


Figure E-29. Log-Normal Distribution Probability Plot, Run 32114, 0.91 m (36 in.) Elevation

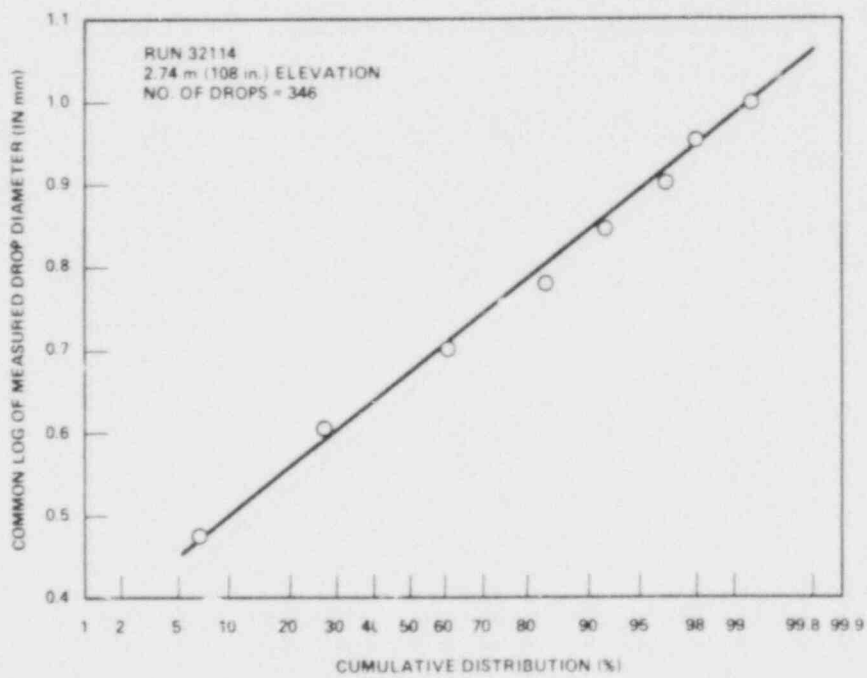


Figure E-30. Log-Normal Distribution Probability Plot, Run 32114, 2.74 m (108 in.) Elevation

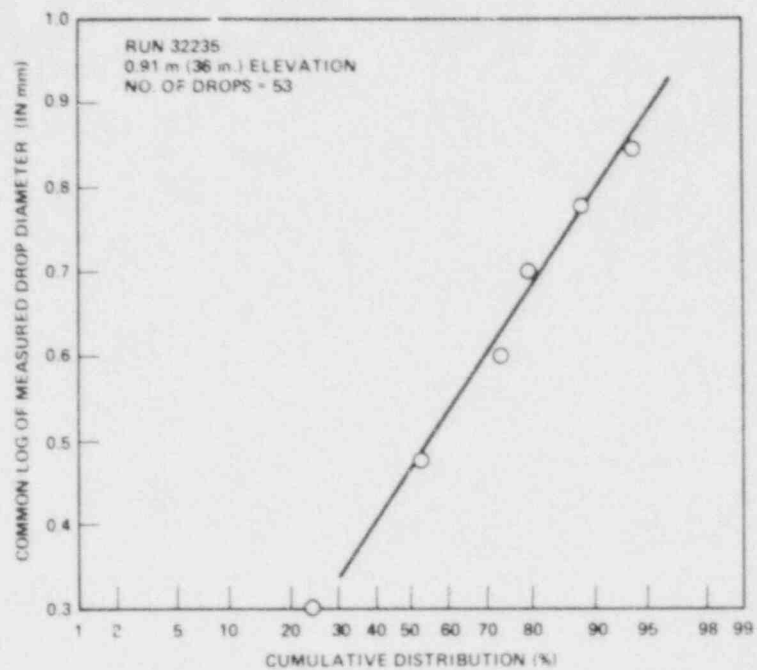


Figure E-31. Log-Normal Distribution Probability Plot, Run 32235

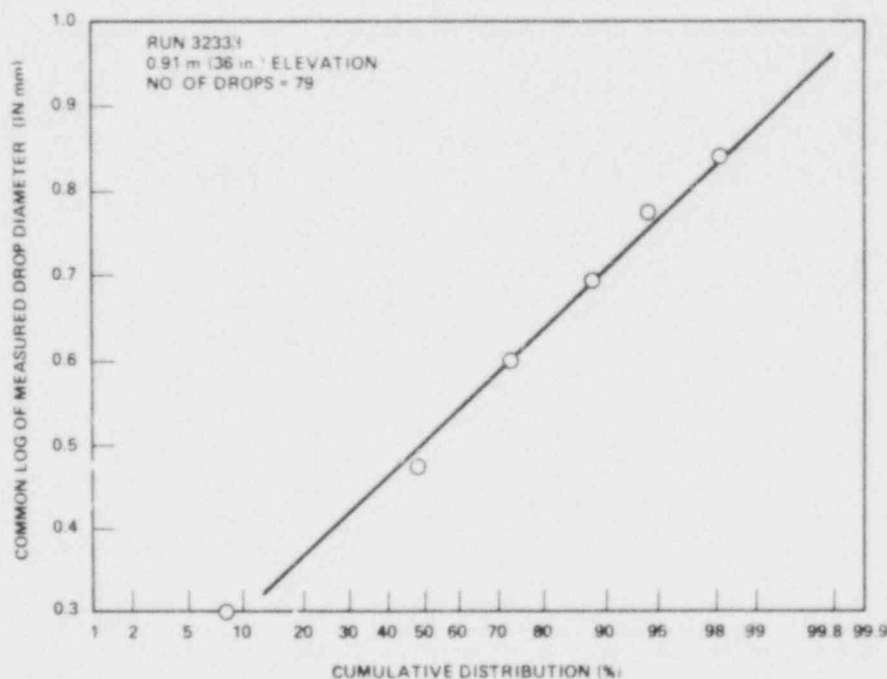


Figure E-32. Log-Normal Distribution Probability Plot, Run 32333, 0.91 m (36 in.) Elevation

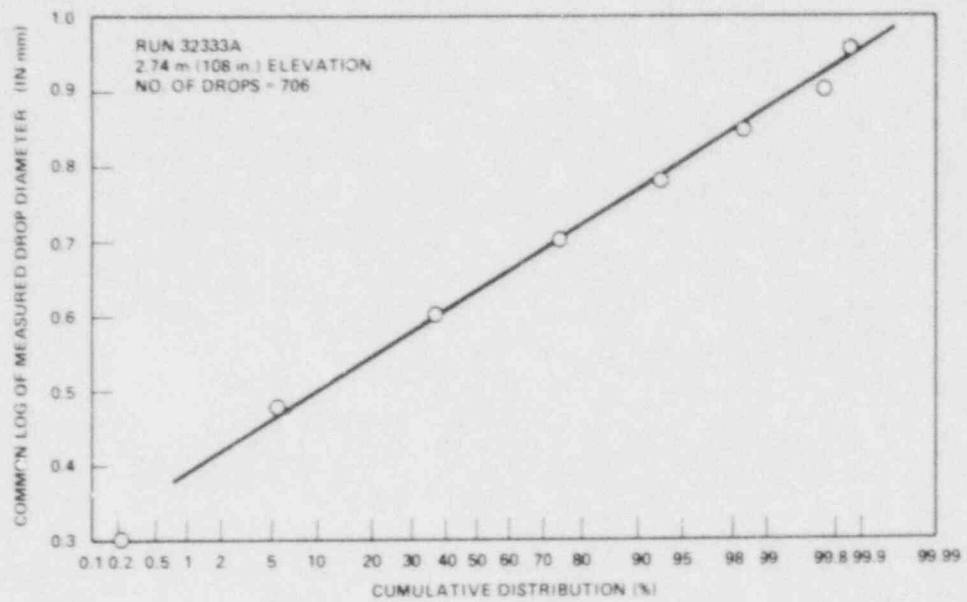


Figure E-33. Log-Normal Distribution Probability Plot, Run 32333A, 2.74 m (108 in.) Elevation

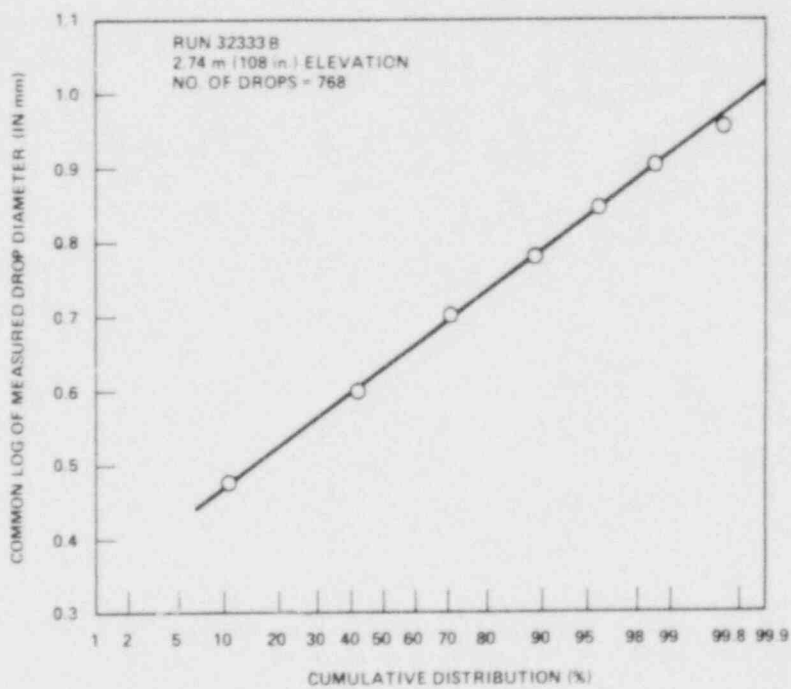


Figure E-34. Log-Normal Distribution Probability Plot, Run 32333B, 2.74 m (108 in.) Elevation

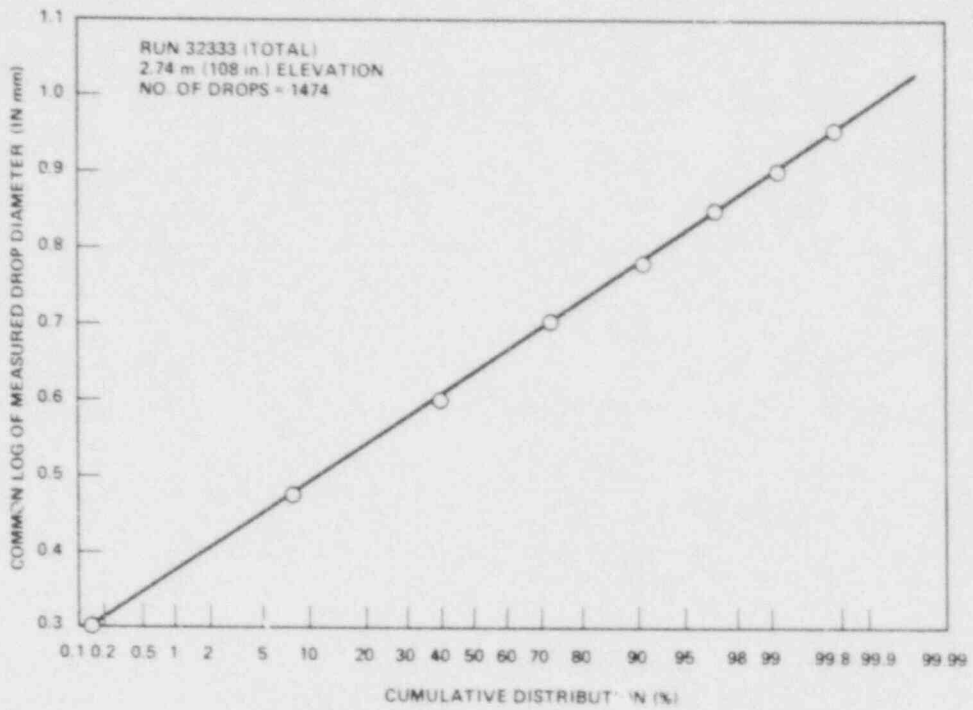


Figure E-35. Log-Normal Distribution Probability Plot, Run 32333 (Total),
2.74 m (108 in.) Elevation

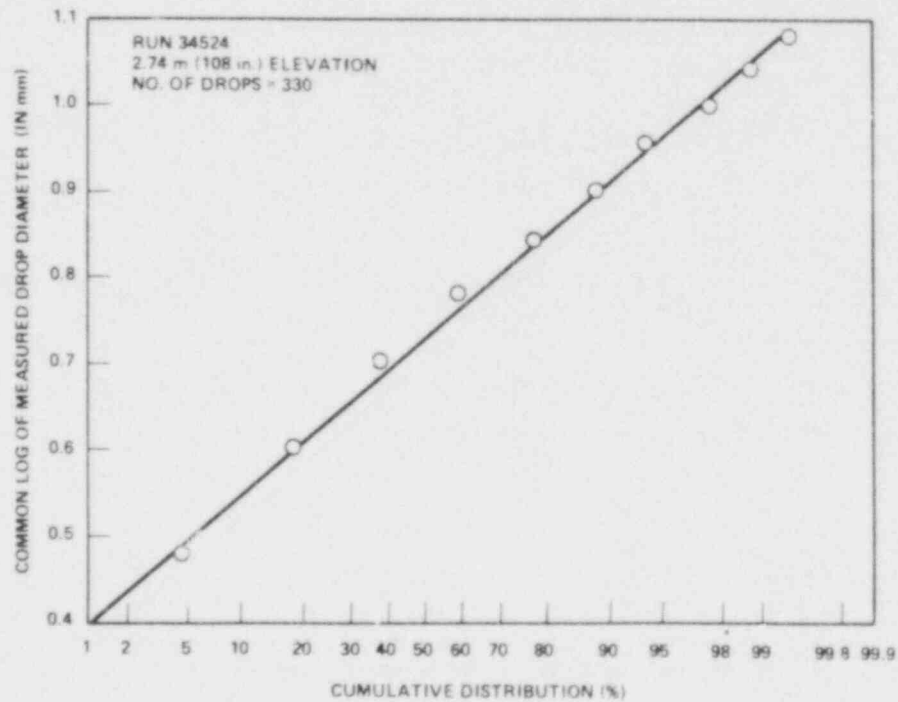


Figure E-36. Log-Normal Distribution Probability Plot, Run 34524

$$\int_{\epsilon}^{\infty} f(x) dx = 1 \quad (E-6)$$

In the droplet diameter distribution, x corresponds to the drop diameter and $f(x)$ is the percent droplet per unit drop diameter at drop diameter x . The variable ϵ was chosen to be zero for all the cases considered. Parameters γ and n were estimated from the droplet data by using the following formulas:

$$\mu = \frac{1}{n} \sum_{i=1}^n \ln (x_i - \epsilon) \quad (E-7)$$

$$S = \left\{ \frac{n \sum_{i=1}^n [\ln (x_i - \epsilon)]^2 - \left[\sum_{i=1}^n \ln (x_i - \epsilon) \right]^2}{n(n-1)} \right\}^{1/2} \quad (E-8)$$

$$\text{with } n = \frac{1}{S} \text{ and } \gamma = \frac{-\mu}{S}$$

where

n = total number of drops

x_i = drop diameter

Parameters obtained with the above formulas were used to generate the log-normal distribution. As shown in figures E-3 through E-20, the log-normal distribution represents the drop diameter distribution fairly well. The estimated parameters (γ , n) of the log-normal distribution are summarized in table E-2.

Drop velocity distributions were also obtained from the movies. They are tabulated in table E-3 and plotted in figures E-37 through E-49.

Information on run conditions, time of movie, mean drop diameter, total number of drops, and quench front elevation is summarized in table E-4.

TABLE E-2
ESTIMATED PARAMETERS FOR LOG-NORMAL DISTRIBUTION

Run	Elevation [m (in.)]		μ	s	η	γ
30518	1.83	(72)	-0.19655	0.36081	2.77153	0.54474
30921A	1.83	(72)	-0.19185	0.31369	3.18790	0.61159
30921B	1.83	(72)	-0.22709	0.26157	3.82307	0.86819
30921C	1.83	(72)	-0.21413	0.28629	3.49295	0.74794
30921T	1.83	(72)	-0.20457	0.29107	3.43560	0.70281
31504	1.83	(72)	-0.32740	0.44155	2.26475	0.74148
31701	0.91	(36)	0.12270	0.33120	3.01936	-0.37047
31701	2.74	(108)	-0.14903	0.32491	3.07774	0.5868
31805	0.91	(36)	-0.18088	0.20520	4.87325	0.88146
31805	1.83	(72)	-0.16237	0.26129	3.82718	0.62143
32114	0.91	(36)	0.02170	0.44162	2.26439	-0.04914
32114	2.74	(108)	-0.11898	0.26529	3.76952	0.44850
32235	0.91	(36)	0.09525	0.43740	2.28622	-0.17204
32333	0.91	(36)	0.15665	0.33033	3.02726	-0.47422
32333A	2.74	(108)	0.02338	0.21460	4.65992	-0.10896
32333B	2.74	(108)	-0.12096	0.25847	3.86889	0.46799
32333T	2.74	(108)	-0.08385	0.23880	4.18750	0.35112
34524	2.74	(108)	0.13332	0.32169	3.10862	-0.41448

TABLE E-3

DROPLET VELOCITY VERSUS DROPLET DIAMETER

RUN 30518
TIME (SEC) = NOT AVAILABLE

ELEVATION = 1.63 (6 FT)

NO.	DIAMETER		VELOCITY	
	MM	IN	M/S	FT/S
1	.77	.0304	4.17	13.67
2	.71	.0281	3.36	11.02
3	.57	.0226	2.93	9.60
4	.57	.0226	3.87	12.71
5	.77	.0304	2.95	9.67
6	.77	.0304	4.34	14.24
7	.67	.0263	4.72	15.47
8	.87	.0341	2.88	9.44
9	.77	.0304	2.46	8.06
10	.57	.0226	5.17	16.97
11	.67	.0263	2.78	9.14
12	.96	.0378	2.86	9.37
13	.96	.0378	2.48	8.14
14	.57	.0226	3.86	12.67
15	.53	.0207	3.00	9.83
16	.67	.0263	2.61	8.56
17	.57	.0226	5.23	17.16
18	1.35	.0530	2.00	6.56
19	1.10	.0433	3.02	9.90
20	.87	.0341	1.71	5.60
21	.57	.0226	3.42	11.21
22	1.35	.0530	3.04	10.28
23	.77	.0304	3.42	11.21
24	1.15	.0451	2.45	8.02
25	.77	.0304	1.91	6.26
26	.77	.0104	1.80	5.91
27	.67	.0263	2.98	9.79
28	.67	.0263	2.69	8.83
29	.71	.0281	2.98	9.79
30	.71	.0281	3.78	12.60
31	1.05	.0415	2.94	9.64
32	.96	.0378	2.90	9.52
33	.71	.0281	2.31	7.56
34	.71	.0281	3.32	10.40
35	.96	.0378	2.07	6.79
36	.77	.0304	2.23	7.33
37	.71	.0281	2.67	8.75
38	.87	.0341	1.98	6.49
39	.71	.0281	2.14	7.03

E-142

TABLE E-3 (Cont)

DROPLET VELOCITY VERSUS DROPLET DIAMETER

40	1.05	.0415	3.98	13.05
41	.77	.0304	2.95	9.67
42	.67	.0263	2.73	8.74
43	.62	.0244	3.87	12.71
44	.91	.0359	2.76	9.06
45	.87	.0341	2.55	8.37
46	.57	.0226	2.55	8.37
47	.57	.0226	2.80	9.17
48	.39	.0152	1.29	4.22
49	1.10	.0423	2.04	6.66
50	.62	.0244	1.37	4.49
51	.71	.0281	3.10	10.17
52	1.49	.0585	3.40	11.17
53	.77	.0304	4.07	13.35
54	.77	.0304	4.27	14.01
55	1.35	.0530	3.69	12.09
56	.67	.0263	3.16	10.36
57	1.17	.0461	3.66	12.02
58	1.08	.0424	3.42	11.21
59	.73	.0266	4.12	13.51
60	.78	.0309	3.81	12.51
61	.78	.0309	2.73	8.94
62	.92	.0364	4.34	14.24
63	.73	.0286	4.69	15.39
64	.73	.0266	2.78	9.14

TABLE E-3 (Cont)

DROPLET VELOCITY VERSUS DROPLET DIAMETER

RUN 30921
TIME (SEC) = 20-26

ELEVATION = 1.83 (6 FT)

NO.	DIAMETER		VELOCITY	
	MM	IN	M/S	FT/S
1	1.22	.0479	7.69	25.22
2	.69	.0272	5.43	17.81
3	.96	.0378	5.09	16.70
4	.78	.0309	6.01	19.73
5	.87	.0341	5.51	18.08
6	.87	.0341	5.44	17.85
7	.78	.0309	4.75	15.58
8	.48	.0189	5.38	17.66
9	.74	.0290	6.26	20.54
10	.74	.0290	5.84	19.15
11	1.12	.0442	5.96	19.24
12	1.12	.0442	5.88	19.31
13	.83	.0327	4.48	14.70
14	.87	.0341	6.00	19.69
15	.61	.0240	5.72	18.77
16	.66	.0258	4.26	13.97
17	.66	.0258	6.84	22.45
18	.87	.0341	5.07	16.62
19	.87	.0341	6.12	20.07
20	1.30	.0511	6.42	21.07
21	.78	.0309	5.67	18.62
22	.78	.0309	5.72	18.77
23	.83	.0327	4.13	13.55
24	.69	.0272	4.38	14.36
25	.74	.0290	6.75	22.15
26	.61	.0240	4.29	14.09
27	.69	.0272	5.92	19.42
28	.87	.0341	5.32	17.46
29	.78	.0309	4.87	15.97
30	1.04	.0410	3.64	11.94
31	.78	.0309	6.34	20.80
32	.69	.0272	5.51	18.08
33	1.04	.0410	5.86	19.23
34	.96	.0378	6.69	21.96
35	.61	.0240	5.88	19.31
36	1.12	.0442	4.67	15.32
37	.69	.0272	5.49	18.06
38	.78	.0309	5.21	17.08

TABLE E-3 (Cont)

DROPLET VELOCITY VERSUS DROPLET DIAMETER

39	.69	.0272	4.67	15.32
40	.53	.0207	4.69	15.39
41	.69	.0272	5.64	18.20
42	1.22	.0479	6.77	22.22
43	.87	.0341	6.79	22.26
44	.61	.0240	5.98	19.61
45	.69	.0272	4.84	15.89
46	.69	.0272	4.68	15.35
47	.78	.0309	5.32	17.46
48	.78	.0309	4.38	14.36
49	.78	.0309	5.92	19.42
50	.61	.0240	6.54	21.46
51	.96	.0378	8.06	26.45
52	.61	.0240	3.74	12.28
53	.87	.0341	5.67	18.62
54	.53	.0207	5.64	18.50
55	.96	.0178	3.99	13.09
56	.87	.0341	4.42	14.51
57	.69	.0272	5.59	18.35
58	.96	.0378	10.38	34.05
59	.91	.0359	8.32	27.24
60	.96	.0378	5.21	17.06
61	.66	.0258	5.64	18.50
62	.82	.0322	7.41	24.30
63	.78	.0309	4.36	14.32
64	.69	.0272	5.92	19.42
65	.78	.0309	5.84	19.13
66	.78	.0309	6.36	20.08
67	.69	.0272	6.18	20.27
68	.73	.0266	6.05	19.84
69	.78	.0309	3.69	12.09
70	.69	.0272	5.59	18.35
71	.78	.0309	5.36	18.23
72	.78	.0309	4.83	15.85
73	.74	.0290	6.28	20.61
74	.96	.0378	5.15	16.89
75	.78	.0309	6.98	22.92
76	.74	.0290	4.82	15.81
77	1.04	.0410	8.62	26.29
78	.69	.0272	5.15	16.89
79	.82	.0322	5.23	17.16
80	1.83	.0719	5.11	16.77
81	.61	.0240	5.00	16.39
82	.56	.0221	4.31	14.13

TABLE E-3 (Cont)

DROPLET VELOCITY VERSUS DROPLET DIAMETER

83	1.22	.0479	6.62	21.73
84	.83	.0327	5.76	18.88
85	.69	.0272	5.56	18.23
86	.61	.0240	5.31	17.43
87	.66	.0258	5.72	18.77
88	.69	.0272	5.49	19.00
89	.53	.0207	5.30	17.39
90	.78	.0309	6.52	21.36
91	1.04	.0410	5.86	19.23
92	.61	.0240	5.08	16.66
93	.87	.0341	3.67	12.05
94	1.04	.0410	5.10	16.74
95	.69	.0272	4.96	16.27
96	.69	.0277	4.95	19.24
97	.61	.0240	5.53	18.16
98	.61	.0246	6.17	20.23
99	1.04	.0410	8.07	26.48
100	.56	.0221	5.51	18.08
101	.87	.0341	5.32	17.40
102	.51	.0203	5.01	16.43
103	.61	.0240	5.45	17.89
104	.78	.0309	4.77	15.66
105	.61	.0240	5.09	16.70
106	.96	.0378	5.97	19.28
107	.87	.0341	6.75	22.15
108	.78	.0309	6.59	21.61
109	.83	.0327	5.60	18.39
110	.87	.0341	5.30	17.39
111	.69	.0272	5.33	17.50
112	.78	.0309	4.89	16.04
113	.69	.0272	4.90	16.08
114	.61	.0240	4.96	16.27
115	.78	.0309	5.74	18.85
116	1.12	.0442	2.50	8.21
117	1.35	.0530	3.72	12.21
118	1.26	.0497	2.46	8.06
119	.96	.0378	3.47	11.40
120	.69	.0272	3.47	11.40
121	.53	.0207	4.70	15.43
122	.83	.0327	6.08	19.96
123	.78	.0309	4.48	14.70
124	.69	.0272	3.84	12.54
125	.61	.0240	5.79	19.00
126	.63	.0249	4.63	15.20

TABLE E-3 (Cont)

DROPLET VELOCITY VERSUS DROPLET DIAMETER

127	1.22	.0479	3.22	10.56
128	.78	.0309	3.45	11.32
129	1.22	.0472	3.38	11.09
130	.69	.0272	5.14	10.85
131	.87	.0341	4.66	15.28
132	.83	.0327	3.28	10.75
133	.83	.0327	3.88	12.74
134	.69	.0272	5.64	18.50
135	.78	.0309	3.78	12.40
136	.61	.0240	4.09	13.43
137	.61	.0240	4.66	15.28
138	.87	.0341	5.51	1d.08
139	.69	.072	4.50	14.78
140	1.22	.0479	3.23	10.59
141	.53	.0207	4.87	15.47
142	.61	.0240	4.70	15.43
143	1.04	.0410	3.28	10.75
144	.96	.0378	3.04	9.98
145	.78	.0309	4.34	14.24
146	.91	.0359	4.17	13.66
147	.66	.0258	4.86	15.93
148	.78	.0309	3.46	11.36
149	1.12	.0442	3.87	12.71
150	.96	.0378	4.29	14.09
151	.78	.0309	3.39	11.13
152	.69	.0272	4.84	15.89
153	.78	.0309	4.21	13.82
154	.53	.0207	6.95	22.60
155	.69	.0272	4.47	14.66
156	.78	.0309	3.35	10.98
157	1.47	.0580	3.54	11.63
158	.69	.0272	5.28	17.31
159	.87	.0341	3.45	11.32
160	.69	.0272	3.11	10.21
161	.69	.0272	3.87	12.71
162	.69	.0272	4.38	14.36
163	.69	.0272	5.18	17.00
164	.74	.0290	4.27	14.01
165	.61	.0240	6.35	20.84
166	.78	.0309	4.77	15.66
167	.78	.0309	5.53	18.16
168	.53	.0207	5.48	17.96
169	.69	.0272	4.36	14.32
170	.61	.0240	4.84	15.89

TABLE E-3 (Cont)

DROPLET VELOCITY VERSUS DROPLET DIAMETER

171	.69	.0272	4.63	15.20
172	1.04	.0410	5.04	16.54
173	1.04	.0410	3.73	12.24
174	.87	.0341	4.71	15.47
175	.69	.0272	3.58	11.75
176	.53	.0207	4.34	14.24
177	.53	.0207	5.29	17.35
178	.83	.0327	4.81	15.78
179	.69	.0272	5.56	18.23
180	1.04	.0410	3.56	11.67
181	1.04	.0410	4.60	15.06
182	1.30	.0511	3.85	12.63
183	.87	.0341	5.76	18.88
184	.78	.0309	4.34	14.24
185	.69	.0272	6.17	20.23
186	.61	.0240	4.80	15.74
187	.66	.0258	5.42	17.77
188	.69	.0272	4.24	13.89
189	.66	.0258	5.08	16.66
190	.96	.0378	4.47	14.66
191	.87	.0341	5.29	17.35
192	.61	.0240	5.12	16.81
193	1.30	.0511	4.84	15.89
194	.78	.0309	5.62	18.42
195	.74	.0290	4.07	13.36
196	.66	.0258	4.08	13.40
197	1.22	.0479	3.19	10.48
198	.78	.0309	3.50	11.40
199	1.22	.0479	2.43	7.78
200	.87	.0341	6.08	19.96
201	.69	.0272	5.01	16.43
202	1.04	.0410	4.14	13.59
203	.69	.0272	3.66	12.01
204	.69	.0272	5.30	17.39
205	.87	.0341	5.05	16.58
206	.69	.0272	5.62	18.42
207	.87	.0341	3.78	12.40
208	1.22	.0479	3.73	12.24
209	.78	.0309	5.64	18.50
210	.87	.0341	4.73	15.91
211	.78	.0309	4.11	13.47
212	.78	.0309	5.55	18.19
213	.66	.0258	3.86	12.67
214	.66	.0258	4.87	15.97

TABLE E-3 (Cont)

DROPLET VELOCITY VERSUS DROPLET DIAMETER

215	.61	.0240	4.90	16.06
216	.61	.0240	3.62	11.86
217	.69	.0272	6.19	20.31
218	.69	.0272	6.32	20.73
219	.69	.0272	3.99	13.09
220	.87	.0341	4.34	14.24
221	.69	.0272	5.23	17.16
222	.69	.0272	4.50	14.78
223	.61	.0240	4.60	15.08
224	.53	.0207	5.08	16.66
225	.61	.0240	4.67	15.32
226	.66	.0258	3.84	12.59
227	.96	.0378	4.12	13.51
228	.78	.0309	4.19	13.74
229	1.04	.0410	3.40	11.17
230	.96	.0378	2.98	9.79
231	.69	.0272	3.94	12.44
232	.96	.0378	4.59	15.05
233	.96	.0378	4.54	14.49
234	.69	.0272	4.19	13.74
235	.61	.0240	3.16	10.36
236	.69	.0272	5.49	18.00
237	.96	.0378	3.93	12.90
238	.78	.0309	4.39	14.34
239	.87	.0341	3.99	13.09
240	1.04	.0410	4.77	15.66
241	.69	.0272	5.10	16.76
242	1.04	.0410	4.63	15.20
243	.78	.0309	5.02	16.47
244	.61	.0240	4.32	14.16
245	1.12	.0442	3.42	11.21
246	1.04	.0410	3.09	10.13
247	.96	.0378	4.50	14.78
248	.91	.0359	3.25	10.67
249	.87	.0341	5.74	18.85
250	.96	.0378	4.32	14.16
251	.87	.0341	4.48	14.70
252	.96	.0378	3.88	12.74
253	.69	.0272	4.80	15.74
254	.87	.0341	3.90	12.78
255	.83	.0327	4.04	13.24
256	.78	.0309	2.63	8.64
257	1.12	.0442	4.24	13.09
258	.87	.0341	3.65	11.48

TABLE E-3 (Cont)

DROPLET VELOCITY VERSUS DROPLET DIAMETER

259	1.04	.0410	1.91	6.26
260	.96	.0378	3.71	12.17
261	.96	.0378	4.02	13.26
262	.96	.0378	3.00	9.83
263	.96	.0378	3.83	12.55
264	.69	.0272	4.09	13.43
265	.78	.0309	4.48	14.70
266	.69	.0272	5.57	18.56
267	.69	.0272	3.19	10.48
268	.69	.0272	4.63	15.20
269	.87	.0341	3.97	13.01
270	1.22	.0479	4.60	15.06
271	.78	.0309	3.31	10.86
272	.66	.0258	4.95	16.24
273	.66	.0258	6.01	19.73
274	.69	.0272	4.29	14.09
275	1.72	.0479	2.40	7.87
276	1.73	.0682	3.30	10.82
277	.83	.0327	4.05	13.26
278	.87	.0341	4.39	14.39
279	1.22	.0479	4.32	14.16
280	.78	.0309	3.97	13.01
281	.61	.0240	5.71	18.73
282	.96	.0378	5.76	18.88
283	.74	.0290	4.68	16.01
284	1.04	.0410	3.10	10.17
285	.83	.0327	4.50	14.78
286	.78	.0309	4.97	16.31
287	1.22	.0479	2.20	7.22
288	.61	.0240	4.54	14.89
289	.69	.0272	5.64	18.56
290	.87	.0341	4.20	13.78
291	.61	.0240	3.28	10.75
292	.69	.0272	4.75	15.58
293	.78	.0309	4.12	13.51
294	1.12	.0442	4.47	14.66
295	1.12	.0442	3.37	11.05
296	.87	.0341	4.91	16.12
297	.61	.0240	5.08	16.66
298	.78	.0309	6.82	22.38
299	1.39	.0548	2.41	7.41
300	.61	.0240	5.92	19.42
301	.87	.0341	3.50	11.48
302	1.30	.0511	4.32	14.16

TABLE E-3 (Cont)

DROPLET VELOCITY VERSUS DROPLET DIAMETER

303	.87	.0341	3.10	10.17
304	.69	.0272	4.39	14.39
305	.53	.0207	6.60	21.65
306	.78	.0309	3.98	13.05
307	.87	.0341	2.88	9.44
308	.78	.0309	4.71	15.47
309	.69	.0272	5.52	18.12
310	.96	.0378	4.42	14.51
311	.56	.0221	3.16	10.36
312	1.12	.0442	3.44	11.28
313	.78	.0309	5.32	17.46
314	.53	.0207	3.71	12.17
315	.69	.0272	4.26	13.97
316	1.22	.0479	2.95	9.67
317	.99	.0392	4.36	14.32
318	.69	.0272	4.60	15.08
319	.78	.0309	3.28	10.75
320	.61	.0240	3.84	12.59
321	.61	.0240	5.32	17.46
322	.87	.0341	4.06	13.32
323	.87	.0341	2.81	9.21
324	.87	.0341	5.78	16.96
325	.69	.0272	4.81	15.76
326	.69	.0272	5.79	19.00
327	.69	.0272	4.84	15.49
328	.96	.0378	4.95	16.24
329	.96	.0378	4.56	14.97
330	.78	.0309	4.08	13.40
331	.66	.0258	5.30	17.39

TABLE E-3 (Cont)

DROPLET VELOCITY VERSUS DROPLET DIAMETER

RUN 31504
TIME (SEC) = 200-265

ELEVATION = 1.83 (6 FT)

NO.	DIAMETER		VELOCITY	
	MM	IN	M/S	FT/S
1	.92	.0364	1.40	4.61
2	.70	.0276	.76	2.50
3	.70	.0276	1.84	6.03
4	.70	.0276	1.10	3.61
5	1.02	.0401	1.06	3.44
6	.81	.0318	1.47	4.84
7	.87	.0341	.44	1.46
8	.60	.0235	1.95	6.41
9	.61	.0240	2.04	6.66
10	1.64	.0645	1.54	5.07
11	.47	.0184	1.64	5.37
12	.84	.0332	1.60	5.26
13	.73	.0286	1.37	4.44
14	.39	.0152	1.95	6.41
15	.41	.0161	2.20	7.22
16	.81	.0318	1.08	3.53
17	1.31	.0516	.98	3.22
18	.54	.0212	1.86	6.10
19	.95	.0392	1.45	4.76
20	.75	.0295	1.25	4.11
21	.48	.0189	1.33	4.38
22	.29	.0115	2.5	6.72
23	1.38	.0544	.80	2.61
24	.97	.0382	1.17	3.84
25	2.01	.0792	.57	1.8
26	.53	.0207	1.90	6.22
27	.89	.0350	1.77	5.80
28	.97	.0362	1.66	5.45
29	1.23	.0464	.85	2.80
30	1.06	.0419	.18	.58
31	.75	.0295	1.53	5.03
32	1.09	.0428	1.79	5.87
33	.62	.0244	2.02	6.64
34	1.17	.0461	1.12	3.68
35	.49	.0193	2.67	8.75
36	.47	.0164	.35	1.12
37	.39	.0152	1.86	6.10
38	1.94	.0765	.74	2.42
39	.69	.0272	1.65	5.41

TABLE E-3 (Cont)

DROPLET VELOCITY VERSUS DROPLET DIAMETER

RUN 3E701
TIME (SEC) = 2-9

ELEVATION = .914 (3 FT)

NO.	DIAMETER		VELOCITY	
	MM	IN	M/S	FT/S
1	1.01	.0398	1.37	4.49
2	1.33	.0524	2.72	8.92
3	1.28	.0504	2.96	9.71
4	.88	.0346	1.59	5.22
5	.91	.0358	1.72	5.64
6	.80	.0315	1.68	5.51
7	.93	.0366	1.08	3.54
8	.96	.0378	1.19	3.90
9	1.33	.0524	.77	2.53
10	.85	.0335	1.39	4.56
11	.91	.0358	.59	1.94
12	1.07	.0421	.63	2.07
13	.93	.0366	1.16	3.81
14	.95	.0374	1.26	4.13
15	1.68	.0661	1.55	5.09
16	1.99	.0783	1.47	4.82
17	1.12	.0441	1.94	6.36
18	.95	.0374	1.14	3.74
19	1.70	.0472	1.89	6.20
20	1.90	.0748	1.38	4.53
21	.98	.0386	2.29	7.51

TABLE E-3 (Cont)

DROPLET VELOCITY VERSUS DROPLET DIAMETER

RUN 31701
TIME (SEC)= 1-8

ELEVATION= 2.74 (9 FT)

NO.	DIAMETER		VELOCITY	
	MM	IN	M/S	FT/S
1	.81	.0318	5.77	19.02
2	1.92	.0758	2.80	9.19
3	1.52	.0600	2.91	9.54
4	1.02	.0400	1.67	5.49
5	.61	.0239	2.89	9.49
6	1.82	.0718	3.27	10.74
7	1.72	.0679	2.62	8.61
8	.77	.0361	3.19	10.67
9	.92	.0361	4.19	13.75
10	1.02	.0400	4.16	13.64
11	1.72	.0679	2.30	7.24
12	.45	.0177	3.92	12.85
13	1.62	.0640	3.73	12.25
14	1.32	.0518	3.52	11.56
15	.81	.0318	2.72	9.11
16	.51	.0200	7.28	23.89
17	1.12	.0440	5.97	19.00
18	.61	.0239	6.35	20.83
19	1.02	.0400	4.79	15.72
20	1.82	.0718	5.22	17.14
21	1.02	.0400	4.12	13.50
22	.51	.0200	3.30	10.83
23	1.12	.0440	5.34	17.52
24	.61	.0239	7.71	22.29
25	.71	.0279	6.67	21.87
26	.61	.0239	6.57	21.54
27	.65	.0256	6.52	21.40
28	.71	.0279	6.64	21.74
29	1.03	.0407	7.21	23.05
30	.93	.0367	6.12	20.07
31	1.45	.0571	5.95	19.52
32	.66	.0259	8.33	27.34
33	.82	.0325	11.02	36.17
34	.82	.0325	7.87	25.83
35	1.03	.0407	6.30	20.67
36	.82	.0325	7.87	25.81
37	1.14	.0449	6.95	29.36
38	.82	.0325	8.10	26.57

TABLE E-3 (Cont)

DROPLET VELOCITY VERSUS DROPLET DIAMETER

39	*.82	*.0325	*.52	1.69
40	1.03	*.0407	.8.54	28.02
41	*.82	*.0325	1.0.12	33.14
42	1.03	*.0407	.9.16	30.04
43	*.62	*.0246	7.71	25.24
44	1.14	*.0449	.9.19	30.15
45	1.03	*.0407	.9.34	30.04
46	1.03	*.0407	.8.64	28.35
47	1.28	*.0489	1.0.17	33.35
48	*.82	*.0325	1.1.10	36.41
49	1.03	*.0407	.8.26	27.04
50	*.93	*.0367	1.0.25	33.62
51	1.28	*.0489	.9.52	31.25
52	1.14	*.0449	7.56	24.74

TABLE E-3 (Cont)

DROPLET VELOCITY VERSUS DROPLET DIAMETER

RUN 31005
TIME (SEC) 10-16

NO.	MM	DIAMETER IN	VELOCITY M/S	VELOCITY FT/S
1	*.70	*.0276	1.446	4.66
2	*.76	*.0299	2.317	7.12
3	*.62	*.0323	2.614	7.02
4	*.85	*.0335	1.73	5.68
5	*.76	*.0299	1.47	4.82
6	*.85	*.0335	1.69	5.54
7	1.07	*.0421	1.93	6.13
8	*.67	*.0264	2.06	6.76
9	1.22	*.0460	2.78	9.12
10	*.91	*.0358	*.96	3.12
11	*.91	*.0358	1.80	5.91
12	*.85	*.0335	1.22	4.00
13	*.88	*.0346	1.07	3.51
14	*.91	*.0358	1.39	4.56
15	*.76	*.0299	1.76	5.77
16	1.07	*.0421	4.29	14.07
17	*.91	*.0358	2.50	8.20
18	*.76	*.0299	1.57	5.15
19	*.91	*.0358	*.94	3.06
20	*.76	*.0299	1.22	4.00
21	*.79	*.0311	1.15	3.77
22	*.97	*.0382	1.64	5.38
23	1.03	*.0406	1.81	5.94
24	*.70	*.0276	1.42	4.76
25	*.64	*.0255	1.92	6.30
26	*.97	*.0362	1.43	4.69
27	*.67	*.0264	1.74	5.71
28	*.85	*.0335	1.16	3.81

TABLE E-3 (Cont)

DROPLET VELOCITY VERSUS DROPLET DIAMETER

RUN 31805 TIME (SEC) = 10-16		ELEVATION = 1.03 (6 FT)		
NO.	DIAMETER	VELOCITY		
	MM	IN	M/S	FT/S
1	.89	.0350	4.19	13.75
2	1.05	.0413	3.85	12.63
3	.80	.0315	4.25	13.94
4	.50	.0197	1.46	4.79
5	.64	.0252	3.67	12.04
6	.82	.0323	3.13	10.27
7	1.03	.0406	3.23	17.16
8	1.19	.0469	3.34	10.96
9	.89	.0350	4.86	15.94
10	.84	.0331	5.02	16.47

TABLE E-3 (Cont)

DROPLET VELOCITY VERSUS DROPLET DIAMETER

RUN 32114
TIME (SEC) = 18-24

ELEVATION = 414 (3 FT)

NO.	DIAMETER		VELOCITY	
	MM	IN	M/S	FT/S
1	.68	.0268	2.90	9.51
2	.87	.0343	2.40	7.87
3	.54	.0213	4.02	13.14
4	.60	.0236	1.48	4.86
5	.71	.0280	2.07	6.79
6	.54	.0213	1.98	6.50
7	.49	.0193	3.41	11.19
8	.62	.0244	1.33	4.36
9	.68	.0268	2.92	9.58
10	.65	.0256	1.78	5.84
11	.76	.0299	1.81	5.94
12	.81	.0319	2.04	6.69
13	.71	.0280	1.52	4.99
14	.68	.0268	2.09	6.86
15	.62	.0244	2.86	9.30
16	.54	.0213	2.05	6.73
17	.82	.0323	2.29	7.51
18	.76	.0299	2.58	8.46
19	.76	.0299	2.24	7.35
20	.96	.0378	1.78	5.84
21	.70	.0276	3.43	11.25
22	.65	.0256	2.40	7.87
23	.62	.0244	2.85	9.35
24	.76	.0299	2.04	6.69
25	.62	.0244	2.24	7.35
26	.62	.0244	3.09	10.14
27	.62	.0244	1.85	6.07
28	.70	.0276	2.34	7.68
29	.68	.0268	2.59	8.50
30	.82	.0323	3.00	10.00
31	.85	.0335	2.26	7.41
32	.85	.0335	2.71	8.89
33	.76	.0299	1.86	6.10
34	.56	.0220	2.76	9.06
35	.65	.0256	2.43	7.97
36	.78	.0307	2.26	7.41
37	1.11	.0437	1.66	5.45
38	.81	.0319	2.95	9.68

TABLE E-3 (Cont)

DROPLET VELOCITY VERSUS DROPLET DIAMETER

39	.83	.0327	1.90	6.23
40	.72	.0263	2.33	7.64
41	.97	.0362	2.22	7.28
42	.56	.0220	2.05	6.73
43	.69	.0272	2.79	9.15
44	.69	.0272	3.24	10.63
45	.69	.0272	2.60	9.53
46	.69	.0272	1.49	4.89
47	.83	.0327	2.49	8.17
48	.86	.0339	2.86	9.36
49	1.35	.0531	1.87	6.14
50	.86	.0339	2.88	9.45
51	1.02	.0402	2.85	9.35
52	1.54	.0606	1.45	4.76
53	.89	.0350	2.22	7.28
54	.94	.0370	2.68	8.79
55	.57	.0224	4.57	14.99
56	1.05	.0417	2.43	7.87
57	.81	.0317	3.26	10.70
58	.81	.0315	3.75	12.30
59	1.08	.0425	3.64	11.94
60	1.16	.0457	1.30	4.27
61	.70	.0276	3.66	12.31
62	1.48	.0583	1.73	5.66
63	1.16	.0457	2.56	8.40
64	.86	.0339	2.93	9.61
65	1.48	.0583	2.11	6.92
66	1.29	.0508	2.41	7.91
67	1.35	.0531	2.16	7.09
68	1.21	.0476	1.98	6.50
69	1.62	.0638	9.63	31.59
70	1.62	.0638	1.32	4.33
71	.67	.0264	3.23	10.60
72	.65	.0256	3.69	12.11
73	.73	.0287	3.30	10.83
74	.70	.0276	2.36	7.74
75	.65	.0256	3.12	10.24
76	.81	.0319	2.09	6.86
77	1.08	.0425	1.67	5.48
78	.81	.0319	1.77	5.81
79	.84	.0331	2.80	9.19
80	.94	.0370	1.45	4.76
81	.76	.0307	2.83	9.28
82	.75	.0295	2.51	8.23

TABLE E-3 (Cont)

DROPLET VELOCITY VERSUS DROPLET DIAMETER

83	.81	.0319	2.12	6.96
84	.81	.0319	2.10	6.84
85	.84	.0331	2.46	6.07
86	.65	.0256	4.21	13.81
87	1.02	.0402	2.23	7.32
88	.73	.0287	2.55	8.17
89	.81	.0319	3.92	12.86
90	.89	.0350	1.98	6.50
91	1.08	.0425	1.88	6.17
92	1.00	.0394	4.81	15.76
93	.65	.0256	3.85	12.63
94	.81	.0319	3.33	10.43
95	.96	.0378	2.66	8.73
96	.85	.0335	2.99	9.81
97	1.16	.0457	2.63	8.63
98	2.48	.0076	1.50	3.32
99	1.43	.0563	1.99	6.53
100	.69	.0272	3.86	12.66
101	1.49	.0587	1.22	4.00
102	3.09	.1217	.97	3.18
103	1.05	.0413	2.70	8.86
104	1.74	.0685	1.11	3.64
105	1.24	.0488	1.95	6.40
106	1.10	.0433	2.7	8.53
107	2.2	.0866	*	2.43
108	1.10	.0433	2.	8.69
109	1.19	.0469	2.34	7.66
110	1.38	.0543	2.59	8.50
111	.88	.0346	4.54	14.89
112	1.41	.0555	2.42	7.44
113	.77	.0303	3.14	10.30
114	.96	.0378	3.12	10.24
115	1.16	.0457	2.39	7.84
116	1.21	.0476	2.04	6.69
117	1.19	.0469	2.32	7.61
118	.97	.0382	3.48	11.42
119	1.49	.0587	1.24	4.07
120	1.70	.0669	2.43	7.47
121	.76	.0299	4.01	13.16
122	1.24	.0488	3.09	10.14
123	1.62	.0638	2.35	7.71
124	.62	.0244	3.80	12.47
125	1.57	.0618	*.88	2.89
126	1.08	.0425	3.35	10.79

TABLE E-3 (Cont)

DROPLET VELOCITY VERSUS DROPLET DIAMETER

127	1.35	.0531	2.40	7.87
128	.95	.0374	2.13	6.49
129	1.57	.0618	2.16	7.09
130	.89	.0350	2.38	7.81
131	.95	.0374	2.02	6.63
132	3.52	.1386	1.74	5.71
133	1.06	.0425	1.83	6.00
134	.81	.0319	3.72	12.20
135	1.22	.0460	1.54	5.06
136	.87	.0343	2.87	9.42
137	.81	.0319	3.68	12.07
138	1.03	.0406	2.67	4.76
139	.68	.0268	3.56	11.60
140	.83	.0327	3.09	12.76
141	1.52	.0198	1.60	5.25
142	1.65	.0650	.79	2.59
143	.83	.0327	3.11	10.20
144	.96	.0378	3.34	10.96
145	.83	.0327	3.41	11.19
146	1.10	.0433	2.34	7.68
147	.96	.0378	2.76	7.06
148	.69	.0272	5.12	16.90
149	1.79	.0705	1.22	4.00
150	.83	.0327	2.41	7.91
151	1.10	.0433	2.18	7.15
152	1.24	.0488	2.92	9.56
153	.55	.0217	3.87	12.70
154	.63	.0248	3.50	11.46
155	1.79	.0705	.84	2.76
156	1.52	.0598	1.31	4.30
157	.69	.0272	3.65	11.97
158	1.10	.0433	2.84	9.32
159	1.38	.0543	2.17	7.12
160	1.65	.0650	1.25	4.10
161	.96	.0378	5.08	16.67
162	.96	.0378	2.85	7.35
163	1.65	.0650	1.78	5.84
164	1.24	.0488	2.62	8.00
165	1.10	.0433	3.23	10.60
166	2.20	.0866	1.76	5.77
167	1.24	.0488	1.40	4.59
168	1.52	.0598	1.49	4.49
169	.77	.0303	3.70	12.14
170	2.34	.0921	.79	2.30

TABLE E-3 (Cont)

DROPLET VELOCITY VERSUS DROPLET DIAMETER

171	.88	.0346	3.11	10.20
172	.83	.0327	2.96	9.71
173	2.07	.0815	2.82	9.25
174	.96	.0378	2.21	7.25
175	1.52	.0598	2.27	7.45
176	.69	.0272	4.13	13.55
177	.69	.0272	3.26	10.70
178	.83	.0327	3.50	11.48
179	1.93	.0760	1.19	3.40
180	1.65	.0650	8.66	28.41
181	2.33	.0917	1.41	4.63
182	1.51	.0594	1.18	3.47
183	1.76	.0701	2.09	6.86
184	2.06	.0811	1.44	4.72
185	1.92	.0756	1.86	5.10
186	2.33	.0917	1.89	6.20
187	1.65	.0650	2.59	8.50
188	1.51	.0594	1.10	3.61
189	1.65	.0650	1.87	6.14
190	1.37	.0539	1.33	4.36
191	1.37	.0539	1.59	5.22
192	1.92	.0756	1.79	5.47
193	.77	.0303	3.23	10.60
194	1.10	.0433	3.18	10.43
195	1.65	.0650	2.62	8.60
196	.82	.0323	3.53	11.58
197	1.37	.0539	2.02	6.63
198	1.65	.0650	1.42	4.66
199	1.51	.0594	1.22	4.00
200	1.24	.0488	2.59	8.50
201	.82	.0323	2.69	8.83
202	.96	.0378	3.61	11.84
203	1.92	.0756	1.24	4.07
204	1.51	.0594	3.00	9.84
205	1.37	.0539	2.59	8.50
206	1.24	.0488	3.48	11.42
207	1.10	.0433	1.90	6.23
208	1.92	.0756	2.77	9.09
209	1.51	.0594	2.72	9.42

TABLE E-3 (Cont)

DROPLET VELOCITY VERSUS DROPLET DIAMETER

RUN 32114
TIME (SEC) = 20-30

ELEVATION = 2.74 (9 FT)

NO.	DIAMETER		VELOCITY	
	MM	IN	M/S	FT/S
1	.90	.0355	9.30	30.51
2	.73	.0286	5.51	18.09
3	.73	.0286	4.59	15.04
4	1.00	.0393	5.04	16.55
5	1.09	.0427	5.54	18.16
6	.64	.0254	6.06	19.87
7	.81	.0318	6.76	22.17
8	.73	.0286	6.36	20.85
9	1.00	.0393	8.36	27.44
10	.73	.0286	6.15	20.16
11	1.93	.0761	5.70	18.69
12	.96	.0379	6.67	21.90
13	.96	.0379	5.66	18.56
14	.81	.0318	6.08	19.46
15	.81	.0318	7.68	24.55
16	.73	.0286	6.51	21.34
17	.81	.0320	8.36	27.44
18	.90	.0355	6.48	21.25
19	.96	.0379	4.75	15.58
20	.48	.0190	5.20	17.07
21	.96	.0379	7.08	23.23
22	.96	.0379	7.33	24.04
23	.96	.0379	6.38	20.94
24	1.13	.0443	6.55	21.48
25	1.00	.0393	7.64	25.08
26	.90	.0355	8.21	26.95
27	.56	.0222	5.30	17.38
28	.48	.0190	4.30	14.11
29	.81	.0318	5.85	19.21
30	.64	.0254	8.00	26.26
31	.81	.0318	5.63	18.47
32	.48	.0190	6.76	22.19
33	1.24	.0489	10.37	34.01
34	1.09	.0427	4.75	15.58
35	.54	.0254	6.72	22.03
36	.64	.0254	5.43	17.80
37	.81	.0318	6.40	20.99
38	.96	.0379	7.24	23.75

E-63

TABLE E-3 (Cont)

DROPLET VELOCITY VERSUS DROPLET DIAMETER

39	.64	.0254	5.78	18.96
40	.98	.0387	4.42	14.51
41	1.09	.0427	9.19	30.16
42	2.11	.0831	6.15	20.16
43	.88	.0345	3.51	11.53
44	.73	.0286	2.28	7.48
45	1.09	.0430	5.04	16.54
46	.82	.0323	6.28	20.61
47	.73	.0286	3.98	13.04
48	.90	.0355	5.35	17.56
49	.73	.0286	7.76	25.46
50	.88	.0345	4.88	16.00
51	1.23	.0483	5.85	19.21
52	1.00	.0395	4.96	16.27
53	.73	.0286	4.73	12.53
54	.73	.0286	7.10	23.30
55	1.09	.0427	3.62	11.86
56	1.00	.0393	5.65	18.54
57	.73	.0286	8.59	28.17
58	.79	.0312	6.59	21.61
59	.88	.0345	4.50	14.76
60	.82	.0323	6.46	21.21
61	.91	.0358	5.92	19.43
62	.91	.0358	5.92	19.43
63	1.09	.0427	6.49	21.30
64	1.09	.0427	5.22	17.14
65	1.81	.0713	7.35	24.10
66	.79	.0312	4.48	14.64
67	.62	.0243	4.41	14.47
68	.73	.0286	4.69	15.38
69	.91	.0358	5.54	18.18
70	1.36	.0534	6.78	22.26
71	1.27	.0499	5.61	18.40
72	.90	.0355	7.76	25.46
73	1.27	.0499	8.07	26.48
74	1.32	.0518	3.30	10.84
75	.96	.0379	5.78	16.96
76	.55	.0216	3.74	12.26
77	.73	.0286	5.16	16.94
78	.90	.0355	6.96	22.83
79	1.81	.0713	4.58	15.02
80	.90	.0355	5.54	18.16
81	1.36	.0534	7.08	23.23
82	.79	.0312	5.26	17.25

TABLE E-3 (Cont)

DROPLET VELOCITY VERSUS DROPLET DIAMETER

83	.88	.0345	6.13	20.10
84	.82	.0323	3.79	12.44
85	.91	.0358	4.67	15.31
86	1.63	.0641	4.85	15.91
87	1.17	.0462	3.71	12.17
88	1.27	.0494	5.65	18.04
89	.81	.0320	10.09	33.12
90	1.49	.0588	4.42	14.49
91	1.14	.0449	4.57	14.70
92	.73	.0286	2.69	8.81
93	1.00	.0395	5.47	17.94
94	1.81	.0713	4.78	15.64
95	1.36	.0534	4.19	13.75
96	1.09	.0427	4.58	15.02
97	1.09	.0427	6.41	21.03
98	.71	.0278	5.07	16.62
99	.88	.0345	5.62	18.43
100	.91	.0358	2.96	9.70
101	.82	.0323	6.76	22.17
102	1.63	.0641	4.88	16.02
103	1.09	.0427	5.27	17.24
104	1.09	.0427	3.49	11.44
105	.81	.0320	8.00	26.26
106	.88	.0345	3.73	12.24
107	.96	.0379	5.16	16.94
108	.91	.0358	3.28	10.75
109	.91	.0358	6.11	20.03
110	1.00	.0393	6.18	20.27
111	1.09	.0427	5.74	18.83
112	1.00	.0393	5.12	16.80
113	1.09	.0427	7.36	24.15
114	.62	.0243	4.00	13.11
115	1.05	.0414	6.01	19.72
116	1.00	.0395	3.98	13.06
117	.91	.0358	5.69	18.67
118	1.17	.0462	4.61	15.13
119	.90	.0355	3.74	12.28
120	.43	.0248	4.70	15.42
121	1.09	.0427	7.05	23.15
122	.71	.0278	5.64	18.52
123	1.14	.0449	4.52	14.82
124	.91	.0358	5.20	17.05
125	.91	.0358	4.27	14.00
126	.54	.0214	5.04	16.54

TABLE E-3 (Cont)

DROPLET VELOCITY VERSUS DROPLET DIAMETER

127	.73	.0286	7.60	24.93
128	1.09	.0427	5.58	18.29
129	1.17	.0462	9.49	31.13
130	.79	.0312	5.80	19.03
131	1.23	.0483	4.16	13.64
132	.55	.0216	4.67	15.31
133	.82	.0323	4.16	13.64
134	1.27	.0499	5.35	17.56
135	.81	.0320	5.50	18.05
136	.63	.0248	6.65	21.81
137	1.63	.0641	6.47	21.23
138	.71	.0278	4.69	15.38
139	1.23	.0483	3.80	12.46
140	1.09	.0430	4.39	14.40
141	.91	.0358	4.95	16.25
142	1.44	.0569	4.16	13.64
143	.90	.0355	5.51	10.09
144	1.17	.0462	5.74	18.83
145	.90	.0353	5.24	17.20
146	.88	.0345	5.43	17.83
147	1.14	.0449	3.88	12.60
148	.73	.0286	4.10	13.44
149	1.09	.0430	4.61	15.13
150	.90	.0355	4.69	15.38
151	.81	.0320	5.73	18.78
152	1.00	.0393	6.33	20.76
153	.90	.0355	6.63	21.74
154	.88	.0345	5.14	16.87
155	1.40	.0353	4.01	13.15
156	.91	.0358	5.40	17.72
157	.73	.0286	4.55	14.93
158	.90	.0355	4.59	15.07
159	.90	.0355	5.94	19.47
160	1.27	.0496	5.58	16.29
161	.90	.0355	5.43	17.80
162	.96	.0379	4.42	14.51
163	1.14	.0449	4.90	16.07
164	1.09	.0430	5.92	19.43
165	.91	.0358	4.41	14.47
166	1.36	.0534	4.52	14.82
167	.81	.0320	5.05	16.56
168	.90	.0355	5.20	17.05
169	1.09	.0427	6.80	22.30
170	.96	.0379	3.48	11.42

TABLE E-3 (Cont)

DROPLET VELOCITY VERSUS DROPLET DIAMETER.

171	.88	.0345	5.07	16.55
172	.91	.0358	5.24	17.18
173	.64	.0251	8.43	27.64
174	1.09	.0427	6.15	20.16
175	.90	.0355	5.20	17.05
176	1.00	.0393	4.84	15.89
177	.90	.0355	7.91	25.95
178	1.40	.0553	4.86	15.96
179	.79	.0312	4.27	14.02
180	.73	.0286	5.79	18.98
181	.73	.0286	4.19	13.75
182	1.17	.0462	3.55	11.66
183	.73	.0286	5.70	18.69
184	1.27	.0499	5.24	17.20
185	1.17	.0462	6.19	20.32
186	1.05	.0414	4.06	13.31
187	.73	.0286	4.61	15.13
188	.73	.0286	4.37	14.33
189	1.09	.0430	6.04	19.83
190	1.27	.0499	6.60	21.65
191	1.00	.0393	5.51	18.29
192	1.17	.0462	4.86	15.93
193	.90	.0355	4.71	15.45
194	1.40	.0553	5.18	16.98
195	.73	.0286	3.71	12.17
196	1.09	.0430	3.41	11.19
197	.73	.0286	6.76	22.17
198	1.09	.0427	4.01	13.15
199	1.44	.0569	5.15	16.89
200	1.27	.0499	5.48	17.98
201	.57	.0224	5.81	19.05
202	.82	.0323	6.65	21.81
203	.73	.0288	5.18	16.98
204	.82	.0323	6.40	20.99
205	.82	.0323	7.17	23.52
206	.57	.0224	6.54	21.45
207	1.31	.0515	7.24	23.75
208	.65	.0256	6.32	20.74
209	.65	.0256	6.61	21.68
210	1.15	.0451	7.00	22.97
211	.65	.0256	6.91	22.68
212	1.15	.0451	6.82	22.39
213	.90	.0355	7.43	24.37
214	.82	.0323	4.14	13.58

TABLE E-3 (Cont)

DROPLET VELOCITY VERSUS DROPLET DIAMETER

215	.82	.0323	6.50	21.32
216	.82	.0323	5.63	18.47
217	.98	.0367	5.77	18.92
218	.73	.0268	6.95	22.79
219	.98	.0367	11.36	37.24
220	.90	.0355	4.88	16.00
221	.82	.0323	6.13	20.12
222	.82	.0323	7.28	23.08
223	.98	.0385	6.91	22.66
224	1.46	.0574	7.60	24.93
225	1.62	.0638	6.50	21.32
226	.81	.0320	7.15	23.46
227	.73	.0288	6.03	19.78
228	.65	.0256	4.71	15.45
229	.81	.0320	7.96	26.11
230	.81	.0320	7.57	24.84
231	.73	.0288	5.47	17.94
232	.90	.0353	5.60	18.38
233	.81	.0320	6.30	20.65
234	.98	.0365	8.05	26.39
235	.90	.0353	7.85	25.75
236	1.14	.0449	7.35	24.12
237	.81	.0320	7.03	25.70
238	.81	.0320	7.12	23.37
239	.90	.0353	10.66	34.96
240	.98	.0385	8.53	27.47
241	.90	.0353	8.32	27.31
242	.81	.0320	8.07	26.46
243	.81	.0320	9.39	30.80
244	.81	.0320	7.87	25.82
245	.81	.0320	7.47	24.50
246	.90	.0353	7.75	25.44
247	.81	.0320	5.68	18.65
248	.98	.0385	5.65	18.54
249	.65	.0256	8.26	27.08
250	.65	.0256	8.12	26.64
251	.81	.0320	6.58	21.59
252	.49	.0192	3.20	10.50
253	.81	.0320	7.98	26.19
254	.98	.0385	7.71	25.30
255	.98	.0385	7.51	24.64
256	.65	.0256	8.08	26.51
257	.98	.0385	7.51	24.64
258	.90	.0353	7.47	24.50

TABLE E-3 (Cont)

DROPLET VELOCITY VERSUS DROPLET DIAMETER

259	.81	.0320	6.25	20.52
260	.65	.0256	8.32	27.31
261	.73	.0288	7.96	26.11
262	1.30	.0513	7.31	23.99
263	.65	.0256	8.89	29.15
264	.82	.0323	9.23	30.27
265	.98	.0387	8.38	27.51
266	.98	.0387	9.84	32.29
267	.98	.0387	9.02	29.60
268	1.15	.0451	9.90	32.47
269	.98	.0387	10.00	32.80
270	.98	.0387	10.09	33.09
271	.82	.0323	9.08	29.00
272	.98	.0387	8.25	27.06
273	.98	.0317	8.20	26.91
274	1.15	.0451	9.59	31.45
275	1.15	.0451	8.52	27.95
276	1.31	.0515	9.44	30.46
277	1.31	.0515	8.20	26.91
278	1.23	.0483	7.31	23.99
279	1.31	.0515	7.20	23.61
280	1.15	.0451	8.97	29.44
281	.97	.0382	7.24	23.77
282	.89	.0350	8.56	29.07
283	.73	.0286	7.29	23.90
284	.97	.0362	9.91	19.30
285	.81	.0318	7.63	25.04
286	.81	.0318	7.81	25.64
287	.81	.0318	9.54	31.24
288	.81	.0318	7.15	23.46
289	1.30	.0510	8.35	27.40
290	.89	.0350	7.28	7.46

TABLE E-3 (Cont)

DROPLET VELOCITY VERSUS DROPLET DIAMETER

RUN 32235
TIME (SEC) = 0-6

ELEVATION = .914 (3 FT)

NO.	DIAMETER		VELOCITY M/S	FT/S
	MM	IN		
1	.61	.0240	2.40	7.87
2	.61	.0240	2.24	7.35
3	.61	.0240	1.79	5.87
4	.61	.0240	2.00	6.56
5	.61	.0240	1.82	5.97
6	.61	.0240	3.03	9.94
7	.61	.0240	2.65	8.69
8	.61	.0240	1.46	4.79
9	.61	.0240	1.23	4.04
10	.61	.0240	2.36	7.74
11	.92	.0362	1.11	3.64
12	.61	.0240	2.38	7.81
13	.92	.0362	2.00	6.56
14	.92	.0362	1.30	4.21
15	.92	.0362	2.42	7.97
16	1.23	.0484	.88	2.99
17	1.23	.0484	1.48	4.86
18	.92	.0362	1.64	5.36
19	1.84	.0724	3.02	9.91
20	1.53	.0602	2.64	8.66
21	1.23	.0484	1.15	3.77
22	1.23	.0484	2.86	9.30
23	.61	.0240	1.53	5.02
24	.92	.0362	1.70	5.58
25	.92	.0362	2.09	6.86
26	2.15	.0846	1.26	4.20
27	1.53	.0602	1.38	4.53
28	.92	.0362	1.48	4.86
29	.92	.0362	1.38	4.53
30	1.23	.0484	1.88	6.17
31	2.45	.0965	.87	2.85
32	.92	.0362	2.41	7.91
33	1.84	.0724	.52	1.71
34	1.23	.0484	1.52	4.99
35	1.53	.0602	1.25	4.10
36	2.15	.0846	1.53	5.02
37	.92	.0362	2.59	8.50
38	1.84	.0724	2.67	8.76

TABLE E-3 (Cont)

DROPLET VELOCITY VERSUS DROPLET DIAMETER

39	1.23	.0484	1.69	5.54
40	2.15	.0846	1.15	3.77
41	2.45	.0965	2.19	7.18
42	1.84	.0724	1.48	4.86

TABLE E-3 (Cont)

DROPLET VELOCITY VERSUS DROPLET DIAMETER

RUN 32333
TIME (SEC) = 0-6

ELEVATION = .914 (3 FT)

NO.	DIAMETER		VELOCITY	
	MM	IN	M/S	FT/S
1	.96	.0378	2.52	8.60
2	1.12	.0441	4.47	14.67
3	.96	.0378	2.60	8.53
4	.96	.0378	3.12	10.24
5	.96	.0378	1.85	6.07
6	.96	.0378	2.66	8.73
7	1.28	.0504	2.11	6.92
8	1.59	.0626	1.69	5.54
9	2.23	.0878	1.31	4.30
10	.80	.0315	1.80	5.91
11	1.44	.0567	.94	3.08
12	.96	.0378	1.32	4.33
13	.96	.0378	1.19	3.90
14	.96	.0378	.90	2.95
15	1.28	.0504	1.17	3.84
16	1.91	.0752	.49	1.61
17	.80	.0315	1.34	4.40
18	1.44	.0567	.57	1.87
19	.96	.0378	1.28	4.20
20	1.12	.0441	.88	2.89
21	1.59	.0626	.49	1.61
22	.80	.0315	1.25	4.10
23	.80	.0315	1.48	4.86
24	.96	.0378	1.54	5.05
25	.94	.0370	1.65	5.41
26	1.57	.0618	.58	1.90
27	1.88	.0740	1.15	3.77
28	.94	.0370	1.89	6.20
29	1.25	.0492	.27	.09
30	1.25	.0492	.46	1.51
31	.63	.0248	2.29	7.51
32	.94	.0370	1.02	3.35
33	2.19	.0862	.76	2.49
34	.78	.0307	.94	3.08
35	1.25	.0492	2.03	6.66
36	1.25	.0492	.84	2.76
37	1.25	.0492	.46	1.51
38	1.25	.0492	2.82	9.25

TABLE E-3 (Cont)

DROPLET VELOCITY VERSUS DROPLET DIAMETER

39	1.41	.0555	.77	2.53
40	1.25	.0492	.62	2.03
41	1.41	.0555	.88	2.09
42	1.41	.0555	1.29	4.23
43	.94	.0370	1.99	6.53
44	1.57	.0618	1.25	4.10

TABLE E-3 (Cont)

DROPLET VELOCITY VERSUS DROPLET DIAMETER

RUN 32333
TIME (SEC) = 50-61

ELEVATION = 2,746 FT

NO.	MM	DIAMETER IN	VELOCITY M/S	VELOCITY FT/S	TIME (SEC) = 50-61	
					ELEVATION = 2,746 FT	ELEVATION = 2,746 FT
1	.71	.0279	9.14	29.99		
2	1.06	.0418	9.07	29.77		
3	1.77	.0697	6.35	20.85		
4	.89	.0349	9.36	30.70		
5	.80	.0315	7.42	24.36		
6	1.16	.0455	1.72	5.63		
7	1.42	.0558	5.5	15.04		
8	.98	.0385	5.83	19.13		
9	1.06	.0418	4.01	13.16		
10	1.16	.0455	5.41	17.76		
11	1.06	.0418	2.62	8.59		
12	.71	.0279	3.67	12.05		
13	.89	.0349	7.1	22.32		
14	.89	.0349	1.49	4.88		
15	1.06	.0418	7.75	24.8		
16	.80	.0315	1.65	5.41		
17	.89	.0349	2.03	6.57		
18	1.06	.0418	1.02	3.36		
19	.89	.0349	2.93	9.63		
20	.98	.0385	1.10	3.61		
21	.71	.0279	1.71	5.61		
22	.89	.0349	3.04	9.38		
23	.61	.0240	3.96	12.99		
24	1.02	.0400	4.37	14.33		
25	1.12	.0440	4.92	16.15		
26	1.32	.0519	3.33	10.94		
27	.92	.0361	3.70	12.15		
28	1.02	.0400	6.94	22.77		
29	1.02	.0400	7.97	26.15		
30	1.02	.0400	11.46	37.65		
31	1.02	.0400	6.13	26.66		
32	.81	.0318	9.13	24.97		
33	1.42	.0561	12.92	42.37		
34	1.02	.0400	11.66	38.31		
35	.81	.0318	6.29	21.21		
36	1.42	.0561	7.24	23.72		
37	1.22	.0479	9.09	29.82		
38	1.22	.0479	10.47	34.36		

TABLE E-3 (Cont)

DROPLET VELOCITY VERSUS DROPLET DIAMETER

39	1.02	* 0400	7.73	25.37
40	1.12	* 0440	6.94	16.20
41	1.07	* 0400	8.51	27.92
42	1.12	* 0440	6.41	14.48
43	1.02	* 0400	6.64	15.24
44	1.27	* 0479	6.87	22.54
45	1.02	* 0400	7.96	26.13
46	1.02	* 0400	3.84	12.58
47	* 92	* 0361	7.05	23.12
48	* 81	* 0318	7.79	25.25
49	1.02	* 0400	6.60	21.65
50	1.32	* 0519	5.49	18.02
51	1.02	* 0400	7.51	24.64
52	1.02	* 0400	6.75	22.13
53	1.06	* 0415	6.74	15.57
54	1.22	* 0479	7.49	24.56
55	1.42	* 0561	5.41	17.76
56	1.42	* 0561	6.98	22.89
57	1.22	* 0479	7.62	24.99
58	1.22	* 0479	5.24	17.21
59	1.22	* 0479	7.80	25.60
60	1.02	* 0400	5.23	17.16
61	1.42	* 0561	6.13	26.66
62	1.12	* 0440	4.91	16.10
63	1.02	* 0400	4.51	14.78
64	1.02	* 0400	4.31	14.15
65	1.02	* 0400	5.91	19.30
66	* 81	* 0318	5.00	16.40
67	* 92	* 0361	4.28	14.05
68	1.42	* 0561	7.87	25.82
69	1.08	* 0425	9.67	31.74
70	1.16	* 0458	3.85	12.63
71	1.06	* 0415	6.45	21.15
72	1.37	* 0540	5.36	17.59
73	* 85	* 0334	4.11	13.47
74	1.06	* 0415	6.40	21.00
75	1.06	* 0415	4.76	15.62
76	1.69	* 0667	6.87	22.54
77	1.06	* 0415	6.62	21.73
78	1.52	* 0600	6.68	21.91
79	1.39	* 0549	6.08	19.94
80	* 85	* 0334	7.51	24.64
81	* 90	* 0355	5.24	17.10
82	* 00	* 0394	5.92	19.43

TABLE E-3 (Cont)

DROPLET VELOCITY VERSUS DROPLET DIAMETER

8.3	1.06	* 0.415	3.25	10.66
8.4	1.31	* 0.515	3.84	12.61
8.5	* 90	* 0.355	3.77	12.38
8.6	1.06	* 0.415	3.32	10.69
8.7	1.48	* 0.502	5.69	19.67
8.8	1.00	* 0.394	6.48	21.28
8.9	* 90	* 0.355	6.99	22.44
9.0	1.69	* 0.657	4.44	14.08
9.1	* 91	* 0.358	5.66	18.27
9.2	1.64	* 0.656	3.83	12.56
9.3	* 97	* 0.382	7.16	23.50
9.4	* 90	* 0.355	7.88	25.85
9.5	1.16	* 0.458	5.92	19.43
9.6	* 96	* 0.376	7.12	23.35
9.7	1.22	* 0.479	5.71	19.72
9.8	* 90	* 0.355	5.68	18.62
9.9	1.27	* 0.600	6.03	19.70
1.00	1.25	* 0.491	5.28	17.33
1.01	* 96	* 0.376	3.95	16.96
1.02	1.00	* 0.394	6.22	20.42
1.03	1.69	* 0.667	6.35	20.82
1.04	1.16	* 0.458	6.24	20.47

TABLE E-3 (Cont)

DROPLET VELOCITY VERSUS DROPLET DIAMETER

RUN 34524
TIME (SEC) = 0-24

ELEVATION = 2.74 (9 FT)

NO.	DIAMETER		VELOCITY	
	M	IN	M/S	FT/S
1	.39	.0152	1.64	5.36
2	.76	.0300	1.41	4.61
3	.58	.0228	1.93	6.33
4	.39	.0152	1.34	4.40
5	.76	.0300	2.99	9.82
6	.76	.0300	2.92	8.26
7	.76	.0300	3.52	11.54
8	.39	.0152	2.95	9.67
9	.76	.0300	4.28	14.04
10	.58	.0228	5.56	18.23
11	.58	.0228	3.95	12.76
12	.58	.0228	6.51	21.37
13	.76	.0300	6.05	19.86
14	.76	.0300	4.39	14.40
15	.58	.0228	1.55	5.09
16	.58	.0228	7.58	24.86
17	.76	.0300	3.07	10.07
18	.76	.0300	7.00	22.96
19	.76	.0300	6.22	20.40
20	.58	.0228	6.06	19.49
21	.76	.0300	5.86	19.23
22	.96	.0376	5.13	16.82
23	1.34	.0528	5.67	18.59
24	.76	.0300	5.91	19.38
25	.76	.0300	6.40	21.00
26	.76	.0300	5.98	19.62
27	1.34	.0528	4.41	14.47
28	.96	.0376	6.61	21.70
29	.96	.0376	6.05	19.86
30	.76	.0300	5.17	16.97
31	1.34	.0528	3.72	12.21
32	.76	.0300	5.13	16.45
33	.76	.0300	5.40	17.72
34	.96	.0376	4.41	14.47
35	.96	.0376	4.22	13.83
36	.76	.0300	4.54	15.22
37	.96	.0376	5.95	19.53
38	.76	.0300	5.62	18.44

TABLE E-3 (Cont.)

DROPLET VELOCITY VERSUS DROPLET DIAMETER

39	.96	.0376	4.00	13.14
40	.76	.0300	5.42	17.78
41	.58	.0228	6.10	20.01
42	1.15	.0452	4.24	13.92
43	1.15	.0452	5.36	17.60
44	2.11	.0832	4.45	14.62
45	1.53	.0604	4.24	13.92
46	.76	.0300	7.36	24.14
47	.76	.0300	2.65	8.68
48	1.15	.0452	4.00	13.14
49	.76	.0300	4.19	13.74
50	.76	.0300	5.34	17.51
51	.58	.0228	5.35	17.54
52	1.15	.0452	4.76	15.61
53	.96	.0376	4.40	14.44
54	1.34	.0528	4.35	14.28
55	.58	.0228	4.79	15.73
56	1.15	.0452	4.94	16.21
57	.76	.0300	5.13	16.85
58	.96	.0376	5.49	18.02
59	1.34	.0528	5.58	18.29
60	.76	.0300	5.82	19.11
61	.96	.0376	6.57	21.55
62	.76	.0300	6.37	20.88
63	.96	.0376	5.83	15.14
64	.96	.0376	5.61	16.41
65	1.34	.0528	6.15	20.19
66	.96	.0376	5.48	17.99
67	1.15	.0452	5.41	17.75
68	.96	.0376	5.36	17.60
69	1.15	.0452	5.75	18.87
70	1.15	.0452	5.45	17.87
71	1.73	.0680	4.07	13.35
72	1.15	.0452	6.69	21.94
73	.76	.0300	5.14	16.88
74	1.53	.0604	4.68	15.34
75	.96	.0376	7.16	23.51
76	1.34	.0528	4.96	16.27
77	1.15	.0452	4.09	13.41
78	1.34	.0528	5.85	19.20
79	1.15	.0452	5.33	17.46
80	1.73	.0680	5.11	16.76
81	1.34	.0528	3.38	11.04
82	.58	.0228	3.55	11.66

TABLE E-3 (Cont)

DROPLET VELOCITY VERSUS DROPLET DIAMETER

		13.83
83	1.34	*0.528
84	1.15	*0.452
85	.76	*0.300
86	.96	*0.376
87	2.88	*11.32
88	.76	*0.300
89	1.15	*0.452
90	.96	*0.376
91	.76	*0.300
92	.96	*0.376
93	.76	*0.300
94	1.15	*0.452
95	.96	*0.376
96	1.53	*0.604
97	1.53	*0.604
98	1.15	*0.452
99	.76	*0.300
100	.96	*0.376
101	1.53	*0.604
102	.76	*0.300
103	1.34	*0.528
104	1.15	*0.452
105	2.30	*0.904
106	.96	*0.376
107	1.15	*0.452
108	.76	*0.300
109	1.15	*0.452
110	1.53	*0.604
111	.76	*0.300
112	1.34	*0.528
113	1.34	*0.528
114	1.73	*0.660
115	1.73	*0.660
116	1.15	*0.452
117	1.15	*0.452
118	1.53	*0.604
119	.96	*0.376
120	.76	*0.300
121	1.15	*0.452
122	1.34	*0.528
123	.96	*0.376
124	1.34	*0.528
125	2.11	*0.832
126	1.53	*0.604

TABLE E-3 (Cont)

DROPLET VELOCITY VERSUS DROPLET DIAMETER

1.27	1.73	* 0.680	4.62	15.16
1.28	1.34	* 0.528	4.33	14.19
1.29	1.92	* 0.756	4.73	15.52
1.30	1.15	* 0.452	4.35	14.28
1.31	1.15	* 0.652	5.63	14.47
1.32	1.34	* 0.528	4.91	16.09
1.33	1.15	* 0.452	3.47	11.39
1.34	1.15	* 0.452	6.37	20.71
1.35	1.92	* 0.756	4.22	13.83
1.36	1.15	* 0.452	4.34	14.22
1.37	1.15	* 0.452	6.79	22.27
1.38	.96	* 0.376	3.98	13.05
1.39	1.34	* 0.528	4.86	15.94
1.40	1.34	* 0.528	5.04	16.54
1.41	.96	* 0.376	5.71	18.74
1.42	1.15	* 0.452	3.27	10.73
1.43	1.53	* 0.604	5.56	18.23
1.44	1.34	* 0.528	5.69	18.65
1.45	1.53	* 0.604	5.46	14.65
1.46	1.15	* 0.452	3.91	12.34
1.47	1.34	* 0.528	3.83	12.57
1.48	1.53	* 0.604	4.12	13.57
1.49	1.15	* 0.452	3.45	11.33
1.50	.76	* 0.300	5.12	13.23
1.51	1.15	* 0.452	5.57	18.26
1.52	.96	* 0.376	6.90	22.63
1.53	1.34	* 0.528	4.44	14.56
1.54	.96	* 0.376	5.92	12.87
1.55	1.92	* 0.756	5.38	11.04
1.56	1.15	* 0.452	3.70	12.14
1.57	1.34	* 0.528	4.13	13.56
1.58	.96	* 0.376	5.32	14.16
1.59	.96	* 0.376	5.48	11.42
1.60	.96	* 0.376	6.17	21.06
1.61	.96	* 0.376	5.82	19.11
1.62	1.15	* 0.452	6.90	22.63
1.63	.96	* 0.376	5.81	19.08
1.64	1.15	* 0.452	3.23	10.61
1.65	.96	* 0.376	6.96	22.84
1.66	.96	* 0.376	7.84	25.74
1.67	.76	* 0.300	4.94	16.21
1.68	1.73	* 0.680	4.40	14.84
1.69	1.15	* 0.452	4.73	15.52
1.70	1.15	* 0.452	4.67	15.31

TABLE E-3 (Cont.)

DROPLET VELOCITY VERSUS DROPLET DIAMETER

171	1.32	.0328	6.22	20.40
172	1.34	.0528	7.61	24.98
173	1.53	.0604	6.09	19.78
174	.96	.0376	6.26	20.55
175	1.34	.0528	6.02	19.74
176	.96	.0376	5.78	18.46
177	.96	.0376	5.70	18.71
178	.96	.0376	6.66	21.85
179	1.53	.0604	9.65	15.25
180	1.92	.0756	5.23	17.15
181	.96	.0376	6.39	20.97
182	.96	.0376	5.82	19.11
183	.96	.0376	6.68	21.71
184	1.92	.0756	5.13	16.35
185	1.73	.0680	5.62	18.44
186	1.15	.0452	5.24	17.18
187	1.34	.0528	3.55	11.63
188	1.53	.0604	4.92	16.15
189	1.53	.0604	5.89	19.32
190	1.73	.0680	4.96	16.27
191	1.92	.0756	6.56	21.52
192	1.92	.0756	6.22	20.40
193	1.34	.0528	5.70	19.66
194	1.92	.0756	7.32	24.02
195	1.15	.0452	7.13	23.34
196	1.15	.0452	7.13	23.39
197	1.62	.0716	6.27	20.58
198	1.15	.0452	7.12	23.36
199	.96	.0376	7.99	26.22
200	1.53	.0604	7.52	24.66
201	1.53	.0604	7.16	23.51
202	1.53	.0604	9.10	29.86
203	1.53	.0604	7.84	25.71
204	1.15	.0452	4.83	15.85
205	1.73	.0680	6.68	21.91
206	1.53	.0604	7.22	23.09
207	1.34	.0528	7.67	25.16
208	.96	.0376	7.20	23.63
209	1.34	.0528	7.28	23.90
210	1.53	.0604	7.78	25.53
211	2.30	.0904	6.27	20.58
212	1.34	.0528	8.15	26.73
213	1.06	.0416	6.56	21.52
214	2.01	.0792	5.91	19.36

TABLE E-3 (Cont)

DROPLET VELOCITY VERSUS DROPLET DIAMETER

215	2.01	.0792	5.90	19.35
216	1.34	.0528	4.68	15.37
217	1.53	.0604	8.43	27.66
218	1.43	.0564	7.01	22.94
219	1.25	.0492	6.16	20.22
220	1.43	.0564	4.99	16.30
221	2.01	.0792	5.07	16.63
222	2.88	.1132	4.77	15.64
223	1.25	.0492	8.32	27.30
224	1.53	.0604	7.48	24.53
225	1.53	.0604	9.34	30.65
226	1.63	.0640	5.51	18.08
227	1.63	.0640	4.68	12.34
228	1.15	.0452	8.16	26.76
229	1.53	.0604	7.24	23.75
230	1.34	.0528	7.61	24.45
231	1.15	.0452	7.86	25.80
232	1.06	.0416	7.94	26.04
233	1.15	.0452	7.29	23.93
234	1.73	.0680	6.90	22.63
235	1.73	.0680	7.72	25.31
236	1.34	.0528	7.73	25.34
237	1.15	.0452	8.18	26.82
238	1.15	.0452	6.63	28.30
239	1.43	.0564	6.90	22.63
240	1.06	.0416	4.99	16.36
241	1.25	.0492	6.37	20.86
242	1.34	.0528	9.14	24.99
243	1.34	.0528	8.35	27.34
244	1.43	.0564	7.88	25.86
245	1.34	.0528	7.62	25.01
246	1.34	.0528	7.80	25.59
247	.96	.0376	6.29	20.64
248	1.73	.0680	7.73	25.37
249	1.15	.0452	8.76	28.75
250	1.06	.0416	9.87	32.40
251	1.82	.0716	7.75	25.43
252	1.73	.0680	10.92	35.83
253	1.25	.0492	11.50	37.73
254	1.15	.0452	11.55	37.86
255	1.01	.0398	10.68	35.05
256	1.63	.0640	7.33	24.05
257	1.73	.0680	6.97	22.87
258	1.15	.0452	9.39	30.80

TABLE E-3 (Cont)

DROPLET VELOCITY VERSUS DROPLET DIAMETER

259	2.01	.0792	8.27	27.12
260	1.53	.0604	8.11	26.61
261	1.39	.0546	10.54	34.60
262	.96	.0376	9.16	30.05
263	1.36	.0535	10.49	34.42
264	1.43	.0564	9.43	30.75
265	1.30	.0514	9.68	31.76
266	1.97	.0774	8.24	27.03
267	1.43	.0564	8.78	28.81
268	1.15	.0452	11.69	39.36
269	1.39	.0546	10.74	35.23
270	1.39	.0546	10.64	35.56
271	.96	.0376	8.72	28.60
272	1.27	.0499	8.97	29.41
273	1.27	.0499	8.97	29.41
274	1.01	.0398	7.05	23.11
275	1.43	.0564	8.35	27.39
276	1.77	.0698	10.46	34.32
277	1.11	.0438	10.35	33.96
278	1.15	.0452	9.69	31.79
279	1.25	.0492	10.08	33.06
280	1.15	.0452	13.91	45.63
281	1.64	.0647	10.22	33.54
282	1.30	.0510	9.29	30.47
283	1.06	.0416	10.73	35.20
284	.92	.0362	9.10	29.86
285	.96	.0376	8.98	29.47
286	1.32	.0521	9.08	29.80
287	1.19	.0470	8.57	28.12
288	.76	.0300	9.20	30.20
289	1.53	.0604	9.41	30.86
290	1.19	.0470	10.31	33.81
291	1.06	.0416	10.11	33.18
292	.96	.0376	12.33	40.44

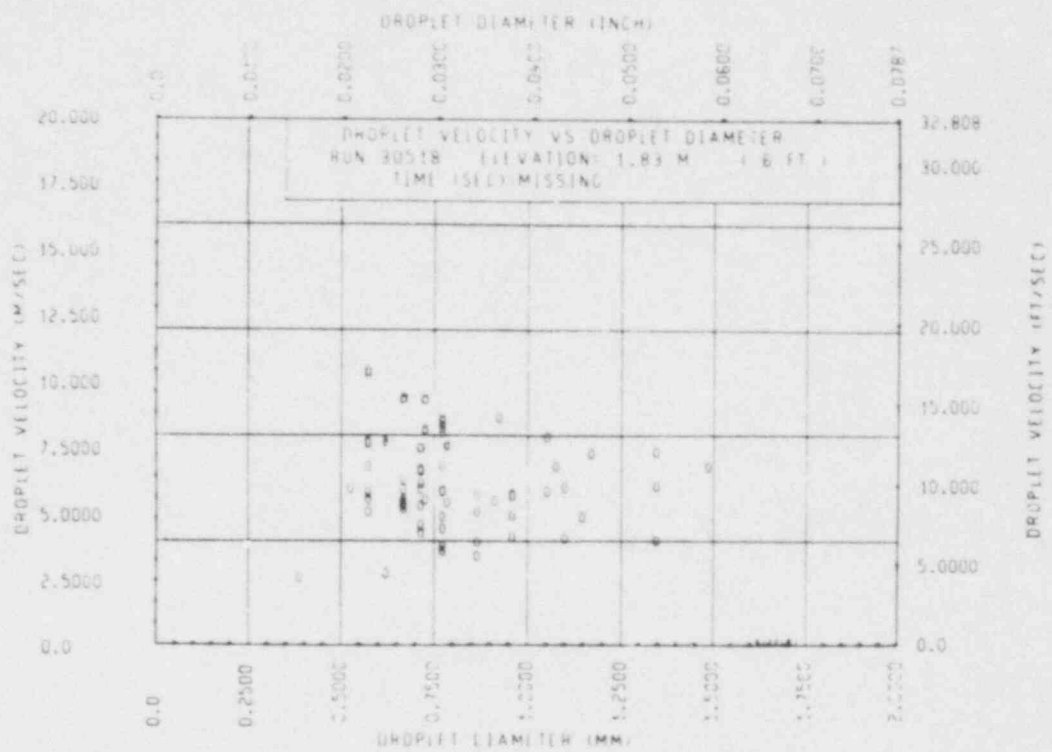


Figure E-37. Droplet Velocity Versus Droplet Diameter, Run 30518

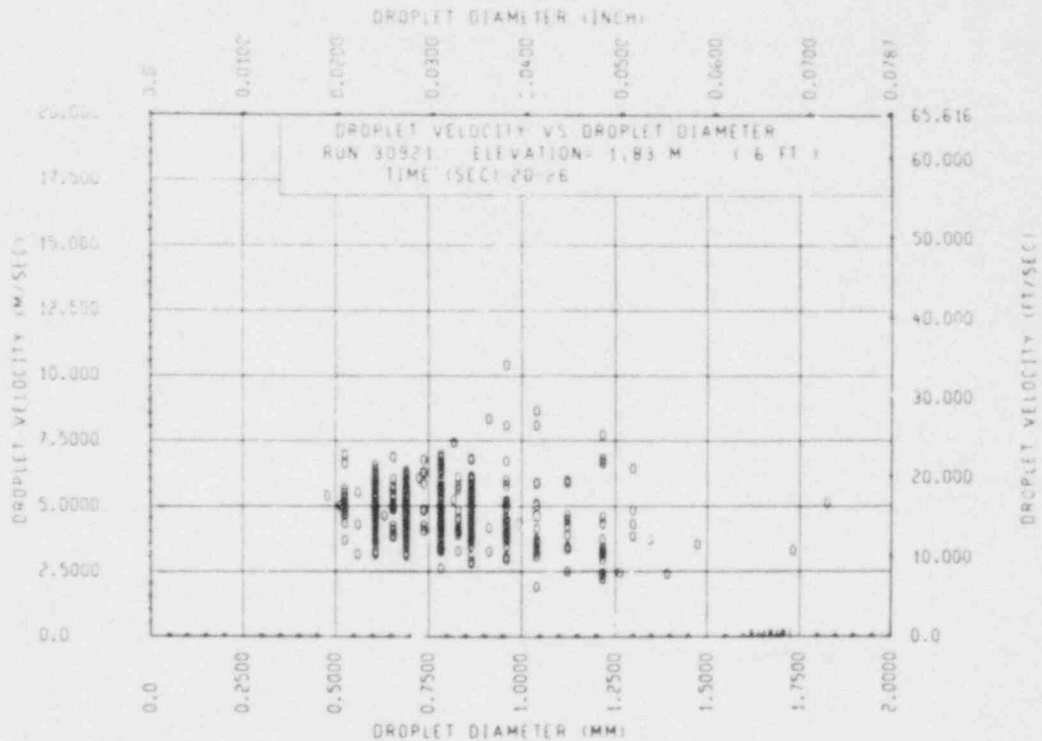


Figure E-38. Droplet Velocity Versus Droplet Diameter, Run 30921

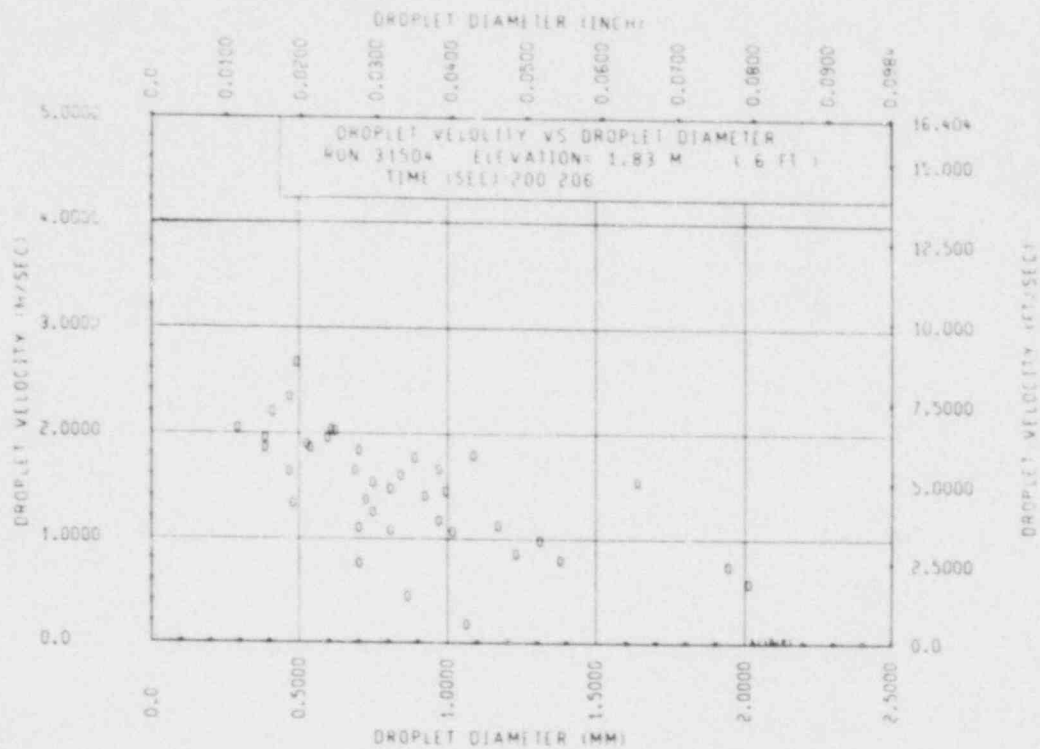


Figure E-39. Droplet Velocity Versus Droplet Diameter, Run 31504

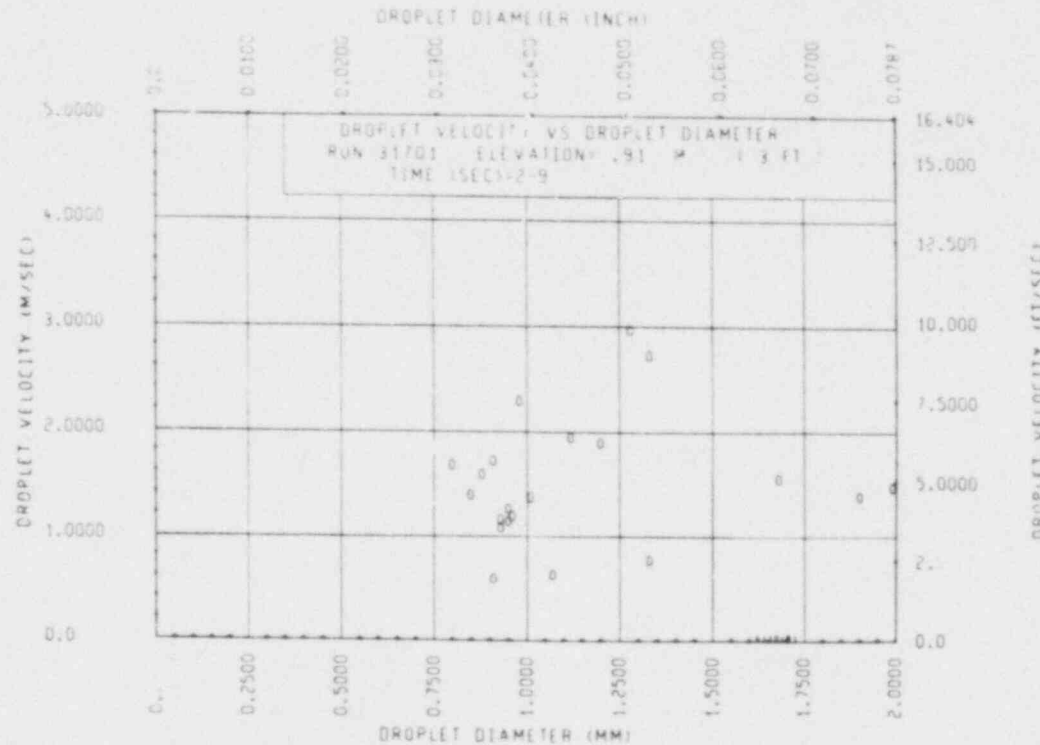


Figure E-40. Droplet Velocity Versus Droplet Diameter, Run 31701, 0.91 m (36 in.) Elevation

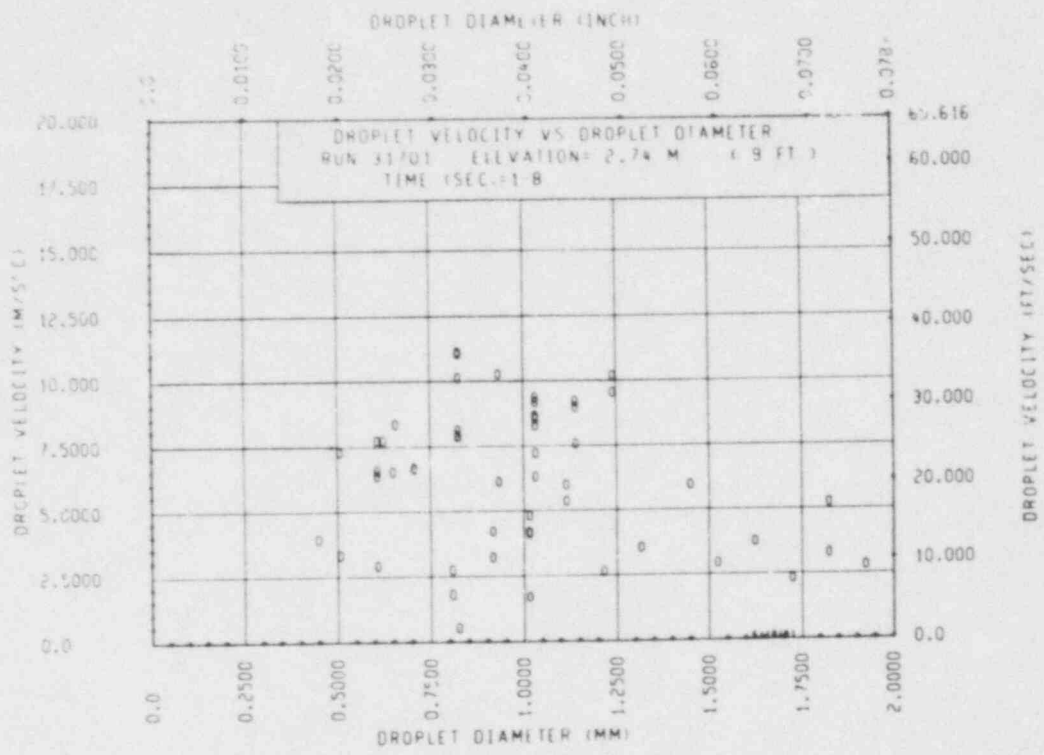


Figure E-41. Droplet Velocity Versus Droplet Diameter, Run 31701, 2.74 m (108 in.) Elevation

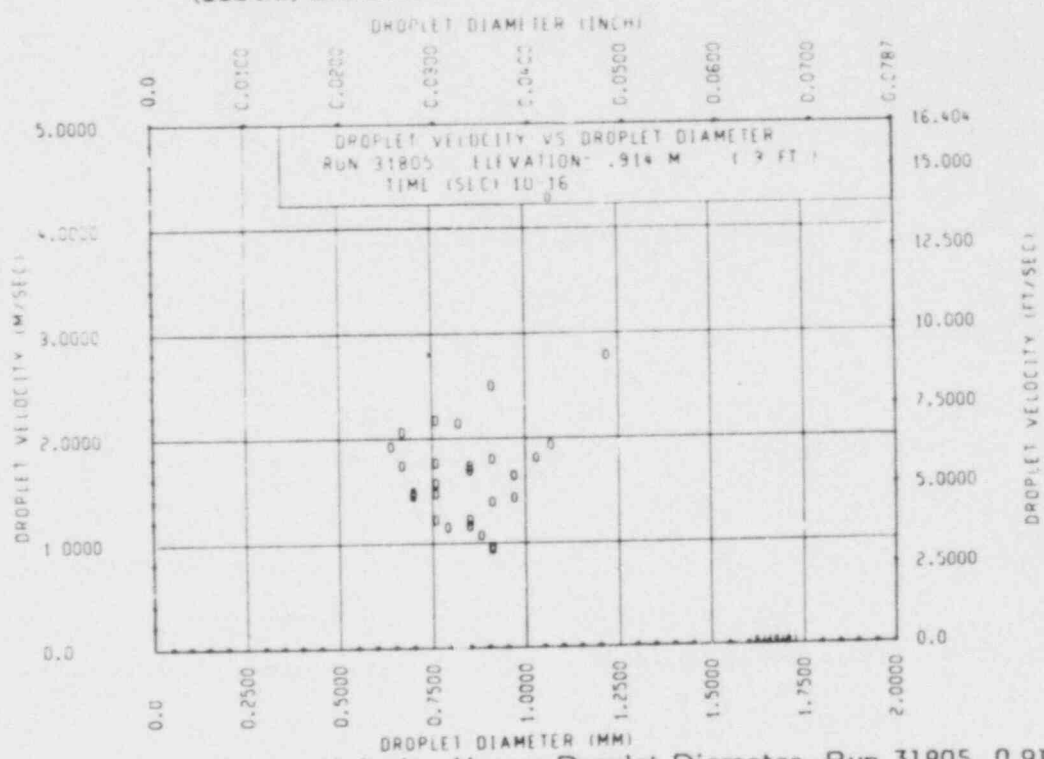


Figure E-42. Droplet Velocity Versus Droplet Diameter, Run 31805, 0.91 m (36 in.) Elevation

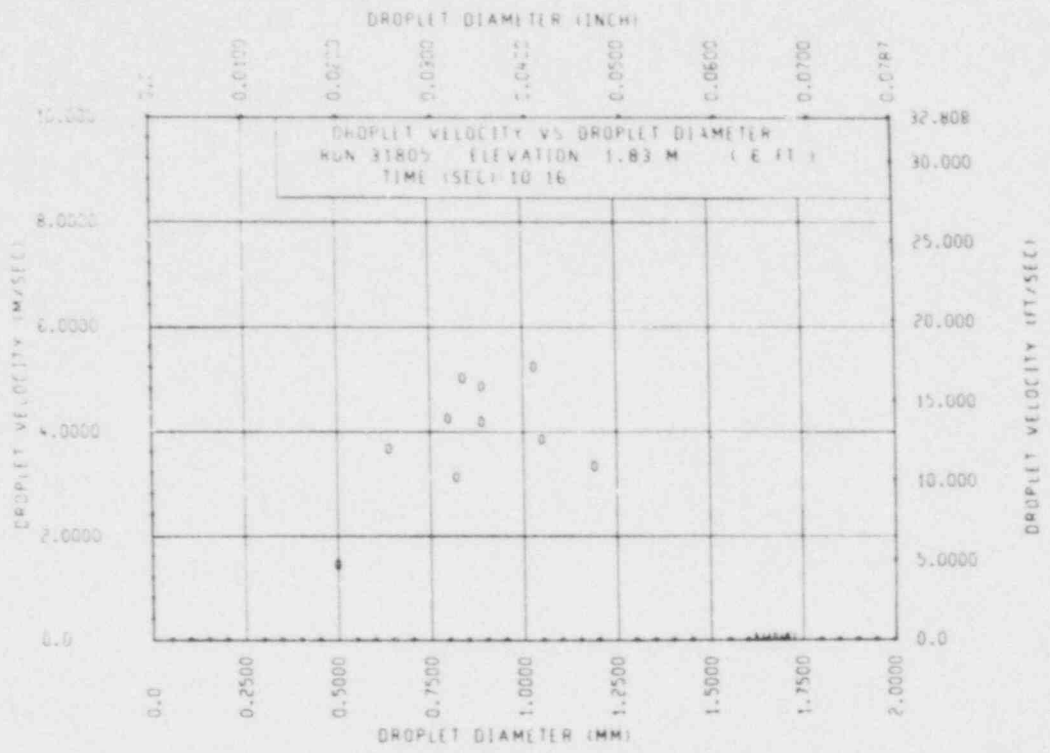


Figure E-43. Droplet Velocity Versus Droplet Diameter, Run 31805, 1.83 m (72 in.) Elevation

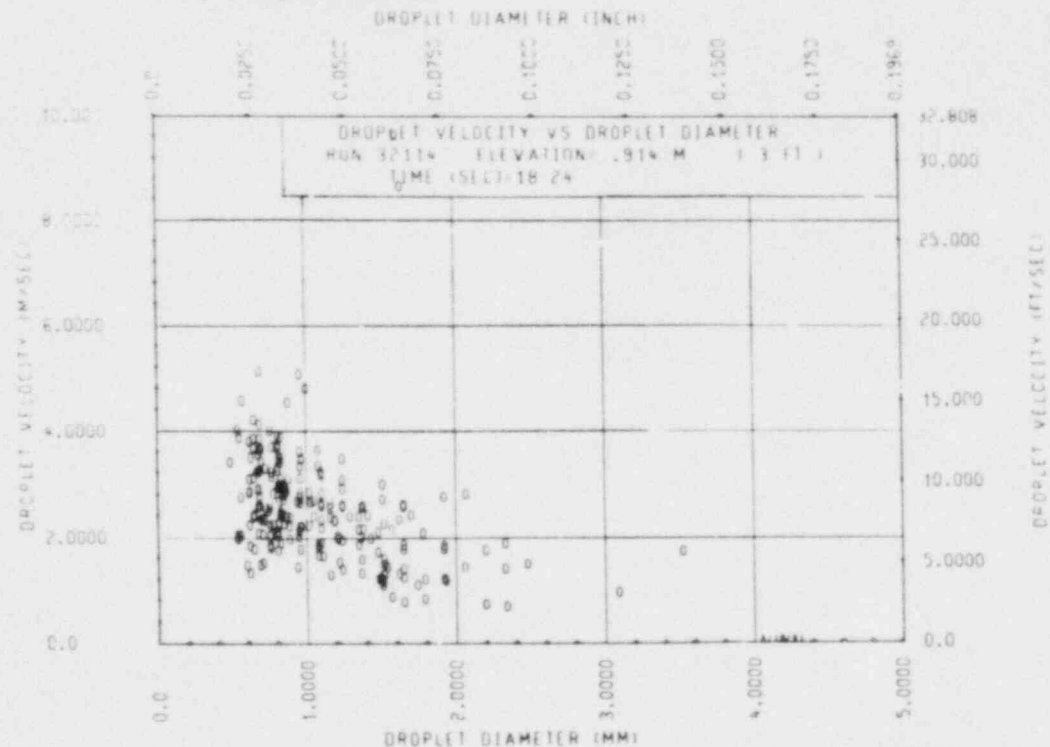


Figure E-44. Droplet Velocity Versus Droplet Diameter, Run 32114, 0.91 m (36 in.) Elevation

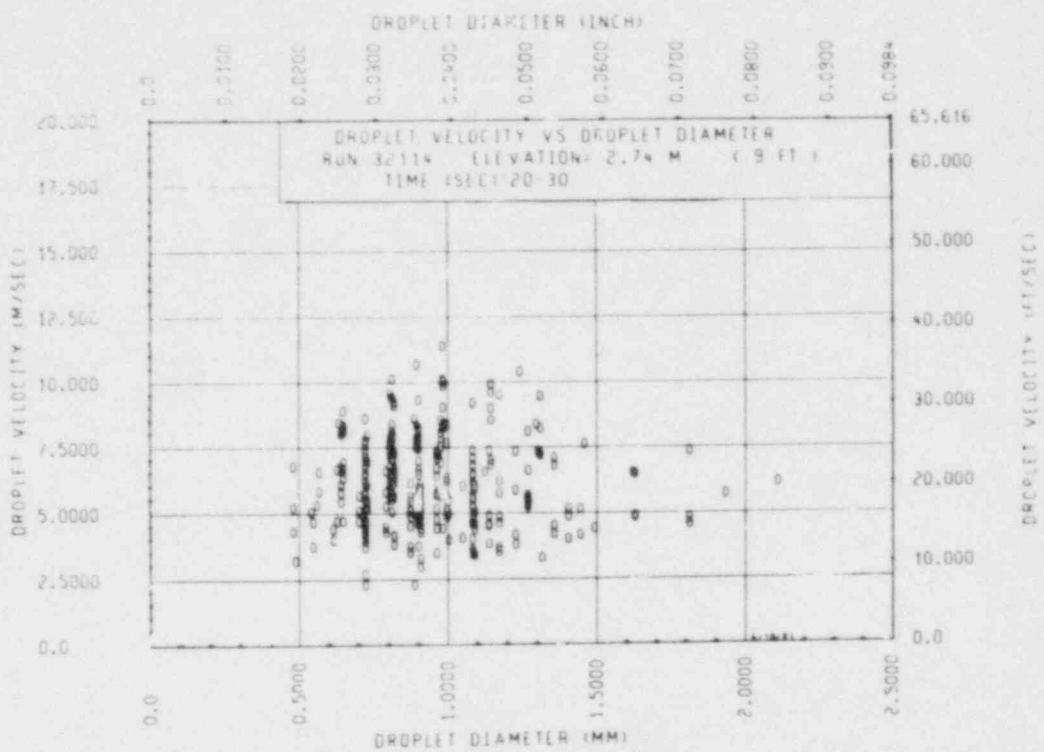


Figure E-45. Droplet Velocity Versus Droplet Diameter, Run 32114, 2.74 m (108in.) Elevation

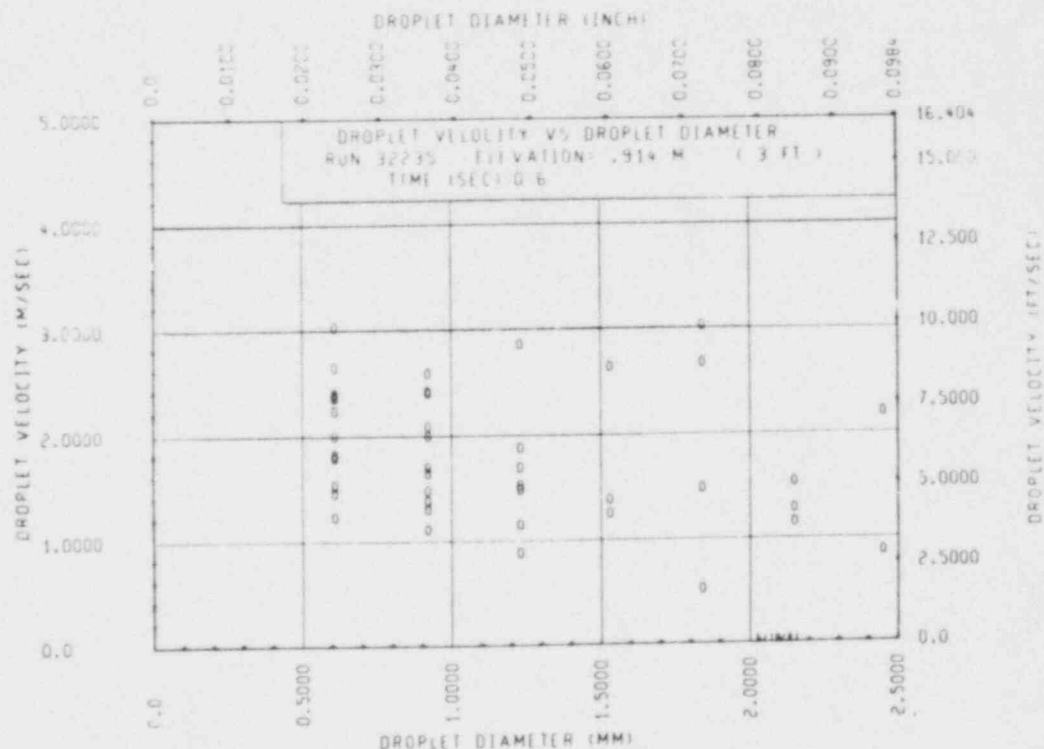


Figure E-46. Droplet Velocity Versus Droplet Diameter, Run 32235

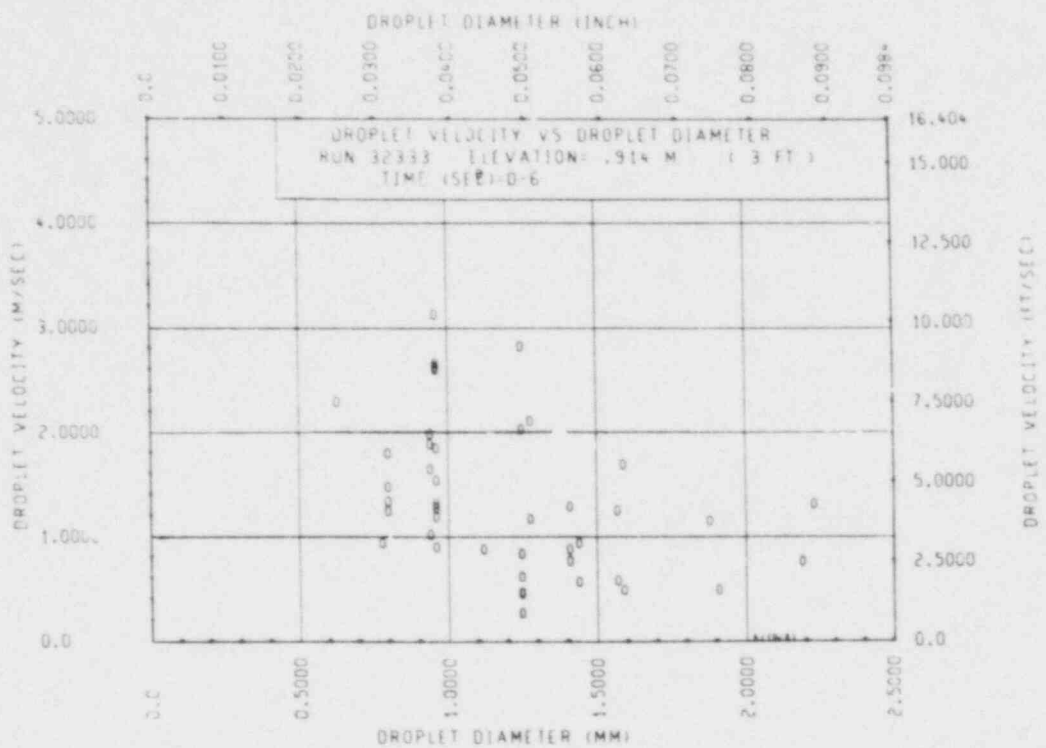


Figure E-47. Droplet Velocity Versus Droplet Diameter, Run 32333, 0.91 m (36 in.) Elevation

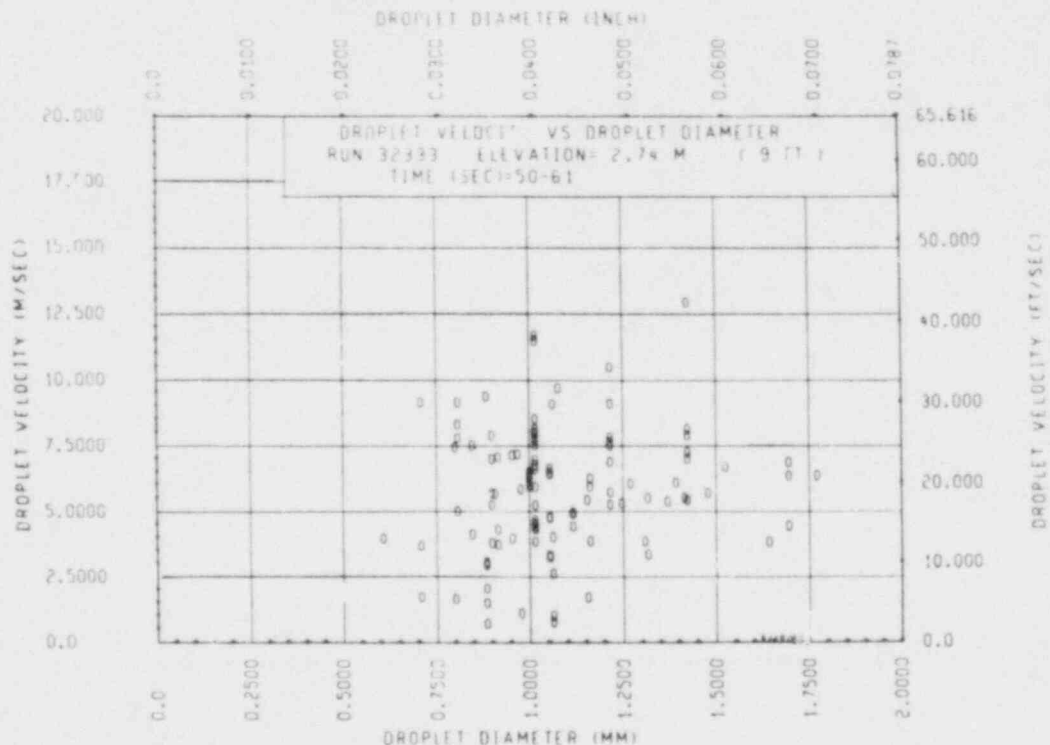


Figure E-48. Droplet Velocity Versus Droplet Diameter, Run 32333, 2.74 m (108 in.) Elevation

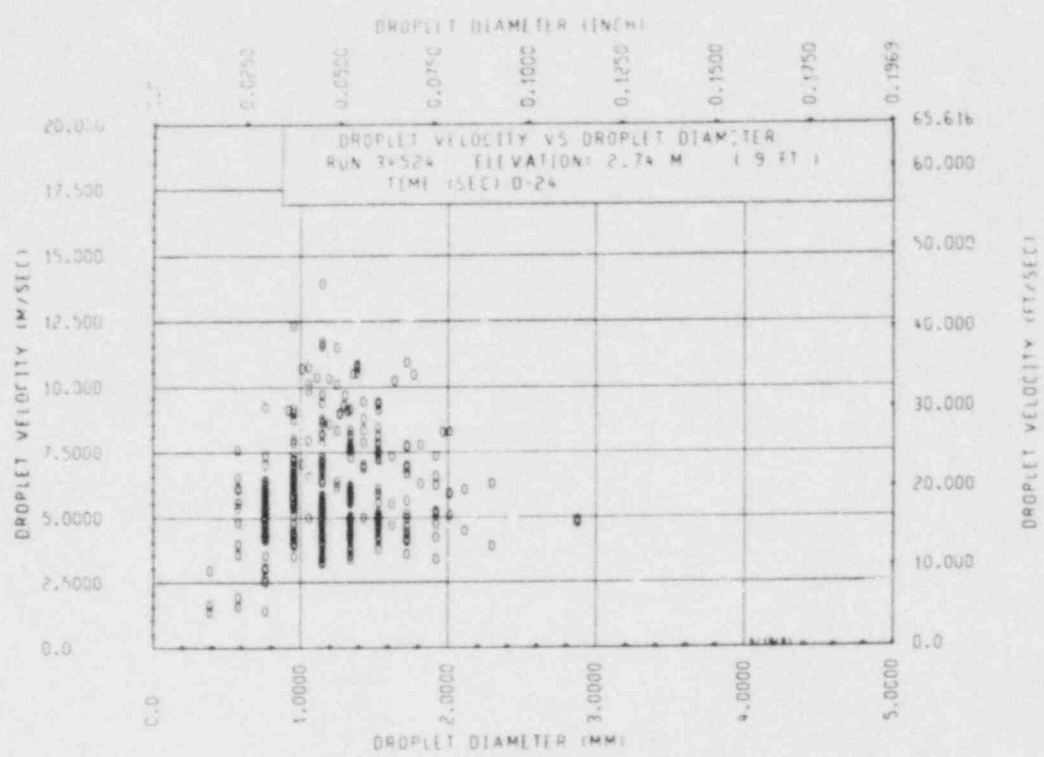


Figure E-49. Droplet Velocity Versus Droplet Diameter, Run 34524

SUMMARY

Run	Elevation [m (in.)]	Pressure [Mpa (psia)]	Peak Power [kw/m (kw/ft)]	Flooding Rate [mm/sec (in./sec)]	Coolant Tempera- ture [$^{\circ}$ C ($^{\circ}$ F)]	Bundie Power Profile
30518	1.83 (72)	0.28 (40)	2.3 (0.7)	38.9 (1.53)	52 (126)	Uniform
30921	1.83 (72)	0.27 (39)	1.3 (0.4)	38.9 (1.53)	52 (126)	Uniform
31504	1.83 (72)	0.28 (40)	2.3 (0.7)	24.6 (0.97)	51 (123)	Uniform
31701	0.91 (36)	0.28 (40)	2.3 (0.7)	155 (6.1)	53 (127)	Uniform
31701	2.74 (108)	0.28 (40)	2.3 (0.7)	155 (6.1)	53 (127)	Uniform
31805	0.91 (36)	0.28 (40)	2.3 (0.7)	20.6 (0.81)	51 (124)	Uniform
31805	1.83 (72)	0.28 (40)	2.3 (0.7)	20.6 (0.81)	51 (124)	Uniform
32114	0.91 (36)	0.28 (40)	2.3 (0.7)	25.4 + 31.0 (1.0 + 1.22)	125 (257)	Uniform
32114	2.74 (108)	0.28 (40)	2.3 (0.7)	25.4 + 31.0 (1.0 + 1.22)	125 (257)	Uniform
32235	0.91 (36)	0.14 (20)	2.3 (0.7)	166 (6.53) 5 sec 24.9 (0.98) 200 sec 15.7 (0.62) onward	31 (88)	Uniform
32333	0.91 (36)	0.28 (40)	2.3 (0.7)	166 (6.36) 5 sec 15.7 (0.82) onward	52 (125)	Uniform
32333	2.74 (108)	0.28 (40)	2.3 (0.7)	166 (6.36) 5 sec 20.8 (0.82) onward	52 (125)	Uniform
34524	2.74 (108)	0.28 (40)	3.3 (1.0)	39.9 (1.57)	52 (125)	Uniform

TABLE E-4

OF MOVIE DROPLET DATA

Hottest Rod and Elevation [m (in.)]	Initial Rod Temperature [$^{\circ}$ C ($^{\circ}$ F)]	Maximum Rod Temperature [$^{\circ}$ C ($^{\circ}$ F)]	Time of Movie (sec)	Mean Drop Diameter [mm (in.)]	Number of Drops	Quench Front [m (in.)]
8H-1.98 (78)	257 (494)	653 (1208)	Missing	0.89 (0.035)	334	Missing
9I-1.78 (70)	879 (1614)	949 (1740)	20-26	0.86 (0.034)	2039	0.38 (14.9)
8K-1.98 (78)	863 (1585)	1149 (2101)	200-206	0.81 (0.032)	101	1.53 (6.01)
	872 (1601)		2-9	1.19 (0.047)	153	0.75 (29.4)
	872 (1601)		1-8	0.91 (0.036)	108	0.39 (15.6)
	871 (1600)		10-16	0.86 (0.034)	32	0.42 (16.6)
	871 (1600)		10-16	0.86 (0.034)	12	0.42 (16.6)
6L-1.88 (74)	893 (1639)	1194 (2172)	18-24	1.14 (0.045)	316	0.18 (7.2)
6L-1.88 (74)	893 (1639)	1194 (2172)	20-30	0.91 (0.036)	346	0.21 (8.2)
6K-1.98 (78)	888 (1630)	1147 (2096)	0-6	1.19 (0.047)	53	0.20 (8.0)
6L-1.98 (78)	888 (1631)	1148 (2099)	0-6	1.24 (0.049)	79	0.16 (6.2)
6L-1.93 (76)	888 (1631)	1148 (2099)	50-61	0.97 (0.038)	1474	0.92 (36.2)
7J-1.83(72)	878 (1612)	1204 (2199)	0-24	1.19 (0.047)	330	0.26 (10.2)

E-5. DISCUSSION

The drop size spectra of droplets entrained in the dispersed flow ahead of the quench front in the rod bundle is found to be represented well by the log-normal distribution. As summarized in table E-4, the mean drop diameter varies from 0.81 mm (0.032 in.) to 1.24 mm (0.049 in.). Lindsted, et al., observed an elliptical droplet shape and found an average axis ratio of about 0.6.⁽¹⁾ In the present study, the droplets seen in the movies were mostly spherical in shape; no significant distortion from a spherical shape was observed, as shown in figures E-1 and E-2.

It is believed that the drop diameter distribution depends on many variables. Among them are system pressure, bundle power, coolant injection rate (flooding rate), coolant subcooling, initial rod temperature, quench front elevation, and bundle geometry. The present drop diameter distribution results do not provide sufficient information for a thorough parametric study. The effects of only a few of the parameters mentioned above can be obtained. The 0.91 m (36 in.) elevation movies of runs 32235 and 32333 show that the effect of system pressure on the mean drop diameter is small within the pressure range of 0.14 to 0.28 MPa (20 to 40 psia). The 0.91m (36 in.) elevation movies of runs 31701, 31805, and 32333 show that the mean drop diameter increases with flooding rate. It appears that flooding rate is an important parameter affecting the drop size. Movies of runs 31701, 31805, and 32114 show the effect of elevation. The mean drop diameter decreased by about 20 percent for runs 31701 and 32114 from the 0.91 m (36 in.) elevation to the 2.74 m (108 in.) elevation, but remained unchanged for run 31805 between the 0.91 m (36 in.) and the 1.83 m (72 in.) elevations. However, the number of drops observed and recorded for run 31805 was much less than for the other runs (see table E-1); hence the results of run 31805 may not be conclusive. The effect of quench front elevation on the drop size is not clear.

The drop velocity versus drop diameter plots (figures E-38, E . . . 41, E-46, E-46, and E-47) show a trend of decreasing velocity with increasing drop diameter. The existence of drop acceleration is also observed. Runs 31701, 31805, and 32114 show that droplets

I. Lindsted, R. D., et al., "Droplet and Flow Pattern Data, Vertical, Two-Phase (Air-Water) Flow Using Axial Photography," NRC Public Document Room, Accession No. 7904110139 (1979).

were accelerated as they moved up the bundle. The droplet velocity at the higher elevation was considerably larger than that at the lower elevation. Although the drop diameter distributions follow closely the log-normal distribution, wide scattering is found in almost all the drop velocity versus drop diameter plots. The large variation in the velocity of drops having the same drop diameter may be due to the rapid change in bundle flow conditions at the beginning of flooding (for example, the mass flow rate above the quench front increases rapidly at the beginning of reflood); also, the net upward force acting on a droplet may depend strongly on the position of the droplet relative to the surrounding rods.

APPENDIX F

CALCULATION OF DROPLET SIZE AND DROP VELOCITY IN DISPERSED FLOW REGIME

F-1. GENERAL

The following paragraphs describe how the drop size and drop velocity from the transition front to the bundle exit were calculated. The calculated drop sizes and drop velocities were then compared with the measured data from the movies (appendix E), to determine the drop size distributions at the transition front. The input data required to perform the calculations are summarized in appendix C. One-dimensional quasi-steady-state axial flow is assumed. In the following paragraphs, the axial dependence of various parameters is omitted from the equations for simplicity.

F-2. BASIC EQUATIONS

Because of the assumption of quasi-steady-state, the bundle total (vapor plus droplet) mass flux and the droplet number flux (number of droplets per unit area passing a given elevation per second) are constants above the transition front. The droplet number flux is related to the measured drop size spectrum and mass flow by

$$\dot{N}_{di} = \frac{6(1-x)m_T v_i}{\pi \rho_l \sum_{j=1}^{N_d} v_j d_j^3} \quad (F-1)$$

where

\dot{N}_{di} = droplet number flux of i-th drop size group
[drops/m²-sec (drops/ft²-sec)]

x = steam quality

- \dot{m}_T = total (vapor plus droplet) mass flux [$\text{kg}/\text{m}^2\text{-sec}$
 $(\text{lbm}/\text{ft}^2\text{-sec})$]
 ρ_l = saturation liquid mass density [kg/m^3 (lbm/ft^3)]
 N_d = total number of drop size groups
 v_i = measured frequency of i -th drop size group
 d_i = diameter of i -th drop size group [m (ft)]

At the transition front, the vapor and droplet mass flux are calculated by

$$\dot{m}_v = x \dot{m}_T \quad (\text{F-2})$$

$$\dot{m}_{di} = \frac{1}{6} \pi d_i^3 \rho_l N_{di} \quad (\text{F-3})$$

where

$$\dot{m}_v = \text{vapor mass flux } [\text{kg}/\text{m}^2\text{-sec} (\text{lbm}/\text{ft}^2\text{-sec})]$$

$$\dot{m}_{di} = \text{droplet mass flux of } i\text{-th drop size group } [\text{kg}/\text{m}^2\text{-sec} (\text{lbm}/\text{ft}^2\text{-sec})]$$

The droplet velocity is assumed to be equal to the terminal velocity at the transition front. Assuming that the drag force and the gravitational and buoyancy forces are the only forces active on the drop, the terminal velocity condition is expressed by

$$0.75 \left(\frac{\rho_v}{\rho_l} \right) \left(\frac{C_{di} \Delta u_i^2}{d_i} \right) - g \left(1 - \frac{\rho_v}{\rho_l} \right) = 0 \quad (F-4)$$

where

ρ_v = vapor mass density [(kg/ft^3) (lbm/ft^3)]

C_{di} = drop force coefficient for i-th drop size group

Δu_i = velocity difference between vapor and i-th drop size group [m/sec (ft/sec)]

g = gravitational acceleration [m/sec^2 (ft/sec^2)]

The drag coefficient is an empirical fit of data for a solid sphere:⁽¹⁾

$$C_{di} = \frac{24}{Re_{di}} + \frac{1}{1 + \sqrt{Re_{di}}} + 0.4 \quad 0 < Re_{di} < 2 \times 10^5 \quad (F-5)$$

where

$$Re_{di} = \frac{\Delta u_i d_i}{v_v} \quad (F-6)$$

v_v = kinematic viscosity of vapor [m^2/sec (ft^2/sec)]

It should be noted that the drag force coefficient, C_{di} , is itself a function of Δu_i ; thus equations (F-4) and (F-5) may be solved simultaneously for Δu_i by iteration. The vapor and drop velocities at the quench front can then be calculated from the velocity difference, Δu_i , by the following iterative scheme. A value for the vapor void fraction at the quench front is first assumed and the velocities computed by:

1. White, F. M., Viscous Fluid Flows, McGraw-Hill, New York, 1974, p 209.

$$u_v = \frac{m''}{\rho_v \alpha} \quad (F-7)$$

$$u_{di} = u_v - \Delta u_i \quad (F-8)$$

where:

u_v = vapor velocity [m/sec or (ft/sec)]

α = vapor void fraction

u_{di} = drop velocity of i-th drop size group
[m/sec or (ft/sec)]

Using the calculated droplet velocities, a droplet volume fraction is defined:

$$\alpha_{di} = \frac{m''_{di}}{\rho_l u_{di}} \quad (F-9)$$

where α_{di} = droplet volume fraction of the i-th drop size group.

The following relation is then checked with the assumed vapor void fraction and the computed liquid volume fractions:

$$l = \alpha + \sum_{i=1}^{N_d} \alpha_{di} \quad (F-10)$$

If the above relation is not satisfied (to within a specified error margin; 10^{-8} is used in the present calculations), a new value for the vapor void fraction is assumed, and the calculations are repeated until convergence is achieved.

It should also be mentioned that in the numerical calculation, the terminal velocity condition in equation (F-4) is represented by

$$(1 + 10^{-6}) \cdot g \left(1 - \frac{\rho_v}{\rho_l}\right) > 0.75 \left(\frac{\rho_v}{\rho_l}\right) \left(\frac{C_{di} \Delta u_i^2}{d_i}\right) > g \left(1 - \frac{\rho_v}{\rho_l}\right) \quad (F-11)$$

so as to ensure a finite positive acceleration for the droplets right above the transition front.

Above the transition front, the drop is accelerated according to

$$\frac{\Delta u_{di}}{\Delta z} = \frac{1}{u_{di}} \left[0.75 \left(\frac{\rho_v}{\rho_l}\right) \left(\frac{C_{di} \Delta u_i^2}{d_i}\right) - g \left(1 - \frac{\rho_v}{\rho_l}\right) \right] \quad (F-12)$$

where

Δz = axial increment [m (ft)]

Δu_{di} = drop velocity of i -th drop size group at $z + \Delta z$
minus that at z [m/sec (ft/sec)]

Drop velocity above the transition front is computed from equation (F-12) by a forward difference numerical technique. That is, in order to compute the drop velocity at $z + \Delta z$, the right-hand side of equation (F-12) is evaluated at z and the droplet velocity computed by

$$u_{di}(z + \Delta z) = u_{di}(z) + \left[\frac{\Delta u_{di}}{\Delta z} (z) \right] \Delta z \quad (F-13)$$

If the calculated droplet velocities of certain drop size groups exceed their respective terminal velocities, the droplet velocities of these groups are assumed to be equal to their terminal velocities.

The assumption that the droplet velocity is calculated by the terminal velocity condition at the transition front is not critical. An overestimate (or underestimate) of the droplet velocity at the transition front will result in an underestimation (or overestimate) of the droplet acceleration [through the Δu_i term in equation (F-12)], and so tend to "correct" for the droplet velocity at subsequent axial nodes. This self-correcting effect of the velocity calculations ensures that the droplet velocity, at a distance sufficiently far from the transition front [> 0.30 m (12 in.)], is independent of the assumed boundary value.⁽¹⁾

Assuming that the droplet evaporation rate is proportional to the product of the droplet surface area and the vapor-droplet heat transfer coefficient, the droplet mass flux of each drop size group is given by

$$\dot{\Delta m}_{di} = - \frac{n_{di} d_i \text{Nu}_{di}}{N_d} \dot{m}_T \Delta x$$

$$\sum_{j=1}^{N_d} (n_{dj} d_j \text{Nu}_{dj})$$
(F-14)

$$\dot{m}_{di}''(z + \Delta z) = \dot{m}_{di}''(z) + \dot{\Delta m}_{di}''(z)$$
(F-15)

The vapor-droplet heat transfer Nusselt number is computed by the Lee and Ryley correlation:⁽²⁾

$$\text{Nu}_{di}'' = 2 + 0.55 \sqrt{\text{Re}_{di}} \text{Pr}^{1/3}$$
(F-16)

where Pr = vapor Prandtl number.

The term n_{di}'' in equation (F-14) is the droplet number density of the i -th drop size group (number of drops per unit volume) and is related to the droplet number flux and droplet velocity by

$$n_{di}'' = \frac{\dot{N}_{di}}{\dot{u}_{di}}$$
(F-17)

1. Lilly, G. P., et al., "PWR FLECHT Skewed Profile Low Flooding Rate Test Series Evaluation Report," WCAP-9183, November, 1977.
2. Lee, K., and Ryley, D. J., "The Evaporation of Water Droplets in Superheated Steam," J. Heat Transfer 90, ASME, 445-451 (1968).

The droplet diameter is related to the droplet number flux and mass flux by

$$d_i = \left(\frac{6 m_{di}^*}{\pi \rho_l N_{di}} \right)^{1/3} \quad (F-18)$$

Finally, the droplet volume fractions and vapor void fraction are calculated by equations (F-9) and (F-10), respectively, and the vapor velocity is computed by equation (F-7).

To ensure that the calculations described above do not give nonphysical results, two additional assumptions are made. First, it is assumed that all drop size groups will survive through the bundle exit; that is, no drop will evaporate completely before it reaches the bundle exit. Hence, when the following condition is encountered for the k-th drop size group:

$$\Delta m_{dk}^* (z) \geq m_{dk}^* (z) \quad (F-19)$$

equation (F-14) will be replaced by

$$\Delta m_{dk}^* (z) = 1/2 m_{dk}^* (z) \quad (F-20)$$

$$\begin{aligned} \dot{m}_{di}^* &= - \frac{n_{di} d_i \dot{N}_{di}}{N_d} (m_T^* \Delta x - \Delta m_{dk}^*), i \neq k \\ &\sum_{j \neq k} (n_{dj} d_j \dot{N}_{dj}) \end{aligned} \quad (F-21)$$

Equation (F-19) implies that the drops belonging to the k-th drop size group will completely evaporate between elevations z and z + Δz. When this happens, the magnitude of Δm_{dk}^* and d_k are usually at least an order of magnitude smaller than the average drop size group, and have negligible effect on the behavior of the rest of the drop size groups. Equations (F-20) and (F-21) serve to keep d_k from evaporating

completely in the numerical calculations; these equations are introduced solely for the purpose of efficient programming.

Second, it is required that if the size of the drop (drop A) is greater (or smaller) than the size of another drop (drop B) at the transition front, then the size of drop A should remain greater (or smaller) than the size of drop B throughout the entire bundle length (although the relative difference in size of the two drops may change). Hence, if

$$d_k(z) > d_n(z) \quad (F-22)$$

but the computed drop sizes [by equation (F-18)] at $z + \Delta z$ are such that

$$d_k(z + \Delta z) \leq d_n(z + \Delta z) \quad (F-23)$$

then equation (F-14) will be replaced by

$$\frac{\partial m}{\partial d_k} = - \frac{(0.5)^m n_{dk} d_k N_{dk}}{\left[\sum_{j \neq k}^{N_d} n_{dj} d_j N_{dj} + (0.5)^m n_{dk} d_k N_{dk} \right]} \frac{\partial m}{\partial x} \quad (F-24)$$

$$\frac{\partial m}{\partial d_i} = - \frac{n_{di} d_i N_{di}}{\left[\sum_{j \neq k}^{N_d} n_{dj} d_j N_{dj} + (0.5)^m n_{dk} d_k N_{dk} \right]} \frac{\partial m}{\partial x}; i \neq k \quad (F-25)$$

where m is equal to 1. The calculations of equations (F-15) through (F-18) will then be repeated for all drop size groups. It is necessary to repeat the calculations for all drop size groups in order to preserve mass balance in the bundle. If the condition of equation (F-23) still persists, then the process is repeated with m set equal to 2, 3, and so forth, until

$$d_k(z + \Delta z) > d_n(z + \Delta z) \quad (F-26)$$

F-3. CALCULATION METHODS

Based on the measured drop size distribution at the camera or window location, a drop size distribution at the transition front is first assumed. The calculations described in the above paragraph are then performed through the movie camera location. The calculated drop sizes are then compared with the measured drop size spectrum. A better estimate of the drop sizes at the transition front is then made and the calculations are repeated until the computed drop sizes agree with the movie data to within a specified margin (an error margin of 1 percent is used in the present calculations); the calculations are then continued through the bundle exit.

F-4. FLECHT SEASET TEST RUNS ANALYZED

Droplet motion movies are available for nine reflood test runs (see table E-4, appendix E). Out of these nine test runs, four were analyzed according to the descriptions given in paragraphs F-1 and F-2. These are runs 30921, 31504, 31701, and 32114. Analysis of the above tests was limited to time periods during which the droplet movies were taken (see also table 6-1). Reasons for not performing the analysis for the other five test runs are summarized below:

- The exact movie time for run 30518 is not available.
- FLEMB (mass and energy balance program for reflood tests) results for runs 31805 and 34524 at early times (shortly after flooding) are not adequate for the present analysis. For example, steam quality at the transition front is obtained by extrapolating steam probe data (see appendix C); extrapolating the steam probe data for run 34524 at early times gives negative steam qualities at the quench front, as shown in figure F-1.
- Runs 32235 and 32333 are variable flooding rate tests. FLEMB results are not available for variable flooding rate cases; also, the assumption of quasi-steady-state is invalid as the flooding rate varies.

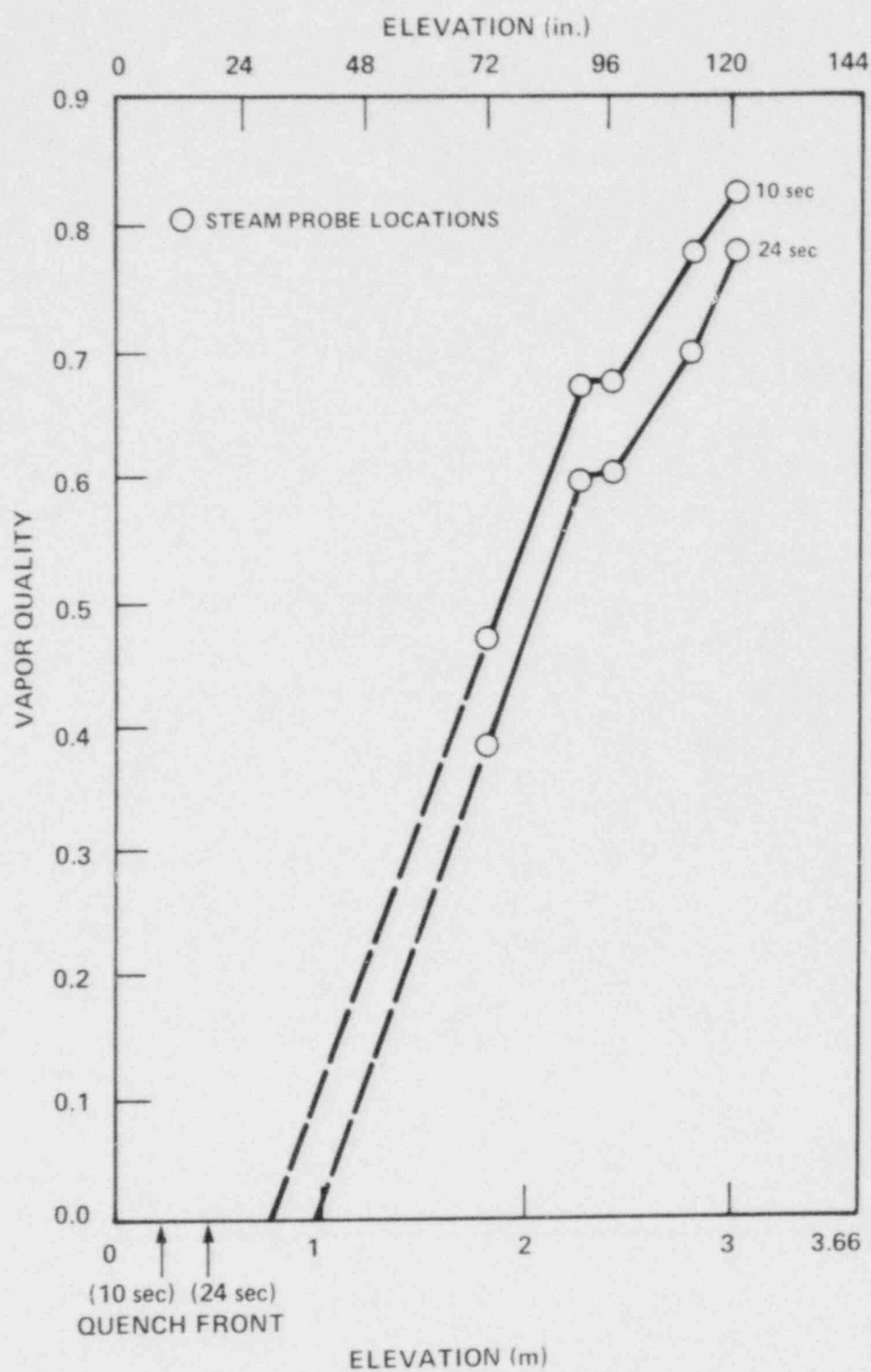


Figure F-1. Data-Based Steam Quality for Run 34524 Shortly After Flooding

F-5. RESULTS AND CONCLUSIONS

Tables F-1 through F-5 show the measured drop sizes at the camera location and also the calculated drop sizes at the transition front. The data show that the large drops evaporate more than the smaller drops since they have a lower velocity, and thus there is more time for evaporation. A Sauter Mean Diameter (SMD) at the transition front is also calculated:

$$SMD = \frac{\sum_{i=1}^{N_d} v_i d_i^3}{\sum_{i=1}^{N_d} v_i d_i^2} \quad (F-27)$$

It is shown in paragraph 6-8 that replacing the drop size spectrum by the SMD gives satisfactory heat transfer results.

Figures F-2 through F-7 show the comparisons of the calculated droplet velocities with data. Three factors are thought to have contributed to the discrepancy between predictions and data. First, the assumption of terminal velocities at the transition front may have overestimated the droplet velocities near the transition front. Figure F-2, for example, shows the results for run 31504 at 200 and 210 seconds at the 1.83 m (72 in.) elevation. The transition fronts at 200 and 210 seconds are at 1.75 m (69 in.) and 1.80 m (71 in.), respectively. The comparisons shown in figure F-2 thus suggest that the boundary conditions for the droplet velocities may have been overstated. Second, the drag coefficient given in equation (F-5) is an empirical fit for a solid sphere; it may not be adequate for accelerating droplets under nonequilibrium dispersed flow conditions. Third, the assumption of quasi-steady-state implies that

$$\frac{dV_d}{dt} = V_d \frac{\partial V_d}{\partial z} + \frac{\partial V_d}{\partial t} \approx V_d \frac{\partial V_d}{\partial z}$$

This assumption may not be valid, especially for high flooding rate tests. Indeed, the worst comparisons with data come from run 31701 (figures F-4 and F-5), which was a high flooding rate test with a water injection rate of 155 mm/sec (6.1 in./sec).

From the results presented above, it is clear that more detailed and fundamental studies of the hydrodynamic interactions between dispersed droplets and steam and the droplet formation mechanisms at the quench front are required to give more accurate evaluation of dispersed two-phase flow conditions during reflood.

TABLE F-1
MEASURED DROP SIZES AT CAMERA LOCATION AND
CALCULATED DROP SIZES AT TRANSITION FRONT,
RUN 30921

Movie time = 20 - 26 sec Calculation times = 20, 23, and 26 sec		Camera location = 1.83 m (72 in.) Transition front at 20 sec = 0.62 m (24.6 in.) at 23 sec = 0.69 m (27.0 in.) at 26 sec = 0.73 m (28.8 in.)		
Drop Group Number	Measured Drop Size at Camera Location [mm (in.)]	Calculated Drop Size at Transition Front at 20 sec [mm (in.)]	Calculated Drop Size at Transition Front at 23 sec [mm (in.)]	Calculated Drop Size at Transition Front at 26 sec [mm (in.)]
1	0.37 (0.0145)	0.41 (0.0163)	0.42 (0.0164)	0.42 (0.0167)
2	0.55 (0.0215)	0.59 (0.0233)	0.59 (0.0234)	0.60 (0.0236)
3	0.73 (0.0286)	0.77 (0.0304)	0.77 (0.0305)	0.78 (0.0307)
4	0.90 (0.0355)	0.95 (0.0373)	0.95 (0.0374)	0.96 (0.0377)
5	1.08 (0.0425)	1.12 (0.0443)	1.13 (0.0444)	1.13 (0.0446)
6	1.31 (0.0517)	1.36 (0.0535)	1.36 (0.0536)	1.37 (0.0539)
7	1.44 (0.0565)	1.48 (0.0583)	1.48 (0.0584)	1.49 (0.0587)
8	1.61 (0.0635)	1.66 (0.0653)	1.66 (0.0654)	1.68 (0.0660)
9	1.79 (0.0706)	1.85 (0.0727)	1.85 (0.0730)	1.87 (0.0734)
10	1.97 (0.0775)	2.03 (0.0799)	2.03 (0.0800)	2.06 (0.0811)
11	2.14 (0.0845)	2.23 (0.0877)	2.23 (0.0877)	2.28 (0.0896)
Calculated Sauter Mean Diameter at transition front		1.07 (0.0421)	1.08 (0.0426)	1.08 (0.0426)

TABLE F-2
MEASURED DROP SIZES AT CAMERA LOCATION AND
CALCULATED DROP SIZES AT TRANSITION FRONT,
RUN 31504

Movie time = 200 - 206 sec Calculations time = 200 and 210 sec		Camera location = 1.83 m (72 in.) Transition front at 200 sec = 1.75 m (69 in.) at 210 sec = 1.80 m (70.8 in.)	
Drop Group Number	Measured Drop Size at Camera Location [mm (in.)]	Calculated Drop Size at Transition Front at 200 sec [mm (in.)]	Calculated Drop Size at Transition Front at 210 sec [mm (in.)]
1	0.27 (0.0104)	0.27 (0.0107)	0.27 (0.0106)
2	0.41 (0.0160)	0.41 (0.0161)	0.41 (0.0160)
3	0.55 (0.0215)	0.55 (0.0216)	0.55 (0.0215)
4	0.67 (0.0265)	0.67 (0.0266)	0.67 (0.0265)
5	0.80 (0.0316)	0.80 (0.0317)	0.80 (0.0316)
6	0.93 (0.0365)	0.93 (0.0366)	0.93 (0.0365)
7	1.07 (0.0420)	1.07 (0.0421)	1.07 (0.0420)
8	1.21 (0.0475)	1.21 (0.0476)	1.21 (0.0475)
9	1.34 (0.0526)	1.34 (0.0527)	1.34 (0.0526)
10	1.46 (0.0575)	1.46 (0.0576)	1.46 (0.0575)
11	1.60 (0.0630)	1.60 (0.0631)	1.60 (0.0630)
12	1.74 (0.0685)	1.74 (0.0686)	1.74 (0.0685)
13	1.87 (0.0736)	1.87 (0.0737)	1.87 (0.0736)
14	1.99 (0.0785)	2.00 (0.0786)	1.99 (0.0785)
Calculated Sauter Mean Diameter at transition front		1.18 (0.0463)	1.17 (0.0462)

TABLE F-3
MEASURED DROP SIZES AT CAMERA LOCATION AND
CALCULATED DROP SIZES AT TRANSITION FRONT,
RUN 31701

Movie time = 2 - 9 sec Calculation time = 5 and 10 sec		Camera location = 0.91 m (36 in.) Transition front at 5 sec = 0.88 m (34.8 in.) at 10 sec = 1.22 m (48 in.)	
Drop Group Number	Measured Drop Size at Camera Location [mm (in.)]	Calculated Drop Size at Transition Front at 5 sec [mm (in.)]	Calculated Drop Size at Transition Front at 10 sec [mm (in.)]
1	0.55 (0.0215)	0.55 (0.0216)	0.55 (0.0216)
2	0.81 (0.0320)	0.82 (0.0322)	0.82 (0.0322)
3	1.08 (0.0425)	1.08 (0.0426)	1.08 (0.0426)
4	1.36 (0.0535)	1.36 (0.0536)	1.36 (0.0536)
5	1.64 (0.0646)	1.64 (0.0647)	1.64 (0.0647)
6	1.91 (0.0750)	1.91 (0.0751)	1.91 (0.0751)
7	2.17 (0.0856)	2.18 (0.0857)	2.18 (0.0857)
8	2.45 (0.0965)	2.45 (0.0966)	2.45 (0.0966)
9	2.73 (0.0108)	2.73 (0.0108)	2.73 (0.0108)
Calculated Sauter Mean Diameter at transition front		1.5 (0.0590)	1.5 (0.0590)

TABLE F-3 (cont)
 MEASURED DROP SIZES AT CAMERA LOCATION AND
 CALCULATED DROP SIZES AT TRANSITION FRONT,
 RUN 31701

Movie time = 1 - 8 sec Calculation time = 5 and 10 sec		Camera location = 2.74 m (108 in.) Transition front at 5 sec = 0.91 m (36 in.) at 10 sec = 1.22 m (48 in.)	
Drop Group Number	Measured Drop Size at Camera Location [mm (in.)]	Calculated Drop Size at Transition Front at 5 sec [mm (in.)]	Calculated Drop Size at Transition Front at 10 sec [mm (in.)]
1	0.41 (0.0160)	0.83 (0.0329)	0.75 (0.0296)
2	0.61 (0.0240)	1.02 (0.0401)	0.94 (0.0372)
3	0.81 (0.0320)	1.21 (0.0476)	1.14 (0.0449)
4	1.01 (0.0400)	1.41 (0.0554)	1.34 (0.0527)
5	1.22 (0.0480)	1.60 (0.0631)	1.54 (0.0605)
6	1.42 (0.0560)	1.81 (0.0712)	1.74 (0.0686)
7	1.64 (0.0646)	2.03 (0.0798)	1.96 (0.0773)
8	1.85 (0.0730)	2.24 (0.0882)	2.18 (0.0857)
Calculated Sauter Mean Diameter at transition		1.44 (0.0568)	1.38 (0.0544)

TABLE F-4
 MEASURED DROP SIZES AT CAMERA LOCATION AND
 CALCULATED DROP SIZES AT TRANSITION FRONT,
 RUN 32114

Movie time = 18 - 24 sec Calculation times = 18, 21, and 24 sec		Camera location = 0.91 m (36 in.) Transition front at 18 sec = 0.29 m (11.4 in.) at 21 sec = 0.40 m (15.6 in.) at 24 sec = 0.44 m (17.4 in.)		
Drop Group Number	Measured Drop Size at Camera Location [mm (in.)]	Calculated Drop Size at Transition Front at 18 sec [mm (in.)]	Calculated Drop Size at Transition Front at 21 sec [mm (in.)]	Calculated Drop Size at Transition Front at 24 sec [mm (in.)]
1	0.55 (0.0215)	0.55 (0.0216)	0.55 (0.0217)	0.55 (0.0216)
2	0.83 (0.0325)	0.83 (0.0328)	0.84 (0.0329)	0.83 (0.0328)
3	1.11 (0.0436)	1.12 (0.0439)	1.12 (0.0438)	1.12 (0.0438)
4	1.37 (0.0540)	1.38 (0.0545)	1.38 (0.0545)	1.38 (0.0545)
5	1.64 (0.0646)	1.65 (0.0650)	1.65 (0.0650)	1.65 (0.0650)
6	1.92 (0.0755)	1.93 (0.0760)	1.93 (0.0761)	1.93 (0.0760)
7	2.20 (0.0865)	2.21 (0.0870)	2.21 (0.0871)	2.21 (0.0870)
8	2.48 (0.0976)	2.50 (0.0983)	2.50 (0.0983)	2.50 (0.0982)
9	2.76 (0.108)	2.78 (0.110)	2.78 (0.110)	2.78 (0.109)
10	3.02 (0.113)	3.05 (0.120)	3.05 (0.120)	3.04 (0.120)
11	3.29 (0.129)	3.32 (0.131)	3.31 (0.130)	3.32 (0.131)
12	3.57 (0.141)	3.60 (0.142)	3.61 (0.142)	3.60 (0.142)
13	3.85 (0.152)	6.34 (0.250)	5.95 (0.234)	5.76 (0.227)
Calculated Sauter Mean Diameter at transition front		2.07 (0.0814)	2.00 (0.0788)	1.98 (0.0778)

TABLE F-5
 MEASURED DROP SIZES AT CAMERA LOCATION AND
 CALCULATED DROP SIZES AT TRANSITION FRONT,
 RUN 30921

Movie time = 20 - 30 sec Calculation times = 20, 26, and 30 sec		Camera location = 2.74 m (108 in.) Transition front at 20 sec = 0.38 m (15 in.) at 26 sec = 0.47 m (18.6 in.) at 30 sec = 0.53 m (21 in.)		
Drop Group Number	Measured Drop Size at Camera Location [mm (in.)]	Calculated Drop Size at Transition Front at 20 sec [mm (in.)]	Calculated Drop Size at Transition Front at 26 sec [mm (in.)]	Calculated Drop Size at Transition Front at 30 sec [mm (in.)]
1	0.52 (0.0205)	0.57 (0.0226)	0.76 (0.0300)	0.79 (0.0310)
2	0.67 (0.0270)	0.74 (0.0290)	0.93 (0.0366)	0.95 (0.0376)
3	0.85 (0.0335)	0.91 (0.0358)	1.10 (0.0433)	1.12 (0.0442)
4	1.03 (0.0406)	1.09 (0.0430)	1.30 (0.0510)	1.31 (0.0517)
5	1.21 (0.0475)	1.27 (0.0502)	1.49 (0.0586)	1.51 (0.0594)
6	1.37 (0.0540)	1.44 (0.0569)	1.67 (0.0659)	1.69 (0.0666)
7	1.54 (0.0605)	1.62 (0.0638)	1.87 (0.0736)	1.87 (0.0738)
8	1.72 (0.0676)	1.82 (0.0716)	2.09 (0.0822)	2.09 (0.0822)
9	1.89 (0.0745)	2.03 (0.0798)	2.32 (0.0914)	2.32 (0.0912)
10	2.07 (0.0815)	6.61 (0.260)	5.09 (0.201)	4.57 (0.180)
Calculated Sauter Mean Diameter at transition front		2.21 (0.0870)	1.65 (0.0650)	1.55 (0.0612)

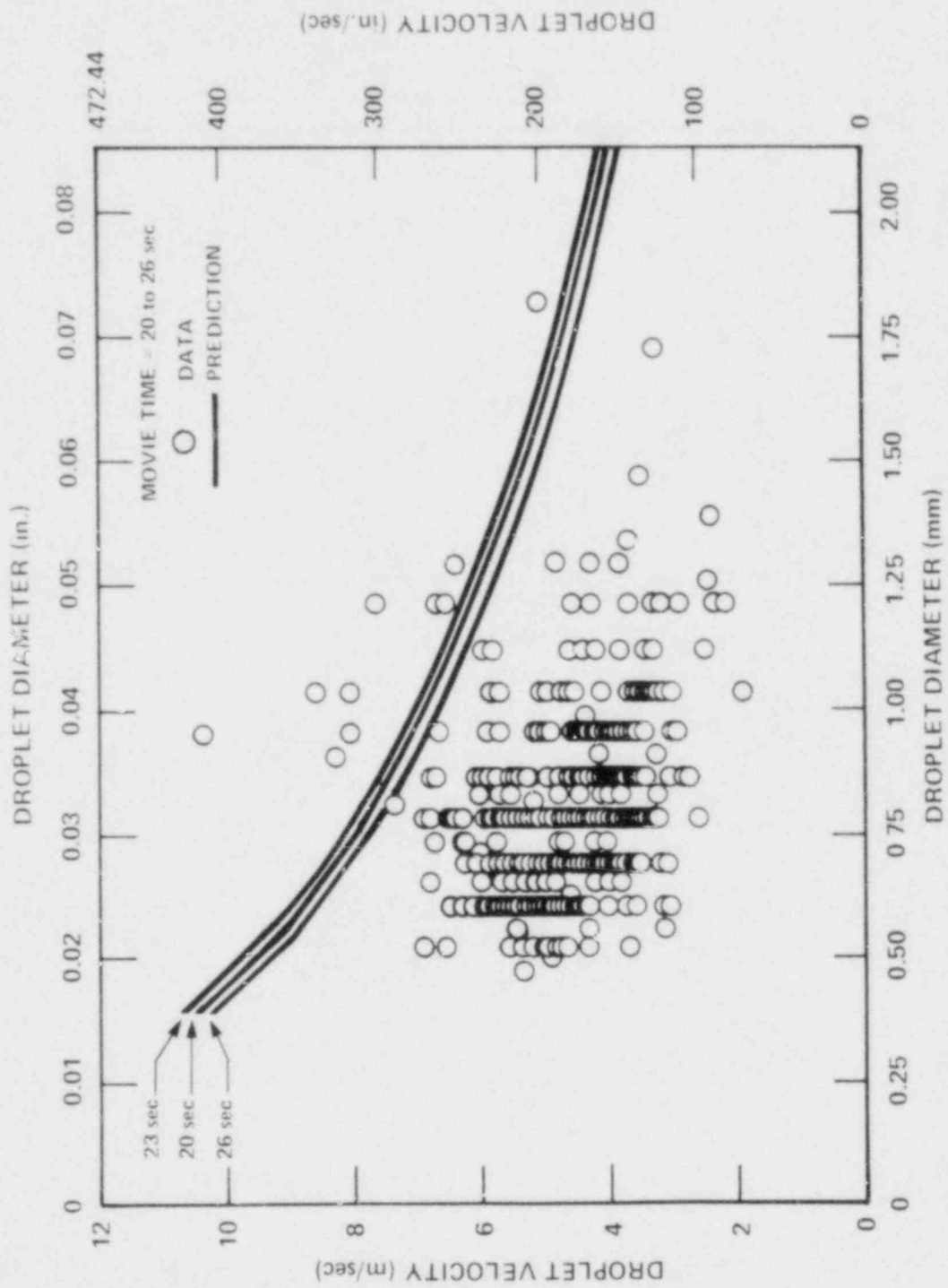


Figure F-2. Comparison of Calculated and Measured Drop Velocities,
Run 30921, 1.83 m (72 in.) Elevation

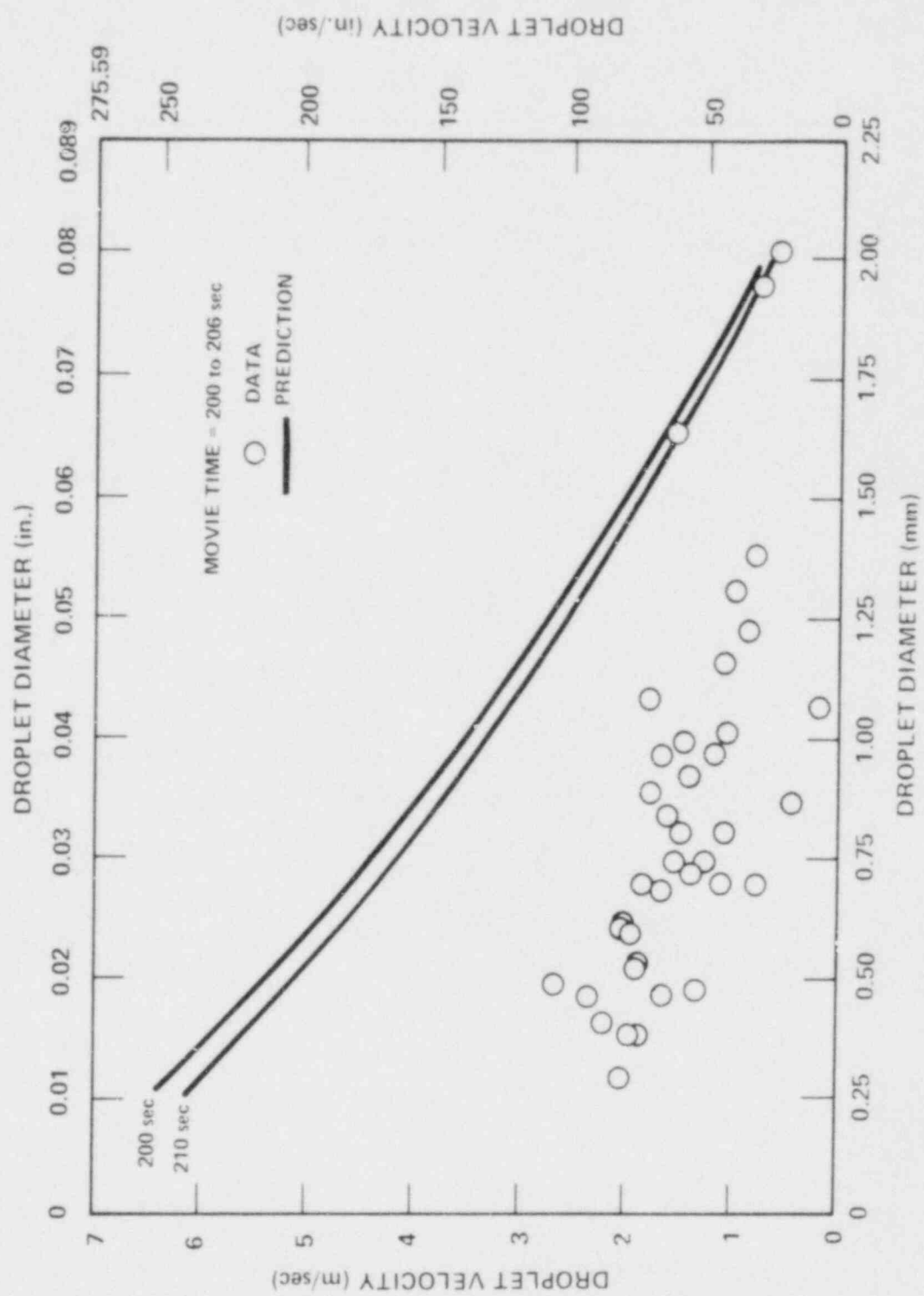


Figure F-3. Comparison of Calculated and Measured Drop Velocities, Run 31504, 1.83 m (72 in.) Elevation

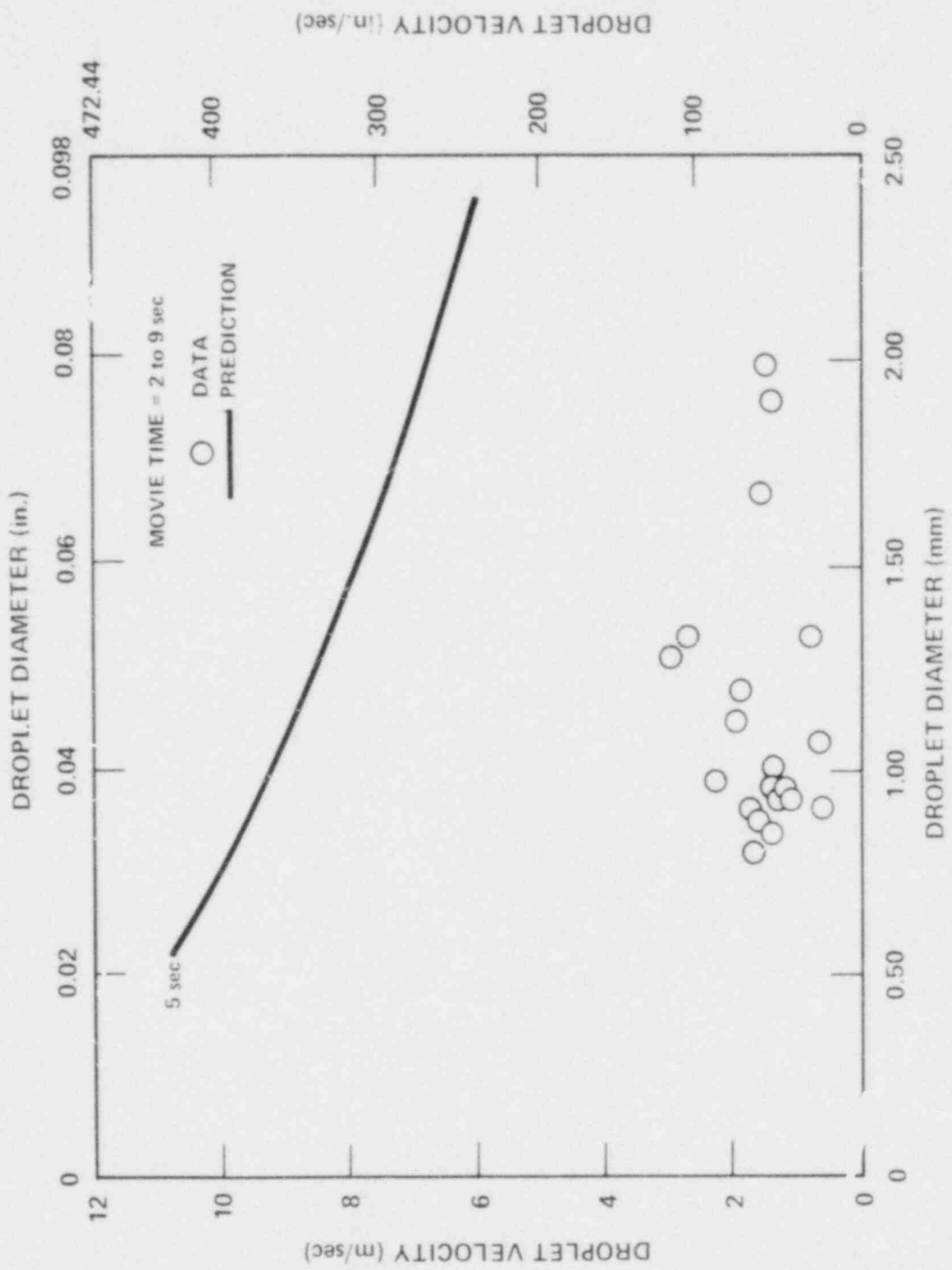


Figure F-4. Comparison of Calculated and Measured Drop Velocities,
Run 31701, 0.91 m (36 in.) Elevation

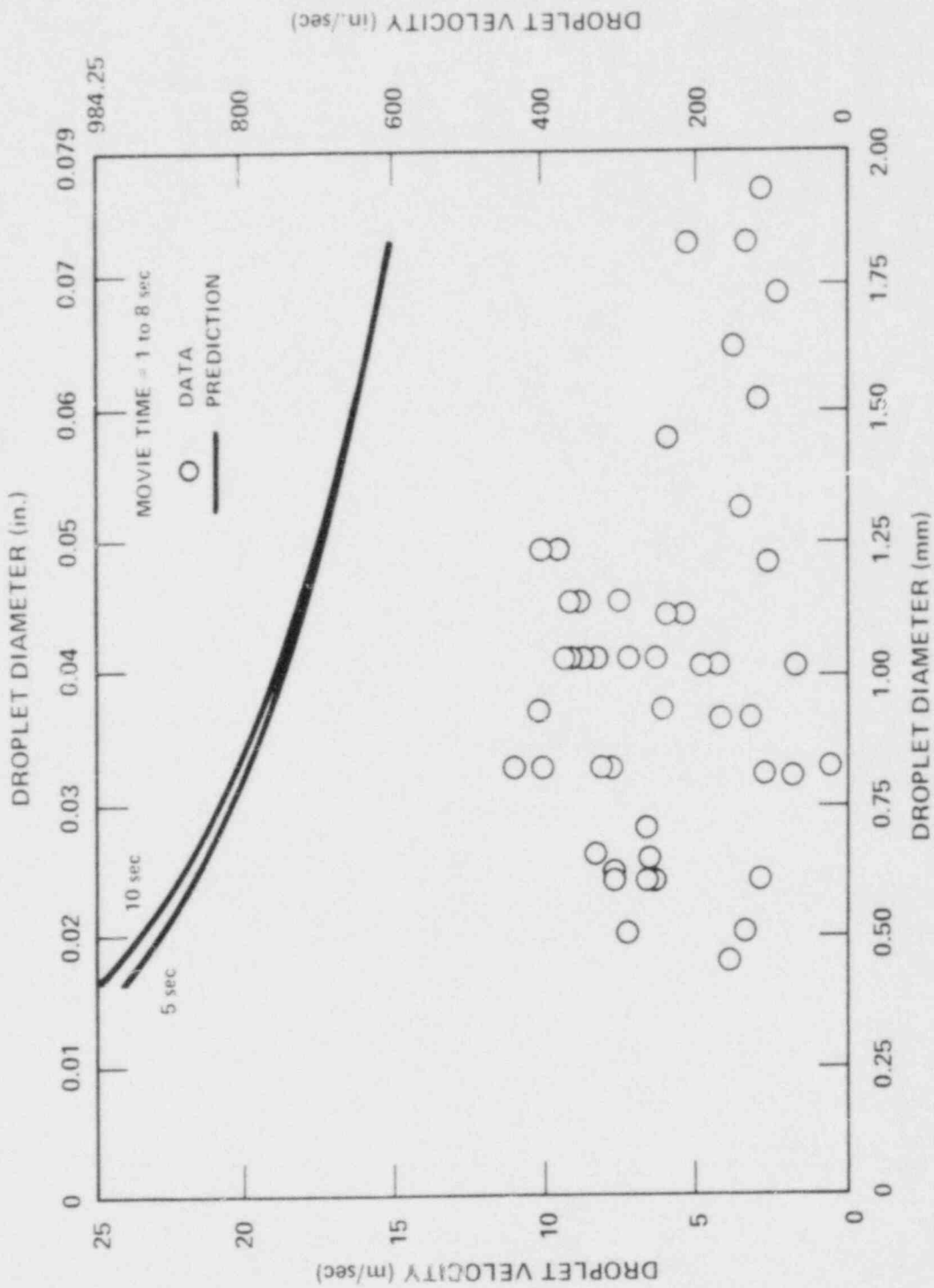


Figure F-5. Comparison of Calculated and Measured Drop Velocities,
Run 31701, 2.74 m (108 in.) Elevation

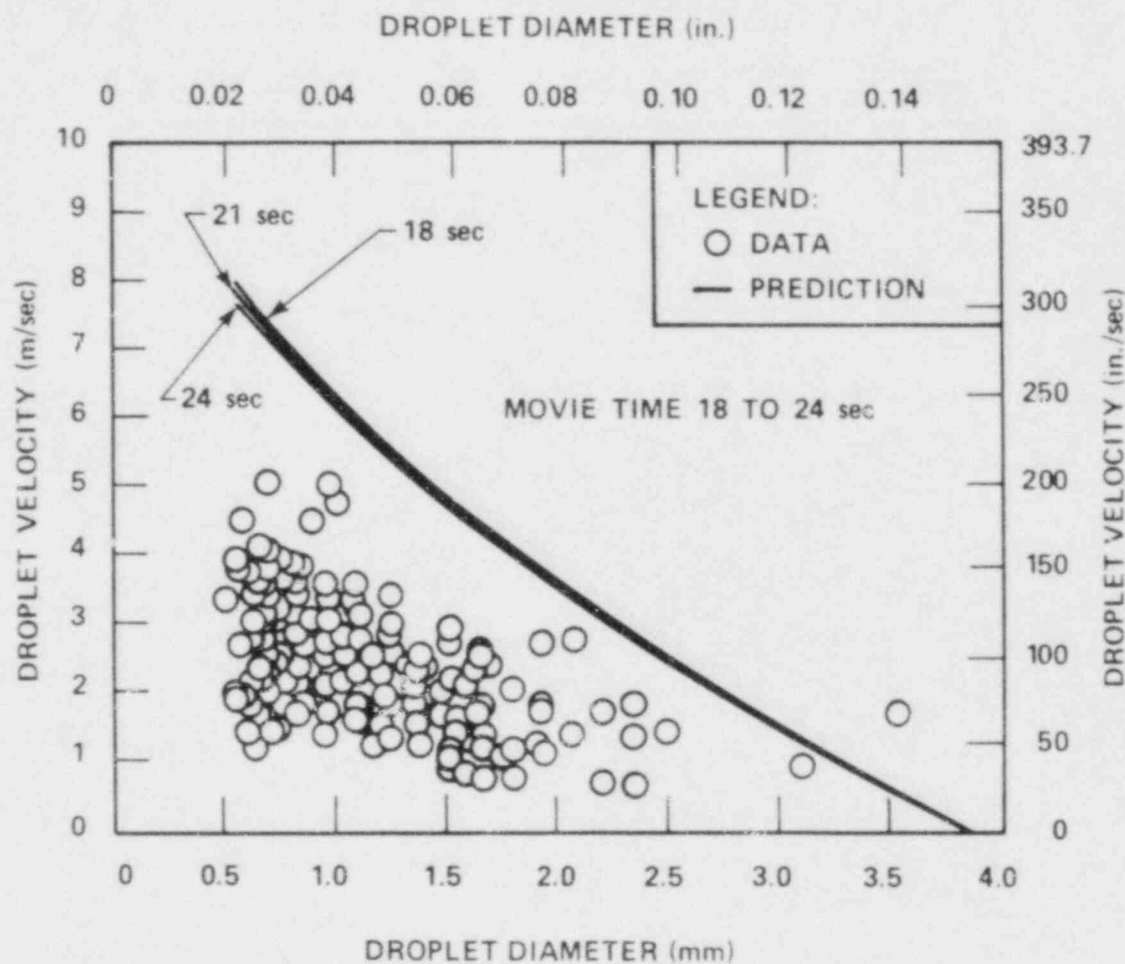


Figure F-6. Comparison of Calculated and Measured Drop Velocities,
Run 32114, 0.91 m (36 in.) Elevation

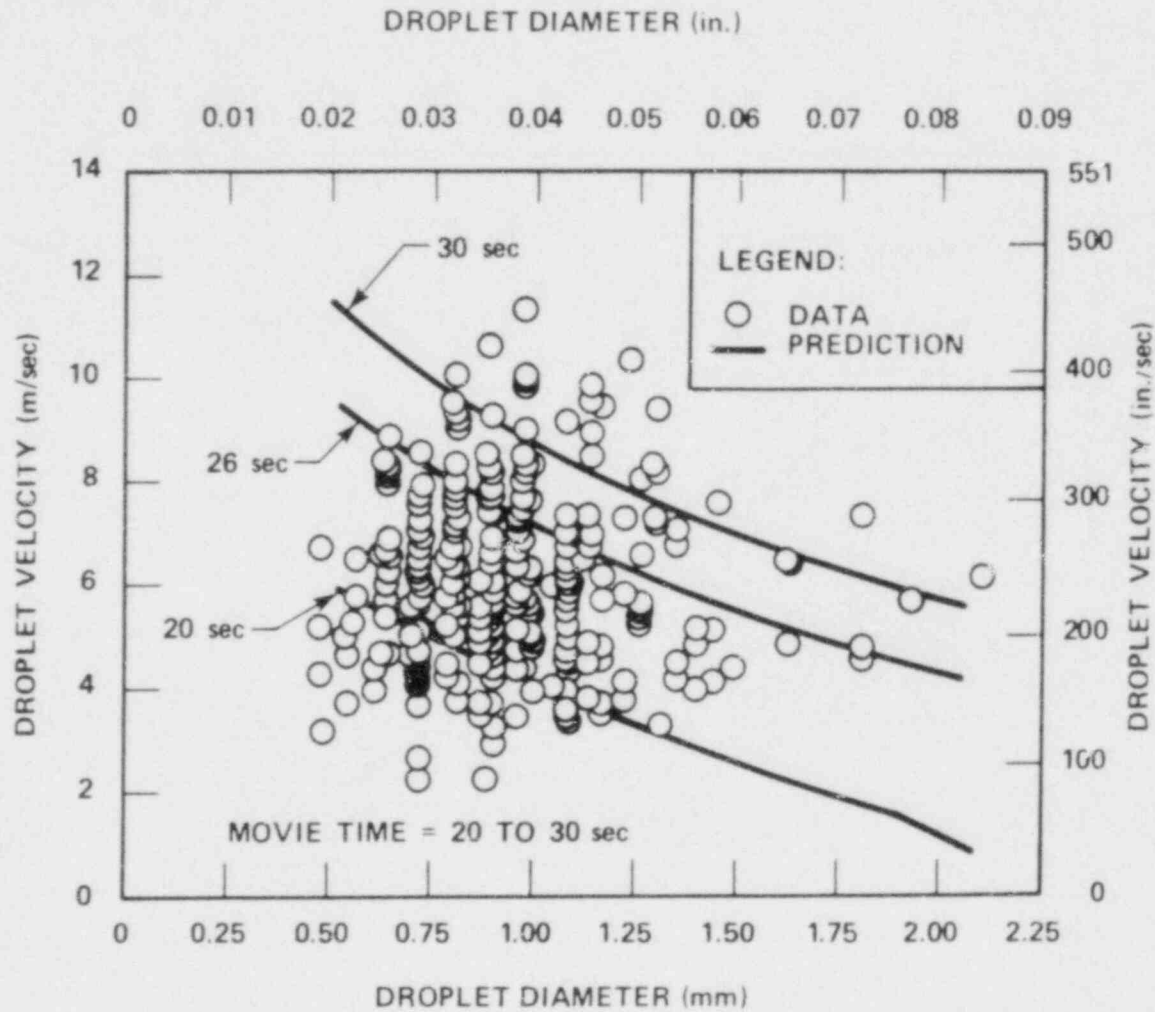


Figure F-7. Comparison of Calculated and Measured Drop Velocities,
Run 32114, 2.74 m (108 in.) Elevation

APPENDIX G

COMPARISON OF HEAT TRANSFER CORRELATION WITH DATA FOR OVERLAP RUNS

Data from overlap runs 31203 (FLECHT SEASET), 03113 (FLECHT cosine power), and 11618 (FLECHT skewed power) have been compared with the heat transfer correlation of this work in paragraph 8-2. Comparison for the remaining sets of overlap runs are presented in figures G-1 through G-34. Run conditions are summarized in table G-1.

G-2

TABLE G-1
OVERLAP RUNS

Run	Peak Power [kw/m (kw/ft)]	Flooding Rate [mm/sec (in./sec)]	Initial Clad Temperature [°C (°F)]	Inlet Subcooling [°C (°F)]	Pressure [MPa (psia)]	Bundle Geometry(a)
30817	2.3 (0.7)	38.1 (1.5)	538 (1000)	77 (140)	0.28 (40)	A
00904	2.8 (0.85)	37.6 (1.48)	538 (998)	77 (140)	0.28 (41)	B
11719	1.5 (0.45)	38.1 (1.5)	538 (1001)	79 (142)	0.28 (41)	C
30518	2.3 (0.7)	38.1 (1.5)	260 (500)	77 (140)	0.28 (40)	A
02005	2.8 (0.84)	38.4 (1.51)	274 (525)	78 (141)	0.28 (40)	B
12720	1.5 (0.45)	38.1 (1.5)	262 (508)	78 (141)	0.28 (40)	C
30619	2.3 (0.7)	38.1 (1.5)	260 (500)	77 (140)	0.14 (20)	A
03709	2.7 (0.81)	38.1 (1.5)	317 (603)	78 (141)	0.14 (20)	B
11821	1.5 (0.45)	41.7 (1.64)	263 (506)	79 (143)	0.14 (20)	C
31805	2.3 (0.7)	20.3 (0.8)	871 (1600)	77 (140)	0.14 (40)	A
02414	2.8 (0.84)	20.6 (0.81)	871 (1600)	77 (138)	0.14 (40)	B
34006	1.3 (0.4)	15.2 (0.6)	871 (1600)	77 (140)	0.14 (40)	A
07836	2.4 (0.74)	15.7 (0.62)	871 (1600)	78 (141)	0.14 (40)	B
36026	2.3 (0.7)	25.4 (1)	871 (1600)	77 (140)	0.14 (40)	A
05132	3.1 (0.95)	25.1 (0.99)	871 (1600)	77 (140)	0.14 (40)	B
32333	2.3 (0.7)	152.4 (6) 5 sec 20.3 (0.8) onward	871 (1600)	77 (140)	0.14 (40)	A
04516	3.1 (0.95)	152.4 (6) 5 sec 20.3 (0.8) onward	871 (1600)	77 (140)	0.14 (40)	B

- a. A - 17 x 17 cosine power
 B - 15 x 15 cosine power
 C - 15 x 15 skewed power

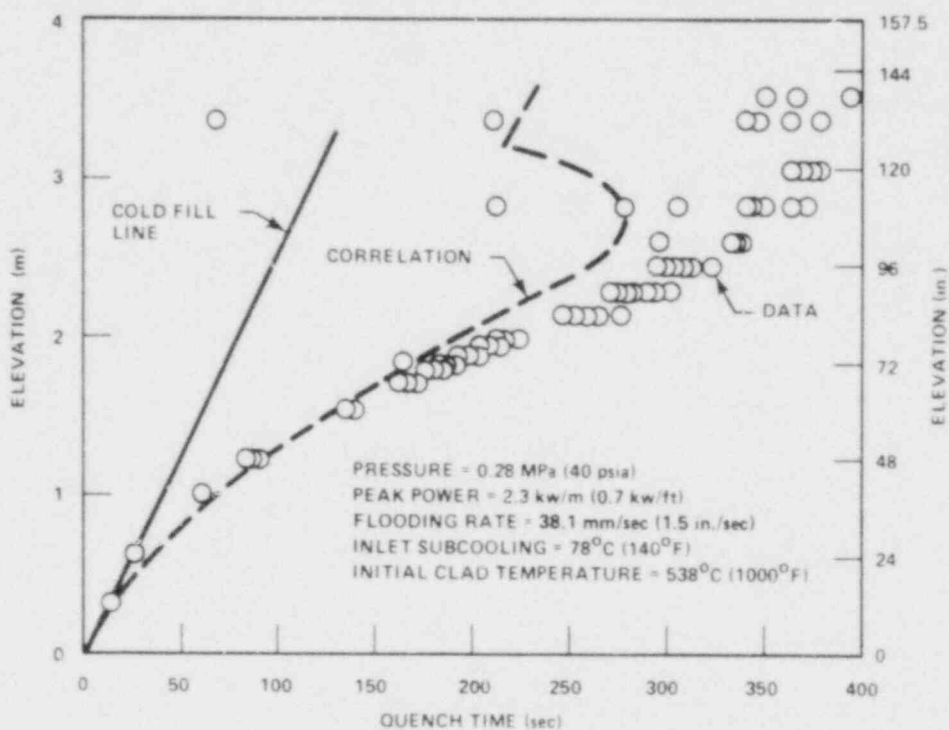


Figure G-1. Quench Correlation Versus Data,
FLECHT SEASET Run 30817

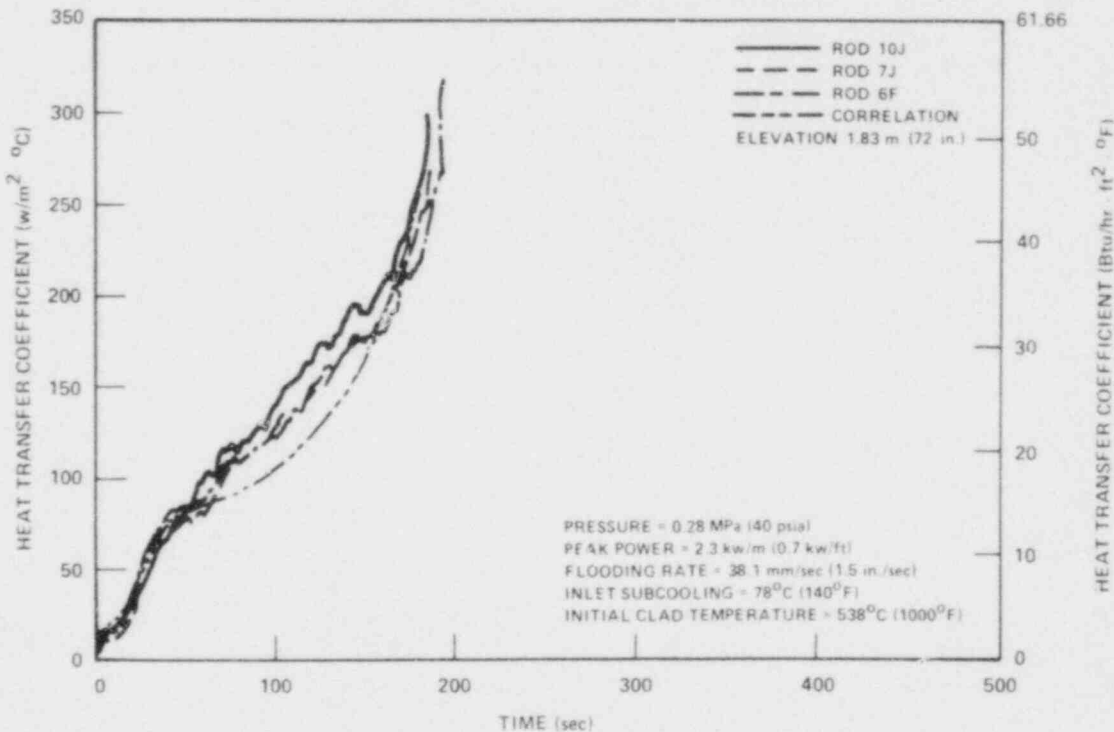


Figure G-2. Heat Transfer Coefficient Correlation Versus Data,
FLECHT SEASET Run 30817

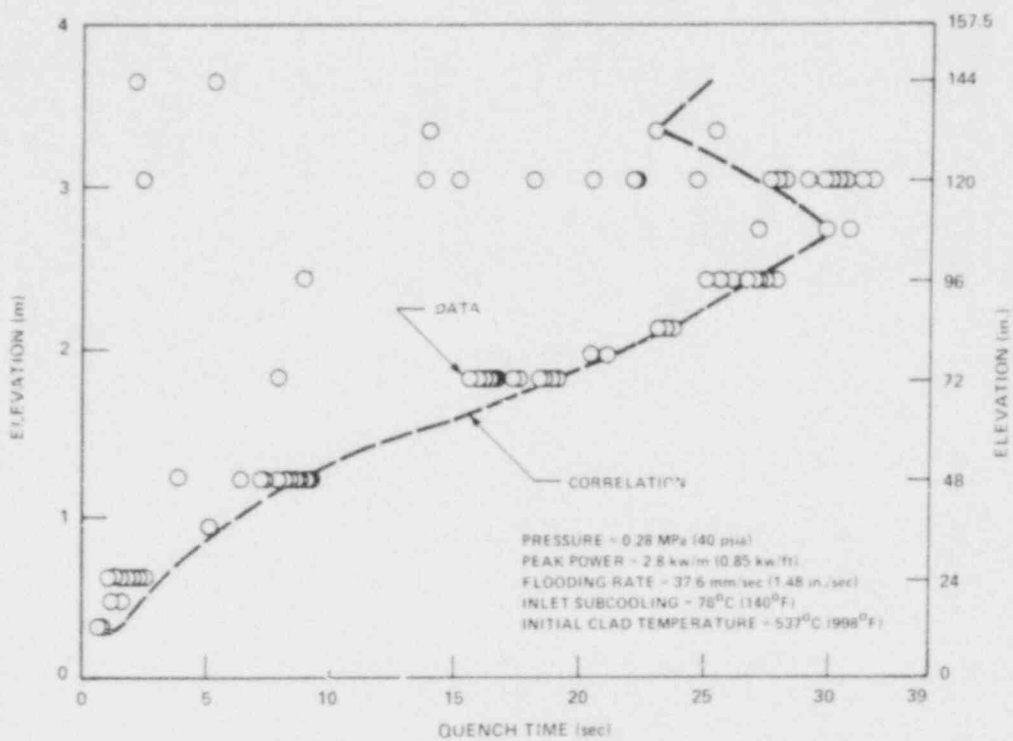


Figure G-3. Quench Correlation Versus Data,
Cosine Power Run 00904

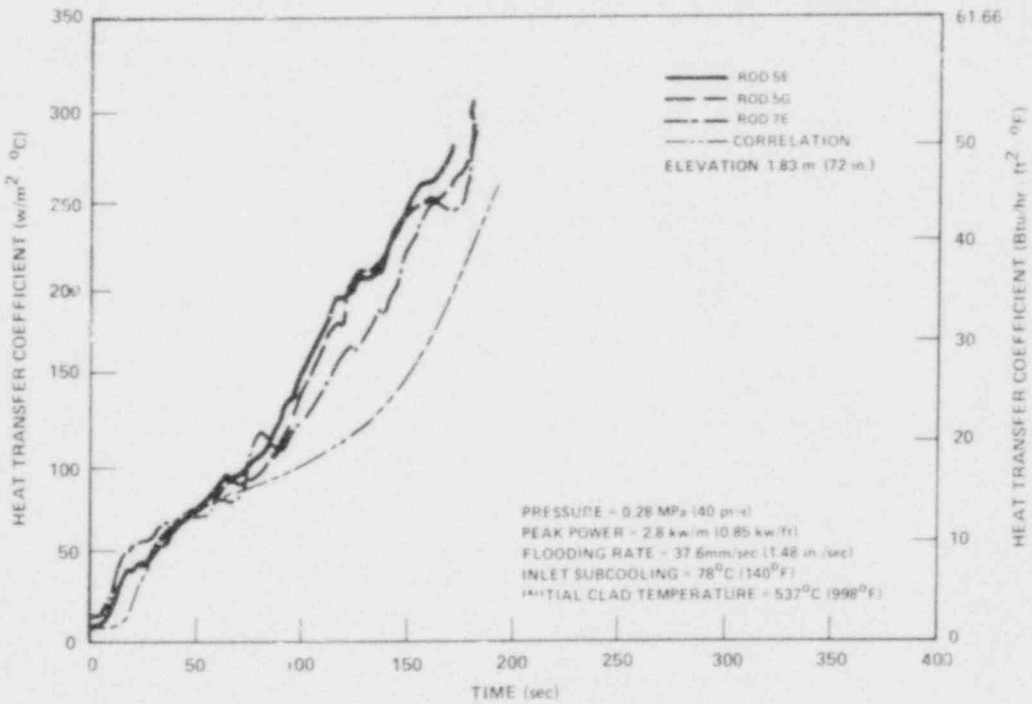


Figure G-4. Heat Transfer Coefficient Correlation Versus Data, Cosine Power Run 00904

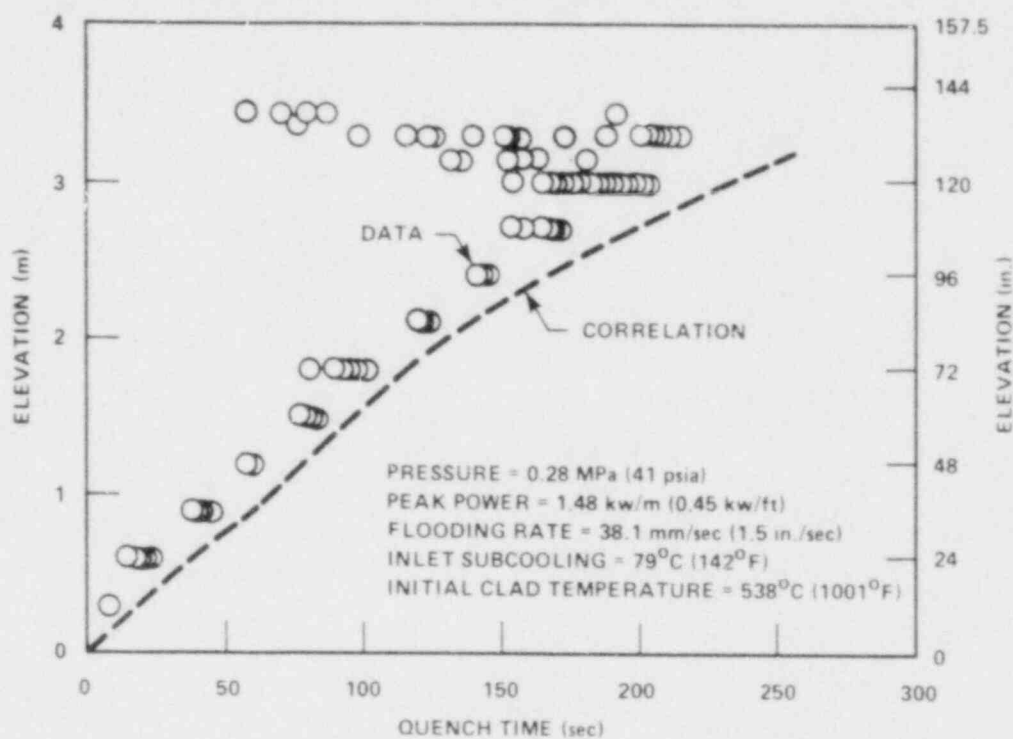


Figure G-5. Quench Correlation Versus Data,
Skewed Power Run 11719

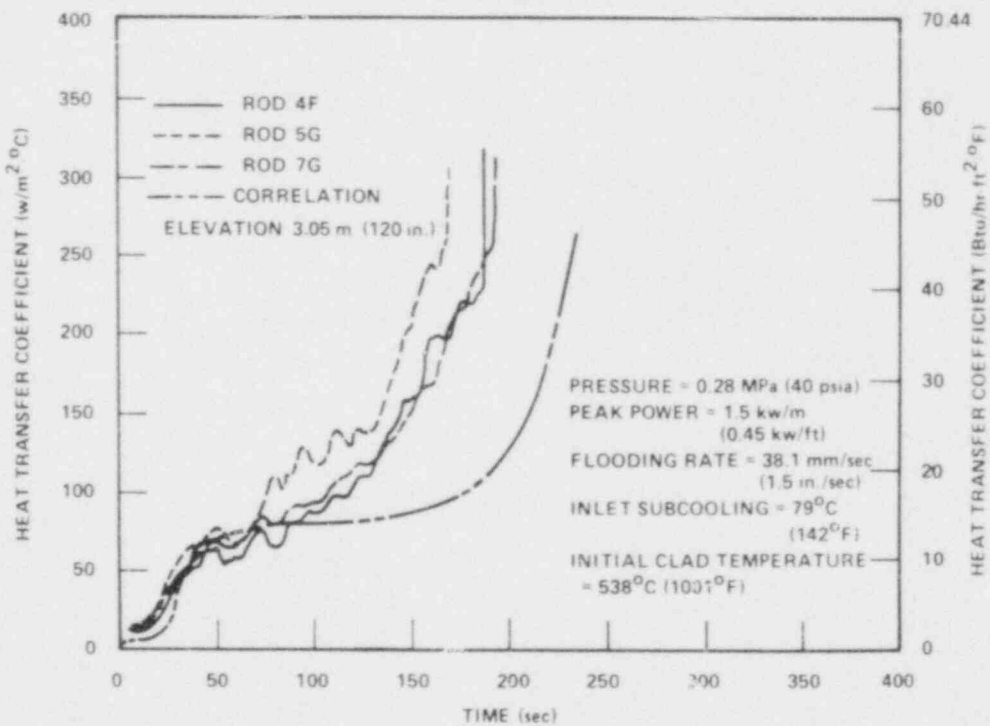


Figure G-6. Heat Transfer Coefficient Correlation
Versus Data, Skewed Power Run 11719

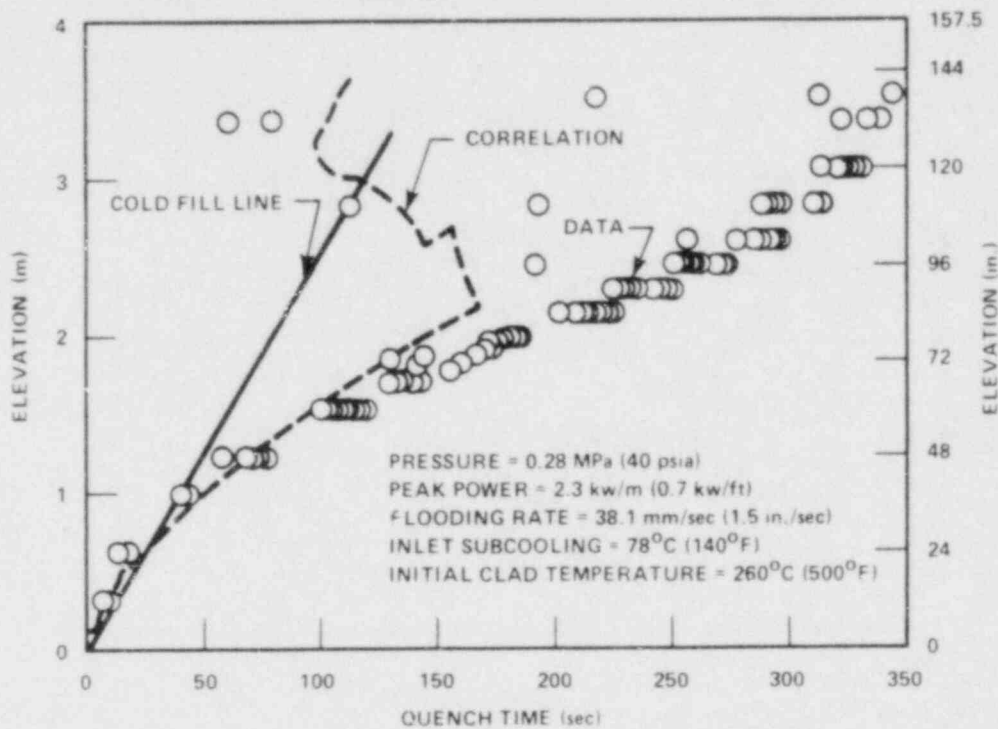


Figure G-7. Quench Correlation Versus Data,
 FLECHT SEASET Run 30518

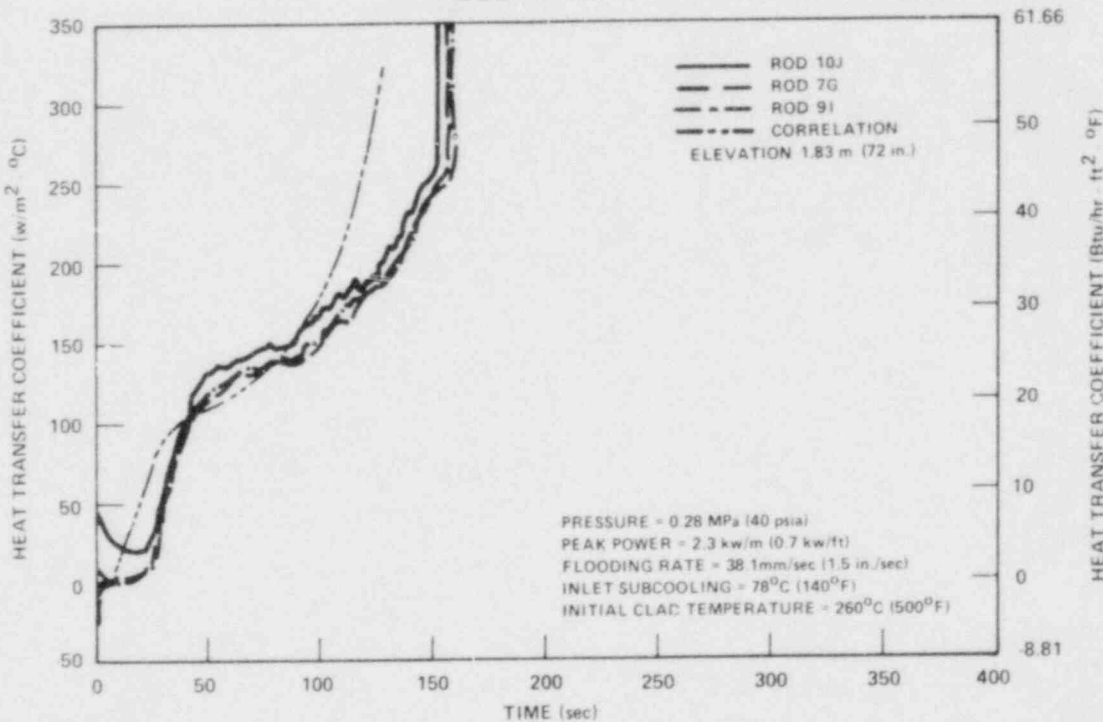


Figure G-8. Heat Transfer Coefficient Correlation
 Versus Data, FLECHT SEASET Run 30518

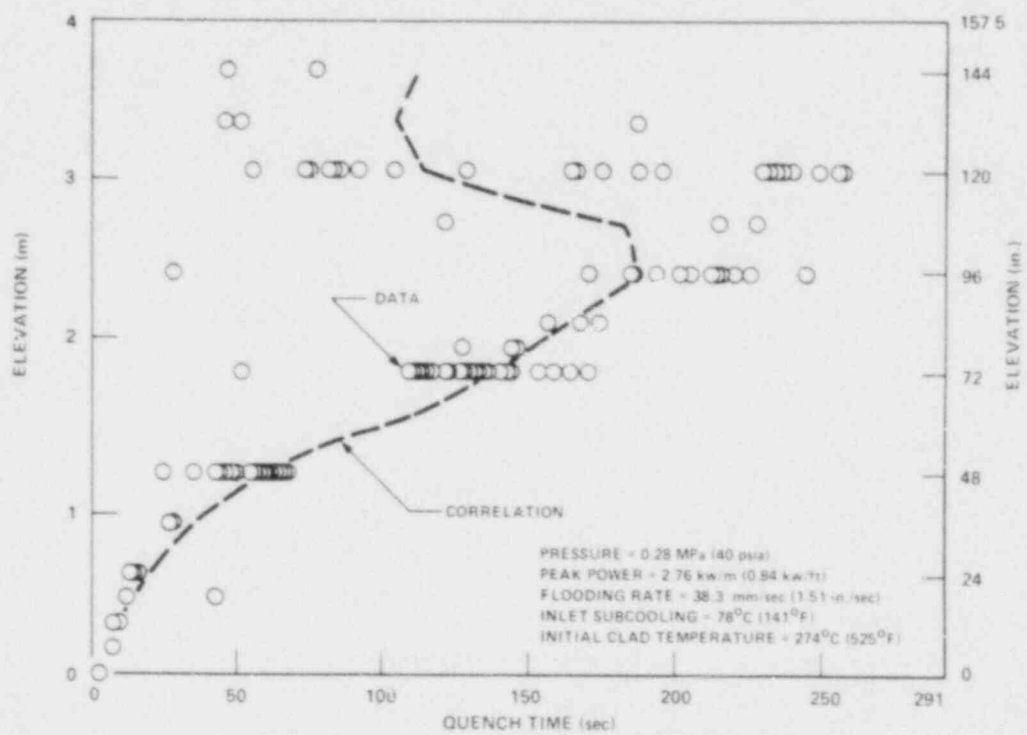


Figure G-9. Quench Correlation Versus Data,
Cosine Power Run 02005

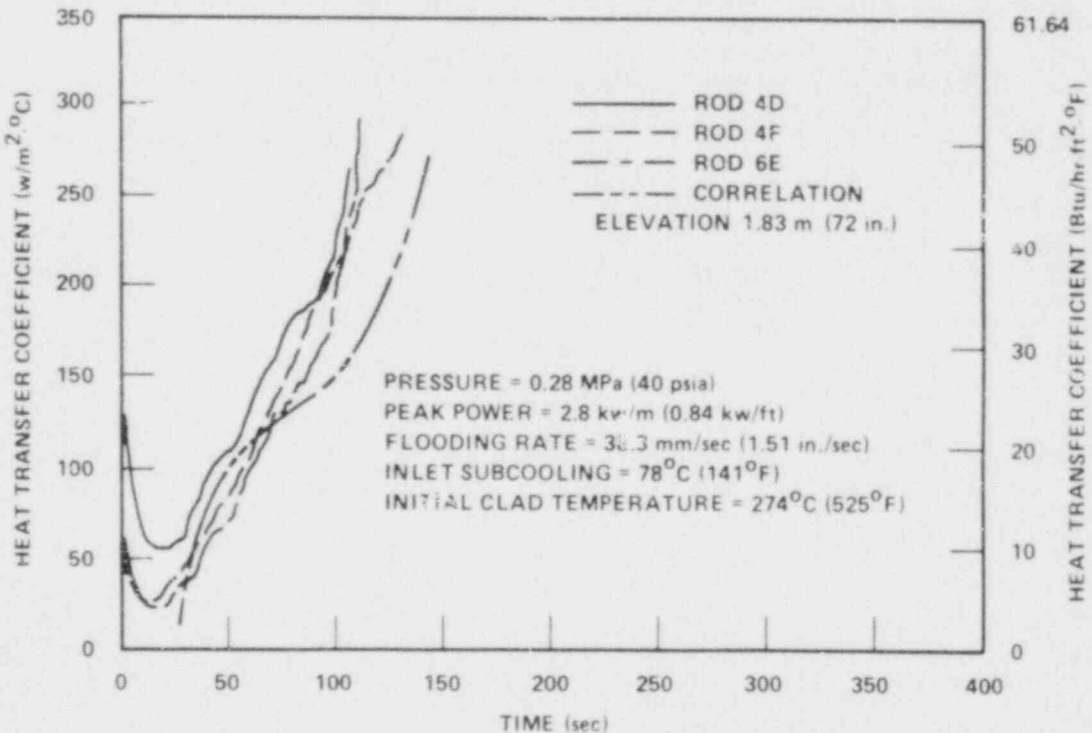


Figure G-10. Heat Transfer Coefficient Correlation
Versus Data, Cosine Power Run 02005

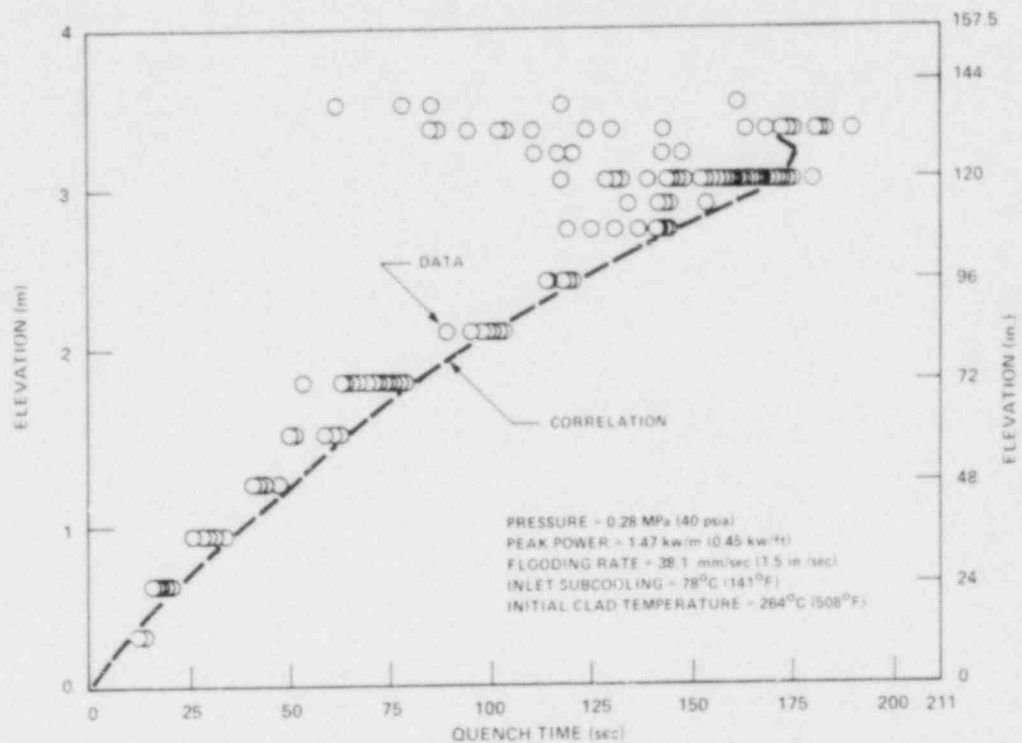


Figure G-11. Quench Correlation Versus Data,
Skewed Power Run 12720

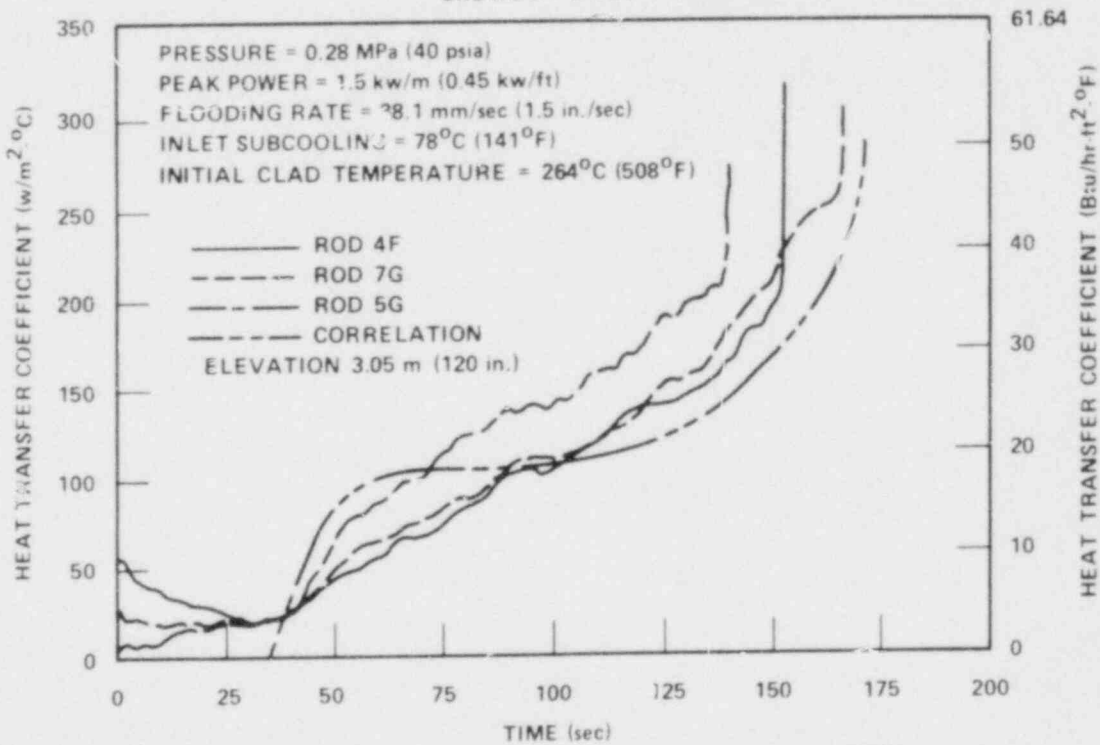


Figure G-12. Heat Transfer Coefficient Correlation
Versus Data, Skewed Power Run 12720

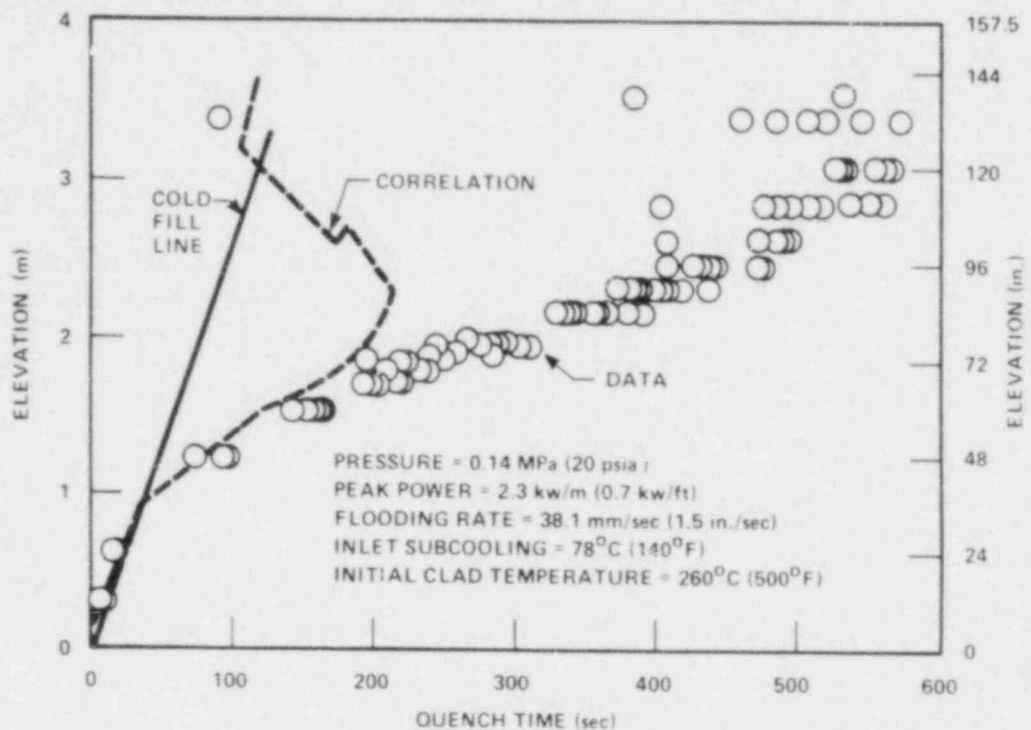


Figure G-13. Quench Correlation Versus Data,
 FLECHT SEASET Run 30619

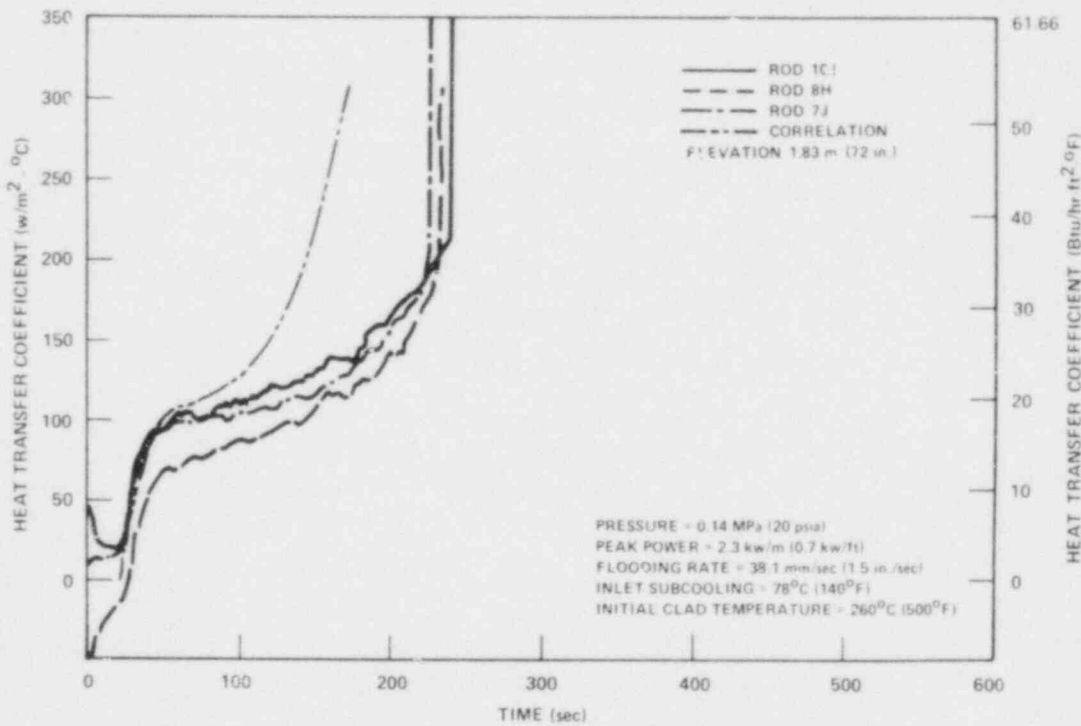


Figure G-14. Heat Transfer Coefficient Correlation
 Versus Data, FLECHT SEASET Run 30619

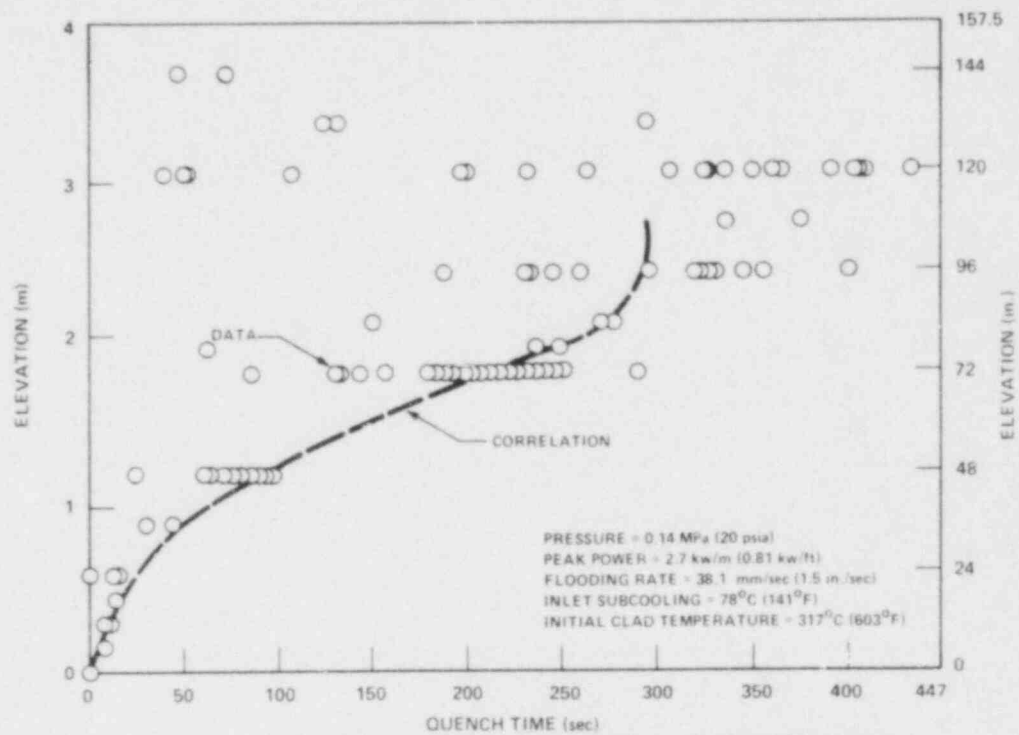


Figure G-15. Quench Correlation Versus Data, Cosine Power Run 03709

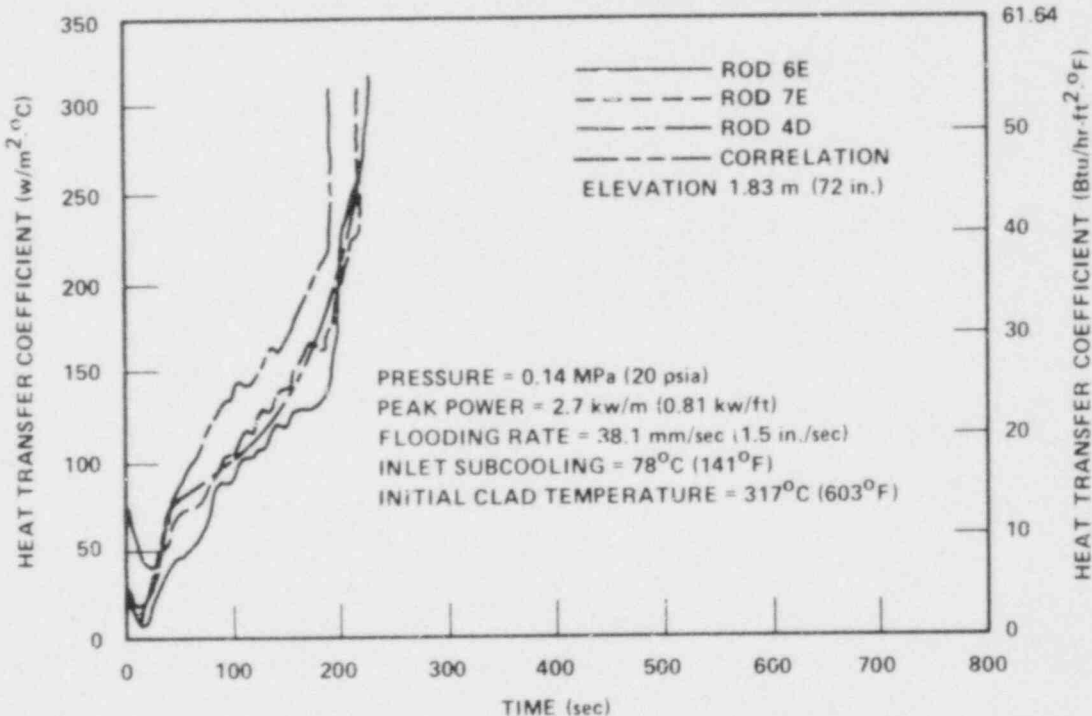


Figure G-16. Heat Transfer Coefficient Correlation Versus Data, Cosine Power Run 03709

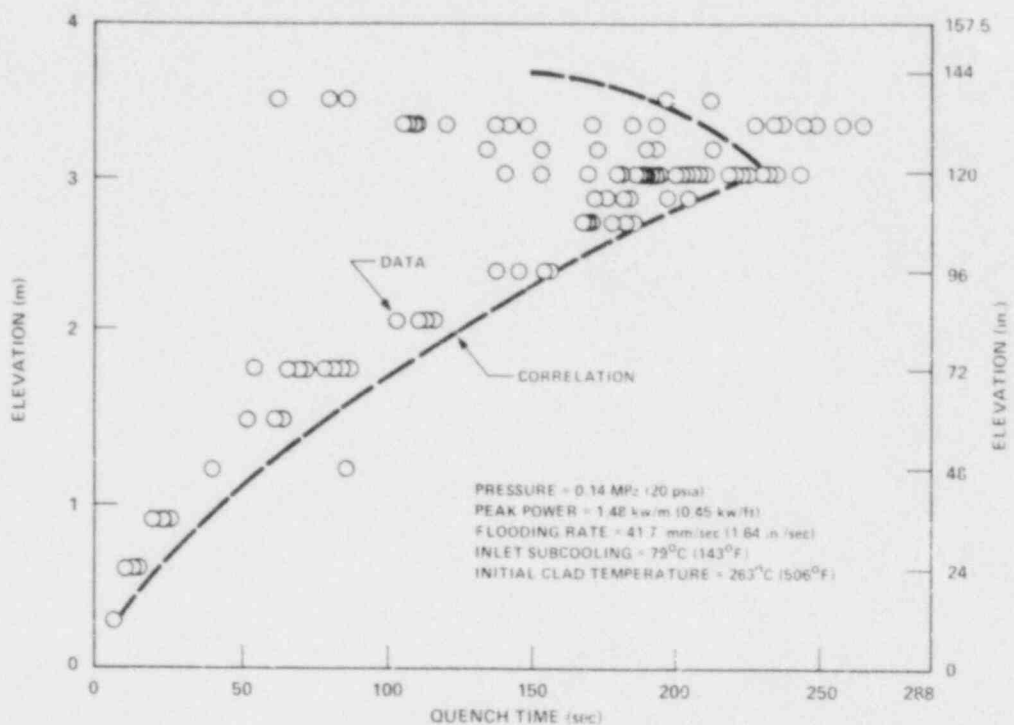


Figure G-17. Quench Correlation Versus Data, Skewed Power Run 11821

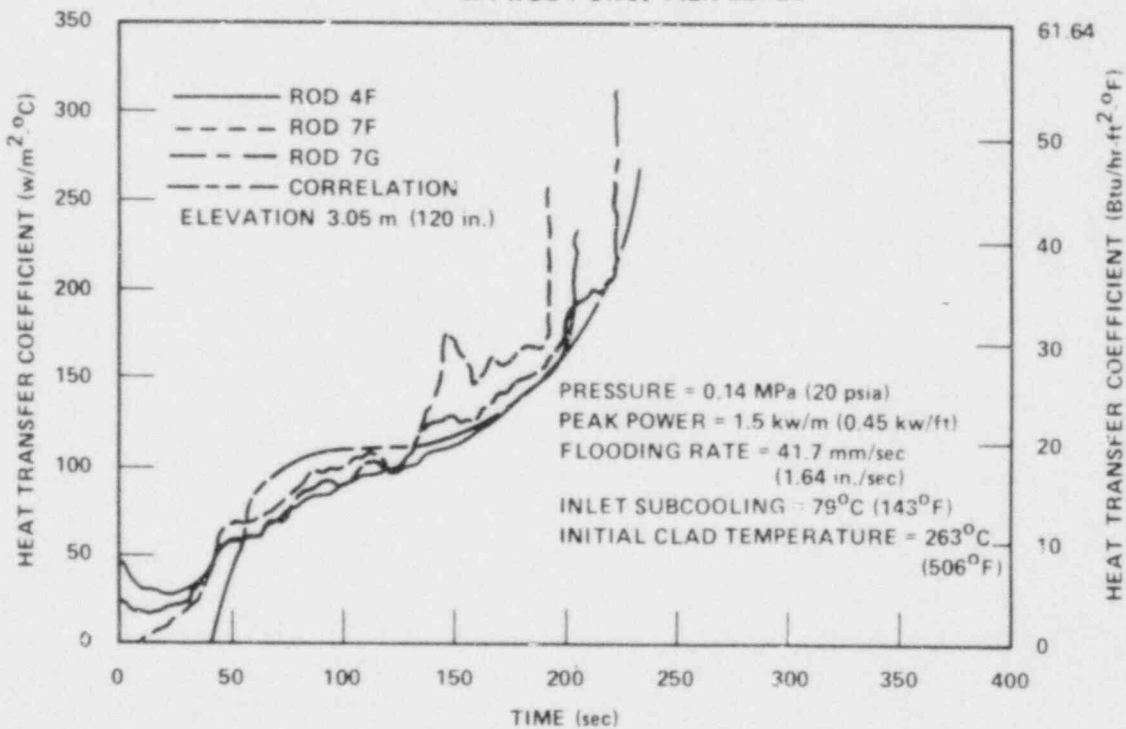


Figure G-18. Heat Transfer Coefficient Correlation Versus Data, Skewed Power Run 11821

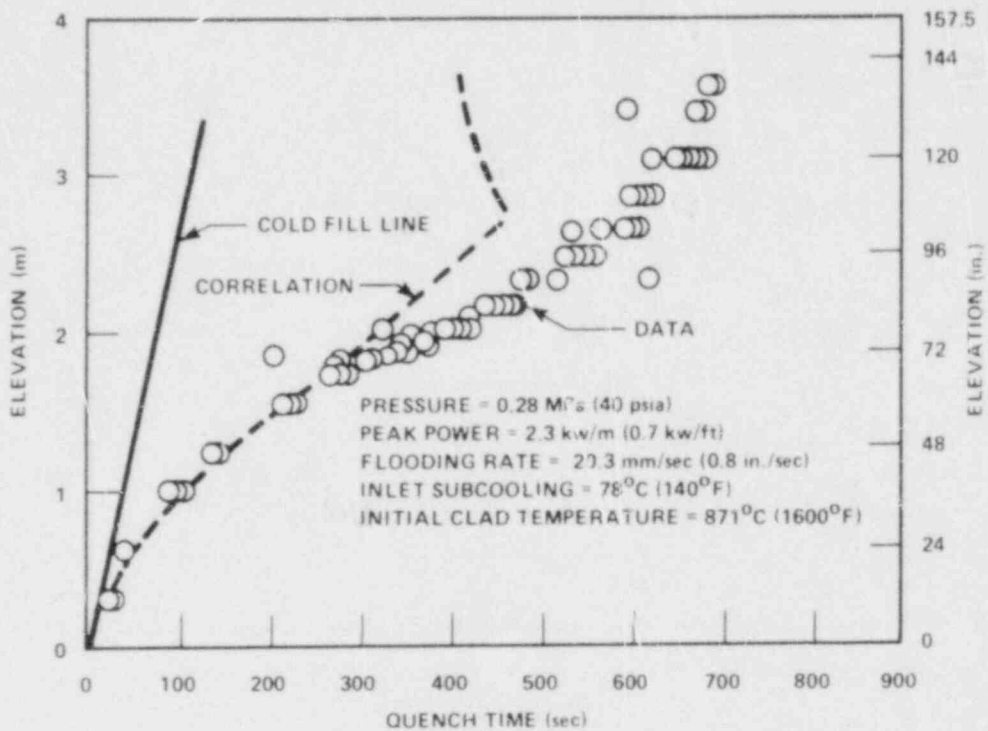


Figure G-19. Quench Correlation Versus Data, FLECHT SEASET Run 31805

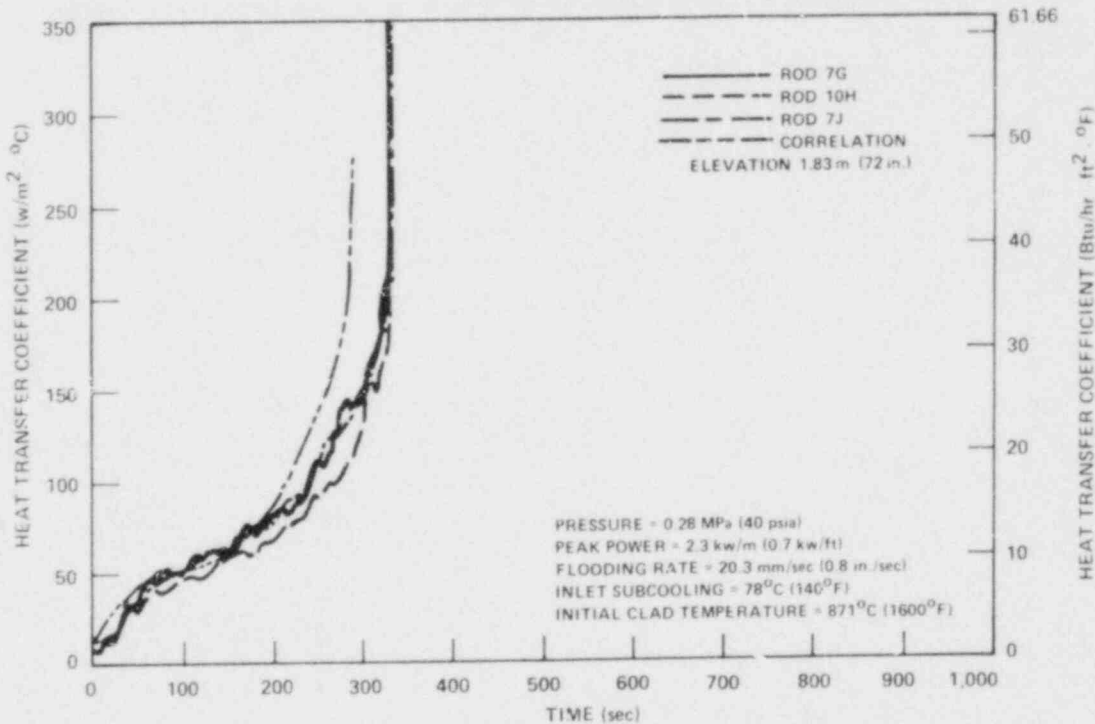


Figure G-20. Heat Transfer Coefficient Correlation Versus Data, FLECHT SEASET Run 31805

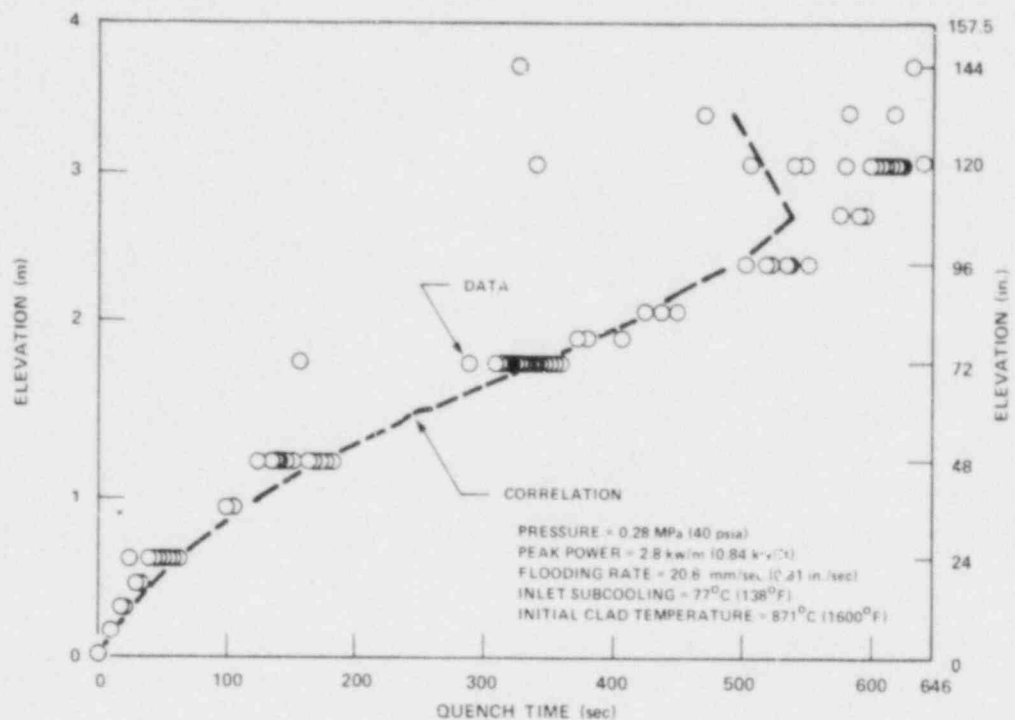


Figure G-21. Quench Correlation Versus Data, Cosine Power Run 02414

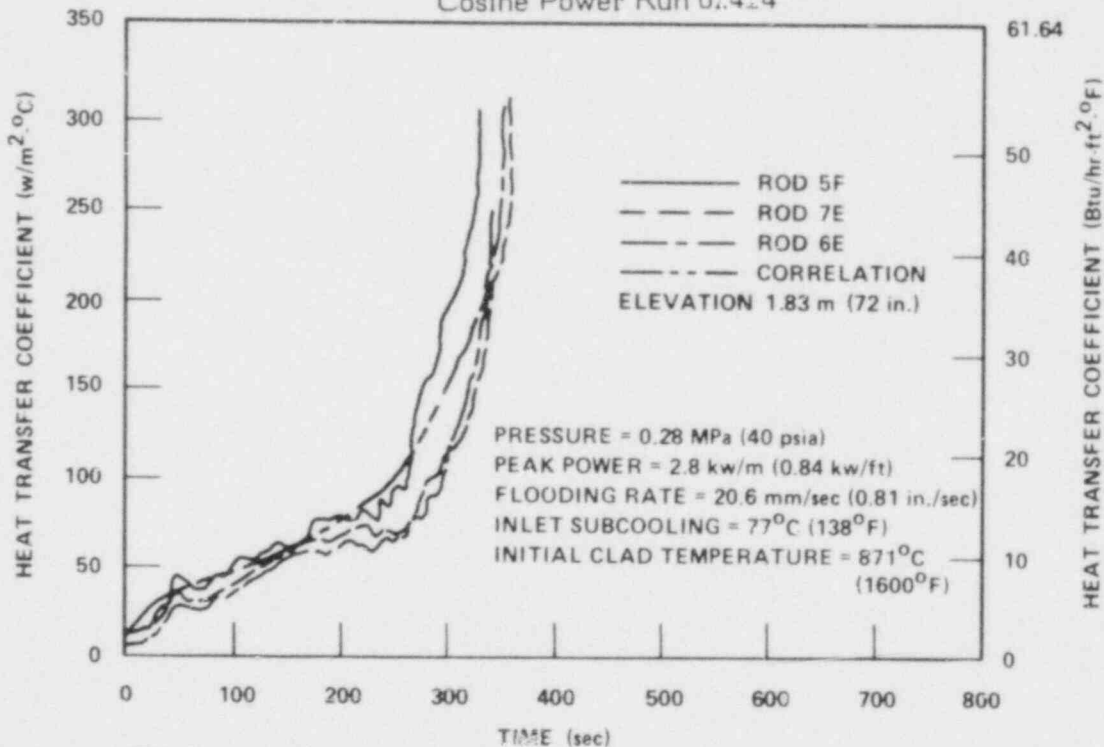


Figure G-22. Heat Transfer Coefficient Correlation Versus Data, Cosine Power Run 02414

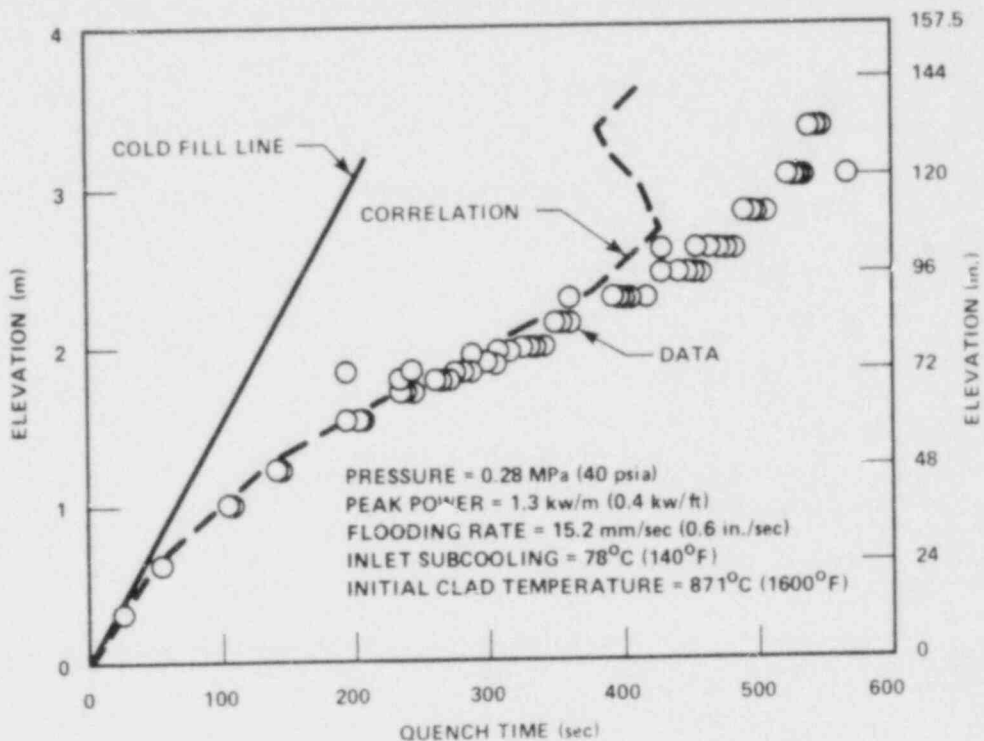


Figure G-23. Quench Correlation Versus Data,
FLECHT SEASET Run 34006

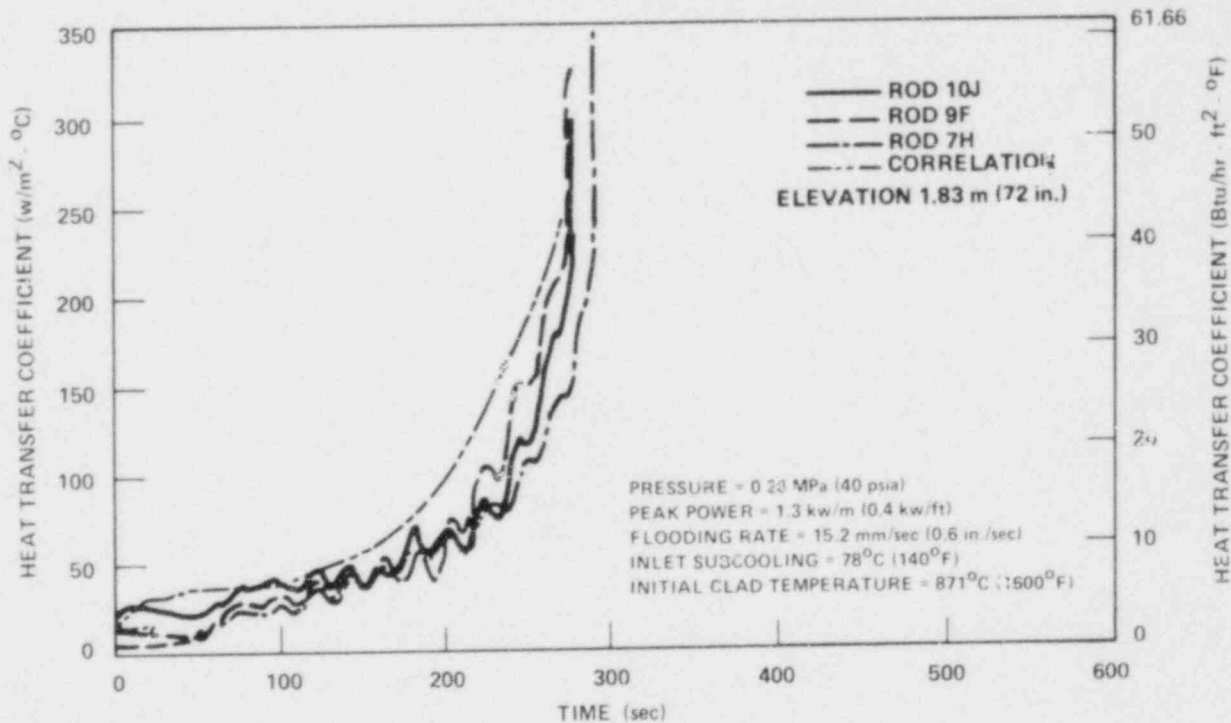


Figure G-24. Heat Transfer Coefficient Correlation
Versus Data, FLECHT SEASET Run 34006

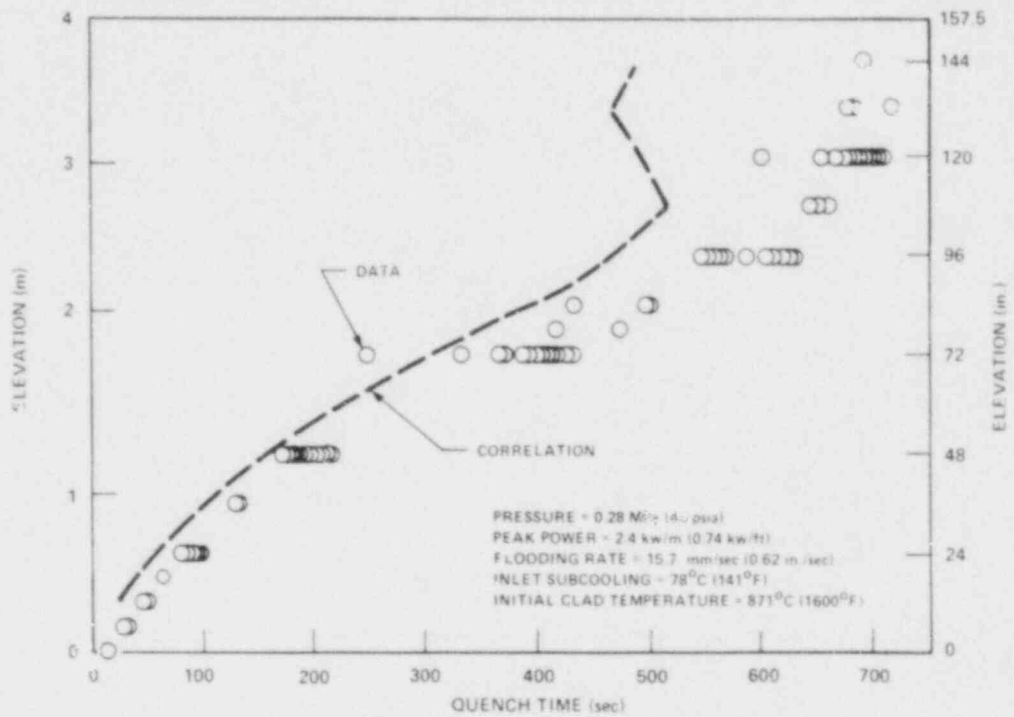


Figure G-25. Quench Correlation Versus Data, Cosine Power Run 07836

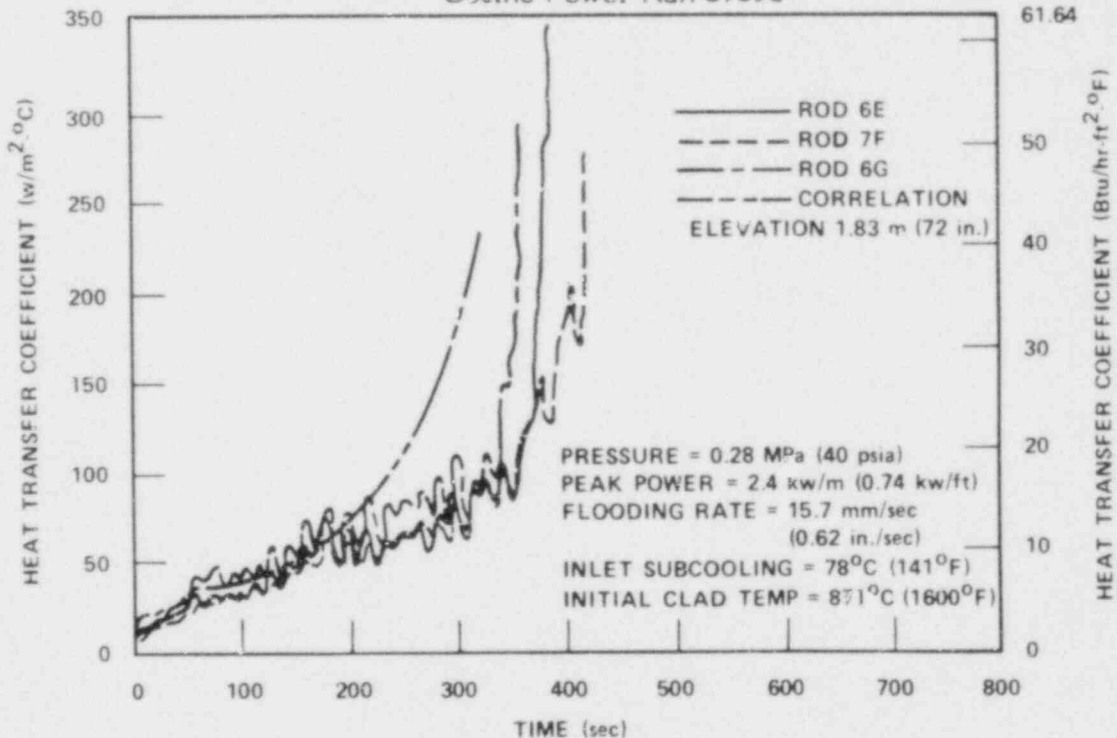


Figure G-26. Heat Transfer Coefficient Correlation Versus Data, Cosine Power Run 07836

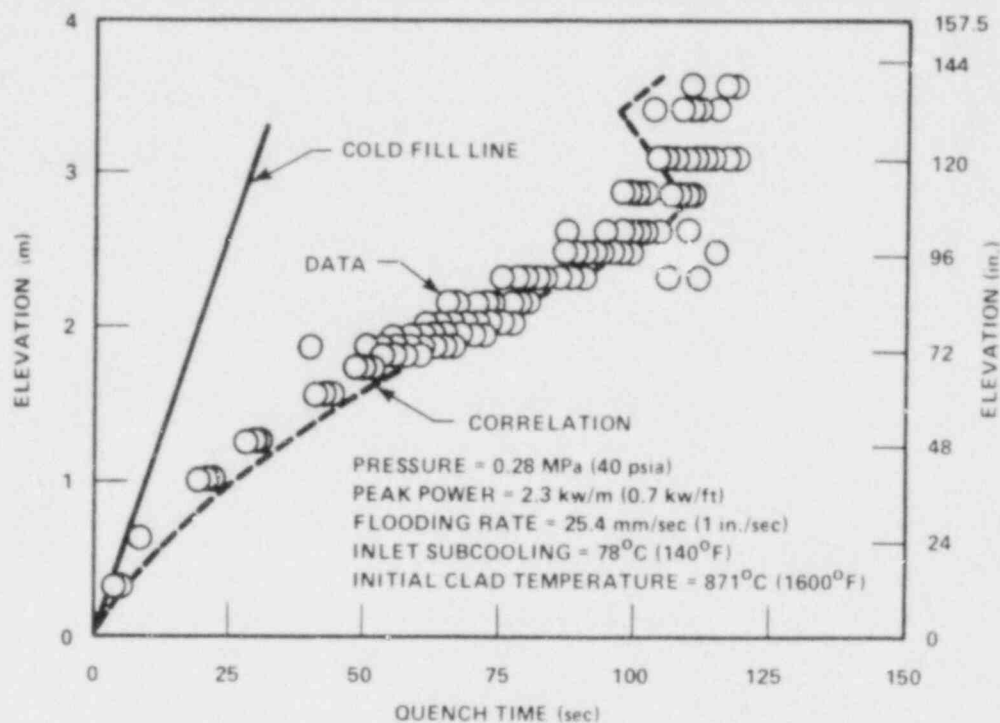


Figure G-27. Quench Correlation Versus Data, FLECHT SEASET Run 36026

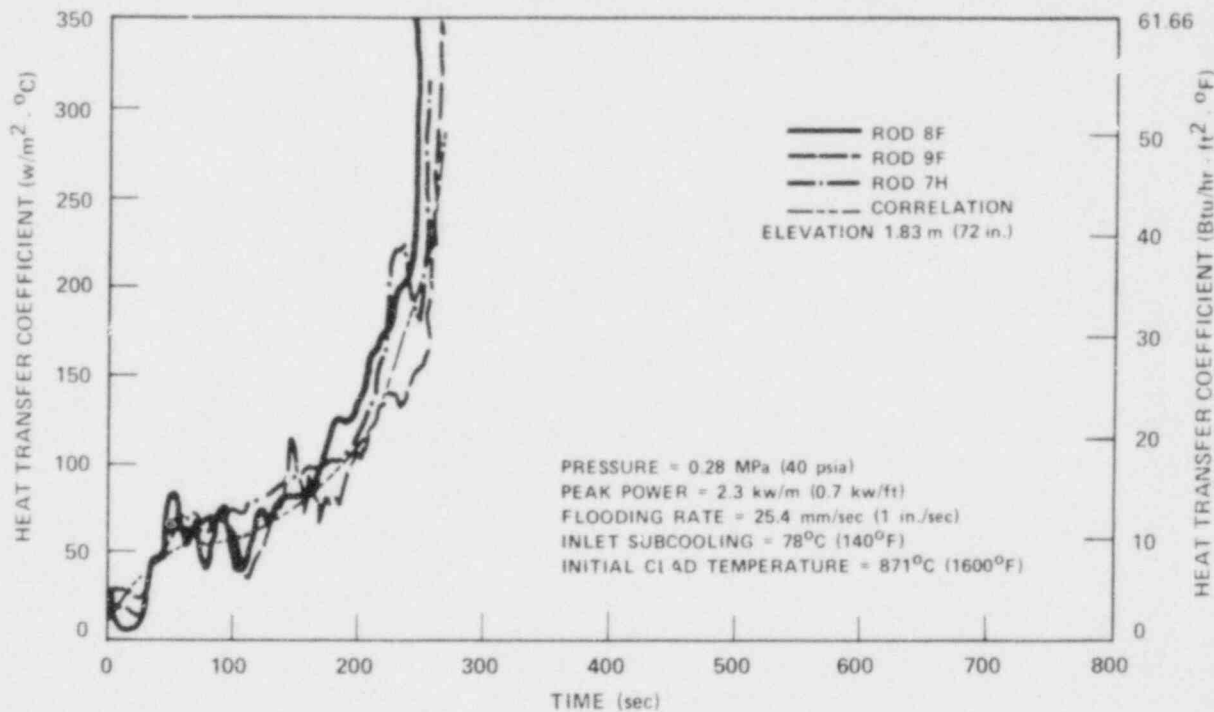


Figure G-28. Heat Transfer Coefficient Correlation Versus Data, FLECHT SEASET Run 36026

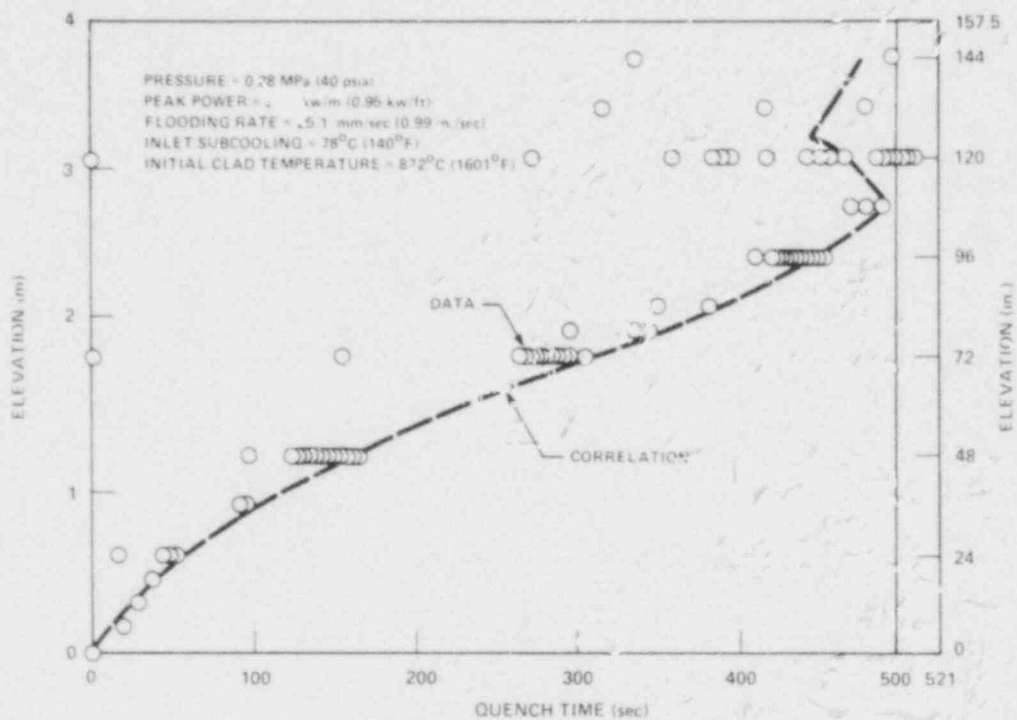


Figure G-29. Quench Correlation V_e vs Data,
 Cosine Power Run 05131

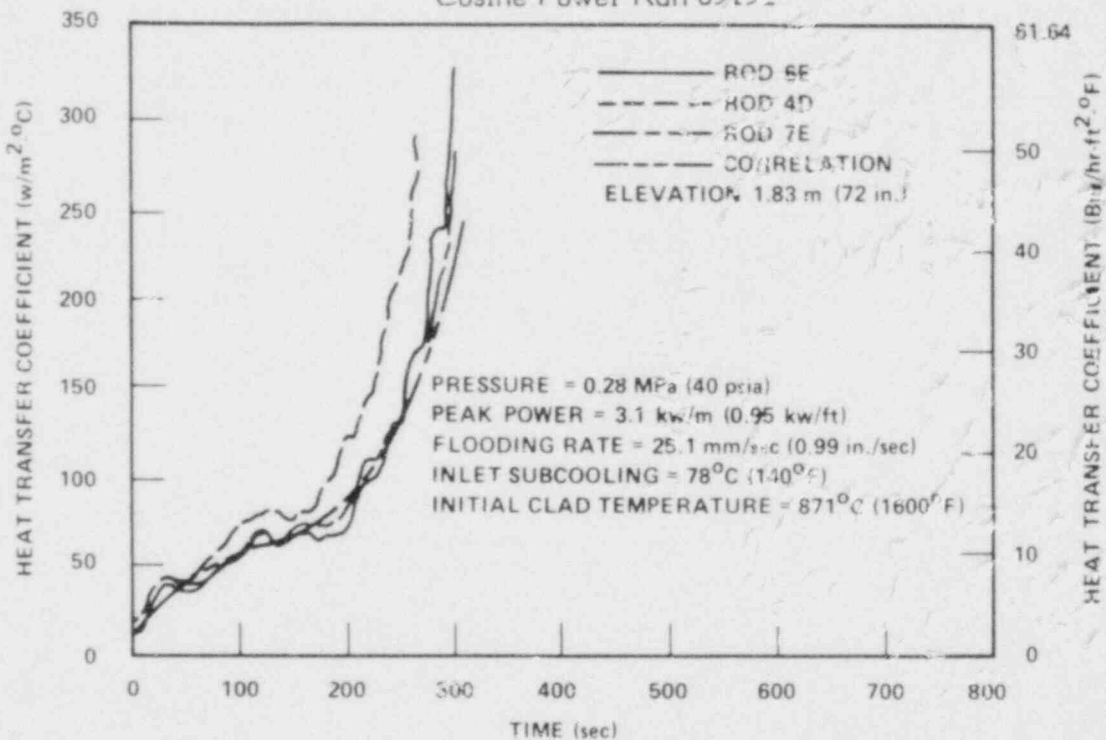


Figure G-30. Heat Transfer Coefficient Correlation
 Versus Data, Cosine Power Run 05132

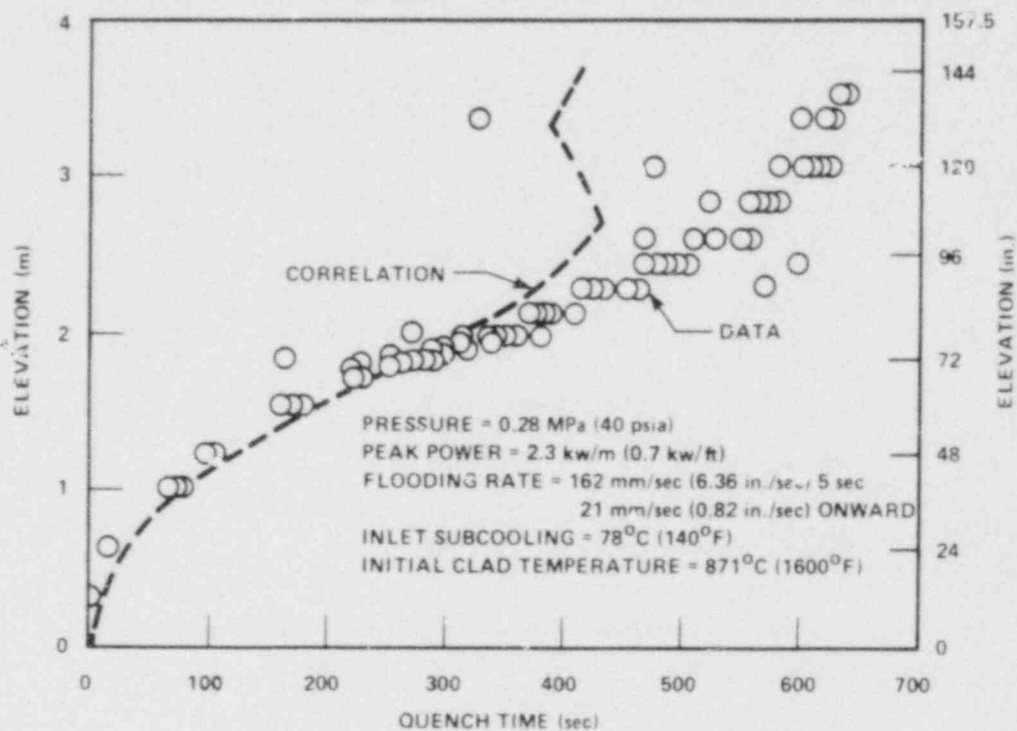


Figure G-31. Quench Correlation Versus Data,
FLECHT SEASET Run 32333

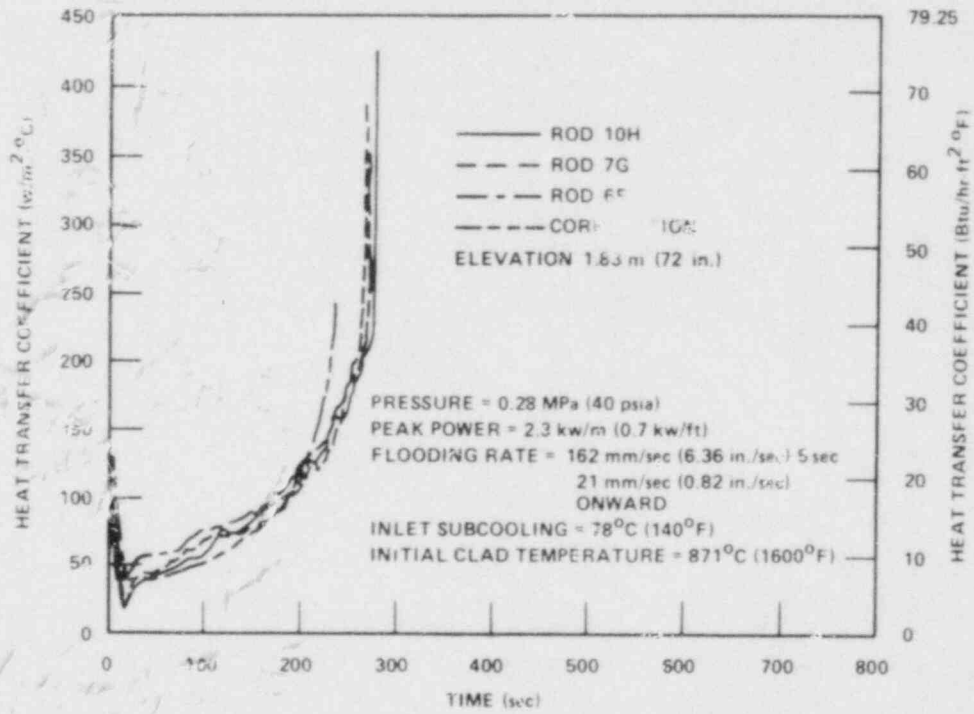


Figure G-32. Heat Transfer Coefficient Correlation
Versus Data, FLECHT SEASET Run 32333

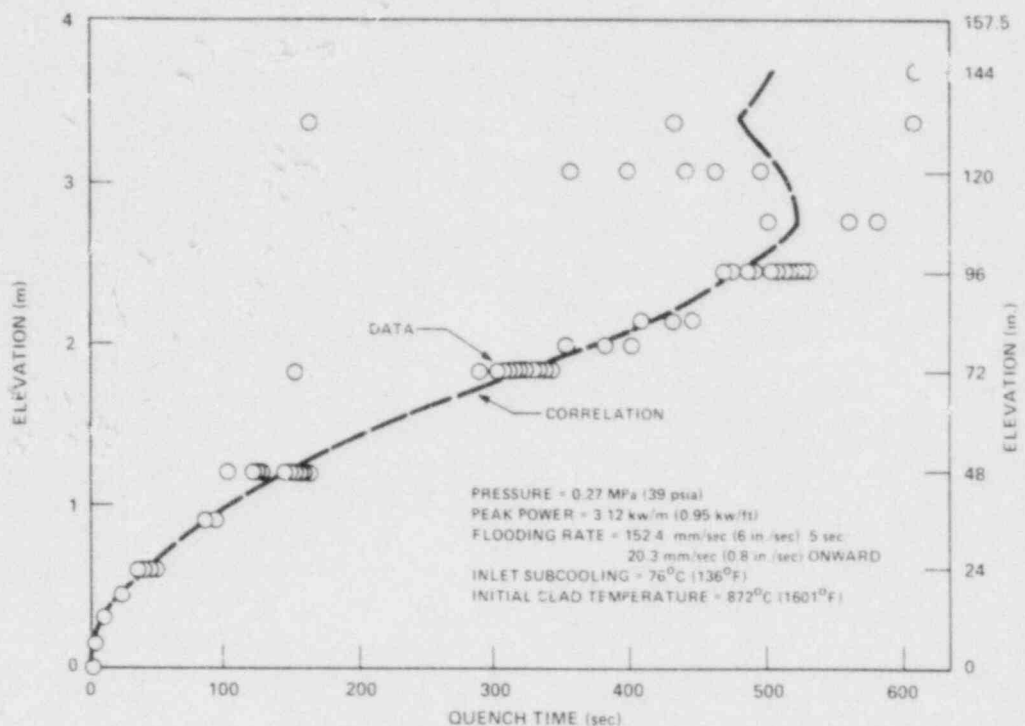


Figure G-33. Quench Correlation Versus Data, Cosine Power Run 04516

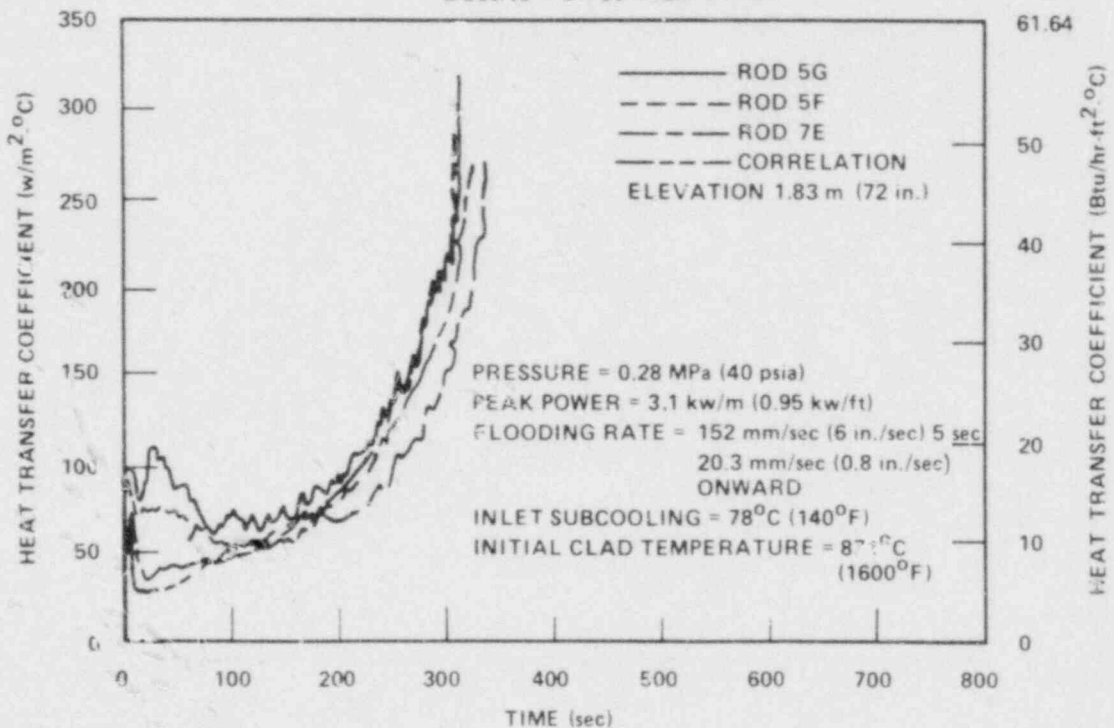


Figure G-34. Heat Transfer Coefficient Correlation Versus Data, Cosine Power Run 04516

APPENDIX H

COMPARISON OF HEAT TRANSFER CORRELATION WITH DATA FOR NONOVERLAP RUNS

Data from the FLECHT SEASET nonoverlap runs (table H-1) are compared with the correlation of this work in figures H-1 through H-16. Data from the cosine power test nonoverlap runs (table H-2) are compared with the correlation in figures H-17 through H-26. Data from the skewed power test nonoverlap runs (table H-3) are compared with the correlation in figures H-27 through H-40.

TABLE H-1
FLECHT SEASET NONOVERLAP RUN DATA

Run	Peak Power [kw/m (kw/ft)]	Flooding Rate [mm/sec (in./sec)]	Initial Clad Temperature [°C (°F)]	Inlet Subcooling [°C (°F)]	Pressure [MPa (psia)]
31701	2.3 (0.7)	152 (6)	871 (1600)	78 (140)	0.28 (40)
31302	2.3 (0.7)	76 (3)	871 (1600)	78 (140)	0.28 (40)
31504	2.3 (0.7)	25.4 (1)	871 (1600)	78 (140)	0.28 (40)
34209	2.3 (0.7)	25.4 (1)	871 (1600)	78 (140)	0.14 (20)
32013	2.3 (0.7)	25.4 (1)	871 (1600)	78 (140)	0.41 (60)
35114	2.3 (0.7)	25.4 (1)	871 (1600)	2.7 (5)	0.28 (40)
31922	1.3 (0.4)	25.4 (1)	871 (1600)	78 (140)	0.14 (20)
32235	2.3 (0.7)	152 → 25.4 → 15.2 (6 → 1 → 0.6)	871 (1600)	78 (140)	0.14 (20)

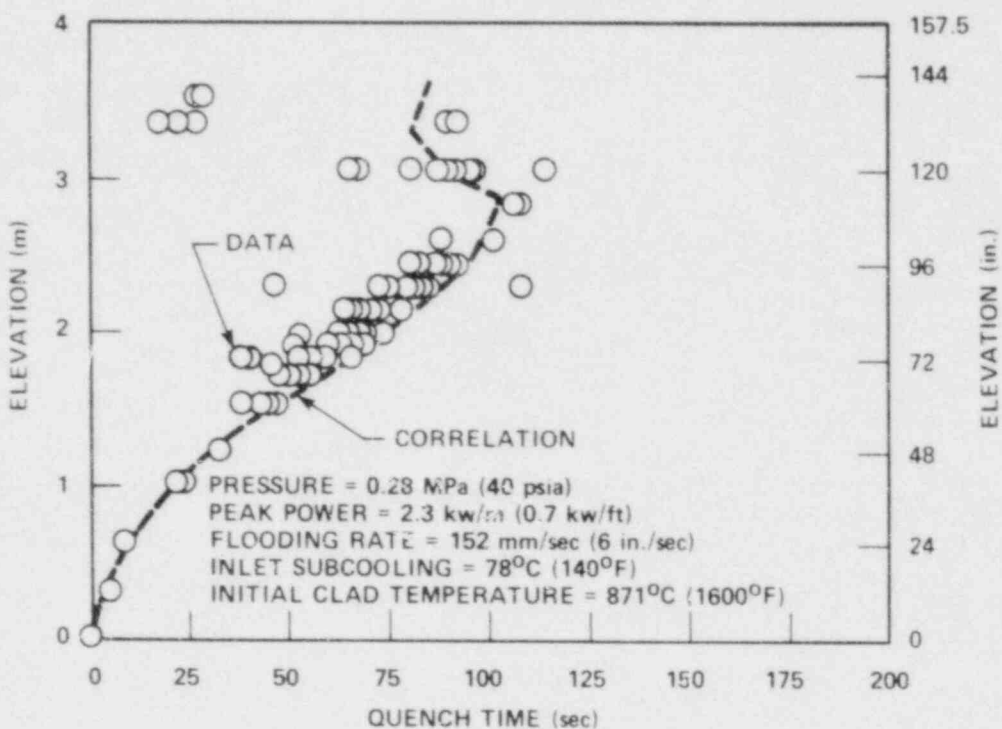


Figure H-1. Quench Correlation Versus Data,
FLECHT SEASET Run 31701

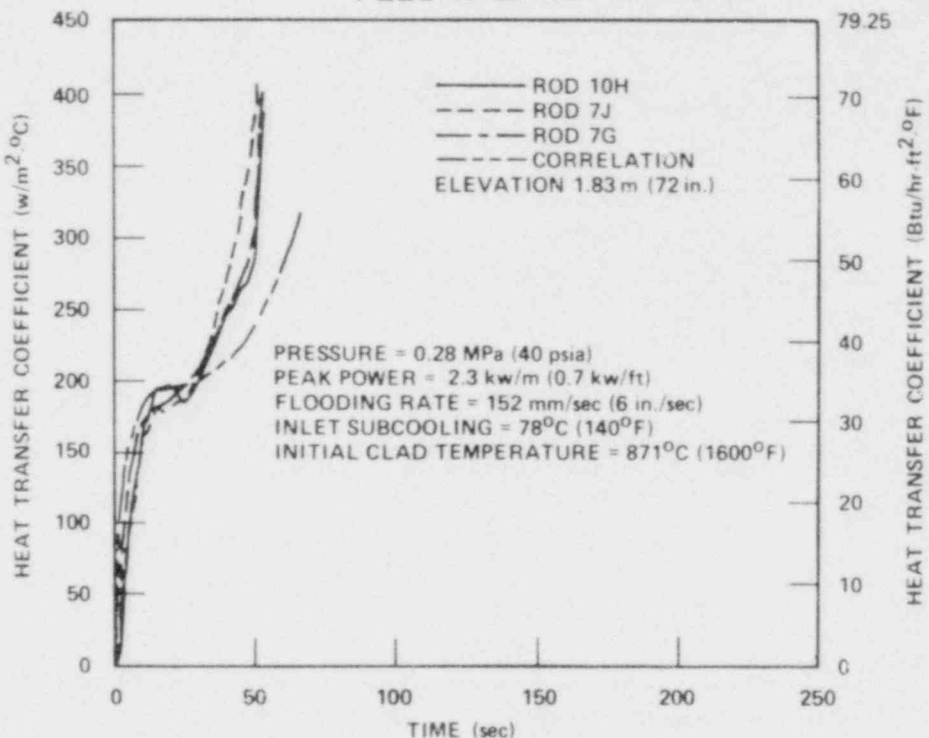


Figure H-2. Heat Transfer Coefficient Correlation
Versus Data, FLECHT SEASET Run 31701

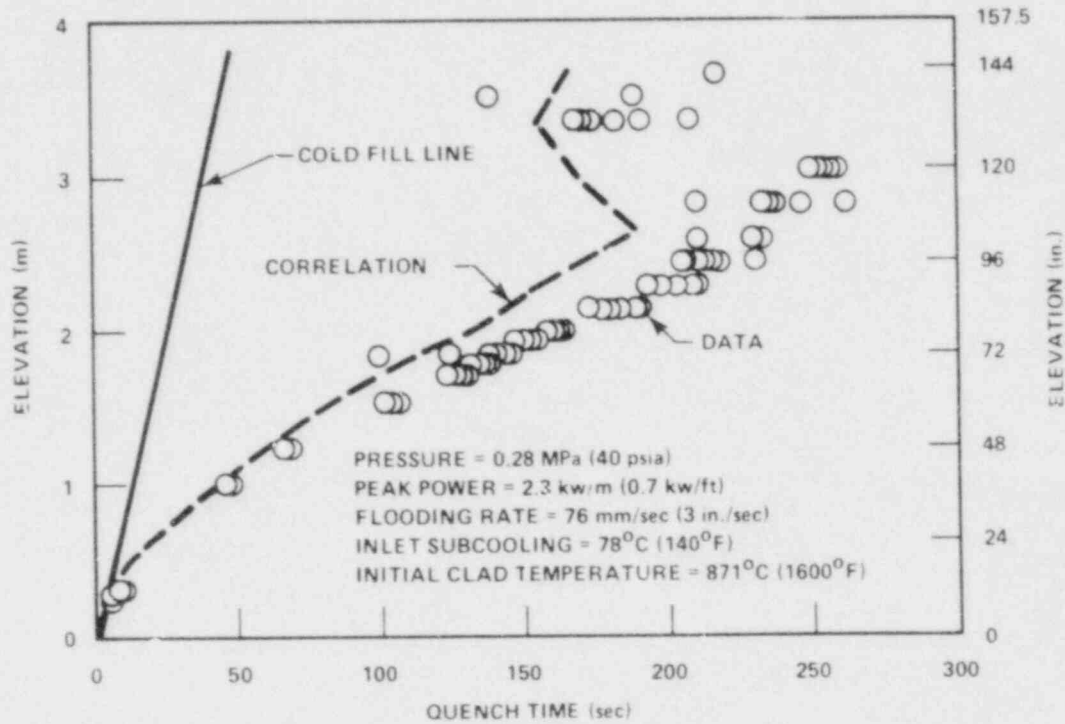


Figure H-3. Quench Correlation Versus Data,
 FLECHT SEASET Run 31302

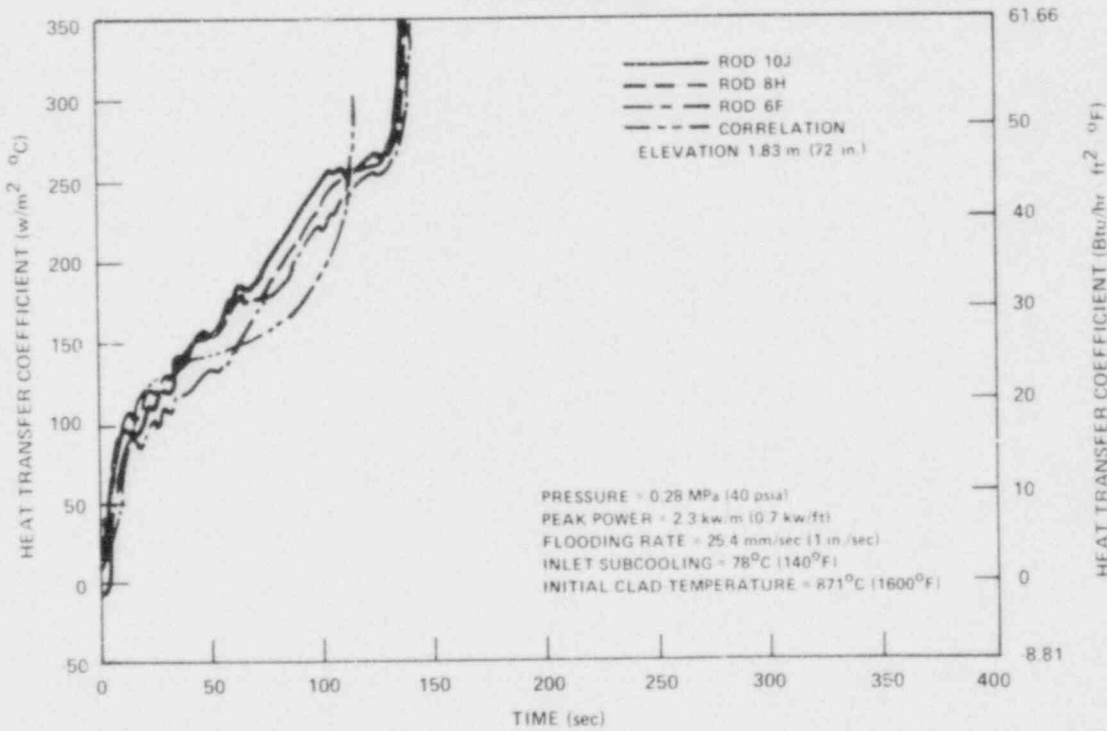


Figure H-4. Heat Transfer Coefficient Correlation Versus Data,
 FLECHT SEASET Run 31302

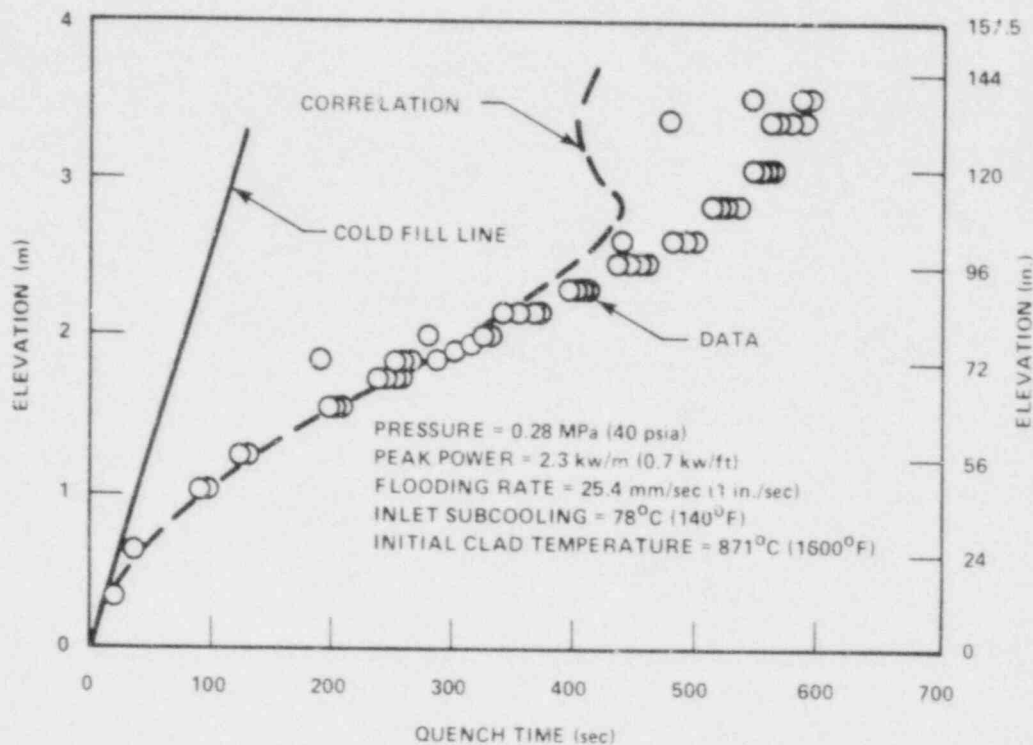


Figure H-5. Quench Correlation Versus Data,
FLECHT SEASET Run 31504

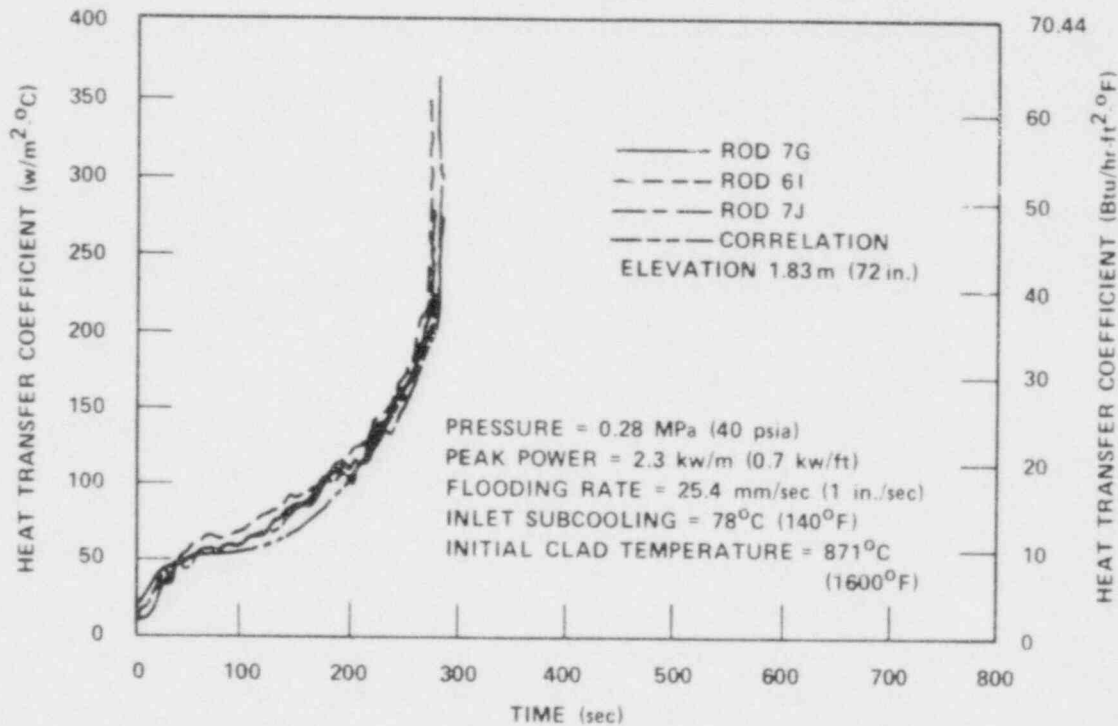


Figure H-6. Heat Transfer Coefficient Correlation
Versus Data, FLECHT SEASET Run 31504

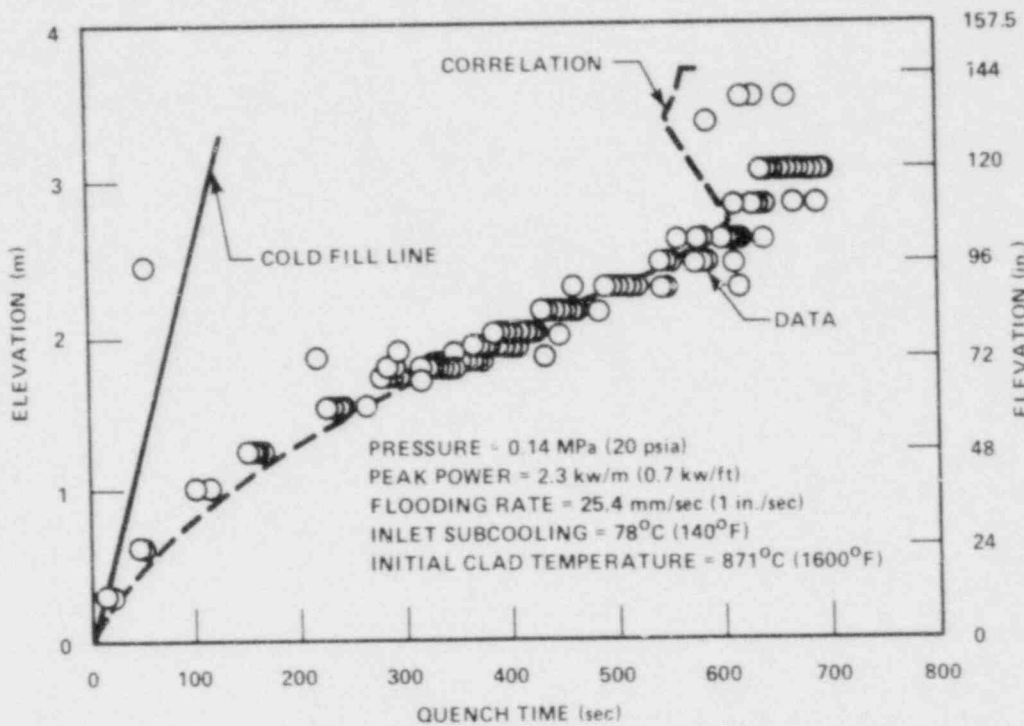


Figure H-7. Quench Correlation Versus Data,
FLECHT SEASET Run 34209

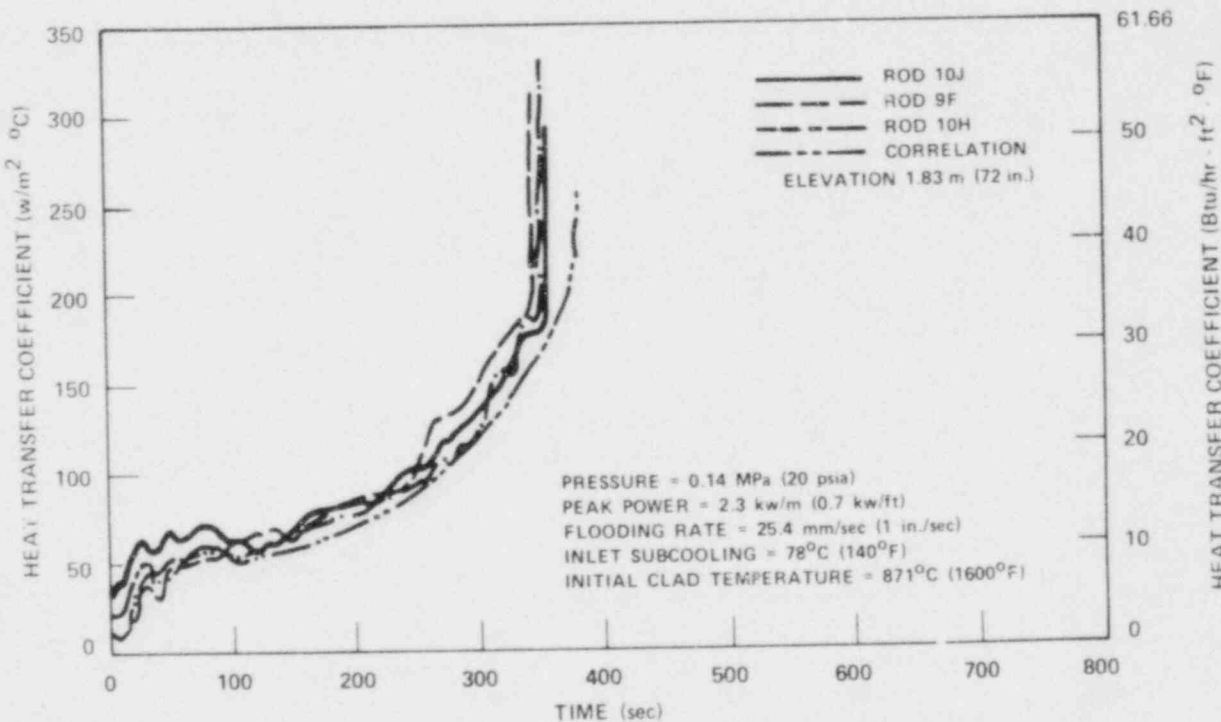


Figure H-8. Heat Transfer Coefficient Correlation
Versus Data, FLECHT SEASET Run 34209

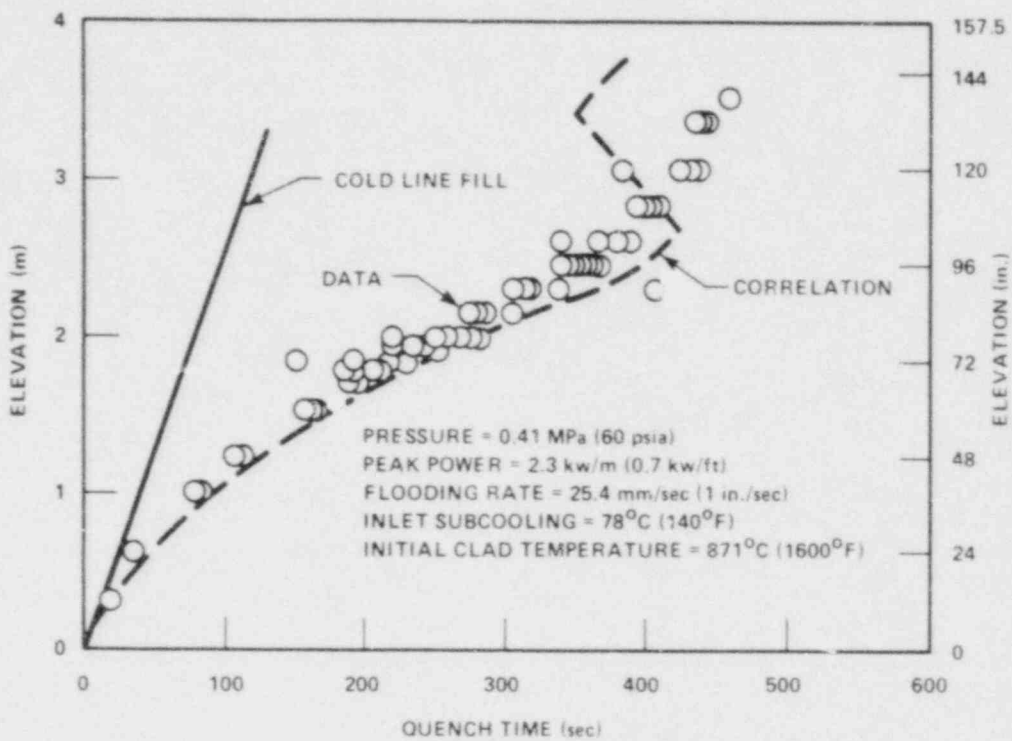


Figure H-9. Quench Correlation Versus Data,
 FLECHT SEASET Run 32013

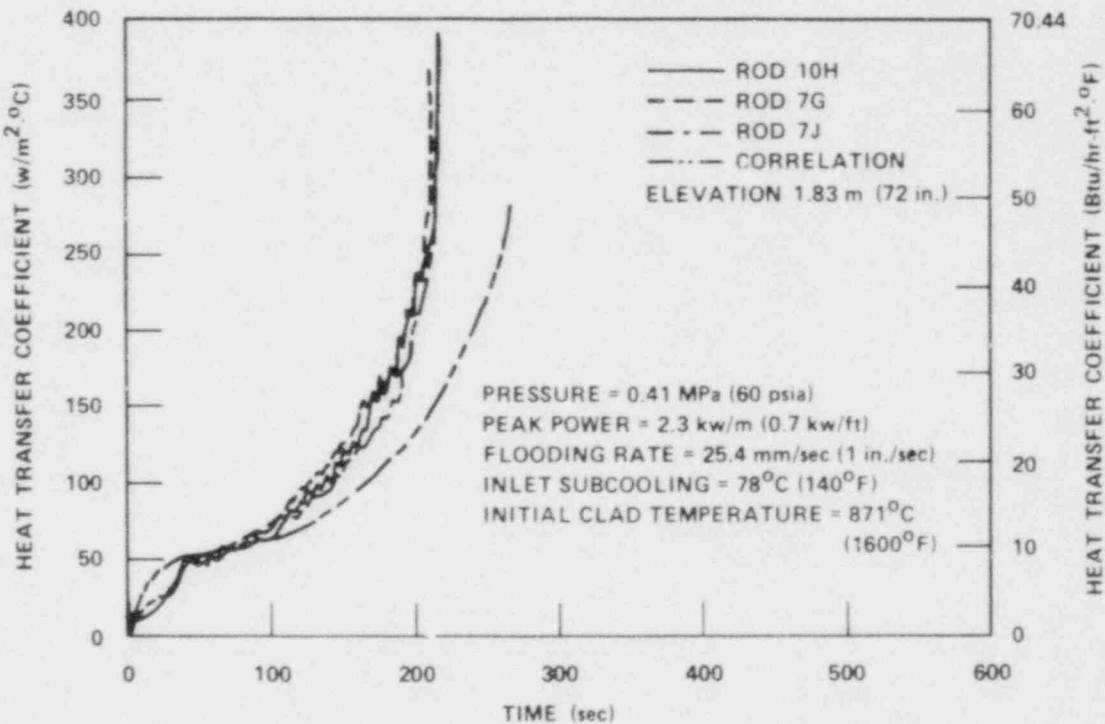


Figure H-10. Heat Transfer Coefficient Correlation
 Versus Data, FLECHT SEASET Run 32013

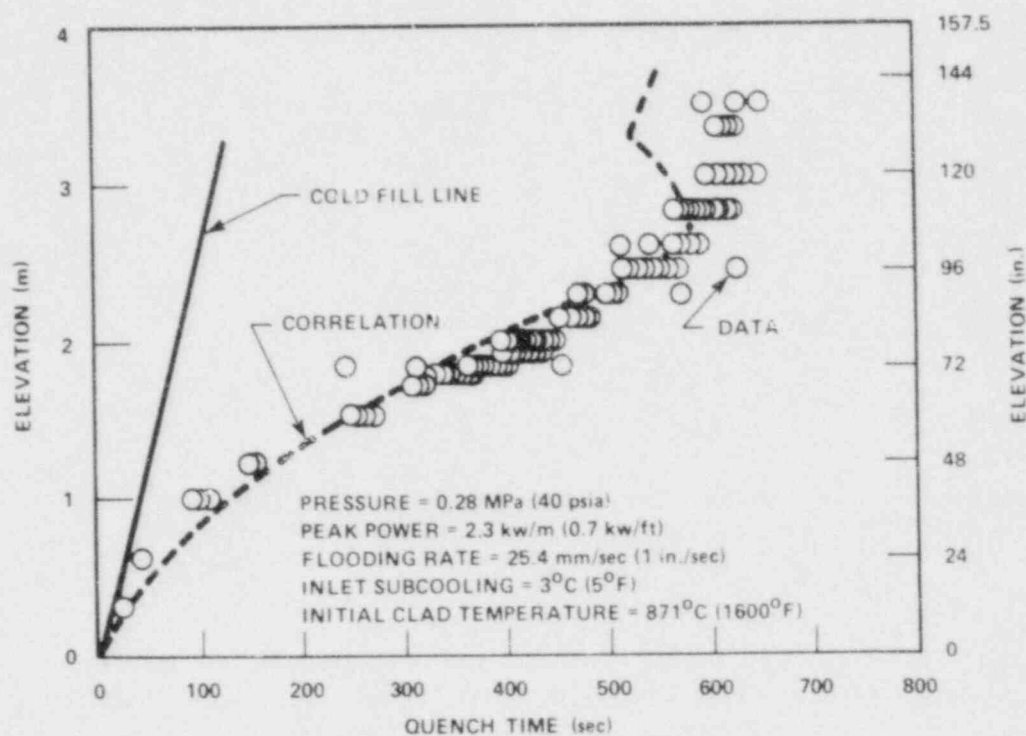


Figure H-11. Quench Correlation Versus Data,
 FLECHT SEASET Run 35114

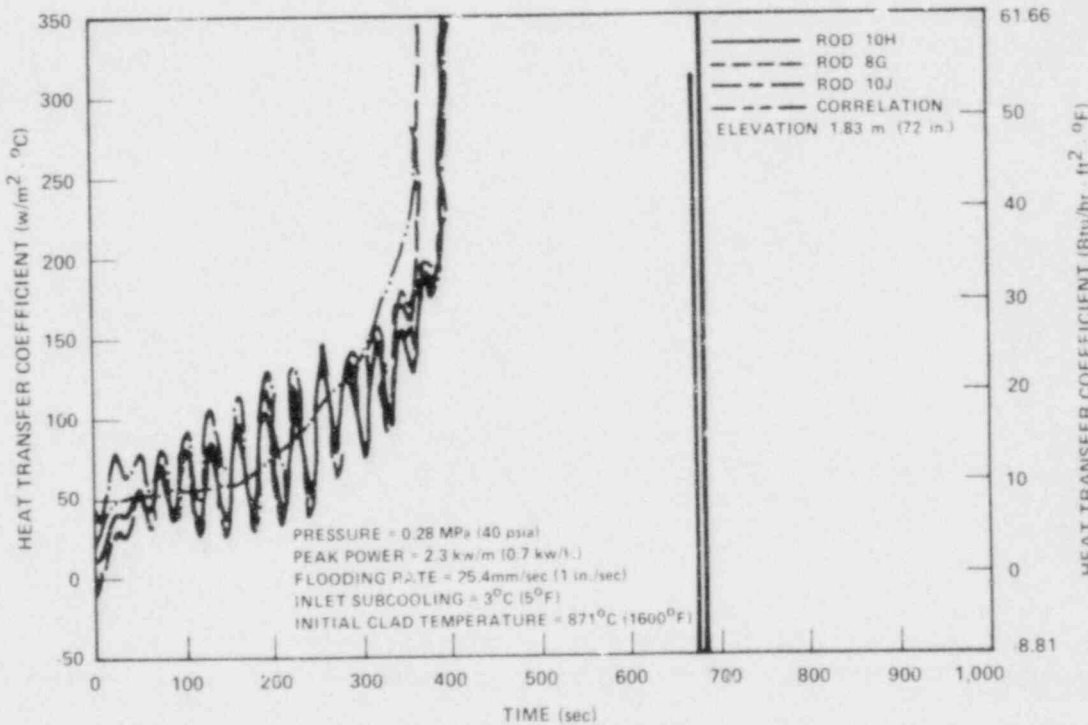


Figure H-12. Heat Transfer Coefficient Correlation
 Versus Data, FLECHT SEASET Run 35114

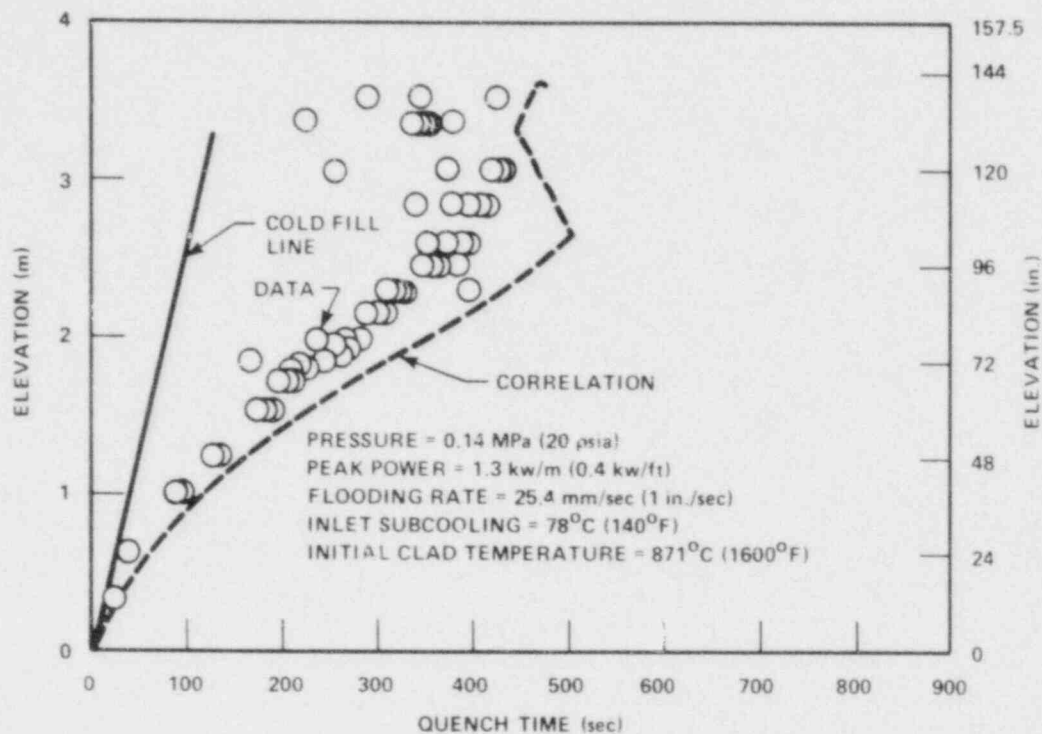


Figure H-13. Quench Correlation Versus Data,
 FLECHT SEASET Run 31922

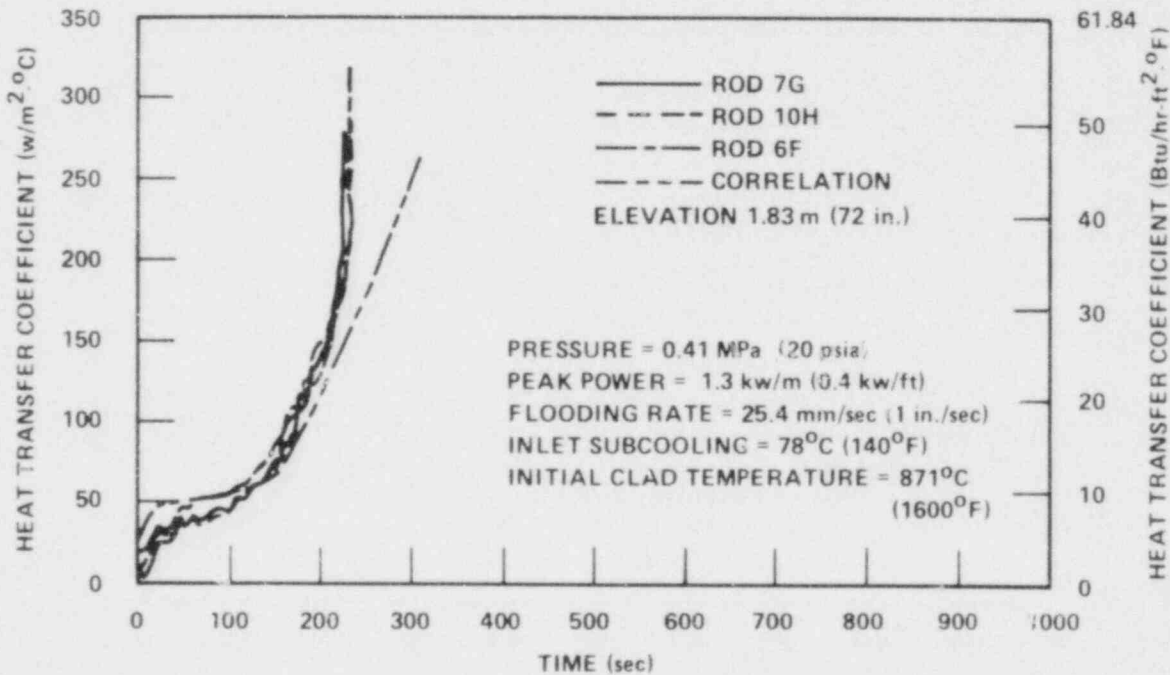


Figure H-14. Heat Transfer Coefficient Correlation
 Versus Data, FLECHT SEASET Run 39122

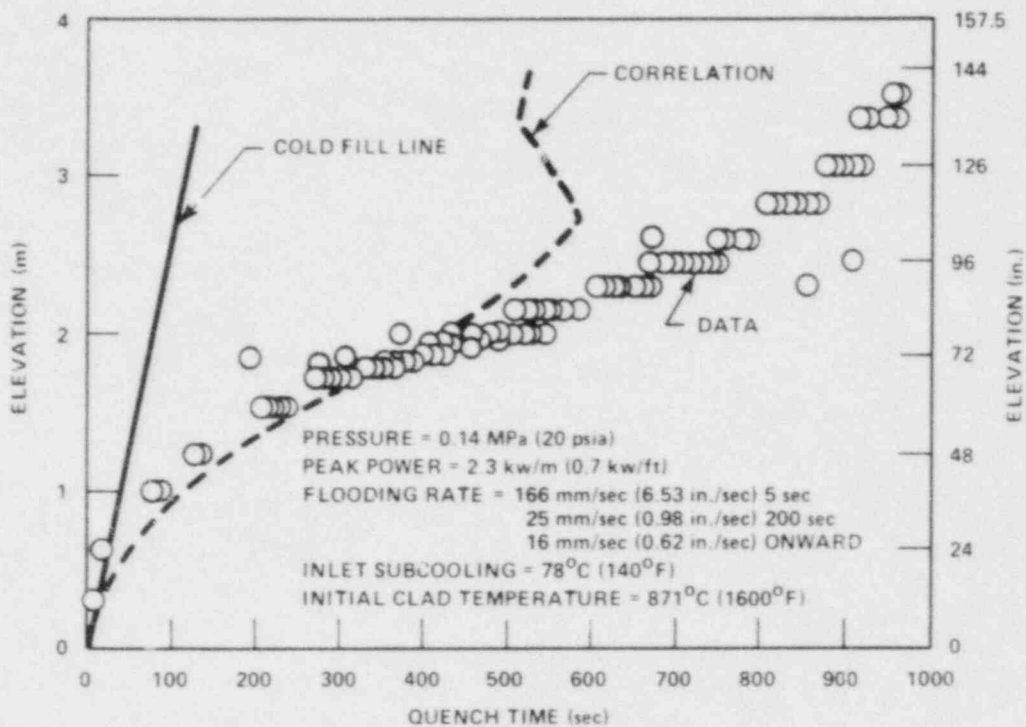


Figure H-15. Quench Correlation Versus Data,
FLECHT SEASET Run 32335

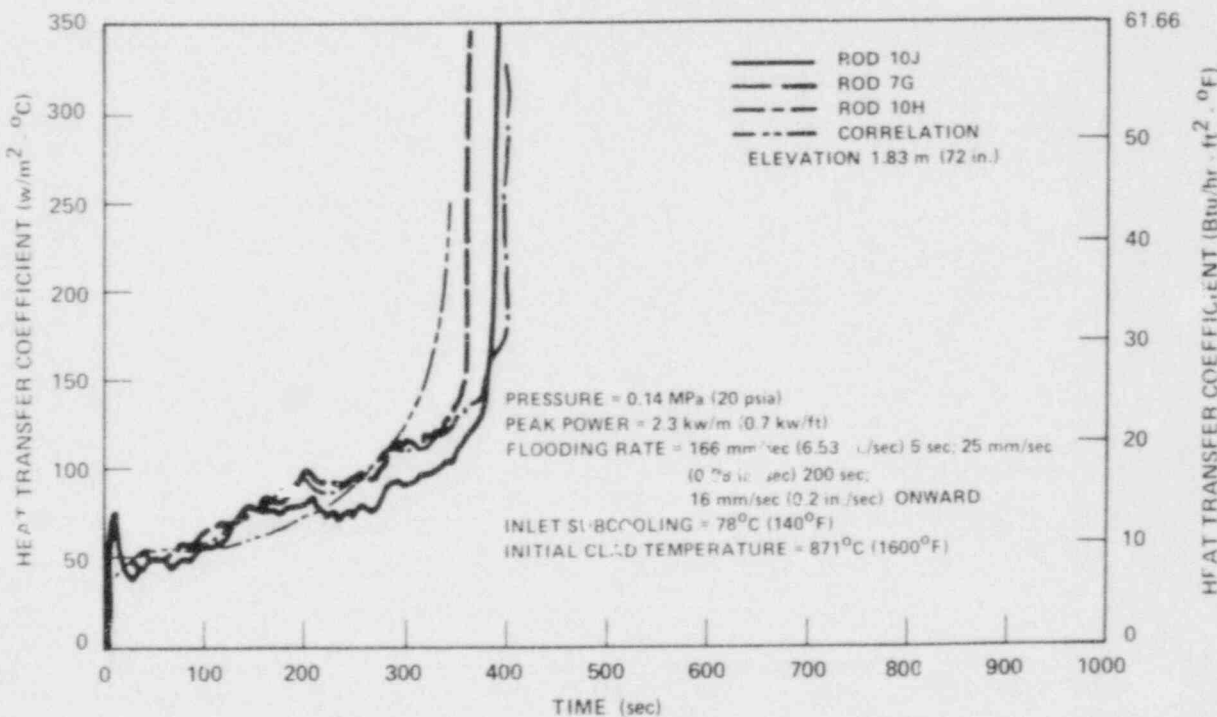


Figure H-16. Heat Transfer Coefficient Correlation
Versus Data, FLECHT SEASET Run 32235

TABLE H-2
COSINE POWER NONOVERLAP RUN DATA

Run	Peak Power [kw/m (kw/ft)]	Flooding Rate [mm/sec (in./sec)]	Initial Clad Temperature [$^{\circ}$ C ($^{\circ}$ F)]	Inlet Subcooling [$^{\circ}$ C ($^{\circ}$ F)]	Pressure [MPa (psia)]
02603	2.7 (0.81)	20.6 (0.81)	556 (1032)	77 (138)	0.28 (40)
04930	1.7 (0.51)	20.3 (0.8)	872 (1601)	77 (138)	0.28 (40)
04831	3.1 (0.95)	38.1 (1.5)	871 (1600)	79 (142)	0.28 (40)
06638	3.1 (0.95)	20.8 (0.82)	871 (1600)	79 (143)	0.14 (20)
05342	3.1 (0.95)	20.3 (0.8)	872 (1601)	11 (19)	0.28 (40)

H-2

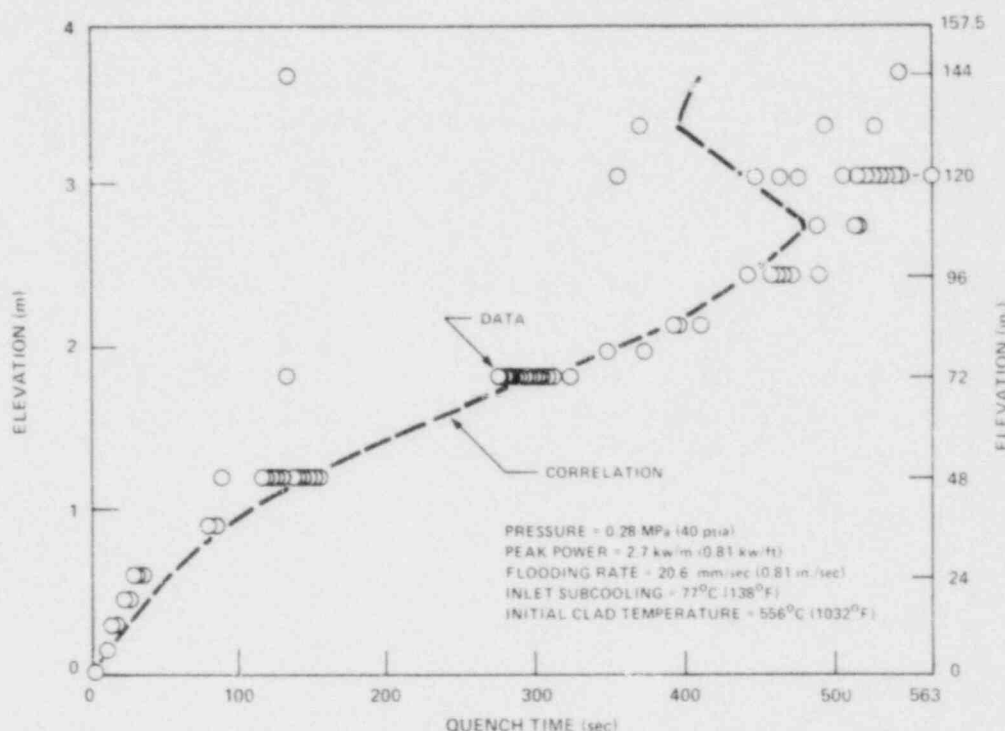


Figure H-17. Quench Correlation Versus Data,
Cosine Power Run 02603

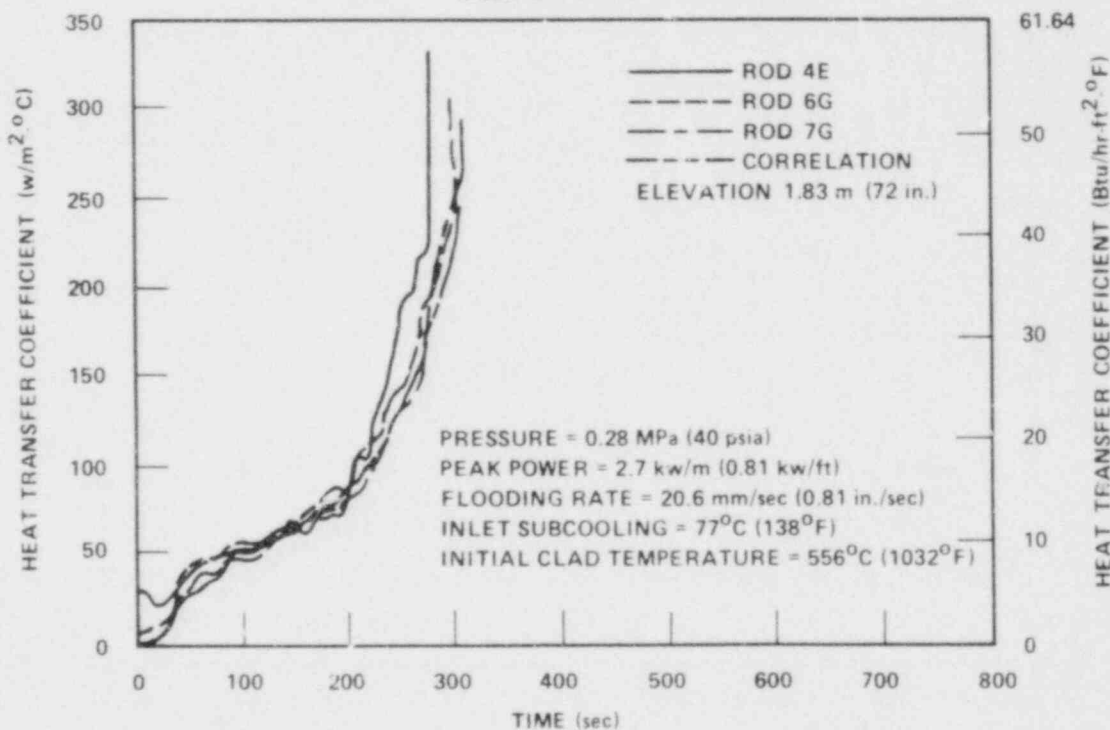


Figure H-18. Heat Transfer Coefficient Correlation
Versus Data, Cosine Power Run 02603

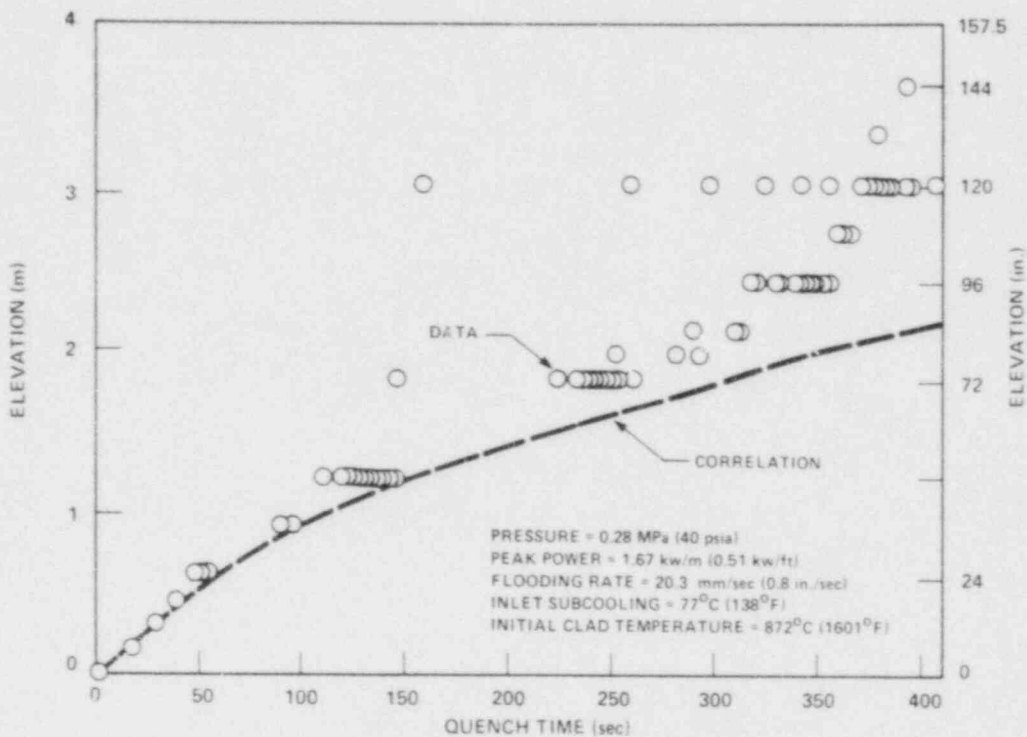


Figure H-19. Quench Correlation Versus Data,
Cosine Power Run 04930

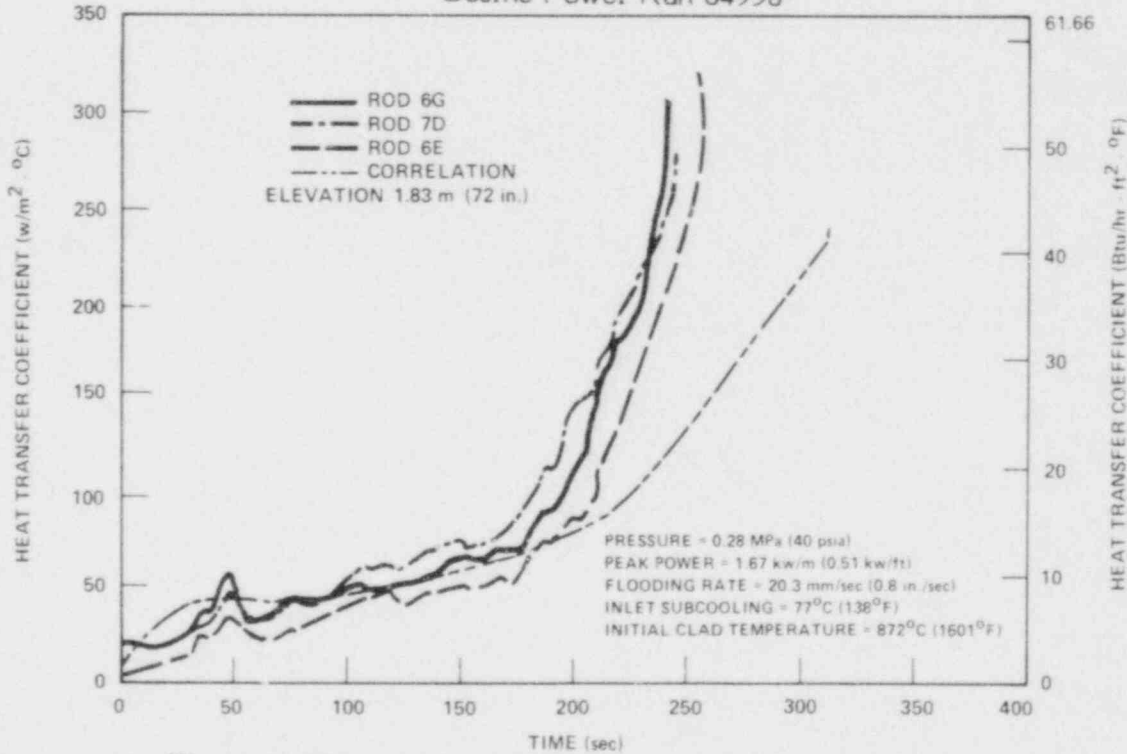


Figure H-20. Heat Transfer Coefficient Correlation
Versus Data, Cosine Power Run 04930

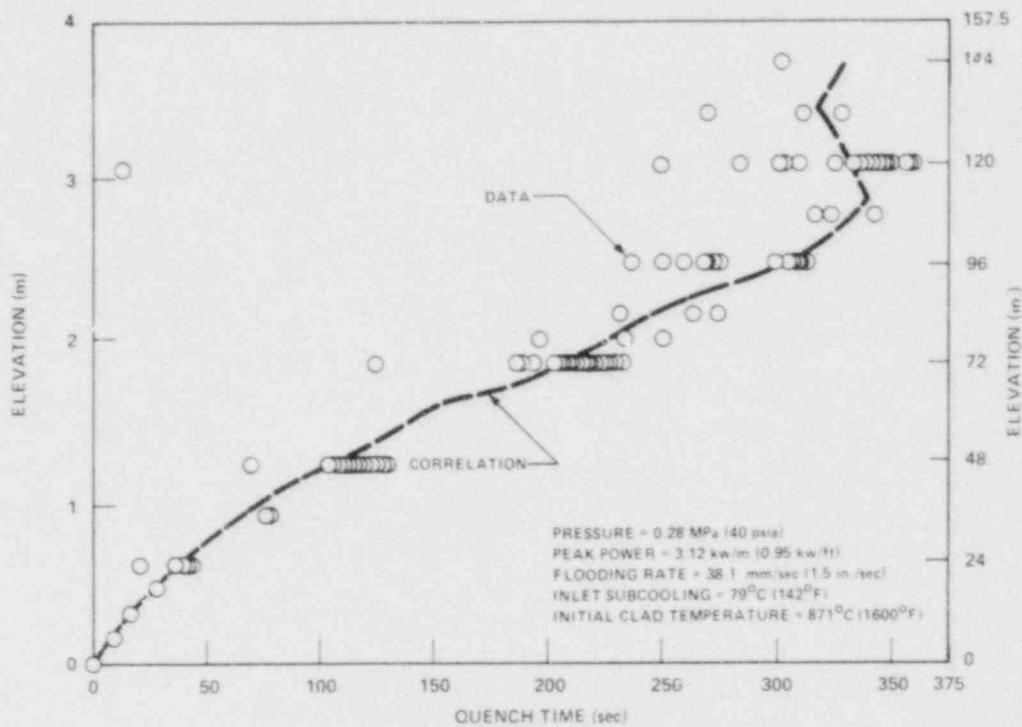


Figure H-21. Quench Correlation Versus Data, Cosine Power Run 04831

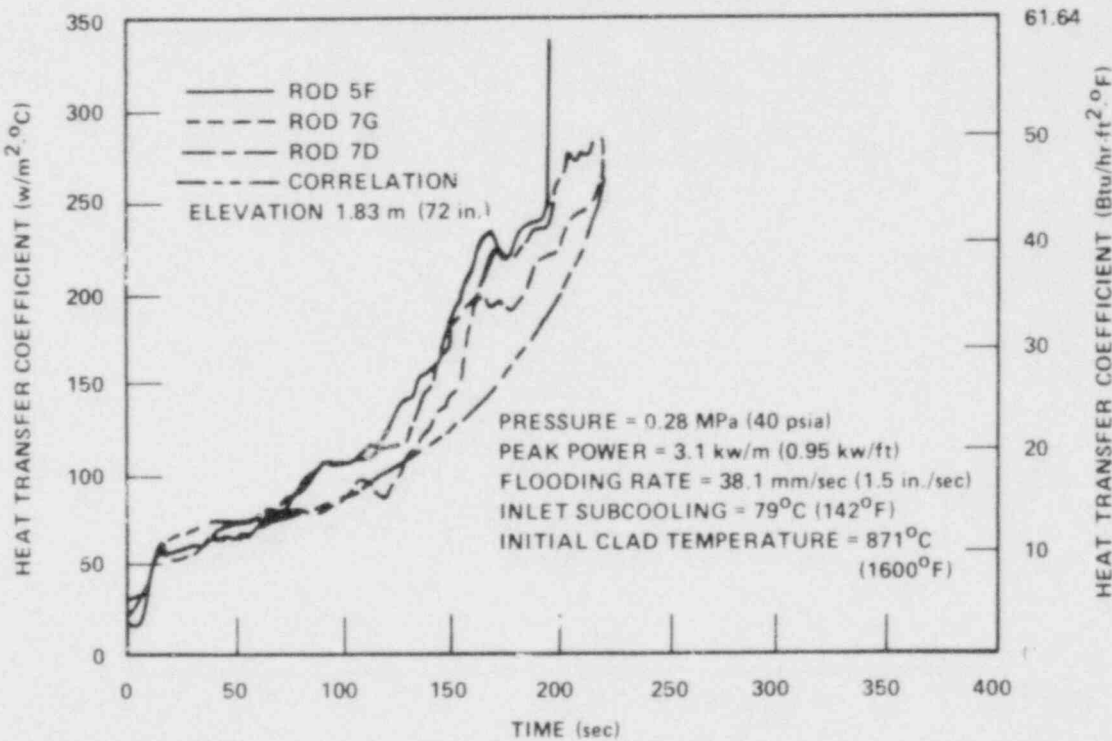


Figure H-22. Heat Transfer Coefficient Correlation Versus Data, Cosine Power Run 04831

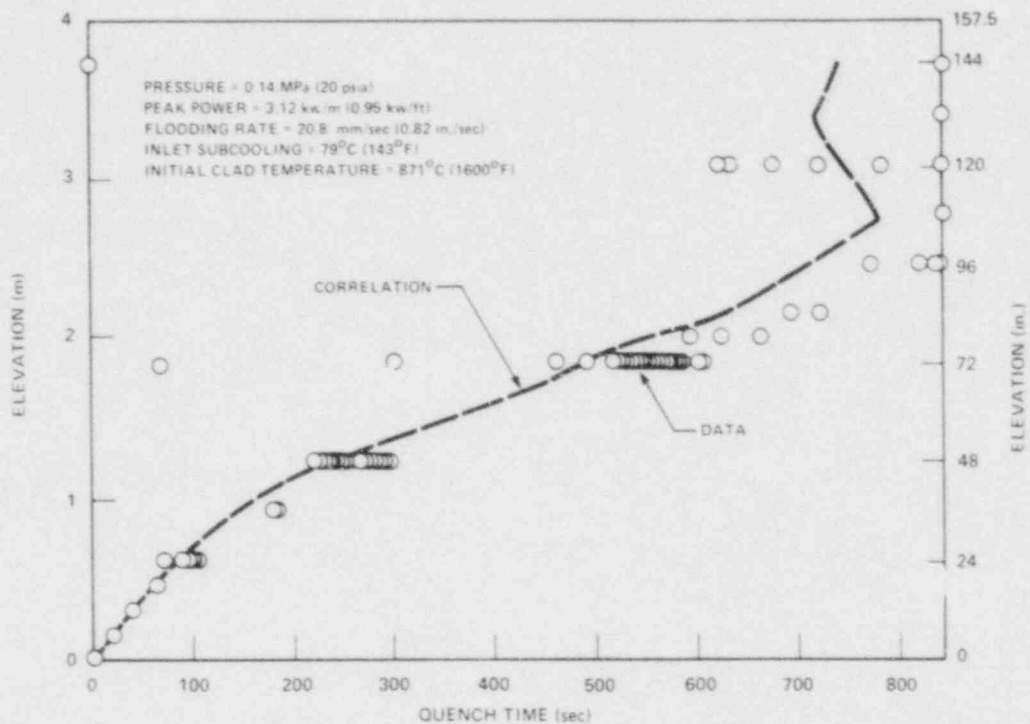


Figure H-23. Quench Correlation Versus Data, Cosine Power Run 06638

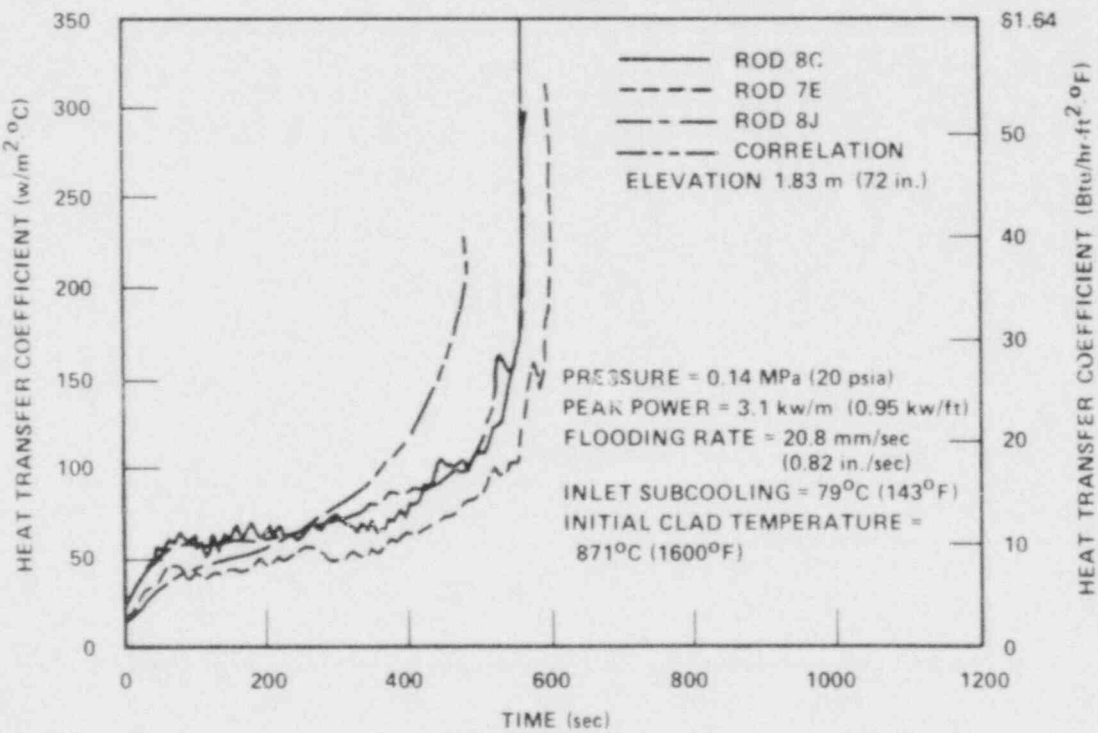


Figure H-24. Heat Transfer Coefficient Correlation Versus Data, Cosine Power Run 06638

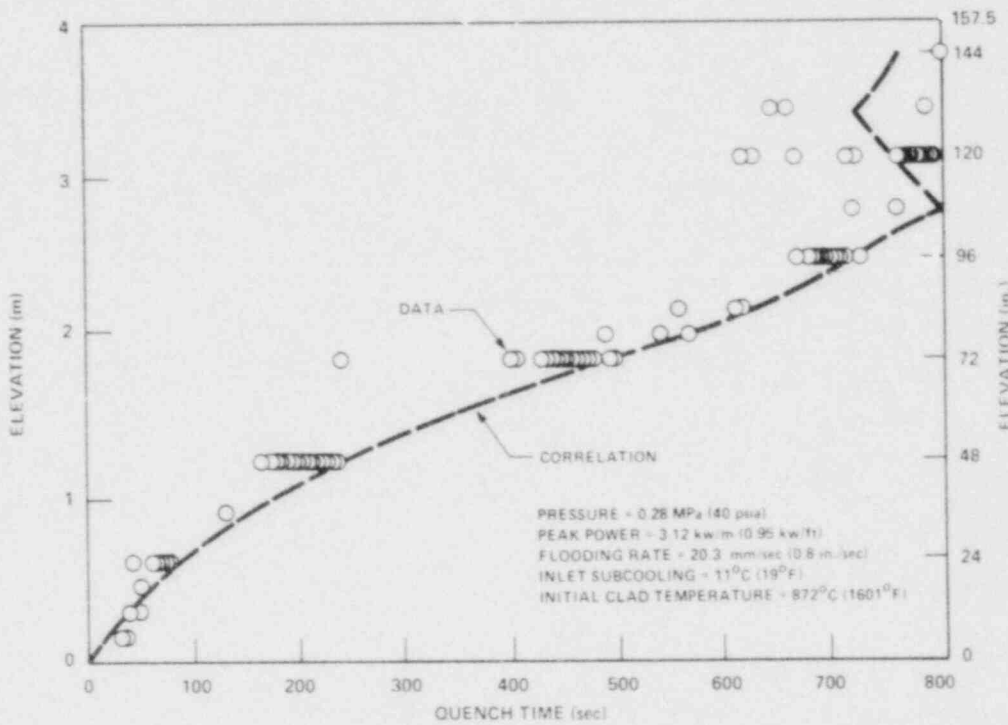


Figure H-25. Quench Correlation Versus Data, Cosine Power Run 05342

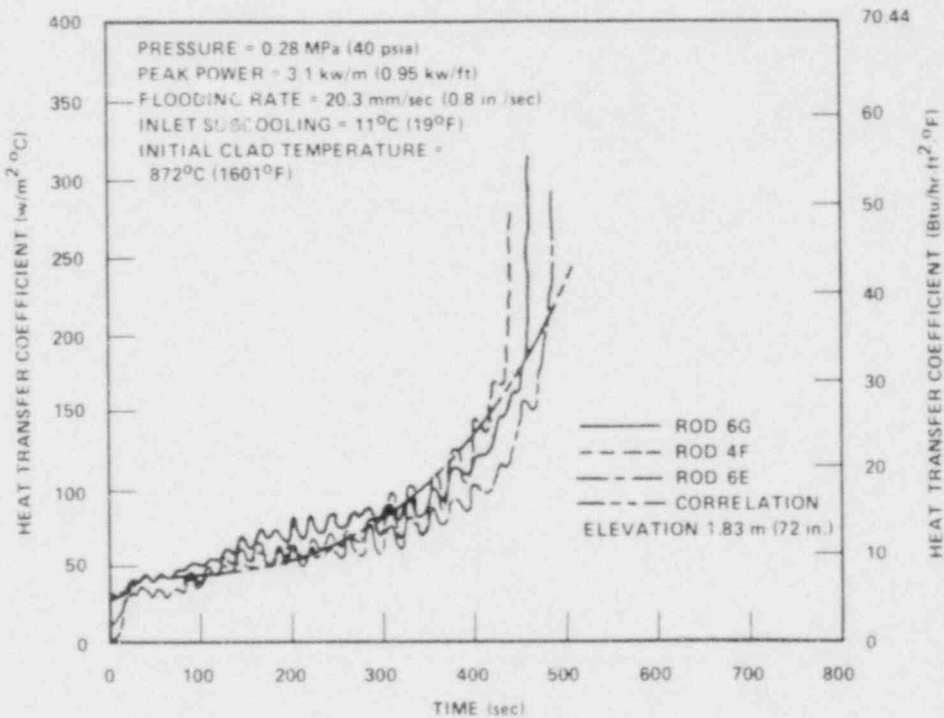


Figure H-26. Heat Transfer Coefficient Correlation Versus Data, Cosine Power Run 05342

TABLE H-3
SKEWED POWER NONOVERLAP RUN DATA

Run	Peak Power [kw/m (kw/ft)]	Flooding Rate [mm/sec (in./sec)]	Initial Clad Temperature [$^{\circ}$ C ($^{\circ}$ F)]	Inlet Subcooling [$^{\circ}$ C ($^{\circ}$ F)]	Pressure [MPa (psia)]
13303	2.3 (0.7)	38.1 (1.5)	871 (1600)	78 (141)	0.28 (41)
15305	2.3 (0.7)	20.3 (0.8)	871 (1600)	78 (140)	0.28 (40)
16110	2.3 (0.7)	20.3 (0.8)	881 (1617)	73 (132)	0.14 (20)
15713	2.3 (0.7)	25.4 (1)	875 (1607)	1 (2)	0.28 (40)
12816	2.3 (0.7)	38.1 (1.5)	264 (507)	78 (141)	0.28 (40)
16022	3.3 (1)	38.1 (1.5)	891 (1636)	77 (139)	0.28 (40)
15132	2.3 (0.7)	152 → 20.3 (6 → 0.8)	846 (1555)	77 (139)	0.27 (39)

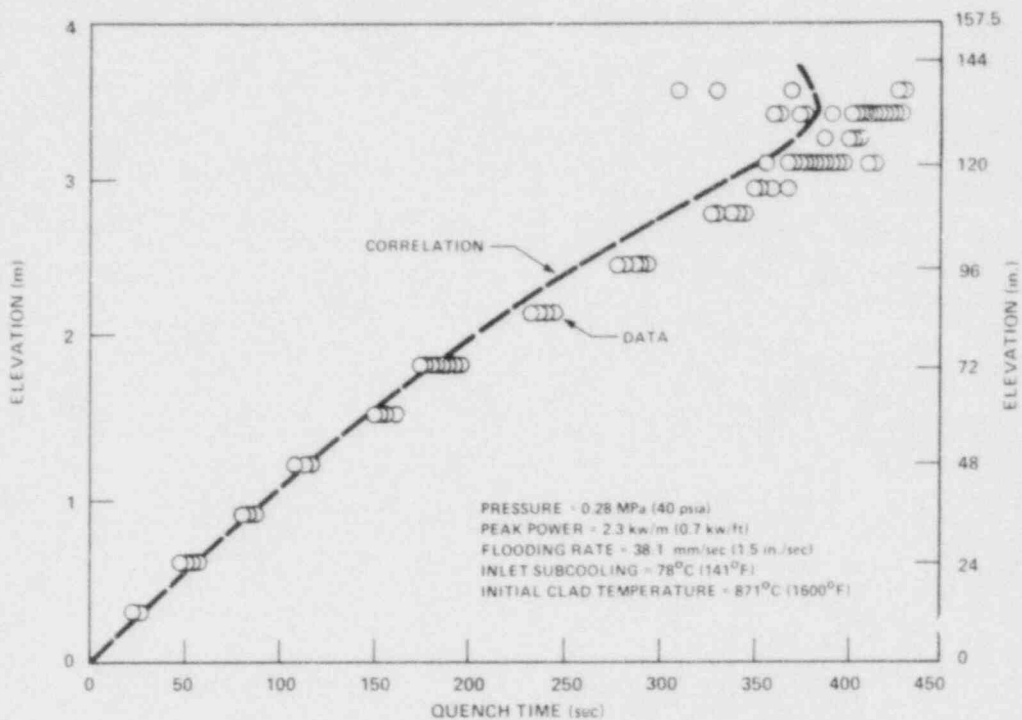


Figure H-27. Quench Correlation Versus Data, Skewed Power Run 13303

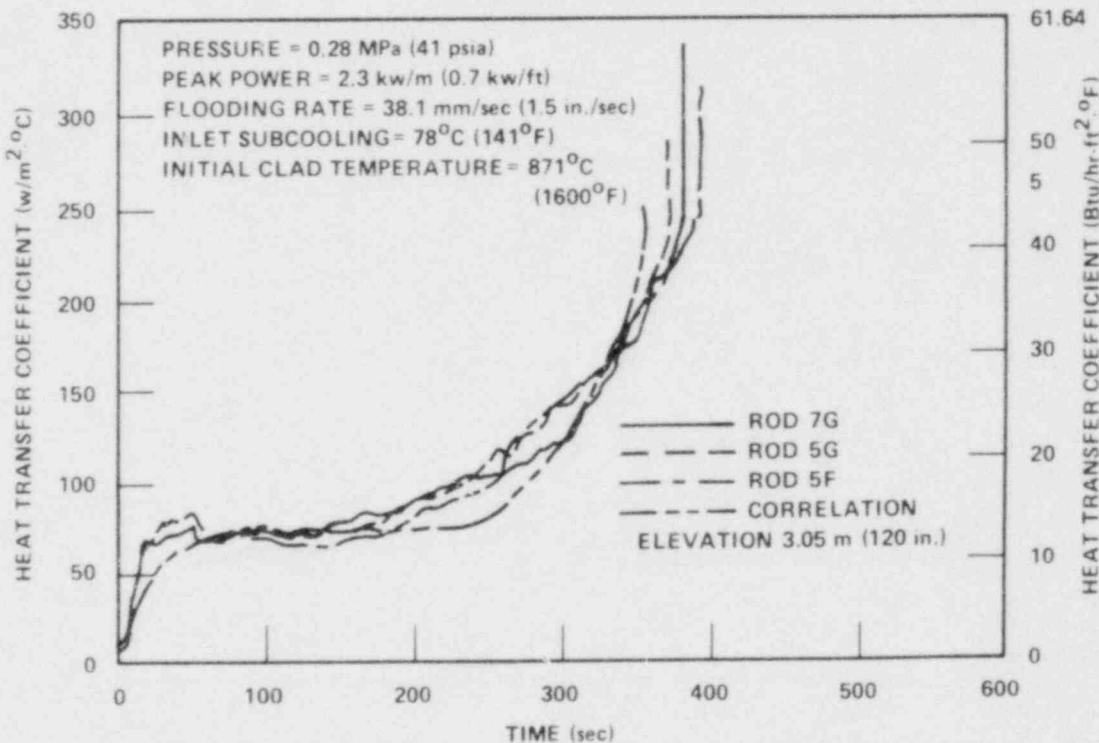


Figure H-28. Heat Transfer Coefficient Correlation Versus Data, Skewed Power Run 13303

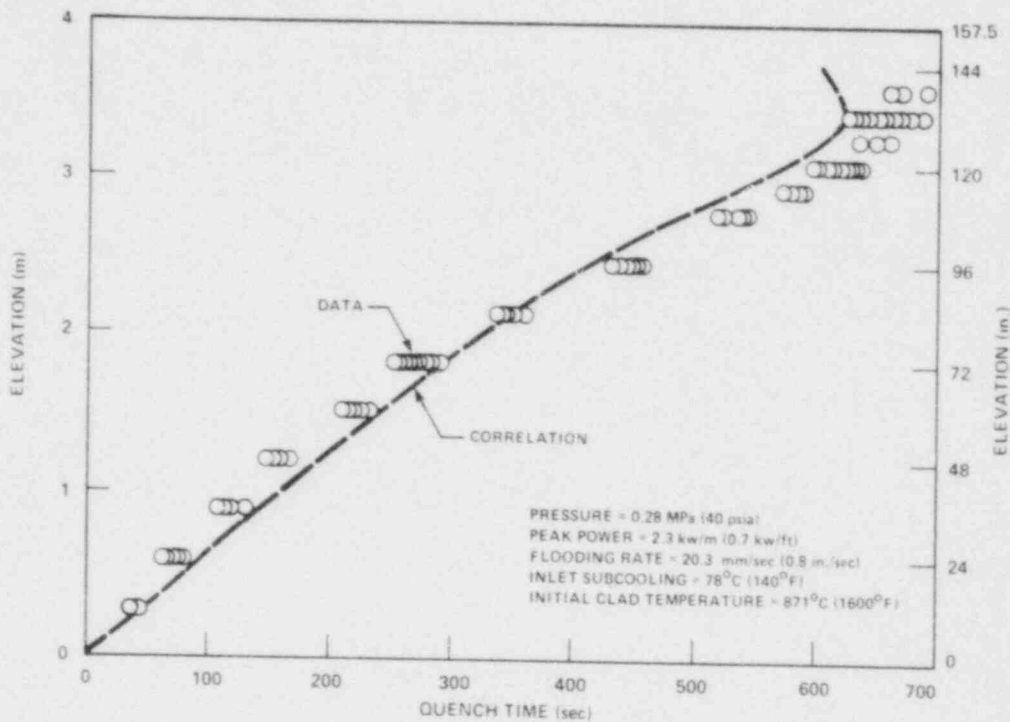


Figure H-29. Quench Correlation Versus Data,
Skewed Power Run 15305

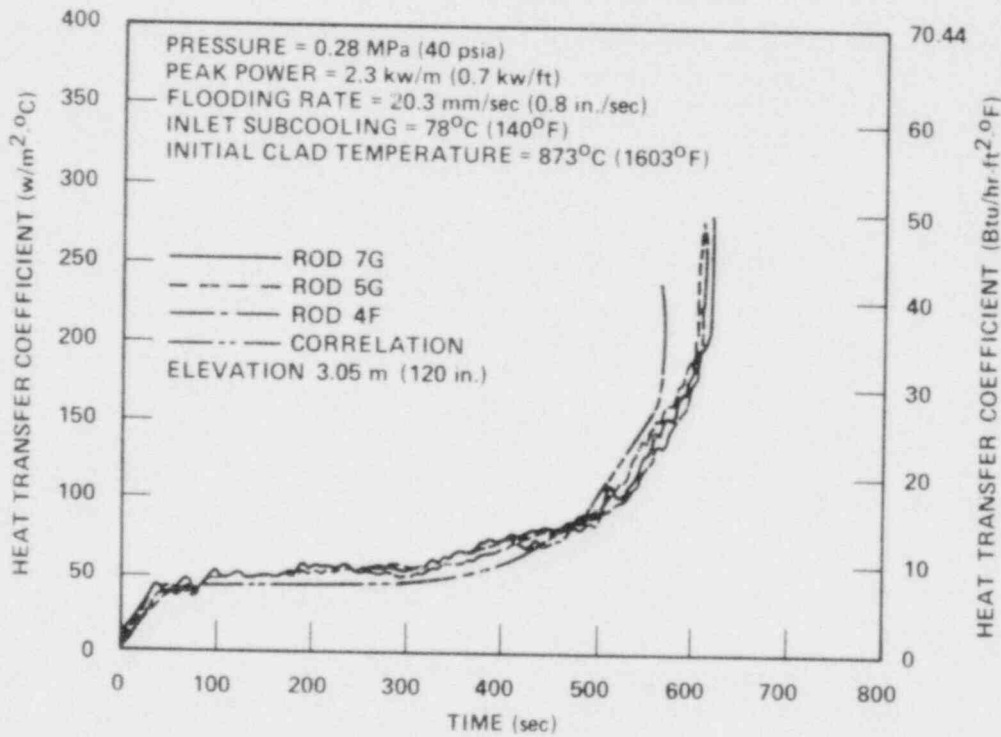


Figure H-30. Heat Transfer Coefficient Correlation
Versus Data, Skewed Power Run 15305

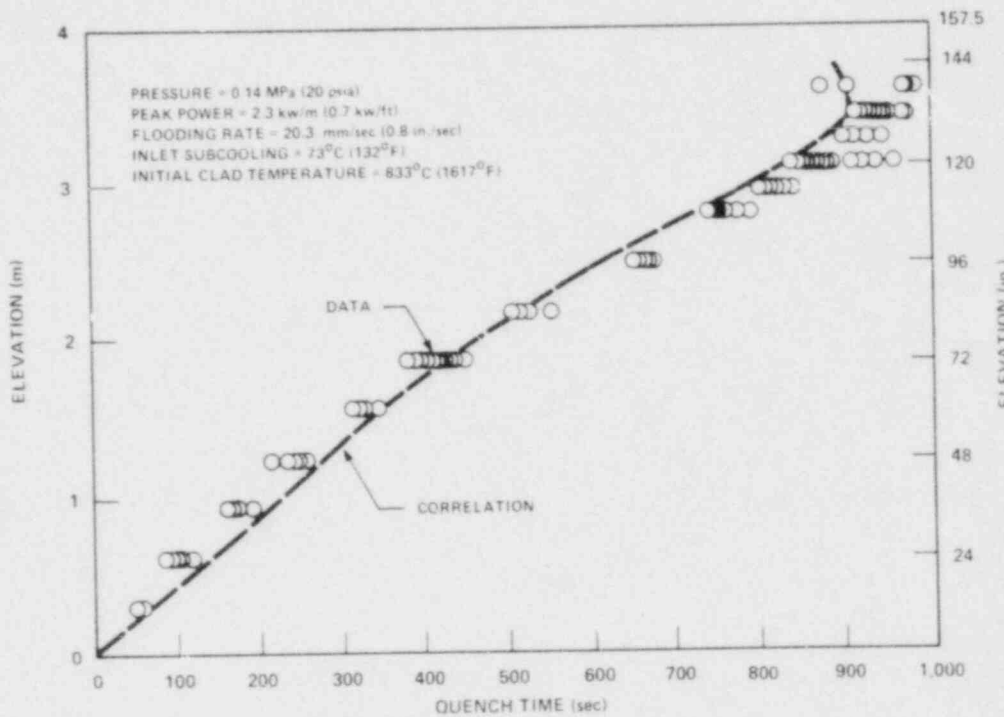


Figure H-31. Quench Correlation Versus Data, Skewed Power Run 16110

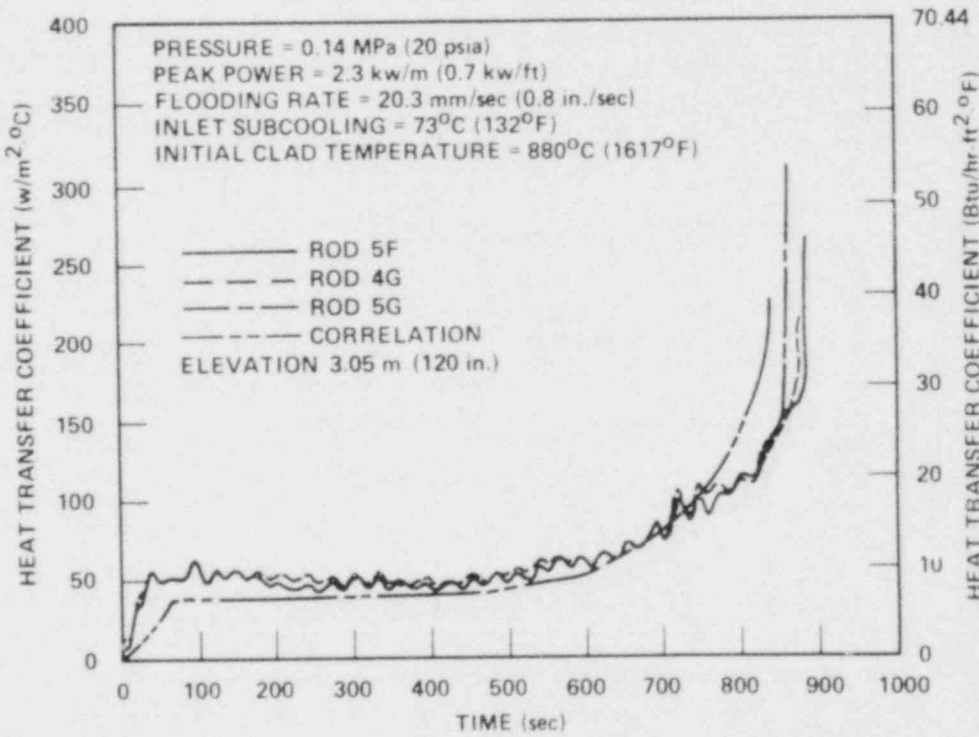


Figure H-32. Heat Transfer Coefficient Correlation Versus Data, Skewed Power Run 16110

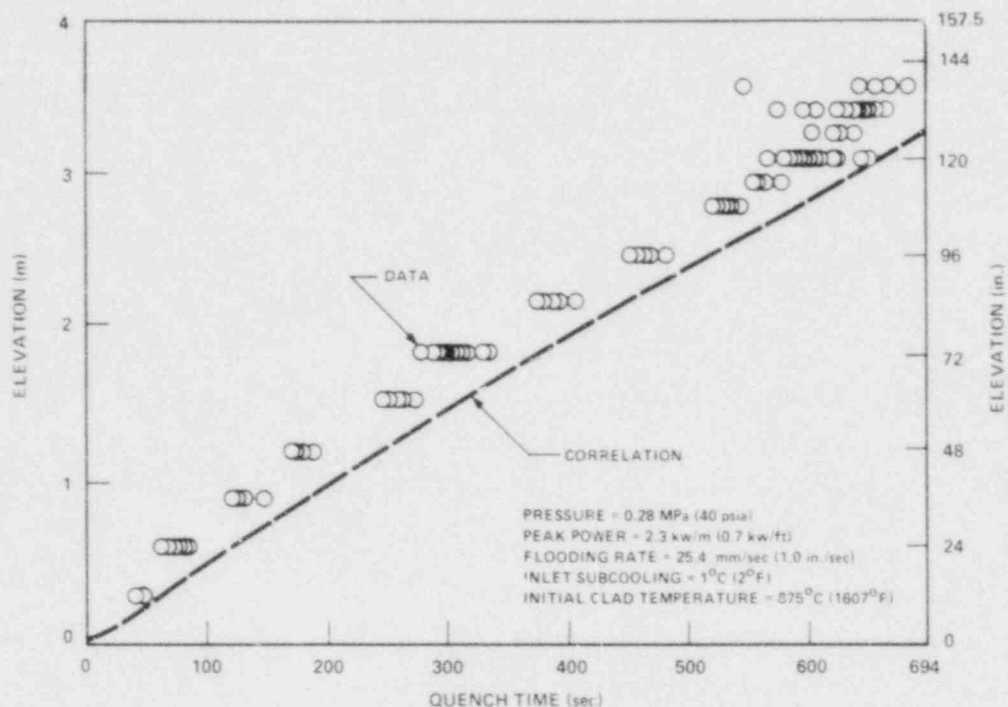


Figure H-33. Quench Correlation Versus Data,
Skewed Power Run 15713

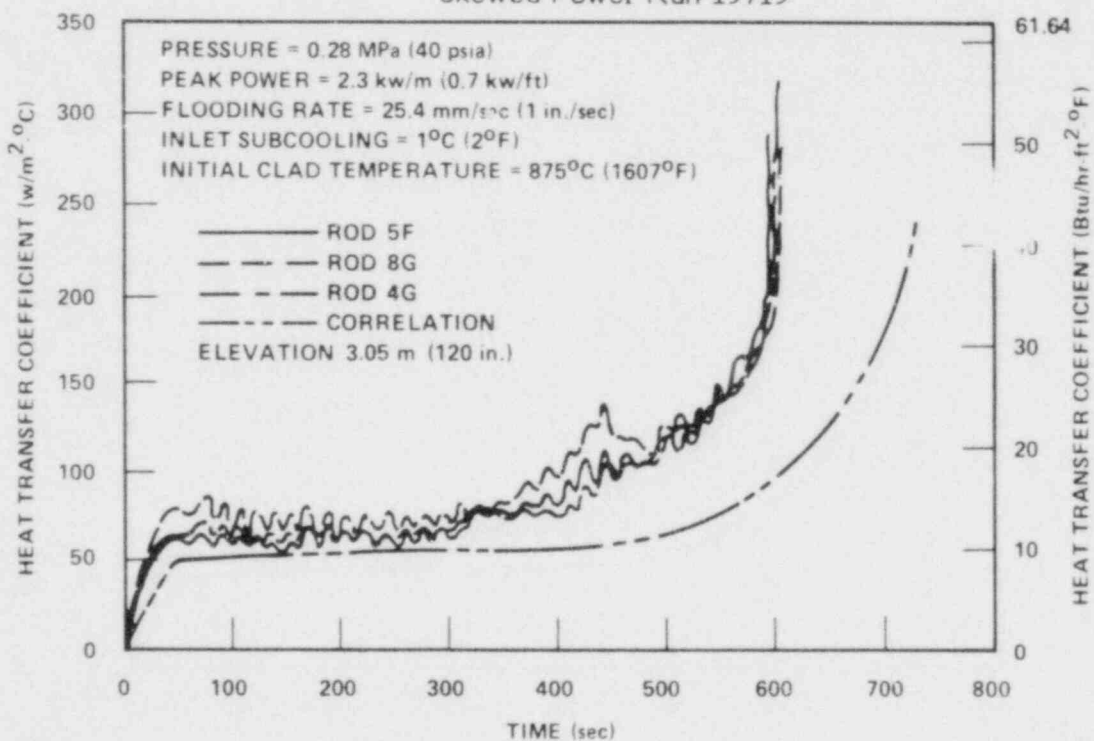


Figure H-34. Heat Transfer Coefficient Correlation
Versus Data, Skewed Power Run 15713

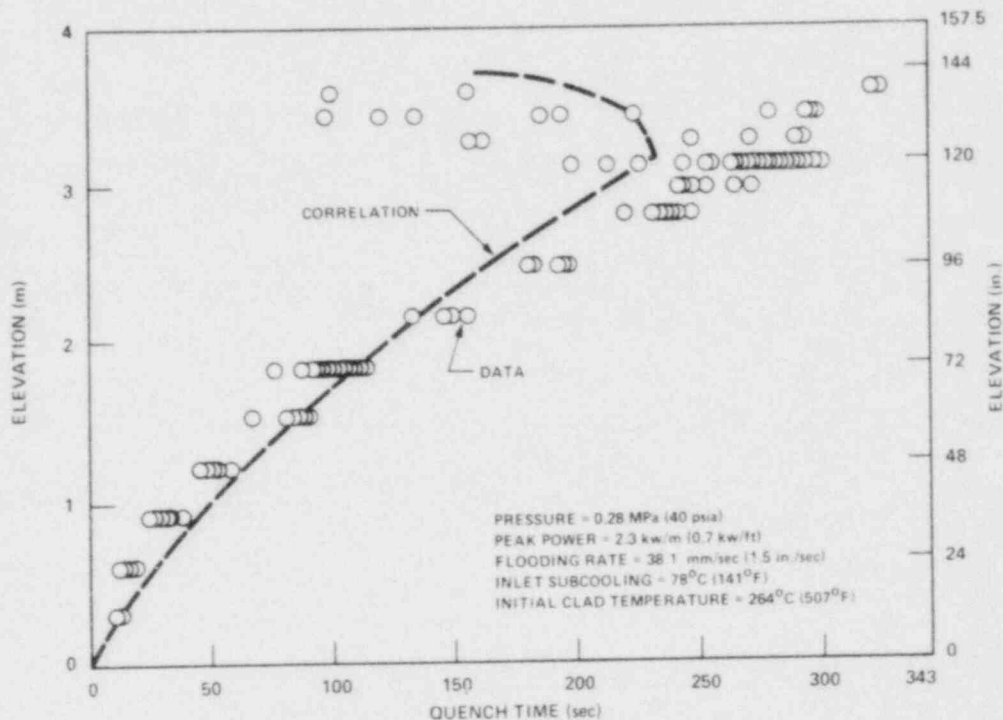


Figure H-35. Quench Correlation Versus Data, Skewed Power Run 12816

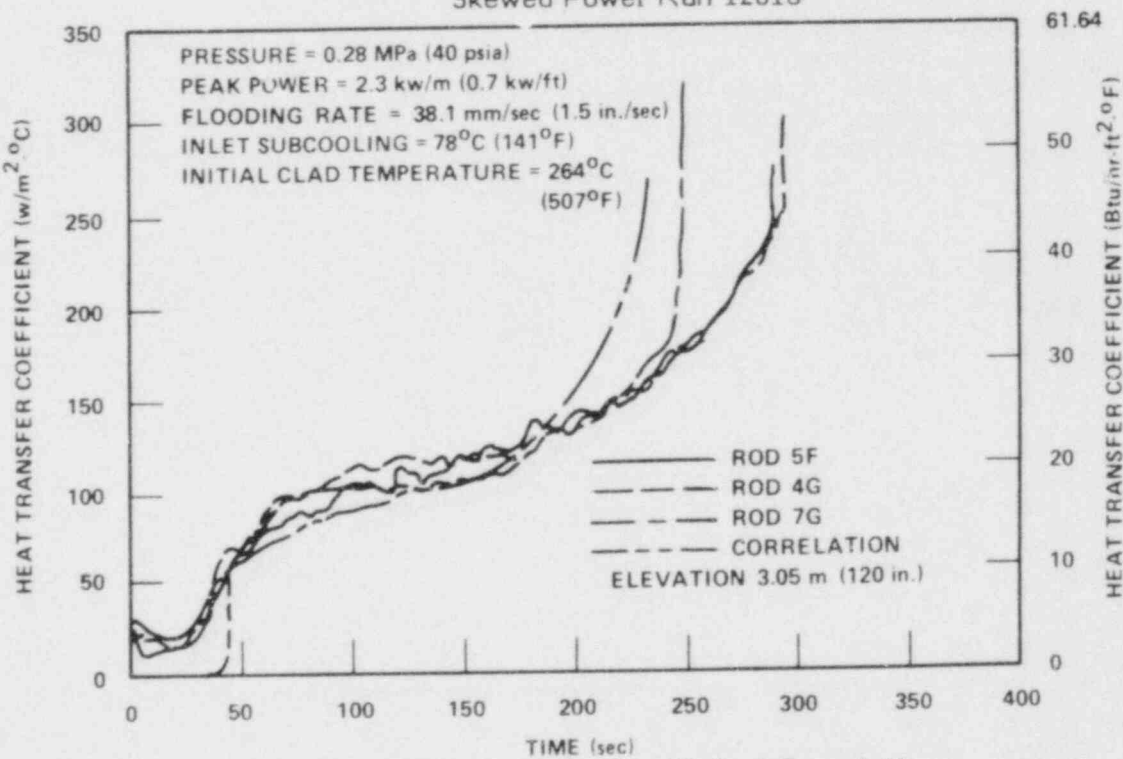


Figure H-36. Heat Transfer Coefficient Correlation Versus Data, Skewed Power Run 12816

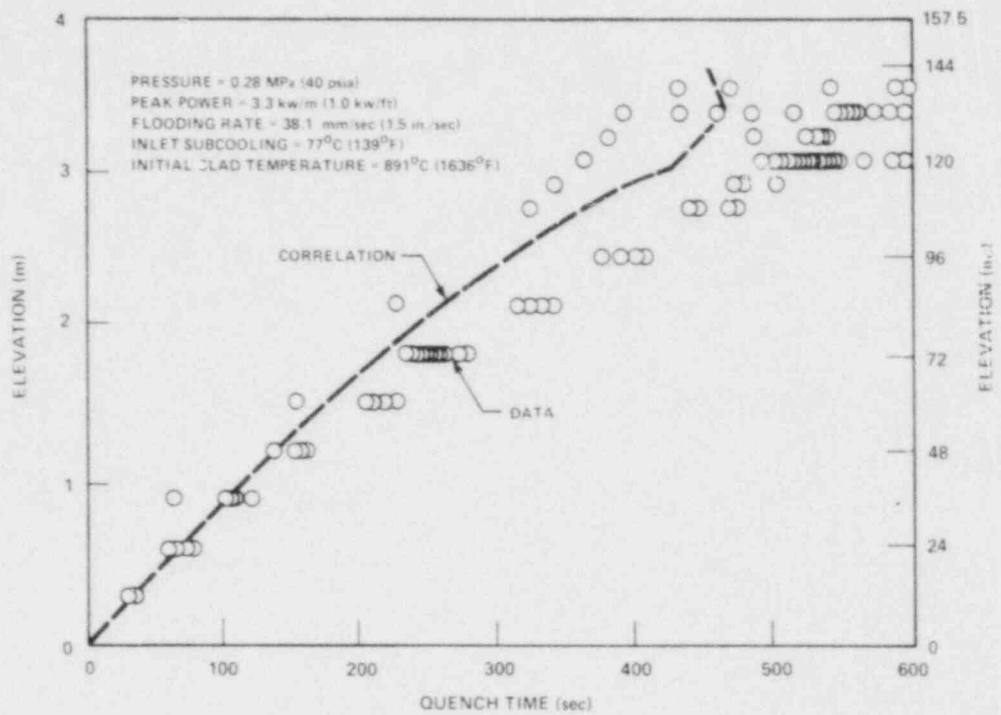


Figure H-37. Quench Correlation Versus Data, Skewed Power Run 16022

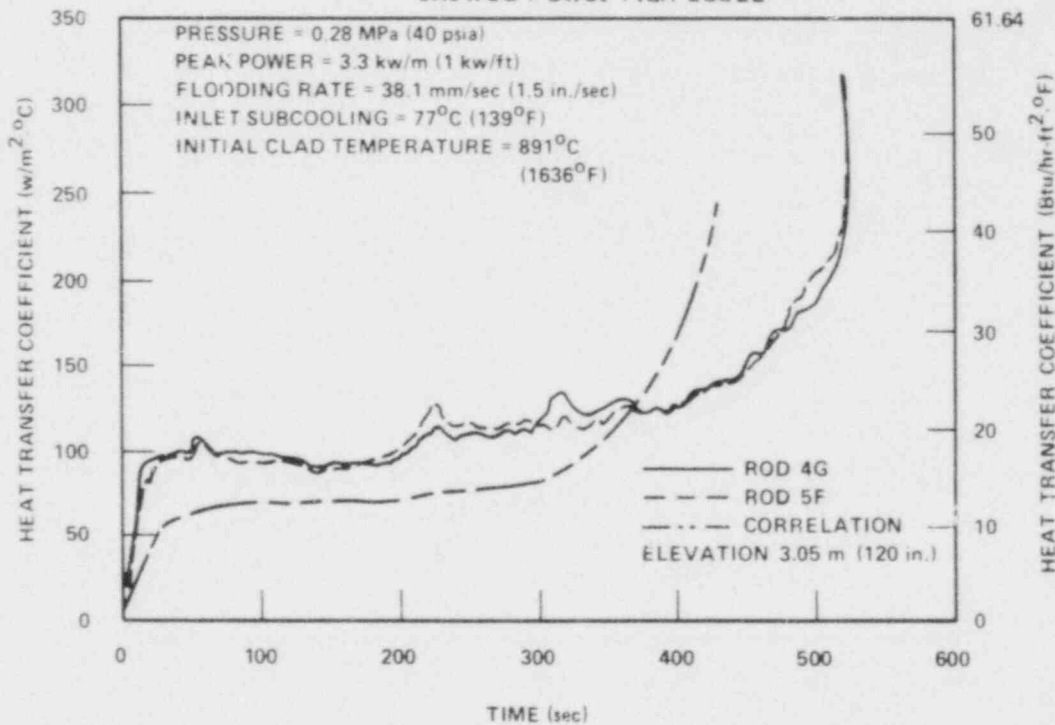


Figure H-38. Heat Transfer Coefficient Correlation Versus Data, Skewed Power Run 16022

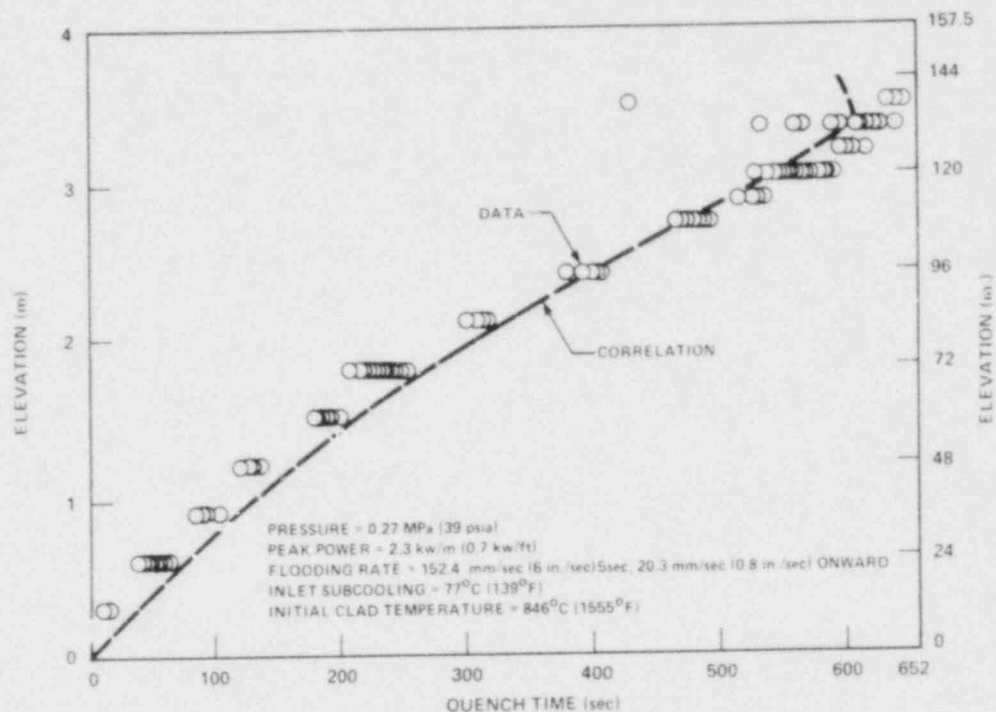


Figure H-39. Quench Correlation Versus Data, Skewed Power Run 15132

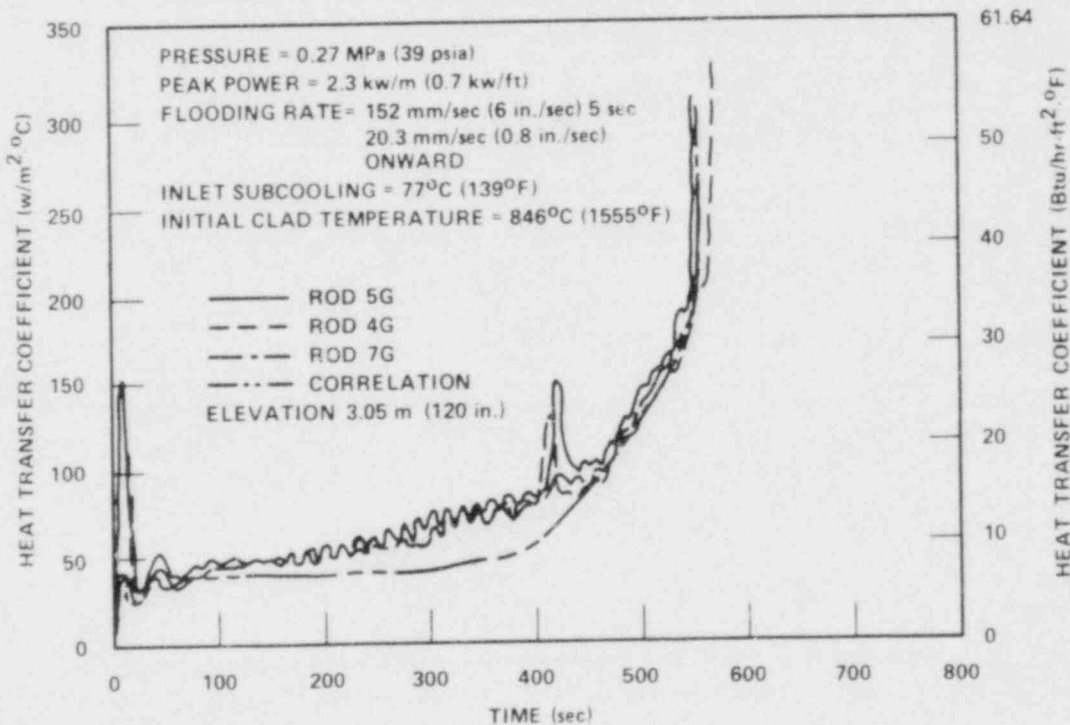


Figure H-40. Heat Transfer Coefficient Correlation Versus Data, Skewed Power Run 15132

APPENDIX I

HEAT TRANSFER CORRELATION COMPUTER PROGRAM

The computer program for calculating the quench front elevation and the heat transfer coefficient correlation of section 6 is listed in this appendix. An example of calculation for run 31805 is given at the end of this appendix. The inputs and outputs for the program are described below:

NRUN = run number

DTSUB = inlet subcooling ($^{\circ}$ F)

P = pressure (psia)

TINIT = initial clad temperature at peak elevation ($^{\circ}$ F)

QM_{AX} = peak power (kw/ft)

TSAT = saturation temperature ($^{\circ}$ F)

Z = elevation at which the heat transfer coefficient is to be computed (ft)

Z PEAK = peak temperature elevation (ft)

TIME = time (sec)

H = heat transfer coefficient in English units (Btu/hr-ft²- $^{\circ}$ F)

H(SI) = heat transfer coefficient in SI units (w/m²- $^{\circ}$ C)

ZQ(F1) = quench front elevation (ft)

ZQ(M) = quench front elevation (m)

Input table for flooding rate:

$$VINTM(J) = \text{time } t_j \text{ (sec)}$$

$$VINTB(J) = \text{flooding rate at time } t_j \text{ (in./sec)}$$

In reactor applications, if the power decay and the axial power shape are different from those in FLECHT or FLECHT SEASET tests, then the "Table of Normalized Power Decay," "Table of Axial Power Shape Factor," and "Table of Normalized Integral of Power" in the following computer program must be replaced. These tables are defined as follows:

-- Table of Normalized Power Decay

$$PDCT(J) = \text{time } t_j \text{ (sec)}$$

$$PDCAY(J) = \frac{\int_0^{t_j} \frac{Q'(Z,t)}{Q'(Z,0)}}{\left[\int_0^{t_j} \frac{Q'(Z,t)}{Q'(Z,0)} \right] \text{decay curve B}}$$

where the normalized FLECHT power decay curve B is shown in figure I-1. The table of PDCAY(J) in the following computer program is for the ANS + 20% power decay curve.

-- Table of Axial Power Shape Factor

$$FAXZ(J) = \text{elevation } Z_j \text{ (ft)}$$

$$FAXTB(J) = Q'(Z_j, 0)/Q'_{\max} \quad \text{for FLECHT cosine power or FLECHT SEASET}$$

$$FAXZS(J), FAXTBS(J) = \begin{aligned} & \text{same as } FAXZ(J) \text{ and } FAXTB(J), \text{ respectively,} \\ & \text{for FLECHT skewed power} \end{aligned}$$

1-1

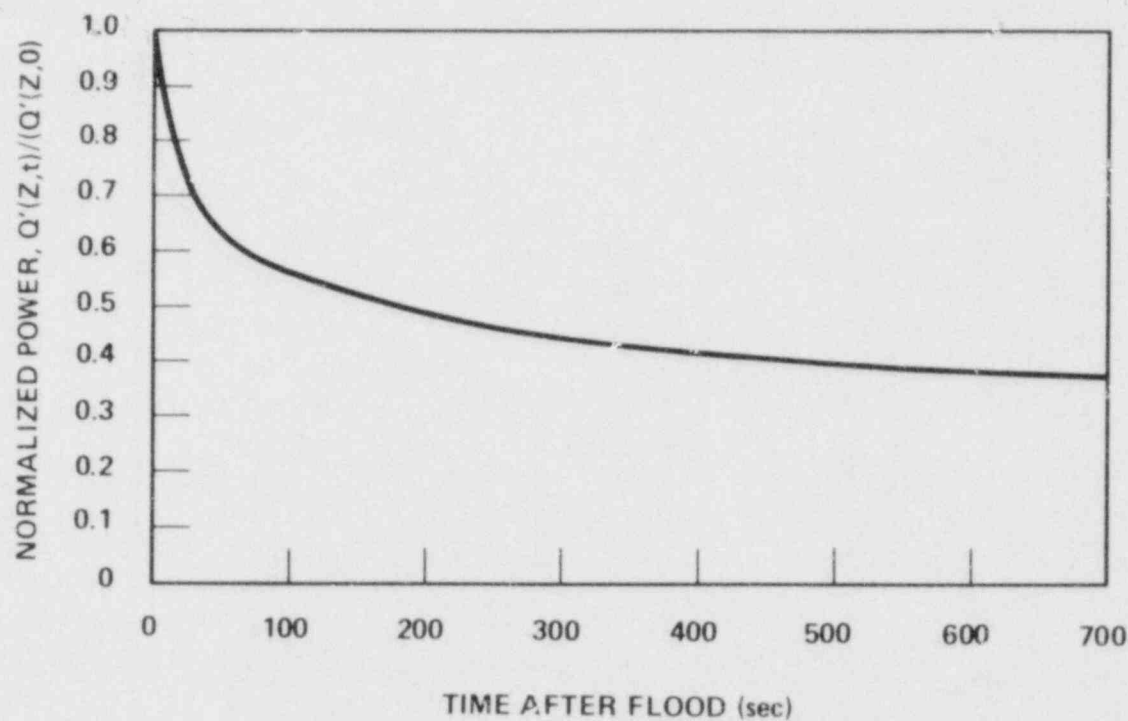


Figure I-1. FLECHT Power Decay Curve B Normalized With Initial Power

-- Table of Normalized Integral of Power

QAXZQ(J) = elevation Z_j (ft)

$$QAXTB(J) = \int_0^{Z_j} \frac{Q'(Z,0)}{Q'_{\max}} dZ \text{ for FLECHT cosine power or FLECHT SEASET}$$

QAXZQS(J), QAXTB3S(J) = same as QAXZQ(J) and QAXTB(J), respectively, for
FLECHT skewed power

Subroutine INTERP is used for linear interpolation between tabulated values.

Steam properties are evaluated with the Westinghouse steam table functions. These functions and their functional performances are as follows:

$$HG = HSV(P, TSAT, S, VOLG) \quad h, T, s, v = f(P)$$

$$VOLF = VCL(P, TSAT) \quad v = f(P, T)$$

$$CPF = CPL(P, TSAT) \quad C_{pf} = f(P, T)$$

$$HF = HSL(TSAT) \quad h_f = f(T)$$

$$VISF = VISL(P, TSAT) \quad \mu_f = f(P, T)$$

$$KF = CONDL (P, TSAT) \quad k_f = f(P, T)$$

$$KG = CONDV (P, TSAT) \quad K_g = f(P, T)$$

These functions may be replaced by appropriate functions or the values of the steam properties given as inputs.

HEAT TRANSFER CORRELATION COMPUTER PROGRAM

```
TYPE YHTDL.F4
00100 C FLECHT-SEASET UNBLOCKED BUNDLE EVALUATION REPORT
00200 C REFLOOD HEAT TRANSFER COEFFICIENT CORRELATION IN
00300 C DIMENSIONLESS FORM DEVELOPED BY YEH.
00500 REAL KF,KG,NU1,NU2,NU3,NU
00600 DIMENSION QAXZQ(92),QAXTB(92),FAXTB(93),FAXZ(93)
00700 1,PDCAV(111),PDCT(111),QAXTBS(99),QAXZQS(99),FAXTBS(99),
00800 2FAXZS(99),VINTM(111),VINTB(111),QAXZQ4(99),QAXTB4(99),
00900 3FAXZQ4(99),FAXTB4(99),FTQTB(99),FTQZQS(99),
01000 4,QAXZQ3(33),QAXTB3(33),FAXZQ3(33),FAXTB3(33),
01100 SFTQZQ3(33),FTQTB3(33),ZQTM(55),ZQTB(55)
01200 10 CONTINUE
01300 TYPE 950
01400 950 FORMAT(' MR=1 FOR FLECHT POWER, MR=2 FOR UNIFORM POWER')
01500 TYPE 900
01600 900 FORMAT (' M=1 FOR COSINE, M=2 FOR SKEW')
01800 1' MBDL=15 FOR 15X15, MBDL=17 FOR 17X17')
01900 TYPE 1000
02000 1000 FORMAT(' ENTER RUN DTSUB P TINT QMAX TSAT
02100 1 M MR Z ZPEAK MBDL')
02200 ACCEPT 1002,NRUN,DTSUB,P,TINIT,QMAX,TSAT,M,MR,
02300 1 Z,ZPEAK,MBDL
02400 1002 FORMAT (11G)
02500 TYPE 1100
02600 1100 FORMAT(' ENTER VIN TABLE BELOW')
02700 TYPE 1110
02800 1110 FORMAT(' ENTER NO. OF POINTS')
02900 ACCEPT 1112, NVIN
03000 1112 FORMAT(I)
03100 TYPE 1102
03200 1102 FORMAT(' ENTER TIME(10/LINE)')
03300 ACCEPT 1104, (VINTM(J),J=1,NVIN)
03400 1104 FORMAT((10G))
03500 TYPE 1106
03600 1106 FORMAT(' ENTER VIN(10/LINE)')
03700 ACCEPT 1104, (VINTB(J),J=1,NVIN)
03800 IF (MZQ .NE. 1) GO TO 1300
03900 TYPE 1200
04000 1200 FORMAT(' ENTER ZQ TABLE BELOW')
04100 TYPE 1210
04200 1210 FORMAT(' ENTER NO. OF POINTS')
04300 ACCEPT 1112, NZQ
04400 TYPE 1202
04500 1202 FORMAT(' ENTER TIME (10/LINE)')
04600 ACCEPT 1104, (ZQTM(J),J=1,NZQ)
04700 TYPE 1206
```

```

04800 1206 FORMAT(' ENTER ZQ (10/LINE) ')
04900      ACCEPT 1104, (ZQTB(J),J=1,NZQ)
05000 1300 CONTINUE
05100 C
05200 C TABLE OF NORMALIZED POWER DECAY
05300 C
05500      DATA (PDCAY(J),J=1,17)/1., 1.085, 1.153, 1.198, 1.226
05600      1, 1.244, 1.255, 1.262, 1.27, 1.28, 1.298, 1.311, 1.319
05700      2, 1.324, 1.327, 1.328, 1.33/
05800      DATA (PDCT(J),J=1,17)/0., 20., 40., 60., 80.
05900      1, 100., 120., 140., 160., 200., 280., 360., 440.
06000      2, 520., 600., 680., 2000./
06800      IF (M .NE. 1) GO TO 12
06900 C
07000 C TABLE OF NORMALIZED INTEGRAL OF POWER FOR FLECHT COSINE
07100 C POWER BUNDLE
07200 C
07300      DATA (QAXZQ(J),J=1,17)/0., 1.83, 2.34, 3., 3.58,
07400      1 4.17, 4.83, 5.42, 6., 6.58, 7.17, 7.83, 8.42, 9.,
07500      2 9.66, 10.17, 12./
07600      DATA (QAXTB(J),J=1,17)/0., .53, .735, 1.088,
07700      11.478, 1.935, 2.534, 3.096, 3.6795, 4.263, 4.825,
07800      2 5.424, 5.881, 6.271, 6.624, 6.829, 7.359/
07900 C
08000 C TABLE OF AXIAL POWER SHAPE FACTOR FOR FLECHT COSINE
08100 C PWER BUNDLE
08200 C
08300      DATA (FAXTB(J),J=1,30)/.289, .289, .41, .41, .53, .53
08400      1, .669, .669, .783, .783, .898, .898, .964, .964, 1., 1.
08500      2, .964, .964, .898, .898, .783, .783, .669, .669, .53, .53
08600      3, .41, .41, .289, .289/
08700      DATA (FAXZ(J),J=1, 30)/0., 1.83, 1.84, 2.33, 2.34, 3.
08800      1, 3.01, 3.58, 3.59, 4.17, 4.18, 4.83, 4.84, 5.42, 5.43
08900      2, 6.58, 6.59, 7.17, 7.18, 7.83, 7.84, 8.42, 8.43
09000      3, 9., 9.01, 9.67, 9.68, 10.17, 10.18, 12./
09100      GO TO 16
09200 12 CONTINUE
09300 C
09400 C TABLE OF NORMALIZED INTEGRAL OF POWER FOR FLECHT SKEWED
09500 C POWER BUNDLE
09600 C
09700      IF (M .NE. 2) GO TO 13
09800      DATA (QAXZQS(J),J=1,14)/0., 1.5, 2.5, 3.5, 4.5, 5.5
09900      1, 6.5, 7.5, 8.5, 9.25, 10.25, 10.75, 11.25, 12./
10000      DATA (QAXTBS(J),J=1,14)/0., .722, 1.285, 1.907, 2.589
10100      1, 3.33, 4.13, 4.989, 5.915, 6.643, 7.643, 8.098
10200      2, 8.494, 8.845/
10240 C
10250 C TABLE OF AXIAL POWER SHAPE FACTOR FOR FLECHT SKEWED POWER
10260 C BUNDLE
10270 C

```

```

10300      DATA (FAXZS(J),J=1,26)/0., 1.5, 1.51, 2.5, 2.51, 3.5
10400      1, 3.51, 4.5, 4.51, 5.5, 5.51, 6.5, 6.51, 7.5, 7.51
10500      2, 8.5, 8.51, 9.25, 9.26, 10.25, 10.26, 10.75, 10.76
10600      3, 11.25, 11.26, 12./
10700      DATA (FAXTBS(J),J=1,26)/.4815, .4815, .563, .563, .622
10800      1, .622, .681, .681, .741, .741, .8, .8, .859, .859
10900      2, .926, .926, .97, .97, 1., 1., .911, .911, .793, .793
11000      3, .5259, .5259/
11500      GO TO 16
11600      13  CONTINUE
14900      16  CONTINUE
14950      TYPE 2100
15000      2100  FORMAT (3X,4HTIME,8X,1HH,4X,6HZQ(FT)
15100      1,4X,5HH(SI),1X,5HZQ(M))
15200      IX=30
15300      IF(M.EQ.1)CALL INTERP(FAXZ,FAXTB,IX,Z,FAX,FAXUZQ)
15400      IX=26
15500      IF(M.EQ.2)CALL INTERP(FAXZS,FAXTBS,IX,Z,FAX,FAXUZQ)
16000      TINITZ=(TINIT-TSAT)*FAX+TSAT
16100      RCPA=.05562
16200      IF (MBDL .EQ. 17) RCPA=.03851
16300      H1=.215*QMAX*.9481*FAX/RCPA*(1.-EXP(-(TINITZ-700.)/435.))
16350      IF (TINITZ .LT. 700.) H1=0.
16370      C
16375      C STEAM PROPERTIES---THE FOLLOWING ARE WESTINGHOUSE STEAM
16380      C TABLE FUNCTIONS. THEY MAY BE REPLACED BY APPROPRIATE
16385      C FUNCTIONS OR GIVEN AS INPUTS.
16390      C
16400      HG=HSV(P,TSAT,S,VOLG)
16405      C THIS FUNCTION PERFORMS H,T,S,V=F(P)
16406      C WHERE ENTROPY S IS NOT USED.
16410      VOLF=VCL(P,TSAT)
16415      CPF=CPL(P,TSAT)
16420      HF=HSL(TSAT)
16425      VISF=VISL(P,TSAT)
16430      KF=CONDL(P,TSAT)/3600.
16435      KG=CONDV(P,TSAT)/3600.
16440      C
16500      A=.00123
16600      IF (MBDL .EQ. 17) A=.0009455
16600      RHOG=1./VOLG
16900      RHOF=1./VOLF
17000      RHOGF=RHOG/RHOF
17100      CT=(TINIT-TSAT)/(500.-TSAT)
17400      HFG=HG-HF
17500      DR=.422/12.
17600      DE=.04451
17630      IF (MBDL .EQ. 15) RCPAF=.00123
17635      IF (MBDL .EQ. 15) RCPAR=.05562
17640      IF (MBDL .EQ. 17) RCPAF=.0009455
17645      IF (MBDL .EQ. 17) RCPAR=.0385

```

```

17700      IF (MBDL .EQ. 17) DE=.03863
17800      IF (MBDL .EQ. 17) DR=.374/12.
18300      H=H1
18400      HSI=H*5.67826
18500      T=0.
18600      ZQ=0.
19100      DZQ=.005
19200      CALL INTERP(VINTM,VINTB,NVIN,0.,VIN,VINSL)
19300      JTYPE=0
19400      JSTYPE=0
19500      J=1
19600 15      CONTINUE
19800 19      CONTINUE
19900 C
20000 C COMPUTE QUENCH FRONT ELEVATION
20100 C
20200      ZQ=ZQ+DZQ
22000 60      CONTINUE
22100      DO 40 IVQ=1,2
22200      IF (IVQ .EQ. 1) ZQ=ZQ-.0005
22300      IF (IVQ .EQ. 2) ZQ=ZQ+.0005
22400      IX=17
22500      IF (M .EQ. 1) CALL INTERP(QAXZQ,QAXTB,IX,ZQ,QAX,QAXSLF)
22600      IX=14
22700      IF (M .EQ. 2) CALL INTERP(QAXZS,QAXTBS,IX,ZQ,QAX,QAXSLF)
24050      QEQ1=QMAX
24100      IF (MR .EQ. 2) QEQ1=QEQ1*1.1
24500      IX=30
24600      IF (M .EQ. 1) CALL INTERP(FAXZ,FAXTB,IX,ZQ,FAX,FAXVZQ)
24700      IX=26
24800      IF (M .EQ. 2) CALL INTERP(FAXZS,FAXTBS,IX,ZQ,FAX,FAXVZQ)
25300      QEQ=QEQ1
25400      TINIT=(TINIT-TSAT)*FAX+TSAT
25430      DTC=800.
25440      DTE=DTC/(1.+60.**(1.08*(TINIT-TSAT)/DTC-1.26))
25450      TE=TINIT+DTE
25460      TEZ=TSAT+(TE-TSAT)*FAX
25500      QEFFZ=.7*FAX*.9481
25600      CALL INTERP(VINTM,VINTB,NVIN,T,VIN,VINSL)
25800      RE=VIN/12.*RHOF*DE/VISF
25850      FH=1./{1.+70.**(1.-.0133*(ZPEAK/DR))})
25900      ZS=6329.*{RE+4000.}**(-1.468)*VIN/12.*RHOF
26000      1*CPF*DE*DE/KF*FH
26050      ZAD=51.*RCPAF*DTSUB*VIN/12./QMAX/.9481-.234*RCPAR
26055      1*(TINIT-TSAT)*VIN/12./QMAX/.9481+1.147*FH
26057      IF (ZAD .LE. 0.) ZAD=0.
26100      FDTSUB=EXP(-10.09*(CPF*DTSUB/HFG))
26200      FVIN1=1.-EXP(-.00008137*RE/RHOGF**.262)
26300      FVIN2=1.3*EXP(-1.652E-9*RE*RE/RHOGF**.524)
26400      FVIN3=EXP(-7.293E-9*RE*RE/RHOGF**.524)
26500      FVIN4=66203.*RHOGF**.2882/RE**1.1-2.8*EXP(-.000122*

```

```

26600      1RE/RHOGF**.262)
26700      FVIN5=1.+.5/(1.+50**(-2.-.00008137*RE/RHOGF**.262))
26800      FP1=1.+.5*EXP(-5.6251E+08*RHOGF*RHOGF*RHOGF)
26900      FP2=17.3*EXP(-5.6251E+08*RHOGF*RHOGF*RHOGF)
27000      FP3=FP1
27100      FP4=1.+.32/(1.+50.**(-2520.*RHOGF))
27200      CT=(TINITE-TSAT)/(500.-TSAT)
27300      FT1=1.01552+.01388*CT
27400      FT2=1.05*EXP(-.66-.59*CT)
27500      FT=FT1+FT2
27600      FVSUB=.3+.7*(1.-EXP(-10.31E-8*RE*RE/RHOGF**.524
27700      1))-2.9E-11*RE*RE*RE/RHOGF**.786*EXP(-9.3E-8*RE*RE
27800      2/RHOGF**.524)/(1.+50.**(-15.75*(CPF#DTSUB/HFG)+1.333))
27900      DO 20 K=1,3
28000      IF (M.EQ.1) QDLS=.9481*3.6795/RHOF/A/VIN*12./HFG
28100      IF (M.EQ.2) QDLS=.9481*7.393/RHOF/A/VIN*12./HFG
28200      CQ=QE0*QDLS
28300      FVQ1=-.7*(1.-EXP(-.0000801*RE/RHOGF**.262))
28400      FVQ2=6.458E-5*RE**1.938/RHOGF**.5078*(CQ*DR/ZPEAK)**1.5
28500      FVQ=FVQ1+FVQ2
28600      FQ=1.16/(1.+70.**(1250.*(DR/ZPEAK)-5.45))
28700      1/(1.+80.**((7.14*CQ-4.93)))
28800      TQ=(FDTSUB*FVQ*(FP1+FVIN2+FP2*FVIN3)
28900      1+FVIN4*FP3)*(FT1-FT2*FVIN5*FP4)*FVSUB*FQ
29000      TQ=ZPEAK/VIN*.00228*RE*RHOGF**(-.262)*TQ
29100      FR1=.5
29200      FR2=9.
29300      IF (M.EQ.1) QR=QAX/3.6795
29400      IF (M.EQ.2) QR=QAX/7.393
29500      FQ=QR+FR1*GR*EXP(-FR2*QR*QR)
29600      TQ=TQ*FQ
29700      TQ=ZQ/VIN*12.+(TQ-ZQ/VIN*12.)/(1.+50.**
29800      1(-(TINITE-400.)/(400.-TSAT)))
29900      IX=16
30000      CALL INTERP(PDCT,PDCAY,IX,TQ,PDECAY,PDCP)
30100      QE0=QE01*PDECAY
30200      CONTINUE
30300      20      C      TYPE 3000, NS,T,TQ,HSI,ZQM
30400      IF (IVQ.EQ.1) ZQ1=ZQ
30500      IF (IVQ.EQ.1) TQ1=TQ
30600      IF (IVQ.EQ.2) ZQ2=ZQ
30700      IF (IVQ.EQ.2) TQ2=TQ
30800      40      C      CONTINUE
30900      VQ=(ZQ2-ZQ1)/(TQ2-TQ1)
31000      20      C      VQINCH=VQ*12.
31100      C      COMPUTE HEAT TRANSFER COEFFICIENT
31200      C
31300      70      C      CONTINUE
31400      ZQM=ZQ*.3048
31500      C      TYPE 3000, NS,T,TQ,HSI,ZQM

```

```

33300      IF(J.EQ.1) TYPE 2200,T,H,ZQ,HSI,ZQM
33400      T=T+DZQ/VQ
33600      X=4.*(ZQ-ZAD)/ZS
33650      NU1=H1/3600.*DE/KG
33900      H3=QEFFF/(TEZ-TSAT)/DR*1.21*(1.-EXP(-.0000305*RE/RHUGF
34000      1**.262))
34100      2*(.714+.286*(1.-EXP(-3.05E-4*RHUGF**1.524/RE/RE)))
34200      NU3=H3*DE/KG
34500      NU2=NU3+108.*EXP(-.0000183*RE/RHUGF**.262)*
34600      1EXP(-.0534*(Z-ZQ)/DE)
34650      IF(ZQ.LE.ZAD) NU=NU1
34700      IF(ZQ.LT.(ZS+ZAD).AND.ZQ.GT.ZAD) NU=NU1*
34800      1(1.-EXP(2.5*X-10.))+(NU2-NU1*(1.-EXP(2.5*X-10.)))
34810      2*(1.-EXP(-X)-.9*X*EXP(-X*X))
34900      IF(ZQ.GE.(ZS+ZAD)) NU=NU2
34930      IF(Z.LE.ZPEAK) GO TO 27
34935      IF(M.EQ.1) CALL INTERP(FAXZ,FAXTB,30,Z,FAX,FAXV)
34940      IF(M.EQ.2) CALL INTERP(FAXZS,FAXTBS,26,Z,FAX,FAXV)
34955      CONTINUE
35000      IF(Z.GT.ZPEAK) NU=NU-44.2*(1.-FAX)*EXP(-.00304
35100      1*(Z-ZPEAK)/DE)
35200      JTYPE=JTYPE+1
35300      JSTYPE=JSTYPE+1
35400      H=NU*KG*3600./DE
35500      HSI=H*5.67826
35600      IF(ZQ.LE.ZS.AND.JSTYPE.EQ.40.AND.JTYPE.NE.100)
35700      1 TYPE 2200,T,H,ZQ,HSI,ZQM
35800      ZMZQ=Z-ZQ
35900      IF(JTYPE.EQ.100)TYPE 2200,T,H,ZQ,HSI,ZQM
36000      2200 FORMAT(F7.0,F11.2,F7.1,F9.0,F6.2)
36100      IF(JSTYPE.EQ.40)JSTYPE=0
36200      IF(JTYPE.EQ.100) JTYPE=0
36300      IF(ZQ.GE.12.) GO TO 30
36400      J=J+1
36500      GO TO 15
36600      30 CONTINUE
36800      STOP
36900      END
37000      SUBROUTINE INTERP(X,Y,L,X1,Y1,SLOPE)
37100      DIMENSION X(100),Y(100)
37200      DO 100 K=1,L
37300      K1=K
37400      IF((X(K1)-X1).LT.100,100,200
37500      100 CONTINUE
37600      200 Y1=Y(K1-1)+((X1-X(K1-1))/(X(K1)-X(K1-1)))
37700      1*(Y(K1)-Y(K1-1))
37800      SLOPE=(Y(K1)-Y(K1-1))/(X(K1)-X(K1-1))
37900      RETURN
38000      END

```

EXAMPLE OF CALCULATION (RUN 31805)

RUN YHTDL

MR=1 FOR FLECHT POWER, MR=2 FOR UNIFORM POWER
M=1 FOR COSINE, M=2 FOR SKEW
MBDL=15 FOR 15X15, MBDL=17 FOR 17X17
ENTER RUN DTSUB P TINT QMAX TSAT M MR Z ZPEAK MBDL
31805, 140., 40., 1600., .7, 267., 1, 2, 6., 6., 17

ENTER VIN TABLE BELOW
ENTER NO. OF POINTS
2

ENTER TIME(10/LINE)
0., 1000.

ENTER VIN(10/LINE)
.8, .8

TIME	H	ZQ(FT)	H(SI)	ZQ(M)
0.	3.24	0.0	18.	0.00
5.	3.24	0.2	18.	0.06
10.	3.24	0.4	18.	0.12
13.	3.24	0.5	18.	0.15
15.	3.24	0.6	18.	0.18
20.	3.55	0.8	20.	0.24
25.	5.27	1.0	30.	0.30
30.	6.71	1.2	38.	0.37
37.	7.33	1.5	42.	0.46
54.	7.68	2.0	44.	0.61
75.	7.84	2.5	45.	0.76
93.	8.16	3.0	46.	0.91
117.	8.79	3.5	50.	1.07
142.	10.07	4.0	57.	1.22
174.	12.61	4.5	72.	1.37
209.	17.68	5.0	100.	1.52
247.	27.81	5.5	158.	1.68
287.	48.01	6.0	273.	1.83
326.	88.35	6.5	502.	1.98
362.	168.86	7.0	959.	2.13
394.	329.58	7.5	1871.	2.29
419.	650.36	8.0	3693.	2.44
435.	1290.67	8.5	7329.	2.59
460.	2568.77	9.0	14586.	2.74
456.	5119.91	9.5	29072.	2.90
442.	10212.13	10.0	57987.	3.05
410.	20376.46	10.5	115703.	3.20
418.	40665.03	11.0	230907.	3.35
427.	81162.08	11.5	460859.	3.51
436.	161996.38	12.0	919858.	3.66

U.S. NUCLEAR REGULATORY COMMISSION
BIBLIOGRAPHIC DATA SHEET

1. REPORT NUMBER (Assigned by DDCI)

NUREG/CR-2256

4. TITLE AND SUBTITLE (Add Volume No., if appropriate)

PWR FLECHT SEASET Unblocked Bundle, Forced and Gravity
 Reflood Task Data Evaluation and Analysis Report
 NRC/EPRI/Westinghouse Report No. 10

2. (Leave blank)

3. RECIPIENT'S ACCESSION NO.

7. AUTHOR(S)

N. Lee, S. Wong, H.C. Yeh, L. E. Hochreiter

5. DATE REPORT COMPLETED

MONTH	YEAR
September	1981

9. PERFORMING ORGANIZATION NAME AND MAILING ADDRESS (Include Zip Code)

Westinghouse Electric Corporation
 Nuclear Energy Systems
 P. O. Box 355
 Pittsburgh, PA 15230

DATE REPORT ISSUED

MONTH	YEAR
November	1981

6. (Leave blank)

8. (Leave blank)

12. SPONSORING ORGANIZATION NAME AND MAILING ADDRESS (Include Zip Code)

U. S. Nuclear Regulatory Commission Electric Power Res. Inst.
 Office of Nuclear Regulatory P. O. Box 10412
 Research Palo Alto, CA 94303
 Division of Accident Evaluation
 Washington, D.C. 20555

10. PROJECT/TASK/WORK UNIT NO.

11. CONTRACT NO.
 NRC-04-77-127
 FIN B6204

13. TYPE OF REPORT

PERIOD COVERED (Inclusive dates)

Technical Topical Report

April 1980 - January 1981

15. SUPPLEMENTARY NOTES

14. (Leave blank)

16. ABSTRACT (200 words or less)

This analysis of the unblocked bundle task data provides further understanding of reflood heat transfer mechanisms, which can be used for assessing prediction models. A new heat transfer correlation has been developed and shown to predict the FLECHT SEASET data as well as the older FLECHT data. The scaling logic of maintaining the same integrated power per unit flow area has been proved valid, and a method has been developed to calculate steam quality just above the quench front. Improved models for estimating effluence rate and preliminary exploration of the transition zone above the quench front are discussed. Droplet size and velocity data deduced from high-speed movies taken during the tests have led to better understanding of these parameters. A model has been proposed to predict the onset of droplet entrainment, and an analytical expression to predict critical void fraction developed. A network analysis of radiation heat exchange and calculation of convective heat transfer are among efforts expected to give better prediction for heat transfer and wall temperature transients. Recommendations evolving from the data analysis are also included.

17. KEY WORDS AND DOCUMENT ANALYSIS

17a. DESCRIPTORS

17b. IDENTIFIERS/OPEN-ENDED TERMS

18. AVAILABILITY STATEMENT

Unlimited

19. SECURITY CLASS (This report)

Unclassified

21. NO. OF PAGES

20. SECURITY CLASS (This page)

Unclassified

22. PRICE

\$

UNITED STATES
NUCLEAR REGULATORY COMMISSION
WASHINGTON, D. C. 20555

OFFICIAL BUSINESS
PENALTY FOR PRIVATE USE, \$300

POSTAGE AND FEES PAID
U.S. NUCLEAR REGULATORY
COMMISSION



120555064215 2 ANR1R2R4
US NRC
ADM DOCUMENT CONTROL DESK
PDR
016
WASHINGTON

DC 20555